

About the Author

Mohamad S. Qatu received his undergraduate engineering degree from Yarmouk University in Jordan in 1985. He then obtained his M.S. and Ph.D. degrees from the Ohio State University in 1986 and 1989, respectively. His academic experience includes working as the director of the mechanical engineering technology program at Franklin University (1992–1995), and as associate professor of mechanical engineering at Lake Superior State University (1995–1997) and an adjunct professor at Oakland University (2002–present). His industrial experience includes working for Dresser Industries (1989–1991), Honda of America (1994), Dana Corporation (1997–2000) and Ford Motor Company (2000–present). He is the author of more than 60 research papers, review articles and book reviews, in addition to numerous abstracts. He is a registered professional engineer in both Ohio and Michigan. His research interests are noise, vibration and harshness (NVH), composite structures, and computer-aided engineering (CAE). He has two patent on noise suppression, several technical awards, and few manuals to his credit. He is working on two books. He has developed courses for Society of Manufacturing Engineers and others. He recently established the new journal “International Journal of Vehicle Noise and Vibration,” and is serving as its executive editor.

Preface

This is the first book on the title subject. There are many reasons for presenting this book to the engineering community at large. Among which are the enormous literature that appeared during the past decades on the subject, the new applications of composite structures, and the added attention given to vibration issues by engineering customers. Many engineering designs are driven by vibrations in today's engineering environment. This book documents some of the latest research in the field of vibration of composite shells and plates and fills certain gaps in this area of research.

The literature on the subject have exploded during the past few decades necessitating such a book. This subject received no or little attention three decades ago. In fact, the monographs published then on vibration of plates and vibration of shells by Leissa dealt mainly with isotropic plates and shells. It touched only briefly on shells other than isotropic. New survey articles revealed that the literature on composite shells and their vibrations have expanded rapidly since then. In fact, the literature found on shell vibrations between 1989 and 2000 was more than all that found prior to 1970.

Furthermore, laminated composite shells are increasingly being used in various engineering applications including aerospace, mechanical, marine, and automotive engineering. With the increasing awareness of, and sensitivity to, structural noise and vibration, research covering the vibration of composite plates and shells has received considerable attention.

The book is laid down in various chapters. The first chapter is an introduction with some historical remarks. The second chapter reviews the various theories used for analyzing composite shells. It covers three-dimensional, shear deformation and classical shell theories. The equations are written in curvilinear coordinates so that they can be easily specialized later for beams, plates and different shell geometries. Less attention is given to nonlinear theories or layer-wise theories. The third chapter of the book overviews the methods used for analyzing such structural components. In particular, special attention is given to linear analysis using the Ritz, Galerkin and finite element methods. These methods will be used in the subsequent chapters.

Chapter four is about vibration of curved beams. This chapter covers the fundamental theories used for analyzing composite curved beams and the fundamental equations used in each theory. It also presents results for various configurations including different boundary conditions and lamination sequences. Emphasis is on the in-plane vibration of curved beams.

Chapter five covers vibration of plates. Fundamental theories are presented. Analysis is given for various plates having rectangular, triangular, trapezoidal and circular

planforms. Mode shapes are also presented for various rectangular plate boundary conditions and lamination configurations.

Chapter six covers shallow shell vibrations. In addition to fundamental equations, the chapter covers analyses made for such shells on rectangular, triangular, trapezoidal and circular planforms. The interesting problem of rectangular lamination, which leads to rectangular orthotropy, on a circular planform is also discussed.

Cylindrical shells are the subject of Chapter seven. Theories and the accompanying equations are presented for these widely used structures. Results are presented for open and closed cylindrical shells having circular cross-section. Closed cylindrical shells with non-circular cylindrical cross-section are also treated. This chapter also covers shells with initial curvature in the axial direction of the shells. Such shells are often referred to as barrel shells.

Other shells, mainly spherical and conical shells are the subjects of Chapters eight and nine. Fundamental equations are presented. Results for selected shell configurations and boundary conditions are also presented in these chapters.

Literature on complicating effects is presented in Chapter ten. These include dynamic loading, thermal stresses, rotating, stiffened, imperfect, piezoelectric, damped and visco-elastic structures. Classical complicating effects like shear deformation consideration is covered in earlier chapters and is not treated in this chapter. Literature treating shells imbedded in (or filled with) elastic or fluid media is also reviewed.

This book is intended to be a reference for researchers in the field and practicing engineers. It can also be used as a text book, or a reference book, for a graduate course on plates and shells, composite structures or vibrations of continuous systems. Prior courses on vibrations, elasticity, variational methods, plates and shells and composite structures are beneficial before treating this book.

I wish to thank various people whose support was vital to the completion of this task. I thank first Dr. Leissa, adjunct professor at Colorado State University and Professor Emeritus at Ohio State University, whose guidance and encouragement was vital for completing this effort. I also thank Professors Ali and Adnan Nayfeh, who set an example for me to follow and built the founding blocks of my interest in mechanics. Also, I would like to thank Mr. Pinfield and Ms. Blatchford of Elsevier and Elsevier's editorial staff, who made this a reality. The author thanks the reviewers who reviewed this work before its publication. The initial review and continued support of my graduate students at Oakland university is also appreciated. In particular, the author thanks Mr. Iqbal, Mr. Sirafi, Mr. Chen, Mr. Abdalla, and Mrs. Sun for their initial review. The author thanks Ms. Cooper and Ms. Swan for their proof-reading and editorial help. Finally, the author thanks his wife Rajaa and children, Abdullah, Mossab, Khalil, Osayd and Zaynab-Haleema; whose understanding, support and sacrifice gave fruit to this work.

MOHAMAD SUBHI QATU
Bloomfield, Michigan

Chapter 1

Introduction

The use of laminated composite plates and shells in many engineering applications has been expanding rapidly in the past three decades. This resulted in considerably more research and interest in their dynamic behavior. In fact, a 1973 monograph by Leissa (1973a) that reviewed shell vibration research up to that point and included about 1000 references listed only few (less than 20) articles that touched on composite shells. A similar observation can be made on plate vibration research (Leissa 1969). As can be seen from the list of references in a recent survey article by the author (Qatu 2002a); approximately 400 papers are listed between 1989 and 2000 alone on composite shell dynamics. Additionally, homogeneous shells received the attention of approximately 600 articles during the same time (Qatu 2002b).

Structures composed of composite materials offer lower weight and higher strength and stiffness than those composed of most metallic materials. That, coupled with advances in the manufacturing of composite materials and structures, gave them a competitive edge when compared with normal engineering materials and led to their extensive use. Composite plates and/or shell components now constitute a large percentage of recent aerospace and submarine structures. They have found increasing use in areas like automotive engineering and other applications. In this chapter we will review some historical aspects of the theory and applications of composite plates and shells as well as their vibration behavior.

1.1. HISTORICAL REMARKS

The discussion in this section is intended to review the historical development of the subject at hand. It is neither meant to be comprehensive nor complete. Rather, it only introduces the reader to some of the early developments in mechanics which were used as the foundation for treating vibration of composite structures.

1.1.1 Development of the theory of plates and shells

Bernoulli developed the first accurate equation for beams as early as 1735 (Soedel 1993). His equations led to interesting discussion with Euler and solutions to several beam boundary conditions. The equations developed by Bernoulli assume pure bending, and thus, both axial and shear deformations were ignored. It is now known that such equations are valid for thin beams undergoing small deformations. It was noted as early as 1877 that

rotary inertia terms are important in the analysis of vibrating systems by Rayleigh (1877). More than 40 years later, Timoshenko (1921) showed that shear deformation terms are at least as important.

The first accurate treatment of plates can be attributed to Germain (1821) and Lagrange (1811) early in the 19th century. A good historical review of the development can be referred to in the books of Soedel (1993) and Timoshenko (1983). This theory is now referred to as the classical plate theory (CPT). It uses the pure bending concept of plates in the development of the equation, where normals to the midsurface remain straight and normal. It is valid for small deformation of thin plates. The inclusion of shear deformation in the fundamental equations of plates is due to Reissner (1945) and Mindlin (1951). Theories that account for shear deformation are now referred to as thick plate theories or shear deformation plate theories (SDPT).

The first accurate shell theory may be attributed to Love (1892). In this theory, Love introduced his first approximation for bending analysis of shells. This approximation defines a linear analysis of thin shells, in which various assumptions were introduced. Among these assumptions, strains and displacements are assumed to be small such that second and higher order terms can be neglected. In addition, Love assumed the thickness of the shell to be small compared with other shell parameters, the transverse stress to be small compared with other stresses in shells, and normals to the undeformed surface to remain straight and normal to the deformed surface. Since then, other shell theories were introduced that were based on the same Love's approximation but differed in the detailed derivation.

Since the introduction of these shell theories, inconsistencies appeared in many of them. Leissa (1973a,b) reported some of these inconsistencies with regard to rigid body motion and unsymmetric differential operators. To overcome some or all of these inconsistencies, various theories were introduced including that of Sanders (1959) and Vlasov's (1949). Among the additional developments that should be stated are the work of Reissner (1941), Novozhilov (1958), Timoshenko and Woinowsky-Krieger (1959), Flugge (1962), Donnell (1976) and Mushtari (1961). Review of these developments and theories can be found in the monograph by Leissa (1973a,b) and the books by Kraus (1967) and Soedel (1993).

Since then, researchers realized that for thick beams, plates or shells, both rotary inertia and shear deformation have to be included in any reliable theory of such components. Various studies, however, like that of Koiter (1967) and Gol'denveizer (1961), concluded that for thin and moderately thick shells, the transverse normal stress remains small compared with other stresses in the shell. The inclusion of shear deformation (and rotary inertia) led to a necessary relaxation of some of the assumptions in Love's first approximation, and shear deformation shell theories were born. Among the first of such theories were those of Vlasov (1949), Reissner (1941) and others.

1.1.2 Development of the theory of laminated plates and shells

Among the first to work on composite plates was Smith (1953). He analyzed the bending behavior of a two-layer rectangular plywood plate in which the fibers of the layers are oriented at angles $+\theta$ and $-\theta$ to the axis of the plate. A consistent theory for symmetrically laminated plates was presented by Reissner and Stavski (1961). There is evidence that some Russian scientists may indeed have considered the problem earlier. Ambartsumian (1961, 1970) and Lekhnitski (1968), published probably the first books in the area of composite plates and shells. They presented the fundamental equations and solved for stresses and deformation under static loads. Librescu (1976) covered areas of stability and flutter. Vinson and Sierakowski (1986) presented analysis of composite beams, plates and shells, while Whitney (1987) analyzed laminated plates.

The beam, plate and shell theories used for isotropic materials need further treatment when composite materials are in consideration. This is because such materials offer higher shear deformation than typical metallic materials. Also, laminated structures introduce the stretching–bending coupling phenomenon (when the lamination is unsymmetric) and new coefficients need to be determined. Such coupling exists for isotropic shells and curved beams and does not exist for straight beams or flat plates.

The inclusion of shear deformation was made for beams by Timoshenko (1921) and expanded for plates by Reissner (1945) and Mindlin (1951). It was shown as early as 1970 that shear deformation effects are higher for laminated plates than they are for isotropic ones (Whitney 1969; Whitney and Sun 1973; Pagano 1970; Srinivas *et al.* 1970).

Orthotropic cylindrical shells were considered by Dong (1968) and Rath and Das (1973). The latter presented equations that included rotary inertia and shear deformation. Among other shear deformation theories developed for shells are those of Reddy (1984a,b) and Librescu *et al.* (1989a,b). The latter included higher order terms as did Lim and those obtained by Liew (1995a,b). Such theories ignored the trapezoidal shape of the shell cross-section in the integration of the stress resultant (i.e., the $1 + z/R$ term). Leissa and Chang (1996) did consider this term but truncated it using a geometric series expansion. Qatu integrated the term exactly for curved beams (Qatu 1993a,b) and shells (Qatu 1999a).

In addition to the previous articles, more recent literature on composite shell vibrations research can be found in various conference proceedings and journals. Other review articles like those by Kapania (1989), Qatu (1992b), Noor and Burton (1990), and Noor *et al.* (1991) covered much of the research done in the *earlier* decades (prior to 1990). Liew *et al.* (1997a,b) reviewed the literature on shallow shell vibrations. Soldatos (1999) reviewed the literature on non-circular cylindrical shells. Computational aspects of the research were covered by Noor *et al.* (1996) and Noor and Venneri (1992).

This book will focus only on the *linear free vibration* of composite shells and plates. Curved beams are also covered. Other subjects of research like shell buckling,

postbuckling, and stress analysis are not included in this book, although much of the fundamental equations and analyses can be expanded to these classes of problems.

1.1.3 Vibration of composite shells and plates

This book presents a unified treatment of the theories being used. These theories include thin and thick beam/plate/shell theories (including three-dimensional theories), shallow and deep shell theories and others. The book focuses only on linear analysis. Most theories are classified based on the thickness ratio of the element being treated (defined as the ratio of the thickness of the structural element to the shortest of the span lengths or radii of curvature for shells and curved beams), its shallowness ratio for shells (defined as the ratio of the shortest span length to one of the radii of curvature or *vice versa*), and the magnitude of displacement (compared mainly to the shell's thickness). Fundamental equations are listed. Comparisons among various theories are also made.

The book also overviews a few methods used frequently in the vibration analysis of laminated beams, plates and shells. Among the methods being used are exact methods, the Ritz method, finite elements and others. Various geometries of plates and shells are considered. Plates (and shallow shells) can have various planforms including rectangular, triangular, circular and others. Among classical shell geometries treated in this book are the cylindrical, spherical and conical shells.

The book also reviews recent advances regarding several complicating effects to the problem at hand. The classical complicating effects of anisotropy and shear deformation are naturally a part of the context of the book. Other classical complicating effects include added mass and spring, and elastic supports. Recent articles showed specific attention to geometric imperfection, piezoelectric materials, initial stresses and rotating condition of the shell as well as others.

1.2. FUNDAMENTAL EQUATIONS OF ELASTICITY IN RECTANGULAR COORDINATES

The fundamental engineering question in mechanics is to determine the fundamental laws that govern the motion (or deformation) of engineering bodies as a result of the application of external (and internal) loads. Once determined, the motion and/or deformation of engineering bodies can be predicted under a given set of loading and boundary conditions for a specified body. The approach followed in mechanics is to first relate the external forces to internal stresses (or stress resultants) through external to internal force and moment equilibrium. This analysis and the resulting equations will be referred to as kinetics. Second, the deformation of the engineering body is related to engineering strains or “average” deformation. This analysis and the resulting equations are referred to as kinematics. Once the state of stress and that of strains are determined

independently, the constitutive (i.e., stress–strain) relations can be used to complete the set of equations needed to solve the problem. Solution to the problem is nothing but finding the deformation (and/or motion) of an engineering body as a result of the application of forces and/or moments. It is assumed here, unless stated otherwise, that the materials are perfectly elastic. In this section, we will cover the fundamental equations that govern the mechanics of elastic laminated bodies in rectangular coordinates.

1.2.1 Kinematic relations

It is assumed that the structure being treated has enough constraints to prevent rigid body motion. The only displacement within the body treated here is related to its deformation. Furthermore, only small deformations (and rotations) are treated here. The deformation of the body is broken into components u , v and w parallel to the α , β and z coordinates (Figure 1.1).

Consider a simple differential element of a body with the point O as its origin undergoing the deformation u , v and w . The displacement of an adjacent point A along the α -axis is $u + (\partial u / \partial \alpha) d\alpha$. The increase in length of the element OA is thus $(\partial u / \partial \alpha) d\alpha$. The unit elongation (or strain ε_α) in the α direction then becomes $(\partial u / \partial \alpha)$. Similarly, the unit elongation in the β and z directions are $(\partial v / \partial \beta)$ and $(\partial w / \partial z)$, respectively. Hence, the strain displacement relations can be written as

$$\begin{aligned}\varepsilon_\alpha &= \frac{\partial u}{\partial \alpha} \\ \varepsilon_\beta &= \frac{\partial v}{\partial \beta} \\ \varepsilon_z &= \frac{\partial w}{\partial z}\end{aligned}\tag{1.1}$$

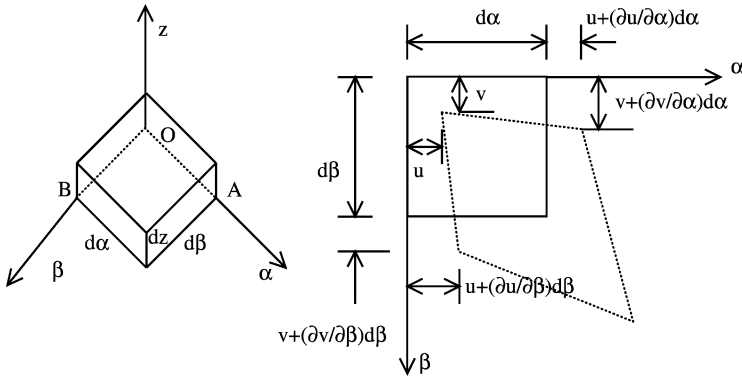


Figure 1.1. Simple differential elements in rectangular coordinates.

Taking a top view of the first differential element (Figure 1.1), the deformation of point A along the α -axis in the β direction will be $v + (\partial v / \partial \alpha) d\alpha$. Similarly the deformation of a point B along the β -axis in the α direction is $u + (\partial u / \partial \beta) d\beta$. The distortion of the right angle at point O is $(\partial v / \partial \alpha + \partial u / \partial \beta)$, which is defined as the shear strain in the $\alpha\beta$ plane. Similarly, shear strains can be found in the αz and βz planes

$$\begin{aligned}\gamma_{\alpha\beta} &= \frac{\partial v}{\partial \alpha} + \frac{\partial u}{\partial \beta} \\ \gamma_{\alpha z} &= \frac{\partial w}{\partial \alpha} + \frac{\partial u}{\partial z} \\ \gamma_{\beta z} &= \frac{\partial w}{\partial \beta} + \frac{\partial v}{\partial z}\end{aligned}\tag{1.2}$$

1.2.2 Stress-strain relations

In order to derive stress-strain relations, consider a laminated composite thin structure constructed from very thin layers of composite material laminae. The materials of each lamina consist of parallel, continuous fibers of one material (e.g., glass, boron, graphite) embedded in a matrix material (e.g., epoxy resin). The matrix material has the primary purpose of transferring shear stress between the fibers as needed. Unless stated otherwise, we will make the following assumptions:

1. The fibers are parallel to the upper and lower surfaces of their layer within the shell, plate or beam.
2. The fibers do not follow straight lines for shells or curved beams. Instead, the curvature of these fibers follow that of the shell maintaining the same distance from the upper and lower surfaces.
3. The angle between the fibers in one layer to those in another layer remains constant.

Plates and shells can have various types of orthotropy depending on the fiber orientations. The fibers may follow rectangular orthotropy. This can happen when one finds a rectangular coordinate system for each layer where the fibers in that layer are parallel to one coordinate and perpendicular to other coordinates. This defines rectangular orthotropy, as compared with circular or polar orthotropy. In the latter, for each layer there exist polar coordinate systems where the fibers are either in the radial or tangential directions. This consideration will introduce a fundamental concern in the formulation of the problem which is no longer a function of only the boundaries or the geometrical shape. The material and its orthotropy must be considered in the formulation of the equations at a fundamental level. A challenge will rise when a circular plate, for example, is made out of materials having rectangular orthotropy. The analyst then faces the problem of whether to formulate the problem using rectangular or polar coordinates. Such problems are seldom treated analytically. A treatment will be introduced later in this book for such plates.

On a macroscopic level, each layer will be regarded as being homogeneous and orthotropic. However, the fibers of a typical layer may not be parallel to the coordinates in which the equations are expressed. This yields anisotropy at the macro-level of the laminate.

For an orthotropic layer, the stress–strain relations can be presented in terms of the layers' fiber directions (or coordinates) in three dimensions as

$$\begin{bmatrix} \sigma_1 \\ \sigma_2 \\ \sigma_3 \\ \sigma_{23} \\ \sigma_{13} \\ \sigma_{12} \end{bmatrix} = \begin{bmatrix} Q_{11} & Q_{12} & Q_{13} & 0 & 0 & 0 \\ Q_{12} & Q_{22} & Q_{23} & 0 & 0 & 0 \\ Q_{13} & Q_{23} & Q_{33} & 0 & 0 & 0 \\ 0 & 0 & 0 & Q_{44} & 0 & 0 \\ 0 & 0 & 0 & 0 & Q_{55} & 0 \\ 0 & 0 & 0 & 0 & 0 & Q_{66} \end{bmatrix} \begin{bmatrix} \varepsilon_1 \\ \varepsilon_2 \\ \varepsilon_3 \\ \gamma_{23} \\ \gamma_{13} \\ \gamma_{12} \end{bmatrix} \quad (1.3)$$

Note that we described the fiber coordinates of the laminate as 1 and 2, where direction 1 is parallel to the fibers and 2 is perpendicular to them. The material constants Q_{ij} are defined in terms of the material properties of the orthotropic laminae.

$$\begin{aligned} Q_{11} &= E_{11} \frac{1 - \nu_{23}\nu_{32}}{\Delta}, & Q_{22} &= E_{22} \frac{1 - \nu_{31}\nu_{13}}{\Delta} \\ Q_{33} &= E_{33} \frac{1 - \nu_{12}\nu_{21}}{\Delta}, & Q_{44} &= G_{23}, & Q_{55} &= G_{13}, & Q_{66} &= G_{12} \\ Q_{12} &= E_{11} \frac{\nu_{21} + \nu_{31}\nu_{23}}{\Delta} = E_{22} \frac{\nu_{12} + \nu_{32}\nu_{13}}{\Delta} \\ Q_{13} &= E_{11} \frac{\nu_{31} + \nu_{21}\nu_{32}}{\Delta} = E_{22} \frac{\nu_{13} + \nu_{12}\nu_{23}}{\Delta} \\ Q_{23} &= E_{22} \frac{\nu_{32} + \nu_{12}\nu_{31}}{\Delta} = E_{33} \frac{\nu_{23} + \nu_{21}\nu_{13}}{\Delta} \\ \Delta &= 1 - \nu_{12}\nu_{21} - \nu_{23}\nu_{32} - \nu_{31}\nu_{13} - 2\nu_{21}\nu_{32}\nu_{13} \end{aligned} \quad (1.4)$$

where E_{11} , E_{22} and E_{33} are moduli of elasticity in the 1, 2 and 3 directions, respectively; G_{12} , G_{23} , and G_{13} are moduli of rigidity and ν_{ij} ($i, j = 1, 2, 3, i \neq j$) are Poisson's ratios. It should be noted that the Poisson's ratios are governed by the equation $\nu_{ij}/E_{ii} = \nu_{ji}/E_{jj}$. There are only nine independent material properties for each layer. These are E_{11} , E_{22} , E_{33} , G_{12} , G_{23} , G_{13} , ν_{12} , ν_{23} and ν_{13} .

Consider a stress element shown in Figure 1.2. The orientation of the fiber makes the angle θ with the rectangular coordinates α and β . The transformation of stresses (and strains) from the 1, 2 coordinates (Figure 1.3) to the $\alpha\beta$ coordinates can be performed by

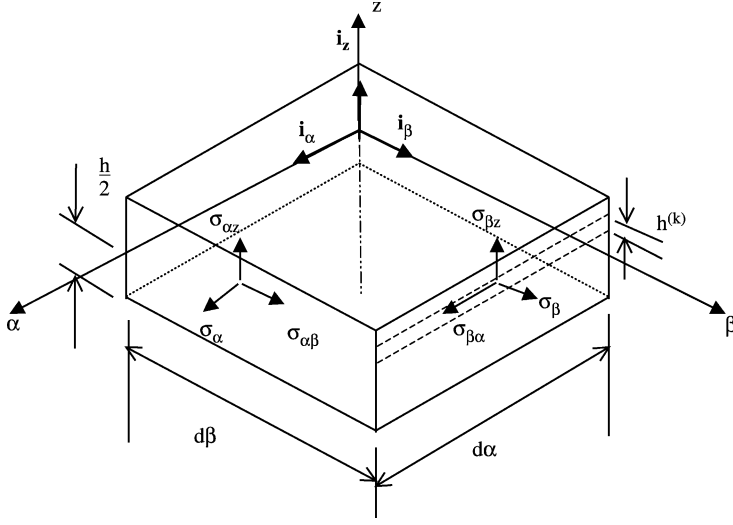


Figure 1.2. Notations in rectangular coordinates.

using the transformation matrix T . This matrix is

$$T = \begin{bmatrix} m^2 & n^2 & 0 & 0 & 0 & 2mn \\ n^2 & m^2 & 0 & 0 & 0 & -2mn \\ 0 & 0 & 1 & 0 & 0 & 0 \\ 0 & 0 & 0 & m & -n & 0 \\ 0 & 0 & 0 & n & m & 0 \\ -mn & mn & 0 & 0 & 0 & (m^2 - n^2) \end{bmatrix} \quad (1.5)$$

where $m = \cos(\theta)$ and $n = \sin(\theta)$. Note that the inverse of the transformation matrix T can be found by replacing θ with $-\theta$. The transformation from fiber coordinates 1 and 2 to global coordinates α and β can be done now as follows:

$$\begin{bmatrix} \sigma_\alpha \\ \sigma_\beta \\ \sigma_z \\ \sigma_{\beta z} \\ \sigma_{\alpha z} \\ \sigma_{\alpha\beta} \end{bmatrix} = T^{-1} \begin{bmatrix} \sigma_1 \\ \sigma_2 \\ \sigma_3 \\ \sigma_{23} \\ \sigma_{13} \\ \sigma_{12} \end{bmatrix}, \quad \text{and} \quad \begin{bmatrix} \varepsilon_\alpha \\ \varepsilon_\beta \\ \varepsilon_z \\ \varepsilon_{\beta z} \\ \varepsilon_{\alpha z} \\ \varepsilon_{\alpha\beta} \end{bmatrix} = T^{-1} \begin{bmatrix} \varepsilon_1 \\ \varepsilon_2 \\ \varepsilon_3 \\ \gamma_{23} \\ \gamma_{13} \\ \gamma_{12} \end{bmatrix} \quad (1.6)$$

The stress–strain relationship for a typical n th lamina (typically called monoclinic) in a laminated composite shell becomes

$$\begin{bmatrix} \sigma_\alpha \\ \sigma_\beta \\ \sigma_z \\ \sigma_{\beta z} \\ \sigma_{\alpha z} \\ \sigma_{\alpha\beta} \end{bmatrix} = \begin{bmatrix} \bar{Q}_{11} & \bar{Q}_{12} & \bar{Q}_{13} & 0 & 0 & \bar{Q}_{16} \\ \bar{Q}_{12} & \bar{Q}_{22} & \bar{Q}_{23} & 0 & 0 & \bar{Q}_{26} \\ \bar{Q}_{13} & \bar{Q}_{23} & \bar{Q}_{33} & 0 & 0 & \bar{Q}_{36} \\ 0 & 0 & 0 & \bar{Q}_{44} & \bar{Q}_{45} & 0 \\ 0 & 0 & 0 & \bar{Q}_{45} & \bar{Q}_{55} & 0 \\ \bar{Q}_{16} & \bar{Q}_{26} & \bar{Q}_{36} & 0 & 0 & \bar{Q}_{66} \end{bmatrix} \begin{bmatrix} \varepsilon_\alpha \\ \varepsilon_\beta \\ \varepsilon_z \\ \gamma_{\beta z} \\ \gamma_{\alpha z} \\ \gamma_{\alpha\beta} \end{bmatrix} \quad (1.7)$$

where as discussed earlier, σ_α , σ_β , and σ_z are normal stress components; $\sigma_{\alpha z}$, $\sigma_{\beta z}$, and $\sigma_{\alpha\beta}$ are shear stress components; ε_α , ε_β , and ε_z are normal strain components and $\gamma_{\alpha\beta}$, $\gamma_{\alpha z}$ and $\gamma_{\beta z}$ are the engineering shear strains. The positive directions of the stresses are shown in Figure 1.2.

The constants \bar{Q}_{ij} are the elastic stiffness coefficients, which are found from the equations

$$[\bar{Q}] = [T]^{-1}[Q][T] \quad (1.8)$$

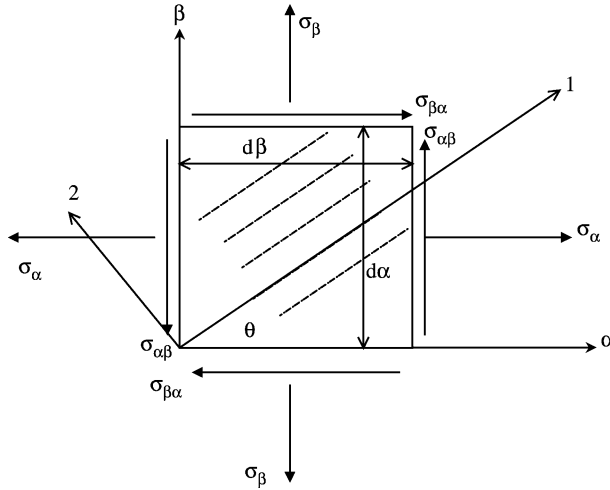


Figure 1.3. Coordinate systems of fiber reinforced materials.

Performing the matrix multiplication in the above equation, the stiffness coefficients \bar{Q}_{ij} can be written as

$$\begin{aligned}
 \bar{Q}_{11} &= Q_{11}m^4 + 2(Q_{12} + 2Q_{66})m^2n^2 + Q_{22}n^4 \\
 \bar{Q}_{12} &= (Q_{11} + Q_{22} - 4Q_{66})m^2n^2 + Q_{12}(m^4 + n^4) \\
 \bar{Q}_{13} &= Q_{13}m^2 + Q_{23}n^2 \\
 \bar{Q}_{16} &= -mn^3Q_{22} + m^3nQ_{11} - mn(m^2 - n^2)(Q_{12} + 2Q_{66}) \\
 \bar{Q}_{22} &= Q_{11}n^4 + 2(Q_{12} + 2Q_{66})m^2n^2 + Q_{22}m^4 \\
 \bar{Q}_{23} &= Q_{23}m^2 + Q_{13}n^2 \\
 \bar{Q}_{33} &= Q_{33} \\
 \bar{Q}_{26} &= mn^3Q_{11} - m^3nQ_{22} - mn(m^2 - n^2)(Q_{12} + 2Q_{66}) \\
 \bar{Q}_{36} &= (Q_{13} - Q_{23})mn \\
 \bar{Q}_{66} &= (Q_{11} + Q_{22} - 2Q_{12})m^2n^2 + Q_{66}(m^2 - n^2)^2 \\
 \bar{Q}_{44} &= Q_{44}m^2 + Q_{55}n^2 \\
 \bar{Q}_{55} &= Q_{55}m^2 + Q_{44}n^2 \\
 \bar{Q}_{45} &= (Q_{55} - Q_{44})mn
 \end{aligned} \tag{1.9}$$

1.2.3 Equations of motion and boundary conditions

The equations of motion can be derived directly from Newton's second law of motion, where the sum of forces is equal to the mass multiplied by the acceleration. Consider the stress differential element shown in Figure 1.4.

Consider also body forces in each of the three direction. In order to get the forces on each plane, one needs to multiply each stress vector by the area upon which it is acting. Summing the forces first in the α direction yields

$$\begin{aligned}
 &-\sigma_\alpha d\beta dz + \left(\sigma_\alpha + \frac{\partial \sigma_\alpha}{\partial \alpha} d\alpha \right) d\beta dz \\
 &-\sigma_{\alpha\beta} d\alpha dz + \left(\sigma_{\alpha\beta} + \frac{\partial \sigma_{\alpha\beta}}{\partial \beta} d\beta \right) d\alpha dz \\
 &-\sigma_{\alpha z} d\alpha d\beta + \left(\sigma_{\alpha z} + \frac{\partial \sigma_{\alpha z}}{\partial z} dz \right) d\alpha d\beta + q_\alpha d\alpha d\beta dz = \rho dV \frac{\partial^2 u}{\partial t^2}
 \end{aligned} \tag{1.10}$$

Note that $dV = d\alpha d\beta dz$, where V is volume. Divide the above equation by dV . It yields

$$\frac{\partial \sigma_\alpha}{\partial \alpha} + \frac{\partial \sigma_{\alpha\beta}}{\partial \beta} + \frac{\partial \sigma_{\alpha z}}{\partial z} + q_\alpha = \rho \frac{\partial^2 u}{\partial t^2} \tag{1.11}$$

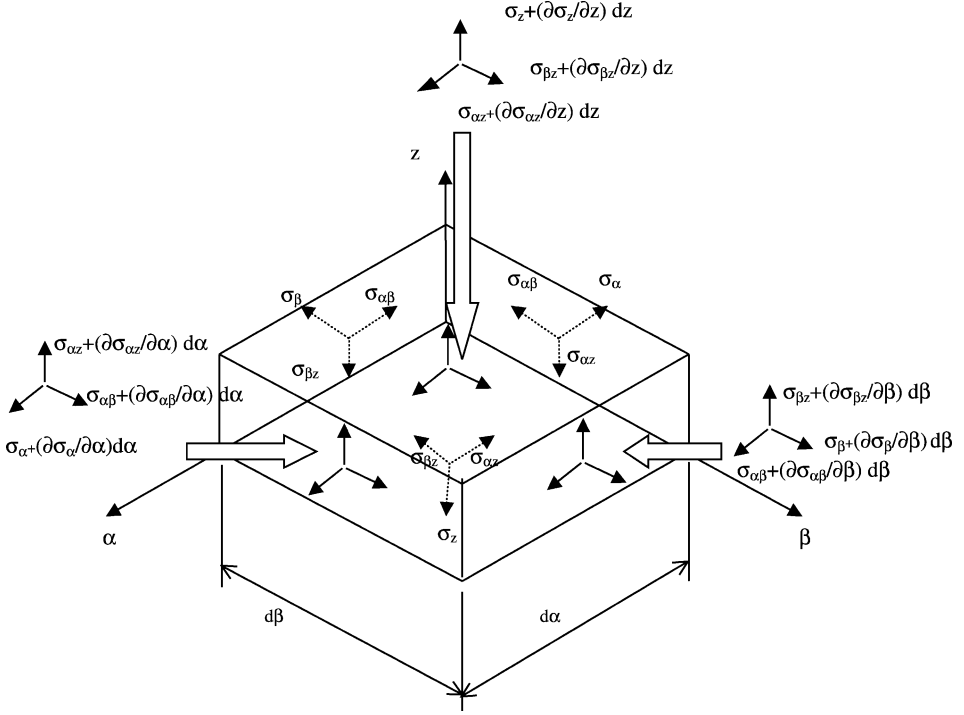


Figure 1.4. Stress notations in rectangular coordinates.

Similarly, summing the forces in the β and z directions yield the other two differential equations

$$\begin{aligned} \frac{\partial \sigma_{\alpha\beta}}{\partial \alpha} + \frac{\partial \sigma_{\beta}}{\partial \beta} + \frac{\partial \sigma_{\beta z}}{\partial z} + q_{\beta} &= \rho \frac{\partial^2 v}{\partial t^2} \\ \frac{\partial \sigma_{\alpha z}}{\partial \alpha} + \frac{\partial \sigma_{\beta z}}{\partial \beta} + \frac{\partial \sigma_z}{\partial z} + q_z &= \rho \frac{\partial^2 w}{\partial t^2} \end{aligned} \quad (1.12)$$

The boundary terms have to be obtained by physical arguments. For the boundaries with $z = \text{constant}$, these boundary conditions are

$$\begin{aligned} \sigma_{0z} - \sigma_z &= 0 & \text{or} & & w^0 &= 0 \\ \sigma_{0\alpha z} - \sigma_{\alpha z} &= 0 & \text{or} & & u^0 &= 0 \\ \sigma_{0\beta z} - \sigma_{\beta z} &= 0 & \text{or} & & v^0 &= 0 \end{aligned} \quad (1.13)$$

where σ_{0z} , $\sigma_{0\alpha z}$ and $\sigma_{0\beta z}$ are surface tractions and u^0 , v^0 and w^0 are specified displacement functions at $z = \text{constant}$. Similarly for the boundaries $\alpha = \text{constant}$ and $\beta = \text{constant}$.

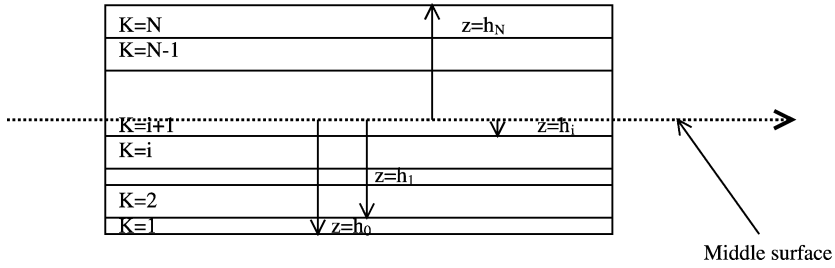


Figure 1.5. Nomenclature for stacking sequence.

A three-dimensional element has six surfaces. With three equations describing boundary conditions at each surface, a total of 18 equations can be obtained.

It should be mentioned that the above equations are developed for single-layered bodies. For multiple layered shells (Figure 1.5), the subject of this book, both displacements and stresses have to be continuous going from the layer k to the next layer $k + 1$ in a laminate having N number of layers. The following conditions should be met to ensure that there are no free internal surfaces (i.e., delamination) between the layers.

$$\left. \begin{aligned} u(\alpha, \beta, z = h_k)]_{\text{layer } k} &= u(\alpha, \beta, z = h_k)]_{\text{layer } k+1} \\ v(\alpha, \beta, z = h_k)]_{\text{layer } k} &= v(\alpha, \beta, z = h_k)]_{\text{layer } k+1} \\ w(\alpha, \beta, z = h_k)]_{\text{layer } k} &= w(\alpha, \beta, z = h_k)]_{\text{layer } k+1} \\ \sigma_z(\alpha, \beta, z = h_k)]_{\text{layer } k} &= \sigma_z(\alpha, \beta, z = h_k)]_{\text{layer } k+1} \\ \sigma_{\alpha z}(\alpha, \beta, z = h_k)]_{\text{layer } k} &= \sigma_{\alpha z}(\alpha, \beta, z = h_k)]_{\text{layer } k+1} \\ \sigma_{\beta z}(\alpha, \beta, z = h_k)]_{\text{layer } k} &= \sigma_{\beta z}(\alpha, \beta, z = h_k)]_{\text{layer } k+1} \end{aligned} \right\} \quad \text{for } k = 1, \dots, N - 1 \quad (1.14)$$

1.2.4 Conditions of compatibility

Studying Eqs. (1.1) and (1.2) closely, one finds that there are three independent unknowns: u , v and w . There are, however, six equations. One immediately concludes that the strains cannot be independently defined. There are conditions that should be set on these strains to assure unique displacement functions u , v and w . These conditions can easily be found. For example, derive the first equation in Eq. (1.1) twice with respect to β , and the second twice with respect to α . This yields

$$\begin{aligned} \frac{\partial^2 \varepsilon_\alpha}{\partial \beta^2} &= \frac{\partial^3 u}{\partial \alpha \partial \beta^2} \\ \frac{\partial^2 \varepsilon_\beta}{\partial \alpha^2} &= \frac{\partial^3 v}{\partial \beta \partial \alpha^2} \end{aligned} \quad (1.15)$$

Taking the derivative of the first equation in Eq. (1.2) with respect to α and β yields

$$\frac{\partial^2 \gamma_{\alpha\beta}}{\partial \alpha \partial \beta} = \frac{\partial^3 v}{\partial \alpha^2 \partial \beta} + \frac{\partial^3 u}{\partial \beta^2 \partial \alpha} \quad (1.16)$$

Eqs. (2.15) and (2.16) show that

$$\frac{\partial^2 \varepsilon_\alpha}{\partial \beta^2} + \frac{\partial^2 \varepsilon_\beta}{\partial \alpha^2} = \frac{\partial^2 \gamma_{\alpha\beta}}{\partial \beta \partial \alpha} \quad (1.17a)$$

which is a constraint that should be met by the strain field. Similarly, the remaining compatibility equations can be derived. These are

$$\begin{aligned} \frac{\partial^2 \varepsilon_\alpha}{\partial z^2} + \frac{\partial^2 \varepsilon_z}{\partial \alpha^2} &= \frac{\partial^2 \gamma_{\alpha z}}{\partial z \partial \alpha} \\ \frac{\partial^2 \varepsilon_z}{\partial \beta^2} + \frac{\partial^2 \varepsilon_\beta}{\partial z^2} &= \frac{\partial^2 \gamma_{\beta z}}{\partial \beta \partial z} \\ 2 \frac{\partial^2 \varepsilon_\alpha}{\partial \beta \partial z} &= \frac{\partial}{\partial \alpha} \left(\frac{\partial \gamma_{\alpha\beta}}{\partial z} + \frac{\partial \gamma_{\alpha z}}{\partial \beta} - \frac{\partial \gamma_{\beta z}}{\partial \beta} \right) \\ 2 \frac{\partial^2 \varepsilon_\beta}{\partial \alpha \partial z} &= \frac{\partial}{\partial \beta} \left(\frac{\partial \gamma_{\alpha\beta}}{\partial z} - \frac{\partial \gamma_{\alpha z}}{\partial \beta} + \frac{\partial \gamma_{\beta z}}{\partial \beta} \right) \\ 2 \frac{\partial^2 \varepsilon_z}{\partial \alpha \partial \beta} &= \frac{\partial}{\partial z} \left(-\frac{\partial \gamma_{\alpha\beta}}{\partial z} + \frac{\partial \gamma_{\alpha z}}{\partial \beta} + \frac{\partial \gamma_{\beta z}}{\partial \beta} \right) \end{aligned} \quad (1.17b)$$

The above equations are sufficient to ensure the existence and uniqueness of a set of displacement functions that correspond to a given set of strains. These equations are important when the set of solution functions are “guessed”. If these guessed solutions are in terms of displacements, as is usually done in vibration problems, the equations of compatibility are identically satisfied. If these functions are in terms of stresses or strains, the above equations are needed to assure unique displacement fields.

1.3. ENERGY AND VARIATIONAL PRINCIPLES

Energy and variational principles offered great simplification to many derivations of fundamental equations in elasticity. They also have been used to introduce and implement approximation techniques for structural systems. Energy and variational principles are covered in many textbooks (Lanczos 1986; Reddy 1984b). In this book, we will introduce the definitions for strain energy, external work and kinetic energy. We will also show how Hamilton’s principle can be used to derive the equations of equilibrium and boundary conditions.

1.3.1 Strain, potential and kinetic energy

Strain energy is defined as the work done by the internal stresses as they cause elongation or shear strains. For a stress element undergoing three-dimensional deformation (and exposed to three-dimensional stresses), the strain energy is

$$U = \frac{1}{2} \iiint (\sigma_\alpha \varepsilon_\alpha + \sigma_\beta \varepsilon_\beta + \sigma_z \varepsilon_z + \sigma_{\alpha\beta} \gamma_{\alpha\beta} + \sigma_{\alpha z} \gamma_{\alpha z} + \sigma_{\beta z} \gamma_{\beta z}) d\alpha d\beta dz \quad (1.18)$$

Eqs. (1.1) and (1.2) can now be substituted in the above equation to write the energy functional in terms of stresses and displacement.

$$U = \frac{1}{2} \iiint \left[\sigma_\alpha \frac{\partial u}{\partial \alpha} + \sigma_\beta \frac{\partial v}{\partial \beta} + \sigma_z \frac{\partial w}{\partial z} + \sigma_{\alpha\beta} \left(\frac{\partial v}{\partial \alpha} + \frac{\partial u}{\partial \beta} \right) + \sigma_{\alpha z} \left(\frac{\partial w}{\partial \alpha} + \frac{\partial u}{\partial z} \right) \gamma_{\alpha z} + \sigma_{\beta z} \left(\frac{\partial w}{\partial \beta} + \frac{\partial v}{\partial z} \right) \right] d\alpha d\beta dz \quad (1.19)$$

Note that the strain energy can also be written in terms of strains by substituting Eq. (1.7) in Eq. (1.18).

The work done by body forces (additional energy input to the system) is defined as

$$W = \iiint [uq_\alpha + vq_\beta + wq_z] d\alpha d\beta dz \quad (1.20)$$

The work done by traction forces can be found from various books on elasticity (Timoshenko and Goodier 1970). The kinetic energy (for constant density ρ) is

$$T = \frac{\rho}{2} \iiint \left[\left(\frac{\partial u}{\partial t} \right)^2 + \left(\frac{\partial v}{\partial t} \right)^2 + \left(\frac{\partial w}{\partial t} \right)^2 \right] d\alpha d\beta dz \quad (1.21)$$

The use of the above energy expressions is illustrated through the discussion of Hamilton's principle.

1.3.2 Hamilton's principle

Hamilton's principle is a general principle that applies to a large class of problems in mechanics. It can be viewed as an axiom, from which other axioms like Newton's second law, can be derived (Soedel 1993). Let us define the potential energy to be $\Pi = U - W$, and the Lagrangian as the function $L = T - \Pi = T - U + W$. Hamilton's principle states that the actual displacement that the body actually goes through from instant t_1 to instant t_2 , out of many possible paths, is that which achieves an extremum of the line integral of the Lagrangian function. This is achieved if the variation of the time integral of

the Lagrangian is set to 0:

$$\delta \int_{t_0}^{t_1} (T + W - U) dt = 0 \quad (1.22)$$

Hamilton's principle can be used to find the compatible set of equations of motion and boundary conditions for given stresses and strains. This is done by substituting the equations for strain energy (U), external work (W) and kinetic energy (T), into the above equation, performing the integration by parts, and setting the coefficients of the displacement variations (also called virtual displacement) equal to 0. The Lagrangian for the three-dimensional elasticity problem in rectangular coordinates (subjected to body forces) is

$$\begin{aligned} L &= T - \Pi = T - U + W \\ &= \iiint \left[\begin{aligned} &\frac{\rho}{2} \left\{ \left(\frac{\partial u}{\partial t} \right)^2 + \left(\frac{\partial v}{\partial t} \right)^2 + \left(\frac{\partial w}{\partial t} \right)^2 \right\} + \{ u q_\alpha + v q_\beta + w q_z \} \\ &- \frac{1}{2} \left\{ \sigma_\alpha \frac{\partial u}{\partial \alpha} + \sigma_\beta \frac{\partial v}{\partial \beta} + \sigma_z \frac{\partial w}{\partial z} + \sigma_{\alpha\beta} \left(\frac{\partial v}{\partial \alpha} + \frac{\partial u}{\partial \beta} \right) \right. \\ &\quad \left. + \sigma_{\alpha z} \left(\frac{\partial w}{\partial \alpha} + \frac{\partial u}{\partial z} \right) \gamma_{\alpha z} + \sigma_{\beta z} \left(\frac{\partial w}{\partial \beta} + \frac{\partial v}{\partial z} \right) \right\} \end{aligned} \right] d\alpha d\beta dz \quad (1.23) \end{aligned}$$

Applying Hamilton's principle yields

$$\begin{aligned} \delta \int_{t_0}^{t_1} (T + W - U) dt &= 0 \\ &= \int_{t_0}^{t_1} \iiint \left[\begin{aligned} &\rho \left\{ \left(\frac{\partial u}{\partial t} \frac{\partial \delta u}{\partial t} \right) + \left(\frac{\partial v}{\partial t} \frac{\partial \delta v}{\partial t} \right) + \left(\frac{\partial w}{\partial t} \frac{\partial \delta w}{\partial t} \right) \right\} \\ &+ \{ q_\alpha \delta u + q_\beta \delta v + q_z \delta w \} \\ &- \left\{ \sigma_\alpha \frac{\partial \delta u}{\partial \alpha} + \sigma_\beta \frac{\partial \delta v}{\partial \beta} + \sigma_z \frac{\partial \delta w}{\partial z} + \sigma_{\alpha\beta} \left(\frac{\partial \delta v}{\partial \alpha} + \frac{\partial \delta u}{\partial \beta} \right) \right. \\ &\quad \left. + \sigma_{\alpha z} \left(\frac{\partial \delta w}{\partial \alpha} + \frac{\partial \delta u}{\partial z} \right) \gamma_{\alpha z} + \sigma_{\beta z} \left(\frac{\partial \delta w}{\partial \beta} + \frac{\partial \delta v}{\partial z} \right) \right\} \end{aligned} \right] d\alpha d\beta dz dt \quad (1.24) \end{aligned}$$

Taking the integration by part yields

$$\begin{aligned}
 & \delta \int_{t_0}^{t_1} (T + W - U) dt = 0 \\
 & = \int \int \int \left[\int_{t_0}^{t_1} - \left\{ \left(\frac{\partial}{\partial t} \rho \frac{\partial u}{\partial t} \right) \delta u + \left(\frac{\partial}{\partial t} \rho \frac{\partial v}{\partial t} \right) \delta v + \left(\frac{\partial}{\partial t} \rho \frac{\partial w}{\partial t} \right) \delta w \right\} dt \right. \\
 & \quad \left. + \rho \left\{ \frac{\partial u}{\partial t} \delta u + \frac{\partial v}{\partial t} \delta v + \frac{\partial w}{\partial t} \delta w \right\} \right]_{t_0}^{t_1} d\alpha d\beta dz \\
 & \quad - \int_{t_0}^{t_1} \left[\int \int \int \left\{ q_\alpha \delta u + q_\beta \delta v + q_z \delta w \right\} d\alpha d\beta dz \right. \\
 & \quad \left. + \left\{ \int \int \left\{ \sigma_\alpha \delta u - \int \delta u \frac{\partial \sigma_\alpha}{\partial \alpha} d\alpha \right\} d\beta dz + \int \int \left\{ \sigma_\beta \delta v - \int \delta v \frac{\partial \sigma_\beta}{\partial \beta} d\beta \right\} d\alpha dz \right. \right. \\
 & \quad \left. + \int \int \left\{ \sigma_z \delta w - \int \delta w \frac{\partial \sigma_z}{\partial z} dz \right\} d\alpha d\beta + \int \int \left\{ \sigma_{\alpha\beta} \delta u - \int \delta u \frac{\partial \sigma_{\alpha\beta}}{\partial \beta} d\beta \right\} d\alpha dz \right. \\
 & \quad \left. + \int \int \left\{ \sigma_{\alpha\beta} \delta v - \int \delta v \frac{\partial \sigma_{\alpha\beta}}{\partial \alpha} d\alpha \right\} d\beta dz + \int \int \left\{ \sigma_{\alpha z} \delta u - \int \delta u \frac{\partial \sigma_{\alpha z}}{\partial z} dz \right\} d\alpha d\beta \right. \\
 & \quad \left. + \int \int \left\{ \sigma_{\alpha z} \delta w - \int \delta w \frac{\partial \sigma_{\alpha z}}{\partial \alpha} d\alpha \right\} d\beta dz + \int \int \left\{ \sigma_{\beta z} \delta v - \int \delta v \frac{\partial \sigma_{\beta z}}{\partial z} dz \right\} d\alpha d\beta \right. \\
 & \quad \left. + \int \int \left\{ \sigma_{\beta z} \delta w - \int \delta w \frac{\partial \sigma_{\beta z}}{\partial \beta} d\beta \right\} d\alpha dz \right\} dt \quad (1.25)
 \end{aligned}$$

Assuming zero variations at the beginning and end of the time interval; and collecting the coefficients of the terms δu , δv and δw yields

$$\begin{aligned}
 & \delta \int_{t_0}^{t_1} (T + W - U) dt = 0 \\
 & = \int_{t_0}^{t_1} \int \int \int \left[\left\{ \frac{\partial \sigma_\alpha}{\partial \alpha} + \frac{\partial \sigma_{\alpha\beta}}{\partial \beta} + \frac{\partial \sigma_{\alpha z}}{\partial z} + q_\alpha - \left(\frac{\partial}{\partial t} \rho \frac{\partial u}{\partial t} \right) \right\} \delta u \right. \\
 & \quad \left. + \left\{ \frac{\partial \sigma_{\alpha\beta}}{\partial \alpha} + \frac{\partial \sigma_\beta}{\partial \beta} + \frac{\partial \sigma_{\beta z}}{\partial z} + q_\beta - \left(\frac{\partial}{\partial t} \rho \frac{\partial v}{\partial t} \right) \right\} \delta v \right. \\
 & \quad \left. + \left\{ \frac{\partial \sigma_{\alpha z}}{\partial \alpha} + \frac{\partial \sigma_{\beta z}}{\partial \beta} + \frac{\partial \sigma_z}{\partial z} + q_z - \left(\frac{\partial}{\partial t} \rho \frac{\partial w}{\partial t} \right) \right\} \delta w \right] d\alpha d\beta dz dt + \text{B.T.} \quad (1.26)
 \end{aligned}$$

where B.T. are terms resulting from energy values obtained by traction forces at the boundaries. Setting the coefficients of δu , δv and δw to 0 yields the equations of motion.

Hamilton's principle has proven to be useful in deriving the equations of motion of complicated systems (like shells). Its power is in the straightforward mathematical task that needs to be done, once the energy functionals are defined. We will use this principle in the upcoming chapters to derive the equations of motion as well as the proper expressions for boundary conditions.

The material covered in this chapter introduces fundamental equations for laminated structures and the fundamental principles used in mechanics to treat such structures. The books of Vinson and Sierakowski (1986), Lekhnitski (1957) and Whitney (1987) as well as others are necessary for a more fundamental treatment of composite laminates. The books of Timoshenko and Goodier (1970) and Saada (1987), as well as others, on elasticity are necessary for detailed treatment of the subject. The books of Lanczos (1986) and Reddy (1984b) as well as many other texts may be needed for a more fundamental treatment of variational principles.

Chapter 2

Shell Theories

This chapter will focus mainly on shell theories. The treatment of plates and beams will be presented later as special cases of shells. In other words, when certain simplifications are made, the shell equations collapse to those of plates and/or beams. Both plates and beams are discussed in independent chapters later.

Shells are three-dimensional (3D) bodies bounded by two, relatively close, curved surfaces. The 3D equations of elasticity are complicated when written in curvilinear, or shell, coordinates. Most engineers who dealt with shells tried to simplify such shell equations by making certain assumptions for particular applications. Almost all shell theories (thin and thick, deep and shallow, etc.) reduce the 3D elasticity problem into a 2D one. This is done usually by eliminating the coordinate normal to the shell surface in the development of the shell equations. The accuracy of thin and thick shell theories can only be established if the results obtained by these theories are compared with those obtained using the 3D theory of elasticity.

A summary of the equations of laminated composite shells will be made in this chapter. In particular, the strain–displacement equations, the stress–strain equations and the equations of motion will be described. These equations and the associated boundary conditions constitute a complete set of equations.

The development of shell equations matured over the last century. The expansion of the shell equations to laminated composites occurred mostly in the second half of the 20th century by mainly a group of Russian researchers. The method that is followed in this chapter is to start with the 3D elasticity theory in curvilinear coordinates. This is followed by introducing the necessary assumptions to reduce the 3D elasticity equations to those which take simpler forms and are applicable to beams, plates and shells.

2.1. THREE DIMENSIONAL ELASTICITY THEORY IN CURVILINEAR COORDINATES

A shell is a 3D body confined by two surfaces. If these surfaces are parallel, the shell will have a constant thickness. In general, the distance between those surfaces (i.e., the thickness) is small compared with other shell parameters like length, width and radii of curvature. In this section, the equations of the 3D theory of elasticity in curvilinear coordinates are presented.

2.1.1 *Theory of surfaces*

It will be assumed here that the deformation of the shells is completely determined by the displacement of its middle surface. This, by itself, does not add constraints to the 3D

theory of elasticity. However, this will simplify the treatment of the shell structure by taking the coordinate system to be at the middle surface of the shell. Let the equations of the undeformed surface be written in terms of the coordinates α and β by the vector

$$\vec{r} = \vec{r}(\alpha, \beta) \quad (2.1)$$

The increment of the vector \vec{r} moving from the point (α, β) on the surface to the point $(\alpha + d\alpha, \beta + d\beta)$ is (Figure 2.1)

$$d\vec{r} = \vec{r}_{,\alpha} d\alpha + \vec{r}_{,\beta} d\beta \quad (2.2)$$

The arc length of the surface between the two points is

$$ds^2 = d\vec{r} \cdot d\vec{r} = A^2 d\alpha^2 + 2AB \cos \chi (d\alpha)(d\beta) + B^2 d\beta^2 \quad (2.3)$$

where

$$A^2 = \vec{r}_{,\alpha} \cdot \vec{r}_{,\alpha}, \quad B^2 = \vec{r}_{,\beta} \cdot \vec{r}_{,\beta}, \quad \text{and} \quad AB \cos \chi = \vec{r}_{,\alpha} \cdot \vec{r}_{,\beta}$$

The right hand side of the above equation is called the “first fundamental form” of the surface. The angle χ between the coordinates α and β and the unit vectors tangent to the surface coordinates are

$$\begin{aligned} \chi &= \cos^{-1}(\vec{i}_{,\alpha} \cdot \vec{i}_{,\beta}) \\ \vec{i}_{,\alpha} &= \vec{r}_{,\alpha}/A \\ \vec{i}_{,\beta} &= \vec{r}_{,\beta}/B \end{aligned} \quad (2.4)$$

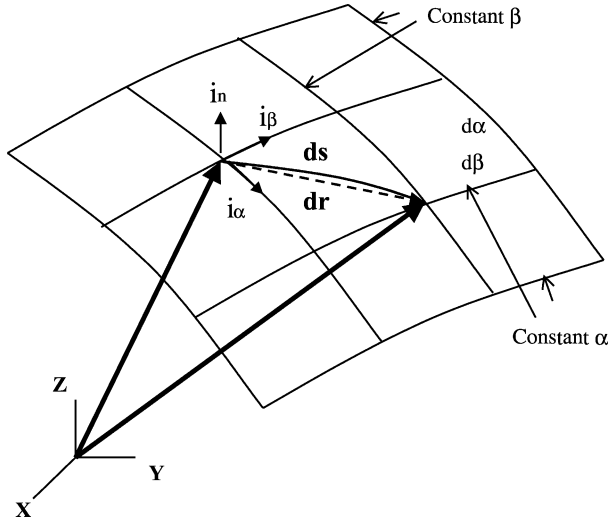


Figure 2.1. Coordinates of the shell's middle surface.

The unit vector normal to the surface is defined by

$$\vec{i}_n = \vec{i}_{,\alpha} \times \vec{i}_{,\beta} / \sin \chi \quad (2.5)$$

The second quadratic form concept of a surface comes up when one finds the curvature of a curve on a surface. If $\vec{r} = \vec{r}(s)$ is the equation of a curve on the surface with s being the arc length, the unit vector tangential to the curve is

$$\vec{\tau} = \frac{d\vec{r}}{ds} = \vec{r}_{,\alpha} \frac{d\alpha}{ds} + \vec{r}_{,\beta} \frac{d\beta}{ds} \quad (2.6)$$

The derivative of the above vector gives the curvature, according to Frenet's formula (Kreyszig 1993)

$$\frac{d\vec{\tau}}{ds} = \frac{\vec{N}}{\rho} \quad (2.7)$$

where $1/\rho$ is the curvature of the curve and \vec{N} is the unit vector of the principal normal to the curve.

Substitution of $\vec{\tau}$ into the above equations yields

$$\frac{\vec{N}}{\rho} = \vec{r}_{,\alpha\alpha} \left(\frac{d\alpha}{ds} \right)^2 + 2\vec{r}_{,\alpha\beta} \left(\frac{d\alpha}{ds} \right) \left(\frac{d\beta}{ds} \right) + \vec{r}_{,\beta\beta} \left(\frac{d\beta}{ds} \right)^2 + \vec{r}_{,\alpha} \frac{d^2\alpha}{ds^2} + \vec{r}_{,\beta} \frac{d^2\beta}{ds^2} \quad (2.8)$$

If ϕ is the angle between the normal \vec{i}_n to the surface and the principal normal to the curve \vec{N} ; then

$$\cos(\phi) = \vec{i}_n \cdot \vec{N} \quad (2.9)$$

Multiply both sides of Eq. (2.8) by \vec{i}_n (and noting that $\vec{i}_n \cdot \vec{r}_{,\alpha} = \vec{i}_n \cdot \vec{r}_{,\beta} = 0$) yields

$$\frac{\cos \phi}{\rho} = \frac{L(d\alpha)^2 + 2M(d\alpha)(d\beta) + N(d\beta)^2}{ds^2} \quad (2.10)$$

where

$$L = \vec{r}_{,\alpha\alpha} \cdot \vec{i}_n, \quad M = \vec{r}_{,\alpha\beta} \cdot \vec{i}_n = \vec{r}_{,\beta\alpha} \cdot \vec{i}_n, \quad \text{and} \quad N = \vec{r}_{,\beta\beta} \cdot \vec{i}_n,$$

The numerator of the above equation's right hand side is called the "second quadratic form", and L , M and N are its coefficient.

The above equation is instrumental in finding the normal curvature. The direction of the vector \vec{i}_n is the positive normal to the surface, opposite to the vector \vec{N} , then $\phi = \pi$ is used, yielding

$$-\frac{1}{R} = \frac{L(d\alpha)^2 + 2M(d\alpha)(d\beta) + N(d\beta)^2}{A^2(d\alpha)^2 + 2AB \cos \chi(d\alpha)(d\beta) + B^2(d\beta)^2} \quad (2.11)$$

The curvature values of the α and β curves are obtained by setting $\beta = \text{constant}$ and $\alpha = \text{constant}$, respectively. This yields

$$\frac{1}{R_\alpha} = -\frac{L}{A^2}, \quad \frac{1}{R_\beta} = -\frac{N}{B^2} \quad (2.12)$$

and the twist curvature of the surface is

$$\frac{1}{R_{\alpha\beta}} = -\frac{M}{AB} \quad (2.13)$$

The second derivatives of the vector \vec{r} can now be performed and written in the matrix form as follows

$$\begin{bmatrix} \vec{r}_{,\alpha\alpha} \\ \vec{r}_{,\alpha\beta} \\ \vec{r}_{,\beta\beta} \end{bmatrix} = \begin{bmatrix} \Gamma_{11}^1 & \Gamma_{11}^2 & L \\ \Gamma_{12}^1 & \Gamma_{12}^2 & M \\ \Gamma_{22}^1 & \Gamma_{22}^2 & N \end{bmatrix} \begin{bmatrix} \vec{r}_{,\alpha} \\ \vec{r}_{,\beta} \\ \vec{i}_n \end{bmatrix} \quad (2.14)$$

where Γ_{jk}^i is the Christoffel symbols, which can be expressed as (Gol'denveizer 1961)

$$\begin{aligned} \Gamma_{11}^1 &= \frac{1}{A} \frac{\partial A}{\partial \alpha}, \quad \Gamma_{11}^2 = -\frac{A}{B^2} \frac{\partial A}{\partial \beta}, \quad \Gamma_{12}^1 = \frac{1}{A} \frac{\partial A}{\partial \beta}, \\ \Gamma_{12}^2 &= \frac{1}{B} \frac{\partial B}{\partial \alpha}, \quad \Gamma_{22}^1 = -\frac{B}{A^2} \frac{\partial B}{\partial \alpha}, \quad \Gamma_{22}^2 = \frac{1}{B} \frac{\partial B}{\partial \beta} \end{aligned} \quad (2.15)$$

Since $\vec{i}_n \cdot \vec{i}_n = 1$, taking the derivative with respect to α and β yields

$$\vec{i}_n \cdot \vec{i}_{n,\alpha} = \vec{i}_n \cdot \vec{i}_{n,\beta} = 0 \quad (2.16)$$

Furthermore, deriving the expressions $\vec{i}_n \cdot \vec{r}_{,\alpha} = \vec{i}_n \cdot \vec{r}_{,\beta} = 0$ with respect to α and β and substituting them into the expressions of L , M and N in Eq. (2.10) yields

$$\begin{aligned} L &= -\vec{r}_{,\alpha} \cdot \vec{i}_{n,\alpha} \\ M &= -\vec{r}_{,\alpha} \cdot \vec{i}_{n,\beta} = -\vec{r}_{,\beta} \cdot \vec{i}_{n,\alpha} \\ N &= -\vec{r}_{,\beta} \cdot \vec{i}_{n,\beta} \end{aligned} \quad (2.17)$$

Using Eqs. (2.12) and (2.13) with the above expressions yields the Weingarten formulas

$$\begin{aligned} \vec{i}_{n,\alpha} &= \frac{A}{R_\alpha} \vec{i}_\alpha + \frac{A}{R_{\alpha\beta}} \vec{i}_\beta \\ \vec{i}_{n,\beta} &= \frac{B}{R_\beta} \vec{i}_\beta + \frac{B}{R_{\alpha\beta}} \vec{i}_\alpha \end{aligned} \quad (2.18)$$

The derivatives of the unit vectors in Eqs. (2.4) and (2.5) can now be found by using Eqs. (2.14) and (2.18). They can be written as

$$\begin{aligned} \frac{\partial}{\partial \alpha} \begin{bmatrix} \vec{i}_\alpha \\ \vec{i}_\beta \\ \vec{i}_n \end{bmatrix} &= \begin{bmatrix} 0 & -\frac{1}{B} \frac{\partial A}{\partial \beta} & -\frac{A}{R_\alpha} \\ \frac{1}{B} \frac{\partial A}{\partial \beta} & 0 & -\frac{A}{R_{\alpha\beta}} \\ \frac{A}{R_\alpha} & \frac{A}{R_{\alpha\beta}} & 0 \end{bmatrix} \begin{bmatrix} \vec{i}_\alpha \\ \vec{i}_\beta \\ \vec{i}_n \end{bmatrix} \\ \frac{\partial}{\partial \beta} \begin{bmatrix} \vec{i}_\alpha \\ \vec{i}_\beta \\ \vec{i}_n \end{bmatrix} &= \begin{bmatrix} 0 & \frac{1}{A} \frac{\partial B}{\partial \alpha} & -\frac{B}{R_{\alpha\beta}} \\ -\frac{1}{A} \frac{\partial B}{\partial \alpha} & 0 & -\frac{B}{R_\beta} \\ \frac{B}{R_{\alpha\beta}} & \frac{B}{R_\beta} & 0 \end{bmatrix} \begin{bmatrix} \vec{i}_\alpha \\ \vec{i}_\beta \\ \vec{i}_n \end{bmatrix} \end{aligned} \quad (2.19)$$

In addition, the following identities can be established

$$\begin{aligned} (\vec{i}_{\alpha,\alpha})_{,\beta} &= (\vec{i}_{\alpha,\beta})_{,\alpha} \\ (\vec{i}_{\beta,\alpha})_{,\beta} &= (\vec{i}_{\beta,\beta})_{,\alpha} \\ (\vec{i}_{n,\alpha})_{,\beta} &= (\vec{i}_{n,\beta})_{,\alpha} \end{aligned} \quad (2.20)$$

Using Eq. (2.19) and the above identities, one obtains

$$\begin{aligned} \frac{\partial}{\partial \beta} \left(\frac{A}{R_\alpha} \right) &= \frac{1}{R_\beta} \frac{\partial A}{\partial \beta} + \frac{1}{B} \frac{\partial}{\partial \alpha} \left(\frac{B^2}{R_{\alpha\beta}} \right) \\ \frac{\partial}{\partial \alpha} \left(\frac{B}{R_\beta} \right) &= \frac{1}{R_\alpha} \frac{\partial B}{\partial \alpha} + \frac{1}{A} \frac{\partial}{\partial \beta} \left(\frac{A^2}{R_{\alpha\beta}} \right) \\ \frac{\partial}{\partial \alpha} \left(\frac{1}{A} \frac{\partial B}{\partial \alpha} \right) + \frac{\partial}{\partial \beta} \left(\frac{1}{B} \frac{\partial A}{\partial \beta} \right) &= -\frac{AB}{R_\alpha R_\beta} + \frac{AB}{R_{\alpha\beta}^2} \end{aligned} \quad (2.21)$$

The first two of the above equations are known as the Mainardi–Codazzi equations, and the last is known as Gauss characteristic equation.

If one assumes an arbitrary vector

$$\vec{U} = U_\alpha \vec{i}_\alpha + U_\beta \vec{i}_\beta + U_n \vec{i}_n \quad (2.22)$$

Taking the derivative of the above vector with respect to α and β , respectively; and using Eq. (2.19) yields

$$\begin{aligned}\vec{U}_{,\alpha} &= \left(U_{\alpha,\alpha} + \frac{1}{B} \frac{\partial A}{\partial \alpha} U_\beta + \frac{A}{R_\alpha} U_n \right) \vec{i}_\alpha + \left(U_{\beta,\alpha} - \frac{1}{B} \frac{\partial A}{\partial \beta} U_\alpha + \frac{A}{R_{\alpha\beta}} U_n \right) \vec{i}_\beta \\ &\quad + \left(U_{n,\alpha} - \frac{A}{R_\alpha} U_\alpha - \frac{A}{R_{\alpha\beta}} U_\beta \right) \vec{i}_n \\ \vec{U}_{,\beta} &= \left(U_{\alpha,\beta} - \frac{1}{A} \frac{\partial B}{\partial \alpha} U_\beta + \frac{B}{R_{\alpha\beta}} U_n \right) \vec{i}_\alpha + \left(U_{\beta,\beta} + \frac{1}{A} \frac{\partial B}{\partial \alpha} U_\alpha + \frac{B}{R_\beta} U_n \right) \vec{i}_\beta \\ &\quad + \left(U_{n,\beta} - \frac{B}{R_\beta} U_\beta - \frac{B}{R_{\alpha\beta}} U_\alpha \right) \vec{i}_n\end{aligned}\tag{2.23}$$

These equations will be used in Section 2.1.2.

2.1.2 Kinematic relations

Consider a point on the midsurface of the shell with the coordinates $(\alpha, \beta, 0)$. The position of the point is $\vec{r}_0(\alpha, \beta)$ before deformation and $\vec{r}'_0(\alpha, \beta)$ after deformation. The displacement vector at the point is defined as

$$\vec{r}'_0(\alpha, \beta) = \vec{r}_0(\alpha, \beta) + \vec{U}_0\tag{2.24}$$

The deformation at the point can be represented by the displacement vector

$$\vec{U}_0 = u_0 \vec{i}_\alpha + v_0 \vec{i}_\beta + w_0 \vec{i}_n\tag{2.25}$$

where \vec{i}_α , \vec{i}_β , and \vec{i}_n are unit vectors in the α , β and z directions, respectively.

Consider an arc length parallel to the α curve and denote that as $ds_{0\alpha} (= A d\alpha)$. This arc length will become $ds'_{0\alpha} (= A' d\alpha)$ after deformation. The extensional strain is now defined as

$$\varepsilon_{0\alpha} = \frac{(ds'_{0\alpha} - ds_{0\alpha})}{ds_{0\alpha}} = \frac{(A' - A)}{A} \quad \text{or} \quad A' = A(1 + \varepsilon_{0\alpha})\tag{2.26}$$

The following equation for strain at the middle surface can now be obtained by deriving Eq. (2.24) and dividing it by A .

$$(1 + \varepsilon_{0\alpha}) \vec{i}'_\alpha = \vec{i}_\alpha + \frac{\vec{U}_{0,\alpha}}{A}\tag{2.27}$$

Assume that the rotation of the shell about its normal is small; or $\vec{i}'_\alpha \cdot \vec{i}_\alpha = 1$. This assumption allows us to neglect nonlinear terms in the subsequent derivation. It will also allow us to refer the analysis to the original configuration of the shell. Then

$$\varepsilon_{0\alpha} = \frac{\vec{U}_{0,\alpha}}{A} \cdot \vec{i}_\alpha \quad (2.28)$$

The term $\vec{U}_{0,\alpha}$ is defined as in Eq. (2.23). Similarly, one can obtain

$$\begin{aligned} \varepsilon_{0\beta} &= \frac{\vec{U}_{0,\beta}}{B} \cdot \vec{i}_\beta \\ \varepsilon_{0\alpha\beta} &= \frac{\vec{U}_{0,\alpha}}{A} \cdot \vec{i}_\beta \\ \varepsilon_{0\beta\alpha} &= \frac{\vec{U}_{0,\beta}}{B} \cdot \vec{i}_\alpha \end{aligned} \quad (2.29)$$

$$\text{or} \quad \gamma_{0\alpha\beta} = \frac{\vec{U}_{0,\alpha}}{A} \cdot \vec{i}_\beta + \frac{\vec{U}_{0,\beta}}{B} \cdot \vec{i}_\alpha$$

$$\gamma_{0\alpha z} = \frac{\vec{U}_{0,\alpha}}{A} \cdot \vec{i}_n + \vec{U}_{0,z} \cdot \vec{i}_\alpha$$

$$\gamma_{0\beta z} = \frac{\vec{U}_{0,\beta}}{B} \cdot \vec{i}_n + \vec{U}_{0,z} \cdot \vec{i}_\beta$$

The last two equations are shear strains in the z direction. The length of an infinitesimal element of thickness dz located at distance z from the shell mid-surface is

$$\begin{aligned} ds_\alpha^{(z)} &= \frac{A d\alpha}{R_\alpha} (R_\alpha + z) = A(1 + z/R_\alpha) d\alpha = A^\circ d\alpha \\ ds_\beta^{(z)} &= \frac{B d\beta}{R_\beta} (R_\beta + z) = B(1 + z/R_\beta) d\beta = B^\circ d\beta \end{aligned} \quad (2.30)$$

where A and B are Lamé parameters of the middle surface. The terms A , B , R_α , R_β and $R_{\alpha\beta}$ are connected together by the Lamé equations, which are extensions of Eq. (2.21) to the surface at a distance z from the middle surface (Figure 2.2).

The strain–displacement relations can be derived from the above equations as

$$\begin{aligned}
 \varepsilon_\alpha &= \frac{1}{(1+z/R_\alpha)} \left(\frac{1}{A} \frac{\partial u}{\partial \alpha} + \frac{v}{AB} \frac{\partial A}{\partial \beta} + \frac{w}{R_\alpha} \right) \\
 \varepsilon_\beta &= \frac{1}{(1+z/R_\beta)} \left(\frac{1}{B} \frac{\partial v}{\partial \beta} + \frac{u}{AB} \frac{\partial B}{\partial \alpha} + \frac{w}{R_\beta} \right) \\
 \varepsilon_z &= \frac{\partial w}{\partial z} \\
 \gamma_{\alpha\beta} &= \frac{1}{(1+z/R_\alpha)} \left(\frac{1}{A} \frac{\partial v}{\partial \alpha} - \frac{u}{AB} \frac{\partial A}{\partial \beta} + \frac{w}{R_{\alpha\beta}} \right) \\
 &\quad + \frac{1}{(1+z/R_\beta)} \left(\frac{1}{B} \frac{\partial u}{\partial \beta} - \frac{v}{AB} \frac{\partial B}{\partial \alpha} + \frac{w}{R_{\alpha\beta}} \right) \\
 \gamma_{\alpha z} &= \frac{1}{A(1+z/R_\alpha)} \frac{\partial w}{\partial \alpha} + A(1+z/R_\alpha) \frac{\partial}{\partial z} \left(\frac{u}{A(1+z/R_\alpha)} \right) - \frac{v}{R_{\alpha\beta}(1+z/R_\alpha)} \\
 \gamma_{\beta z} &= \frac{1}{B(1+z/R_\beta)} \frac{\partial w}{\partial \beta} + B(1+z/R_\beta) \frac{\partial}{\partial z} \left(\frac{v}{B(1+z/R_\beta)} \right) - \frac{u}{R_{\alpha\beta}(1+z/R_\beta)}
 \end{aligned} \tag{2.33}$$

The above equations constitute the fundamental kinematic relations of a 3D body in curvilinear coordinates. It should be mentioned that other than the assumption of small displacements, no additional assumptions are made in the derivation. The range of applications of the above equations is indeed wide. They can be easily specialized to some of the frequently encountered components like flat plates and cylindrical shells.

2.1.3 Stress–strain relations

The assumptions made earlier of fibers being parallel to the upper and lower surfaces of their layer within the shells and that they follow the curved surface of the shells are maintained here. In general, it is assumed that the stiffness parameters are constant. It will be shown later that for general shells and plates, this assumption is not easy to maintain for circular plates, spherical and conical shells. The orthotropy of the material is assumed here to follow the coordinates chosen (or *vice versa*). For materials with rectangular orthotropy, rectangular coordinates are chosen. Similarly for materials having polar, elliptical or other types of orthotropy. In addition, the angle between the fibers in one layer to those in another layer is to remain constant. This assumption will make it necessary for the fibers in an angle-ply laminate to have a curvature that may not necessarily be constant. Such arrangement is encountered for building angle-ply circular plates and some shells.

The stress–strain relationships for a typical n th lamina (typically called monoclinic) in a laminated composite shell are the same as those derived earlier (Eq. (1.7)).

2.1.4 Equations of motion

In order to develop a consistent set of equations, the boundary conditions and the equations of motion will be derived using Hamilton's principle (Eq. (1.22)). Substituting the equations for strain energy (U), external work (W) and kinetic energy (T), performing the integration by parts, and setting the coefficients of the displacement variations equal to 0, in a normal manner, yields the equations of motion (Saada 1987; p. 178).

$$\begin{aligned}
 & \frac{\partial(B\sigma_\alpha)}{\partial\alpha} + \frac{\partial(A\sigma_{\alpha\beta})}{\partial\beta} + \frac{\partial(AB\sigma_{\alpha z})}{\partial z} + \sigma_{\alpha\beta}\frac{\partial A}{\partial\beta} + \sigma_{\alpha z}B\frac{\partial A}{\partial z} - \sigma_\beta\frac{\partial B}{\partial\alpha} + ABq_\alpha = \rho\frac{\partial u^2}{\partial t^2} \\
 & \frac{\partial(B\sigma_{\alpha\beta})}{\partial\alpha} + \frac{\partial(A\sigma_\beta)}{\partial\beta} + \frac{\partial(AB\sigma_{\beta z})}{\partial z} + \sigma_{\beta z}A\frac{\partial B}{\partial z} + \sigma_{\alpha\beta}\frac{\partial B}{\partial\alpha} - \sigma_\alpha\frac{\partial A}{\partial\beta} + ABq_\beta = \rho\frac{\partial v^2}{\partial t^2} \quad (2.34) \\
 & \frac{\partial(B\sigma_{\alpha z})}{\partial\alpha} + \frac{\partial(A\sigma_{\beta z})}{\partial\beta} + \frac{\partial(AB\sigma_z)}{\partial z} - \sigma_\beta A\frac{\partial B}{\partial z} - \sigma_\alpha B\frac{\partial A}{\partial z} + ABq_z = \rho\frac{\partial w^2}{\partial t^2}
 \end{aligned}$$

The above equations do not depend on the shell material. Hamilton's principle will also yield boundary terms that are consistent with these equations. The terms for the boundaries with $z = \text{constant}$ are given in Eq. (1.13). Similar terms can be found for the boundaries $\alpha = \text{constant}$ and $\beta = \text{constant}$. A 3D shell element, in curvilinear coordinates, has six surfaces. With three equations at each surface, a total of 18 equations can be obtained for a single-layered shell. Eq. (1.14) applies for multiple layered shells, where continuity between layers must be assured.

2.1.5 Recent developments

The recent research that used the 3D elasticity theory in the analysis of laminates shell structures is covered in a recent book (Ye 2003). In addition, the following work should be reported. Bhimaraddi (1991) obtained results based on the 3D theory of elasticity for doubly curved composite shallow shells. Others, including Wang *et al.* (1995), Jiang (1997) and Tsai (1991), obtained results based on the 3D theory of elasticity for closed cylindrical shells. 3D solutions for cylindrical shells with initial stresses are found by Xu *et al.* (1997). Ye and Soldatos (1996, 1997) used 3D elasticity theory to treat cylindrical shells with arbitrary point supports and clamped edge boundaries, respectively. Chen and Shen (1998) used 3D analysis to study orthotropic piezoelectric circular cylindrical shells. Chen *et al.* (1998a,b) presented 3D study for free vibration of transversely isotropic cylindrical panels. Ding and Tang (1999) studied 3D free vibration of thick laminated cylindrical shells with clamped edges. Yin (1999) found simplifications for the frequency equation of multilayered cylinders and developed some recursion formulae of Bessel functions. Chern and Chao (2000) used 3D theory to study the natural frequencies of laminated curved panels. A review of the 3D literature can be found in Soldatos (1994).

2.2. THICK SHELL THEORY

The first reliable approximation for bending analysis of shells was introduced by Love (1892). Love made several assumptions to reduce the general 3D equation of elasticity in curvilinear coordinates to 2D equations that can be applied for shells. First, he assumed that strains and displacements are small such that second and higher order terms can be neglected. Love's second assumption was that the thickness of the shell is small compared with other shell parameters. His third assumption was that the transverse stress is small compared with other stresses in shells. Finally, Love assumed that normals to the undeformed surface remain straight and normal to the deformed surface. The first of these assumptions defines a linear analysis of shells (Timoshenko and Woinowsky-Krieger 1959). This assumption needs to be relaxed if the strains and/or displacements become large. Displacement is considered definitely large if it exceeds the thickness of the shell. This is typical for thin shells. Nonlinear behavior can be observed even before this level of deformation for various boundary conditions. A recent study (Qatu 1994a) concluded that this assumption generally applies to most of the analyses of thick shells. This is because stresses exceed allowable values before the deflection becomes large enough for the nonlinear terms to be important.

The remaining assumptions in Love's first approximation need to be re-examined when thick shells are treated. For thick shells, the thickness is no longer small compared with other shell parameters, nor do the normals of the undeformed surface remain as such. Various studies (Koiter 1969; Gol'denveiser 1961; and Noor 1990) concluded that even for thicker shells the transverse normal stress (and strain) remains small compared with other stresses (and strains) in the shell.

As pointed earlier, many shell theories were derived based on Love's first approximation. Inconsistencies, however, appeared in many of these theories and were reported in much of the literature on shell theory during the middle of the 20th century (Leissa 1973a). For example, the strain-displacement relations used by Naghdi and Berry (1964) are inconsistent with regard to rigid body motion. Other theories including Love (1892) and Timoshenko and Woinowsky-Krieger (1959), although free from rigid body motion inconsistencies, introduced unsymmetrical differential operators, which contradicts the theorem of reciprocity and yields imaginary numbers for natural frequencies in a free vibration analysis. Other inconsistencies appeared when the assumption of small thickness (h/R and $z/R \ll 1$) is imposed and symmetric stress resultants (i.e., $N_{\alpha\beta} = N_{\beta\alpha}$ and $M_{\alpha\beta} = M_{\beta\alpha}$) are obtained. This is not true for shells that are not spherical. To overcome some or all the above inconsistencies, various theories were introduced including that of Sanders (1959). Vlasov (1949) tried to resolve some of these inconsistencies by expanding usually negligible terms appearing in the denominator of the stress resultant equations using a Taylor series.

On the other hand, Rayleigh noted the importance of rotary inertia terms in the analysis of vibrating systems (Rayleigh 1877). Timoshenko (1921) showed that shear deformation terms are at least as important. This led to a necessary relaxation of some of the assumptions in Love's first approximation and shear deformation shell theories (SDST) were born. Among the first of such theories were those of Vlasov (1949), Reissner (1941, 1952), Naghdi and Cooper (1956) and others.

Ambartsumian (1961) expanded the stress resultant equations of earlier theories to those for anisotropic shells. Orthotropic cylindrical shells were considered by Dong (1968) and Rath and Das (1973). The latter presented equations that included rotary inertia and shear deformation. Various survey articles appeared on the treatment of homogeneous and laminated composite shells (Ambartsumian 1962; Bert *et al.* 1969b; Noor 1990; Soldatos 1994; Liew *et al.* 1997a,b; Qatu 2002a,b). These articles reviewed theories and analyses of laminated composite shells. It was found that shear deformation effects for laminated composite materials are generally more important than those for isotropic materials. Unfortunately, while SDST, including higher order ones, include shear deformation and rotary inertia, they fail to consider the $1 + z/R$ terms in the stress resultant equations. This led to inaccurate results in the constitutive equations used for laminated deep thick shells. This was initially observed by Bert (1967) and investigated thoroughly only recently by Qatu (1993a,b) for curved beams and Leissa and Chang (1996) and Qatu (1995a, 1999a) for laminated shells. Leissa and Chang truncated this term using a geometric series expansion. Qatu integrated the term exactly. Results obtained using this theory show closer comparison with 3D theory of elasticity (Qatu 1999a, 2002a). Other shear deformation theories included higher order terms for shear strains, but neglected the $1 + z/R$ (Reddy 1984a; Reddy and Liu 1985; and Librescu *et al.* 1989a,b). Interestingly, the results obtained by these authors were presented for shallow shells. For such shells the term $(1 + z/R)$ is less important.

2.2.1 Kinematic relations

Thick shells are defined here as shells with a thickness smaller by approximately one order of magnitude when compared with other shell parameters, like its vibration mode shape wavelength and/or radii of curvature (thickness is less than (1/10)th of the smallest of the wave lengths and/or radii of curvature). Thick shells require the inclusion of shear deformation and rotary inertia factors in a vibration analysis. Thin shells, on the other hand are shells with the thickness smaller than (1/20)th (probably smaller for composite materials) of the smallest of the wave lengths and/or radii of curvature. For such shells, both shear deformation and rotary inertia can be neglected. Theories that include shear deformation are referred to as thick shell theories, or SDST. A consistent set of equations is presented here for both thick and thin shell theories (Leissa and Qatu 1991; Qatu 1999a,b, 2002a, 2004).

In thick shell theories, the midplane shell displacements are expanded in terms of shell thickness. Such an expansion can be of a first or a higher order. In the case of first order expansion, the theories are referred to as first order shear deformation theories. The 3D elasticity theory can then be reduced to a 2D theory using the *assumption* that the normal strains acting on the plane parallel to the middle surface are negligible compared with other strain components. This assumption is generally valid except within the vicinity of a highly concentrated force. In other words, no stretching is assumed in the z direction (i.e., $\varepsilon_z = 0$).

Assuming that normals to the midsurface strains remain straight during deformation but not normal to the midsurface, the displacements can be written as

$$\begin{aligned} u(\alpha, \beta, z) &= u_0(\alpha, \beta) + z\psi_\alpha(\alpha, \beta) \\ v(\alpha, \beta, z) &= v_0(\alpha, \beta) + z\psi_\beta(\alpha, \beta) \\ w(\alpha, \beta, z) &= w_0(\alpha, \beta) \end{aligned} \quad (2.35)$$

where u_0 , v_0 and w_0 are midsurface displacements of the shell and ψ_α and ψ_β are midsurface rotations. The third of the above equations yields $\varepsilon_z = 0$. An alternative derivation can be made with the assumption $\sigma_z = 0$ (Librescu 1976). The subscript (0) will refer to the middle surface in the subsequent equations. The above equations describe a typical first order SDST and will constitute the only assumption made in this theory when compared with the 3D theory of elasticity described earlier. Eq. (2.35) can be substituted in Eq. (2.33). The strains at any point in the shells can then be written in terms of midsurface strains and curvature changes as

$$\begin{aligned} \varepsilon_\alpha &= \frac{1}{(1 + z/R_\alpha)}(\varepsilon_{0\alpha} + z\kappa_\alpha) \\ \varepsilon_\beta &= \frac{1}{(1 + z/R_\beta)}(\varepsilon_{0\beta} + z\kappa_\beta) \\ \varepsilon_{\alpha\beta} &= \frac{1}{(1 + z/R_\alpha)}(\varepsilon_{0\alpha\beta} + z\kappa_{\alpha\beta}) \\ \varepsilon_{\beta\alpha} &= \frac{1}{(1 + z/R_\beta)}(\varepsilon_{0\beta\alpha} + z\kappa_{\beta\alpha}) \\ \gamma_{\alpha z} &= \frac{1}{(1 + z/R_\alpha)}(\gamma_{0\alpha z} + z(\psi_\alpha/R_\alpha)) \\ \gamma_{\beta z} &= \frac{1}{(1 + z/R_\beta)}(\gamma_{0\beta z} + z(\psi_\beta/R_\beta)) \end{aligned} \quad (2.36)$$

The contribution of the terms $z\psi_\alpha/R_\alpha$ and $z\psi_\beta/R_\beta$ to the overall accuracy of the theory needs to be determined. The midsurface strains are (obtained by setting $z = 0$ in

Eq. (2.33))

$$\begin{aligned}
 \varepsilon_{0\alpha} &= \frac{1}{A} \frac{\partial u_0}{\partial \alpha} + \frac{v_0}{AB} \frac{\partial A}{\partial \beta} + \frac{w_0}{R_\alpha} \\
 \varepsilon_{0\beta} &= \frac{1}{B} \frac{\partial v_0}{\partial \beta} + \frac{u_0}{AB} \frac{\partial B}{\partial \alpha} + \frac{w_0}{R_\beta} \\
 \varepsilon_{0\alpha\beta} &= \frac{1}{A} \frac{\partial v_0}{\partial \alpha} - \frac{u_0}{AB} \frac{\partial A}{\partial \beta} + \frac{w_0}{R_{\alpha\beta}} \\
 \varepsilon_{0\beta\alpha} &= \frac{1}{B} \frac{\partial u_0}{\partial \beta} - \frac{v_0}{AB} \frac{\partial B}{\partial \alpha} + \frac{w_0}{R_{\alpha\beta}} \\
 \gamma_{0\alpha z} &= \frac{1}{A} \frac{\partial w_0}{\partial \alpha} - \frac{u_0}{R_\alpha} - \frac{v_0}{R_{\alpha\beta}} + \psi_\alpha \\
 \gamma_{0\beta z} &= \frac{1}{B} \frac{\partial w_0}{\partial \beta} - \frac{v_0}{R_\beta} - \frac{u_0}{R_{\alpha\beta}} + \psi_\beta
 \end{aligned} \tag{2.37}$$

and the curvature and twist changes are

$$\begin{aligned}
 \kappa_\alpha &= \frac{1}{A} \frac{\partial \psi_\alpha}{\partial \alpha} + \frac{\psi_\beta}{AB} \frac{\partial A}{\partial \beta}, & \kappa_\beta &= \frac{1}{B} \frac{\partial \psi_\beta}{\partial \beta} + \frac{\psi_\alpha}{AB} \frac{\partial B}{\partial \alpha} \\
 \kappa_{\alpha\beta} &= \frac{1}{A} \frac{\partial \psi_\beta}{\partial \alpha} - \frac{\psi_\alpha}{AB} \frac{\partial A}{\partial \beta}, & \kappa_{\beta\alpha} &= \frac{1}{B} \frac{\partial \psi_\alpha}{\partial \beta} - \frac{\psi_\beta}{AB} \frac{\partial B}{\partial \alpha}
 \end{aligned} \tag{2.38}$$

Eqs. (2.36)–(2.38) constitute the strain–displacement relations needed for first order SDST.

2.2.2 Stress resultants

The force and moment resultants (Figures 2.3 and 2.4) are obtained by integrating the stresses over the shell thickness. The normal and shear force resultants are

$$\begin{aligned}
 \begin{bmatrix} N_\alpha \\ N_{\alpha\beta} \\ Q_\alpha \end{bmatrix} &= \int_{-h/2}^{h/2} \begin{bmatrix} \sigma_\alpha \\ \sigma_{\alpha\beta} \\ \sigma_{\alpha z} \end{bmatrix} (1 + z/R_\beta) dz \\
 \begin{bmatrix} N_\beta \\ N_{\beta\alpha} \\ Q_\beta \end{bmatrix} &= \int_{-h/2}^{h/2} \begin{bmatrix} \sigma_\beta \\ \sigma_{\alpha\beta} \\ \sigma_{\beta z} \end{bmatrix} (1 + z/R_\alpha) dz
 \end{aligned} \tag{2.39}$$

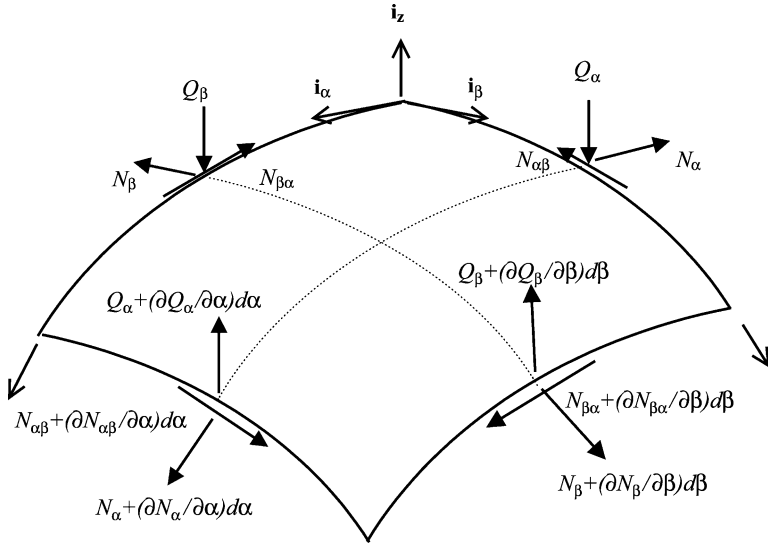


Figure 2.3. Force resultants in shell coordinates.

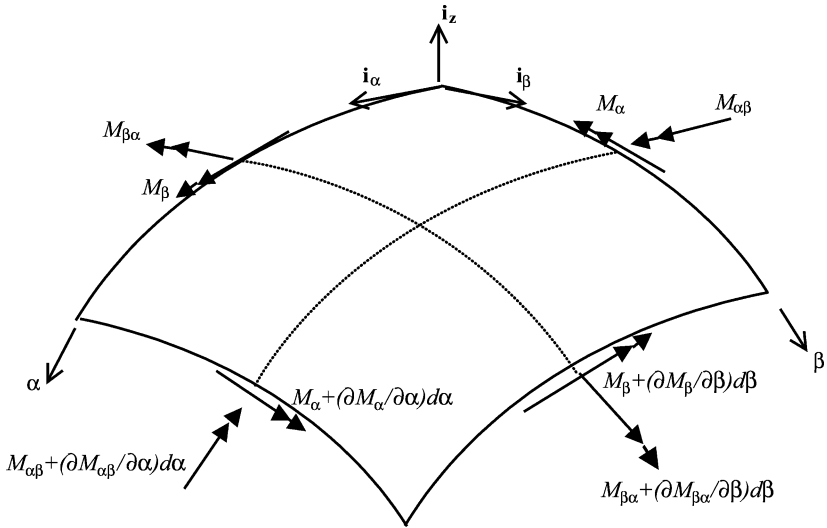


Figure 2.4. Moment resultants in shell coordinates.

The bending and twisting moment resultants and higher order shear resultant terms are

$$\begin{bmatrix} M_\alpha \\ M_{\alpha\beta} \\ P_\alpha \end{bmatrix} = \int_{-h/2}^{h/2} \begin{bmatrix} \sigma_\alpha \\ \sigma_{\alpha\beta} \\ \sigma_{\alpha z} \end{bmatrix} (1 + z/R_\beta) z \, dz \quad (2.40)$$

$$\begin{bmatrix} M_\beta \\ M_{\beta\alpha} \\ P_\beta \end{bmatrix} = \int_{-h/2}^{h/2} \begin{bmatrix} \sigma_\beta \\ \sigma_{\alpha\beta} \\ \sigma_{\beta z} \end{bmatrix} (1 + z/R_\alpha) z \, dz$$

where P_α and P_β are higher order shear terms. It should be noted here that the actual contribution of these terms to the accuracy of the shell equations needs to be determined. These terms will be kept here.

Force resultants have dimensions of force per unit length. The moment resultants are the moments per unit length. It should be mentioned that, although the stresses $\sigma_{\alpha\beta}$ and $\sigma_{\beta\alpha}$ are equal, the stress resultants $N_{\alpha\beta}$ and $N_{\beta\alpha}$ are not equal. Similarly, $M_{\alpha\beta}$ and $M_{\beta\alpha}$ are not equal. These stress resultants will be equal ($N_{\alpha\beta} = N_{\beta\alpha}$; $M_{\alpha\beta} = M_{\beta\alpha}$) only if $R_\alpha = R_\beta$, which is the case only for spherical shells or flat plates.

The above equations include the term $(1 + z/R_n)$, where n is α or β in the denominator. This term creates difficulties in carrying out the integration. Such difficulties do not exist for plates. The term was ignored in most thin shell theories (Leissa 1973a). In some thin shell theories (e.g., Vlasov's), the term was expanded in a geometric series form. Numerical investigations revealed that such expansion did not introduce better results for isotropic thin shells. This is understandable for thin shells because the term $(1 + z/R_n)$ is close to 1.

For thick shells, shear deformation and rotary inertia should be considered. However, many researchers failed to include the above term in the stress resultant equations (Librescu *et al.* 1989a,b; Bhimaraddi 1991). When the term was included, results closer to those of the 3D elasticity theory were obtained (Qatu 1999a). Including the term $(1 + z/R_n)$ yields the following stress resultant equations (Qatu 1999a, 2002a):

$$\begin{bmatrix} N_\alpha \\ N_\beta \\ N_{\alpha\beta} \\ N_{\beta\alpha} \\ M_\alpha \\ M_\beta \\ M_{\alpha\beta} \\ M_{\beta\alpha} \end{bmatrix} = \begin{bmatrix} \bar{A}_{11} & A_{12} & \bar{A}_{16} & A_{16} & \bar{B}_{11} & B_{12} & \bar{B}_{16} & B_{16} \\ A_{12} & \hat{A}_{22} & A_{26} & \hat{A}_{26} & B_{12} & \hat{B}_{22} & B_{26} & \hat{B}_{26} \\ \bar{A}_{16} & A_{26} & \bar{A}_{66} & A_{66} & \bar{B}_{16} & B_{26} & \bar{B}_{66} & B_{66} \\ A_{16} & \hat{A}_{26} & A_{66} & \hat{A}_{66} & B_{16} & \hat{B}_{26} & B_{66} & \hat{B}_{66} \\ \bar{B}_{11} & B_{12} & \bar{B}_{16} & B_{16} & \bar{D}_{11} & D_{12} & \bar{D}_{16} & D_{16} \\ B_{12} & \hat{B}_{22} & B_{16} & \hat{B}_{16} & D_{12} & \hat{D}_{22} & D_{26} & \hat{D}_{26} \\ \bar{B}_{16} & B_{26} & \bar{B}_{66} & B_{66} & \bar{D}_{16} & D_{26} & \bar{D}_{66} & D_{66} \\ B_{16} & \hat{B}_{26} & B_{66} & \hat{B}_{66} & D_{16} & \hat{D}_{26} & D_{66} & \hat{D}_{66} \end{bmatrix} \begin{bmatrix} \varepsilon_{0\alpha} \\ \varepsilon_{0\beta} \\ \varepsilon_{0\alpha\beta} \\ \varepsilon_{0\beta\alpha} \\ \kappa_\alpha \\ \kappa_\beta \\ \kappa_{\alpha\beta} \\ \kappa_{\beta\alpha} \end{bmatrix} \quad (2.41)$$

$$\begin{bmatrix} Q_\alpha \\ Q_\beta \\ P_\alpha \\ P_\beta \end{bmatrix} = \begin{bmatrix} \bar{A}_{55} & A_{45} & \bar{B}_{55} & B_{45} \\ A_{45} & \hat{A}_{44} & B_{45} & \hat{B}_{44} \\ \bar{B}_{55} & B_{45} & \bar{D}_{55} & D_{45} \\ B_{45} & \hat{B}_{44} & D_{45} & \hat{D}_{44} \end{bmatrix} \begin{bmatrix} \gamma_{0\alpha z} \\ \gamma_{0\beta z} \\ \psi_\alpha/R_\alpha \\ \psi_\beta/R_\beta \end{bmatrix} \quad (2.42)$$

where A_{ij} , B_{ij} , D_{ij} , \bar{A}_{ij} , \bar{B}_{ij} , \bar{D}_{ij} , \hat{A}_{ij} , \hat{B}_{ij} and \hat{D}_{ij} are defined as follows:

$$\left. \begin{aligned} A_{ij} &= \sum_{k=1}^N \bar{Q}_{ij}^{(k)} (h_k - h_{k-1}) \\ B_{ij} &= \frac{1}{2} \sum_{k=1}^N \bar{Q}_{ij}^{(k)} (h_k^2 - h_{k-1}^2) \\ D_{ij} &= \frac{1}{3} \sum_{k=1}^N \bar{Q}_{ij}^{(k)} (h_k^3 - h_{k-1}^3) \end{aligned} \right\} \quad i, j = 1, 2, 6$$

$$\left. \begin{aligned} A_{ij} &= \sum_{k=1}^N K_i K_j \bar{Q}_{ij}^{(k)} (h_k - h_{k-1}) \\ B_{ij} &= \frac{1}{2} \sum_{k=1}^N K_i K_j \bar{Q}_{ij}^{(k)} (h_k^2 - h_{k-1}^2) \\ D_{ij} &= \frac{1}{3} \sum_{k=1}^N K_i K_j \bar{Q}_{ij}^{(k)} (h_k^3 - h_{k-1}^3) \end{aligned} \right\} \quad i, j = 4, 5 \quad (2.43)$$

$$\left. \begin{aligned} \bar{A}_{ij} &= A_{ij\alpha} + \frac{B_{ij\alpha}}{R_\beta}, \quad \hat{A}_{ij} = A_{ij\beta} + \frac{B_{ij\beta}}{R_\alpha}, \\ \bar{B}_{ij} &= B_{ij\alpha} + \frac{D_{ij\alpha}}{R_\beta}, \quad \hat{B}_{ij} = B_{ij\beta} + \frac{D_{ij\beta}}{R_\alpha}, \\ \bar{D}_{ij} &= D_{ij\alpha} + \frac{E_{ij\alpha}}{R_\beta}, \quad \hat{D}_{ij} = D_{ij\beta} + \frac{E_{ij\beta}}{R_\alpha}, \end{aligned} \right\} \quad i, j = 1, 2, 4, 5, 6$$

where K_i and K_j are shear correction coefficients, typically taken at 5/6 (Timoshenko 1921), and where

$$\left. \begin{aligned} A_{ijn} &= \sum_{k=1}^N \int_{h_{k-1}}^{h_k} \bar{Q}_{ij}^{(k)} \frac{dz}{1+z/R_n} = R_n \sum_{k=1}^N \bar{Q}_{ij}^{(k)} \ln \left(\frac{R_n + h_k}{R_n + h_{k-1}} \right) \\ B_{ijn} &= \sum_{k=1}^N \int_{h_{k-1}}^{h_k} \bar{Q}_{ij}^{(k)} \frac{z dz}{1+z/R_n} = R_n \sum_{k=1}^N \bar{Q}_{ij}^{(k)} \left[(h_k - h_{k-1}) - R_n \ln \left(\frac{R_n + h_k}{R_n + h_{k-1}} \right) \right] \\ D_{ijn} &= \sum_{k=1}^N \int_{h_{k-1}}^{h_k} \bar{Q}_{ij}^{(k)} \frac{z^2 dz}{1+z/R_n} = R_n \sum_{k=1}^N \bar{Q}_{ij}^{(k)} \left[\frac{1}{2} \{ (R_n + h_k)^2 - (R_n + h_{k-1})^2 \} \right. \\ &\quad \left. - 2R_n(h_k - h_{k-1}) - R_n^2 \ln \left(\frac{R_n + h_k}{R_n + h_{k-1}} \right) \right] \\ E_{ijn} &= \sum_{k=1}^N \int_{h_{k-1}}^{h_k} \bar{Q}_{ij}^{(k)} \frac{z^3 dz}{1+z/R_n} = R_n \sum_{k=1}^N \bar{Q}_{ij}^{(k)} \left[\frac{1}{3} \{ (R_n + h_k)^3 - (R_n + h_{k-1})^3 \} \right. \\ &\quad \left. + \frac{3}{2} R_n \{ (R_n + h_k)^2 - (R_n + h_{k-1})^2 \} - 3R_n^2(h_k - h_{k-1}) - R_n^3 \ln \left(\frac{R_n + h_k}{R_n + h_{k-1}} \right) \right] \end{aligned} \right\} \quad (2.44)$$

$n = \alpha, \beta$

One can also use the truncated equations (Leissa and Chang 1996), for better numerical stability. The term $1/(1+z/R_n)$ is expanded in a geometric series as

$$\frac{1}{1+z/R_n} = 1 - \frac{z}{R_n} + \frac{z^2}{R_n^2} + (\text{Higher order terms}) \quad (2.45)$$

The terms having orders higher than $(z/R_n)^2$ are truncated. Then the Eq. (2.43) are replaced by the following equations

$$\left. \begin{aligned} \bar{A}_{ij} &= A_{ij} - c_0 B_{ij}, \quad \hat{A}_{ij} = A_{ij} + c_0 B_{ij}, \\ \bar{B}_{ij} &= B_{ij} - c_0 D_{ij}, \quad \hat{B}_{ij} = B_{ij} + c_0 D_{ij} \\ \bar{D}_{ij} &= D_{ij} - c_0 E_{ij}, \quad \hat{D}_{ij} = D_{ij} + c_0 E_{ij} \end{aligned} \right\} \quad i, j = 1, 2, 4, 5, 6 \quad (2.46)$$

where

$$\left. \begin{aligned} A_{ij} &= \sum_{k=1}^N \bar{Q}_{ij}^{(k)} (h_k - h_{k-1}) \\ B_{ij} &= \frac{1}{2} \sum_{k=1}^N \bar{Q}_{ij}^{(k)} (h_k^2 - h_{k-1}^2) \\ D_{ij} &= \frac{1}{3} \sum_{k=1}^N \bar{Q}_{ij}^{(k)} (h_k^3 - h_{k-1}^3) \\ E_{ij} &= \frac{1}{4} \sum_{k=1}^N \bar{Q}_{ij}^{(k)} (h_k^4 - h_{k-1}^4) \end{aligned} \right\} \quad i, j = 1, 2, 6 \quad (2.47)$$

and

$$\left. \begin{aligned} A_{ij} &= \sum_{k=1}^N K_i K_j \bar{Q}_{ij}^{(k)} (h_k - h_{k-1}) \\ B_{ij} &= \frac{1}{2} \sum_{k=1}^N K_i K_j \bar{Q}_{ij}^{(k)} (h_k^2 - h_{k-1}^2) \\ D_{ij} &= \frac{1}{3} \sum_{k=1}^N K_i K_j \bar{Q}_{ij}^{(k)} (h_k^3 - h_{k-1}^3) \end{aligned} \right\} \quad i, j = 4, 5$$

where

$$c_0 = \left(\frac{1}{R_\alpha} - \frac{1}{R_\beta} \right) \quad (2.48)$$

h_k is the distance from the midsurface to the surface of the k th layer having the farthest z coordinate (Figure 1.5). For shells which are laminated symmetrically with respect to their midsurfaces, all the B_{ij} terms become 0's. The above truncated equations are similar to those obtained by Leissa and Chang (1996).

2.2.3 Energy functionals

The energy functionals are important for their use in approximate methods as well as deriving a consistent set of equations of motion and boundary conditions. The strain energy of a shell element is defined as

$$\begin{aligned} U &= \frac{1}{2} \int_V \{ \sigma_\alpha \varepsilon_\alpha + \sigma_\beta \varepsilon_\beta + \sigma_z \varepsilon_z + \sigma_{\alpha\beta} \gamma_{\alpha\beta} + \sigma_{\alpha z} \gamma_{\alpha z} + \sigma_{\beta z} \gamma_{\beta z} \} dV \\ &= \frac{1}{2} \int_\alpha \int_\beta \int_{-h/2}^{+h/2} \{ \sigma_\alpha \varepsilon_\alpha + \sigma_\beta \varepsilon_\beta + \sigma_z \varepsilon_z + \sigma_{\alpha\beta} \gamma_{\alpha\beta} + \sigma_{\alpha z} \gamma_{\alpha z} + \sigma_{\beta z} \gamma_{\beta z} \} \\ &\quad (1 + z/R_\alpha)(1 + z/R_\beta) AB \, d\alpha \, d\beta \, dz \end{aligned} \quad (2.49)$$

Substituting Eqs. (2.36), (2.39) and (2.40) into the above equation yields

$$\begin{aligned} U &= \frac{1}{2} \int_\alpha \int_\beta \{ N_\alpha \varepsilon_{0\alpha} + N_\beta \varepsilon_{0\beta} + N_{\alpha\beta} \varepsilon_{0\alpha\beta} + N_{\beta\alpha} \varepsilon_{0\beta\alpha} + M_\alpha \kappa_\alpha + M_\beta \kappa_\beta + M_{\alpha\beta} \kappa_{\alpha\beta} \\ &\quad + M_{\beta\alpha} \kappa_{\beta\alpha} + Q_\alpha \gamma_{0\alpha z} + Q_{\beta\alpha} \gamma_{0\beta z} + P_\alpha \psi_\alpha / R_\alpha + P_\beta \psi_\beta / R_\beta \} AB \, d\alpha \, d\beta \end{aligned} \quad (2.50)$$

The external work is

$$W = \int_\alpha \int_\beta \{ q_\alpha u_0 + q_\beta v_0 + q_n w_0 + m_\alpha \psi_\alpha + m_\beta \psi_\beta \} AB \, d\alpha \, d\beta \quad (2.51)$$

where q_α , q_β and q_n are the distributed forces in the α , β and z directions, respectively. Also, m_α and m_β are the distributed couples about the middle surface of the shell.

The kinetic energy of the shell can be expressed as

$$\begin{aligned}
 T &= \frac{1}{2} \int_V \{ \dot{u}^2 + \dot{v}^2 + \dot{w}^2 \} dV \\
 &= \frac{1}{2} \int_{\alpha} \int_{\beta} \int_{-h/2}^{+h/2} (\dot{u}_0^2 + \dot{v}_0^2 + \dot{w}_0^2 + z^2 \dot{\psi}_{\alpha}^2 + z^2 \dot{\psi}_{\beta}^2 + 2z\dot{u}_0\dot{\psi}_{\alpha} + 2z\dot{v}_0\dot{\psi}_{\beta}) \\
 &\quad (1 + z/R_{\alpha})(1 + z/R_{\beta}) AB \, d\alpha \, d\beta \, dz
 \end{aligned} \tag{2.52}$$

Expanding the terms yields

$$\begin{aligned}
 T &= \frac{1}{2} \int_{\alpha} \int_{\beta} \int_{-h/2}^{+h/2} \left\{ (\dot{u}_0^2 + \dot{v}_0^2 + \dot{w}_0^2) \left(1 + z \left(\frac{1}{R_{\alpha}} + \frac{1}{R_{\beta}} \right) + \frac{z^2}{R_{\alpha}R_{\beta}} \right) \right. \\
 &\quad + z^2 (\dot{\psi}_{\alpha}^2 + \dot{\psi}_{\beta}^2) \left(1 + z \left(\frac{1}{R_{\alpha}} + \frac{1}{R_{\beta}} \right) + \frac{z^2}{R_{\alpha}R_{\beta}} \right) \\
 &\quad \left. + 2z(\dot{u}_0\dot{\psi}_{\alpha} + \dot{v}_0\dot{\psi}_{\beta}) \left(1 + z \left(\frac{1}{R_{\alpha}} + \frac{1}{R_{\beta}} \right) + \frac{z^2}{R_{\alpha}R_{\beta}} \right) \right\} AB \, dz \, d\alpha \, d\beta
 \end{aligned} \tag{2.53}$$

Carrying out the integration yields

$$\begin{aligned}
 T &= \frac{1}{2} \int_{\alpha} \int_{\beta} \left\{ (\dot{u}_0^2 + \dot{v}_0^2 + \dot{w}_0^2) \left(I_1 + I_2 \left(\frac{1}{R_{\alpha}} + \frac{1}{R_{\beta}} \right) + \frac{I_3}{R_{\alpha}R_{\beta}} \right) \right. \\
 &\quad + (\dot{\psi}_{\alpha}^2 + \dot{\psi}_{\beta}^2) \left(I_3 + I_4 \left(\frac{1}{R_{\alpha}} + \frac{1}{R_{\beta}} \right) + \frac{I_5}{R_{\alpha}R_{\beta}} \right) \\
 &\quad \left. + (\dot{u}_0\dot{\psi}_{\alpha} + \dot{v}_0\dot{\psi}_{\beta}) \left(I_2 + I_3 \left(\frac{1}{R_{\alpha}} + \frac{1}{R_{\beta}} \right) + \frac{I_4}{R_{\alpha}R_{\beta}} \right) \right\} AB \, d\alpha \, d\beta
 \end{aligned} \tag{2.54}$$

where the inertia terms are

$$[I_1, I_2, I_3, I_4, I_5] = \sum_{k=1}^N \int_{h_{k-1}}^{h_k} \rho^{(k)} [1, z, z^2, z^3, z^4] dz \tag{2.55}$$

$\rho^{(k)}$ is the mass density of the k th layer of the shell per unit midsurface area. The energy expressions described here are used to derive the equations of motion.

2.2.4 Equations of motion

The equations of motion can be obtained by taking a differential element of a shell having thickness h and midsurface lengths $A \, d\alpha$ by $B \, d\beta$ (Figures 2.3 and 2.4), and requiring the sums of the external and internal body forces and moments each to be 0.

Figure 2.3 shows such an element (although the thickness is not described) with all the internal forces (per unit length) acting upon it. These include the force resultants N_α , N_β , $N_{\alpha\beta}$, $N_{\beta\alpha}$ tangent to the midsurface (also called “membrane force resultants”) described earlier, and the transverse shearing force resultants Q_α and Q_β . Figure 2.4 depicts the element with the moment resultants acting upon it. Summing moments on the element, including both the moment resultants and the force resultants, yield the remaining equilibrium equations. m_α and m_β represent possible body couples (moments per unit length) which may be applied to the shell. Hamilton’s principle can also be used to derive the consistent equations of motion and boundary conditions. The equations of motion are

$$\begin{aligned}
& \frac{\partial}{\partial \alpha}(BN_\alpha) + \frac{\partial}{\partial \beta}(AN_{\beta\alpha}) + \frac{\partial A}{\partial \beta}N_{\alpha\beta} - \frac{\partial B}{\partial \alpha}N_\beta + \frac{AB}{R_\alpha}Q_\alpha + \frac{AB}{R_{\alpha\beta}}Q_\beta + ABq_\alpha \\
& \quad = AB(\bar{I}_1\ddot{u}_0^2 + \bar{I}_2\ddot{\psi}_\alpha^2) \\
& \frac{\partial}{\partial \beta}(AN_\beta) + \frac{\partial}{\partial \alpha}(BN_{\alpha\beta}) + \frac{\partial B}{\partial \alpha}N_{\beta\alpha} - \frac{\partial A}{\partial \beta}N_\alpha + \frac{AB}{R_\beta}Q_\beta + \frac{AB}{R_{\alpha\beta}}Q_\alpha + ABq_\beta \\
& \quad = AB(\bar{I}_1\ddot{v}_0^2 + \bar{I}_2\ddot{\psi}_\beta^2) \\
& -AB\left(\frac{N_\alpha}{R_\alpha} + \frac{N_\beta}{R_\beta} + \frac{N_{\alpha\beta} + N_{\beta\alpha}}{R_{\alpha\beta}}\right) + \frac{\partial}{\partial \alpha}(BQ_\alpha) + \frac{\partial}{\partial \beta}(AQ_\beta) + ABq_n = AB(\bar{I}_1\ddot{w}_0^2) \quad (2.56) \\
& \frac{\partial}{\partial \alpha}(BM_\alpha) + \frac{\partial}{\partial \beta}(AM_{\beta\alpha}) + \frac{\partial A}{\partial \beta}M_{\alpha\beta} - \frac{\partial B}{\partial \alpha}M_\beta - ABQ_\alpha + \frac{AB}{R_\alpha}P_\alpha + ABm_\alpha \\
& \quad = AB(\bar{I}_2\ddot{u}_0^2 + \bar{I}_3\ddot{\psi}_\alpha^2) \\
& \frac{\partial}{\partial \beta}(AM_\beta) + \frac{\partial}{\partial \alpha}(BM_{\alpha\beta}) + \frac{\partial B}{\partial \alpha}M_{\beta\alpha} - \frac{\partial A}{\partial \beta}M_\alpha - ABQ_\beta + \frac{AB}{R_\beta}P_\beta + ABm_\beta \\
& \quad = AB(\bar{I}_2\ddot{v}_0^2 + \bar{I}_3\ddot{\psi}_\beta^2)
\end{aligned}$$

where q_α , q_β and q_n represent external forces (per unit area) applied either to the surface or as body forces and where the two dots represent the second derivative of these terms with respect to time, and where

$$\bar{I}_i = \left(I_i + I_{i+1} \left(\frac{1}{R_\alpha} + \frac{1}{R_\beta} \right) + \frac{I_{i+2}}{R_\alpha R_\beta} \right), \quad i = 1, 2, 3 \quad (2.57)$$

where the terms I_i are defined in Eq. (2.55).

The sixth equation of motion is typically ignored in shell analysis. Although it may not be identically satisfied, the non-zero residual that will be found on its right hand side after the solution is substituted into it, which may be interpreted as a body moment about the n -axis, will typically be small.

Boundary conditions for a shell may be derived by physical arguments or by using energy functionals and the Hamilton's principle. On each boundary one must specify five conditions. The boundary terms for the boundaries with $\alpha = \text{constant}$ are

$$\begin{aligned}
 N_{0\alpha} - N_{\alpha} &= 0 & \text{or} & & u_0 &= 0 \\
 N_{0\alpha\beta} - N_{\alpha\beta} &= 0 & \text{or} & & v_0 &= 0 \\
 Q_{0\alpha} - Q_{\alpha} &= 0 & \text{or} & & w_0 &= 0 \\
 M_{0\alpha} - M_{\alpha} &= 0 & \text{or} & & \psi_{\alpha} &= 0 \\
 M_{0\alpha\beta} - M_{\alpha\beta} &= 0 & \text{or} & & \psi_{\beta} &= 0
 \end{aligned} \tag{2.58}$$

Similar equations can be obtained for $\beta = \text{constant}$. The above boundary conditions produce eight possible combinations for each of the classical boundary conditions (free, simple support, clamped). These are given in Table 2.1.

Boundaries may also be elastically constrained, with the constraints being represented as translational and rotational springs distributed along the boundaries. In such cases the boundary conditions can be generalized (Qatu and Leissa 1991a,b) to include elastic constraints.

The above set of equations describe a first order shear deformation theory. This theory was recently used to analyze thick shallow shells and closed circular cylindrical shells by Qatu (1999a). This theory will be specialized later for beams, plates and various shells. Higher order shear deformation theories can also be generated by choosing different displacement fields from those of Eq. (2.35). A displacement field that will allow the shear to be quadratic as a function of thickness. This will allow the shell surfaces to be free of shear (as they should be). Such displacement, however, will introduce terms at the boundaries that are not easily applicable or yet understood. Higher order theories will not be described here.

Thick shell theories have been used for thickness ratios (thickness to the smallest of wavelength and radii of curvature) as large as 1/10 and arguably for thickness ratios up to 1/5. It should be stated that including shear deformation increases the order of the differential equations from 8 to 10 (for first order shear deformation theories) or more (for higher order shear deformation theories) when compared with thin shell theories.

2.2.5 Recent developments

Many recent research papers appeared where thick, or shear deformation, shell theories have been used. Such theories were used by Kabir (1998), Kabir and Chaudhuri (1991, 1994a,b), Nosier and Reddy (1992), Piskunov *et al.* (1994, 1995), Soldatos (1991), Wang and Schweizerhof (1996a,b, 1997), Sivadas (1995a,b), Sharma *et al.* (1999), Xi *et al.* (1996), Argyris and Tenek (1996), Chonan, (1988), Ding *et al.* (1997) and Toorani and Lakis (2000).

Table 2.1. Combinations of boundary conditions for thick shells at each edge $\alpha = \text{constant}$.

Boundary type	Conditions
<i>Free boundaries</i>	
F1	$Q_\alpha = M_\alpha = u = v = \psi_\beta = 0$
F2	$Q_\alpha = M_\alpha = N_\alpha = v = \psi_\beta = 0$
F3	$Q_\alpha = M_\alpha = u = N_{\alpha\beta} = \psi_\beta = 0$
F4	$Q_\alpha = M_\alpha = N_\alpha = N_{\alpha\beta} = \psi_\beta = 0$
F5	$Q_\alpha = M_\alpha = u = v = M_{\alpha\beta} = 0$
F6	$Q_\alpha = M_\alpha = N_\alpha = v = M_{\alpha\beta} = 0$
F7	$Q_\alpha = M_\alpha = u = N_{\alpha\beta} = M_{\alpha\beta} = 0$
F8	$Q_\alpha = M_\alpha = N_\alpha = N_{\alpha\beta} = M_{\alpha\beta} = 0$
<i>Simple support boundaries</i>	
S1	$w = M_\alpha = u = v = \psi_\beta = 0$
S2	$w = M_\alpha = N_\alpha = v = \psi_\beta = 0$
S3	$w = M_\alpha = u = N_{\alpha\beta} = \psi_\beta = 0$
S4	$w = M_\alpha = N_\alpha = N_{\alpha\beta} = \psi_\beta = 0$
S5	$w = M_\alpha = u = v = M_{\alpha\beta} = 0$
S6	$w = M_\alpha = N_\alpha = v = M_{\alpha\beta} = 0$
S7	$w = M_\alpha = u = N_{\alpha\beta} = M_{\alpha\beta} = 0$
S8	$w = M_\alpha = N_\alpha = N_{\alpha\beta} = M_{\alpha\beta} = 0$
<i>Clamped boundaries</i>	
C1	$w = \psi_\alpha = u = v = \psi_\beta = 0$
C2	$w = \psi_\alpha = N_\alpha = v = \psi_\beta = 0$
C3	$w = \psi_\alpha = u = N_{\alpha\beta} = \psi_\beta = 0$
C4	$w = \psi_\alpha = N_\alpha = N_{\alpha\beta} = \psi_\beta = 0$
C5	$w = \psi_\alpha = u = v = M_{\alpha\beta} = 0$
C6	$w = \psi_\alpha = N_\alpha = v = M_{\alpha\beta} = 0$
C7	$w = \psi_\alpha = u = N_{\alpha\beta} = M_{\alpha\beta} = 0$
C8	$w = \psi_\alpha = N_\alpha = N_{\alpha\beta} = M_{\alpha\beta} = 0$

Higher order shear deformation theories were developed and used for composite shells by Librescu *et al.* (1989a,b), Mizusawa (1996), Ma and He (1998), Messina and Soldatos (1999a,b) and Timarci and Soldatos (1995). Thick circular cylindrical shells were considered by Birlik and Mengi (1989), Sivadas and Ganesan (1991a,b, 1993), Kolesnikov (1996), Sun *et al.* (1997), Zenkour (1998), Soldatos and Messina (1998) and Mizusawa (1996). Non-circular cylindrical shells were reviewed by Soldatos (1999). Spherical thick shells were studied by several researchers (Chao and Chern, 1988; Dasgupta and Huang, 1997; Gautham and Ganesan, 1994). Lu *et al.* (1996), Ramesh and Ganesan (1993) and Sivadas and Ganesan (1992) considered thick conical shells.

The second approach to the development of shell theories is a stress-based approach. The work of Reissner is the first to adopt this approach, which has recently been used by Yong and Cho (1995), Carrera (1999a,b) and Xi *et al.* (1996). This will not be described here.

2.3. THIN SHELL THEORY

If the shell thickness is less than $1/20$ of the *wavelength* of the deformation mode and/or radii of curvature, a thin shell theory, where both shear deformation and rotary inertia are negligible, is generally acceptable. Some researchers question the value of $1/20$ and choose a smaller value, particularly for laminated composite materials. Depending on various assumptions made during the derivation of the strain–displacement relations, stress–strain relations, and the equilibrium equations, various thin shell theories can be derived. Among the most common of these are the Love, Reissner, Naghdi, Sander and Flügge shell theories. All these theories were initially derived for isotropic shells and expanded later for laminated composite shells by applying the appropriate integration through lamina and stress–strain relations.

Leissa (1973a) showed that most thin shell theories yield similar results. The exceptions were the membrane theory and that of Donnell and Mushtari. The equations of Donnell and Mushtari describe shallow shells and are shown later as a part of shallow shell theory. The equations shown in this section are equivalent to those of Reissner and Naghdi (Leissa 1973a) with the extension to laminated composite thin shells. The reason for adopting these equations is the fact that they offer the simplest, most accurate and consistent equations for laminated thin shells.

2.3.1 Kinematic relations

For very thin shells, the following additional assumptions simplify the shell equations and reduce their order:

1. The shell is thin such that the ratio of the thickness compared to any of the shell's radii of curvature or its width or length is negligible compared to unity. In vibration analysis, the length of the shell is replaced by the wave length.
2. The normals to the middle surface remain straight and normal to the midsurface when the shell undergoes deformation.

The first of the above assumptions assures that certain parameters in the shell equations (including the z/R term mentioned earlier in the thick shell theory) can be neglected. The second of the above assumptions allows for neglecting shear deformation in the kinematics equations. It allows for making the inplane displacement to be linearly varying through the shell's thickness:

$$\begin{aligned}\varepsilon_\alpha &= \varepsilon_{0\alpha} + z\kappa_\alpha \\ \varepsilon_\beta &= \varepsilon_{0\beta} + z\kappa_\beta \\ \gamma_{\alpha\beta} &= \gamma_{0\alpha\beta} + z\tau\end{aligned}\tag{2.59}$$

where the midsurface strains and curvature and twist changes are

$$\begin{aligned}\varepsilon_{0\alpha} &= \frac{1}{A} \frac{\partial u_0}{\partial \alpha} + \frac{v_0}{AB} \frac{\partial A}{\partial \beta} + \frac{w_0}{R_\alpha} \\ \varepsilon_{0\beta} &= \frac{1}{B} \frac{\partial v_0}{\partial \beta} + \frac{u_0}{AB} \frac{\partial B}{\partial \alpha} + \frac{w_0}{R_\beta} \\ \gamma_{0\alpha\beta} &= \frac{1}{A} \frac{\partial v_0}{\partial \alpha} - \frac{u_0}{AB} \frac{\partial A}{\partial \beta} + \frac{1}{B} \frac{\partial u_0}{\partial \beta} - \frac{v_0}{AB} \frac{\partial B}{\partial \alpha} + 2 \frac{w_0}{R_{\alpha\beta}} \\ \kappa_\alpha &= \frac{1}{A} \frac{\partial \psi_\alpha}{\partial \alpha} + \frac{\psi_\beta}{AB} \frac{\partial A}{\partial \beta}, \quad \kappa_\beta = \frac{1}{B} \frac{\partial \psi_\beta}{\partial \beta} + \frac{\psi_\alpha}{AB} \frac{\partial B}{\partial \alpha} \\ \tau &= \frac{1}{A} \frac{\partial \psi_\beta}{\partial \alpha} - \frac{\psi_\alpha}{AB} \frac{\partial A}{\partial \beta} + \frac{1}{B} \frac{\partial \psi_\alpha}{\partial \beta} - \frac{\psi_\beta}{AB} \frac{\partial B}{\partial \alpha}\end{aligned}\tag{2.60}$$

where

$$\psi_\alpha = \frac{u_0}{R_\alpha} + \frac{v_0}{R_{\alpha\beta}} - \frac{1}{A} \frac{\partial w_0}{\partial \alpha}, \quad \psi_\beta = \frac{v_0}{R_\beta} + \frac{u_0}{R_{\alpha\beta}} - \frac{1}{B} \frac{\partial w_0}{\partial \beta}\tag{2.61}$$

2.3.2 Stress resultants

Applying the Kirchhoff hypothesis of neglecting shear deformation and the assumption that ε_z is negligible, the stress-strain equations for an element of material in the k th

lamina may be written as

$$\begin{bmatrix} \sigma_\alpha \\ \sigma_\beta \\ \sigma_{\alpha\beta} \end{bmatrix}_k = \begin{bmatrix} \bar{Q}_{11} & \bar{Q}_{12} & \bar{Q}_{16} \\ \bar{Q}_{12} & \bar{Q}_{22} & \bar{Q}_{26} \\ \bar{Q}_{16} & \bar{Q}_{26} & \bar{Q}_{66} \end{bmatrix}_k \begin{bmatrix} \varepsilon_\alpha \\ \varepsilon_\beta \\ \gamma_{\alpha\beta} \end{bmatrix}_k \quad (2.62)$$

Although the layers are orthotropic in their material coordinates, the above equations are the same as those of material with general anisotropy. This is a result of the lamination at an angle other than 0 or 90° with respect to the global coordinates. In other words, the \bar{Q}_{16} and \bar{Q}_{26} coefficients result from a coordinate transformation and arise only if the shell coordinates (α, β) are not parallel nor perpendicular to the fibers. Subsequently, if the shell coordinates (α, β) are parallel or perpendicular to the fibers, then the terms \bar{Q}_{16} and \bar{Q}_{26} are 0.

The stresses over the shell thickness (h) are integrated to obtain the force and moment resultants. Note that, for a thin shell, the terms z/R_α and z/R_β are much less than unity and may, therefore, be neglected. Doing so results in equal inplane shear force resultants (i.e., $N_{\alpha\beta} = N_{\beta\alpha}$), and twisting moments (i.e., $M_{\alpha\beta} = M_{\beta\alpha}$). Thus the force and moment resultants are

$$\begin{bmatrix} N_\alpha \\ N_\beta \\ N_{\alpha\beta} \end{bmatrix} = \int_{-h/2}^{h/2} \begin{bmatrix} \sigma_\alpha \\ \sigma_\beta \\ \sigma_{\alpha\beta} \end{bmatrix} dz \quad (2.63)$$

$$\begin{bmatrix} M_\alpha \\ M_\beta \\ M_{\alpha\beta} \end{bmatrix} = \int_{-h/2}^{h/2} \begin{bmatrix} \sigma_\alpha \\ \sigma_\beta \\ \sigma_{\alpha\beta} \end{bmatrix} z dz$$

Substituting Eqs. (2.59), (2.60) and (2.62) into Eq. (2.63) and carrying out the integration over the thickness, from layer to layer, yields

$$\begin{bmatrix} N_\alpha \\ N_\beta \\ N_{\alpha\beta} \\ - \\ M_\alpha \\ M_\beta \\ M_{\alpha\beta} \end{bmatrix} = \begin{bmatrix} A_{11} & A_{12} & A_{16} & B_{11} & B_{12} & B_{16} \\ A_{12} & A_{22} & A_{26} & B_{12} & B_{22} & B_{26} \\ A_{16} & A_{26} & A_{66} & B_{16} & B_{26} & B_{66} \\ - & - & - & - & - & - \\ B_{11} & B_{12} & B_{16} & D_{11} & D_{12} & D_{16} \\ B_{12} & B_{22} & B_{26} & D_{12} & D_{22} & D_{26} \\ B_{16} & B_{26} & B_{66} & D_{16} & D_{26} & D_{66} \end{bmatrix} \begin{bmatrix} \varepsilon_{0\alpha} \\ \varepsilon_{0\beta} \\ \gamma_{0\alpha\beta} \\ - \\ k_\alpha \\ k_\beta \\ \tau \end{bmatrix} \quad (2.64)$$

where A_{ij} , B_{ij} and D_{ij} are the stiffness coefficients arising from the piecewise integration over the shell thickness:

$$\begin{aligned} A_{ij} &= \sum_{k=1}^N Q_{ij}^{(k)} (z_k - z_{k-1}) \\ B_{ij} &= \frac{1}{2} \sum_{k=1}^N Q_{ij}^{(k)} (z_k^2 - z_{k-1}^2) \\ D_{ij} &= \frac{1}{3} \sum_{k=1}^N Q_{ij}^{(k)} (z_k^3 - z_{k-1}^3) \end{aligned} \quad (2.65)$$

and where z_k is the distance from the midsurface to the surface of the k th layer having the farthest z coordinate (Figure 1.5). For shells which are laminated symmetrically with respect to their midsurfaces, all the B_{ij} terms become 0. Note that the above equations for thin shells are the same as those for laminated plates (Ambartsumian 1970; Whitney 1987). This is a consequence of neglecting terms of the type z/R in comparison with unity. This is also made in many of the isotropic deep shell theories, but not all of them (Flügge 1962).

2.3.3 Energy functionals

The energy functionals are important for their use in approximate methods as well as deriving a consistent set of equations of motion and boundary conditions. The strain energy of a shell element is defined as

$$\begin{aligned} U &= \frac{1}{2} \int_V \{ \sigma_\alpha \varepsilon_\alpha + \sigma_\beta \varepsilon_\beta + \sigma_{\alpha\beta} \gamma_{\alpha\beta} \} dV \\ &= \frac{1}{2} \int_\alpha \int_\beta \int_{-h/2}^{+h/2} \{ \sigma_\alpha \varepsilon_\alpha + \sigma_\beta \varepsilon_\beta + \sigma_{\alpha\beta} \gamma_{\alpha\beta} \} AB \, d\alpha \, d\beta \, dz \end{aligned} \quad (2.66)$$

The strain energy can also be written in terms of the midsurface strains and stress resultants as

$$U = \frac{1}{2} \int_\alpha \int_\beta \{ N_\alpha \varepsilon_{0\alpha} + N_\beta \varepsilon_{0\beta} + N_{\alpha\beta} \gamma_{0\alpha\beta} + M_\alpha \kappa_\alpha + M_\beta \kappa_\beta + M_{\alpha\beta} \tau \} AB \, d\alpha \, d\beta \quad (2.67)$$

The external work is

$$W = \int_\alpha \int_\beta \{ q_\alpha u_0 + q_\beta v_0 + q_n w_0 \} AB \, d\alpha \, d\beta \quad (2.68)$$

The kinetic energy of the thin shell can be expressed as (note that rotary inertia terms are neglected)

$$T = \frac{1}{2} \int_V \{\dot{u}^2 + \dot{v}^2 + \dot{w}^2\} dV = \frac{1}{2} \int_\alpha \int_\beta \int_{-h/2}^{+h/2} (\dot{u}_0^2 + \dot{v}_0^2 + \dot{w}_0^2) AB d\alpha d\beta dz \quad (2.69)$$

Expanding the terms yields and carrying out the integration yields

$$T = \frac{1}{2} \int_\alpha \int_\beta \{(\dot{u}_0^2 + \dot{v}_0^2 + \dot{w}_0^2)(I_1)\} AB d\alpha d\beta \quad (2.70)$$

The energy expression described here are used to derive the equations of motion.

2.3.4 Equations of motion

Using Hamilton's principle, in the manner similar to that described earlier, yields the following equations of motion:

$$\begin{aligned} \frac{\partial}{\partial \alpha}(BN_\alpha) + \frac{\partial}{\partial \beta}(AN_{\beta\alpha}) + \frac{\partial A}{\partial \beta}N_{\alpha\beta} - \frac{\partial B}{\partial \alpha}N_\beta + \frac{AB}{R_\alpha}Q_\alpha + \frac{AB}{R_{\alpha\beta}}Q_\beta + ABq_\alpha &= AB(I_1\ddot{u}_0^2) \\ \frac{\partial}{\partial \beta}(AN_\beta) + \frac{\partial}{\partial \alpha}(BN_{\alpha\beta}) + \frac{\partial B}{\partial \alpha}N_{\beta\alpha} - \frac{\partial A}{\partial \beta}N_\alpha + \frac{AB}{R_\beta}Q_\beta + \frac{AB}{R_{\alpha\beta}}Q_\alpha + ABq_\beta &= AB(I_1\ddot{v}_0^2) \quad (2.71) \\ -AB\left(\frac{N_\alpha}{R_\alpha} + \frac{N_\beta}{R_\beta} + \frac{N_{\alpha\beta} + N_{\beta\alpha}}{R_{\alpha\beta}}\right) + \frac{\partial}{\partial \alpha}(BQ_\alpha) + \frac{\partial}{\partial \beta}(AQ_\beta) + ABq_n &= AB(I_1\ddot{w}_0^2) \end{aligned}$$

where

$$\begin{aligned} ABQ_\alpha &= \frac{\partial}{\partial \alpha}(BM_\alpha) + \frac{\partial}{\partial \beta}(AM_{\beta\alpha}) + \frac{\partial A}{\partial \beta}M_{\alpha\beta} - \frac{\partial B}{\partial \alpha}M_\beta \\ ABQ_\beta &= \frac{\partial}{\partial \beta}(AM_\beta) + \frac{\partial}{\partial \alpha}(BM_{\alpha\beta}) + \frac{\partial B}{\partial \alpha}M_{\beta\alpha} - \frac{\partial A}{\partial \beta}M_\alpha \end{aligned}$$

where I_1 is defined in Eq. (2.55). Rotary inertia terms are omitted from the right hand sides of the above equations because, as it is known, they are less important than shear deformation effects, which are being neglected in the present analysis.

It should be noted that the summation of forces and moments actually yield five equations of equilibrium. Two of these (the moment summation equations considered) can be substituted in the third equation (summation of forces in the normal direction). This reduces the five equations to the three equations described in Eq. (2.71).

The following boundary conditions can be obtained for thin shells (for $\alpha = \text{constant}$):

$$\begin{aligned}
 N_{0\alpha} - N_\alpha &= 0 \quad \text{or} \quad u_0 = 0 \\
 \left(N_{0\alpha\beta} - \frac{M_{0\alpha\beta}}{R_\beta} \right) - \left(N_{\alpha\beta} - \frac{M_{\alpha\beta}}{R_\beta} \right) &= 0 \quad \text{or} \quad v_0 = 0 \\
 \left(Q_{0\alpha} - \frac{1}{B} \frac{\partial M_{0\alpha\beta}}{\partial \beta} \right) - \left(Q_\alpha - \frac{1}{B} \frac{\partial M_{\alpha\beta}}{\partial \beta} \right) &= 0 \quad \text{or} \quad w_0 = 0 \\
 M_{0\alpha} - M_\alpha &= 0 \quad \text{or} \quad \psi_\alpha = 0 \\
 M_{0\alpha\beta} w \Big|_{\beta_1}^{\beta_2} &= 0
 \end{aligned} \tag{2.72}$$

Similar equations can be obtained for $\beta = \text{constant}$. Because of the coupling between the inplane displacements (u and v) and the out-of-plane displacement (w), the classical boundary conditions of simply supported, clamped and free that exist for homogeneous plates have to be revisited. For general shells and unsymmetrically laminated plates, each of the mentioned boundary conditions can exist in one of four forms. For example, a clamped boundary condition at $\alpha = \alpha_0$ can take the following forms:

$$\begin{aligned}
 \text{C1} \quad & u_0(\alpha_0, \beta) = v_0(\alpha_0, \beta) = w_0(\alpha_0, \beta) = \psi_\alpha(\alpha_0, \beta) = 0, \text{ (completely clamped)} \\
 \text{C2} \quad & v_0(\alpha_0, \beta) = w_0(\alpha_0, \beta) = \psi_\alpha(\alpha_0, \beta) = 0, \quad N_{0\alpha} - N_\alpha = 0 \\
 \text{C3} \quad & u_0(\alpha_0, \beta) = w_0(\alpha_0, \beta) = \psi_\alpha(\alpha_0, \beta) = 0, \quad \left(N_{0\alpha\beta} - \frac{N_{0\alpha\beta}}{R_\beta} \right) - \left(N_{\alpha\beta} - \frac{N_{\alpha\beta}}{R_\beta} \right) = 0 \\
 \text{C4} \quad & w_0(\alpha_0, \beta) = \psi_\alpha(\alpha_0, \beta) = 0, \quad N_{0\alpha} - N_\alpha = 0, \quad \left(N_{0\alpha\beta} - \frac{N_{0\alpha\beta}}{R_\beta} \right) - \left(N_{\alpha\beta} - \frac{N_{\alpha\beta}}{R_\beta} \right) = 0
 \end{aligned} \tag{2.73}$$

Similarly, there are four possible simply supported boundary conditions:

$$\begin{aligned}
 \text{S1} \quad & u_0(\alpha_0, \beta) = v_0(\alpha_0, \beta) = w_0(\alpha_0, \beta) = 0, \quad M_{0\alpha} - M_\alpha = 0 \\
 \text{S2} \quad & v_0(\alpha_0, \beta) = w_0(\alpha_0, \beta) = 0, \quad N_{0\alpha} - N_\alpha = 0, \quad M_{0\alpha} - M_\alpha = 0 \text{ (Shear diaphragm)} \\
 \text{S3} \quad & u_0(\alpha_0, \beta) = w_0(\alpha_0, \beta) = 0, \quad \left(N_{0\alpha\beta} - \frac{M_{0\alpha\beta}}{R_\beta} \right) - \left(N_{\alpha\beta} - \frac{M_{\alpha\beta}}{R_\beta} \right) = 0, \quad M_{0\alpha} - M_\alpha = 0 \\
 \text{S4} \quad & w_0(\alpha_0, \beta) = 0, \quad N_{0\alpha} - N_\alpha = 0, \quad \left(N_{0\alpha\beta} - \frac{M_{0\alpha\beta}}{R_\beta} \right) - \left(N_{\alpha\beta} - \frac{M_{\alpha\beta}}{R_\beta} \right) = 0, \quad M_{0\alpha} - M_\alpha = 0
 \end{aligned} \tag{2.74}$$

The S2 boundary condition is of particular interest. It is a reasonable presentation of stiff thin perpendicular plate attached to the end of the structure at hand. Such end will prevent translation in the out-of-plane direction as well as the direction tangential to the boundary,

but permits translation normal to the boundary. It also permits slope at the boundary because of its small thickness.

Four possible free boundary conditions can also be described:

$$\begin{aligned}
 \text{F1} \quad & u_0(\alpha_0, \beta) = v_0(\alpha_0, \beta) = 0, \quad \left(Q_{0\alpha} - \frac{1}{B} \frac{\partial M_{0\alpha\beta}}{\partial \beta} \right) - \left(Q_\alpha - \frac{1}{B} \frac{\partial M_{\alpha\beta}}{\partial \beta} \right) = 0, \\
 & M_{0\alpha} - M_\alpha = 0 \\
 \text{F2} \quad & v_0(\alpha_0, \beta) = 0, \quad N_{0\alpha} - N_\alpha = 0, \quad \left(Q_{0\alpha} - \frac{1}{B} \frac{\partial M_{0\alpha\beta}}{\partial \beta} \right) - \left(Q_\alpha - \frac{1}{B} \frac{\partial M_{\alpha\beta}}{\partial \beta} \right) = 0, \\
 & M_{0\alpha} - M_\alpha = 0 \\
 \text{F3} \quad & u_0(\alpha_0, \beta) = 0, \quad \left(N_{0\alpha\beta} - \frac{M_{0\alpha\beta}}{R_\beta} \right) - \left(N_{\alpha\beta} - \frac{M_{\alpha\beta}}{R_\beta} \right) = 0, \\
 & \left(Q_{0\alpha} - \frac{1}{B} \frac{\partial M_{0\alpha\beta}}{\partial \beta} \right) - \left(Q_\alpha - \frac{1}{B} \frac{\partial M_{\alpha\beta}}{\partial \beta} \right) = 0, \quad M_{0\alpha} - M_\alpha = 0 \\
 \text{F4} \quad & \text{No displacement boundaries specified} \quad (\text{Completely free}), \quad N_{0\alpha} - N_\alpha = 0, \\
 & \left(N_{0\alpha\beta} - \frac{M_{0\alpha\beta}}{R_\beta} \right) - \left(N_{\alpha\beta} - \frac{M_{\alpha\beta}}{R_\beta} \right) = 0, \\
 & \left(Q_{0\alpha} - \frac{1}{B} \frac{\partial M_{0\alpha\beta}}{\partial \beta} \right) - \left(Q_\alpha - \frac{1}{B} \frac{\partial M_{\alpha\beta}}{\partial \beta} \right) = 0, \quad M_{0\alpha} - M_\alpha = 0
 \end{aligned} \tag{2.75}$$

2.3.5 Recent developments

We will describe some of the recent literature in which thin shell theories were used to analyze composites. Love's shell theory was used by Sivadas and Ganesan (1992), Ip *et al.* (1996), Shu (1996) and Lam and Loy (1995a,b). Sanders' theory was employed by Selmane and Lakis (1997a–d), Lam and Loy (1995a,b), Mohd and Dawe (1993a,b) and Bhattacharyya and Vendhan (1991). Flugge's theory was used by Narita *et al.* (1993), Lam and Loy (1995a,b) and Sivadas and Ganesan (1991a,b, 1993). Loy *et al.* (1999) studied cylindrical panels with different boundary conditions. Recently, Qatu (1999b) presented a theory for isotropic and laminated barrel thin shells, and used it to study vibrations.

2.4. LAYER-WISE THEORIES

Other thick shell theories exist. Among these are layer-wise theories. In these theories, each layer in a laminated shell is considered to be a shell, and compatibility conditions are applied between various layers. Layer-wise shell theories have been used by Huang and

Dasgupta (1995), Dasgupta and Huang (1997) and Gautham and Ganesan (1994) for free vibrations of thick composite cylindrical and spherical panels. Carrera used layer-wise theories to evaluate doubly curved shells. Xavier *et al.* (1995) used one to study the effect of various curvatures. Basar and Omurtag (2000) examined vibrations of laminated structures using layer-wise shell models. These types of theories will not be covered in this book.

2.5. NONLINEAR THEORIES

The magnitude of transverse displacement compared to shell thickness is another criterion used in classifying shell equations. It can be shown that if such magnitude approaches the thickness of the shell (often earlier than that), the results of a linear analysis can be in gross error. The nonlinear terms were neglected in the thin, thick and 3D shell theories described earlier. In nonlinear shell theories, such terms are retained. In many cases, they are expanded using perturbation methods, and smaller orders of the rotations are retained. Most frequently the first order only is retained and, recently, even third orders have been included in a nonlinear shell theory by Pai and Nayfeh (1992a,b, 1994). In some shell dynamics problems, the material used can also be nonlinear (e.g., rubber, plastics and others). Theories that include nonlinear material behavior are also referred to as nonlinear shell theories (Klosowski *et al.* 1995). The vast majority of shell theories, however, deal with geometric nonlinearity only.

A nonlinear thin shell theory was used to study open cylindrical shells by Selmane and Lakis (1997a,b) and closed ones by Li (1996) and Ganapathi and Varadan (1996). A nonlinear shallow thin shell theory was used by Raouf and Palazotto (1994), Li (1993) and Xu and Chia (1994a,b). Doubly curved shallow shells having simple supports were treated by Shin (1997) using a nonlinear shell theory. Shallow shells of revolution including spherical and conical shells were also studied by Li (1992). Effects of shear nonlinearity on the free vibration of laminated shells was discussed by Xi *et al.* (1999).

In various research articles both shear deformation and nonlinear terms were included (Reddy 1989). It is argued that such theories will solve only a limited number of problems and are not needed for general composites (Qatu, 1994a). Large deformation of open doubly curved shallow shells was treated by Tsai and Palazotto (1991), Noor *et al.* (1991, 1994) and recently by Shin (1997) and Wang *et al.* (1997). Xu *et al.* (1996) studied truncated thick shallow shells. Shallow spherical shells were considered by Xu and Chia (1994a,b) and Sathyamoorthy (1995).

Tang and Chen (1998) studied the nonlinear analysis of laminated composite cylindrical panels. Fu and Chia (1989a,b, 1993), Ganapathi and Varadan, (1995, 1996), Soldatos (1992), Cederbaum (1992a,b) and Iu and Chia (1988) studied thick circular cylindrical shells. Selmane and Lakis (1997a) and Lakis *et al.* (1998) studied the influence

of geometric nonlinearities on the free vibrations of orthotropic open and closed cylindrical shells. Roussos and Mason (1998) studied the nonlinear radial vibrations of a hyperelastic cylindrical tube. Pai and Nayfeh (1992a,b, 1994) presented equations that included higher order shear deformation terms as well as higher order nonlinearities for composite cylindrical shells. Gummadi and Palazotto (1999) used finite elements to analyze nonlinear dynamics of composite cylindrical shells considering large rotations. Conical shells were considered by Xu *et al.* (1996). Zarutski (1998) developed approximate nonlinear equations of motion of cylindrical shells. Abe *et al.* (2000) studied the nonlinear vibration of clamped composite shallow shells. Cho *et al.* (2000) studied nonlinear behavior of composite shells under impact using finite elements. Other studies on nonlinear dynamics of composite shells include Nayfeh and Riveccio (2000).

2.6. SYNTHESIS OF LAMINATED SHELL EQUATIONS

The equations presented thus far are complete in the sense that the number of equations is equal to the number of unknowns for each of the theories presented. Table 2.2 summarizes the number of equations and unknowns for each of the theories. As seen there, the number of equations using 3D elasticity theory is 15. The difficulty of these equations is not in

Table 2.2. Synthesis of shell equations (Qatu, 2002a).

	3D (per layer)	Thick	Thin
<i>Unknowns</i>			
Displacements/rotation	u, v, w	$u_0, v_0, w_0, \psi_\alpha, \psi_\beta$	u_0, v_0, w_0
Stresses at a point (3D) or	$\sigma_\alpha, \sigma_\beta, \sigma_z$	$N_\alpha, N_\beta, N_{\alpha\beta}, N_{\beta\alpha}, Q_\alpha, Q_\beta$	$N_\alpha, N_\beta, N_{\alpha\beta}$
Stress resultants	$\tau_{\alpha\beta}, \tau_{\alpha z}, \tau_{\beta z}$	$M_\alpha, M_\beta, M_{\alpha\beta}, M_{\beta\alpha}, P_\alpha, P_\beta$	$M_\alpha, M_\beta, M_{\alpha\beta}$
Strains at a point (3D) or	$\epsilon_\alpha, \epsilon_\beta, \epsilon_z$	$\epsilon_{0\alpha}, \epsilon_{0\beta}, \epsilon_{0\alpha\beta}, \epsilon_{0\beta\alpha}, \gamma_{0\alpha z}, \gamma_{0\beta z}$	$\epsilon_{0\alpha}, \epsilon_{0\beta}, \gamma_{0\alpha\beta}$
Strains at the middle surface	$\gamma_{\alpha\beta}, \gamma_{\alpha z}, \gamma_{\beta z}$	$\kappa_\alpha, \kappa_\beta, \kappa_{\alpha\beta}, \kappa_{\beta\alpha}$	$\kappa_\alpha, \kappa_\beta, \tau$
Total	15	27	15
<i>Equations</i>			
Motion	3	5	3
Strain–displacement	6	10	6
Stress–strain	6	12	6
Total	15	27	15

the number of equations (as they are less than those needed in some of the other theories, particularly thick shell theories) but in the fact that such equations present three independent space variables (α , β and z). Other shell theories use only two variables (α and β). The 3D elasticity theory requires the satisfaction of three boundary conditions at each boundary. 2D thin shell theories require the satisfaction of four conditions at each of the edges of the shell, along with an additional one at each of the free corners.

The assumption needed to reduce the 3D theory to a 2D one is given by Eq. (2.35). The accuracy of this assumption depends heavily on how the unknowns are assumed to vary with the thickness. Indeed, one can expand Eq. (2.35) to include higher order terms. Generally, this yields results closer to that of the 3D elasticity theory. This is established in the literature for plates (Khdeir 1986, 1988a,b). It has also been shown here that accurate treatment of a first order expansion for shells yielded rather sophisticated stress resultant equations. The degree of difficulty is expected to become even higher when third orders are included in Eq. (2.35) (yielding higher order shear deformation theories). Such equations, once derived properly, may indeed yield results closer to those obtained using the 3D elasticity equations. As stated earlier, such equations will introduce boundary terms that are not easily conceptualized.

Chapter 3

Methods of Analysis

The equations described for shells using curvilinear coordinates show the level of complexity that can be reached when treating laminated composite structures. This complexity in the equations of motion and the associated boundary conditions resulted only in a limited number of problems where exact solutions are possible. In general, however, it is known that there is no exact solution for a laminated structure (solid, plate or shell) with general boundary conditions and/or lamination sequence. This resulted in seeking solutions using experimental and computational methods.

3.1. INTRODUCTION

Researchers have searched for information about the dynamic behavior of laminated composite structures using various methods. Some used experimental methods for determining the frequencies and mode shapes of such structures, while others used analytical methods. This is an overview of these methods.

3.1.1 *Experimental methods*

Experimental results for laminated composite shells were obtained by a limited number of studies (Sivak 1998). Some of these studies included using scaled down models and similitude theory (Rezaeepazhand *et al.* 1996a,b). The use of similitude was explained for isotropic shells by Soedel (1993).

Influence of enclosed air on vibration modes of a shell structure was discussed by Isaksson *et al.* (1995). Experiments show that enclosed air in a thin walled structure affects some modes of vibration significantly. Air coupling between vibrating sides of the structure cannot always be neglected, and frequencies may not be predicted accurately if calculations are performed as if in a vacuum. Optical modal analysis of the real, physical, violin model has been performed by using electronic holography (Isaksson *et al.* 1995). Calculated modes of vibration were compared with experimental ones. For the lowest modes, a good agreement between measured and calculated frequencies was reached. A mixed numerical and experimental approach for the dynamic modeling of a composite shell was discussed by Swider *et al.* (1996). More discussion of experimental analysis of shell dynamics can be found in the article by Noor *et al.* (1996) and Qatu (2002a).

3.1.2 Exact solutions

The term “exact solutions” is used here to mean finding a solution that satisfies both the differential equations and boundary conditions exactly. It will not mean finding an exact solution to the 3D elasticity equations. Instead, the exact solutions will be searched for and presented only for the various theories that were described and will be given in further details for more specific geometries like curved beams, plates and shallow and cylindrical shells. Finding an exact solution to the set of shell equations and boundary conditions for a general lamination sequence and/or boundary conditions is out of reach. Only a limited number of boundary conditions and lamination sequences have exact solutions. Generally speaking, untwisted (i.e., $R_{\alpha\beta} = \infty$), symmetric and unsymmetric cross-ply (e.g., $[0^\circ, 90^\circ]$) laminated singly or doubly curved shells (and plates) with two opposite edges having shear diaphragm boundaries permit exact solutions (Librescu, *et al.* 1989a). Exact solutions can also be found for plates with antisymmetric (e.g., $[-45^\circ, 45^\circ]$) lamination sequence with S3 boundaries at opposite edges. Such solution cannot be expanded for shells. Details of these solutions will be discussed later. The complexity of the analysis and solution available for such shells with two opposite edges simply supported, while the others are arbitrary, prevented many researchers from getting results. For closed shells, cylindrical or barrel, and open doubly curved shells or flat plates having all four edges with shear diaphragms, the solution becomes relatively simple. That is the reason for using such a solution in many publications on the subject.

3D solutions for cylinders were presented by Soldatos (1994). Recently, laminated cross-ply, thin, noncircular cylindrical shells were analyzed exactly for their natural frequencies by Suzuki *et al.* (1994). Laminated thick noncircular cylindrical shells were analyzed exactly as well by Suzuki *et al.* (1996).

Exact solutions will be discussed later for the specific structural elements discussed here (curved beams, plates or shells). On the other hand, numerous approximation methods are available for researchers to study shell dynamics and obtain natural frequencies and mode shapes. The most used analytical methods will be the emphasis of this section. The various experimental methods used by researchers to obtain the needed information for laminated shell and plate vibrations will not be treated in this chapter.

3.1.3 Approximate solutions

In the previous chapters, variational and energy methods were presented and used to obtain the governing differential equations and boundary conditions of solids, plates and shells using Hamilton’s principle. The methods described here can be used to obtain approximate solutions. The methods fundamentally assume a solution with undetermined coefficients. These coefficients are minimized to achieve a stationary value for certain functionals or minimize errors. In the Ritz analysis this functional is the energy functional (i.e., Lagrangian). In other methods like the weighted residuals methods, this functional is

some expression of deviation from the solution (i.e., error). The assumed functions can be continuous functions describing the whole structure or a linear combination of various functions. Unless the assumed functions are actually the exact solution itself, which is rarely the case, errors are introduced. As the number of terms, or functions, increases, error is reduced, and convergence is observed. An issue that is treated considerably in the literature about these methods is to find whether these solutions converge to the exact solution or to some other solution within the vicinity of the exact solution.

It is worth mentioning here that the analytical models described earlier, including the 3D elasticity model, are themselves approximate. The shell theories derived earlier are based on, and an approximation of, the 3D theory of elasticity. Thus, the accuracy of these theories in analyzing the actual physical problem is less than that of the 3D theory of elasticity. Approximate solutions introduce less accurate results when compared with exact solution, unless proper convergence characteristics are established.

The variational or energy methods used for vibration analysis of continuous systems are the Ritz, and Ritz-based finite element methods (FEM). The most widely used weighted residuals methods are the Galerkin method and Galerkin-based FEM. The FEM are piecewise applications of Galerkin and Ritz methods. Finite elements, however, is the dominant method used by application engineers to study the vibration behavior of structures including composite ones. Other variational methods are also used to a lesser degree by researchers in the field. Most of these are other weighted residual methods including Trefftz, collocation and point matching.

There are other approximate methods used in the literature. One method that was used frequently by researchers is the finite difference method. This method approximates the derivatives in the governing differential equations by difference equations. While this method received considerable attention decades ago (Kraus 1967), it is receiving less attention in recent literature. We will briefly describe the Ritz method and the weighted residual Galerkin method in Sections 3.2 and 3.3, respectively. The reader is encouraged to consult other texts for a comprehensive review of these methods (Reddy 1984b; Langhaar 1962; Washizu 1982).

3.2. THE RITZ METHOD

The Rayleigh and Ritz methods are among the most common approximate methods used in the vibration analysis of continuous systems. A displacement field is assumed in both methods. The coefficients of the displacement field are completely determined beforehand in the method of Rayleigh. In the Ritz method, undetermined coefficients are used in the displacement field. The displacement field is then substituted in the energy functional (i.e., Lagrangian). The Lagrangian is then minimized by taking its derivatives with respect to these coefficients and making them equal to zero. This yields equations that can be written

in a matrix form and give the displacement in a static analysis and natural frequencies in a vibration analysis. The method of Rayleigh, which assumes a completely determined mode shape, generally yields a less accurate frequency corresponding to the assumed mode shape when compared with the Ritz method.

For free vibration analysis, the motion is assumed to be harmonic, and the displacements take the form

$$\begin{aligned} u(\varphi_1, \varphi_2, \varphi_3, t) &= U(\varphi_1, \varphi_2, \varphi_3) \sin \omega t \\ v(\varphi_1, \varphi_2, \varphi_3, t) &= V(\varphi_1, \varphi_2, \varphi_3) \sin \omega t \\ w(\varphi_1, \varphi_2, \varphi_3, t) &= W(\varphi_1, \varphi_2, \varphi_3) \sin \omega t \end{aligned} \quad (3.1)$$

where φ_1 , φ_2 and φ_3 are the coordinates used in the problem and t is time. In the Ritz method, displacement functions U , V and W are approximated by using certain functions or a linear combination of such functions. For example, the displacements in a 3D problem can be approximated by using

$$\begin{aligned} U(\varphi_1, \varphi_2, \varphi_3) &= \sum_{i=0}^I \sum_{j=0}^J \sum_{k=0}^K \alpha_{ijk} f_{ijk}(\varphi_1, \varphi_2, \varphi_3) \\ V(\varphi_1, \varphi_2, \varphi_3) &= \sum_{l=0}^L \sum_{m=0}^M \sum_{n=0}^N \beta_{lmn} f_{lmn}(\varphi_1, \varphi_2, \varphi_3) \\ W(\varphi_1, \varphi_2, \varphi_3) &= \sum_{p=0}^P \sum_{q=0}^Q \sum_{r=0}^R \gamma_{pqr} f_{pqr}(\varphi_1, \varphi_2, \varphi_3) \end{aligned} \quad (3.2)$$

where α_{ijk} , β_{lmn} and γ_{pqr} are the undetermined coefficients and f_{ijk} , f_{lmn} and f_{pqr} are the assumed functions. These functions will need to be determined first. They must satisfy two conditions for the solution to be of any value. First, they should be continuous (for a continuous structure), linearly independent and differentiable to the degree needed in the problem. Second, they should satisfy at least the geometric boundary conditions. They do not need to satisfy the forced boundary conditions (Reddy 1984b). Numerical investigations, however, showed that when these assumed displacements satisfy the forced boundary conditions, a more rapid convergence would be observed. In order to guarantee convergence to the exact solutions, an additional condition must be met. This condition is that the series of these functions (frequently referred to as trial functions or shape functions) need to be mathematically complete. Mathematical completeness of a series of functions will mean that any function (actual displacements) can be adequately represented by these complete functions. Completeness has been proven for many series of functions (Kreyszig 1989, 1993). These include both algebraic polynomials and trigonometric functions. Both are widely used with the Ritz method to obtain natural frequencies. The method of least squares in curve fitting proves that practically any

function can be represented by an infinite series of algebraic polynomials (Kreyszig 1993). Fourier series expansion proves the same for trigonometric series of functions. For a detailed discussion on completeness of functions, one can consult the books by Kantorovich and Krylov (1964) and Kreyszig (1989, 1993).

For algebraic polynomials, Eq. (3.2) can be written as

$$\begin{aligned}
 U(\varphi_1, \varphi_2, \varphi_3) &= \sum_{i=0}^I \sum_{j=0}^J \sum_{k=0}^K \alpha_{ijk} \varphi_1^i \varphi_2^j \varphi_3^k \\
 V(\varphi_1, \varphi_2, \varphi_3) &= \sum_{l=0}^L \sum_{m=0}^M \sum_{n=0}^N \beta_{lmn} \varphi_1^l \varphi_2^m \varphi_3^n \\
 W(\varphi_1, \varphi_2, \varphi_3) &= \sum_{p=0}^P \sum_{q=0}^Q \sum_{r=0}^R \gamma_{pqr} \varphi_1^p \varphi_2^q \varphi_3^r
 \end{aligned} \tag{3.3}$$

The first equation in Eq. (3.3) can be expanded as

$$\begin{aligned}
 U(\varphi_1, \varphi_2, \varphi_3) &= \sum_{i=0}^I \sum_{j=0}^J \sum_{k=0}^K \alpha_{ijk} \varphi_1^i \varphi_2^j \varphi_3^k \\
 &= \alpha_{000} + \alpha_{001} \varphi_3 + \alpha_{010} \varphi_2 + \alpha_{100} \varphi_1 + \alpha_{111} \varphi_1 \varphi_2 \varphi_3 + \alpha_{112} \varphi_1 \varphi_2 \varphi_3^2 \\
 &\quad + \alpha_{113} \varphi_1 \varphi_2 \varphi_3^3 + \cdots + \alpha_{11K} \varphi_1 \varphi_2 \varphi_3^K + \alpha_{121} \varphi_1 \varphi_2^2 \varphi_3 + \alpha_{131} \varphi_1 \varphi_2^3 \varphi_3 \\
 &\quad + \cdots + \alpha_{1J1} \varphi_1 \varphi_2^J \varphi_3 + \alpha_{211} \varphi_1^2 \varphi_2 \varphi_3 + \alpha_{311} \varphi_1^3 \varphi_2 \varphi_3 + \cdots \\
 &\quad + \alpha_{I11} \varphi_1^I \varphi_2 \varphi_3 + \alpha_{222} \varphi_1^2 \varphi_2^2 \varphi_3^2 + \cdots
 \end{aligned} \tag{3.4}$$

It should be noted here that no higher order term should be used unless the needed lower order term is used for the same power series. The needed lower order terms are all the lower order terms that do not violate the necessary geometric boundary conditions.

Once the displacement field or assumed functions are determined, they need to be directly substituted in the Lagrangian energy functional $L = T - U + W$. The total expression of the Lagrangian needs to be minimized in search of a stationary value. This search requires minimization of the expression with respect to the undetermined coefficients:

$$\begin{aligned}
 \frac{\partial L}{\partial \alpha_{ijk}} &= 0, \quad i = 0, 1, \dots, I, \quad j = 0, 1, \dots, J, \quad k = 0, 1, \dots, K, \\
 \frac{\partial L}{\partial \beta_{lmn}} &= 0, \quad l = 0, 1, \dots, L, \quad m = 0, 1, \dots, M, \quad n = 0, 1, \dots, N, \\
 \frac{\partial L}{\partial \gamma_{pqr}} &= 0, \quad p = 0, 1, \dots, P, \quad q = 0, 1, \dots, Q, \quad r = 0, 1, \dots, R
 \end{aligned} \tag{3.5}$$

In a typical problem with no geometric constraints, this yields a system of equations of the size $(I + 1)(J + 1)(K + 1) + (I + 1)(M + 1)(N + 1) + (P + 1)(Q + 1)(R + 1)$. In order to avoid the trivial zero solution, the determinant must be taken to zero. In a free vibration analysis, this yields a set of eigenvalues.

It should be mentioned that for the class of problems treated in this book, symmetric stiffness and mass matrices will result from the Ritz analysis. Furthermore, generally speaking, the force resultants and stresses obtained by using the Ritz method will be less accurate when compared with displacements and frequencies.

The assumed displacements in a Ritz analysis converge to the exact frequencies only if a complete set of assumed functions is used. Since that is not the case in typical problems where the series get truncated at some level, the assumed displacement field usually represents a stiffer system than the actual one. This results in higher frequencies than the exact solution. This is established numerically by observing the convergence characteristics of the natural frequencies. These frequencies converge monotonically from above in a Ritz analysis.

The Ritz method has been widely used in mechanics for a variety of problems, most notably in vibrations of continuous systems. The method can be used in nonlinear vibration analysis, resulting in a nonlinear system of algebraic equations. These equations are then solved using numerical techniques leading to more than one answer. The method of Ritz permits obtaining as many natural frequencies as needed. If a complete set of functions is used, the Ritz method has excellent convergence characteristics and is relatively easy to program (Qatu 1989). The Ritz method, sometimes referred to as Rayleigh–Ritz, has been used successfully to analyze thin cylindrical shells (Ip *et al.* 1996; Sharma *et al.* 1996; Kumar and Singh 1996; Heyliger and Jilani 1993). It has also been used to study thin shallow shells (Chun and Lam 1995; Qatu and Leissa 1991a,b; Qatu 1993a, 1994b,c, 1995b,c; Messina and Soldatos 1999a,b, Sheinman and Reichman 1992). The Ritz method has also been used to study thick shallow shells by Singh and Kumar (1996) and spherical shells by Chao and Chern (1988), and other shells by Lee (1988). Raouf and Palazotto (1992) used the Ritz method with harmonic balance to analyze nonlinear vibrations of shells.

One has to start with a displacement field that satisfies at least the geometric boundary conditions when using the Ritz method. Furthermore, it is somewhat difficult to obtain a displacement field for a relatively complex shell structure or set of such structures. For example, a problem of a plate attached to a shell at a certain angle is challenging if the Ritz method is to be used, as found by Young and Dickinson (1997). Special treatments were introduced to overcome the difficulty of using the Ritz method with general boundary conditions (Kumar and Singh 1996; Li and Mirza 1997).

3.3. THE GALERKIN METHOD

The Ritz method is used to obtain approximate solution to problems having an energy (or variational) expression. There are problems in mechanics which do not allow for such an expression. The weighted residual methods are basically a generalization of the Ritz method to handle problems that do not allow an energy expression. The Galerkin method is a special case of the general weighted residual methods. In these methods, the governing differential equations and corresponding boundary conditions are needed. For a typical problem treated in this text, the governing equations can be written in the form

$$\begin{bmatrix} L_{11} & L_{12} & L_{13} \\ L_{21} & L_{22} & L_{23} \\ L_{31} & L_{32} & L_{33} \end{bmatrix} \begin{bmatrix} U \\ V \\ W \end{bmatrix} = \begin{bmatrix} p_1 \\ p_2 \\ p_3 \end{bmatrix} \quad (3.6)$$

where the L_{ij} terms are the differential operators (which may contain derivatives with respect to time), U , V and W are the displacement fields and p_1 , p_2 and p_3 are the forcing function. Additional boundary terms will represent specified boundary conditions. The solution of the displacement field using the Galerkin method is searched for in a form similar to Eq. (3.1) for a free vibration analysis. The displacement field is approximated with trial functions, similar to Eq. (3.2). This displacement field is directly substituted in the governing differential equations (3.6). This yields an expression for the residual (error) that can be written as

$$\begin{bmatrix} E_1 \\ E_2 \\ E_3 \end{bmatrix} = \begin{bmatrix} L_{11} & L_{12} & L_{13} \\ L_{21} & L_{22} & L_{23} \\ L_{31} & L_{32} & L_{33} \end{bmatrix} \begin{bmatrix} \sum_{i=0}^I \sum_{j=0}^J \sum_{k=0}^K \alpha_{ijk} f_{ijk}(\varphi_1, \varphi_2, \varphi_3) \\ \sum_{l=0}^L \sum_{m=0}^M \sum_{n=0}^N \beta_{lmn} f_{lmn}(\varphi_1, \varphi_2, \varphi_3) \\ \sum_{p=0}^P \sum_{q=0}^Q \sum_{r=0}^R \gamma_{pqr} f_{pqr}(\varphi_1, \varphi_2, \varphi_3) \end{bmatrix} - \begin{bmatrix} p_1 \\ p_2 \\ p_3 \end{bmatrix} \quad (3.7)$$

where the E_1 , E_2 and E_3 are expressions for the residual terms. They are functions of the undetermined coefficients, the forcing functions and the coordinate system. The weighted residual methods require these coefficients to be orthogonal to some weight functions ψ_i . This is achieved by setting the integral below to 0.

$$\int_V \psi_i E_n dV = 0, \quad i = 1, 2, \dots, n \quad (3.8)$$

The term n in the above equation includes all the undetermined coefficients in the problem. This yields a system of equations that is equal to the undetermined coefficients. To avoid a nontrivial solution, the determinant is set to 0, which yields the eigenvalues.

Various weighted residual methods differ from each other in the selection of the weight functions. Galerkin's method requires those functions to be the trial functions themselves. Interestingly, for many problems this yields computations similar to those of the Ritz method.

The Galerkin method has been used mainly to study nonlinear vibration problems. It was used to analyze doubly curved shallow shells in many research articles (Ohnabe 1995; Shin 1997; Raouf and Palazotto 1994; Heuer 1994; Chaudhuri and Kabir 1992, 1994). The Galerkin method was also used to study the nonlinear vibration of cylindrical shells in various studies (Palazotto and Linnemann 1991; Tighe and Palazotto 1994; Fu and Chia 1993). Other researchers used the method to deal with conical shells (Khatri and Asnani 1995, 1996; Khatri 1996; Xu *et al.* 1996). Spherical shells were studied by Chao *et al.* (1991), Narasimhan and Alwar (1992), and Xu and Chia (1994a,b, 1995). Other shells were considered by Fu and Chia (1989a,b).

3.4. THE FINITE ELEMENT METHODS

The FEM have been growing rapidly in the last three decades. Most of these methods have been based upon the Ritz method (minimizing the energy functional) or other weighted residual methods including Galerkin on an element level to obtain an element stiffness matrix. FEM overcome the difficulties the Ritz and Galerkin methods have in dealing with various boundary conditions and relatively complex shapes. For simple structures, the Ritz method shows better convergence and less computational needs. For complex structures, loading functions and/or boundary conditions, the FEM have proven to be an excellent tool. A considerable number of FEM commercial codes and packages exist to obtain vibration results. Good literature survey articles on the subject were presented by Noor and Burton (1992), Noor *et al.* (1993) and Reddy (1989).

The main difference the finite element methods have from the previous methods is that the equations are derived at the subdomain (called finite element) level. The finite elements themselves are simple in shape. Algebraic polynomials are typically used as the trial functions at the element level which makes the computation relatively straightforward. The undetermined coefficients are the values of dependent variables at certain selected points within the structure (called nodes). Finite element analysis will be described briefly here. For a detailed derivation, the reader is advised to consult one of the major texts on the subject.

In today's commercial finite element packages, the actual computations are transparent to the user. What the user actually encounters are three fundamental components of the finite element package. The first is the preprocessor. In this component, a finite element model is built. This modeling part constitutes the major task done by today's finite element engineers. In this task, the structure at hand is divided into elements.

The user must decide whether solid elements, shell elements or other elements are to be used. There are some general guidelines on the applicability and usage of each of these elements. These guidelines are driven by the accuracy needed, the complexity of the structure at hand, and the computational time available. Generally speaking, smaller element sizes (i.e., larger number of elements for the whole structure) will need more computational time and deliver more accurate results. If shell elements are used, only the middle surface needs to be defined in the model and the thickness is presented as an element property. As a general rule, the element side lengths used when modeling a structure using shell elements should be larger than the thickness by one order of magnitude. Otherwise, solid elements should be selected. Also, if solid elements are used, there should be at least two, preferably four, elements across the thickness. Once the general type of elements is decided (e.g., solid *versus* shell), the type of element should be further specified. There are many different solid and shell elements available to the user. For solid elements, the user can use tetrahedron elements, parallel-piped ones (referred to as brick elements) or others. Each type of these has its own advantages and shortcomings. For shell elements, the user often has to choose triangular, rectangular or other element. For each of these, there are multiple derivatives. For example, there are four-noded rectangular elements, eight-noded ones and others. Again, advantages and shortcomings are reported for each. The user can also mix elements relatively easily when elements are chosen from the same category (e.g., solids), and with great care when elements from different categories are connected together (e.g., connecting solid elements with shell elements). The mismatch of the degrees of freedom (DOF) at the nodes when shell

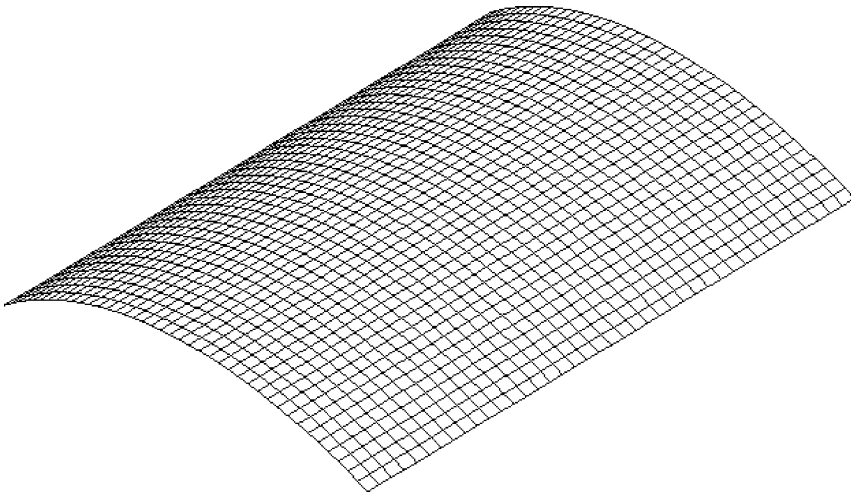


Figure 3.1. A shell modeled by shell elements.

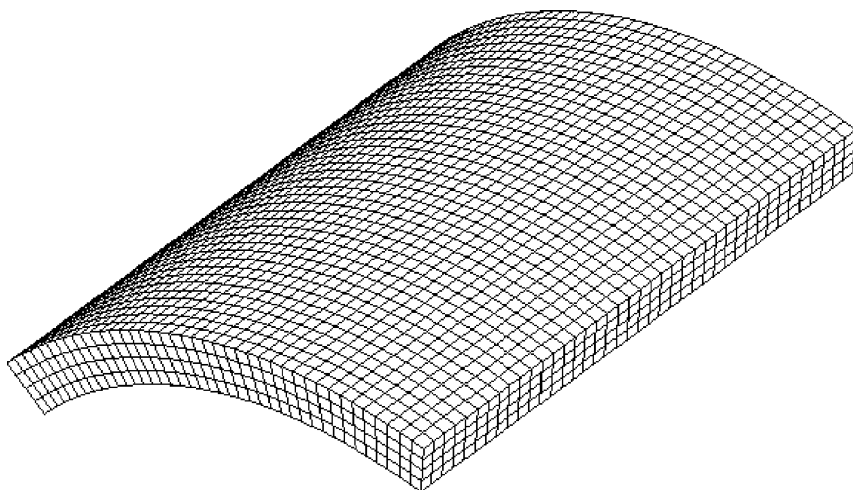


Figure 3.2. A shell modeled by solid elements.

elements are connected to solid elements should be treated very carefully. Figures 3.1 and 3.2 display a shell modeled by shell elements and solid elements, respectively.

Once the model is built, most commercial packages have a variety of tools to check the model. Among the most important checks is the inner-connectivity of the elements. This is important to avoid unintended internal boundaries between the elements. For shell elements, the normals of the elements should be in the same direction. Once the finite element is built, it produces a file which is used as an input data file for the processor, which is the main component of the finite element package.

The finite element processor code reads the input data prepared by the preprocessor. This code contains material properties of each element, nodal coordinate data as well as the nodes surrounding each element. The code is usually editable by the user. The processor itself is usually transparent to the user and is the portion that requires considerable computational timing depending on the refinement of the model and the speed of the computing machine. The processor produces an output data file which is read by a post-processor to view and evaluate results. The description that follows is a brief summary of the computations performed by the processor portion of the code.

3.4.1 Deriving element parameters

A finite element formulation begins with a formulation at the element level. The undetermined coefficients used in the previously described methods of Ritz and weighted residuals are replaced by unknown values (e.g., displacements) at the nodes. Algebraic polynomials that represent the displacements over the element are derived based upon

the nodal values of the displacements. For solid elements, the nodal displacements u_i , v_i and w_i (where i is a typical node) constitute the DOF used at each node. For the least possible tetrahedron element that has four nodes, with 3 DOF per node, a total of 12 DOF will be needed per element. For shell elements, midsurface displacements u_{0i} , v_{0i} and w_{0i} (where i is a typical node) as well as the slopes (see, e.g., Eq. (2.60)) represent the needed DOF per node. This yields a total of 5 DOF per node. For a triangular shell element, with three nodes, this results in at least 15 DOF over the element. Appropriate algebraic polynomials are then carefully selected for the u , v and w displacements over the domain of the element with the same number of undetermined coefficients. For shell elements that include shear deformation, five independent variables exist at each boundary. This, in principle, added complexity to the problem at hand. Interestingly, the treatment of elements with shear deformation is easier than that of classical shell elements. The reason is the condition of compatibility.

For classical shell elements, compatibility requires both displacements and slopes to be continuous across the boundary of the elements (and not only at the nodal points). For classical elements, this requires a higher degree polynomial over the domain. For elements with shear deformation and with higher number of DOF per node, the polynomial needed is of lesser degree, and thus the formulation is simpler. A typical displacement function within the element can be represented by the following polynomial:

$$\begin{aligned}
 U(\varphi_1, \varphi_2, \varphi_3) = & \alpha_{000} + \alpha_{001}\varphi_3 + \alpha_{010}\varphi_2 + \alpha_{100}\varphi_1 + \alpha_{110}\varphi_1\varphi_2 + \alpha_{101}\varphi_1\varphi_3 \\
 & + \alpha_{011}\varphi_2\varphi_3 + \alpha_{200}\varphi_1^2 + \alpha_{020}\varphi_2^2 + \alpha_{002}\varphi_3^2 + \alpha_{111}\varphi_1\varphi_2\varphi_3 \\
 & + \alpha_{210}\varphi_1^2\varphi_2 + \alpha_{201}\varphi_1^2\varphi_3 + \alpha_{021}\varphi_2^2\varphi_3 + \alpha_{120}\varphi_1\varphi_2^2 + \alpha_{102}\varphi_1\varphi_3^2 \\
 & + \alpha_{012}\varphi_2\varphi_3^2 + \alpha_{300}\varphi_1^3 + \alpha_{030}\varphi_2^3 + \alpha_{003}\varphi_3^3 + \alpha_{112}\varphi_1\varphi_2\varphi_3^2 \\
 & + \alpha_{121}\varphi_1\varphi_2^2\varphi_3 + \alpha_{211}\varphi_1^2\varphi_2\varphi_3 + \dots
 \end{aligned} \tag{3.9}$$

The above expression is written carefully such that it begins with a constant term α_{000} followed by three linear terms. These four terms would be enough interpolation functions for a solid element. If a higher order element is selected, then quadratic terms must be included. Some or all of the quadratic terms described in the above equations can be selected for that purpose.

Similar displacement functions can be written for other displacements like V and W (and shear functions for shear deformable shell elements). The coefficients in the polynomial are determined by using proper interpolation functions that achieve a displacement (or curvature) value at one of the nodes.

The stiffness matrix for the element is determined by using either the Ritz method or one of the weighted residual methods. If the Ritz method is used, the trial functions of Eq. (3.9) are substituted into the Lagrangian expression, which in turn needs to be

minimized using

$$\frac{\partial L}{\partial \alpha_{ijk}} = 0 = \sum_{j=1}^n K_{ij}^e u_j^e - F_i^e \quad (3.10)$$

The superscript (e) is used to refer to a particular element. The K_{ij} terms refer to stiffness and inertia terms, u_j refers to the DOF, and F_i refers to the force vector at the prescribed DOF.

The stiffness matrices of laminated shell and plate elements exist in the literature and are available in many books including those of Reddy (1984b, 2003).

Coordinate transformation is needed to write the above equations in the global coordinates used in the total system, which are typically different than those used at the element level.

3.4.2 Assembly of the elements

Once the stiffness (and mass) matrix as well as the force vector are written for each element in terms of global coordinates, the elements need to be connected together to obtain one global stiffness matrix and another mass matrix as well as a force vector.

Each node will have a global displacement in a certain direction. This displacement must be the same for each of the surrounding elements at that node. A total energy expression (Π) can be reached by summing all the potential energies of the elements

$$\Pi = \sum_{i=1}^N \Pi_i \quad (3.11)$$

where N is the total number of elements. The variation of the total energy is then taken to be 0, satisfying the principle of minimum potential energy for the whole system. This yields

$$\frac{\partial \Pi}{\partial U_I} = 0, \quad I = 1, 2, \dots, n \quad (3.12)$$

The above expression yields equations for each DOF for the global system. This, when connected together, can be written as a global matrix of the form

$$K_{ij} u_i = F_i \quad (3.13)$$

Note that the K_{ij} terms include both stiffness and mass coefficients needed in a dynamic analysis. The resulting stiffness and mass matrices are symmetric.

3.4.3 Imposing the boundary conditions and post-processing

The boundary conditions need to be imposed on the global equations. The specified boundaries can either be written in terms of specified displacements or specified forces

(at any of the nodes). If the displacement is specified at a certain node, then the row and column corresponding to the node should be deleted. The force column should be modified by subtracting the product of the stiffness coefficient in the column with the specified displacement. For applied forces at any node, the internal forces should be equal to the external forces at that node (equilibrium at the node).

Once the system is fully determined with only the displacements as unknown, typical mathematical procedures can be applied to obtain a solution (i.e., find the displacements at each of the nodes). Forces can then be computed at each of the boundaries as well as the nodes.

3.4.4 Recent literature

Various finite elements for composite shells were discussed by Carrera (2001, 2002). Thin shell elements were used to analyze the vibrations of composite shells by many researchers (Cyr *et al.* 1988; Singh *et al.* 1990; Lee and Saravanos 2000; Lakshminarayana and Dwarakanath 1992a,b; Chen *et al.* 1993; Gotsis and Guptill 1995; Isaksson *et al.* 1995; Soares *et al.* 1995; Chang and Shyong 1994; Lakis and Sinno 1992). Thin and thick shallow shell elements were developed and used for composite shell vibration research in various studies (Beakou and Touratier 1993; Singh and Kumar 1996; Chakravorty *et al.* 1995a,b, 1996; Argyris and Tenek 1996; Kapania and Mohan 1996; Kosmatka 1994; Zhu 1996).

Finite elements were also developed using various shear deformation theories (Sivadas and Ganesan 1991a,b, 1993; Chakravorty *et al.* 1996; Touratier and Faye 1995; Chun and Dong 1998). Vibration and damping analysis of pretwisted composite blades was performed by Nabi and Ganesan (1993). FEM were used to analyze stiffened shells by many authors (Rao *et al.* 1993; Liao and Cheng 1994a,b; Goswami and Mukhopadhyay 1995; Lee and Lee 1995; Bouabdallah and Batoz 1996). Predictor–corrector procedures for stress and free vibration analyses of multilayered composite plates and shells were performed by Noor *et al.* (1990).

Sanders' shell theory was modified to include shear deformation and used to develop conforming finite elements by Abu-Farsakh and Qatu (1995). Thick conical shells were analyzed using finite elements by Sivadas (1995a,b). Hybrid-mixed formulations were used to study vibrations of composite shells (Wilt *et al.* 1990; Gendy *et al.* 1997; Selmane and Lakis 1997a,b). A higher-order, partial hybrid stress, FEM formulation was given by Yong and Cho (1995). Bardell *et al.* (1999) used h-p FEM to study the vibration of open conical sandwich panels.

3D elements were also used in the analysis of composite shells by Dasgupta and Huang (1997). A discrete layer analysis using FEM was performed for cylindrical shells by Ramesh and Ganesan (1992, 1993, 1994) and Gautham and Ganesan (1992, 1994).

Finite elements were developed for the new piezoelectric materials. FEM models were generated for shells with embedded layers of these materials by Jia and Rogers (1990). Other models were developed for shells made of such materials by many researchers (Lammering 1991; Hussein and Heyliger 1996; Tzou and Bao 1995; Tzou and Gadre 1989; Tzou and Ye 1996). Shells made of shape memory alloys were treated by Hurlbut and Regelbrugge (1996). Berger and Gabbert (2000) used finite element analysis to design piezoelectric controlled smart structures.

Nonlinear vibration analysis was performed by many researchers using various types of composite shell elements (Martin and Lung 1991; Lakis and Laveau 1991). Flutter was considered by Chowdary *et al.* (1994) and Liao and Sun (1993). Kapania and Byun (1992) considered imperfections using finite element analysis.

3.5. OTHER METHODS

Other techniques exist for solving the vibration problem of composite shells including finite differences, boundary element methods (BEM), differential quadrature and others. Differential quadrature is evolving rapidly lately, and the same is true for BEM.

Differential quadrature was used to analyze laminated conical shells by Shu (1996) and Wu and Wu (2000). Argyris and Tenek (1996) developed the “natural mode method” and used it in their analysis. Boundary domain elements were employed to analyze free vibration of thick shells by Wang and Schweizerhof (1996a,b, 1997) and Beskos (1997). A spline strip method was used to analyze thick cylindrical shells by Mizusawa and Kito (1995) and Mizusawa (1996). Boundary continuous displacement based Fourier analysis was conducted for laminated panels using a classical shallow shell theory by Chaudhuri and Kabir (1992). Li and Mirza (1997) used a method based on the superposition and state-space techniques to study the free vibration of cross-ply laminated composite shell panels with general boundary conditions.

The relative ease, accuracy and dependability of the Ritz method for linear analysis and the Galerkin method for nonlinear analysis has proved to be valuable for simple structures and/or boundary conditions. The FEM have also been widely used and accepted for complex structures and boundary configuration. The availability of commercial codes in obtaining natural frequencies using the FEM and the user friendliness of these codes have made finite elements the industry standard in many applications that involve dynamic analysis of composite structures.

Chapter 4

Curved Beams

Laminated composite materials are used to build components like beams, plates or shells. Often encountered among various applications are laminated beams. The same structural component can be referred to as a beam, a rod, a column or a shaft. The name is a function of the loading encountered by this component. It is a rod or a bar when under tension, a column when under compression and a shaft when under torsional loads. Beams support mainly bending and shear loads. These structural components are also called “beams” when they are under combined loading including bending.

Beams can be straight or curved. Curved beams can have deep or shallow curvature and can be open or closed. Closed beams are often called rings, and open curved beams are often referred to as arches. This chapter addresses the vibration of laminated curved beams and rings. The treatment includes both thin and thick beams.

It should be mentioned here that the treatment presented in this chapter considers beams vibrating (or deforming) in their plane of curvature. This will help build some significant insight to their behavior and the impact of curvature on the beam’s vibration. The difference between the vibration of straight and curved beams will constitute an introduction to build insight about the difference between flat plates and shells. Out-of-plane vibration of laminated beams is beyond the scope of this book.

Vibration analysis of curved beams was the subject of few survey studies (Chidamparam and Leissa 1993; Markus and Nanasi 1981; Laura and Maurizi 1987). These studies list more than 200 references on the subject. Almost all the references dealt with isotropic beams. Only a limited number of these references dealt with composite beams. The work of Kao and Ross (1968) should be reported to be among the first to deal with composite beams. The in-plane, or planar, vibration treated here received most interest by researchers.

The finite element method was used to study the dynamic response of sandwich curved beams (Ahmed 1971, 1972). Elements having three, four and five degrees of freedom (DOF) per node were analyzed (Ahmed 1971). Shear deformation and rotary inertia effects on the natural frequencies were further studied (Ahmed 1972). Free and forced vibrations of a three-layer damped ring were investigated (DiTaranto 1973). The same problem was solved using analytical formulation (Lu 1976; Nelson 1977). Transient response was analyzed for three-layer rings (Sagartz 1977). Damping properties of curved sandwich beams with viscoelastic layer were studied (Tatemichi *et al.* 1980). Viscoelastic damping in the middle core layer was emphasized. A consistent set of equations was developed for slightly curved laminated beams (Qatu 1992a) and results were obtained for such beams having different boundary conditions. It was shown that

the stretching–bending coupling due to lamination have significant effect on the natural frequencies. Thin and thick theories for laminated curved beams were presented and used in vibration analysis by Qatu (1993b).

This chapter is concerned with the development of the fundamental equations and energy functionals for laminated composite curved beams and closed rings and present results using both exact and approximate solutions, which can be useful for design engineers. Equations for straight beam can be derived by setting the curvature to zero (i.e., radius of curvature goes to infinity). Two theories are developed for laminated curved beams. In the first theory, thin beams are studied where effects of shear deformation and rotary inertia are neglected. This theory will be referred to as thin beam theory or classical beam theory (CBT). In the second theory, shear deformation and rotary inertia effects are considered. This theory will be referred to as thick beam theory or shear deformation beam theory (SDBT). Kinematical relations, force and moment resultants, equations of motion and boundary condition are derived and shown to be consistent for both theories. Stretching–bending coupling due to both curvature and unsymmetrical lamination are distinguished. Natural frequencies are presented for simply supported open curved beams and closed rings by exact and approximate methods. Shear deformation and rotary inertia effects as well as those of the thickness and orthotropy ratios and lamination sequence upon the natural frequencies are studied.

4.1. FUNDAMENTAL THEORY OF THIN BEAMS

A CBT will be developed here to treat thin beams. A laminated curved beam is characterized by its middle surface, which is defined by the polar coordinate α (Figure 4.1), where

$$\alpha = R\theta \quad (4.1)$$

The constant R identifies the radius of curvature of the beam (Figure 4.1). The equations derived earlier for deep shells can be specialized to those for curved beams by deleting all derivatives with respect to the out-of-plane axis and all terms containing displacement in the out-of-plane direction. The equations derived here are for curved beams subjected to in-plane loading and/or vibrating in the α – z plane.

4.1.1 Kinematic relations

Middle surface strain and curvature change are obtained from Eqs. (2.59) and (2.60). This is done by introducing constant Lamé parameters and ignoring out-of-plane components.

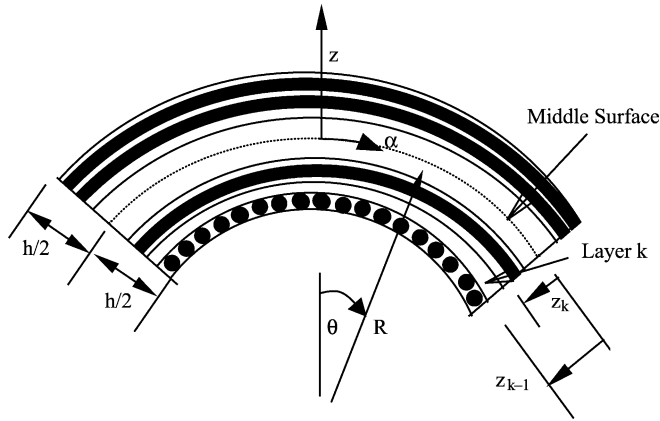


Figure 4.1. Parameters used for laminated curved beams.

This results in the following equations for midsurface strains and curvature change:

$$\varepsilon_0 = \frac{\partial u_0}{\partial \alpha} + \frac{w_0}{R}, \quad k = -\frac{\partial^2 w_0}{\partial \alpha^2} + \frac{1}{R} \frac{\partial u_0}{\partial \alpha} \quad (4.2)$$

The strain at an arbitrary point can be found from

$$\varepsilon = (\varepsilon_0 + zk) \quad (4.3)$$

where u_0 and w_0 are displacements of the beam's middle surface in the α and z directions, respectively. Note that the term z/R is small in comparison with unity and is neglected for thin beams. The well-known Kirchhoff hypothesis (normals to the middle surface remain straight and normal during deformation) was used.

4.1.2 Force and moment resultants

Consider now a laminated curved beam composed of composite material laminae. The fibers of a typical layer may not be parallel to the coordinate in which the beam equations are expressed (i.e., the α coordinate). The stress-strain equations for an element of material in the k th lamina may be written as

$$\sigma = Q_{11}\varepsilon \quad (4.4)$$

where σ is the normal stress component. The constant Q_{11} is the elastic stiffness coefficient for the material. The subscript (11) could be omitted but is maintained here for the direct use and comparison with the shell equations. Vinson and Sierakowski (1986) used a different constant that takes into consideration the effects of Poisson's ratio and free surfaces.

The force and moment resultants are the integrals of the stresses over the beam thickness (h):

$$[N, M] = b \int_{-h/2}^{h/2} [1, z] \sigma dz \quad (4.5)$$

where b is the width of the beam. Keeping in mind that beams of n number of layers are considered, then the above equations may be rewritten as

$$[N, M] = b \sum_{k=1}^n \int_{h_{k-1}}^{h_k} [1, z] \sigma dz \quad (4.6)$$

Substituting Eq. (4.4) into Eq. (4.6), utilizing Eq. (4.3), and carrying out the integration over the thickness piecewise, from layer to layer, yields

$$\begin{bmatrix} N \\ M \end{bmatrix} = \begin{bmatrix} A_{11} & B_{11} \\ B_{11} & D_{11} \end{bmatrix} \begin{bmatrix} \varepsilon_0 \\ \kappa \end{bmatrix} \quad (4.7)$$

where the A_{11} , B_{11} and D_{11} are the stiffness coefficients arising from the piecewise integration (Eq. (2.65))

$$[A_{11}, B_{11}, D_{11}] = \sum_{k=1}^N b Q_{11}^{(k)} \left[(z_k - z_{k-1}), \frac{1}{2}(z_k^2 - z_{k-1}^2), \frac{1}{3}(z_k^3 - z_{k-1}^3) \right] \quad (4.8)$$

where z is the distance from the midsurface to the surface of the k th layer having the largest z -coordinate. The above equations are valid for cylindrical bending of beams. For beams with free stress surfaces, the above equations can be modified. This approach can be found in the book of Vinson and Sierakowski (1986).

4.1.3 Equations of motion

The equations of motion may be obtained by taking a differential element of a beam having thickness h and midsurface length $d\alpha$ (Figure 4.2) and requiring the sum of the external and internal forces in the α and z directions and the sum of the external and internal moments in the out-of-plane direction to be zero. The equations of motion can also be obtained by specializing the thin shell equations derived in Chapter 2 to those of beams. The equations of motion are

$$\begin{aligned} \frac{\partial N}{\partial \alpha} + \frac{Q}{R} &= I_1 \frac{\partial^2 u_0}{\partial t^2} - p_\alpha \\ -\frac{N}{R} + \frac{\partial Q}{\partial \alpha} &= I_1 \frac{\partial^2 w_0}{\partial t^2} - p_n \\ \frac{\partial M}{\partial \alpha} - Q &= 0 \end{aligned} \quad (4.9)$$

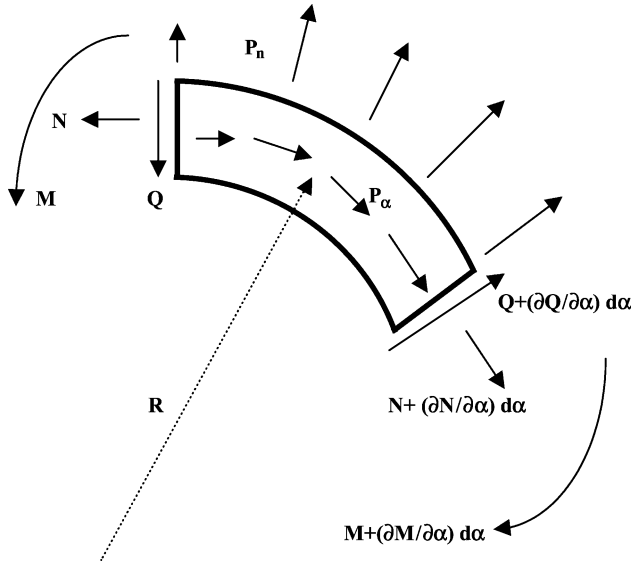


Figure 4.2. A differential curved beam element.

where $I_1 = \sum_{k=1}^N \int_{h_{k-1}}^{h_k} \rho^{(k)} dz = \sum_{k=1}^N b \rho^{(k)} (h_k - h_{k-1})$; N , Q and M are the normal and shear forces and the bending moment, respectively; and p_α and p_n are external force (or body force) components tangent and normal to the beam midsurface, respectively. Solving the third equation in Eq. (4.9) for Q , and substituting this into the second equation, the equations of motion become

$$\frac{\partial N}{\partial \alpha} + \frac{1}{R} \frac{\partial M}{\partial \alpha} = I_1 \frac{\partial^2 u_0}{\partial t^2} - p_\alpha, \quad -\frac{N}{R} + \frac{\partial^2 M}{\partial \alpha^2} = I_1 \frac{\partial^2 w_0}{\partial t^2} - p_n \quad (4.10)$$

Multiplying the last of Eq. (4.10) through by -1 and substituting Eqs. (4.2) and (4.7) into Eq. (4.10), the equations of motion may be expressed in terms of the midsurface displacements in matrix form as

$$\begin{bmatrix} L_{11} & L_{12} \\ L_{21} & L_{22} \end{bmatrix} \begin{bmatrix} u_0 \\ w_0 \end{bmatrix} + \begin{bmatrix} -I_1 & 0 \\ 0 & I_1 \end{bmatrix} \frac{\partial^2}{\partial t^2} \begin{bmatrix} u_0 \\ w_0 \end{bmatrix} = \begin{bmatrix} -p_\alpha \\ +p_n \end{bmatrix} \quad (4.11)$$

where

$$L_{11} = A_{11} \frac{\partial^2}{\partial \alpha^2} + 2 \frac{B_{11}}{R} \frac{\partial^2}{\partial \alpha^2} + \frac{D_{11}}{R^2} \frac{\partial^2}{\partial \alpha^2}$$

$$L_{22} = D_{11} \frac{\partial^4}{\partial \alpha^4} - 2 \frac{B_{11}}{R} \frac{\partial^2}{\partial \alpha^2} + \frac{A_{11}}{R^2}$$

and

$$L_{12} = L_{21} = -B_{11} \frac{\partial^3}{\partial \alpha^3} + \frac{A_{11}}{R} \frac{\partial}{\partial \alpha} - \frac{D_{11}}{R} \frac{\partial^3}{\partial \alpha^3} + \frac{B_{11}}{R^2} \frac{\partial}{\partial \alpha}$$

For symmetrically laminated beams, all terms containing B_{11} vanish. Note that even when the curved beam is symmetrically laminated, there exist coupling between in-plane and transverse displacements. Only if the beam is straight and symmetrically laminated that the in-plane and transverse displacements are decoupled.

4.1.4 Energy functionals

The strain energy stored in a beam during elastic deformation is

$$U = \frac{1}{2} \int_V (\sigma \epsilon) dV = \frac{1}{2} \int (N \epsilon_0 + M \kappa) d\alpha \quad (4.12)$$

where V is the volume. Writing the strain energy functional for the k th lamina, and summing for n number of laminates yields

$$U = \frac{1}{2} \int_L [A_{11}(\epsilon_0)^2 + 2B_{11}\epsilon_0\kappa + D_{11}\kappa^2] d\alpha \quad (4.13)$$

The above equations can also be derived straightforwardly by substituting Eq. (4.7) into Eq. (4.12). Substituting the strain–displacement and curvature–displacement equations (4.2) into Eq. (4.13) yields the strain energy functional in terms of the displacements

$$U = \frac{1}{2} \int_L \left(A_{11} \left(\frac{\partial u_0}{\partial \alpha} + \frac{w_0}{R} \right)^2 + D_{11} \left(-\frac{\partial^2 w_0}{\partial \alpha^2} + \frac{1}{R} \frac{\partial u_0}{\partial \alpha} \right)^2 + 2B_{11} \left(\frac{\partial u_0}{\partial \alpha} + \frac{w_0}{R} \right) \left(-\frac{\partial^2 w_0}{\partial \alpha^2} + \frac{1}{R} \frac{\partial u_0}{\partial \alpha} \right) \right) d\alpha \quad (4.14)$$

Using the distributed external force components p_α in the tangential (polar) direction, and p_n in the normal direction, the work done by the external forces as the beam displaces is

$$W = \int_L (p_\alpha u_0 + p_n w_0) d\alpha \quad (4.15)$$

The kinetic energy for each lamina is

$$T_k = \frac{1}{2} b \rho^{(k)} \int_{L_k} \int_{z_{k-1}}^{z_k} \left[\left(\frac{\partial u_0}{\partial t} \right)^2 + \left(\frac{\partial w_0}{\partial t} \right)^2 \right] d\alpha \quad (4.16)$$

where $\rho^{(k)}$ is the lamina density per unit volume, and t is time. The kinetic energy of the entire beam is (neglecting rotary inertia terms):

$$T = \sum_{k=1}^N T_k = \frac{I_1}{2} \int \left[\left(\frac{\partial u_0}{\partial t} \right)^2 + \left(\frac{\partial w_0}{\partial t} \right)^2 \right] d\alpha \quad (4.17)$$

where I_1 is the average mass density of the beam per unit length.

The above energy expressions can be shown to be consistent with the equations of motion, strain–displacement relations and boundary conditions by means of Hamilton's principle. This requires taking the variation of the Lagrangian energy functional ($T - U + W$), at time t ,

$$\begin{aligned} \delta(T - U + W) = & \int \left(-N \delta\epsilon_0 - M \delta\kappa + I_1 \frac{\partial u_0}{\partial t} \delta \frac{\partial u_0}{\partial t} + I_1 \frac{\partial w_0}{\partial t} \delta \frac{\partial w_0}{\partial t} + p_\alpha \delta u_0 + p_n \delta w_0 \right) d\alpha \\ & - \left(\left(N + \frac{M}{R} \right) \delta u_0 \Big|_{-a/2}^{a/2} + \frac{\partial M}{\partial \alpha} \delta w_0 \Big|_{-a/2}^{a/2} - M \delta \left(\frac{\partial w_0}{\partial \alpha} \right) \Big|_{-a/2}^{a/2} \right) \\ & + \text{initial conditions} \end{aligned} \quad (4.18)$$

Hamilton's principle require the coefficients of δu and δw to vanish independently. The two equations of motion (Eq. (4.10)) can be obtained by separating the terms multiplied by the variation of u_0 (i.e., δu_0) and w_0 , respectively.

4.1.5 Boundary conditions

Boundary conditions can be obtained from the last terms of the variational equation. On each boundary, one must specify three conditions:

$$\begin{aligned} u_0 = 0 \quad & \text{or} \quad N + \frac{M}{R} = 0 \\ w_0 = 0 \quad & \text{or} \quad Q = 0 \\ \frac{\partial w_0}{\partial \alpha} = 0 \quad & \text{or} \quad M = 0 \end{aligned} \quad (4.19)$$

Note that there is an additional term, (M/R) , in the first boundary condition. This term does not exist for straight or slightly curved beams (Qatu 1992a). Boundaries may also be elastically constrained, with the constraints being represented as translational and rotational springs at the beam edges. In such cases, the boundary conditions are generalized to

$$\begin{aligned} k_u u_0 + \left(N + \frac{M}{R} \right) &= 0 \\ k_w w_0 + Q &= 0 \\ k_\psi \frac{\partial w_0}{\partial \alpha} - M &= 0 \end{aligned} \quad (4.20)$$

at the edge $\alpha = -a/2$, where k_u and k_w are translational spring stiffnesses and k_ψ is the rotational spring stiffness. The signs of N , M and Q in the above equations change at the edge $\alpha = a/2$.

The above equations constitute a complete and consistent set of equations for the static and dynamic analyses of laminated composite curved thin beams. By introducing the stiffness and kinematical relationships into the equations of motion, they have been expressed in terms of displacements. If the assumed displacement functions have sufficient continuity, then the equations of compatibility are identically satisfied.

4.2. FUNDAMENTAL THEORY OF MODERATELY THICK BEAMS

A SDBT will be developed here to treat thick beams. The equations derived for moderately thick beams are different from those derived for thin beams. Shear deformation and rotary inertia should be included in the derivation of a thick beam theory. An accurate formulation is made for the stress resultants of thick beams (including the z/R term).

4.2.1 Kinematic relations

Specializing the equations derived in Chapter 2 for thick shells (Eqs. (2.36)–(2.38)) to those of beams, in a manner similar to that described earlier for thin beams, yields the following middle surface strain and curvature change

$$\varepsilon_0 = \frac{\partial u_0}{\partial \alpha} + \frac{w_0}{R}, \quad \kappa = \frac{\partial \psi}{\partial \alpha} \quad (4.21)$$

$$\gamma = \frac{\partial w_0}{\partial \alpha} + \psi - \frac{u_0}{R} \quad (4.22)$$

where γ is the shear strain at the neutral axis, and ψ is rotation of a line element originally perpendicular to the longitudinal direction, about the out-of-plane direction.

Normal strain at an arbitrary point can be found from

$$\varepsilon = \frac{1}{(1 + z/R)} (\varepsilon_0 + z\kappa) \quad (4.23)$$

4.2.2 Force and moment resultants

The force and moment resultants are the integrals of the stresses over the beam thickness (h):

$$[N, M, Q] = b \int_{-h/2}^{h/2} [\sigma, \sigma z, \tau] dz \quad (4.24)$$

where b is the width of the beam. For a laminated beam, with n number of layers, the above equations may be rewritten as

$$[N, M, Q] = b \sum_{k=1}^n \int_{h_{k-1}}^{h_k} [\sigma, \sigma z, \tau] dz \quad (4.25)$$

Substituting Eq. (4.21) into Eq. (4.25), utilizing Eq. (4.23), and carrying out the integration over the thickness yields

$$\begin{bmatrix} N \\ M \\ Q \end{bmatrix} = \begin{bmatrix} A_{11} & B_{11} & 0 \\ B_{11} & D_{11} & 0 \\ 0 & 0 & A_{55} \end{bmatrix} \begin{bmatrix} \varepsilon_0 \\ \kappa \\ \gamma \end{bmatrix} \quad (4.26)$$

where the A_{11} , B_{11} , D_{11} and A_{55} are the stiffness coefficients arising from the integration. The integration is carried exactly, with the z/R term of Eq. (4.23) included

$$\begin{aligned} A_{11} &= R \sum_{k=1}^N b Q_{11}^{(k)} \ln \left(\frac{R + h_k}{R + h_{k-1}} \right) \\ B_{11} &= R \sum_{k=1}^N b Q_{11}^{(k)} \left((h_k - h_{k-1}) - R \ln \left(\frac{R + h_k}{R + h_{k-1}} \right) \right) \\ D_{11} &= R \sum_{k=1}^N b Q_{11}^{(k)} \left(\frac{1}{2} ([R + h_k]^2 - [R + h_{k-1}]^2) - 2R(h_k - h_{k-1}) \right. \\ &\quad \left. + R^2 \ln \left(\frac{R + h_k}{R + h_{k-1}} \right) \right) \\ A_{55} &= \frac{5}{4} \sum_{k=1}^N b Q_{11}^{(k)} \left[(h_k - h_{k-1}) - \frac{4}{3h^2} (h_k^3 - h_{k-1}^3) \right] \end{aligned} \quad (4.27)$$

Table 4.1 shows a comparison between the above terms when both Eqs. (4.27) and (4.8) are used. Eq. (4.27) is accurate and the comparison should give a hint on the limitation of the constitutive relations used in the thin curved beam theory. The difference becomes large as the orthotropy ratio increases. This difference reaches approximately 8% for beams with an orthotropy ratios of 15 and 40 and thickness ratio h/R of 0.2, which is taken as the limit of thick beam theories. This should also be a benchmark for establishing the limitations of shell equations. In general, the z/R term should be included to obtain accurate equations for thick beams (or shells).

Table 4.1. A comparison between approximate and accurate equations for the coefficients A_{11} , B_{11} and D_{11} of $[0^\circ, 90^\circ]$ curved beams.

h/R	Approximate equations (4.8)			Accurate equations (4.27)		
	A_{11}/E_2bR	B_{11}/E_2bR^2	D_{11}/E_2bR^3	A_{11}/E_2bR	B_{11}/E_2bR^2	D_{11}/E_2bR^3
$E_1/E_2 = 1$ (i.e., single layer)						
0.01	0.01	0	0.00000008	0.01000008	-0.00000008	0.00000008
0.02	0.02	0	0.00000067	0.02000067	-0.00000067	0.00000067
0.05	0.05	0	0.00001042	0.05001004	-0.00001042	0.00001042
0.10	0.10	0	0.00008333	0.10008346	-0.00008346	0.00008346
0.20	0.20	0	0.00066667	0.20067070	-0.00067070	0.00067070
Δ^*	-0.3%	-	-0.6%			
$E_1/E_2 = 15$						
0.01	0.08	0.000175	0.00000067	0.07982566	0.00017434	0.00000066
0.02	0.16	0.000700	0.00000533	0.15930530	0.00069470	0.00000530
0.05	0.40	0.004375	0.00008333	0.39570700	0.00429300	0.00008200
0.10	0.80	0.017500	0.00066667	0.78314576	0.01685424	0.00064576
0.20	1.60	0.070000	0.00533333	1.53501321	0.06498679	0.00501321
Δ^*	4.2%	7.7%	6.4%			
$E_1/E_2 = 40$						
0.01	0.205	0.0004875	0.00000171	0.20451420	0.00048579	0.00000170
0.02	0.410	0.0019500	0.00001367	0.40806357	0.00193643	0.00001357
0.05	1.025	0.0121875	0.00021354	1.01302231	0.01197769	0.00020981
0.10	2.050	0.0487500	0.00170833	2.00289986	0.04710014	0.00164986
0.20	4.100	0.1950000	0.01366667	3.91776771	0.18223229	0.01276771
Δ^*	4.7%	7.0%	7.0%			

The percentage difference between Eqs. (4.8) and (4.27) for $h/R = 0.2$.

4.2.3 Equations of motion

Considering rotary inertia terms, the equations of motion become

$$\begin{aligned}
 \frac{\partial N}{\partial \alpha} + \frac{Q}{R} &= \bar{I}_1 \frac{\partial^2 u}{\partial t^2} + \bar{I}_2 \frac{\partial^2 \psi}{\partial t^2} - p_\alpha \\
 -\frac{N}{R} + \frac{\partial Q}{\partial \alpha} &= \bar{I}_1 \frac{\partial^2 w}{\partial t^2} - p_n \\
 \frac{\partial M}{\partial \alpha} - Q &= \bar{I}_2 \frac{\partial^2 u}{\partial t^2} + \bar{I}_3 \frac{\partial^2 \psi}{\partial t^2}
 \end{aligned} \tag{4.28}$$

where

$$(\bar{I}_1, \bar{I}_2, \bar{I}_3) = \left(I_1 + \frac{I_2}{R} + \frac{I_3}{R}, I_2 + \frac{I_3}{R}, I_3 \right) \quad (4.29)$$

$$[I_1, I_2, I_3] = \sum_{k=1}^N \int_{h_{k-1}}^{h_k} \rho^{(k)} [1, z, z^2] dz$$

or

$$[I_1, I_2, I_3] = \sum_{k=1}^N b\rho^{(k)} \left((h_k - h_{k-1}), \frac{1}{2}(h_k^2 - h_{k-1}^2), \frac{1}{3}(h_k^3 - h_{k-1}^3) \right)$$

The term (\bar{I}_2) is of particular interest. It may be referred to as the coupling inertia and only appears if the material density is not symmetric about the middle surface, which is rarely the case. This term does not exist for symmetrically laminated plates and even unsymmetrically laminated plates if the material used is the same, regardless of the fiber orientation.

It will be shown later that the above equations are consistent with the energy functionals. Multiplying the second equation in Eq. (4.28) of the equations of motion through by -1 and substituting Eqs. (4.22) and (4.26) into Eq. (4.28), the equations of motion may be expressed in terms of the midsurface displacements and slope in matrix form as:

$$\begin{bmatrix} L_{11} & L_{12} & L_{13} \\ L_{21} & L_{22} & L_{23} \\ L_{31} & L_{32} & L_{33} \end{bmatrix} \begin{bmatrix} u_0 \\ w_0 \\ \psi \end{bmatrix} + \begin{bmatrix} \bar{I}_1 & 0 & \bar{I}_2 \\ 0 & -\bar{I}_1 & 0 \\ \bar{I}_2 & 0 & \bar{I}_3 \end{bmatrix} \frac{\partial^2}{\partial t^2} \begin{bmatrix} u_0 \\ w_0 \\ \psi \end{bmatrix} = \begin{bmatrix} -p_\alpha \\ +p_n \\ 0 \end{bmatrix} \quad (4.30)$$

where

$$L_{11} = A_{11} \frac{\partial^2}{\partial \alpha^2} - \frac{A_{55}}{R^2}$$

$$L_{12} = L_{21} = \left(\frac{A_{11}}{R} + \frac{A_{55}}{R} \right) \frac{\partial}{\partial \alpha}$$

$$L_{13} = L_{31} = B_{11} \frac{\partial^2}{\partial \alpha^2} + \frac{A_{55}}{R^2}$$

$$L_{22} = \frac{A_{11}}{R^2} - A_{55} \frac{\partial^2}{\partial \alpha^2}$$

$$L_{23} = L_{32} = B_{11} \frac{\partial}{\partial \alpha} - A_{55} \frac{\partial}{\partial \alpha}$$

$$L_{33} = D_{11} \frac{\partial^2}{\partial \alpha^2} + A_{55}$$

For symmetrically laminated beams, all terms containing B_{11} vanish. Similar to CBT, both curvature and unsymmetric lamination cause the coupling between tangential and transverse deformation.

4.2.4 Energy functionals

The strain energy stored in a beam during elastic deformation is

$$U = \frac{1}{2} \int \left(N \varepsilon_0 + M \frac{\partial \psi}{\partial \alpha} + Q \gamma \right) d\alpha \quad (4.31)$$

Writing the strain energy functional for the k th lamina, and summing for n number of layers yields

$$U = \frac{1}{2} \int_L [A_{11}(\varepsilon_0)^2 + B_{11}\varepsilon_0\kappa + D_{11}\kappa^2 + A_{55}\gamma^2] d\alpha \quad (4.32)$$

The above equations can also be derived straightforwardly by substituting Eq. (4.26) into Eq. (4.31). Substituting Eqs. (4.21) and (4.22) into the above energy expression yields the strain energy functional in terms of the slope and displacements

$$U = \frac{1}{2} \int_L \left(A_{11} \left(\frac{\partial u_0}{\partial \alpha} + \frac{w_0}{R} \right)^2 + D_{11} \left(\frac{\partial \psi}{\partial \alpha} \right)^2 + 2B_{11} \left(\frac{\partial u_0}{\partial \alpha} + \frac{w_0}{R} \right) \frac{\partial \psi}{\partial \alpha} + A_{55} \left(\frac{\partial w_0}{\partial \alpha} + \psi - \frac{u_0}{R} \right)^2 \right) d\alpha \quad (4.33)$$

The work done by the external force components (p_α in the tangential (polar) direction, and p_n in the normal direction) as the beam displaces is

$$W = \int_L (p_\alpha u_0 + p_n w_0) d\alpha \quad (4.34)$$

The kinetic energy for the entire beam (including rotary inertia) is

$$\begin{aligned} T &= \frac{b}{2} \int_{l_k} \int \rho \left[\left(\left(1 + \frac{z}{R} \right) \frac{\partial u_0}{\partial t} + z \frac{\partial \psi}{\partial t} \right)^2 \right] dz d\alpha \\ &= \frac{b}{2} \int_L \int \rho \left[\left(\left(1 + \frac{z}{R} \right) \frac{\partial u_0}{\partial t} \right)^2 + 2 \left(1 + \frac{z}{R} \right) z \frac{\partial u_0}{\partial t} \frac{\partial \psi}{\partial t} + \left(z \frac{\partial \psi}{\partial t} \right)^2 + \left(\frac{\partial w_0}{\partial t} \right)^2 \right] dz d\alpha \end{aligned}$$

Integrating over z and summing for N number of layers yields

$$T = \sum_{k=1}^N T_k = \frac{b}{2} \int_L \left[\bar{I}_1 \left(\frac{\partial u_0}{\partial t} \right)^2 + \bar{I}_1 \left(\frac{\partial w_0}{\partial t} \right)^2 + 2\bar{I}_2 \left(\frac{\partial \psi}{\partial t} \frac{\partial u_0}{\partial t} \right) + \bar{I}_3 \left(\frac{\partial \psi}{\partial t} \right)^2 \right] d\alpha \quad (4.35)$$

Hamilton's principle is used again to show that the above energy functionals are consistent with the equations of motion and the kinematical relations. This requires taking the variation of the Lagrangian energy functional ($T - U + W$), at time t ,

$$\begin{aligned}
 \delta(T - U + W) = & - \int \left(N \delta \varepsilon_0 + M \delta \kappa + Q \delta \gamma - \bar{I}_1 \delta \frac{\partial u_0}{\partial t} \frac{\partial u_0}{\partial t} - \bar{I}_1 \delta \frac{\partial w_0}{\partial t} \frac{\partial w_0}{\partial t} \right. \\
 & - \bar{I}_2 \frac{\partial \psi}{\partial t} \delta \frac{\partial u_0}{\partial t} - \bar{I}_2 \frac{\partial u_0}{\partial t} \delta \frac{\partial \psi}{\partial t} - \bar{I}_3 \frac{\partial \psi}{\partial t} \delta \frac{\partial \psi}{\partial t} \\
 & \left. - p_\alpha \delta u_0 - p_n \delta w_0 \right) d\alpha \\
 = & \int \left(\frac{\partial N}{\partial \alpha} \delta u_0 - \frac{N}{R} \delta w_0 + \frac{\partial M}{\partial \alpha} \delta \psi + \frac{\partial Q}{\partial \alpha} \delta w_0 - Q \delta \psi + \frac{Q}{R} \delta u_0 \right. \\
 & + p_\alpha \delta u_0 + p_n \delta w_0 - \bar{I}_1 \frac{\partial^2 u_0}{\partial t^2} \delta u_0 - \bar{I}_1 \frac{\partial^2 w_0}{\partial t^2} \delta w_0 \\
 & \left. - \bar{I}_2 \frac{\partial^2 \psi}{\partial t^2} \delta u_0 - \bar{I}_2 \frac{\partial^2 u_0}{\partial t^2} \delta \psi - \bar{I}_3 \frac{\partial^2 \psi}{\partial t^2} \delta \psi \right) d\alpha \\
 & - \left(N \delta u_0 \Big|_{-a/2}^{a/2} + Q \delta w_0 \Big|_{-a/2}^{a/2} - M \delta \psi \Big|_{-a/2}^{a/2} \right) \\
 & + \text{initial conditions}
 \end{aligned} \tag{4.36}$$

Again, the equations of motion can be obtained by separating the terms multiplied by the variations of u (i.e., δu_0), w_0 and ψ , respectively.

4.2.5 Boundary conditions

One can get the consistent boundary conditions from the last terms of the variational equation. On each boundary, one must specify three conditions.

$$\begin{aligned}
 u = 0 & \quad \text{or} \quad N = 0 \\
 w = 0 & \quad \text{or} \quad Q = 0 \\
 \psi = 0 & \quad \text{or} \quad M = 0
 \end{aligned} \tag{4.37}$$

It is worth mentioning that for moderately thick curved beams, the term M/R in the first of the above equations drops. This is hard to find without the variational derivation. For elastically constrained boundaries, with the constraints being represented as translational

and rotational springs at the beam edges, the boundary conditions are generalized to

$$\begin{aligned} k_u u_0 + N &= 0 \\ k_w w_0 + Q &= 0 \\ k_\psi \psi - M &= 0 \end{aligned} \quad (4.38)$$

at the edge $\alpha = -a/2$. The signs of N , M and Q in the above equations change at the edge $\alpha = a/2$.

The simple support boundary conditions can take two forms for curved beams at one boundary, namely:

$$\begin{aligned} \text{S1 :} \quad w_0 = N = M &= 0 \quad \text{on} \quad \alpha = -a/2, a/2 \\ \text{S2 :} \quad w_0 = u_0 = M &= 0 \quad \text{on} \quad \alpha = -a/2, a/2 \end{aligned} \quad (4.39a)$$

Similarly, the free boundary conditions can take the following forms:

$$\begin{aligned} \text{F1 :} \quad Q = N = M &= 0 \quad (\text{completely free}) \\ \text{F2 :} \quad Q = u_0 = M &= 0 \end{aligned} \quad (4.39b)$$

and the clamped boundary conditions can take the following forms:

$$\begin{aligned} \text{C1 :} \quad w_0 = N = \psi &= 0 \\ \text{C2 :} \quad w_0 = u_0 = \psi &= 0 \quad (\text{completely clamped}) \end{aligned} \quad (4.39c)$$

This completes the set of equations for the analysis of laminated composite moderately thick curved beams. The equations of compatibility will be identically satisfied if the assumed displacement functions have sufficient continuity, which is less than that of thin beams.

4.3. SIMPLY SUPPORTED BEAMS AND CLOSED RINGS

Simply supported curved beams (with S1 boundary condition) will be studied in this section. For such beams, straightforward exact solution can be used. Vibration analysis is conducted to compare the thin and moderately thick beam theories derived earlier in this chapter. Thin beams will be considered first, followed by thick ones.

4.3.1 Thin beams

The above S1 boundary conditions are exactly satisfied at both ends ($\alpha = -a/2$ and $\alpha = a/2$) by choosing

$$[u_0, w_0] = \sum_{m=1}^m [A_m \sin(\alpha_m \alpha), C_m \cos(\alpha_m \alpha)] \sin(\omega t) \quad (4.40)$$

where $\alpha_m = m\pi/a$, m is proper integer and A_m and C_m are arbitrary constants.

The external forces (important in a static or dynamic analyses) can be expanded in a Fourier series in α :

$$[p_\alpha, p_z] = \sum_{m=1}^m [p_{\alpha m} \sin(\alpha_m \alpha), p_{zm} \cos(\alpha_m \alpha)] \sin(\omega t) \quad (4.41)$$

where

$$p_{\alpha m} = \frac{2}{a} \int p_\alpha \sin(\alpha_m \alpha) d\alpha \quad \text{and} \quad p_{zm} = \frac{2}{a} \int p_z \cos(\alpha_m \alpha) d\alpha$$

Substituting Eqs. (4.40) and (4.41) into the equations of motion written in terms of displacement

$$\begin{bmatrix} C_{11} & C_{12} \\ C_{21} & C_{22} \end{bmatrix} \begin{bmatrix} A_m \\ C_m \end{bmatrix} + \omega^2 \begin{bmatrix} \rho & 0 \\ 0 & -\rho \end{bmatrix} \begin{bmatrix} A_m \\ C_m \end{bmatrix} + \begin{bmatrix} p_{\alpha m} \\ -p_{zm} \end{bmatrix} = \begin{bmatrix} 0 \\ 0 \end{bmatrix} \quad (4.42)$$

where

$$\begin{aligned} C_{11} &= -\alpha_m^2 [A_{11} + 2B_{11}/R + D_{11}/R^2] \\ C_{22} &= +(D_{11}\alpha_m^4) + 2(B_{11}/R)\alpha_m^2 + (A_{11}/R^2) \end{aligned}$$

and

$$C_{21} = -C_{12} = [B_{11}\alpha_m^3] + \alpha_m [(A_{11}/R) + (B_{11}/R^2)] + D_{11}/R$$

Eq. (4.42) is actually valid for problems of forced vibrations. The static problem results when the frequency is set to 0. The free vibration problem arises by setting the pressure terms equal to 0. If one assumes that $u_0 = \cos(\alpha_m \alpha) \sin(\omega t)$; and $w_0 = \sin(\alpha_m \alpha) \sin(\omega t)$ in Eq. (4.40), then the problem of laminated curved beams having vertical hinge supports (i.e., $u_0 = \partial w_0 / \partial \alpha = Q = 0$) is solved. This will yield a frequency determinant which is the same as that of simply supported beams, and consequently, and interestingly, the same natural frequencies.

4.3.2 Moderately thick beams

Similar to thin curved beams, The simple support S1 boundary conditions for thick beams at $\alpha = -a/2; a/2$ are

$$S1 : \quad w_0 = N_\alpha = \frac{\partial \psi}{\partial \alpha} = 0 \quad \text{on} \quad \alpha = -a/2, a/2 \quad (4.43)$$

The above S1 boundary conditions are exactly satisfied by choosing

$$[u_0, w_0, \psi] = \sum_{m=1}^m [A_m u_{0m}, C_m w_{0m}, B_m \psi_m] \sin(\omega t) \quad (4.44)$$

where $u_{0m} = \sin(\alpha_m \alpha)$, $w_{0m} = \cos(\alpha_m \alpha)$, $\psi_m = \sin(\alpha_m \alpha)$ and $\alpha_m = m\pi/a$.

The external forces can be expanded in a Fourier series as in Eq. (4.41). Substituting Eqs. (4.43) and (4.44) into the equations of motion written in terms of displacement for moderately thick beams Eq. (4.30) yields

$$\begin{bmatrix} C_{11} & C_{12} & C_{13} \\ C_{21} & C_{22} & C_{23} \\ C_{31} & C_{32} & C_{33} \end{bmatrix} \begin{bmatrix} A_m \\ C_m \\ B_m \end{bmatrix} + \omega^2 \begin{bmatrix} \bar{I}_1 & 0 & \bar{I}_2 \\ 0 & -\bar{I}_1 & 0 \\ \bar{I}_2 & 0 & \bar{I}_3 \end{bmatrix} \begin{bmatrix} A_m \\ C_m \\ B_m \end{bmatrix} + \begin{bmatrix} p_{\alpha m} \\ -p_{zm} \\ 0 \end{bmatrix} = \begin{bmatrix} 0 \\ 0 \\ 0 \end{bmatrix} \quad (4.45)$$

where

$$C_{11} = -\alpha_m^2 A_{11} - A_{55}/R^2$$

$$C_{22} = A_{11}/R^2 + A_{55}\alpha_m^2$$

$$C_{33} = -D_{11}\alpha_m^2 - A_{55}$$

$$C_{21} = -C_{12} = \alpha_m[(A_{11}/R) + (A_{55}/R)]$$

$$C_{31} = C_{13} = -B_{11}\alpha_m^2 + (A_{55}/R)$$

and

$$C_{23} = -C_{32} = \alpha_m[(B_{11}/R) - A_{55}]$$

Again, Eq. (4.45) is actually valid for problems of forced vibrations. The static problem results when the frequency is set to 0, and the free vibration problem arises when the pressure terms are 0s. Similar to thin beams, if one assumes that $u_{0m} = \cos(\alpha_m \alpha)$, $w_{0m} = \sin(\alpha_m \alpha)$ and $\psi_m = \cos(\alpha_m \alpha)$ in Eq. (4.44) then the problem of laminated curved beam having vertical hinge supports (i.e., $u_0 = \psi = Q = 0$) is solved.

It should be mentioned that the above exact solutions are exact with respect to the theory presented here. They are not exact with respect to the theory of elasticity.

4.3.3 Closed rings

The analysis of closed rings can be performed by assuming $u_0 = \sin(m\theta)$, $w_0 = \cos(m\theta)$, in Eq. (4.40) and integrating over θ instead of α using Eq. (4.1). This will yield a determinant similar to that of Eq. (4.42) for thin rings. Similar treatment can be made for moderately thick rings by further assuming $\psi_m = \sin(m\theta)$, which will yield a third order determinant similar to that of Eq. (4.45).

4.3.4 Numerical results

Table 4.2 shows a comparison of the first four natural frequencies obtained for simply supported beams using equations of slightly curved beams (Qatu 1992a) or shallow

Table 4.2. Exact frequency parameters $\Omega = \omega a^2 \sqrt{12I_1/E_{11}h^2}$ for simply supported $[0^\circ, 90^\circ]$ laminated curved thin beams using deep and shallow beam theories, $a/h = 100$.

a/R	Deep beam theory (Eq. (4.42))				Shallow beam theory (Qatu 1992a)			
	m = 1	m = 2	m = 3	m = 4	m = 1	m = 2	m = 3	m = 4
<i>$E_{11}/E_{22} = 1$ (i.e., single layer)</i>								
0.0	9.8702	39.491	88.892	158.12	9.8702	39.477	88.826	157.91
0.1	9.8549	39.475	88.876	158.11	9.8642	39.473	88.820	157.91
0.2	9.8102	39.431	88.830	158.06	9.8493	39.460	88.807	157.89
0.3	9.7364	39.356	88.757	157.99	9.8249	39.434	88.781	157.87
0.5	9.4993	39.116	88.516	157.75	9.7490	39.352	88.702	157.79
0.8	8.9473	38.538	87.935	157.16	9.5683	39.162	88.510	157.59
1.0	8.4516	38.000	87.335	156.42	9.4024	38.987	88.330	157.42
<i>$E_{11}/E_{22} = 15$</i>								
0.0	4.7037	18.810	42.320	75.222	4.7037	18.810	42.320	75.222
0.1	4.6936	18.795	42.295	75.181	4.6987	18.805	42.307	75.202
0.2	4.6707	18.767	42.255	75.131	4.6911	18.792	42.291	75.179
0.3	4.6348	18.721	42.198	75.059	4.6783	18.777	42.271	75.151
0.5	4.5176	18.593	42.049	74.881	4.6400	18.731	42.214	75.082
0.8	4.2483	18.296	41.721	74.509	4.5491	18.629	42.094	74.940
1.0	4.0115	18.030	41.431	74.188	4.4725	18.539	41.992	74.823
<i>$E_{11}/E_{22} = 40$</i>								
0.0	4.0072	16.024	36.040	64.061	4.0072	16.024	36.040	64.061
0.1	3.9938	16.011	36.017	64.021	4.0027	16.015	36.032	64.043
0.2	3.9758	15.980	35.985	63.976	3.9938	16.006	36.013	64.021
0.3	3.9442	15.944	35.933	63.918	3.9848	15.989	35.997	63.994
0.5	3.8432	15.831	35.805	63.757	3.9533	15.953	35.945	63.936
0.8	3.6179	15.576	35.521	63.433	3.8710	15.863	35.845	63.811
1.0	3.4153	15.349	35.271	63.156	3.8105	15.786	35.753	63.708

Table 4.3. Exact frequency parameters $\Omega = \omega a^2 \sqrt{12I_1/E_{11}h^2}$ for simply supported $[0^\circ, 90^\circ]$ laminated curved thin and moderately thick beams, $a/R = 1.0$, $G_{12}/E_2 = G_{13}/E_3 = 0.5$.

h/a	Classical beam theory (Eq. (4.42))				Shear deformation beam theory (Eq. (4.45))			
	$m = 1$	$m = 2$	$m = 3$	$m = 4$	$m = 1$	$m = 2$	$m = 3$	$m = 4$
$E_f/E_2 = 1$ (i.e., single layer)								
0.01	8.4520	38.001	87.335	156.41	8.4508	37.980	87.229	156.07
0.02	8.4520	37.998	87.331	156.41	8.4478	37.919	86.909	155.06
0.05	8.4488	37.985	87.300	156.35	8.4270	37.504	84.790	148.58
0.10	8.4401	37.938	87.183	156.12	8.3546	36.153	78.546	131.57
0.20	8.4047	37.730	86.558	154.40	8.0874	32.122	63.760	98.806
$E_f/E_2 = 15$								
0.01	4.0116	18.031	41.432	74.190	4.0094	18.000	41.286	73.738
0.02	3.9960	17.949	41.227	73.786	3.9885	17.839	40.681	72.095
0.05	3.9471	17.690	40.526	72.278	3.9109	17.089	37.667	64.041
0.10	3.8656	17.212	39.083	68.854	3.7419	15.329	31.300	49.452
0.20	3.7015	16.118	35.403	59.676	3.3312	11.808	21.481	31.295
$E_f/E_2 = 40$								
0.01	3.4145	15.349	35.270	63.157	3.4108	15.298	35.034	62.438
0.02	3.4014	15.274	35.081	62.778	3.3871	15.093	35.220	60.178
0.05	3.3559	15.034	34.424	61.355	3.2932	14.111	30.283	50.017
0.10	3.2809	14.591	33.077	58.157	3.0814	11.964	23.180	35.118
0.20	3.1315	13.592	29.743	49.981	2.5935	8.3979	14.446	20.425

beams, and those presented here for thin beams with deep curvature. The nondimensional frequency parameter $\Omega = \omega a^2 \sqrt{12I_1/E_{11}h^2}$ ($= \omega a^2 \sqrt{I_1 A/E_{11} \bar{I}}$), where A is the cross-sectional area and I is the moment of inertia of $bh^3/12$ is used in the comparison. As shown in the results, the shallow beam equations give higher frequencies than the equations of deep beams. As the curvature increases, the difference between both theories increases and reaches a maximum of approximately 10% for the fundamental frequency when a/R reaches 1, which is taken as the limit of the shallow beam equations. This difference decreases for high frequencies because the mode shapes associated with the higher frequencies divide the beam into sections, each of which is shallower (in terms of the half wavelength to radius ratio) than the original beams.

Table 4.3 shows a comparison between the results obtained using classical and shear deformation curved beam equations. The same frequency parameter is used. The thickness ratio h/R is varied from 0.01 to 0.2, which is taken as the limit of the moderately thick beam equations (to be proven when and if these equations are compared with those obtained by 3D theory of elasticity). The results show criteria for establishing the limit of the thin beam theory. The effect of shear deformation and rotary inertia increases as

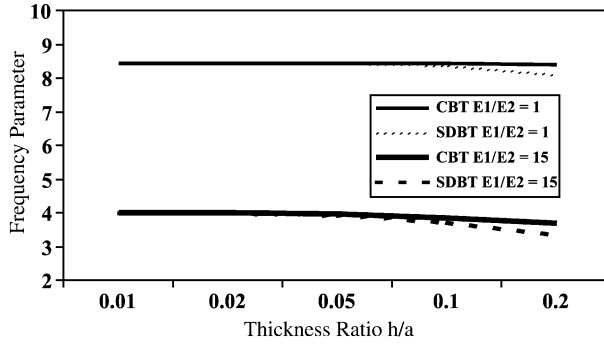


Figure 4.3. The fundamental frequency parameters $\Omega = \omega a^2 \sqrt{12I_1/E_{11}h^2}$ for simply supported $[0^\circ, 90^\circ]$ beams, $a/R = 1.0$, $G_{12}/E_2 = G_{13}/E_3 = 0.5$ using CBT and SDBT.

the orthotropy ratio increases. While the maximum difference (in the fourth frequency) between the frequencies obtained by thin beam equations and moderately thick beam equations is 5.2% for a thickness ratio of 0.05 and single layer beams, this difference is 12.9% for $[0^\circ, 90^\circ]$ cross-ply beams with an orthotropy ratio of 15 and it is 22.7% for an orthotropy ratio of 40. The difference between both theories becomes large, even for the fundamental frequencies, when the thickness ratio exceeds 0.05, which is taken as the limit of the thin beam theory. The results are shown graphically in Figures 4.3 and 4.4 for the first and second modes, respectively. Both orthotropy ratios of 1 and 15 are shown in each figure. The figures show how the difference between CBT and SDBT increases with higher thickness ratio and higher modes.

These results can be used in establishing the limits of shell theories and shell equations. They can also be used as benchmarks for future research on using approximate methods, like the Ritz and finite element methods.

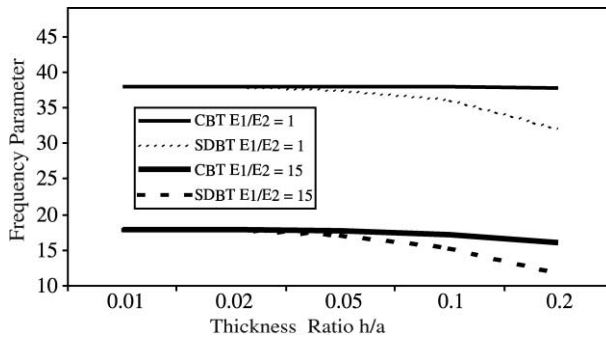


Figure 4.4. The second lowest frequency parameters $\Omega = \omega a^2 \sqrt{12I_1/E_{11}h^2}$ for simply supported $[0^\circ, 90^\circ]$ beams, $a/R = 1.0$, $G_{12}/E_2 = G_{13}/E_3 = 0.5$ using CBT and SDBT.

4.4. LAMINATED CURVED THIN BEAMS WITH ARBITRARY BOUNDARIES

In Section 4.3, exact solutions are presented for laminated curved beams having simply supported boundary conditions. In this section, other boundary conditions will be studied, and their effect on the structural behavior of these components will be explored. Only thin curved beams are considered in this section.

Exact solutions are found for the boundary value problem with arbitrary boundary conditions. A solution procedure is described to obtain frequencies. The Ritz method, known for the shortcoming of being difficult to apply for arbitrary boundaries, will be presented here in a general but simple form which can be used for arbitrary boundary conditions. This is done using the same numerical procedure and computer program. The method can be expanded to plates and shells.

4.4.1 Exact solutions for thin beams

Exact solutions (i.e., solutions which satisfy both the equations of motion and the boundary conditions) are possible for laminated curved beams. For arbitrary boundary conditions, the displacements in the equations of motion can be assumed as

$$u_0(x, t) = C e^{s\alpha} \sin \omega t, \quad w_0(x, t) = D e^{s\alpha} \sin \omega t \quad (4.46)$$

Substituting Eq. (4.46) into the equations of motion yields two equations with the unknown coefficients C and D . In order to avoid the trivial solution of $C = D = 0$, the determinant has to be set to 0. This yields the following equation:

$$Fs^6 + \left[\frac{2F}{R^2} + \rho\omega^2 D_{11} \right] s^4 + \left[-\left[A_{11} + \frac{4}{R} B_{11} + \frac{1}{R^2} D_{11} \right] \rho\omega^2 + \frac{F}{R^2} \right] s^2 + \rho\omega^2 \frac{1}{R} A_{11} - (\rho\omega^2)^2 = 0 \quad (4.47)$$

where $F = A_{11}D_{11} - B_{11}$. This is a third order equation in s^2 , the roots of which can be found. Numerical experimentation of these roots showed that they are all real ones, and typically one of them is negative ($-\nu_1^2$), where ν_1 is positive, and the remaining two are positive (ν_2^2, ν_3^2). These roots yield the following general solution:

$$\begin{aligned} u_0(\alpha) &= C_1 \sin(\nu_1 \alpha) + C_2 \cos(\nu_1 \alpha) + C_3 \sinh(\nu_2 \alpha) + C_4 \cosh(\nu_2 \alpha) \\ &\quad + C_5 \sinh(\nu_3 \alpha) + C_6 \cosh(\nu_3 \alpha) \\ w_0(\alpha) &= D_1 \sin(\nu_1 \alpha) + D_2 \cos(\nu_1 \alpha) + D_3 \sinh(\nu_2 \alpha) + D_4 \cosh(\nu_2 \alpha) \\ &\quad + D_5 \sinh(\nu_3 \alpha) + D_6 \cosh(\nu_3 \alpha) \end{aligned} \quad (4.48)$$

The equations of motion can be used again to determine the ratios (C_i/D_i). Eq. (4.48) involves six independent unknowns which are solved for by using the six boundary conditions (three on each edge). The six resulting equations are written and the

determinant is taken as 0, which yields the frequency parameters. The solution has to be verified by checking the roots $(-\nu_1^2, \nu_2^2, \nu_3^2)$. If these roots are not found as assumed, other forms of solutions have to be found.

The above procedure yields exact frequencies. It does, however, involve considerable amount of work and subsequent programming for finding the roots of the determinant. The solution has to be verified for each frequency. The frequency determinant will be different for each set of edge supports. Symmetry in particular problems can be used to simplify the mathematics.

The above difficulties justify looking for an approximate, but reasonably accurate, solution. This is done by using the Ritz method.

4.4.2 Vibration of curved beams using the Ritz method

The deformation is assumed to be sinusoidal with time. Displacements are thus assumed as:

$$u_0(\alpha, t) = U_0(\alpha)\sin \omega t, \quad w_0(\alpha, t) = W_0(\alpha)\sin \omega t \quad (4.49)$$

Various functions can be used for U_0 and W_0 . Among the mostly used functions are trigonometric functions, beam functions and algebraic polynomials. Beam functions are actually the mode shapes obtained in the analysis of straight beams. They are not widely used because they do not form a complete set of functions and thus cannot guarantee convergence to the exact solution.

Algebraic polynomial trial functions are used in the analysis because they form a mathematically complete set of functions which guarantees convergence to the exact solution as the number of terms taken increases. They are also relatively simple to use in the algebraic manipulation and computer programming subsequently required and can be differentiated and integrated exactly in the energy functionals needed. Using algebraic polynomial, one can solve for all possible combinations of boundary conditions for these beams. Thus, the displacement functions U_0 and W_0 are written in terms of the nondimensional coordinate ξ as

$$U_0(\xi) = \sum_{i=i_0}^I \alpha_i \xi^{i_0} (1 - \xi)^{j_0} \quad (4.50)$$

$$W_0(\xi) = \sum_{l=l_0}^L \gamma_l \xi^{l_0} (1 - \xi)^{m_0} \quad (4.51)$$

where $\xi = \alpha/a$, and α_i and γ_i are arbitrary coefficients to be determined subsequently.

The Ritz method requires the satisfaction of the geometric “forced” boundary conditions only. Thus by suitable selection of i_0 and l_0 , one can solve for any boundary conditions at $\xi = 0$, and by suitable selection of j_0 and m_0 , one can solve for

Table 4.4. Values of i_0, j_0, l_0 and m_0 required in the Ritz method for various boundary conditions at $\xi = 0$ and 1.

Boundary conditions	At $\xi = 0$		At $\xi = 1$	
	i_0	l_0	j_0	m_0
F1 (completely free)	0	0	0	0
F2	1	0	1	0
S1	0	1	0	1
S2	1	1	1	1
C1	0	2	0	2
C2 (completely clamped)	1	2	1	2

any boundary conditions at the other end (i.e., $\xi = 1$). For example, if one chooses the cantilever boundary conditions, where the edge at $\xi = 0$ is clamped and that at $\xi = 1$ is free, then one should satisfy $u_0 = w_0 = dw_0/d\alpha = 0$ at $\xi = 0$. This is done by choosing i_0 as 1 to satisfy $u_0 = 0$ and $l_0 = 2$ to satisfy $w_0 = dw_0/d\alpha = 0$. One needs to satisfy no geometric boundary conditions at $\xi = 1$, which results in the selection of j_0 and m_0 as 0s. Table 4.4 shows these values for six possible boundary conditions per edge.

In order to make the subsequent analysis and computer programming easier, the terms $(1 - \xi)^{j_0}$ and $(1 - \xi)^{m_0}$ are expanded in the following forms:

$$(1 - \xi)^{j_0} = f_1 - f_2\xi, \quad (1 - \xi)^{m_0} = f_3 - 2f_4\xi + f_5\xi^2, \quad (4.52)$$

$$j_0 = 0 \text{ or } 1 \quad \text{and} \quad m_0 = 0, 1 \text{ or } 2$$

For example, if j_0 is 0 then $f_1 = 1$ and $f_2 = 0$, and if m_0 is 2 then $f_3 = 1, f_4 = 1$ and $f_5 = 1$, and so on.

The Ritz method requires minimization of the functional $L = T - U$ in a free vibration analysis, where U and T are the maximum strain and kinetic energies, respectively. This can be accomplished by taking the derivatives:

$$\frac{\partial L_m}{\partial \alpha_p} = 0, \quad p = i_0, i_0 + 1, \dots, I$$

$$\frac{\partial L_m}{\partial \gamma_q} = 0, \quad q = l_0, l_0 + 1, \dots, L \quad (4.53)$$

This yields simultaneous, linear equations in an equal number of unknowns α_p , and γ_q :

$$\begin{aligned}
 \frac{\partial L_m}{\partial \alpha_p} = & \sum_{i=i_0}^I \frac{\alpha_i}{2} \left(2s_1 a^{(i+p+1)} \left(\frac{f_1^2 i p}{i+p-1} - \frac{f_1 f_2 p(i+1)}{i+p} - \frac{f_1 f_2 i(p+i)}{i+p} + \frac{f_2^2 (i+1)(p+1)}{i+p+1} \right) \right. \\
 & \left. - 2\omega^2 I_1 a^{(i+q+3)} \left(\frac{f_1^2}{i+p+1} - \frac{2f_1 f_2}{p+i+2} + \frac{f_2^2}{i+p+3} \right) \right) \\
 & + \sum_{l=l_0}^L \frac{\gamma_l}{2} \left(s_2 a^{(p+l+3)} \left(\frac{f_1 f_3 p}{p+l} - \frac{2f_1 f_4 p}{l+p+1} + \frac{f_1 f_5 p}{p+l+2} - \frac{f_2 f_3 (p+1)}{p+l+1} \right. \right. \\
 & \left. \left. + 2 \frac{f_2 f_4 (p+1)}{p+l+2} - \frac{f_2 f_5 (p+1)}{p+l+3} \right) \right) \\
 & + s_3 a^{(l+p+1)} \left(\frac{f_1 f_3 p l (l-1)}{p+l-2} - 2 \frac{f_1 f_4 p l (l+1)}{p+l-1} + \frac{f_1 f_5 p (l+2)(l+1)}{l+p} \right. \\
 & \left. - \frac{f_3 f_2 l (p+1)(l-1)}{l+p-1} + \frac{2f_2 f_4 l (p+1)(l+1)}{l+p} \right. \\
 & \left. \left. - \frac{f_2 f_5 (l+2)(p+1)(l+1)}{l+p+1} \right) \right) \Bigg)
 \end{aligned} \tag{4.54}$$

$$\begin{aligned}
 \frac{\partial L_m}{\partial \gamma_q} = & \sum_{i=i_0}^I \frac{\alpha_i}{2} \left(s_2 a^{(i+q+3)} \left(\frac{f_1 f_3 i}{i+q} - \frac{2f_1 f_4 i}{i+q+1} + \frac{f_1 f_5 i}{i+q+2} - \frac{f_2 f_3 (i+1)}{i+q+1} + 2 \frac{f_2 f_4 (i+1)}{i+q+2} - \frac{f_2 f_5 (i+1)}{i+q+3} \right) \right. \\
 & + s_3 a^{(i+q+1)} \left(\frac{f_1 f_3 i q (q-1)}{i+q-2} - \frac{2f_1 f_4 i q (q+1)}{i+q-1} + \frac{f_1 f_5 i (q+2)(q+1)}{q+i} - \frac{f_3 f_2 q (i+1)(q-1)}{q+i-1} \right. \\
 & \left. \left. + \frac{2f_2 f_4 q (i+1)(q+1)}{q+1} - \frac{f_2 f_5 (q+2)(i+1)(q+1)}{q+i+1} \right) \right) \\
 & + \sum_{l=l_0}^L \frac{\gamma_l}{2} \left(s_4 a^{(l+q+3)} \left(\frac{f_3^2 l (l-1)}{q+l-1} - \frac{2f_3 f_4 l (l+1)}{q+l} + \frac{f_3 f_5 (l+2)(l+1)}{l+q+1} \right. \right. \\
 & \left. \left. - \frac{2f_3 f_4 l (l-1)}{l+q} + \frac{4f_4^2 l (l+1)}{q+l+1} - \frac{2f_4 f_5 (l+2)(l+1)}{q+l+2} \right. \right. \\
 & \left. \left. + \frac{f_3 f_5 l (l-1)}{q+l+1} - \frac{2f_4 f_5 (l+1)l}{q+l+2} + \frac{f_5^2 (l+2)(l+1)}{q+l+3} \right. \right. \\
 & \left. \left. + \frac{f_3^2 q (q-1)}{q+l-1} - \frac{2f_3 f_4 q (q+1)}{q+l} + \frac{f_3 f_5 (q+2)(q+1)}{l+q+1} \right. \right. \\
 & \left. \left. - \frac{2f_3 f_4 q (q-1)}{q+l} + \frac{4f_4^2 q (q+1)}{q+l+1} - \frac{2f_4 f_5 (q+2)(q+1)}{q+l+2} \right) \right)
 \end{aligned}$$

$$\begin{aligned}
& + \frac{f_3 f_5 q(q-1)}{q+l+1} - \frac{2f_4 f_5 (q+1)l}{q+l+2} + \frac{f_5^2 (q+2)(q+1)}{q+l+3} \Bigg) \\
& + 2s_5 a^{(l+q+1)} \left(\frac{f_3^2 q(q-1)l(l-1)}{q+l-3} - \frac{2f_3 f_4 q(q+1)l(l-1)}{q+l-2} \right. \\
& + \frac{f_3 f_5 l(l-1)(q+2)(q+1)}{l+q-1} - \frac{2f_3 f_4 q(q-1)l(l+1)}{l+q-2} + \frac{4f_4^2 q(q+1)l(l+1)}{q+l-1} \\
& - \frac{2f_4 f_5 q(q+1)(q+2)l(l+1)}{q+l} + \frac{f_3 f_5 q(q-1)(l+2)(l+1)}{q+l-1} \\
& \left. - \frac{2f_4 f_5 q(q+1)(l+1)(l+2)}{q+l} + \frac{f_5^2 (q+1)(q+2)(l+1)(l+2)}{q+l+1} \right) \\
& + 2s_6 a^{(l+q+5)} \left(\frac{f_3^2}{q+l+1} - \frac{4f_3 f_4}{q+l+2} + \frac{2f_3 f_5}{q+l+3} + \frac{4f_4^2}{q+l+3} - \frac{4f_4 f_5}{q+l+4} \right. \\
& + \frac{f_5^2}{q+l+5} \Bigg) - 2\omega^2 I_1 a^{(l+q+5)} \left(\frac{f_3^2}{q+l+1} - \frac{4f_4 f_5}{q+l+2} + \frac{2f_3 f_5}{q+l+3} \right. \\
& \left. \left. + \frac{4f_4^2}{q+l+3} - \frac{4f_4 f_5}{q+l+4} + \frac{f_5^2}{q+l+5} \right) \right)
\end{aligned} \tag{4.55}$$

where

$$\begin{aligned}
s_1 &= A_{11} + \frac{2B_{11}}{R} + \frac{D_{11}}{R^2}, \quad s_2 = \frac{2A_{11}}{R} + \frac{2B_{11}}{R^2} \\
s_3 &= -\frac{2D_{11}}{R} - 2B_{11}, \quad s_4 = -\frac{2B_{11}}{R} \\
s_5 &= D_{11}, \quad s_6 = \frac{A_{11}}{R^2}
\end{aligned} \tag{4.56}$$

The above equations can be described by

$$(K - \Omega^2 M)A = 0 \tag{4.57}$$

where K and M are the stiffness and mass matrices, respectively; Ω is the frequency parameter, and A is the vector of unknown coefficients.

The determinant of the coefficient matrix is set equal to zero which will yield a set of eigenvalues. Substituting each eigenvalue back into Eqs. (4.50) and (4.51) yields the corresponding eigenvector (amplitude ratios). The mode shape corresponding to each frequency can be determined by substituting the eigenvector back into Eqs. (4.50) and (4.51).

4.4.3 Convergence studies

Table 4.5 shows convergence studies made for the first six frequency parameters of laminated curved beams with a typical curvature ratio (a/R) of 0.5 and various orthotropy ratios for S1 and S2 boundary conditions at both edges. The ratio a/h is held constant at 100 and two orthotropy ratios are used. Table 4.6 shows a similar convergence study for C1 and C2 boundary conditions. The first row shows results obtained by using six terms in both the U and W functions. This yields a total of $2 \times 6 = 12$ DOF.

The convergence studies start with $2 \times 6 = 12$ terms. The frequency parameters obtained using these terms are good for the first three and not as good for the last three in

Table 4.5. Convergence of the frequency parameters $\Omega = \omega a^2 \sqrt{12I_1/E_{11}h^2}$ for simply supported $[0^\circ, 90^\circ]$ laminated curved beam, $a/R = 0.5$, $a/h = 100$.

DOF	$m = 1$	$m = 2$	$m = 3$	$m = 4$	$m = 5$	$m = 6$
<i>S1 boundary conditions, $E_1/E_2 = 1$ (i.e., single layer)</i>						
2×6	9.5004	40.982	93.003	215.81	523.25	869.78
2×7	9.5003	39.116	92.911	167.76	304.65	868.46
2×8	9.5000	39.116	88.531	164.82	270.11	430.04
2×9	9.5000	39.105	88.527	157.91	256.49	406.57
2×10	9.5000	39.105	88.452	157.79	247.77	368.90
2×11	9.5000	39.105	88.452	157.54	246.96	359.41
<i>$E_1/E_2 = 15$</i>						
2×6	4.5177	19.365	45.859	155.77	258.14	529.58
2×7	4.5174	18.604	44.578	81.859	231.48	418.65
2×8	4.5173	18.598	42.121	81.203	130.60	326.60
2×9	4.5173	18.593	42.097	75.150	130.58	195.28
2×10	4.5173	18.593	42.050	75.119	117.93	194.45
2×11	4.5173	18.593	42.050	74.884	117.92	194.40
<i>S2 boundary conditions, $E_1/E_2 = 1$ (i.e., single layer)</i>						
2×6	38.871	83.269	167.448	168.07	509.64	865.70
2×7	38.861	82.334	163.895	165.58	273.72	856.14
2×8	38.860	82.296	157.651	165.45	270.22	406.09
2×9	38.860	82.284	157.497	165.25	251.26	402.71
2×10	38.860	82.284	157.292	165.25	250.97	359.11
2×11	38.860	82.283	157.290	165.25	249.83	358.67
<i>$E_1/E_2 = 15$</i>						
2×6	18.445	38.332	81.389	116.14	273.16	396.87
2×7	18.434	37.974	77.631	103.68	157.91	386.67
2×8	18.434	37.940	74.809	102.25	155.00	193.68
2×9	18.434	37.935	74.645	100.08	144.55	190.00
2×10	18.434	37.935	74.551	99.985	144.17	170.16
2×11	18.434	37.935	74.549	99.888	143.10	169.68

Table 4.6. Convergence of the frequency parameters $\Omega = \omega a^2 \sqrt{12I_1/E_{11}h^2}$ for clamped $[0^\circ, 90^\circ]$ laminated curved beams arch, $a/R = 0.2$, $a/h = 100$

DOF	$m = 1$	$m = 2$	$m = 3$	$m = 4$	$m = 5$	$m = 6$
<i>C1 boundary conditions $E_1/E_2 = 1$ (i.e., single layer)</i>						
2×6	21.976	70.713	134.05	254.86	383.38	551.70
2×7	21.976	61.401	133.98	215.97	341.87	550.87
2×8	21.967	61.400	120.89	215.82	318.18	456.75
2×9	21.967	61.300	120.89	200.41	315.93	443.95
2×10	21.967	61.300	120.51	200.40	299.96	436.27
2×11	21.967	61.299	120.51	199.50	299.91	420.06
<i>$E_1/E_2 = 15$</i>						
2×6	10.449	33.262	66.208	243.233	335.78	464.84
2×7	10.449	29.200	66.200	112.473	312.84	446.17
2×8	10.445	29.200	57.588	112.470	173.96	393.14
2×9	10.445	29.145	57.588	95.882	173.93	252.84
2×10	10.445	29.145	57.291	95.882	144.65	252.57
2×11	10.445	29.145	57.291	94.837	144.65	244.85
<i>C2 boundary conditions $E_1/E_2 = 1$ (i.e., single layer)</i>						
2×6	61.124	103.12	169.22	215.52	363.12	549.70
2×7	61.025	103.10	168.97	200.81	321.78	535.05
2×8	61.025	102.96	168.41	200.02	307.39	443.36
2×9	61.025	102.96	168.40	199.14	303.68	430.01
2×10	61.025	102.96	168.39	199.12	302.07	420.95
2×11	61.025	102.96	168.39	199.10	301.96	417.32
<i>$E_1/E_2 = 15$</i>						
2×6	29.069	51.552	112.18	114.26	180.60	445.51
2×7	29.016	51.506	95.736	114.21	180.10	257.36
2×8	29.015	51.350	95.697	111.84	152.19	252.40
2×9	29.015	51.350	94.664	111.83	152.18	204.85
2×10	29.015	51.348	94.663	111.64	149.21	204.60
2×11	29.015	51.348	94.637	111.64	149.21	198.58

the cases of S1 and C1 supports. Better convergence is observed for S2 and C2 supports. The number of terms is increased in both α and z directions until 2×11 terms are reached. The convergence is fairly good, and the frequencies converged to the first three significant figures in almost all the parameters presented in these results (except for the sixth frequency). The maximum difference between the 20 and 22-term solutions is less than 1.0% in all the cases (except for the sixth frequency). From the above analysis it is observed that convergence is achieved with $2 \times 10 = 20$ terms for all the results. Subsequently, 20 terms will be used in the following analysis. Only the first five frequency parameters will be reported.

4.4.4 Numerical results

Table 4.7 shows the effect of curvature upon the first five frequency parameters obtained for the S1 type of simply supported arches. The curvature ratios included in the study are 0.01, 0.05, 0.1, 0.2, 0.5, 0.8, 1.0, 2.0 and π . The opening angle θ of the curved beam in radians is the curvature ratio (a/R). This means that the curvature ratio of 2.0 corresponds with an opening angle of 114.6° . The last curvature ratio of π , corresponds to curved beam which is half the closed circle (i.e., $\theta = 180^\circ$). Tables 4.8–4.10 show similar studies for the S2, C1 and C2 boundary conditions, respectively.

The first important observation is the effect of the constraint on the tangential displacement. Increasing the curvature slightly has very limited effects for curved beams with no constraints on the in-plane displacement (i.e., S1 and C1 boundaries). The effect starts to be large when these beams become deep in curvature ($a/R > 1$).

When the constraint on the tangential displacement (u) is introduced (i.e., S2 and C2 boundaries), curvature effects become very large. Very slight curvature or deviation from

Table 4.7. Curvature effects on the frequency parameters $\Omega = \omega a^2 \sqrt{12I_1/E_{11}h^2}$ for simply supported $[0^\circ, 90^\circ]$ laminated curved beams, $a/h = 100$; S1 boundary conditions.

a/R	$m = 1$	$m = 2$	$m = 3$	$m = 4$	$m = 5$
$E_1/E_2 = 1$ (i.e., single layer)					
–	9.8696	39.478	88.827	157.92	247.86
0.01	9.8695	39.478	88.826	157.92	247.86
0.05	9.8659	39.475	88.823	157.92	247.86
0.10	9.8546	39.463	88.812	157.91	247.86
0.20	9.8097	39.418	88.767	157.90	247.85
0.50	9.5000	39.105	88.452	157.79	247.77
0.80	8.9441	38.527	87.870	157.52	247.63
1.00	8.4517	38.000	87.336	157.21	247.48
2.00	4.9512	33.805	82.978	153.76	245.73
π	–	26.480	74.904	146.06	240.74
$E_1/E_2 = 15$					
–	4.7031	18.811	42.320	75.283	118.05
0.01	4.7028	18.810	42.318	75.283	118.04
0.05	4.7003	18.805	42.309	75.280	118.02
0.10	4.6939	18.796	42.294	75.274	118.00
0.20	4.6705	18.766	42.254	75.255	117.96
0.50	4.5173	18.593	42.050	75.119	117.93
0.80	4.2481	18.295	41.720	74.856	117.95
1.00	4.0115	18.030	41.432	74.608	117.98
2.00	2.3449	15.982	39.210	72.531	117.60
π	–	12.482	35.258	68.616	115.10

Table 4.8. Curvature effects on the frequency parameters $\Omega = \omega a^2 \sqrt{12I_1/E_{11}h^2}$ for simply supported $[0^\circ, 90^\circ]$ laminated curved beam, $a/h = 100$; S2 boundary conditions.

a/R	$m = 1$	$m = 2$	$m = 3$	$m = 4$	$m = 5$
$E_1/E_2 = 1$ (i.e., single layer)					
–	9.8696	39.478	88.827	157.92	247.86
0.01	10.351	39.478	88.832	157.92	247.86
0.05	18.430	39.472	88.979	157.91	247.87
0.10	32.467	39.453	89.501	157.89	247.92
0.20	39.378	60.147	93.095	157.82	248.13
0.50	38.860	82.284	157.29	165.25	250.97
0.80	37.925	82.627	156.34	229.93	283.00
1.00	37.092	82.184	155.48	237.09	340.00
2.00	31.058	77.298	148.91	235.50	355.68
π	22.367	68.288	137.92	225.81	349.87
$E_1/E_2 = 15$					
–	6.4291	18.807	44.533	75.166	120.44
0.01	7.9180	18.806	44.781	75.160	120.53
0.05	14.722	18.796	46.079	75.131	120.93
0.10	18.779	22.703	48.751	75.089	121.54
0.20	18.727	32.625	59.743	74.988	123.36
0.50	18.434	37.935	74.551	99.985	144.17
0.80	17.948	38.389	73.925	109.50	169.95
1.00	17.529	38.288	73.410	110.82	169.84
2.00	14.602	36.125	69.880	109.93	169.13
π	10.493	31.874	64.415	105.17	166.52

straightness for these beams results in noticeable increase in the frequency parameters. This deviation can be as small as the thickness of the beam to show this effect. Increasing the curvature ratio from 0 (i.e., straight beam) to 0.5 (i.e., moderately deep curved beam) more than tripled the fundamental frequency for S2 supports and more than doubled it for C2 ones. This is shown in Figure 4.5.

The first natural frequencies correspond to the first symmetric mode. The second frequency corresponds to the first antisymmetric mode. The effect of curvature is very large for the symmetric modes. For these modes, the normal force (N) develops fast as the curvature increases when constraints are imposed to the normal displacement. This normal force is tensile, and so its effect is to increase the frequencies. For the second frequency, which corresponds to the first antisymmetric mode, the effect of curvature is limited. This is also true for the other symmetric and antisymmetric modes.

As the curvature increases, the rapid increase in the frequencies corresponding to the symmetric modes make them exceed the frequencies corresponding to the antisymmetric modes. For single layer beams with S2 boundaries, as the curvature ratio is changed from

Table 4.9. Curvature effects on the frequency parameters $\Omega = \omega a^2 \sqrt{12I_1/E_{11}h^2}$ for clamped $[0^\circ, 90^\circ]$ laminated curved beam, $a/h = 100$; C1 boundary conditions.

a/R	$m = 1$	$m = 2$	$m = 3$	$m = 4$	$m = 5$
<i>$E_1/E_2 = 1$ (i.e., single layer)</i>					
–	22.373	61.673	120.90	199.86	298.75
0.01	22.373	61.677	120.90	199.86	298.74
0.05	22.369	61.669	120.90	199.87	298.76
0.10	22.357	61.658	120.89	199.89	298.80
0.20	22.307	61.613	120.84	199.96	298.95
0.50	21.967	61.300	120.51	200.40	299.96
0.80	21.362	60.724	119.90	200.93	301.51
1.00	20.833	60.199	119.35	201.17	302.64
2.00	17.303	56.068	114.87	199.95	306.18
π	13.358	49.077	106.79	194.01	303.25
<i>$E_1/E_2 = 15$</i>					
–	10.661	29.386	57.601	95.567	143.58
0.01	10.660	29.385	57.599	95.576	143.61
0.05	10.657	29.378	57.587	95.611	143.70
0.10	10.649	29.366	57.569	95.653	143.82
0.20	10.621	29.332	57.522	95.731	144.05
0.50	10.445	29.145	57.291	95.882	144.65
0.80	10.146	28.835	56.928	95.881	145.07
1.00	9.8882	28.562	56.616	95.789	145.23
2.00	8.1941	26.505	54.275	94.248	144.72
π	6.3218	23.130	50.264	90.249	141.92

0.10 to 0.20, the frequency corresponding to the first symmetric mode changes from being the fundamental frequency to being the second frequency. Similar observations can be made for the second and third symmetric modes (the third and fifth frequencies), which, as the curvature ratio increases, become higher frequencies. They change at higher values of curvature because for these higher modes, the curved beam is divided into sections, each of which is shallower than the original arch (per each half sine wave).

This mode overlapping phenomenon happens earlier for $[0^\circ, 90^\circ]$ laminates with 15 orthotropy ratio. The first frequency becomes the second one as the curvature changes from 0.05 to 0.10. Similar observations are made for beams with C2 boundaries. For these boundaries, this mode overlapping occurs at higher curvature ratio.

The natural frequencies tend to reach a maximum value as a/R increases for supports with constraints on the normal displacement (i.e., S2 and C2). The maximum fundamental frequency parameter was obtained when $a/R = 0.1$ for S2 boundary condition and it is 0.3 for C2 boundary condition. For higher frequency parameters, the maximum values are

Table 4.10. Curvature effects on the frequency parameters $\Omega = \omega a^2 \sqrt{12I_1/E_{11}h^2}$ for clamped $[0^\circ, 90^\circ]$ laminated curved beam, $a/h = 100$; C2 boundary conditions.

a/R	$m = 1$	$m = 2$	$m = 3$	$m = 4$	$m = 5$
$E_1/E_2 = 1$ (i.e., single layer)					
–	22.373	61.673	120.90	199.86	298.74
0.01	22.558	61.673	120.91	199.86	298.74
0.05	26.589	61.666	121.07	199.85	298.77
0.10	36.306	61.647	121.58	199.83	298.84
0.20	60.164	61.568	124.16	199.74	299.13
0.50	61.025	102.96	168.39	199.12	302.07
0.80	60.040	107.57	197.99	241.26	316.50
1.00	59.159	107.85	196.98	268.54	349.40
2.00	52.691	103.87	189.29	280.19	428.09
π	43.258	95.119	176.46	271.24	417.50
$E_1/E_2 = 15$					
–	10.661	29.386	57.601	95.208	142.27
0.01	10.866	29.384	57.606	95.204	142.27
0.05	14.941	29.376	57.777	95.185	142.27
0.10	23.265	29.361	58.411	95.155	142.33
0.20	29.311	39.735	62.683	95.074	142.67
0.50	29.015	51.348	94.663	111.64	149.21
0.80	28.513	51.741	94.011	132.79	193.62
1.00	28.074	51.558	93.451	134.45	205.54
2.00	24.936	49.179	89.422	133.17	202.31
π	20.441	44.834	82.723	128.09	173.12

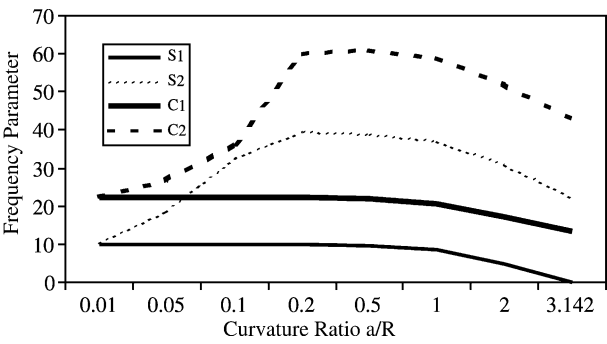


Figure 4.5. Curvature effects on the frequency parameters $\Omega = \omega a^2 \sqrt{12I_1/E_{11}h^2}$ for various boundaries of a curved beam, $a/h = 100$; $E_1/E_2 = 1$.

obtained for higher a/R ratios. It should be mentioned that as the opening angle reaches 180° , the fundamental frequency becomes 0 which represents a rigid body mode.

In conclusion, vibration of laminated thin and thick composite curved beams is studied in this chapter. It is shown that exact solutions are possible. Alternatively, the Ritz method is used to obtain accurate numerical frequencies for arbitrary boundary conditions using CBT. The effects of curvature, in-plane constraints on the frequency parameters are clearly outlined. A similar analysis can be performed for thick curved beams. The material of this section is used as an introduction to the analysis of shells, which will be the subject of later chapters.

Chapter 5

Plates

Plates can be defined as shells with zero curvature, or infinite radii of curvature. If slight curvature exists, the plates can be referred to as “curved plates” or “shallow shells”. More often, these plates are referred to as shallow shells. These shells will be the subject of Chapter 6. There is no need for the term “flat plates”, as all plates are flat. As was indicated earlier, the first accurate equations for plates appeared in the early 19th century. These equations described homogeneous plates. Laminated plates were treated by the middle of the 20th century (Lekhnitski 1957).

Laminated plates were the subject of various studies and books. Hearmon (1946) presented what could be the first study on composite plates. He obtained the fundamental frequency of vibration of rectangular wood and ply-wood plates in a closed form. Ambartsumian (1970) and Ashton and Whitney (1970) presented fundamental equations of laminated plates. Whitney (1987) presented various structural analyses, including free vibrations, of laminated anisotropic plates. The subject was also picked up by Mohan and Kingsbury (1971) as well as Noor (1973) among the many researchers in the field.

In this chapter, the previously derived equations for shells will be specialized to those for plates by setting the curvatures to zero (i.e., setting the radii of curvature to infinity). We will begin with the fundamental equations of thin plates, followed by those for moderately thick plates. Vibrations of rectangular, triangular, trapezoidal and circular plates will then be treated in the later sections of this chapter.

5.1. FUNDAMENTAL EQUATIONS OF THIN PLATES

There are some fundamental differences in the equations of laminated plates as they are compared with those obtained for homogeneous plates. The most important fundamental difference is that for generally laminated plates, the bending is coupled with stretching. This is of great importance, as the equations will be of order eight, just like shells, instead of the fourth order equations, which describe thin homogeneous plates. The equations will reduce to order four only if the lamination sequence is symmetric with respect to the plate’s middle surface. The inplane modes are then totally decoupled from the out-of-plane ones and often ignored in the analysis because they usually are of higher frequencies. The theory described here is referred to as classical plate theory (CPT).

5.1.1 Kinematic relations

Like shells, if the plate thickness is less than 1/20 of the wavelength of the deformation mode, a thin plate theory (also referred to as CPT), where shear deformation and rotary inertia are negligible, provides reasonable accurate results. Some researchers question the value of 1/20 and choose a smaller value. Unlike thin shells, where a variety of shell theories exist, thin plates have one theory that is agreed upon by most researchers.

For thin plates, like shells, the plate is thin enough such that the ratio of the thickness compared to any of the plate's width or length is negligible compared to unity; and the normals to the middle surface remain straight and normal to the surface when it undergoes deformation (Kirchoff's hypothesis). The latter of these assumptions allows for neglecting shear deformation in the kinematics equations. It allows for making the inplane displacement linearly varying through the plate's thickness:

$$\begin{aligned}\varepsilon_\alpha &= \varepsilon_{0\alpha} + z\kappa_\alpha \\ \varepsilon_\beta &= \varepsilon_{0\beta} + z\kappa_\beta \\ \gamma_{\alpha\beta} &= \gamma_{0\alpha\beta} + z\tau\end{aligned}\tag{5.1 (2.59)}$$

where the midsurface strains, curvature and twist changes are

$$\begin{aligned}\varepsilon_{0\alpha} &= \frac{1}{A} \frac{\partial u_0}{\partial \alpha} + \frac{v_0}{AB} \frac{\partial A}{\partial \beta} \\ \varepsilon_{0\beta} &= \frac{1}{B} \frac{\partial v_0}{\partial \beta} + \frac{u_0}{AB} \frac{\partial B}{\partial \alpha} \\ \gamma_{0\alpha\beta} &= \frac{1}{A} \frac{\partial v_0}{\partial \alpha} - \frac{u_0}{AB} \frac{\partial A}{\partial \beta} + \frac{1}{B} \frac{\partial u_0}{\partial \beta} - \frac{v_0}{AB} \frac{\partial B}{\partial \alpha}\end{aligned}\tag{5.2}$$

$$\begin{aligned}\kappa_\alpha &= \frac{1}{A} \frac{\partial \psi_\alpha}{\partial \alpha} + \frac{\psi_\beta}{AB} \frac{\partial A}{\partial \beta}, \quad \kappa_\beta = \frac{1}{B} \frac{\partial \psi_\beta}{\partial \beta} + \frac{\psi_\alpha}{AB} \frac{\partial B}{\partial \alpha} \\ \tau &= \frac{1}{A} \frac{\partial \psi_\beta}{\partial \alpha} - \frac{\psi_\alpha}{AB} \frac{\partial A}{\partial \beta} + \frac{1}{B} \frac{\partial \psi_\alpha}{\partial \beta} - \frac{\psi_\beta}{AB} \frac{\partial B}{\partial \alpha}\end{aligned}\tag{5.3}$$

where

$$\psi_\alpha = -\frac{1}{A} \frac{\partial w}{\partial \alpha}, \quad \psi_\beta = -\frac{1}{B} \frac{\partial w}{\partial \beta}\tag{5.4}$$

We will retain the Lamé parameters in the subsequent analysis. This is done to enable us develop equations for plates other than rectangular rather straightforwardly. Equations specialized for plates with rectangular orthotropy will be described later in this section.

5.1.2 Stress resultants

Like shells, for a laminated composite thin plate constructed with very thin layers of composite material laminae, the materials of each lamina may be regarded as being homogeneous and orthotropic. The fibers of a typical layer may not be parallel to the coordinates in which the equations are expressed and/or the boundaries. For plates treated here, the fibers will need to have a continuous constant angle with respect to the fibers in any other layer.

Applying the Kirchhoff hypothesis of neglecting shear deformation and the assumption that ε_z is negligible, then the stress–strain equations for an element of material in the k th lamina may be written as in Eq. (2.62). The stresses over the plate thickness (h) are integrated to obtain the force and moment resultants. Note that for plates, the inplane force resultants are equal (i.e., $N_{\alpha\beta} = N_{\beta\alpha}$), and so are the twisting moments (i.e., $M_{\alpha\beta} = M_{\beta\alpha}$). Thus, the force and moment resultants are the same as those derived for thin laminated shells (Eqs. (2.63)–(2.65)).

5.1.3 Equations of motion

One could specialize the differential elements considered earlier for shells (Eq. (2.71)) to those for plates. One could also develop a differential element for plates and derive the equations of motion using Newton's second law. Alternatively, Hamilton's principle can also be used. These methods will yield the following equations of motion for thin plates:

$$\begin{aligned} \frac{\partial}{\partial \alpha}(BN_\alpha) + \frac{\partial}{\partial \beta}(AN_{\beta\alpha}) + \frac{\partial A}{\partial \beta}N_{\alpha\beta} - \frac{\partial B}{\partial \alpha}N_\beta + ABq_\alpha &= AB(I_1\ddot{u}_0^2) \\ \frac{\partial}{\partial \beta}(AN_\beta) + \frac{\partial}{\partial \alpha}(BN_{\alpha\beta}) + \frac{\partial B}{\partial \alpha}N_{\beta\alpha} - \frac{\partial A}{\partial \beta}N_\alpha + ABq_\beta &= AB(I_1\ddot{v}_0^2) \\ \frac{\partial}{\partial \alpha}(BQ_\alpha) + \frac{\partial}{\partial \beta}(AQ_\beta) + ABq_n &= AB(I_1\ddot{w}_0^2) \end{aligned} \quad (5.5)$$

where

$$\begin{aligned} ABQ_\alpha &= \frac{\partial}{\partial \alpha}(BM_\alpha) + \frac{\partial}{\partial \beta}(AM_{\beta\alpha}) + \frac{\partial A}{\partial \beta}M_{\alpha\beta} - \frac{\partial B}{\partial \alpha}M_\beta \\ ABQ_\beta &= \frac{\partial}{\partial \beta}(AM_\beta) + \frac{\partial}{\partial \alpha}(BM_{\alpha\beta}) + \frac{\partial B}{\partial \alpha}M_{\beta\alpha} - \frac{\partial A}{\partial \beta}M_\alpha \end{aligned}$$

Again, the Lamé parameter terms A and B are maintained in the above equations to enable us treat various coordinate systems and plate configurations. Note that the last two expressions in the above equations are directly derived from the summation of moments in Newton's second law. Note also that the first two equations of motions are generally decoupled from the third bending equation. This shows that the absence of curvature

eliminated the coupling between the stretching and bending equations (unless unsymmetric lamination causes such coupling). The following boundary conditions can be obtained for thin plates; for $\alpha = \text{constant}$, either by specializing Eq. (2.72) or by means of Hamilton's principle:

$$\begin{aligned}
 N_{0\alpha} - N_{\alpha} &= 0 \quad \text{or} \quad u_0 = 0 \\
 (N_{0\alpha\beta}) - (N_{\alpha\beta}) &= 0 \quad \text{or} \quad v_0 = 0 \\
 \left(Q_{0\alpha} - \frac{1}{B} \frac{\partial M_{0\alpha\beta}}{\partial \beta} \right) - \left(Q_{\alpha} - \frac{1}{B} \frac{\partial M_{\alpha\beta}}{\partial \beta} \right) &= 0 \quad \text{or} \quad w_0 = 0 \\
 M_{0\alpha} - M_{\alpha} &= 0 \quad \text{or} \quad \psi_{\alpha} = 0 \\
 M_{0\alpha\beta} w|_{\beta_1}^{\beta_2} &= 0
 \end{aligned} \tag{5.6}$$

Similar equations can be obtained for $\beta = \text{constant}$. Note that the classification of these boundary conditions shown in Eqs. (2.61)–(2.63) for thin shells will be adopted here for plates.

5.1.4 Equations of thin plates with rectangular orthotropy

Unlike homogeneous plates, where the coordinates are chosen solely based on the plate shape, coordinates for laminated plates should be chosen carefully. There are two main factors for the choice of the coordinate system. The first is the shape of the plate. Meaning that rectangular plates will be best represented by the choice of rectangular (i.e., Cartesian) coordinates. It will be relatively easy to represent the boundaries of such plates with such coordinates. The second factor is the fiber orientation or orthotropy. If the fibers are set straight within each lamina, then rectangular orthotropy would result. It is possible to set the fibers in a radial and circular fashion, which would result in circular orthotropy. Indeed, the fibers can also be set in elliptical directions, which would result in elliptical orthotropy.

Having that in mind, the choice of the coordinate system is of critical importance for laminated plates. This is because plates with rectangular orthotropy can be setting on rectangular, triangular, circular or other boundaries. Composite materials with rectangular orthotropy are the most popular, mainly because of their ease in manufacturing. The equations that follow are developed for materials with rectangular orthotropy. The treatment of the plates having rectangular orthotropy and nonrectangular boundaries will be discussed later.

For a rectangular plate with the Cartesian coordinate system, the Lamé parameters are

$$A = B = 1 \tag{5.7}$$

Note that we will retain the α and β symbols in the following analysis. These coordinates are replaced by x and y in most texts. Midsurface strains and curvature changes are

$$\begin{aligned}\varepsilon_\alpha^0 &= \frac{\partial u_0}{\partial \alpha}, & \varepsilon_\beta^0 &= \frac{\partial v_0}{\partial \beta}, & \gamma_{\alpha\beta}^0 &= \frac{\partial v_0}{\partial \alpha} + \frac{\partial u_0}{\partial \beta} \\ k_\alpha &= -\frac{\partial^2 w_0}{\partial \alpha^2}, & k_\beta &= -\frac{\partial^2 w_0}{\partial \beta^2}, & \tau &= -2\frac{\partial^2 w_0}{\partial \alpha \partial \beta}\end{aligned}\quad (5.8)$$

The stress-strain equations for an element of material in the k th lamina are the same as those given by Eqs. (2.62). The stress resultant relation with the strain and curvature changes is written as in Eqs. (2.63) and (2.64), and the stiffness coefficients are those of Eq. (2.65).

Deleting the body couples, the reduced equations of motion from Eq. (5.5) become

$$\begin{aligned}\frac{\partial N_\alpha}{\partial \alpha} + \frac{\partial N_{\alpha\beta}}{\partial \beta} + p_\alpha &= I_1 \frac{\partial^2 u_0}{\partial t^2} \\ \frac{\partial N_\beta}{\partial \beta} + \frac{\partial N_{\alpha\beta}}{\partial \alpha} + p_\beta &= I_1 \frac{\partial^2 v_0}{\partial t^2} \\ \frac{\partial^2 M_\alpha}{\partial \alpha^2} + 2\frac{\partial^2 M_{\alpha\beta}}{\partial \beta \partial \alpha} + \frac{\partial^2 M_\beta}{\partial \beta^2} + p_n &= I_1 \frac{\partial^2 w_0}{\partial t^2}\end{aligned}\quad (5.9)$$

Substituting Eqs. (2.64) and Eq. (5.8) in Eq. (5.9), and multiplying the last equation by -1 , yields

$$\begin{bmatrix} L_{11} & L_{12} & L_{13} \\ L_{21} & L_{22} & L_{23} \\ L_{31} & L_{32} & L_{33} \end{bmatrix} \begin{bmatrix} u_0 \\ v_0 \\ w_0 \end{bmatrix} + \begin{bmatrix} -I_1 & 0 & 0 \\ 0 & -I_1 & 0 \\ 0 & 0 & I_1 \end{bmatrix} \frac{\partial^2}{\partial t^2} \begin{bmatrix} u_0 \\ v_0 \\ w_0 \end{bmatrix} = \begin{bmatrix} -p_\alpha \\ -p_\beta \\ p_n \end{bmatrix}\quad (5.10)$$

The L_{ij} coefficients of Eq. (5.10) (the equations of motion in terms of displacements) are

$$\begin{aligned}L_{11} &= A_{11} \frac{\partial^2}{\partial \alpha^2} + 2A_{16} \frac{\partial^2}{\partial \alpha \partial \beta} + A_{66} \frac{\partial^2}{\partial \beta^2} \\ L_{12} = L_{21} &= A_{16} \frac{\partial^2}{\partial \alpha^2} + \{A_{12} + A_{66}\} \frac{\partial^2}{\partial \alpha \partial \beta} + A_{26} \frac{\partial^2}{\partial \beta^2} \\ L_{22} &= A_{66} \frac{\partial^2}{\partial \alpha^2} + 2A_{26} \frac{\partial^2}{\partial \alpha \partial \beta} + A_{22} \frac{\partial^2}{\partial \beta^2} \\ L_{13} = L_{31} &= -B_{11} \frac{\partial^3}{\partial \alpha^3} - B_{26} \frac{\partial^3}{\partial \beta^3} - 3B_{16} \frac{\partial^3}{\partial \alpha^2 \partial \beta} - (B_{12} + 2B_{66}) \frac{\partial^3}{\partial \alpha \partial \beta^2} \\ L_{23} = L_{32} &= -B_{16} \frac{\partial^3}{\partial \alpha^3} - B_{22} \frac{\partial^3}{\partial \beta^3} - 3B_{26} \frac{\partial^3}{\partial \alpha \partial \beta^2} - (B_{12} + 2B_{66}) \frac{\partial^3}{\partial \alpha^2 \partial \beta}\end{aligned}$$

$$L_{33} = D_{11} \frac{\partial^4}{\partial \alpha^4} + 4D_{16} \frac{\partial^4}{\partial \alpha^3 \partial \beta} + 2(D_{12} + 2D_{66}) \frac{\partial^4}{\partial \alpha^2 \partial \beta^2} + 4D_{26} \frac{\partial^4}{\partial \alpha \partial \beta^3} + D_{22} \frac{\partial^4}{\partial \beta^4} \quad (5.11)$$

Note that the L_{13} and L_{23} terms are functions of the stiffness parameters B_{ij} . These parameters have zero values if the plate is symmetrically laminated. This leads to decoupling the inplane vibration from the out of plane vibration. The out of plane vibration for symmetrically laminated plate will then collapse to $L_{33}w_0 + I_1 \ddot{w}_0 = 0$. In addition, if the plate is made of cross-ply lamination, the terms D_{16} and D_{26} become zero which will reduce the equation to that of an orthotropic plate.

The above equations can be used to obtain exact solution, and it can also be used with approximate weighted residual methods like Galerkin's method. Energy functionals that are consistent with the above equations of motion can be written as

$$\begin{aligned} U &= \frac{1}{2} \int_A \{N_\alpha \varepsilon_{0\alpha} + N_\beta \varepsilon_{0\beta} + N_{\alpha\beta} \gamma_{0\alpha\beta} + M_\alpha \kappa_\alpha + M_\beta \kappa_\beta + M_{\alpha\beta} \tau\} dA \\ &= \frac{1}{2} \int_A \{[A_{11}(\varepsilon_{0\alpha})^2 + 2B_{11}\varepsilon_{0\alpha}\kappa_\alpha + D_{11}\kappa_\alpha^2] + [A_{22}(\varepsilon_{0\beta})^2 + 2B_{22}\varepsilon_{0\beta}\kappa_\beta + D_{22}\kappa_\beta^2] \\ &\quad + [A_{66}(\gamma_{0\alpha\beta})^2 + 2B_{66}\gamma_{0\alpha\beta}\tau + D_{66}\tau^2] + 2[A_{12}\varepsilon_{0\alpha}\varepsilon_{0\beta} + B_{12}(\varepsilon_{0\alpha}\kappa_\beta + \varepsilon_{0\beta}\kappa_\alpha) \\ &\quad + D_{12}\kappa_\alpha\kappa_\beta] + 2[A_{16}\varepsilon_{0\alpha}\gamma_{0\alpha\beta} + B_{16}(\varepsilon_{0\alpha}\tau + \gamma_{0\alpha\beta}\kappa_\alpha) + D_{16}\kappa_\alpha\tau] \\ &\quad + 2[A_{26}\varepsilon_{0\beta}\gamma_{0\alpha\beta} + B_{26}(\varepsilon_{0\beta}\tau + \gamma_{0\alpha\beta}\kappa_\beta) + D_{26}\kappa_\beta\tau]\} dA \end{aligned} \quad (5.12)$$

Substituting the strain- and curvature-displacement equations into the above equation yields the strain energy in terms of the displacements. This may be expressed as a sum of three parts:

$$U = U_s + U_b + U_{bs} \quad (5.13)$$

where U_s is the part due to stretching alone,

$$\begin{aligned} U_s &= \frac{1}{2} \int_A \left\{ A_{11} \left(\frac{\partial u_0}{\partial \alpha} \right)^2 + A_{22} \left(\frac{\partial v_0}{\partial \beta} \right)^2 + A_{66} \left(\frac{\partial v_0}{\partial \alpha} + \frac{\partial u_0}{\partial \beta} \right)^2 + 2A_{12} \left(\frac{\partial u_0}{\partial \alpha} \right) \left(\frac{\partial v_0}{\partial \beta} \right) \right. \\ &\quad \left. + 2A_{16} \left(\frac{\partial u_0}{\partial \alpha} \right) \left(\frac{\partial v_0}{\partial \alpha} + \frac{\partial u_0}{\partial \beta} \right) + 2A_{26} \left(\frac{\partial v_0}{\partial \beta} \right) \left(\frac{\partial v_0}{\partial \alpha} + \frac{\partial u_0}{\partial \beta} \right) \right\} dA \end{aligned} \quad (5.14)$$

U_b is the part due to bending alone,

$$\begin{aligned} U_b &= \frac{1}{2} \int_A \left\{ D_{11} \left(\frac{\partial^2 w_0}{\partial \alpha^2} \right)^2 + D_{22} \left(\frac{\partial^2 w_0}{\partial \beta^2} \right)^2 + 4D_{66} \left(\frac{\partial^2 w_0}{\partial \alpha \partial \beta} \right)^2 + 2D_{12} \left(\frac{\partial^2 w_0}{\partial \alpha^2} \right) \left(\frac{\partial^2 w_0}{\partial \beta^2} \right) \right. \\ &\quad \left. + 4D_{16} \left(\frac{\partial^2 w_0}{\partial \alpha^2} \right) \left(\frac{\partial^2 w_0}{\partial \alpha \partial \beta} \right) + 4D_{26} \left(\frac{\partial^2 w_0}{\partial \beta^2} \right) \left(\frac{\partial^2 w_0}{\partial \alpha \partial \beta} \right) \right\} dA \end{aligned} \quad (5.15)$$

and U_{bs} is the part due to bending–stretching coupling,

$$\begin{aligned}
 U_{bs} = - \int_A \left\{ B_{11} \left(\frac{\partial u_0}{\partial \alpha} \right) \left(\frac{\partial^2 w_0}{\partial \alpha^2} \right) + B_{22} \left(\frac{\partial v_0}{\partial \beta} \right) \left(\frac{\partial^2 w_0}{\partial \beta^2} \right) \right. \\
 + 2B_{66} \left(\frac{\partial v_0}{\partial \alpha} + \frac{\partial u_0}{\partial \beta} \right) \left(\frac{\partial^2 w_0}{\partial \alpha \partial \beta} \right) \\
 + B_{12} \left[\left(\frac{\partial u_0}{\partial \alpha} \right) \left(\frac{\partial^2 w_0}{\partial \beta^2} \right) + \left(\frac{\partial v_0}{\partial \beta} \right) \left(\frac{\partial^2 w_0}{\partial \alpha^2} \right) \right] \\
 + B_{16} \left[2 \left(\frac{\partial u_0}{\partial \alpha} \right) \left(\frac{\partial^2 w_0}{\partial \alpha \partial \beta} \right) + \left(\frac{\partial v_0}{\partial \alpha} + \frac{\partial u_0}{\partial \beta} \right) \left(\frac{\partial^2 w_0}{\partial \alpha^2} \right) \right] \\
 \left. + B_{26} \left[2 \left(\frac{\partial v_0}{\partial \beta} \right) \left(\frac{\partial^2 w_0}{\partial \alpha \partial \beta} \right) + \left(\frac{\partial v_0}{\partial \alpha} + \frac{\partial u_0}{\partial \beta} \right) \left(\frac{\partial^2 w_0}{\partial \beta^2} \right) \right] \right\} dA \quad (5.16)
 \end{aligned}$$

For symmetrically laminated plates, $B_{ij} = 0$ and, hence, $U_{bs} = 0$. This will result in the inplane deformation being decoupled from out-of-plane one. If one is interested in out-of-plane (or transverse) vibration only, the term U_b will be the only term needed. These functionals can be used for approximate energy methods like the Ritz and the Ritz-based finite element methods.

Using the distributed external force components p_α and p_β in the tangential directions and p_z in the normal direction, the work done by the external forces as the plate displaces is

$$W = \int_\alpha \int_\beta (p_\alpha u_0 + p_\beta v_0 + p_z w_0) d\alpha d\beta \quad (5.17)$$

Therefore, the total potential energy of the plate in its deformed shape is $\Pi = U - W$. The kinetic energy of the entire plate is then found to be (neglecting rotary inertia terms)

$$T = \sum_{k=1}^N T_k = \frac{I_1}{2} \int_A \left[\left(\frac{\partial u_0}{\partial t} \right)^2 + \left(\frac{\partial v_0}{\partial t} \right)^2 + \left(\frac{\partial w_0}{\partial t} \right)^2 \right] dA \quad (5.18)$$

where I_1 is the average mass density of the plate per unit area of the midsurface, as given by

$$I_1 = \sum_{k=1}^N \rho^{(k)} (z_k - z_{k-1}) \quad (5.19)$$

where $\rho^{(k)}$ is the density of the lamina (k) per unit volume, and t is time.

5.2. FUNDAMENTAL EQUATIONS OF THICK PLATES

Thick plates are ones with a thickness smaller by approximately one order of magnitude when compared with other plate parameters, particularly its vibration mode shape wavelength (thickness is smaller than $(1/10)$ th of the smallest of the wave lengths). Thick plate theories (also referred to as shear deformation plate theories, or SDPT) require the inclusion of shear deformation and rotary inertia factors when compared with thin or CPT. This section will present a consistent set of equations that can be used for thick composite plates.

Various thick plate theories can be introduced. The dissertations of Hanna (1990) and Alghothani (1986) offer a good treatment of various theories used for plates including those of Mindlin, Reissner, and Ambartsumian. Both Mindlin and Reissner theories have been extended for laminated plates. The treatment that follows is an extension of Mindlin's theory to laminated plates.

5.2.1 Kinematic relations

In thick plate theories, the midplane plate displacements are expanded in terms of its thickness. Such an expansion can be of a first or a higher order. In the case of first order expansion, the theories are referred to as first order shear deformation theories (Reddy 1984b). Thick plate theories still use the assumption that the normal strains acting on the plane parallel to the middle surface are negligible compared with other strain components. In other words, no stretching is assumed in the z direction (i.e., $\varepsilon_z = 0$). This assumption is generally valid except within the vicinity of a highly concentrated force.

From the equations derived for general plates and *assuming* that normals to the midsurface strains remain straight during deformation but not normal to the midsurface, the displacements are (Eq. (2.35))

$$u(\alpha, \beta, z) = u_0(\alpha, \beta) + z\psi_\alpha(\alpha, \beta)$$

$$v(\alpha, \beta, z) = v_0(\alpha, \beta) + z\psi_\beta(\alpha, \beta) \quad (5.20 \quad (2.35))$$

$$w(\alpha, \beta, z) = w_0(\alpha, \beta)$$

where u_0 , v_0 and w_0 are midsurface displacements of the plate and ψ_α and ψ_β are midsurface rotations. The above equations are the basis of a typical first order SDPT and will constitute the only assumption made in this development when compared with the three dimensional theory of elasticity. The equations for strains can be derived independently for plates or specialized from the general shell Eqs. (2.36) and (2.37) by setting the radii of curvature to be infinity. These equations become

$$\begin{aligned}
\varepsilon_\alpha &= (\varepsilon_{0\alpha} + z\kappa_\alpha) \\
\varepsilon_\beta &= (\varepsilon_{0\beta} + z\kappa_\beta) \\
\varepsilon_{\alpha\beta} &= (\varepsilon_{0\alpha\beta} + z\kappa_{\alpha\beta}) \\
\varepsilon_{\beta\alpha} &= (\varepsilon_{0\beta\alpha} + z\kappa_{\beta\alpha})
\end{aligned} \tag{5.21}$$

or

$$\gamma_{\alpha\beta} = \gamma_{0\alpha\beta} + z\tau, \quad \gamma_{\alpha\beta} = \varepsilon_{\alpha\beta} + \varepsilon_{\beta\alpha}, \quad \text{and} \quad \tau = \kappa_{\alpha\beta} + \kappa_{\beta\alpha}$$

$$\gamma_{\alpha z} = \gamma_{0\alpha z}$$

$$\gamma_{\beta z} = \gamma_{0\beta z}$$

Note that when the shear strains $\varepsilon_{\alpha\beta}$ and $\varepsilon_{\beta\alpha}$ are equal, the engineering shear strain $\gamma_{\alpha\beta}$ ($= \varepsilon_{\alpha\beta} + \varepsilon_{\beta\alpha}$) will be used. Similarly for the change of twist curvature expressions. The midsurface strains are

$$\begin{aligned}
\varepsilon_{0\alpha} &= \frac{1}{A} \frac{\partial u_0}{\partial \alpha} + \frac{v_0}{AB} \frac{\partial A}{\partial \beta}, \quad \varepsilon_{0\beta} = \frac{1}{B} \frac{\partial v_0}{\partial \beta} + \frac{u_0}{AB} \frac{\partial B}{\partial \alpha} \\
\gamma_{0\alpha\beta} &= \frac{1}{A} \frac{\partial v_0}{\partial \alpha} - \frac{u_0}{AB} \frac{\partial A}{\partial \beta} + \frac{1}{B} \frac{\partial u_0}{\partial \beta} - \frac{v_0}{AB} \frac{\partial B}{\partial \alpha} \\
\gamma_{0\alpha z} &= \frac{1}{A} \frac{\partial w_0}{\partial \alpha} + \psi_\alpha, \quad \gamma_{0\beta z} = \frac{1}{B} \frac{\partial w_0}{\partial \beta} + \psi_\beta
\end{aligned} \tag{5.22}$$

and the curvature and twist changes are

$$\begin{aligned}
\kappa_\alpha &= \frac{1}{A} \frac{\partial \psi_\alpha}{\partial \alpha} + \frac{\psi_\beta}{AB} \frac{\partial A}{\partial \beta}, \quad \kappa_\beta = \frac{1}{B} \frac{\partial \psi_\beta}{\partial \beta} + \frac{\psi_\alpha}{AB} \frac{\partial B}{\partial \alpha} \\
\tau &= \frac{1}{A} \frac{\partial \psi_\beta}{\partial \alpha} - \frac{\psi_\alpha}{AB} \frac{\partial A}{\partial \beta} + \frac{1}{B} \frac{\partial \psi_\alpha}{\partial \beta} - \frac{\psi_\beta}{AB} \frac{\partial B}{\partial \alpha}
\end{aligned} \tag{5.23 (2.38)}$$

The subscript (0) will refer to the middle surface in the subsequent equations.

5.2.2 Stress resultants

The force and moment resultants (Figures 2.3 and 2.4) are obtained by integrating the stresses over the plate thickness. The normal and shear force resultants are

$$\begin{bmatrix} N_\alpha \\ N_\beta \\ N_{\alpha\beta} \\ Q_\alpha \\ Q_\beta \end{bmatrix} = \int_{-h/2}^{h/2} \begin{bmatrix} \sigma_\alpha \\ \sigma_\beta \\ \sigma_{\alpha\beta} \\ \sigma_{\alpha z} \\ \sigma_{\beta z} \end{bmatrix} dz \tag{5.24}$$

The bending and twisting moment resultants are

$$\begin{bmatrix} M_\alpha \\ M_\beta \\ M_{\alpha\beta} \end{bmatrix} = \int_{-h/2}^{h/2} \begin{bmatrix} \sigma_\alpha \\ \sigma_\beta \\ \sigma_{\alpha\beta} \end{bmatrix} z \, dz \quad (5.25)$$

Note here that the higher order shear terms that were present for shells are not needed for plates. It should be mentioned that both the inplane shear stresses $\sigma_{\alpha\beta}$ and $\sigma_{\beta\alpha}$ are equal. Also, the stress resultants $N_{\alpha\beta}$ and $N_{\beta\alpha}$ are equal. Similarly for the twisting moment (i.e. $M_{\alpha\beta} = M_{\beta\alpha}$). Carrying out the integration over the thickness, from layer to layer, yields

$$\begin{bmatrix} N_\alpha \\ N_\beta \\ N_{\alpha\beta} \\ - \\ M_\alpha \\ M_\beta \\ M_{\alpha\beta} \end{bmatrix} = \begin{bmatrix} A_{11} & A_{12} & A_{16} & B_{11} & B_{12} & B_{16} \\ A_{12} & A_{22} & A_{26} & B_{12} & B_{22} & B_{26} \\ A_{16} & A_{26} & A_{66} & B_{16} & B_{26} & B_{66} \\ - & - & - & - & - & - \\ B_{11} & B_{12} & B_{16} & D_{11} & D_{12} & D_{16} \\ B_{12} & B_{22} & B_{26} & D_{12} & D_{22} & D_{26} \\ B_{16} & B_{26} & B_{66} & D_{16} & D_{26} & D_{66} \end{bmatrix} \begin{bmatrix} \varepsilon_{0\alpha} \\ \varepsilon_{0\beta} \\ \gamma_{0\alpha\beta} \\ - \\ \kappa_\alpha \\ \kappa_\beta \\ \tau \end{bmatrix} \quad (5.26)$$

$$\begin{bmatrix} Q_\alpha \\ Q_\beta \end{bmatrix} = \begin{bmatrix} A_{55} & A_{45} \\ A_{45} & A_{44} \end{bmatrix} \begin{bmatrix} \gamma_{0\alpha z} \\ \gamma_{0\beta z} \end{bmatrix} \quad (5.27)$$

where A_{ij} , B_{ij} and D_{ij} are defined as in Eq. (2.47) or (2.65).

5.2.3 Equations of motion

The equations for motion can be derived independently for plates or specialized from the general shell equations of motion (2.56) by setting the radii of curvature equal to infinity. The equations of motion are

$$\begin{aligned} \frac{\partial}{\partial \alpha}(BN_\alpha) + \frac{\partial}{\partial \beta}(AN_{\beta\alpha}) + \frac{\partial A}{\partial \beta}N_{\alpha\beta} - \frac{\partial B}{\partial \alpha}N_\beta + ABq_\alpha &= AB(I_1\ddot{u}_0^2 + I_2\ddot{\psi}_\alpha^2) \\ \frac{\partial}{\partial \beta}(AN_\beta) + \frac{\partial}{\partial \alpha}(BN_{\alpha\beta}) + \frac{\partial B}{\partial \alpha}N_{\beta\alpha} - \frac{\partial A}{\partial \beta}N_\alpha + ABq_\beta &= AB(I_1\ddot{v}_0^2 + I_2\ddot{\psi}_\beta^2) + \frac{\partial}{\partial \alpha}(BQ_\alpha) + \frac{\partial}{\partial \beta}(AQ_\beta) + ABq_n = AB(I_1\ddot{w}_0^2) \\ \frac{\partial}{\partial \alpha}(BM_\alpha) + \frac{\partial}{\partial \beta}(AM_{\beta\alpha}) + \frac{\partial A}{\partial \beta}M_{\alpha\beta} - \frac{\partial B}{\partial \alpha}M_\beta - ABQ_\alpha + ABm_\alpha &= AB(I_2\ddot{u}_0^2 + I_3\ddot{\psi}_\alpha^2) \\ \frac{\partial}{\partial \beta}(AM_\beta) + \frac{\partial}{\partial \alpha}(BM_{\alpha\beta}) + \frac{\partial B}{\partial \alpha}M_{\beta\alpha} - \frac{\partial A}{\partial \beta}M_\alpha - ABQ_{\beta\alpha} + ABm_\beta &= AB(I_2\ddot{v}_0^2 + I_3\ddot{\psi}_\beta^2) \end{aligned} \quad (5.28)$$

where the two dots represent the second derivative of these terms with respect to time, and where the inertia terms are defined in Eq. (2.55). The boundary terms for the boundaries with $\alpha = \text{constant}$ are given in Eq. (2.58). Possible combination of boundary conditions at each edge is given in Table 2.1.

5.2.4 Equations of thick plates with rectangular orthotropy

The equations that follow will be developed for materials with rectangular orthotropy. As argued earlier, such materials will be best represented with a rectangular coordinate system.

The middle surface strains and curvature changes for thick plates having constant Lamé parameters (and equal to unity, as in Eq. (5.7)) are

$$\begin{aligned}
 \varepsilon_{0\alpha} &= \frac{\partial u_0}{\partial \alpha}, & \varepsilon_{0\beta} &= \frac{\partial v_0}{\partial \beta}, & \varepsilon_{0\alpha\beta} &= \frac{\partial v_0}{\partial \alpha}, & \varepsilon_{0\beta\alpha} &= \frac{\partial u_0}{\partial \beta}, & \text{or} \\
 \gamma_{0\alpha\beta} &= \frac{\partial v_0}{\partial \alpha} + \frac{\partial u_0}{\partial \beta} \\
 \gamma_{0\alpha z} &= \frac{\partial w_0}{\partial \alpha} + \psi_\alpha, & \gamma_{0\beta z} &= \frac{\partial w_0}{\partial \beta} + \psi_\beta \\
 \kappa_\alpha &= \frac{\partial \psi_\alpha}{\partial \alpha}, & \kappa_\beta &= \frac{\partial \psi_\beta}{\partial \beta}, & \kappa_{\alpha\beta} &= \frac{\partial \psi_\beta}{\partial \alpha}, & \kappa_{\beta\alpha} &= \frac{\partial \psi_\alpha}{\partial \beta}
 \end{aligned} \tag{5.29}$$

The equations of motion are

$$\begin{aligned}
 \frac{\partial N_\alpha}{\partial \alpha} + \frac{\partial N_{\beta\alpha}}{\partial \beta} + q_\alpha &= (I_1 \ddot{u}_0 + I_2 \ddot{\psi}_\alpha^2) \\
 \frac{\partial N_\beta}{\partial \beta} + \frac{\partial N_{\alpha\beta}}{\partial \alpha} + q_\beta &= (I_1 \ddot{v}_0 + I_2 \ddot{\psi}_\beta^2) \\
 \frac{\partial Q_\alpha}{\partial \alpha} + \frac{\partial Q_\beta}{\partial \beta} + q_n &= (I_1 \ddot{w}_0^2) \\
 \frac{\partial M_\alpha}{\partial \alpha} + \frac{\partial M_{\beta\alpha}}{\partial \beta} - Q_\alpha + m_\alpha &= (I_2 \ddot{u}_0^2 + I_3 \ddot{\psi}_\alpha^2) \\
 \frac{\partial M_\beta}{\partial \beta} + \frac{\partial M_{\alpha\beta}}{\partial \alpha} - Q_\beta + m_\beta &= (I_2 \ddot{v}_0^2 + I_3 \ddot{\psi}_\beta^2)
 \end{aligned} \tag{5.30}$$

The equilibrium equations can be written in terms of displacements. These equations are proven useful when exact solutions are desired. The equations can be written as

$$L_{ij}u_i + M_{ij}\ddot{u}_i = q \tag{5.31}$$

The stiffness parameters L_{ij} in Eq. (5.31) are

$$\begin{aligned}
 L_{11} &= A_{11} \frac{\partial^2}{\partial \alpha^2} + 2A_{16} \frac{\partial^2}{\partial \alpha \partial \beta} + A_{66} \frac{\partial^2}{\partial \beta^2} \\
 L_{12} &= A_{16} \frac{\partial^2}{\partial \alpha^2} + (A_{12} + A_{66}) \frac{\partial^2}{\partial \alpha \partial \beta} + A_{26} \frac{\partial^2}{\partial \beta^2} \\
 L_{13} &= 0 \\
 L_{14} &= B_{11} \frac{\partial^2}{\partial \alpha^2} + 2B_{16} \frac{\partial^2}{\partial \alpha \partial \beta} + B_{66} \frac{\partial^2}{\partial \beta^2} \\
 L_{15} &= B_{16} \frac{\partial^2}{\partial \alpha^2} + (B_{12} + B_{66}) \frac{\partial^2}{\partial \alpha \partial \beta} + B_{26} \frac{\partial^2}{\partial \beta^2} \\
 L_{22} &= A_{66} \frac{\partial^2}{\partial \alpha^2} + 2A_{26} \frac{\partial^2}{\partial \alpha \partial \beta} + A_{22} \frac{\partial^2}{\partial \beta^2} \\
 L_{23} &= 0 \\
 L_{24} &= B_{16} \frac{\partial^2}{\partial \alpha^2} + (B_{12} + B_{66}) \frac{\partial^2}{\partial \alpha \partial \beta} + B_{26} \frac{\partial^2}{\partial \beta^2} \\
 L_{25} &= B_{66} \frac{\partial^2}{\partial \alpha^2} + 2B_{26} \frac{\partial^2}{\partial \alpha \partial \beta} + B_{22} \frac{\partial^2}{\partial \beta^2} \\
 L_{33} &= -A_{55} \frac{\partial^2}{\partial \alpha^2} - 2A_{45} \frac{\partial^2}{\partial \alpha \partial \beta} - A_{44} \frac{\partial^2}{\partial \beta^2} \\
 L_{34} &= -A_{55} \frac{\partial}{\partial \alpha} - A_{45} \frac{\partial}{\partial \beta} \\
 L_{35} &= -A_{45} \frac{\partial}{\partial \alpha} - A_{44} \frac{\partial}{\partial \beta} \\
 L_{44} &= -A_{55} + D_{11} \frac{\partial^2}{\partial \alpha^2} + 2D_{16} \frac{\partial^2}{\partial \alpha \partial \beta} + D_{66} \frac{\partial^2}{\partial \beta^2} \\
 L_{45} &= -A_{45} + D_{16} \frac{\partial^2}{\partial \alpha^2} + (D_{12} + D_{66}) \frac{\partial^2}{\partial \alpha \partial \beta} + D_{26} \frac{\partial^2}{\partial \beta^2} \\
 L_{55} &= -A_{44} + D_{66} \frac{\partial^2}{\partial \alpha^2} + 2D_{26} \frac{\partial^2}{\partial \alpha \partial \beta} + D_{22} \frac{\partial^2}{\partial \beta^2}
 \end{aligned} \tag{5.32}$$

The mass parameters in Eq. (5.31) are

$$\begin{aligned}
 M_{ji} &= M_{ij} \\
 M_{11} &= M_{22} = M_{33} = -I_1 \\
 M_{14} &= M_{25} = -I_2 \\
 M_{44} &= M_{55} = -I_3 \\
 \text{all other } M_{ij} &= 0
 \end{aligned} \tag{5.33}$$

where I_i are given in Eq. (2.55). The displacement and loading vectors are

$$u_i = [u_0, v_0, w_0, \psi_\alpha, \psi_\beta]^T, \quad q_i = [-q_\alpha, -q_\beta, -q_n, -m_\alpha, -m_\beta]^T \quad (5.34)$$

The above equation describes a thick plate with general lamination sequence. If the plate is symmetrically laminated, then all the B_{ij} terms vanish. This will make $L_{14} = L_{15} = L_{24} = L_{25} = 0$. The inplane displacements (u_0 and v_0) will then be decoupled from the out-of-plane displacement and shear deformation. This will reduce the equations and subsequent treatment significantly. Eq. (5.31) will include a 3×3 differential operator, for a symmetrically laminated thick plate, instead of the above 5×5 . The order of the whole system of differential equations will reduce from 10 to 6.

Eq. (2.58) represent the correct boundary conditions for thick plates. Energy functional can be derived easily from the above equations in a fashion similar to that done for thin plates.

5.3. VIBRATION OF RECTANGULAR PLATES

We will first consider rectangular plates constructed of composite materials having rectangular orthotropy. These plates are best represented with Cartesian coordinates. Figure 5.1 shows the parameters used in such a plate (dimensions a and b , and thickness h). Plates with circular orthotropy will be dealt with in later sections of this chapter.

Thin rectangular plates with symmetric lamination can have four possible boundary conditions at each edge. Three of these boundary conditions are classical. These are simply supported, clamped or free. The total possible combination of classical boundary conditions for such plates when they are isotropic is 21 (Leissa 1969). Symmetrically

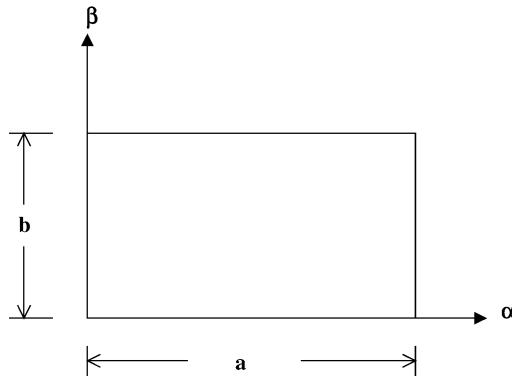


Figure 5.1. Parameters used for rectangular plates.

laminated plates, although they have three possible classical boundaries per edge, will yield even higher number of combinations of boundaries for all edges. This is because of the reduced symmetry in laminated plates as compared with isotropic ones.

Plates that are not symmetrically laminated will have 16 possible boundary conditions for each edge, with 12 of these being classical. This is because of the stretching–bending coupling that has to be considered for such plates. Symmetrically laminated thick plates can have six possible classical boundary conditions at each edge. Unsymmetrically laminated plates can have up to 24 classical possible boundary conditions at each edge (Table 2.1). The combinations of boundary conditions are higher for thick rectangular plates when compared with thin plates.

Among all the boundary combinations, only those that have two opposite edges simply supported permit having exact solutions (for homogeneous plates). The solution is referred to as the Levy solution (Leissa 1973b). When the Levy solution procedure is extended to laminated composite plates, it is found that such exact solution can only be applied to two types of lamination sequences and boundary conditions:

1. *Cross-ply plates with S2 opposite boundaries.* These are plates where the lamination angle for each layer makes either a 0 or 90° with each of the boundaries. In other words, the fibers in each layer can either be parallel or perpendicular to each boundary. These plates could be symmetrically laminated or unsymmetrically (i.e., asymmetrically) laminated about the middle surface. Figure 5.2 shows examples of such lamination sequence. Note that the lamination sequences made of layers having 45 and -45° angles (e.g., $[45^\circ, -45^\circ]$) or 30 and -60° or similar fiber angles for each lamina are *not* considered here as cross-ply because, although these plies make right angles with each other, they do not make right angle with the edges of the plate. Cross-ply plates can have exact solutions when the two simply supported opposite boundaries are of the S2 type (i.e., shear diaphragms).
2. *Antisymmetrically laminated plates.* These plates are constructed with laminates in which the fibers in each lamina above the middle surface making an angle θ with a coordinate is mirror-imaged with another one (of equal thickness) at exactly the same distance in the opposite z direction from the middle surface with fibers making negative the angle (i.e., $-\theta$) with the same coordinate. Figure 5.3 shows example of such lamination sequence. Antisymmetrically laminated plates can have exact solutions when the two opposite boundaries are of the S3 type.

Of particular importance and ease of use is the problem with all edges being simply supported. For these plates the rather lengthy Levy solution can be specialized into a simpler solution form called the Navier solution. This solution will be presented in the upcoming sections for both cross-ply and antisymmetric angle-ply plates. The solution procedure is applicable for both thin plates where CPT is used and moderately thick plates where SDPT is used.

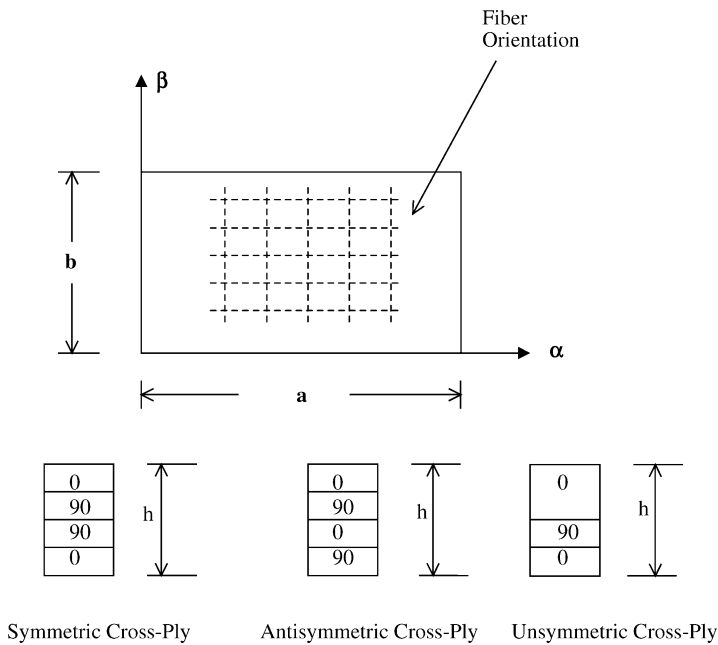


Figure 5.2. Plates with cross-ply lamination sequence.

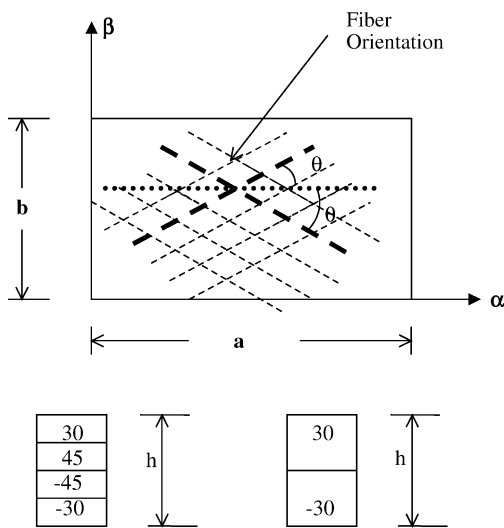


Figure 5.3. Plates with antisymmetric lamination sequence.

5.3.1 Simply supported cross-ply rectangular plates

We will first consider simply supported thin plates. Thick plates will be treated later.

5.3.1.1 Thin plates. Consider a plate that is made of a cross-ply laminate, thus

$$A_{16} = A_{26} = B_{16} = B_{26} = D_{16} = D_{26} = 0 \quad (5.35)$$

The differential parameters in the equations of motion (5.11) L_{ij} become

$$\begin{aligned} L_{11} &= A_{11} \frac{\partial^2}{\partial \alpha^2} + A_{66} \frac{\partial^2}{\partial \beta^2} \\ L_{12} &= L_{21} = (A_{12} + A_{66}) \frac{\partial^2}{\partial \alpha \partial \beta} \\ L_{22} &= A_{66} \frac{\partial^2}{\partial \alpha^2} + A_{22} \frac{\partial^2}{\partial \beta^2} \\ L_{13} &= L_{31} = -B_{11} \frac{\partial^3}{\partial \alpha^3} - (B_{12} + 2B_{66}) \frac{\partial^3}{\partial \alpha \partial \beta^2} \\ L_{23} &= L_{32} = -B_{22} \frac{\partial^3}{\partial \beta^3} - (B_{12} + 2B_{66}) \frac{\partial^3}{\partial \alpha^2 \partial \beta} \\ L_{33} &= D_{11} \frac{\partial^4}{\partial \alpha^4} + 2(D_{12} + 2D_{66}) \frac{\partial^4}{\partial \alpha^2 \partial \beta^2} + D_{22} \frac{\partial^4}{\partial \beta^4} \end{aligned} \quad (5.36)$$

Consider a plate with shear diaphragm (S2) boundaries on all four edges. That is, the following boundary conditions apply:

$$\begin{aligned} N_\alpha &= w_0 = v_0 = M_\alpha = 0 && \text{for the edges } \alpha = 0, a \\ N_\beta &= w_0 = u_0 = M_\beta = 0 && \text{for the edges } \beta = 0, b \end{aligned} \quad (5.37)$$

The following solution satisfies the boundary conditions and the equations of motion:

$$\begin{aligned} u_0(\alpha, \beta, t) &= \sum_{m=0}^M \sum_{n=0}^N U_{mn} \cos(\alpha_m \alpha) \sin(\beta_n \beta) \sin(\omega_{mn} t) \\ v_0(\alpha, \beta, t) &= \sum_{m=0}^M \sum_{n=0}^N V_{mn} \sin(\alpha_m \alpha) \cos(\beta_n \beta) \sin(\omega_{mn} t) \\ w_0(\alpha, \beta, t) &= \sum_{m=0}^M \sum_{n=0}^N W_{mn} \sin(\alpha_m \alpha) \sin(\beta_n \beta) \sin(\omega_{mn} t) \end{aligned} \quad (5.38)$$

where

$$\alpha_m = \frac{m\pi}{a}, \quad \beta_n = \frac{n\pi}{b}$$

ω_{mn} is the natural frequency.

Also, the external forces can be expanded in a Fourier series,

$$\begin{aligned}
 p_\alpha(\alpha, \beta) &= \sum_{m=0}^M \sum_{n=0}^N p_{\alpha mn} \cos(\alpha_m \alpha) \sin(\beta_n \beta) \\
 p_\beta(\alpha, \beta) &= \sum_{m=0}^M \sum_{n=0}^N p_{\beta mn} \sin(\alpha_m \alpha) \cos(\beta_n \beta) \\
 p_z(\alpha, \beta) &= \sum_{m=0}^M \sum_{n=0}^N p_{zmn} \sin(\alpha_m \alpha) \sin(\beta_n \beta)
 \end{aligned} \tag{5.39}$$

where

$$\begin{aligned}
 p_{\alpha mn} &= \frac{4}{ab} \int P_\alpha \cos(\alpha_m \alpha) \sin(\beta_n \beta) d\alpha d\beta \\
 p_{\beta mn} &= \frac{4}{ab} \int P_\beta \sin(\alpha_m \alpha) \cos(\beta_n \beta) d\alpha d\beta \\
 p_{zmn} &= \frac{4}{ab} \int P_z \sin(\alpha_m \alpha) \sin(\beta_n \beta) d\alpha d\beta
 \end{aligned}$$

Substituting Eq. (5.38) into Eq. (5.11), with the differential operator given in Eq. (5.36), yields the following equations of motion:

$$\begin{bmatrix} C_{11} & C_{12} & C_{13} \\ C_{21} & C_{22} & C_{23} \\ C_{31} & C_{32} & C_{33} \end{bmatrix} \begin{bmatrix} U_{mn} \\ V_{mn} \\ W_{mn} \end{bmatrix} + \omega_{mn}^2 \begin{bmatrix} I_1 & 0 & 0 \\ 0 & I_1 & 0 \\ 0 & 0 & -I_1 \end{bmatrix} \begin{bmatrix} U_{mn} \\ V_{mn} \\ W_{mn} \end{bmatrix} = \begin{bmatrix} -p_{\alpha mn} \\ -p_{\beta mn} \\ p_{zmn} \end{bmatrix} \tag{5.40}$$

where

$$\begin{aligned}
 C_{11} &= -A_{11} \alpha_m^2 - A_{66} \beta_n^2 \\
 C_{12} = C_{21} &= -(A_{12} + A_{66}) \alpha_m \beta_n \\
 C_{22} &= -A_{66} \alpha_m^2 - A_{22} \beta_n^2 \\
 C_{13} = C_{31} &= B_{11} \alpha_m^3 + (B_{12} + 2B_{66}) \alpha_m \beta_n^2 \\
 C_{23} = C_{32} &= B_{22} \beta_n^3 + (B_{12} + 2B_{66}) \alpha_m^2 \beta_n \\
 C_{33} &= D_{11} \alpha_m^4 + 2(D_{12} + 2D_{66}) \alpha_m^2 \beta_n^2 + D_{22} \beta_n^4
 \end{aligned} \tag{5.41}$$

The above equations are valid for forced vibration problems. They reduce to static problems if the natural frequency is set to zero, and to free vibrations if the loads are set to

zero. The above solution reduces to a closed form one for symmetric cross-ply plates (Hearmon 1946). This can be expressed as

$$\frac{\omega_{mn}^2 a^4 \rho}{\pi^4} = D_{11} m^4 + 2(D_{12} + 2D_{66}) m^2 n^2 (a/b)^2 + D_{22} n^4 (a/b)^4$$

as was reported by Leissa (1969).

5.3.1.2 Thick plates. Consider a plate that is made of a cross-ply laminate. The differential operators L_{ij} in the equations of motion (5.31) and (5.32) become

$$\begin{aligned} L_{11} &= A_{11} \frac{\partial^2}{\partial \alpha^2} + A_{66} \frac{\partial^2}{\partial \beta^2} \\ L_{12} &= (A_{12} + A_{66}) \frac{\partial^2}{\partial \alpha \partial \beta} + A_{26} \frac{\partial^2}{\partial \beta^2} \\ L_{13} &= 0, \quad L_{14} = B_{11} \frac{\partial^2}{\partial \alpha^2} + B_{66} \frac{\partial^2}{\partial \beta^2}, \quad L_{15} = (B_{12} + B_{66}) \frac{\partial^2}{\partial \alpha \partial \beta} \\ L_{22} &= A_{66} \frac{\partial^2}{\partial \alpha^2} + 2A_{26} \frac{\partial^2}{\partial \alpha \partial \beta} + A_{22} \frac{\partial^2}{\partial \beta^2} \\ L_{23} &= 0, \quad L_{24} = (B_{12} + B_{66}) \frac{\partial^2}{\partial \alpha \partial \beta} \\ L_{25} &= B_{66} \frac{\partial^2}{\partial \alpha^2} + B_{22} \frac{\partial^2}{\partial \beta^2}, \quad L_{33} = -A_{55} \frac{\partial^2}{\partial \alpha^2} - A_{44} \frac{\partial^2}{\partial \beta^2} \\ L_{34} &= -A_{55} \frac{\partial}{\partial \alpha}, \quad L_{35} = -A_{44} \frac{\partial}{\partial \beta} \\ L_{44} &= -A_{55} + D_{11} \frac{\partial^2}{\partial \alpha^2} + D_{66} \frac{\partial^2}{\partial \beta^2} \\ L_{45} &= -A_{45} + (D_{12} + D_{66}) \frac{\partial^2}{\partial \alpha \partial \beta} \\ L_{55} &= -A_{44} + D_{66} \frac{\partial^2}{\partial \alpha^2} + D_{22} \frac{\partial^2}{\partial \beta^2} \end{aligned} \tag{5.42}$$

Consider a plate, with shear diaphragm (S2) boundaries on all four edges. That is, the following boundary conditions apply:

$$\begin{aligned} N_\alpha = w_0 = v_0 = M_\alpha = \psi_\beta &= 0 & \text{for the edges } \alpha = 0, a \\ N_\beta = w_0 = u_0 = M_\beta = \psi_\alpha &= 0 & \text{for the edges } \beta = 0, b \end{aligned} \tag{5.43}$$

The Navier-type solution can be applied to thick plates with shear diaphragm supports to obtain exact solution. The displacement and slope functions take the forms

$$\begin{aligned}
 u_0(\alpha, \beta, t) &= \sum_{m=1}^{\infty} \sum_{n=1}^{\infty} U_{mn} \cos(\alpha_m \alpha) \sin(\beta_n \beta) \sin(\omega_{mn} t) \\
 v_0(\alpha, \beta, t) &= \sum_{m=1}^{\infty} \sum_{n=1}^{\infty} V_{mn} \sin(\alpha_m \alpha) \cos(\beta_n \beta) \sin(\omega_{mn} t) \\
 w_0(\alpha, \beta, t) &= \sum_{m=1}^{\infty} \sum_{n=1}^{\infty} W_{mn} \sin(\alpha_m \alpha) \sin(\beta_n \beta) \sin(\omega_{mn} t) \\
 \psi_{\alpha}(\alpha, \beta, t) &= \sum_{m=1}^{\infty} \sum_{n=1}^{\infty} \psi_{\alpha mn} \cos(\alpha_m \alpha) \sin(\beta_n \beta) \sin(\omega_{mn} t) \\
 \psi_{\beta}(\alpha, \beta, t) &= \sum_{m=1}^{\infty} \sum_{n=1}^{\infty} \psi_{\beta mn} \sin(\alpha_m \alpha) \cos(\beta_n \beta) \sin(\omega_{mn} t)
 \end{aligned} \tag{5.44}$$

where $\alpha_m = m\pi/a$, and $\beta_n = n\pi/b$, and U_{mn} , V_{mn} , W_{mn} , $\psi_{\alpha mn}$, and $\psi_{\beta mn}$ are arbitrary coefficients.

Substituting the above equations into equations of motion and using a Fourier expansion for the loading functions yields

$$[K]\{\Delta\} + (\omega_{mn})^2[M]\{\Delta\} = -\{F\} \tag{5.45}$$

where $[K]$ and $[M]$ are the stiffness and mass symmetric 5×5 matrices; respectively ω_{mn} is the frequency with m number of half sine waves in the α direction and n number of half sine waves in the β direction, $\{F\}$ is the forcing function, and $\{\Delta\} = \{U_{mn}, V_{mn}, W_{mn}, \psi_{\alpha mn}, \psi_{\beta mn}\}^T$. The K_{ij} coefficients are

$$\begin{aligned}
 K_{11} &= -A_{11}\alpha_m^2 - A_{66}\beta_n^2 \\
 K_{12} &= -(A_{12} + A_{66})\alpha_m\beta_n \\
 K_{13} &= 0 \\
 K_{14} &= -B_{11}\alpha_m^2 - B_{66}\beta_n^2 \\
 K_{15} &= -(B_{12} + B_{66})\alpha_m\beta_n \\
 K_{22} &= -A_{66}\alpha_m^2 - A_{22}\beta_n^2 \\
 K_{23} &= 0 \\
 K_{24} &= -(B_{12} + B_{66})\alpha_m\beta_n \\
 K_{25} &= -B_{66}\alpha_m^2 + B_{22}\beta_n^2 \\
 K_{33} &= -A_{55}\alpha_m^2 - A_{44}\beta_n^2 \\
 K_{34} &= -A_{55}\alpha_m \\
 K_{35} &= -A_{44}\beta_n \\
 K_{44} &= -A_{55} - D_{11}\alpha_m^2 - D_{66}\beta_n^2
 \end{aligned}$$

$$\begin{aligned} K_{45} &= -(D_{12} + D_{66})\alpha_m\beta_n \\ K_{55} &= -A_{44} - D_{66}\alpha_m^2 - D_{22}\beta_n^2 \end{aligned} \quad (5.46)$$

If the forcing function $\{F\}$ is assumed to be zero, the above equations can be used directly to find the natural frequencies of free vibration. Unless stated otherwise, the following natural frequency parameter is used in the subsequent analysis:

$$\Omega = \omega a^2 \sqrt{\rho/E_2 h^2} \quad (5.47)$$

Table 5.1 shows the frequency parameter for cross-ply square plates with relatively high orthotropy ratio ($E_1/E_2 = 25$) using SDPT and CPT. Three lamination sequence values are considered $[0^\circ, 90^\circ]$, $[0^\circ, 90^\circ, 0^\circ]$, and $[0^\circ, 90^\circ, 90^\circ, 0^\circ]$. Two thickness ratios (a/h) of 100 and 10 are used. The results are compared with those obtained by Reddy (1984b). The results show that for the thin plate with $a/h = 100$, the difference between the two theories is minimal. Thus the CPT is certainly accurate. For a thick plate with $a/h = 10$, the difference between both theories reaches more than 20%, showing the lack of accuracy that the CPT has in predicting vibrations of thick plates. The results compare well with those obtained by Reddy (1984b), who used practically the same theory (when his equations are specialized to those of plates). Table 5.2 shows another comparison between CPT and SDPT. Various thickness ratios are used in the analysis. The difference between the prediction of SDPT and those of CPT are less than 1% for very thin plates with a thickness ratio (a/h) of 100. The difference reaches 3.2% for plates with thickness ratio of 20, 11.8% for plates with thickness ratio of 10, and 40% for plates with thickness ratios of 5 (where the SDPT is not proven to apply and must be compared with results obtained by the theory of elasticity). It does seem reasonable to assume that CPT applies only for plates having a thickness ratio of 20 or higher. This theory overpredicts the natural frequency as expected. It is also important to note that the nondimensional frequency parameter chosen here does not change with thickness for the

Table 5.1. Frequency parameter $\Omega = \omega a^2 \sqrt{\rho/E_2 h^2}$ for cross-ply plates ($a/b = 1$, $E_1/E_2 = 25$, $G_{12}/E_2 = 0.5$, $G_{13}/E_2 = 0.5$, $G_{23}/E_2 = 0.2$, $\nu_{12} = 0.25$, $K^2 = 5/6$) for SDPT and CPT.

a/h	Lamination theory								
	$[0^\circ, 90^\circ]$			$[0^\circ, 90^\circ, 0^\circ]$			$[0^\circ, 90^\circ, 90^\circ, 0^\circ]$		
	Reddy ^a	SDPT	CPT	Reddy ^a	SDPT	CPT	Reddy ^a	SDPT	CPT
100	9.6873	9.6873	9.6960	15.183	15.183	15.228	12.226	15.184	15.228
10	8.8998	8.9001	9.6436	12.163	12.163	15.228	12.226	12.226	15.228

^aEquations obtained by Reddy (1984b).

Table 5.2. Frequency parameter $\Omega = \omega a^2 \sqrt{\rho/E_2 h^2}$ for cross-ply plates ($a/b = 1$, $E_1/E_2 = 15$, $G_{12}/E_2 = 0.5$, $G_{13}/E_2 = 0.5$, $G_{23}/E_2 = 0.5$, $\nu_{12} = 0.25$, $K^2 = 5/6$) for SDPT and CPT.

a/h	Lamination theory			
	[0°, 90°]	[0°, 90°]	[0°, 90°, 90°, 0°]	[0°, 90°, 90°, 0°]
	SDPT	CPT	SDPT	CPT
100	8.56394	8.56847	12.26147	12.37733
20	8.44807	8.55811	11.90100	12.27733
10	8.11956	8.52569	10.97163	12.27733
5	7.14661	8.39526	8.77840	12.27733

predictions made using CPT for symmetrically laminated cross-ply plates. It does change slightly for asymmetrically laminated plates. Furthermore, the accuracy of CPT in predicting frequencies is higher for asymmetrically laminated plates than it is for symmetrically laminated ones.

5.3.2 Simply supported antisymmetric angle-ply rectangular plates

Consider first simply supported thin plates.

5.3.2.1 Thin plates. The plates treated here are those made of antisymmetric angle-ply laminate, thus

$$A_{16} = A_{26} = B_{11} = B_{12} = B_{22} = B_{66} = D_{16} = D_{26} = 0 \quad (5.48)$$

The differential operators L_{ij} in the equations of motion (5.11) become

$$\begin{aligned}
 L_{11} &= A_{11} \frac{\partial^2}{\partial \alpha^2} + A_{66} \frac{\partial^2}{\partial \beta^2} \\
 L_{12} = L_{21} &= \{A_{12} + A_{66}\} \frac{\partial^2}{\partial \alpha \partial \beta} \\
 L_{22} &= A_{66} \frac{\partial^2}{\partial \alpha^2} + A_{22} \frac{\partial^2}{\partial \beta^2} \\
 L_{13} = L_{31} &= -B_{26} \frac{\partial^3}{\partial \beta^3} - 3B_{16} \frac{\partial^3}{\partial \alpha^2 \partial \beta} \\
 L_{23} = L_{32} &= -B_{16} \frac{\partial^3}{\partial \alpha^3} - 3B_{26} \frac{\partial^3}{\partial \alpha \partial \beta^2} \\
 L_{33} &= D_{11} \frac{\partial^4}{\partial \alpha^4} + 2(D_{12} + 2D_{66}) \frac{\partial^4}{\partial \alpha^2 \partial \beta^2} + D_{22} \frac{\partial^4}{\partial \beta^4}
 \end{aligned} \quad (5.49)$$

Consider a plate, with simple support (S3) boundaries on all four edges. That is, the following boundary conditions apply:

$$\begin{aligned} w_0 = u_0 = N_{\alpha\beta} = M_\alpha = 0 & \quad \text{for the edges } \alpha = 0, a \\ w_0 = v_0 = N_{\alpha\beta} = M_\beta = 0 & \quad \text{for the edges } \beta = 0, b \end{aligned} \quad (5.50)$$

Note the difference between the S3 boundaries and the shear diaphragm boundaries. The shear diaphragm boundaries allow motion in the inplane direction that is perpendicular to the boundary and prevents it in the inplane direction tangential to the boundary. The S3 has opposite treatment of the inplane displacement supports. The following solution satisfies the S3 boundary conditions and the equations of motion exactly:

$$\begin{aligned} u_0(\alpha, \beta, t) &= \sum_{m=0}^M \sum_{n=0}^N U_{mn} \sin(\alpha_m \alpha) \cos(\beta_n \beta) \sin(\omega_{mn} t) \\ v_0(\alpha, \beta, t) &= \sum_{m=0}^M \sum_{n=0}^N V_{mn} \cos(\alpha_m \alpha) \sin(\beta_n \beta) \sin(\omega_{mn} t) \\ w_0(\alpha, \beta, t) &= \sum_{m=0}^M \sum_{n=0}^N W_{mn} \sin(\alpha_m \alpha) \sin(\beta_n \beta) \sin(\omega_{mn} t) \end{aligned} \quad (5.51)$$

where

$$\alpha_m = \frac{m\pi}{a}, \quad \beta_n = \frac{n\pi}{b}$$

ω_{mn} is the frequency with m number of half sine waves in the α direction and n number of half sine waves in the β direction. Also, the external forces can be expanded in a Fourier series. This is done for both static and forced vibration types of analyses.

The equations of motion can now be written as Eq. (5.40) with the coefficients

$$\begin{aligned} C_{11} &= -A_{11}\alpha_m^2 - A_{66}\beta_n^2 \\ C_{12} = C_{21} &= -(A_{12} + A_{66})\alpha_m\beta_n \\ C_{22} &= -A_{66}\alpha_m^2 - A_{22}\beta_n^2 \\ C_{13} = C_{31} &= B_{26}\beta_n^3 + 3B_{16}\alpha_m^2\beta_n \\ C_{23} = C_{32} &= B_{16}\alpha_m^3 + 3B_{26}\alpha_m\beta_n^2 \\ C_{33} &= \{D_{11}\alpha_m^4 + 2(D_{12} + 2D_{66})\alpha_m^2\beta_n^2 + D_{22}\beta_n^4\} \end{aligned} \quad (5.52)$$

The above equations can be used to find the exact frequencies.

5.3.2.2 Thick plates. For antisymmetric angle-ply plate, Eq. (5.48) will reduce the differential operators L_{ij} in the equations of motion (5.31) to

$$\begin{aligned}
L_{11} &= A_{11} \frac{\partial^2}{\partial \alpha^2} + A_{66} \frac{\partial^2}{\partial \beta^2} \\
L_{12} &= (A_{12} + A_{66}) \frac{\partial^2}{\partial \alpha \partial \beta} \\
L_{13} &= 0, \quad L_{14} = 2B_{16} \frac{\partial^2}{\partial \alpha \partial \beta} \\
L_{15} &= B_{16} \frac{\partial^2}{\partial \alpha^2} + B_{26} \frac{\partial^2}{\partial \beta^2} \\
L_{22} &= A_{66} \frac{\partial^2}{\partial \alpha^2} + A_{22} \frac{\partial^2}{\partial \beta^2} \\
L_{23} &= 0 \\
L_{24} &= B_{16} \frac{\partial^2}{\partial \alpha^2} + B_{26} \frac{\partial^2}{\partial \beta^2} \\
L_{25} &= 2B_{26} \frac{\partial^2}{\partial \alpha \partial \beta} \\
L_{33} &= -A_{55} \frac{\partial^2}{\partial \alpha^2} - A_{44} \frac{\partial^2}{\partial \beta^2} \\
L_{34} &= -A_{55} \frac{\partial}{\partial \alpha}, \quad L_{35} = -A_{44} \frac{\partial}{\partial \beta} \\
L_{44} &= -A_{55} + D_{11} \frac{\partial^2}{\partial \alpha^2} + D_{66} \frac{\partial^2}{\partial \beta^2} \\
L_{45} &= (D_{12} + D_{66}) \frac{\partial^2}{\partial \alpha \partial \beta} \\
L_{55} &= -A_{44} + D_{66} \frac{\partial^2}{\partial \alpha^2} + D_{22} \frac{\partial^2}{\partial \beta^2}
\end{aligned} \tag{5.53}$$

Consider a plate, with simple support S3 boundaries on all four edges ($w_0 = M_\alpha = u_0 = N_{\alpha\beta} = \psi_\beta = 0$ at $\alpha = 0$ and a , and $w_0 = M_\beta = u_0 = N_{\alpha\beta} = \psi_\alpha = 0$ at $\beta = 0$ and b). The Navier-type solution can be applied to thick plates to obtain an exact solution. It takes the following form:

$$\begin{aligned}
u_0(\alpha, \beta, t) &= \sum_{m=1}^{\infty} \sum_{n=1}^{\infty} U_{mn} \sin(\alpha_m \alpha) \cos(\beta_n \beta) \sin(\omega_{mn} t) \\
v_0(\alpha, \beta, t) &= \sum_{m=1}^{\infty} \sum_{n=1}^{\infty} V_{mn} \cos(\alpha_m \alpha) \sin(\beta_n \beta) \sin(\omega_{mn} t) \\
w_0(\alpha, \beta, t) &= \sum_{m=1}^{\infty} \sum_{n=1}^{\infty} W_{mn} \sin(\alpha_m \alpha) \sin(\beta_n \beta) \sin(\omega_{mn} t)
\end{aligned}$$

$$\begin{aligned}
\psi_\alpha(\alpha, \beta, t) &= \sum_{m=1}^{\infty} \sum_{n=1}^{\infty} \psi_{\alpha mn} \cos(\alpha_m \alpha) \sin(\beta_n \beta) \sin(\omega_{mn} t) \\
\psi_\beta(\alpha, \beta, t) &= \sum_{m=1}^{\infty} \sum_{n=1}^{\infty} \psi_{\beta mn} \sin(\alpha_m \alpha) \cos(\beta_n \beta) \sin(\omega_{mn} t)
\end{aligned} \tag{5.54}$$

where

$$\alpha_m = \frac{m\pi}{a}, \quad \beta_n = \frac{n\pi}{b}$$

ω_{mn} is the natural frequency and U_{mn} , V_{mn} , W_{mn} , $\psi_{\alpha mn}$ and $\psi_{\beta mn}$ are arbitrary coefficients. Substituting the above equations into equations of motion and using a Fourier expansion for the loading functions yields

$$[K]\{\Delta\} + (\omega_{mn})^2[M]\{\Delta\} = -\{F\} \tag{5.55}$$

where $[K]$ and $[M]$ are the stiffness and mass symmetric 5×5 matrices, respectively, ω_{mn} the frequency, $\{F\}$ the forcing function, and $\{\Delta\} = \{U_{mn}, V_{mn}, W_{mn}, \psi_{\alpha mn}, \psi_{\beta mn}\}^T$. The K_{ij} coefficients are

$$\begin{aligned}
K_{11} &= -A_{11}\alpha_m^2 - A_{66}\beta_n^2 \\
K_{12} &= -(A_{12} + A_{66})\alpha_m\beta_n \\
K_{13} &= 0 \\
K_{14} &= -2B_{16}\alpha_m\beta_n \\
K_{15} &= -B_{16}\alpha_m^2 - B_{26}\beta_n^2 n \\
K_{22} &= -A_{66}\alpha_m^2 - A_{22}\beta_n^2 \\
K_{23} &= 0 \\
K_{24} &= -B_{16}\alpha_m^2 + B_{26}\beta_n^2 \\
K_{25} &= -2B_{26}\alpha_m\beta_n \\
K_{33} &= -A_{55}\alpha_m^2 - A_{44}\beta_n^2 \\
K_{34} &= -A_{55}\alpha_m \\
K_{35} &= -A_{44}\beta_n \\
K_{44} &= -A_{55} - D_{11}\alpha_m^2 - D_{66}\beta_n^2 \\
K_{45} &= -(D_{12} + D_{66})\alpha_m\beta_n \\
K_{55} &= -A_{44} - D_{66}\alpha_m^2 - D_{22}\beta_n^2
\end{aligned} \tag{5.56}$$

As before, the above equations can be used directly to find the natural frequencies of free vibration if the forcing function $\{F\}$ is assumed to be zero.

Table 5.3. Natural frequency parameters $\Omega = \omega a^2 \sqrt{\rho/E_2 h^2}$ for angle-ply square laminated $[45^\circ, -45^\circ, 45^\circ, -45^\circ]$ plates with $E_1/E_2 = 40$, $G_{12}/E_2 = G_{13}/E_2 = 0.6$, $G_{23}/E_2 = 0.5$, $\nu_{12} = 0.25$ and $a/h = 10$, $K^2 = 5/6$.

Mode number	Khdeir (1988a) and Bert and Chen (1978)	Reddy (1979)	CPT
1	18.46	18.61	23.53
2	34.87	35.41	53.74
3	54.27	54.36	98.87
4	75.58	76.41	160.35
5	97.56	105.06	238.72

Table 5.3 shows the frequency parameters $\Omega = \omega a^2 \sqrt{\rho/E_2 h^2}$ for angle-ply square laminated $[45^\circ, -45^\circ, 45^\circ, -45^\circ]$ plates with high orthotropy ratio of 40. The results obtained by Khdeir (1988a) and Bert and Chen (1978) using a theory similar to the one presented here are compared with the results presented by Reddy (1979) using finite elements and CPT. The table particularly shows the failure of CPT in predicting higher frequencies for these plates with thickness ratio of 10. Table 5.4 shows a similar comparison for other stacking sequences.

5.3.3 Cross-ply plates with two opposite edges simply supported

Exact solutions can be found for plates having two opposite edges simply supported. This is true for the same boundaries and lamination sequences described in Section 5.3.2. That is, exact solutions can be found for unsymmetric cross-ply plates with S2 opposite boundaries as well as antisymmetric angle-ply plates with S3 opposite boundaries. Figure 5.4 shows the notations used in describing the possible boundary configurations of CSFS. Note that the letters in the CSFS begin by describing the far left clamped (C) end

Table 5.4. Natural frequency parameters $\Omega = \omega a^2 \sqrt{\rho/E_2 h^2}$ for angle-ply square laminated plates with $E_1/E_2 = 40$, $G_{12}/E_2 = G_{13}/E_2 = 0.6$, $G_{23}/E_2 = 0.5$, $\nu_{12} = 0.25$ and $a/h = 10$, $K^2 = 5/6$.

θ	Lamination	Khdeir (1988a) and Bert and Chen (1978)	Reddy (1979)
30	$[\theta, -\theta]$	12.68	15.00
	$[\theta, -\theta, \theta, -\theta]$	17.63	17.69
45	$[\theta, -\theta]$	13.04	15.71
	$[\theta, -\theta, \theta, -\theta]$	18.46	18.61

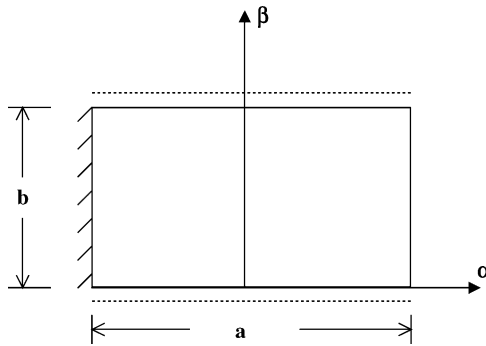


Figure 5.4. A CSFS plate.

(at $\alpha = -a/2$), followed by the simply supported boundary (S) at the bottom ($\beta = 0$), the free (F) one to the right (at $\alpha = a/2$) and finally the top simply supported (S) boundary (at $\beta = b$).

5.3.3.1 Thin plates. Consider a plate that is made of a cross-ply laminate, thus Eq. (5.35) applies for stiffness parameters, and Eq. (5.36) applies for the differential operator in the equations of motion. Consider further the plate having shear diaphragm (S2) boundaries on the two opposite edges $\beta = 0, b$ (i.e., $N_\beta = w_0 = u_0 = M_\beta = 0$; for the edges $\beta = 0, b$) and the other edges $\alpha = -a/2, a/2$ have arbitrary conditions. A displacement field can be chosen to satisfy the simply supported boundaries in the following form:

$$\begin{aligned}
 u_0(\alpha, \beta, t) &= \sum_{m=1}^{\infty} \sum_{n=1}^{\infty} U_{mn} X_m(\alpha) \sin(\beta_n \beta) \sin(\omega_{mn} t) \\
 v_0(\alpha, \beta, t) &= \sum_{m=1}^{\infty} \sum_{n=1}^{\infty} V_{mn} Y_m(\alpha) \cos(\beta_n \beta) \sin(\omega_{mn} t) \\
 w_0(\alpha, \beta, t) &= \sum_{m=1}^{\infty} \sum_{n=1}^{\infty} W_{mn} Z_m(\alpha) \sin(\beta_n \beta) \sin(\omega_{mn} t) \\
 \beta_n &= \frac{n\pi}{b} \quad \omega_{mn} \text{ is the natural frequency.}
 \end{aligned} \tag{5.57}$$

One needs to substitute the above equations into Eq. (5.11) with the operator described in Eq. (5.36) for cross-ply laminates. A direct method has been described in Chapter 4 on laminated curved beams to solve the resulting equations. The method can be extended to treat the equations of plates. Alternatively, in Section 5.3.3.2 we will describe a method for solving the resulting system of differential equations.

5.3.3.2 Thick plates. For thick plates made of a cross-ply laminate, Eq. (5.31) can be used with the differential operator L_{ij} described in Eq. (5.42) for the equations of motion. Let the boundaries on the two opposite edges $\beta = 0, b$ be shear diaphragm (S2) (i.e., $N_\beta = w_0 = u_0 = M_\beta = \psi_\alpha = 0$; for the edges $\beta = 0, b$) and the other edges $\alpha = -a/2, +a/2$ have arbitrary conditions. The following displacement field can be applied to the equations of motion of thick plates:

$$\begin{aligned}
 u_0(\alpha, \beta, t) &= \sum_{m=1}^{\infty} \sum_{n=1}^{\infty} U_{mn} X_m(\alpha) \sin(\beta_n \beta) \sin(\omega_{mn} t) \\
 v_0(\alpha, \beta, t) &= \sum_{m=1}^{\infty} \sum_{n=1}^{\infty} V_{mn} Y_m(\alpha) \cos(\beta_n \beta) \sin(\omega_{mn} t) \\
 w_0(\alpha, \beta, t) &= \sum_{m=1}^{\infty} \sum_{n=1}^{\infty} W_{mn} Z_m(\alpha) \sin(\beta_n \beta) \sin(\omega_{mn} t) \\
 \psi_\alpha(\alpha, \beta, t) &= \sum_{m=1}^{\infty} \sum_{n=1}^{\infty} \psi_{\alpha mn} S_m(\alpha) \sin(\beta_n \beta) \sin(\omega_{mn} t) \\
 \psi_\beta(\alpha, \beta, t) &= \sum_{m=1}^{\infty} \sum_{n=1}^{\infty} \psi_{\beta mn} T_m(\alpha) \cos(\beta_n \beta) \sin(\omega_{mn} t)
 \end{aligned} \tag{5.58}$$

where

$$\beta_n = \frac{n\pi}{b}$$

and U_{mn} , V_{mn} , W_{mn} , $\psi_{\alpha mn}$ and, $\psi_{\beta mn}$ are arbitrary coefficients.

One needs to substitute the above equations into Eq. (5.31) with the operator described in Eq. (5.42) for cross-ply laminates. The resulting equations can be addressed in a manner similar to that of curved beams discussed in Chapter 4 (Lin and King 1974). Alternatively, Khdeir (1986, 1989) used the state space approach (Brogan 1985) for the procedure to obtain solutions to the resulting equations. In this approach, the resulting equations of motion is rewritten as

$$\{\chi'\} = [A]\{\chi\} \tag{5.59}$$

where

$$\begin{aligned}
 \chi_1 &= X_m, & \chi_2 &= X'_m, & \chi_3 &= Y_m, & \chi_4 &= Y'_m, & \chi_5 &= Z_m, \\
 \chi_6 &= Z'_m, & \chi_7 &= S_m, & \chi_8 &= S'_m, & \chi_9 &= T_m, & \chi_{10} &= T'_m
 \end{aligned}$$

where each prime is a derivative with respect to α . The matrix A is a 10×10 matrix and can be found by the references mentioned earlier as well as that of Reddy and Khdeir (1989). While the above equation are written for thick plates, similar equations can be written for thin plates (with a resulting 8×8 matrix). A solution to the above equations is

written as

$$e^{A\alpha} = [\Gamma] \begin{Bmatrix} e^{\lambda_1 \alpha} & 0 & \cdots & 0 \\ 0 & e^{\lambda_2 \alpha} & & 0 \\ \vdots & & \ddots & 0 \\ 0 & 0 & & e^{\lambda_{10} \alpha} \end{Bmatrix} [\Gamma]^{-1} \quad (5.60)$$

where $\lambda_1, \dots, \lambda_{10}$ are eigenvalues and $[\Gamma]$ are eigenvectors.

Substituting Eq. (5.59) into the boundary conditions associated with the two opposite boundaries at $\alpha = -a/2, +a/2$ results in a homogeneous system of equations. The determinant of which has to be set to zero to obtain a nontrivial solution for the frequencies in the normal manner.

Table 5.5 shows the natural frequency parameters $\Omega = \omega a^2 \sqrt{\rho/E_2 h^2}$ of $[0^\circ, 90^\circ]$ square plates with various boundaries at $\alpha = -a/2, a/2$. The table is written starting with the plate of less constraints (FSFS) and ending with the plate with higher constraints (SCSC) with the exception of (SSSS) and (FSCS), which have similar constraint levels.

The first observation made here is the lack of accuracy obtained with CPT for such moderately thick plates ($a/h = 10$), especially for the plates with higher orthotropy ratios. The difference between the CPT prediction and the SDPT ones is almost double for plates with the high orthotropy ratio ($E_1/E_2 = 40$); when compared with plates with the lower orthotropy ratio of 10. The second observation is that the difference between both theories is higher for plates with higher constraints. For $E_1/E_2 = 10$, the difference between the CPT and SDPT is 2.4% for the SFSF plates and almost 11% for the SCSC ones.

Table 5.5. Natural frequency parameters $\Omega = \omega a^2 \sqrt{\rho/E_2 h^2}$ of $[0^\circ, 90^\circ]$ square plates with various boundaries at $\alpha = -a/2, a/2$, $G_{12} = G_{13} = 0.6E_2$, $\nu_{12} = 0.25$, $a/h = 10$, $K^2 = 5/6$ (Khdeir 1989).

Theory	E_1/E_2	FSFS	SSSF	SCSF	SSSS	SCSS	SCSC
CPT	40	7.267	7.636	8.228	11.154	14.223	18.543
SDPT		6.881	7.215	7.741	10.473	12.610	15.152
CPT	20	5.704	6.166	6.681	9.204	11.575	14.899
SDPT		5.511	5.940	6.397	8.810	10.658	12.956
CPT	10	4.694	5.264	5.709	8.032	9.951	12.624
SDPT		4.584	5.104	5.515	7.766	9.352	11.377

Table 5.6. Natural frequency parameters $\Omega = \omega a^2 \sqrt{\rho/E_2 h^2}$ for a $[0^\circ, 90^\circ, 0^\circ]$ square laminated plates with $E_1/E_2 = 40$, $G_{12}/E_2 = G_{13}/E_2 = 0.6$, $G_{23}/E_2 = 0.5$, $\nu_{12} = 0.25$, $K^2 = 5/6$ with various boundaries at $\alpha = -a/2, a/2$ (Khdeir 1988b).

Theory	m , mode number	SFSF	SFSS	SFSC	SSSS	SSSC	SCSC
CPT	1	4.457	5.076	8.269	18.89	28.50	40.74
SDPT	1	4.343	4.914	7.331	14.77	17.18	19.67
CPT	2	17.83	18.47	19.79	26.94	34.53	45.23
SDPT	2	16.21	16.74	17.56	22.16	23.68	25.35
CPT	3	40.11	40.76	41.51	46.21	51.19	59.02
SDPT	3	33.19	33.64	34.02	36.90	37.72	38.65

The third observation is to show how the frequencies actually increase with the added constraints, particularly when the clamped edges are considered. The impact of the constraints at the edges is higher for plates with higher orthotropy ratios.

Table 5.6 shows the natural frequency parameters $\Omega = \omega a^2 \sqrt{\rho/E_2 h^2}$ for symmetrically laminated, three layered square laminated plates with high orthotropy ratio ($E_1/E_2 = 40$), and various boundary conditions at $\alpha = -a/2, a/2$. The table shows results obtained using both CPT and SDPT. The first three half sine waves in the β -direction are considered.

The table shows that the CPT overpredicts the frequencies considerably, especially for the higher modes. These tables show clearly that CPT should not be used for such moderately thick plates. The table further emphasizes the previous observation regarding the clamped constraints for both fundamental and higher modes.

5.3.4 Antisymmetric angle-ply plates with two opposite edges simply supported

Consider first a thin plate that is made of antisymmetric angle-ply laminate. Thus Eqs. (5.48) and (5.49) apply for the stiffness parameters and equations of motion; respectively. Consider further the plate having simple support of the type S3 boundaries: $w_0 = v_0 = N_{\alpha\beta} = M_\beta = 0$ at the edges $\beta = 0$ or b ; the other boundaries are arbitrary. The following solution satisfies the S3 boundary conditions at the edges $\beta = 0, b$ exactly

$$\begin{aligned}
 u_0(\alpha, \beta, t) &= \sum_{m=0}^M \sum_{n=0}^N U_{mn} X_m(\alpha) \cos(\beta_n \beta) \sin(\omega_{mn} t) \\
 v_0(\alpha, \beta, t) &= \sum_{m=0}^M \sum_{n=0}^N V_{mn} Y_m(\alpha) \sin(\beta_n \beta) \sin(\omega_{mn} t) \\
 w_0(\alpha, \beta, t) &= \sum_{m=0}^M \sum_{n=0}^N W_{mn} Z_m(\alpha) \sin(\beta_n \beta) \sin(\omega_{mn} t)
 \end{aligned} \tag{5.61}$$

where

$$\beta_n = \frac{n\pi}{b}$$

Consider an antisymmetric angle-ply thick plate where Eqs. (5.48) and (5.53) apply for the stiffness parameters and equations of motion; respectively. Let the plate have simple support S3 boundaries for the edges $\beta = 0$ and b , and the other boundaries are arbitrary. The following solution satisfies the S3 boundary conditions ($w = M_\alpha = u = N_{\alpha\beta} = \psi_\beta = 0$) exactly

$$\begin{aligned} u_0(\alpha, \beta, t) &= \sum_{m=1}^{\infty} \sum_{n=1}^{\infty} U_{mn} X_m(\alpha_m \alpha) \cos(\beta_n \beta) \sin(\omega_{mn} t) \\ v_0(\alpha, \beta, t) &= \sum_{m=1}^{\infty} \sum_{n=1}^{\infty} V_{mn} Y_m(\alpha_m \alpha) \sin(\beta_n \beta) \sin(\omega_{mn} t) \\ w_0(\alpha, \beta, t) &= \sum_{m=1}^{\infty} \sum_{n=1}^{\infty} W_{mn} Z_m(\alpha_m \alpha) \sin(\beta_n \beta) \sin(\omega_{mn} t) \\ \psi_\alpha(\alpha, \beta, t) &= \sum_{m=1}^{\infty} \sum_{n=1}^{\infty} \psi_{\alpha mn} S_m(\alpha_m \alpha) \sin(\beta_n \beta) \sin(\omega_{mn} t) \\ \psi_\beta(\alpha, \beta, t) &= \sum_{m=1}^{\infty} \sum_{n=1}^{\infty} \psi_{\beta mn} T_m(\alpha_m \alpha) \cos(\beta_n \beta) \sin(\omega_{mn} t) \end{aligned} \quad (5.62)$$

The above solutions can be substituted back into the equations of motion in terms of displacement (Eq. (5.49) for thin plates and Eq. (5.53) for thick ones). A procedure similar to that shown earlier can then be used to solve for the natural frequencies of anti-symmetric angle-ply plates having two opposite edges simply supported of type S3.

Table 5.7 shows the natural frequency parameters $\Omega = \omega a^2 \sqrt{\rho/E_2 h^2}$ for angle-ply square laminated plates with high orthotropy $E_1/E_2 = 40$, $G_{12}/E_2 = G_{13}/E_2 = 0.6$, $G_{23}/E_2 = 0.5$, $\nu_{12} = 0.25$, shear correction factor $K^2 = 5/6$ and a thickness ratio

Table 5.7. Natural frequency parameters $\Omega = \omega a^2 \sqrt{\rho/E_2 h^2}$ for angle-ply square laminated plates with $E_1/E_2 = 40$, $G_{12}/E_2 = G_{13}/E_2 = 0.6$, $G_{23}/E_2 = 0.5$, $\nu_{12} = 0.25$, $K^2 = 5/6$ and $a/h = 10$, using thick plate theory with various boundaries at $\alpha = -a/2, a/2$ (Khdeir 1988a).

θ	Layers	FSFS	SSFS	FSCS	SSSS	SSCS	CSCS
30	$[\theta, -\theta]$	6.95	8.45	8.65	12.68	13.46	14.41
	$[\theta, -\theta, \theta, -\theta]$	9.61	11.72	11.88	17.63	18.27	19.01
45	$[\theta, -\theta]$	4.76	7.13	7.52	13.04	14.23	15.63
	$[\theta, -\theta, \theta, -\theta]$	6.26	10.05	10.36	18.46	19.41	20.48

Table 5.8. Natural frequency parameters $\Omega = \omega a^2 \sqrt{\rho/E_2 h^2}$ for $[45^\circ, -45^\circ, 45^\circ, -45^\circ]$ square laminated plates with $E_1/E_2 = 40$, $G_{12}/E_2 = G_{13}/E_2 = 0.6$, $G_{23}/E_2 = 0.5$, $\nu_{12} = 0.25$, $K^2 = 5/6$ and $a/h = 10$, using thick plate theory with various boundaries at $\alpha = -a/2, a/2$ (Khdeir 1988a).

m	FSFS	SSFS	FSCS	SSSS	SSCS	CSCS
1	6.26	10.05	10.36	18.46	19.41	20.48
2	23.80	26.31	26.32	34.87	34.95	35.03
3	45.82	47.18	47.18	54.27	54.27	54.27
4	68.92	69.66	69.66	75.58	75.59	75.59
5	92.02	92.48	92.48	97.56	97.57	97.58

$a/h = 10$ (Khdeir 1988a). Two angles of lamination at 30° and 45° are considered with two and four layers for each angle. The first observation to be made here is the higher frequencies obtained by the higher number of layers. This may be due to the fact that weaker stretching–bending coupling (smaller B_{ij} terms) are obtained when higher number of layers are treated. The second observation is that more constraints yields, as expected, higher frequencies, particularly when slopes are constrained with the clamped boundaries. Finally, it is interesting to find out that the 30° laminates yielded higher frequencies for the FSFS, SSFS, and FSCS boundaries than the 45° laminates. This is reversed when SSSS, SSCS, and CSCS boundaries are considered.

Table 5.8 shows frequency parameters obtained for a four-layer antisymmetric laminate with a 45° angle (Khdeir 1988a). Higher modes are considered in this analysis. The additional observation made from this analysis is noting that the higher frequency parameters get closer to each other when compared with lower frequency parameters. This may be due to the fact that for higher frequencies, the half sine waves become smaller when compared with the plate dimensions and the boundary conditions influence becomes local at the outer half sine waves. Further comparisons, not shown here, between thick and thin plate theories show that the latter overpredicts the higher frequencies and becomes inaccurate when used for predicting such frequencies.

When the results obtained using the solution presented here with that obtained earlier using Navier solutions for simply supported boundaries at all edges (Table 5.3), the same results were obtained. This is because both methods are exact ones, and the theories used are the same.

5.3.5 Other lamination sequences and boundary conditions

Boundary conditions that are different from those considered earlier or lamination sequences different from those considered in the previous sections (cross-ply and antisymmetric angle-ply) have no exact solutions. Approximate methods must be used in

order to obtain results. The widely used finite element methods have been used by most engineers and researchers in the field to solve practical problems and find the dynamic behavior of composite plates. When parametric studies and/or optimization methods are used to maximize frequencies, finite elements become an expensive tool. Instead, for simple geometries like the flat plates considered here, the less demanding Ritz analysis can be employed. This analysis will be used here.

A series of publications (Leissa 1978, 1981a,b, 1987a,b) listed hundreds of references on the subject. Many of the previous studies concentrated on the theory of the subject, obtaining natural frequencies only for those problems which permit exact solutions (Jones 1973, 1975; Lin 1974).

Simply supported, symmetrically laminated plates were studied by Leissa and Narita (1989). The Ritz method with trigonometric functions was used and reasonably accurate and comprehensive results were obtained. The first eight natural frequencies and mode shapes were obtained for various lamination sequences. Symmetrically laminated cantilevered plates were also analyzed in other studies (Jensen *et al.* 1982; Jensen and Crawley 1984). Experimental and analytical natural frequencies and mode shapes were obtained. The finite element and Ritz methods with beam and plate functions were used. Completely free, symmetrically laminated plates were also analyzed (Sivakumaran 1987). Frequencies obtained by using the finite element method and those obtained by using the Ritz method with algebraic polynomials were compared with experimental results.

The energy functionals derived earlier (Eqs. (5.13)–(5.16)) are consistent with the equations of motion and boundary conditions and, therefore, can be used with energy approaches such as the Ritz method. These equations were successfully applied to obtain the natural frequencies of laminated cantilevered and completely free plates and shells (Qatu 1989; Qatu and Leissa 1991a,b).

The Ritz method with algebraic polynomial displacement functions is used here to solve the vibration problem for laminated composite plates having different boundary conditions. Natural frequencies and mode shapes for plates having two adjacent free edges and the remaining edges either simply supported, clamped or free are presented. Convergence studies are made which demonstrate that accurate results (natural frequencies and mode shapes) can be obtained with this analysis. The effects of various parameters (material, fiber orientation and boundary conditions) upon the natural frequencies and mode shapes are studied.

For free vibrations of a plate having the rectangular planform shown in Figure 5.5, displacements are assumed as

$$\begin{aligned} u(\alpha, \beta, t) &= U(\alpha, \beta) \sin \omega t \\ v(\alpha, \beta, t) &= V(\alpha, \beta) \sin \omega t \\ w(\alpha, \beta, t) &= W(\alpha, \beta) \sin \omega t \end{aligned} \tag{5.63}$$

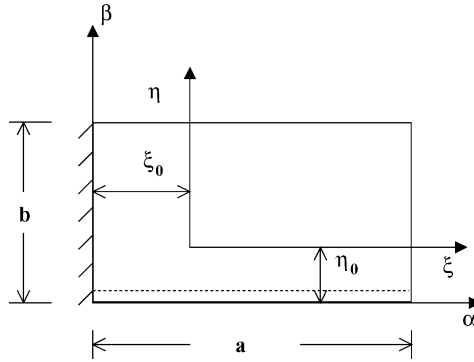


Figure 5.5. Nondimensional coordinates for a CSFF plate.

Trial functions can be used for the displacement functions U , V and W . As stated earlier (Chapter 3), these functions should form a complete set of functions, which guarantees convergence to the exact solution as the number of terms taken increases, and second, they should satisfy the geometric boundary conditions. Several types of functions have been used in the literature. Among the functions used by researchers are trigonometric functions and algebraic ones. Leissa and Narita (1989) have used trigonometric functions. They treated symmetrically laminated simply supported plates. For such plates, the inplane displacements are decoupled for transverse displacements, and only the function W is needed:

$$W(\alpha, \beta) = \sum_{m=1}^M \sum_{n=1}^N \gamma_{mn} \sin\left(\frac{m\pi\alpha}{a}\right) \sin\left(\frac{n\pi\beta}{b}\right) \quad (5.64)$$

Alternatively, algebraic functions can be used. The displacement trial functions, in terms of the nondimensional coordinates ξ and η , are taken as

$$\begin{aligned} U(\xi, \eta) &= \sum_{i=i_0}^I \sum_{j=j_0}^J \alpha_{ij} \xi^i \eta^j \\ V(\xi, \eta) &= \sum_{k=k_0}^K \sum_{l=l_0}^L \beta_{kl} \xi^k \eta^l \\ W(\xi, \eta) &= \sum_{m=m_0}^M \sum_{n=n_0}^N \gamma_{mn} \xi^m \eta^n \end{aligned} \quad (5.65)$$

where $\xi = \alpha/a$ and $\eta = \beta/b$ and ξ_0 and η_0 are defined in Figure 5.5.

The Ritz method requires satisfaction of geometric (forced) boundary conditions only. One can solve for many boundary conditions with the same analytical procedure by using

a suitable selection of the values i_0, j_0, k_0, l_0, m_0 and n_0 . Vibration problems for laminated plates having the boundary conditions XXFF, where X can be simply supported (S), clamped (C), or free (F) can be solved. One should keep in mind that for generally laminated plates there are four types of boundary conditions for each of the simply supported, free and clamped edge conditions (as described in Table 5.9).

For other types of boundary conditions, one can use springs at the free ends. These are springs that cover the whole edge and can actually be functions of the boundary coordinates. These springs will be taken as constants along the boundary at which they are acting (Baharlou and Leissa 1987). Three linear springs and one rotational spring are used at each of the two edges at $\alpha = a$ and at $\beta = b$. For the free edge at $\alpha = a$, a linear spring in the vertical direction (with a spring constant k_z) can be taken to restrain motion vertically; another linear spring is used to restrain motion in the α direction (with a spring constant k_α); a third linear spring can be used to restrain motion in the tangential direction (with a spring constant k_β); finally, a rotational spring about the edge parallel to the β -axis can be used (with a spring constant k_ψ). The strain energy of these springs is

$$U_{\alpha=a} = \frac{1}{2} \int_{\beta=0}^{\beta=b} \left\{ k_\alpha u_0^2(a, \beta) + k_\beta v_0^2(a, \beta) + k_z w_0^2(a, \beta) + k_\psi \left(\frac{\partial w_0(a, \beta)}{\partial \alpha} \right)^2 \right\} d\beta \quad (5.66)$$

Similar treatment can be made for springs at $\beta = b$.

Table 5.9 shows the combinations of i_0, k_0 and m_0 that should be used in the α -direction to get each of the possible boundary conditions at $\alpha = 0$. Similar types of boundary conditions can be obtained at $\beta = 0$ by suitable selection of j_0, l_0 and n_0 . This will enable one to solve for six classical boundary conditions of isotropic, orthotropic or

Table 5.9. Values for values i_0, k_0 and m_0 needed for different boundary conditions at $\alpha = 0$.

B.C. at $\alpha = 0$	i_0	k_0	m_0
F-1	1	1	0
F-2	0	1	0
F-3	1	0	0
F-4	0	0	0
S-1	1	1	1
S-2	0	1	1
S-3	1	0	1
S-4	0	0	1
C-1	1	1	2
C-2	0	1	2
C-3	1	0	2
C-4	0	0	2

anisotropic laminated plates, namely, FFFF, SFFF, SSFF, CFFF, CSFF and CCFF without the need for the added springs at the edges $\alpha = a$ and $\beta = b$. It will also enable one to solve for many combinations of boundary conditions of unsymmetrically laminated plates.

For solving the free vibration problem, the displacement functions are substituted into the energy functional Eqs. (5.13)–(5.16) in order to get an expression for the maximum strain energy (U_{\max}) and into Eq. (5.18) in order to get an expression for the maximum kinetic energy (T_{\max}). The Ritz method requires minimization of the functional ($T_{\max} - U_{\max}$) with respect to the coefficient α_{ij} , β_{kl} , and γ_{mn} , which can be accomplished by setting:

$$\begin{aligned} \frac{\partial(T_{\max} - U_{\max})}{\partial \alpha_{ij}} &= 0, & i &= i_0, i_0 + 1, \dots, I, & j &= j_0, j_0 + 1, \dots, J; \\ \frac{\partial(T_{\max} - U_{\max})}{\partial \beta_{kl}} &= 0, & k &= k_0, k_0 + 1, \dots, K, & l &= l_0, l_0 + 1, \dots, L; \\ \frac{\partial(T_{\max} - U_{\max})}{\partial \gamma_{mn}} &= 0, & m &= m_0, m_0 + 1, \dots, M, & n &= n_0, n_0 + 1, \dots, N, \end{aligned} \quad (5.67)$$

which yields a total of $(I - i_0 + 1) \times (J - j_0 + 1) + (K - k_0 + 1) \times (L - l_0 + 1) + (M - m_0 + 1) \times (N - n_0 + 1)$ simultaneous, linear, homogenous equations in an equal number of unknowns α_{ij} , β_{kl} , and γ_{mn} . Those equations can be described by $\{[K] - \Omega^2[M]\}\{a\} = 0$; where $[K]$ and $[M]$ are the stiffness and mass matrices, respectively, Ω the frequency parameter, and $\{a\}$ the vector of unknown coefficients α_{ij} , β_{kl} , and γ_{mn} .

The determinant of the coefficient matrix is set equal to zero which will yield a set of eigenvalues. Substituting each eigenvalue back into Eq. (5.68) yields the corresponding eigenvector (amplitude ratio) in the usual manner. The mode shape corresponding to each frequency can be determined by substituting the eigenvector back into the displacement functions.

It has been noted that the convergence characteristics and possible matrix ill-conditioning can be improved if one uses the nondimensional coordinates such that they form planes of symmetry. This can be done for the completely free, SSFF and cantilever plates. For that reason, $\xi_0 = \eta_0 = 1/2$ are used for completely free boundaries, where two lines of symmetry are observed. Also, $\xi_0 = 0$ and $\eta_0 = 1/2$ are used for SFFF and CFFF boundaries, where one line of symmetry is observed. Finally, $\xi_0 = \eta_0 = 0$ are used for SSFF, CSFF and CCFF boundary conditions. For the SSFF and CCFF square plates, there exists a diagonal line of symmetry, which cannot be accounted for easily with the present polynomials. It should also be mentioned that the symmetry is preserved only for isotropic or orthotropic rectangular plates, but is lost for generally anisotropic plates.

For symmetrically laminated plates, all of the stretching–bending coupling terms vanish (i.e., $B_{ij} = 0$). This leads to decoupling the inplane displacements from the out-of-plane displacement. Lets keep free boundaries at $\alpha = a$ and $\beta = b$, and thus there is no

need to implement the spring strain energy functionals (Eq. (5.66)). The possible combination of classical boundary conditions at $\alpha = 0$ and at $\beta = 0$, which can be solved by the present method, reduces to six as was mentioned earlier. When the spring strain energy functionals are used to simulate boundary conditions at $\alpha = a$ and at $\beta = b$, then all possible boundary conditions can be treated. Only the last equations of the sets of Eqs. (5.65) and (5.67) are needed for the transverse vibrations of symmetrically laminated plates. This leads to a system of linear, homogenous equations of the order $(M - m_0 + 1) \times (N - n_0 + 1)$. Table 5.10 gives the needed values of m and n for each of the six combinations of boundary conditions. Comparisons among results from the present Ritz analysis and other analytical and experimental ones will be described later.

5.3.5.1 Convergence studies. Convergence studies are made for composite plates representative of those to be analyzed subsequently. These include symmetric laminates of three-layer with stacking sequence $[\theta / - \theta / \theta]$. The angle θ lies between the fibers and the projection of the α -axis upon the plate. Filamentary composite materials of two types were considered, namely E-glass/epoxy (E/E) and graphite/epoxy (G/E). The following material properties were used:

$$\begin{aligned} \text{E-glass/epoxy (E/E): } E_1 &= 60.7 \text{ GPa, } E_2 = 24.8 \text{ GPa, } G_{12} = 12.0 \text{ GPa, } \nu_{12} = 0.23 \\ \text{Graphite/epoxy (G/E): } E_1 &= 138 \text{ GPa, } E_2 = 8.96 \text{ GPa, } G_{12} = 7.1 \text{ GPa, } \nu_{12} = 0.30 \end{aligned} \quad (5.68)$$

The above properties were taken from Vinson and Sierakowski (1986). A typical plate of square planform ($a/b = 1$) is used. Convergence studies of the lowest eight frequency parameters $\Omega = \omega a^2 \sqrt{\rho/E_1 h^2}$ for graphite/epoxy plates having the six boundary conditions which will subsequently be analyzed can be found in Table 5.11. Qatu (1991a,b) listed results for E-glass/epoxy. For each of the six boundary conditions, three solutions are presented. These solutions are obtained by using 36, 49 and 64 terms for the

Table 5.10. Values for m_0 and n_0 used in vibration analysis of symmetrically laminated plates having different boundary conditions at $\alpha = 0$ and $\beta = 0$ and free boundaries at $\alpha = 0$ and $\beta = 0$.

B.C.	m_0	n_0
FFFF	0	0
SFFF	1	0
CFFF	2	0
SSFF	1	1
CSFF	2	1
CCFF	2	2

Table 5.11. Convergence of the frequency parameter $\Omega = \omega a^2 \sqrt{\rho/E_1 h^2}$ for a graphite/epoxy square ($a/b = 1$) plate with $[30^\circ, -30^\circ, 30^\circ]$ lamination using algebraic functions.

B.C.	Determinant size	Ω							
		1	2	3	4	5	6	7	8
FFFF	36	1.6262	2.0910	3.7748	5.1285	5.1924	7.4462	7.9743	9.5453
	49	1.6203	2.0789	3.7177	5.0570	5.1460	7.2263	7.8735	9.1564
	64	1.6202	2.0784	3.7115	5.0517	5.0707	7.0800	7.6870	8.9317
SFFF	36	0.9171	2.5554	3.2899	4.5599	5.8347	7.7369	9.4071	11.792
	49	0.9166	2.5371	3.2786	4.5284	5.7501	7.6644	9.2225	11.255
	64	0.9165	2.5363	3.2754	4.5181	5.6929	7.5070	9.0844	11.085
CFFF	36	0.6519	1.4392	3.1581	4.1996	5.6674	6.7157	8.8263	11.058
	49	0.6513	1.4377	3.1253	4.1881	5.6427	6.6344	8.7529	10.809
	64	0.6507	1.4372	3.1228	4.1839	5.6111	6.5257	8.6460	10.557
SSFF	36	0.4671	1.8437	3.9371	4.6707	6.8341	8.2414	10.919	12.747
	49	0.4656	1.8248	3.9276	4.6559	6.7644	8.1051	10.690	12.395
	64	0.4644	1.8424	3.9263	4.6541	6.7514	8.0780	10.540	12.236
CSFF	36	1.0615	2.4227	5.0125	5.6484	7.9491	9.3699	12.325	14.282
	49	1.0606	2.4211	4.9812	5.6388	7.9011	9.1566	12.059	13.991
	64	1.0600	2.4205	4.9791	5.6243	7.8767	9.0771	11.881	13.713
CCFF	36	1.2913	3.0535	5.5559	6.2780	8.5898	10.367	13.459	14.936
	49	1.2912	3.0518	5.5534	6.2730	8.5715	10.241	12.990	14.570
	64	1.2907	3.0495	5.5463	6.2691	8.5507	10.236	12.970	14.551

first, second, and third solution respectively. Equal number of terms are taken in each of the inplane directions. Zero frequencies corresponding to rigid body modes are not reported.

Convergence is observed to be reasonably good for engineering applications. The maximum difference between the 49- and the 64-term solutions is less than 3% for all the cases. The set of boundary conditions with the poorest convergence is the completely free one. As geometric constraints are imposed on the boundaries, convergence seems to improve, and the fastest convergence is observed for the plate with two adjacent clamped edges (i.e., CCFF plates). The maximum difference in the natural frequencies between the 49- and 64-term solutions for CCFF boundary conditions is 0.07% for E/E material and 0.14% for G/E materials (Qatu 1991a). From these studies, it may be considered that the 64-term solution for plates presents satisfactory convergence for engineering applications. Therefore, unless stated otherwise, 64 terms will be used in the subsequent analyses.

5.3.5.2 Comparison among various results. Table 5.12 shows a comparison made among results from the present method and those taken from Sivakumaran (1987) for a cross-ply *completely free* plate. It also includes results obtained by the finite element method and experimental data obtained by Tracy *et al.* (1985). For this particular laminate, the results show good agreement with experimental results except for the fundamental frequency. It is observed that a fine mesh with 507 degrees of freedom (DOF) was needed for the finite element method to get reasonably accurate results, while only 100-terms are needed (which will result in 100 DOF) in the present analysis to get the converged, accurate frequencies. It is interesting to note that there is major disagreement for at least two frequencies between the results obtained by the Ritz method (Qatu 1991a) and those of Sivakumaran, who also used the Ritz method with algebraic polynomials. It is believed that the present analysis is more accurate because of the convergence obtained. The 100-term solution gave the same results for the first five significant figures as those obtained by using 121 terms. Also, the present method yields closer upper bounds to the exact results with only 100 terms than does that of Sivakumaran with 121 terms. From the data of Table 5.12, it also appears that certain frequencies were missed in the analytical and experimental studies made by Tracy *et al.* (1985).

Another comparison is made in Table 5.13 between the present analysis and that of Sivakumaran for two other laminates and two aspect ratios. The agreement in these cases is excellent – the results agree for the first three significant figures.

Table 5.14 shows a comparison made among results from the present method and analytical and experimental data obtained by Jensen *et al.* (1982) for *cantilevered* plates having six plies. In the latter work, the experimental results were compared with the finite

Table 5.12. Comparison of different analytical frequencies (Hz) with experimental ones. $E_1 = 181$ GPa, $E_2 = 10.3$ GPa, $G_{12} = 7.17$ GPa, $\nu_{12} = 0.28$, $a = 330.2$ mm, $b = 304.8$ mm, $h = 2.29$ mm, $\rho = 1600 \times \text{kg/m}^3$, $[(90, 0, 0)_2, (90, 0)]_s$ laminate.

Ritz analysis (DOF)		Sivakumaran (1987)	Tracy <i>et al.</i> (1985)	
64 DOF	100 DOF	121 DOF	507 DOF (FEM)	Test
44.38	44.38	45.25	44.8	58.7
137.64	137.64	152.33	149.1	152.3
164.26	164.26	168.03	164.0	170.0
172.80	172.79	177.78	–	179.5
194.35	194.34	190.88	–	–
286.50	285.47	293.56	280.0	277.0
379.74	379.67	420.63	405.0	382.0
401.89	401.79	441.02	422.0	409.0
476.23	476.13	462.44	445.0	425.0
494.23	494.09	482.20	461.0	441.0

Table 5.13. Comparison of the frequency parameter $\Omega = \omega a^2 \sqrt{\rho/E_2 h^2}$ obtained by various Ritz analyses.

[(0°, 90°) ₄] _s		[(-45°, 45°) ₄] _s	
Qatu and Leissa (1991a); 100 DOF	Sivakumaran (1987); 121 DOF	Qatu and Leissa (1991a); 100 DOF	Sivakumaran (1987); 121 DOF
<i>a/b</i> = 1			
5.668	5.67	8.608	8.61
17.983	17.98	13.268	13.27
21.318	21.32	17.793	17.79
21.320	21.32	29.019	29.02
24.159	24.16	29.080	29.08
36.338	36.33	39.084	39.08
49.611	49.60	41.627	41.62
52.362	52.35	50.846	50.83
58.738	58.73	56.860	56.85
61.123	61.11	63.315	63.30
<i>a/b</i> = 2			
11.250	11.25	10.676	10.67
21.302	21.30	26.686	26.26
31.299	31.29	34.551	34.54
58.713	58.70	53.719	53.70
67.900	67.88	55.646	55.64
71.990	71.96	76.839	76.81
75.416	75.39	78.327	78.30
88.095	88.05	90.367	90.34
115.16	115.12	123.83	124.16
116.03	115.97	126.21	126.16

element ones and those obtained by using the Ritz method with different combinations of trial functions that consist of three cantilevered beam bending modes, two beam torsional modes, two isotropic plate torsional modes and a chordwise bending mode. Table 5.15 shows further comparisons among the natural frequencies obtained experimentally, by using the finite element method (Crawley 1978, 1979) and ones from the present method (Qatu 1991a). Different laminations and aspect ratios for plates having eight plies are included in both tables.

As can be seen from the comparisons, the present analysis yields a closer upper bound to the exact solution than all the other Ritz solutions. It is also interesting to notice that the present method with only 64 displacement terms, which yields 64 degrees of freedom (DOF), gives more accurate results than those obtained by the finite element method with 365 DOF in Table 5.14, and with 200 DOF when $a = b = 3$ in. and with 365 DOF when $a = 3$ in, $b = 6$ in. in Table 5.15. One can also see that the present method yields results,

Table 5.14. Comparison of analytical and experimental natural frequencies (Hz) for cantilevered plates. $E_1 = 98 \text{ GPa}$, $E_2 = 7.9 \text{ GPa}$, $G_{12} = 5.16 \text{ GPa}$, $\nu_{12} = 0.28$, $a = 304.8 \text{ mm}$, $b = 76.2 \text{ mm}$, $h/\text{ply} = 0.134 \text{ mm}$, $\rho = 1520 \text{ kg/m}^3$.

Qatu and Leissa (1991b)		Jensen <i>et al.</i> (1982)						Test
Ritz 64 DOF	FEA 365 DOF	<i>A</i>	<i>B</i>	<i>C</i>	<i>D</i>	<i>A'</i>	<i>D'</i>	
[0, 0, 90] _s								
11.04	11.1	11.1	11.1	11.1	11.1	11.1	11.1	11.2
69.16	69.5	69.4	69.4	69.3	69.3	69.4	69.3	70.5
39.49	39.5	39.6	39.6	39.6	39.6	40.0	40.0	42.4
[15, 15, 0] _s								
8.923	8.9	8.8	8.8	8.8	8.7	9.0	9.0	9.4
62.52	62.7	67.7	60.5	66.5	59.9	70.3	65.0	66.2
42.82	42.9	50.0	48.8	49.4	48.2	46.5	44.0	45.8
[30, 30, 0] _s								
6.288	6.3	6.3	6.2	6.3	6.2	6.5	6.4	6.6
37.22	37.3	53.3	42.0	52.5	42.0	49.1	41.0	40.0
56.87	56.9	69.9	69.0	60.8	60.7	73.0	59.7	59.1
[45, 45, 0] _s								
4.875	4.9	4.9	4.9	4.9	4.8	5.0	5.0	4.8
30.02	30.1	41.4	32.7	38.5	32.6	39.9	33.0	29.8
49.55	49.4	74.0	73.9	59.1	56.3	74.9	52.4	51.3
[60, 60, 0] _s								
4.179	4.2	4.2	4.2	4.2	4.2	4.3	4.2	4.3
26.04	26.1	30.4	27.0	28.7	26.8	29.9	27.0	27.1
41.81	41.7	65.4	65.4	50.4	47.1	65.6	44.1	47.7
[75, 75, 0] _s								
3.877	3.9	3.9	3.9	3.9	3.9	3.9	3.9	3.8
24.27	24.3	24.9	24.5	24.7	24.4	24.8	24.4	25.1
36.78	36.7	47.2	47.2	40.1	39.2	47.3	37.9	38.9
[90, 90, 0] _s								
3.801	3.8	3.8	3.8	3.8	3.8	3.8	3.8	3.7
23.82	23.9	23.9	23.9	23.9	23.9	23.9	23.9	24.3
35.07	35.1	35.1	35.1	35.1	35.1	35.2	35.2	38.2

which are comparable to the experimental ones. The maximum difference between the present results and experimental ones is within 10%.

5.3.5.3 Natural frequencies and mode shapes. Natural frequencies and contour plots of the mode shapes for different boundary conditions, and the material with the higher

Table 5.15. Comparison of analytical and experimental natural frequencies (Hz) for cantilevered plates. $E_1 = 128$ GPa, $E_2 = 11$ GPa, $G_{12} = 4.48$ GPa, $\nu_{12} = 0.25$, $h/\text{ply} = 0.13$ mm, $\rho = 1500$ kg/m³.

$a = 76.2$ mm, $b = 76.2$ mm			$a = 152.4$ mm, $b = 76.2$ mm		
Qatu and Leissa (1991b)	Crawley (1979)	Test	Qatu and Leissa (1991b)	Crawley (1979)	Test
Ritz 64 DOF	FEA 200 DOF		Ritz 64 DOF	FEA 365 DOF	
[0, 0, 30, -30] _s					
260.3	261.9	234.2	64.9	65.4	58.3
362.1	263.0	262.0	136.9	137.5	148.0
757.6	761.8	728.3	405.8	408.3	362.7
1596.0	1662.0	1449.0	523.0	525.6	508.0
1632.0	1709.0	1503.0	579.9	588.3	546.0
[0, 45, -45, 90] _s					
222.9	224.3	196.4	55.2	55.6	48.6
421.2	421.8	418.0	175.0	175.4	169.0
1010.0	1012.0	960.0	343.4	345.3	303.0
1405.0	1426.0	1215.0	591.0	591.8	554.0
1705.0	1722.0	1550.0	808.8	820.1	739.0
[45, -45, -45, 45] _s					
138.5	138.9	131.2	32.0	31.9	31.3
500.0	499.5	472.0	191.6	191.3	185.8
801.2	805.0	790.5	228.7	228.2	214.0
1319.0	1326.0	1168.0	564.8	565.3	533.0
1640.2	1648.0	1486.0	708.8	708.3	653.0

orthotropy ratio (i.e., G/E) are given in Figures 5.6–5.10. The aspect ratio (a/b) is chosen to be one indicating square plates. Three-layer $[\theta, -\theta, \theta]$ laminates are used. The lamination angle is varied from 0 to 90° with an increment of 15°. For FFFF, SSFF and CCFF square plates, geometric symmetry about the line $\xi = \eta$ exists. This results in the frequencies for plates with the fiber angles $\theta = 60, 75$ and 90° being the same as those with the fiber angles $\theta = 30, 15$ and 0°, respectively.

It is noticed that increasing the fiber angle θ from 0 to 45° increases the lowest two nondimensional frequencies for plates with geometric symmetry about the $\xi = \eta$ line (i.e., FFFF, SSFF and CCFF plates). From the symmetry of the problems, increasing the fiber angle from 45 to 90° decreases these frequencies. This indicates that the maximum fundamental frequencies are obtained with the fiber angle equals to 45° for these boundary conditions. For that angle, the fibers are parallel (or perpendicular) to the line of geometric diagonal symmetry. This observation is true for both materials considered (Qatu 1991a). The effect of the orthotropy ratio is more clear for the second lowest frequency than it is for the first one. Increasing the fiber angle from 0 to 45° increases the second lowest frequency by only 3.4% for E/E material and by 37% for G/E material

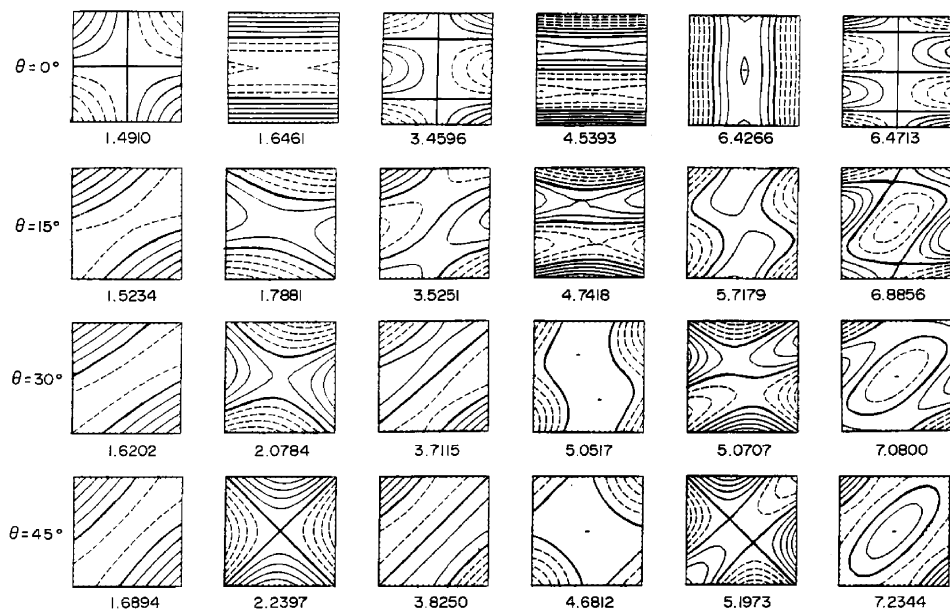


Figure 5.6. Mode shapes and frequency parameters $\Omega = \omega a^2 \sqrt{\rho/E_1 h^2}$ for FFFF, G/E $[\theta, -\theta, \theta]$ square plates.

when the boundary conditions are completely free. Similar observations are true for the other two boundary conditions (i.e., SSFF and CCFF). Mode interaction occurred for the remaining frequencies, but generally maximum frequencies occurred at the fiber angle of 45°. These results are better illustrated by Figures 5.11 and 5.12 which show the impact of the fiber angle on the first and second frequency parameters for various boundary conditions.

For plates with the line of geometric symmetry is $\eta = 0$ (i.e., SFFF and CFFF plates) the behavior is different. For cantilever plates, it is observed that increasing the fiber orientation angle from 0 to 90° decreases the fundamental frequency, which corresponds to the first bending mode. This effect is larger for the material with the higher orthotropy ratio (i.e., G/E). Increasing the fiber angle from 0 to 90° decreases the lowest natural frequency by 75% for G/E materials and only by 35% for E/E materials. For the second lowest frequency, which corresponds to the first twisting mode, the maximum natural frequency is obtained when the fiber angle is 30°. The difference between the maximum second frequency (at the fiber angle $\theta = 30^\circ$) and the minimum one (at the fiber angle $\theta = 0^\circ$) is considerably larger for the plates with higher orthotropy ratio (i.e., G/E material). For SFFF plates, increasing the fiber orientation increases the fundamental

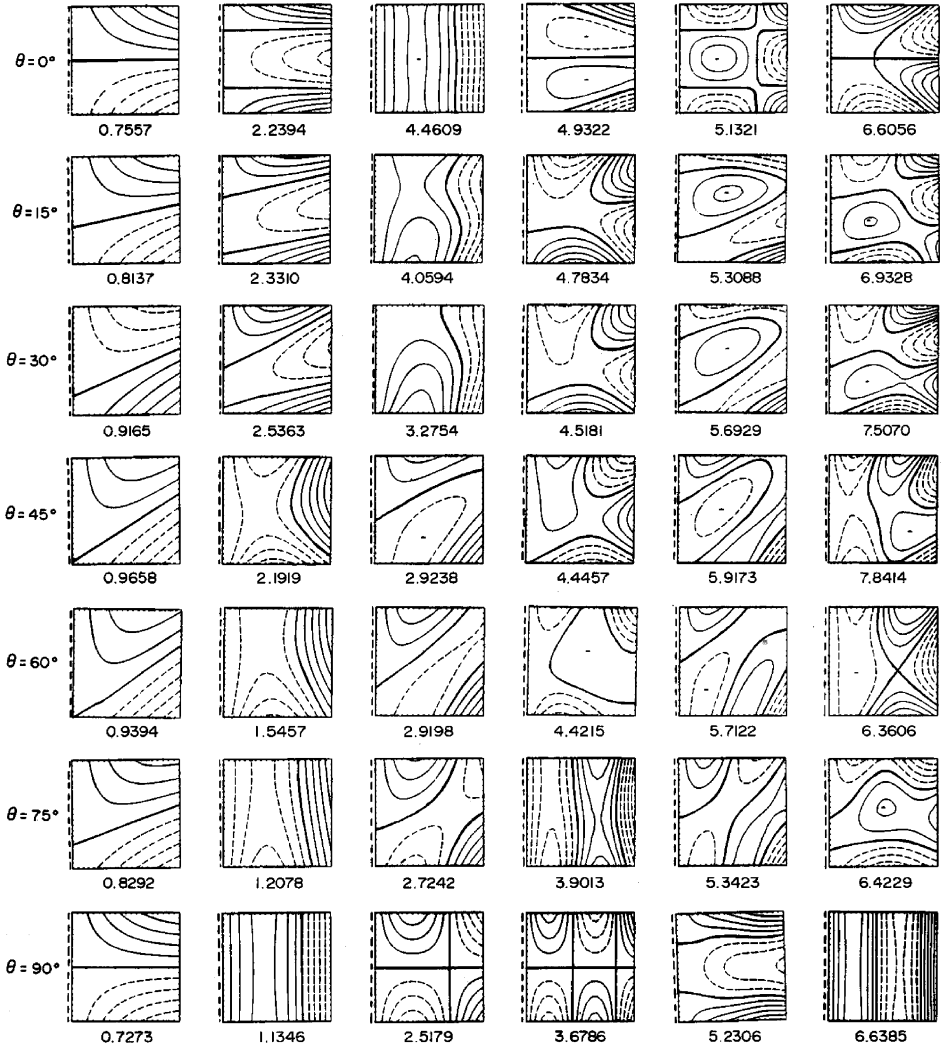


Figure 5.7. Mode shapes and frequency parameters $\Omega = \omega a^2 \sqrt{\rho/E_1 h^2}$ for SFFF, G/E $[\theta, -\theta, \theta]$ square plates.

frequency for the fiber angles from 0 to 45° and decreases it afterwards. This indicates that the fundamental frequency for SFFF plates should be corresponding to the first twisting mode, which is what Figure 5.7 shows. This observation is true for both material and is stronger for the G/E plates.

For CSFF plates, the geometric symmetry is lost, and the fundamental frequency is observed to be maximum when the fiber angle is 15° for E/E materials and is 0° for G/E

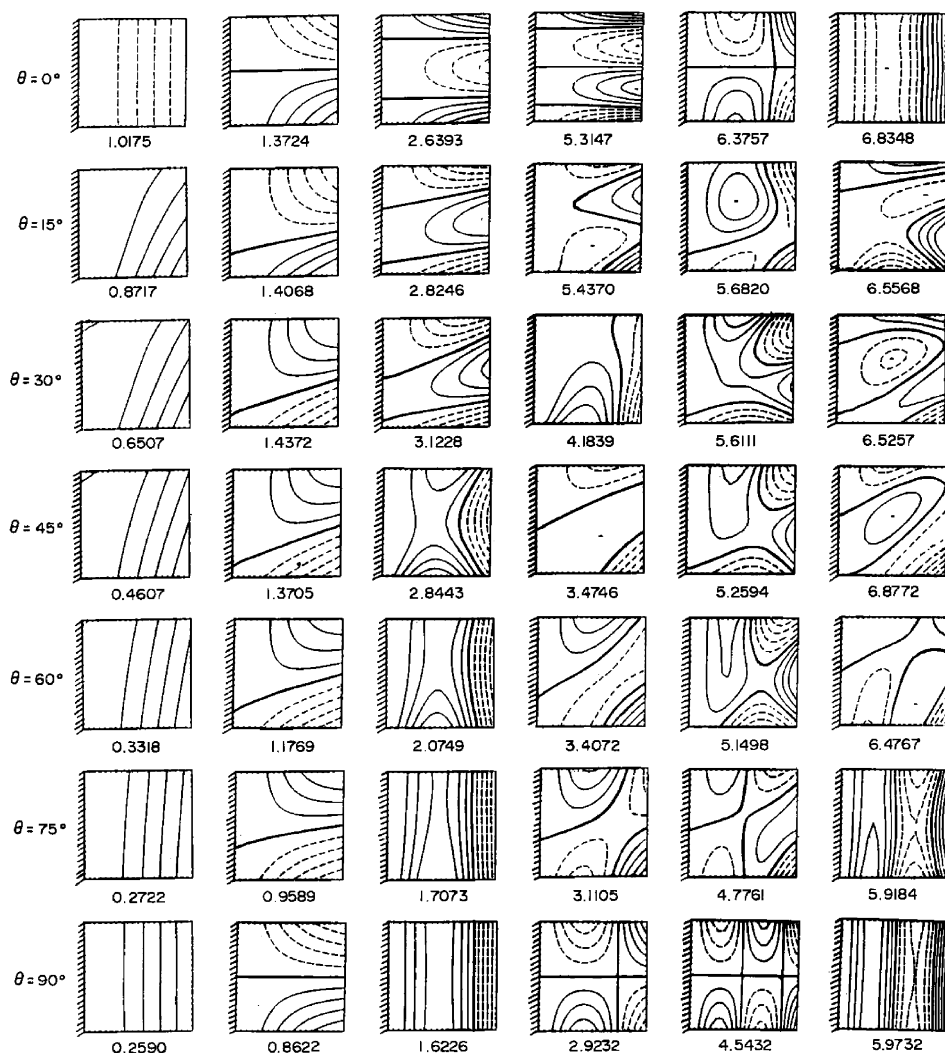


Figure 5.8. Mode shapes and frequency parameters $\Omega = \omega a^2 \sqrt{\rho/E_1 h^2}$ for cantilevered (CFFF), G/E $[\theta, -\theta, \theta]$ square plates.

materials. This is closer to the 0° fiber angle than the 90° one because the clamped boundary condition imposes stronger constraints than does the simple support boundary condition.

Mode shapes for $\theta = 0, 15, 30$ and 45° are shown for completely free, SSFF and CCFF plates. For these boundary conditions, mode shapes for $\theta = 60, 75$ and 90° are similar to

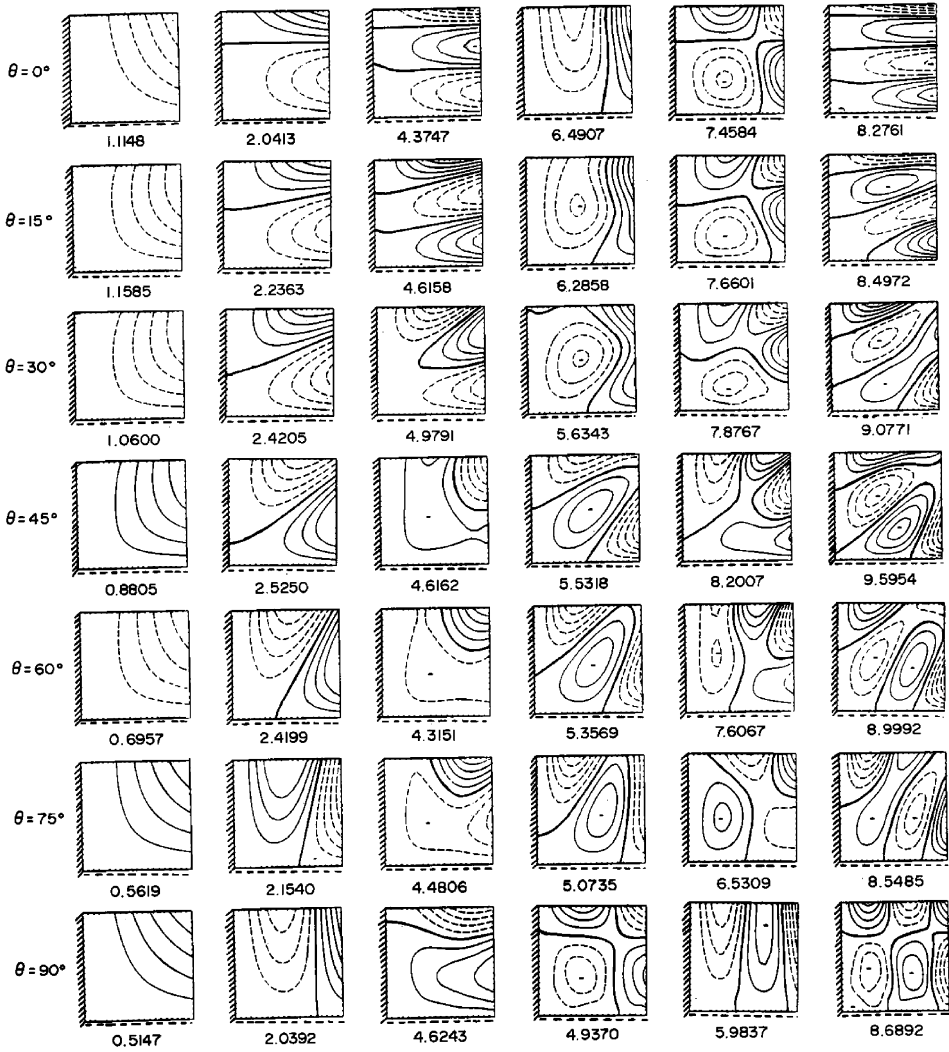


Figure 5.9. Mode shapes and frequency parameters $\Omega = \omega a^2 \sqrt{\rho/E_1 h^2}$ for CSFF, G/E $[\theta, -\theta, \theta]$ square plates.

those given for the $\theta = 30, 15$ and 0° , respectively; and can be easily obtained by changing the coordinates. Heavier lines in the sketches are node lines (i.e., lines with zero displacements). The absolute maximum displacement in the mode shapes is normalized to one. The displacement between the contour lines is one-fifth of the maximum displacement. The first six mode shapes are given.

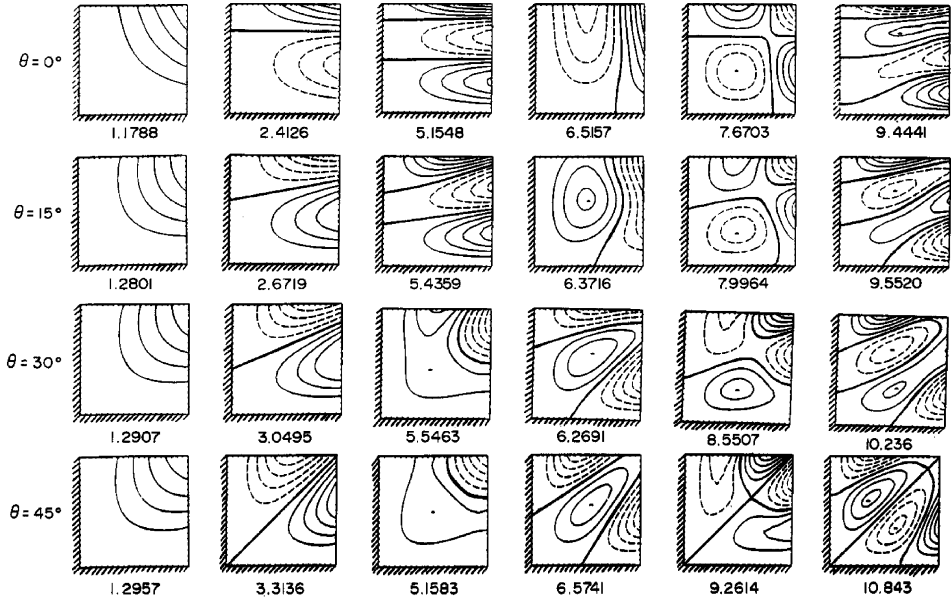


Figure 5.10. Mode shapes and frequency parameters $\Omega = \omega a^2 \sqrt{\rho/E_1 h^2}$ for CCFF, G/E $[\theta, -\theta, \theta]$ square plates.

For the completely free boundary condition, one should note that four possible symmetry classes exist in the displacement functions chosen. For example, one can choose $m = n = 0, 2, 4, \dots$, for the doubly symmetric (i.e., symmetric about both the ξ and

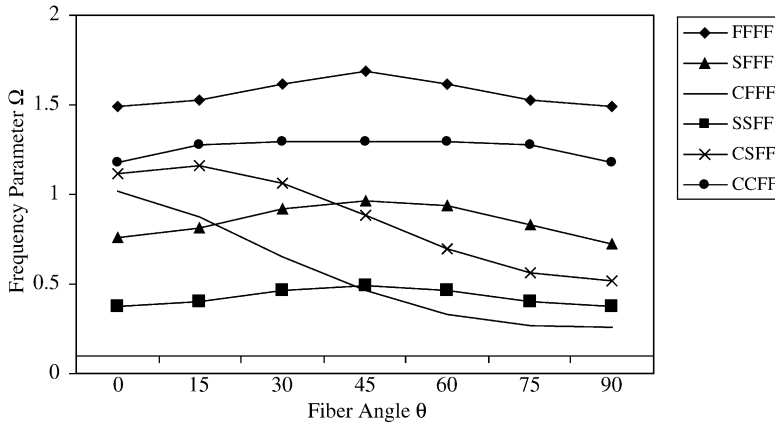


Figure 5.11. Effect of the fiber angle on the first frequency parameter $\Omega = \omega a^2 \sqrt{\rho/E_1 h^2}$ for G/E $[\theta, -\theta, \theta]$ square plates.

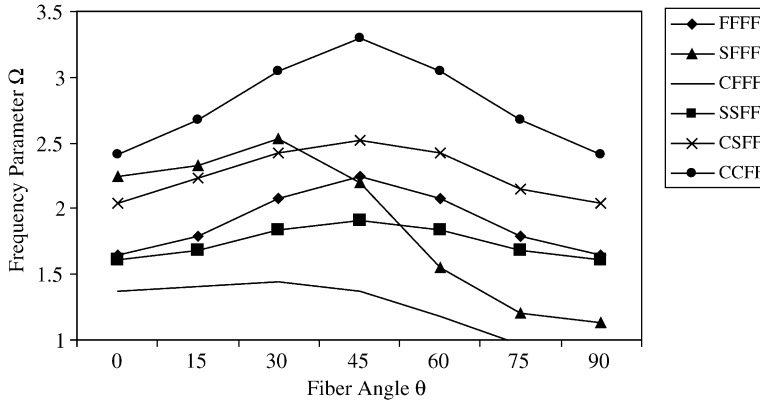


Figure 5.12. Effect of the fiber angle on the second frequency parameter $\Omega = \omega a^2 \sqrt{\rho/E_1 h^2}$ for G/E $[\theta, -\theta, \theta]$ square plates.

η -axes) modes. Similar choices can be made for the other three symmetry classes. These symmetry classes about the ξ and η axes exist for the isotropic, orthotropic and cross-ply plates only. This symmetry is lost for plates with angle-ply lamination, and one should keep all the terms in the polynomials. For the special case of diagonally orthotropic angle-ply laminates which are made of 45° angle layers, the symmetry classes exist about the diagonals (Figure 5.6). The gradual change in contour lines with increasing θ is evident.

For plates with SFFF and CFFF (i.e., cantilever) boundaries, only two classes of symmetry are possible in the displacement functions (i.e., the displacement functions can be either symmetric or antisymmetric about the ξ -axis). Figures 5.7 and 5.8 give the first six mode shapes for these plates. For example, to obtain the symmetric modes one should chose $n = 0, 2, 4, \dots$. This symmetry/antisymmetry in the mode shapes can be seen for isotropic and cross-ply laminated plates. For angle-ply plates, the symmetry classes are lost, and one should keep all the terms in the analysis. One should keep in mind that one zero frequency exists for SFFF plates which corresponds to the rigid body mode (rotation about the η axis). For SFFF plates with $\theta = 0^\circ$ and the fibers are parallel to the α -axis, the second mode shape is the first symmetric mode with two nodal lines parallel to the α -axis. The equivalent to this mode when $\theta = 90^\circ$ (i.e., the fibers are perpendicular to the α -axis) is the fifth mode, and the actual second mode has one nodal line in the direction of the fibers. Similar observations are made for the cantilever plates. This shows that for certain mode shapes, more nodal lines tend to appear parallel to the direction of the fibers.

Plates having CSFF boundary conditions do not permit any symmetry or antisymmetry in the mode shapes. The mode shapes tend to be similar to those obtained for plates with CCFF and SSFF boundary conditions, with curve crossing being replaced

by curve veering in most of the cases. For all laminates, the first mode is the double bending mode. The second mode has one nodal line in the ξ direction for $\theta = 0^\circ$ and one nodal line in the η -direction for $\theta = 90^\circ$. For laminates with other lamination angles, the second mode has one nodal line making an angle with the ξ -axis almost the same as the lamination angle. This shows that the previously mentioned observation of more nodal lines tend to appear in the direction of the fibers is also evident for this boundary condition.

For SSFF and CCFF plates, the mode shapes are very similar, and only those of the CCFF plate are given in Figure 5.10. For these boundary conditions, symmetry about the diagonal $\xi = \eta$ exists only for isotropic and diagonally orthotropic plates with layers making a 45° angle with the ξ -axis. For these laminates, mode shapes can be either symmetric or antisymmetric about the diagonal $\xi = \eta$. The gradual change in contour plots as the angle θ increases is clear.

Leissa and Narita (1989) used trigonometric functions (Eq. (5.64)) to obtain natural frequencies and mode shapes for symmetrically laminated, simply supported plates. Table 5.16 shows the convergence characteristics of these functions for a three-layered $[30^\circ, -30^\circ, 30^\circ]$ graphite/epoxy laminate. Note that Leissa and Narita (1989) used a different frequency parameter. The convergence is reasonably fast, and reliable results were obtained. Similar observations were reported about the convergence characteristics among all studies. Convergence is fastest with the weakest orthotropy ratio (lowest) and highest number of layers.

Table 5.16 also shows convergence studies made for the same material using algebraic polynomials. Eq. (5.66) was used to simulate the boundary conditions at $\alpha = a$ and $\beta = b$ in the energy functional. Interestingly, the algebraic polynomials yielded

Table 5.16. Convergence of the frequency parameter $\Omega = \omega a^2 \sqrt{12\rho(1 - \nu_{12}\nu_{21})/E_1 h^2}$ for a graphite/epoxy square ($a/b = 1$) simply supported plate with $[30^\circ, -30^\circ, 30^\circ]$ lamination using trigonometric functions.

M, N	Determinant size	Ω							
		1	2	3	4	5	6	7	8
<i>Trigonometric trial functions (Leissa and Narita 1989)</i>									
8	64	12.07	22.15	36.05	36.29	49.99	53.87	70.59	72.85
10	100	12.01	22.04	35.95	36.14	49.75	53.95	70.24	72.54
12	144	11.97	21.97	35.88	36.04	49.60	53.43	70.04	72.35
<i>Algebraic trial functions</i>									
	36	11.82	21.82	36.37	41.71	62.73	76.07	107.79	115.61
	49	11.79	21.69	35.89	36.32	50.30	58.06	76.05	91.74
	64	11.76	21.61	35.56	35.83	49.48	54.30	72.98	74.17

Table 5.17. Effect of the lamination angle on the frequency parameter $\Omega = \omega a^2 \sqrt{12\rho(1 - \nu_{12}\nu_{21})/E_1 h^2}$ for a three-layer $[\theta/ - \theta/\theta]$, graphite/epoxy, square ($a/b = 1$), simply supported plate (Leissa and Narita 1989).

Lamination angle (degrees)	Ω							
	1	2	3	4	5	6	7	8
0	11.29	17.13	28.69	40.74	45.16	45.78	54.08	68.53
15	11.46	18.69	31.20	39.15	45.91	48.19	58.70	67.84
30	11.97	21.97	35.88	36.04	49.60	53.43	70.04	72.35
45	12.31	23.72	34.14	38.45	54.10	56.31	66.20	76.63

slightly better accuracy than the trigonometric series for the lower frequencies and worse accuracy for the higher frequencies.

The effect of the lamination angle on both the frequencies and mode shapes were also reported. Table 5.17 shows the effect of the lamination angle on graphite/epoxy three layered square plates. It is interesting to see how maximum frequencies were obtained at a lamination angle of 45° for most, but not all results. These maximum frequencies were underlined. Leissa and Narita (1989) reported more results for different lamination sequences and materials.

Table 5.18 shows a comparison between frequency parameters $\Omega = \omega a^2 \sqrt{\rho/E_1 h^2}$ obtained using exact and Ritz methods for $[0^\circ, 90^\circ, 0^\circ]$ E-glass/Epoxy simply supported square plates. The exact results were obtained by both CPT and SDPT. A thickness ratio of 20 (i.e., $a/h = 20$) is used, which is the limit of CPT. As seen in the table, CPT overpredicts the natural frequencies in general but is still relatively accurate, especially for the first six frequencies, with error less than 5%. It is less accurate for higher frequencies. Furthermore, the Ritz method is overpredicting the frequencies obtained by

Table 5.18. Comparison between frequency parameters obtained using exact, and Ritz methods for $[0^\circ, 90^\circ, 0^\circ]$ E-glass/epoxy simply supported square plates $\Omega = \omega a^2 \sqrt{\rho/E_1 h^2}$.

m	n	Exact CPT	Exact SDPT	Ritz CPT (64 terms)
1	1	4.4345	4.3909	4.4354
1	2	9.8576	9.6648	9.8578
2	1	12.858	12.472	12.904
2	2	17.738	17.075	17.761
1	3	19.215	18.520	19.485
2	3	26.578	25.219	26.907
3	1	27.069	25.421	27.435
3	2	31.649	29.529	32.026

the exact method. The difference between the results obtained by the Ritz and exact analyses is less than 1% for all the results shown. This analysis is building confidence in both the convergence characteristics and accurate prediction of the Ritz method. Further results will be presented for various boundary conditions of E-glass/epoxy laminates.

Table 5.19a shows the fundamental non-zero frequency parameters obtained using exact and Ritz methods with 36-term beam functions (Leissa 1973b). Table 5.19b shows the same fundamental frequencies obtained using the Ritz method with 49-term algebraic polynomials. Both tables show the results for isotropic square plates. All 21 combinations of classical boundary conditions for isotropic square plates are considered in the analysis. The frequency parameters of $\Omega = \omega a^2 \sqrt{\rho/D}$ are used in these results. The table is constructed such that it starts with the least constrained plates and ends with the most constrained ones. This table is constructed as a reference to upcoming studies on composite laminates. It establishes the accuracy of the current analysis. The difference between the results obtained here and those obtained by Leissa is less than 1% for almost all the frequencies, particularly the lower ones.

Table 5.19a. Frequency parameters $\Omega = \omega a^2 \sqrt{\rho/D}$ for isotropic square plates obtained using exact (results below with *) and Ritz methods with 36-term beam functions (Leissa 1973b).

	1	2	3	4	5	6
FFFF	13.489	19.789	24.432	35.024	35.024	61.526
SFFF	6.648	15.023	25.492	26.126	48.711	50.849
CFFF	3.492	8.525	21.429	27.331	31.111	54.443
SSFF	3.369	17.407	19.367	38.291	51.324	53.738
CSFF	5.364	19.171	24.768	43.191	53.000	64.050
CCFF	6.942	24.034	26.681	47.785	63.039	65.833
SFSF*	9.631	16.135	36.726	38.945	46.738	70.740
CFSF	15.285	20.673	39.775	49.730	56.617	77.368
SSSF*	11.685	27.756	41.197	59.066	61.861	90.294
CSSF	16.865	31.138	51.631	64.043	67.646	101.210
CCSF	17.615	36.046	52.065	71.194	74.349	106.280
CFCF	22.272	26.529	43.664	61.466	67.549	79.904
SCSF*	12.687	33.065	41.702	63.015	72.398	90.611
CSCF	23.460	35.612	63.126	66.808	77.502	108.990
CCCF	24.020	40.039	63.193	76.761	80.713	116.800
SSSS*	19.739	49.348	49.348	78.957	98.696	98.696
CSSS*	23.646	51.674	58.646	86.135	100.270	113.228
CCSS	27.056	60.544	60.791	92.865	114.570	114.720
CSCS*	28.951	54.743	69.327	94.585	102.216	129.096
CCCS	31.829	63.347	71.084	100.830	116.400	130.370
CCCC	35.992	73.413	73.413	108.270	131.640	132.240

Table 5.19b. Frequency parameters $\Omega = \omega a^2 \sqrt{\rho/D}$ for isotropic square plates obtained using 49-term algebraic polynomials.

	1	2	3	4	5	6
FFFF	13.469	19.596	24.271	34.808	34.808	62.947
SFFF	6.644	14.902	25.378	26.001	48.454	50.585
CFFF	3.472	8.512	21.293	27.200	30.977	54.204
SSFF	3.367	17.316	19.293	38.211	51.043	53.501
CSFF	5.353	19.078	24.677	43.096	52.718	63.797
CCFF	6.923	23.918	26.589	47.668	62.736	65.574
SFSF*	9.631	16.134	36.721	38.944	46.745	70.732
CFSF	15.140	20.442	39.709	49.274	55.908	78.260
SSSF*	11.684	27.755	41.195	59.061	61.826	91.773
CSSF	16.808	31.104	51.434	64.031	67.520	101.140
CCSF	17.537	36.025	51.825	71.085	74.286	106.010
CFCF	22.181	26.437	43.611	61.208	67.250	82.152
SCSF*	12.689	33.060	41.701	63.017	72.405	91.973
CSCF	23.315	35.703	62.909	66.761	77.346	109.768
CCCF	23.903	39.972	63.240	76.772	80.543	116.663
SSSS*	19.738	49.343	49.345	78.943	100.104	100.123
CSSS*	23.658	51.513	58.877	86.307	101.575	113.499
CCSS	26.907	60.545	60.554	95.934	114.979	115.842
CSCS*	28.902	54.685	69.413	94.766	103.070	129.267
CCCS	31.686	62.914	71.359	100.172	117.285	132.143
CCCC	35.773	73.182	73.374	108.606	134.395	134.445

Appendix A displays the fundamental six non-zero frequency parameter for a three layer $[\theta, -\theta, \theta]$ laminated square plate made of E-glass/epoxy materials. The angle varies from 0 to 90° with 15° increments. Frequencies are listed for all 21 boundary combinations. The frequency parameter $\Omega = \omega a^2 \sqrt{\rho/E_1 h^2}$ is used. Notice that for the FFFF, SSFF, CCFF, SSSS, CCSS, and CCCC boundary condition, the results obtained for 60, 75, and 90° are the same as those obtained for 30, 15, and 0°, respectively. This is because of the symmetrical characteristics of these boundary configurations.

5.4. TRIANGULAR AND TRAPEZOIDAL PLATES

Triangular and trapezoidal plates are encountered in different engineering applications. Only plates with rectangular orthotropy will be treated in this section. The treatment of plates with rectangular orthotropy on planforms other than rectangular presents an interesting problem. This is related to how the problem should be formulated. One alternative is to use a triangular coordinate system, following the geometric boundaries, and

rewriting the equations to follow this coordinate system. The second alternative is to maintain the rectangular coordinates and perform the analysis on the current planform. The second alternative is proven to be relatively easier and will be adopted in the following analysis. Completely free as well as cantilevered laminated plates are treated here.

Although significant attention has been given to other plate configurations (e.g., circular, elliptical, parallelogram, other quadrilaterals, hexagonal, sectorial). Only recently accurate results were presented for completely free triangular (Leissa and Jaber 1992; Kim and Dickinson 1990) and trapezoidal isotropic plates (Qatu *et al.* 1993; Qatu 1994c). Other studies are found in the literature which deal with other boundary conditions.

5.4.1 Completely free

Vibrations of laminated composite angle-ply triangular and trapezoidal plates with completely free boundaries are studied. Similar to the analysis performed earlier for rectangular plates, the Ritz method with algebraic polynomials is used. Detailed convergence studies are made and show that relatively accurate results can be obtained. Results are then obtained and listed for the lowest frequencies and for a set of shapes including right and symmetrical triangular and trapezoidal thin plates.

Consider a plate of arbitrary shape, as shown in Figure 5.13 where its boundary is defined by the four straight lines:

$$\alpha = a_1, \quad \alpha = a, \quad \beta = b\alpha/a, \quad \text{and} \quad \beta = -c\alpha/a \quad (5.69)$$

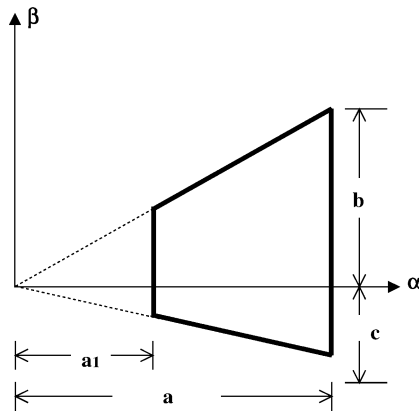


Figure 5.13. Parameters used for triangular and trapezoidal plates.

where a_1 , a , b and c are defined in Figure 5.13. If one chooses a_1 to be zero, then the shape will represent a triangular plate. Any other value of a_1 (less than a) will make the shape trapezoidal.

The displacement functions U , V and W can be written in terms of the nondimensional coordinates in a manner similar to Eq. (5.65) (note that all the coefficients values i_0, j_0, k_0, l_0, m_0 and n_0 are zeros). The Ritz method requires satisfaction of the geometric (forced) boundary conditions only, which do not exist for a completely free case. Subsequently, Eq. (5.65) represents the complete set of polynomials to be used here. The same procedure that was applied for rectangular plates is carried out here, keeping in mind that the double integration of the energy functional and subsequent coefficient minimization is performed in the plate field:

$$U = \frac{1}{2} \int_{a_1}^a \int_{-c\alpha/a}^{ba/a} [] d\beta d\alpha = \frac{1}{2} \int_{\xi_1}^1 \int_{-\eta_1\xi}^{(1-\eta_1)\xi} [] a(b+c) d\eta d\xi \quad (5.70)$$

where $\xi = \alpha/a$, $\eta = \beta/(b+c)$, $\xi_1 = a_1/a$, $\eta_1 = c/(b+c)$. The terms in brackets represent the energy functional differential terms.

5.4.1.1 Convergence studies. The algebraic polynomials used guarantee convergence to the exact solution as the upper limits of the summations are increased. There are two computational limitations. The first one is matrix ill-conditioning because of round-off errors, and the second is computer time and cost. Ill-conditioning is the more serious limitation for the present problems. This difficulty may be greatly alleviated by orthogonalizing the polynomials before using them. However, this process increases the computational time considerably and introduces other numerical difficulties. Another approach to decrease the severity of ill-conditioning is to perform the computations using the highly precise (29 significant figures in double precision) supercomputers (Qatu and Bataineh 1992). For the problem considered here, sufficient accuracy was obtained by using ordinary (i.e., nonorthogonal) polynomials and by performing all computations on a main line computer with double precision (16 significant figures). However, to achieve this, careful convergence studies were conducted.

An equal number of terms is taken in both directions ($I = J$) of the polynomials because, as was found earlier, this yields the least upper bound for most frequencies. The 6×6 (36 term) results are compared with those from the more accurate 7×7 (49 term) and 8×8 (64 term) solutions.

Table 5.20 shows a convergence study for the nondimensional frequencies $\omega a^2 \sqrt{\rho/E_1 h^2}$ of a laminated right (i.e. $c = 0$) triangular ($a_1/a = 0$) and trapezoidal ($a_1/a = 0.25$ and 0.5) plates. As is typical for the Ritz method, convergence of the frequencies is monotonic, with successively closer upper bounds being achieved as

Table 5.20. Convergence of the frequency parameter $\omega a^2 \sqrt{\rho/E_1 h^2}$ for completely free graphite/epoxy right triangular and trapezoidal plates, $[30^\circ, -30^\circ, 30^\circ]$ laminate, $a/b = 1$, $c/b = 0$.

a_1/a	No. of terms	Mode number							
		1	2	3	4	5	6	7	8
0	6×6	2.752	5.164	5.784	7.520	11.86	13.85	16.67	17.47
	7×7	2.742	5.128	5.759	7.470	11.63	13.81	14.38	17.07
	8×8	2.742	5.125	5.752	7.373	11.49	13.45	14.26	17.02
0.25	6×6	2.781	5.215	6.842	8.963	12.68	15.28	17.05	22.22
	7×7	2.770	5.187	6.804	8.906	12.21	14.74	15.15	20.15
	8×8	2.770	5.183	6.744	8.835	12.06	14.62	15.05	19.77
0.5	6×6	2.770	5.550	7.336	12.49	15.63	21.14	22.88	28.64
	7×7	2.754	5.530	7.316	12.08	13.76	19.79	20.50	25.62
	8×8	2.754	5.512	7.220	11.93	13.64	19.62	20.05	23.39

additional terms are taken in the displacement polynomial. The first (i.e., lowest) eight non-zero frequencies are given for various solution sizes. Other convergence studies have also been performed for symmetrical ($c = b$) plates (Qatu 1994b). Only convergence of graphite/epoxy plates is considered because previous studies (Qatu 1989) showed that convergence of materials with a lower orthotropy ratio (e.g., E-glass/epoxy) is faster.

Convergence is observed to be good for the fundamental frequency, where it is achieved for the first three significant figures, for all the plates considered. Higher frequencies do not converge as fast. The slowest convergence occurs for the eighth frequency.

For right plates, the maximum difference between the 7×7 and 8×8 solutions is 2.7% for the sixth frequency of triangular plates. This difference is the highest for the eighth frequency of the trapezoidal plates with $a_1/a = 0.5$, where it is 9.5%. For symmetrical plates, convergence is observed to be even slower. For these plates, the maximum difference between the 7×7 and the more accurate 8×8 solutions is 12.6% for the seventh frequency of triangular plates and 10.6% for trapezoidal plates with $a_1/a = 0.25$ and 19% for trapezoidal plates with $a_1/a = 0.5$. This shows that the convergence is slow for the higher frequencies (typically the seventh or eighth frequency). Convergence is also slower for plates with higher a_1/a ratio. This is why only four significant figures are given in this and all subsequent analyses. Convergence for the first six frequencies is relatively good, and results have converged to within 10% of the most accurate ones for almost all these frequencies. A study will now be presented for a set of triangular and trapezoidal plate configurations. Theoretically, all possible shapes may be achieved by varying the parameters a_1/a , a/b and c/b . Poor convergence and/or ill-conditioning is observed when a trapezoidal plate with high a_1/a ratio is treated.

5.4.1.2 Natural frequencies. Right triangular and trapezoidal plates are first considered. For these plates $c = 0$. Two a/b ratios are considered, namely 1 and 1.732. These values give rise to interesting configurations with a plate “opening” angle (at the left corner of the plate in Figure 5.13) of 45 and 30°, respectively. One triangular plate ($a_1/a = 0$) and two trapezoidal ($a_1/a = 0.25$ and 0.5) are studied (Qatu 1994b); only results for $a_1/a = 0.25$ are presented here. Results are presented in Tables 5.21 and 5.22 for right triangular and trapezoidal plates. In each of these tables, the lamination angle in a three-layer laminate $[\theta, -\theta, \theta]$ is varied from 0 to 90° by an increment of 15°. Results for graphite/epoxy materials are presented here. Results for other materials are found by Qatu (1994b).

For right *triangular* plates with a/b ratio of 1, results obtained for the natural frequencies for $\theta = 60, 75$ and 90° are the same as those obtained for $\theta = 30, 15$ and 0°. This is due to the symmetry in this particular plate configuration. For these plates, the maximum fundamental frequency occurs when the lamination angle equals to 45° (Figure 5.14). The maximum second frequency occurs at the lamination angle of 30° (or 60°). For plates with a/b ratio of 1.732, no such symmetry exist. For these plates the maximum fundamental frequency occurs at an angle of lamination equal to 15°. The maximum second frequency occurs at an angle of 45°, while the maximum third

Table 5.21. Effect of varying the lamination angle θ on the frequency parameter $\omega a^2 \sqrt{\rho/E_1 h^2}$ for free right triangular graphite/epoxy $[\theta, -\theta, \theta]$ plates.

θ (degrees)	Mode number							
	1	2	3	4	5	6	7	8
<i>a/b = 1.0</i>								
0	1.816	3.677	5.021	7.281	9.019	10.04	12.45	16.84
15	2.133	4.453	5.568	7.457	9.584	10.86	15.80	16.66
30	2.742	5.125	5.752	7.373	11.49	13.45	14.26	17.02
45	3.577	4.357	5.555	10.05	10.59	12.50	14.99	19.98
60	2.741	5.125	5.752	7.373	11.49	13.45	14.26	17.02
75	2.133	4.453	5.568	7.457	9.584	10.86	15.80	16.66
90	1.816	3.677	5.021	7.281	9.019	10.04	12.44	16.84
<i>a/b = 1.732</i>								
0	4.020	7.291	10.28	11.89	16.18	20.45	24.68	27.82
15	5.587	7.841	8.925	14.53	19.31	19.98	24.95	28.79
30	5.414	8.068	9.736	14.43	19.26	22.54	25.73	29.69
45	3.619	8.767	10.21	12.62	17.39	22.13	28.19	29.62
60	2.650	6.801	8.852	13.21	15.59	19.21	23.59	28.74
75	2.209	5.625	7.347	10.91	14.34	18.32	21.07	24.30
90	2.013	5.034	6.474	9.700	12.67	16.24	20.66	24.44

Table 5.22. Effect of varying the lamination angle θ on the frequency parameter $\omega a^2 \sqrt{\rho/E_1 h^2}$ for free right trapezoidal graphite/epoxy plates, $[\theta, -\theta, \theta]$ laminate, $a_1/a = 0.25$.

θ (degrees)	Mode number							
	1	2	3	4	5	6	7	8
$a/b = 1.0$								
0	1.927	4.139	5.039	8.167	9.945	12.18	13.84	16.92
15	2.213	4.626	5.603	9.021	10.82	12.06	16.56	17.35
30	2.770	5.183	6.744	8.835	12.06	14.62	15.05	19.77
45	3.740	5.290	6.413	10.42	12.24	14.51	17.23	20.56
60	3.925	5.163	6.057	10.72	12.58	13.44	16.93	20.72
75	3.085	4.618	7.432	8.470	10.16	15.73	16.74	18.70
90	2.510	4.171	6.543	8.581	9.757	12.14	16.70	18.36
$a/b = 1.732$								
0	4.554	8.344	12.18	13.24	17.71	22.02	23.96	27.55
15	5.839	8.348	8.825	10.94	15.71	20.57	23.62	29.14
30	6.806	9.233	10.14	18.01	22.33	24.63	27.07	35.43
45	5.172	9.879	12.10	14.70	21.72	28.10	28.70	33.91
60	3.873	8.906	10.57	15.67	19.16	22.69	29.93	33.38
75	3.224	7.418	8.713	14.60	17.60	21.16	25.06	30.47
90	2.919	6.399	7.939	12.68	15.76	21.21	24.50	26.32

frequency occurs at $\theta = 0^\circ$. Most of the maximum frequencies in the rest of the results occur at an angle of lamination between 0 and 45° . This may give an indication on the type of mode shape (not presented here) corresponding with each of these frequencies.

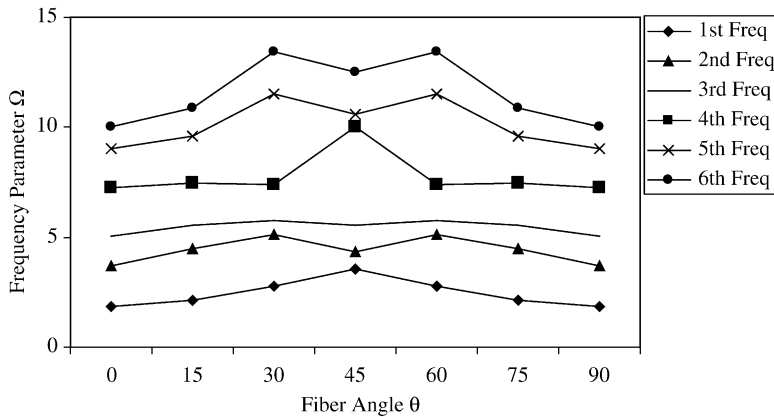


Figure 5.14. Effect of varying the lamination angle θ on the frequency parameter $\omega a^2 \sqrt{\rho/E_1 h^2}$ for free right triangular graphite/epoxy $[\theta, -\theta, \theta]$ plates, $a/b = 1$.

For right *trapezoidal* plates with $a_1/a = 0.25$, the maximum fundamental frequency occurs at the angle $\theta = 60^\circ$ when $a/b = 1.0$ and at $\theta = 30^\circ$ when $a/b = 1.732$. As the value of a_1 increases, the maximum fundamental frequency occurs at a higher angle of lamination. For trapezoidal plates with $a_1/a = 0.5$, the maximum fundamental frequency occurs at $\theta = 75^\circ$ when $a/b = 1.0$ and at $\theta = 45^\circ$ when $a/b = 1.732$ (Qatu 1994b).

Tables 5.23 and 5.24 present the natural frequencies of different symmetrical triangular and trapezoidal plates with $c = b$. Again, for these plates, two values of a/b are taken, namely 1 and 1.732, which correspond to opening angles of 90° and 60° at the left corner of the plate. The later ratio present the interesting *equilateral* plate configuration for triangular plates. Three-layer laminates with variable angle of lamination θ are studied.

For symmetrical *triangular* plates with $a/b = 1$, the maximum fundamental frequency occurs at $\theta = 90^\circ$. The maximum second frequency occurs at a lamination angle of 75° for graphite/epoxy materials (and at an angle of 60° for E-glass/epoxy as per Qatu 1994b). For the equilateral triangle (Table 5.23), the maximum fundamental frequency occurs at a lamination angle of 45° , and the maximum second frequency is at 30° . For this particular triangle, frequencies obtained for the lamination $[-\theta, \theta, -\theta]$ are expected to be the same as those obtained here for $[\theta, -\theta, \theta]$.

For symmetrical trapezoidal plates, the maximum fundamental frequency occurs at the angle of 90° (i.e., when the fibers are parallel to the two parallel edges at $\alpha = a_1$ and a).

Table 5.23. Effect of varying the lamination angle θ on the frequency parameter $\omega a^2 \sqrt{\rho/E_1 h^2}$ for symmetrical triangular graphite/epoxy plates, $[\theta, -\theta, \theta]$ laminate.

θ (degrees)	Mode number							
	1	2	3	4	5	6	7	8
$a/b = 1.0$								
0	0.7596	1.358	2.370	2.630	4.182	4.279	6.457	7.387
15	0.7861	1.441	2.473	2.750	4.418	4.528	6.547	7.842
30	0.8747	1.663	2.692	3.153	4.853	5.288	6.513	8.628
45	1.038	1.962	2.940	3.924	4.684	5.811	7.051	9.281
60	1.246	2.162	3.254	3.663	4.958	6.231	7.788	8.755
75	1.471	2.184	2.895	3.832	5.395	6.013	7.358	8.255
90	1.777	1.960	2.553	4.689	4.760	6.136	6.635	8.829
$a/b = 1.732$								
0	2.115	2.911	5.346	5.884	8.479	9.854	11.46	14.17
15	2.165	3.124	5.418	6.115	8.264	10.33	11.76	14.41
30	2.355	3.275	5.901	6.691	7.499	11.25	13.59	14.34
45	2.555	3.062	6.072	6.617	8.455	11.05	12.89	15.21
60	2.328	3.155	5.740	6.362	8.817	10.58	11.97	14.95
75	2.134	3.182	5.364	6.176	8.158	10.13	11.90	14.00
90	2.100	3.098	5.272	6.692	6.918	10.02	12.29	13.71

Table 5.24. Effect of varying the lamination angle θ on the frequency parameter $\omega a^2 \sqrt{\rho/E_1 h^2}$ for symmetrical trapezoidal graphite/epoxy plates, $[\theta, -\theta, \theta]$ laminate, $a_1/a = 0.25$.

θ (degrees)	Mode number							
	1	2	3	4	5	6	7	8
$a/b = 1.0$								
0	0.7475	1.365	2.348	2.636	4.303	4.477	6.692	7.614
15	0.7717	1.447	2.490	2.778	4.489	4.727	7.158	8.032
30	0.8590	1.674	2.792	3.220	5.084	5.390	8.176	8.916
45	1.029	2.056	3.091	4.028	5.613	6.659	7.456	9.640
60	1.257	2.524	3.353	4.498	5.359	6.672	8.468	9.706
75	1.512	2.878	3.041	4.154	5.909	7.420	8.033	8.829
90	1.804	2.356	3.055	4.914	5.869	6.189	8.341	9.529
$a/b = 1.732$								
0	2.100	2.939	5.350	6.293	10.07	10.15	13.58	14.95
15	2.173	3.195	5.527	6.594	10.19	10.61	13.11	15.23
30	2.407	3.620	6.068	7.401	9.680	11.77	13.46	15.60
45	2.684	3.775	6.669	8.048	8.773	12.77	15.30	16.00
60	2.866	3.680	6.491	7.482	10.15	12.12	13.74	17.36
75	2.890	3.460	6.175	7.583	9.281	11.53	14.10	17.26
90	3.048	3.140	6.659	7.203	8.060	13.17	13.47	16.27

This is true for all configurations. The difference between the highest (at $\theta = 0^\circ$) and the second highest (at $\theta = 75^\circ$) fundamental frequencies increases for plates with higher orthotropy ratio (i.e., graphite/epoxy) and higher a_1/a ratios (Qatu 1994b).

5.4.2 Cantilevered

The natural frequencies for cantilevered laminated composite angle-ply right triangular and trapezoidal plates will be presented using the Ritz method. Similar to the previously treated completely free plates, detailed convergence studies are made to show the accuracy of the obtained results. Comparisons with experimental and analytical frequencies available in the literature for *isotropic* cantilevered triangular plates are made. Results are then obtained and listed for the lowest six frequencies, and for a set of shapes of right triangular and trapezoidal thin plates.

While limited references are available for laminated triangular plates, isotropic cantilevered triangular plates received considerable attention. An early investigation by Gustafson *et al.* (1953) listed frequencies obtained experimentally for the cantilever isotropic triangular plates. This investigation was followed by other analytical ones. Cristensen (1963) used the grid-work approximation. Anderson (1954) and Bhat (1981) used the Ritz method in their analytical solution to the same problem. Mirza and Bijlani

(1983) obtained frequencies by using the finite element method. In two recent publications by Kim and Dickinson (1990, 1992), the Ritz method was used to obtain natural frequencies for right and generally shaped triangular plates. Recently, Qatu (1994c) presented results for cantilevered triangular and trapezoidal laminated plates.

This section will present results for laminated composite cantilevered plates. We will also study the effects of parameters like the lamination angle and orthotropy ratio on the natural frequencies of these plates.

Consider a right-angled plate, as shown in Figure 5.15 where its boundary is defined by the four straight lines:

$$\alpha = a_1, \quad \alpha = a, \quad \beta = b\alpha/a, \quad \text{and} \quad \beta = 0 \quad (5.71)$$

where a_1 , a and b are defined in Figure 5.15. Again, if one chooses a_1 to be zero, then the shape will represent a triangular plate. Any other value of a_1 less than a will make the shape trapezoidal.

The Ritz method, in a fashion quite similar to that used for the completely free triangular plates, is used for cantilevered plates. The main difference is the coefficients in Eq. (5.65). For cantilevered triangular (and/or trapezoidal) plate, with clamped boundaries along $\beta = 0$, the coefficients $i_0 = k_0 = m_0 = 0$, $j_0 = l_0 = 1$, and $n_0 = 2$ are chosen to satisfy the geometric boundary conditions, as was done for rectangular plates (Table 5.2). Attention should also be given to the integration which should be carried over the domain of the triangular and/or trapezoidal plate as was done in Eq. (5.70), with the special consideration that $\eta_1 = 0$ because we will only treat right cantilevered plates here (Figure 5.15).

For symmetrically laminated plates, all of the stretching–bending coupling (i.e., $B_{ij} = 0$) terms vanish, and the inplane displacements are decoupled from the

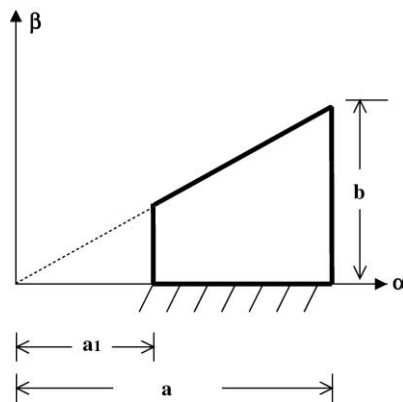


Figure 5.15. Parameters used for triangular and trapezoidal cantilevered plates.

out-of-plane one. This leads to a system of linear, homogenous equations of the order $(M + 1) \times (N - 1)$.

5.4.2.1 Convergence studies. Convergence studies of composite plates representative of those to be analyzed subsequently are conducted. The laminates considered here are symmetric with the stacking sequence $[\theta, -\theta, \theta]$. An equal number of terms is taken in both inplane directions of the plate ($I = J$).

Table 5.25 shows a convergence study for the nondimensional frequencies of a laminated graphite/epoxy triangular ($a_1/a = 0$) and trapezoidal ($a_1/a = 0.25$ and 0.5) plates. The first (i.e., lowest) six frequencies are given for various solution sizes.

Convergence is shown to be particularly good for all the plate configurations discussed earlier. In fact, frequencies converged to the first three significant figures in almost all the results. Furthermore, convergence is observed to be the fastest for triangular plates. For these plates, the maximum difference between the frequencies obtained by using 7×7 terms and those obtained by using 8×8 terms is less than 0.03% for all the results. Convergence is slightly slower for plates, which are trapezoidal. Such difference is less than 0.1% for plates with $a_1/a = 0.25$ and less than 0.2% for ones with $a_1/a = 0.5$. This is an excellent convergence (compared with the completely free case studied earlier).

5.4.2.2 Comparison with other results. Table 5.26 shows a comparison of the natural frequencies obtained by different methods for cantilevered isotropic triangular plates with a/b ratios of 1 and 0.5. The experimental results obtained by Gustafson (1953) were nondimensionalized by assuming a Young's modulus value of 28.5×10^6 psi

Table 5.25. Convergence of the frequency parameters $\omega a^2 \sqrt{\rho/E_1 h^2}$ for $[30^\circ, -30^\circ, 30^\circ]$ laminated cantilevered graphite/epoxy plate with $a/b = 1$ (Qatu 1994c).

a_1/a	No. of terms	Mode number					
		1	2	3	4	5	6
0	6×6	0.7260	3.095	4.464	7.594	11.15	14.45
	7×7	0.7259	3.094	4.460	7.589	11.06	14.05
	8×8	0.7259	3.094	4.459	7.588	11.05	14.04
0.25	6×6	0.6694	2.931	4.000	7.299	10.67	13.64
	7×7	0.6689	2.930	3.996	7.295	10.63	13.35
	8×8	0.6686	2.930	3.991	7.293	10.62	13.27
0.5	6×6	0.5351	2.636	3.716	7.139	11.22	13.94
	7×7	0.5348	2.634	3.705	7.135	11.12	13.49
	8×8	0.5344	2.633	3.698	7.132	11.11	13.48

Table 5.26. Comparison of frequency parameters $\omega b^2 \sqrt{\rho h/D}$ for isotropic plates obtained by different methods ($\nu = 0.3$).

Source	Method	Mode number					
		1	2	3	4	5	6
<i>a/b = 1</i>							
Present (Qatu 1994c)	Ritz (8 × 8 terms)	6.1646	23.457	32.669	56.148	76.426	99.323
	Ritz (9 × 9 terms)	6.1640	23.456	32.664	56.147	76.413	99.312
Kim and Dickinson	Ritz (9 × 9 terms)	6.1640	23.457	32.664	56.149	76.422	99.312
Bhat	Ritz	6.1732	23.477	32.716	56.405	78.207	107.79
Cristensen	Grid-work	6.16	23.70	32.54	55.01	75.87	85.31
Mirza and Bijlani	FEM (25 elements)	6.1588	23.061	33.289	55.915	74.487	99.466
Gustafson <i>et al.</i>	Experiment	5.93	23.4	32.7	55.9	75.8	99.4
Walton	Finite difference	6.20	23.7	32.7	55.7	73.6	96.5
	Experimental	5.88	23.2	32.4	55.4	75.2	98.5
<i>a/b = 0.5</i>							
Present	Ritz (8 × 8 terms)	6.6224	28.436	49.402	69.660	116.80	133.05
	(9 × 9 terms)	6.6216	28.435	49.397	69.651	116.79	132.94
Kim and Dickinson	Ritz (9 × 9)	6.6217	28.435	49.398	69.651	116.79	132.94
Anderson	Ritz	5.887	25.40	—	—	—	—
Mirza and Bijlani	FEM (25 elements)	6.6963	29.499	51.011	77.759	122.77	167.78

(196.5×10^9 Pa), a Poisson's ratio of 0.3 and a material density of 0.281 lb/in.^3 (7778 kg/m^3) which are typical values for steel. Kim and Dickinson (1990) used a Ritz analysis similar to the present one with edge functions to satisfy the clamped boundary conditions. Bhat (1981) used a Ritz analysis with beam functions. Different nonconforming triangular plate elements were used by Mirza and Bijlani (1983).

Results obtained here agree well with those obtained by Kim and Dickinson. This is no surprise because Kim and Dickinson used a similar analysis. The present results agree very well with those of Mirza and Bijlani and the experimental ones for all the lowest six frequencies when $a/b = 1$. Results obtained by Bhat and Cristensen are seen to differ by approximately 10% for the sixth frequency. The results obtained by different methods for $a/b = 0.5$ seem to have good agreement especially those presented here and those given by Kim and Dickinson. The finite element method overpredicts the higher frequencies considerably.

It should be mentioned here that not all the above methods guarantee convergence to the exact solution. The use of nonconforming elements does not guarantee this for all the finite element results presented here. Orthogonal beam functions do not form a complete set of functions which, again, does not guarantee convergence to the exact solution.

5.4.2.3 Natural frequencies. Three a/b ratios are considered (0.577, 1 and 1.732). These values result in interesting configurations with a plate “opening” angle (at the left corner of the plate in Figure 5.13) of 60, 45 and 30°, respectively. For each of these ratios, the results of one triangular plate ($a_1/a = 0$) and another trapezoidal ($a_1/a = 0.25$) are presented. Other results for $a_1/a = 0.5$ are available (Qatu 1994c). Results are presented for the triangular and trapezoidal plates in Tables 5.27 and 5.28, respectively. The lamination angle in a three-layer laminate $[\theta, -\theta, \theta]$ is varied from 0 to 90° by an increment of 15°.

The highest fundamental frequency for all triangular plates is found at a lamination angle of $\theta = 75^\circ$ (Figure 5.16). This is interesting because of the interaction between the triangular planform and the clamped boundary. In the case of rectangular plates, previous studies showed that the maximum fundamental frequency always occurs at an angle perpendicular to the clamped edge. This would be a fiber angle of 90° for our case because the clamped edge is at $\alpha = 0$. The difference between the highest fundamental frequency

Table 5.27. Effect of varying θ on the frequency parameters $\omega a^2 \sqrt{\rho/E_1 h^2}$ for composite triangular plates; $[\theta, -\theta, \theta]$ graphite/epoxy.

θ (degrees)		Mode number					
		1	2	3	4	5	6
$a/b = 0.577$	0	0.1694	0.731	1.544	1.801	3.253	3.815
	15	0.1847	0.800	1.847	1.948	3.609	4.416
	30	0.2323	0.994	2.270	2.478	4.474	5.497
	45	0.3361	1.145	1.418	2.543	3.543	5.837
	60	0.4966	2.048	2.541	5.081	6.425	7.799
	75	0.6202	2.220	2.732	5.515	6.710	7.607
	90	0.5631	1.870	2.954	4.661	6.420	8.089
$a/b = 1$	0	0.4857	2.047	3.146	5.065	7.604	9.650
	15	0.5438	2.345	3.729	5.732	9.160	10.66
	30	0.7259	3.094	4.459	7.588	11.05	14.04
	45	1.082	4.386	5.019	10.97	12.43	13.69
	60	1.490	4.775	6.410	10.93	14.19	16.33
	75	1.691	4.419	7.857	9.317	14.99	16.31
	90	1.529	3.926	7.737	8.691	12.87	16.27
$a/b = 1.732$	0	1.351	5.024	7.278	12.72	17.20	22.22
	15	1.553	6.303	7.921	15.54	19.83	22.58
	30	2.164	8.500	9.341	19.63	23.34	24.60
	45	3.156	9.350	13.42	19.39	28.49	31.55
	60	4.059	9.591	16.63	19.33	28.07	33.42
	75	4.505	9.186	15.82	22.09	24.85	36.11
	90	4.174	8.486	14.63	22.11	23.25	37.29

Table 5.28. Effect of varying θ on the frequency parameters $\omega a^2 \sqrt{\rho/E_1 h^2}$ for composite trapezoidal plates; $[\theta, -\theta, \theta]$ graphite/epoxy, $a_1/a = 0.25$.

θ (degrees)		Mode number					
		1	2	3	4	5	6
$a/b = 0.577$	0	0.1623	0.7111	1.425	1.792	3.222	3.782
	15	0.1739	0.7719	1.608	1.929	3.562	4.307
	30	0.2110	0.9421	1.910	2.343	4.390	5.351
	45	0.2978	1.326	2.296	3.310	5.819	6.510
	60	0.4431	2.001	2.259	4.914	5.926	7.660
	75	0.5942	2.010	2.727	5.022	6.709	7.436
	90	0.5618	1.807	2.922	4.497	6.190	8.006
$a/b = 1$	0	0.4740	1.965	2.936	5.029	7.431	9.641
	15	0.5205	2.241	3.292	5.651	8.870	10.60
	30	0.6686	2.930	3.991	7.293	10.61	13.27
	45	0.9881	4.356	4.404	10.40	11.32	13.63
	60	1.426	4.429	6.289	9.672	14.18	16.15
	75	1.683	4.296	7.852	8.612	13.95	15.88
	90	1.529	3.915	7.660	8.610	12.44	15.87
$a/b = 1.732$	0	1.342	4.771	7.114	12.45	16.71	21.80
	15	1.521	5.851	7.732	14.68	18.99	22.04
	30	2.078	7.776	9.290	17.12	23.33	24.51
	45	3.081	8.876	13.16	17.58	27.28	29.65
	60	4.049	9.460	16.05	18.91	25.24	33.25
	75	4.505	9.181	15.73	22.01	24.01	32.88
	90	4.173	8.486	14.60	22.01	23.21	30.79

obtained at $\theta = 75^\circ$ and the second highest fundamental frequency obtained at $\theta = 90^\circ$ becomes larger as the orthotropy and/or aspect (a/b) ratios increase. The second fundamental frequency occur at $\theta = 75^\circ$ also for triangular plates with $a/b = 0.577$ and at $\theta = 60^\circ$ for $a/b = 1.732$. All higher frequencies occur at a lamination angle between 45 and 90° .

For trapezoidal plates with $a_1/a = 0.25$, the highest fundamental frequency occurs at the lamination angle $\theta = 60^\circ$ and the second highest occurs at $\theta = 75^\circ$ when $a/b = 0.577$. The highest second frequency occurs at $\theta = 75^\circ$. For the other two aspect ratios (a/b) the maximum fundamental frequency occurs at $\theta = 75^\circ$ and the maximum second frequency occurs at $\theta = 60^\circ$. All higher frequencies occurs at an angle between $\theta = 45$ and 90° .

For the remaining trapezoidal plates with $a_1/a = 0.5$, the highest fundamental frequency occurs at the lamination angle of 90° for a/b ratios of 0.577 and 1.0 and at $\theta = 60^\circ$ for $a/b = 1.732$. The configuration of these trapezoidal plates is closer to the rectangular one, and subsequently, the results show trends similar to those of rectangular plates (Qatu 1994c).

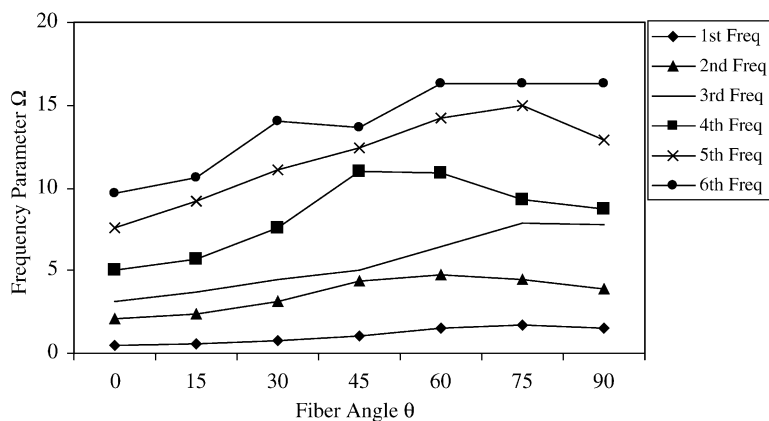


Figure 5.16. Effect of varying the lamination angle θ on the frequency parameters $\omega\alpha^2\sqrt{\rho/E_1h^2}$ for composite triangular plates; $[\theta, -\theta, \theta]$ graphite/epoxy laminate, $a/b = 1$.

5.5. CIRCULAR PLATES

Circular plates made of isotropic materials have received considerable attention in the literature. The earlier monograph of Leissa (1969) listed more than 40 papers on the subject prior to 1969. Orthotropic circular plates, on the other hand, received much less attention. Orthotropic circular plates can exist in many engineering applications including such plates made of wood or concrete. Fiber-reinforced laminated composite circular plates have received much less attention. This can be due to the difficulty in constructing such plates. One can use traditional fibers to construct circular plates in different ways. The first of these is to actually construct the laminates with rectangular orthotropy, cut the plates (or sheets) in circular shapes and then build the laminates from such sheets.

On the other hand, one can also construct the sheets such that the fibers take a circular shape around the center of the plates and circular orthotropy will result from this, which requires special treatment. In the later case, difficulty may rise in constructing these sheets with fibers oriented in the radial direction from the center of the plate. This is because these fibers have constant diameters and the space between the fibers increases as the fibers are extended farther from the center of the plate. This will result in elastic constants that are functions of the radius of the plates, and treatment of such plates is doable but not straightforward. One can also introduce additional fibers as the spacing between the original fibers starting at the center becomes large enough to allow adding additional fibers. Other possible fiber orientations will be presented in this section.

The analysis of circular plates will be treated for only two types:

1. Plates that are made with sheets having rectangular orthotropy and then are cut in circular shapes;
2. Plates that are made of single layers having circular orthotropy.

5.5.1 Circular plates with rectangular orthotropy

These plates can be treated in a manner similar to that of Section 5.4 on triangular plates with special attention to the integration of the energy functional over a circular area (rather than rectangular or triangular as was done earlier) as in Figure 5.17. An earlier paper treated isotropic plates on curvilinear planforms using rectangular coordinates (Narita and Leissa 1986). Such treatment can be extended for laminated circular plates. The energy functional of thin plates (Eqs. (5.11)–(5.16)) can be used for a vibration analysis. For such analysis, the integration of the area should be conducted over the circular plate field:

$$U = \frac{1}{2} \int_{-a}^a \int_{-\sqrt{1-(\alpha/a)^2}}^{\sqrt{1-(\alpha/a)^2}} [] d\alpha d\beta = \frac{1}{2} \int_{-1}^1 \int_{-\sqrt{1-\xi^2}}^{\sqrt{1-\xi^2}} [] d\xi d\eta \quad (5.72)$$

where $\xi = \alpha/a$, $\eta = \beta/b$. The term in bracket represents the terms from the energy functional. A Ritz analysis can then be performed. This formulation is actually valid for plates with curvilinear planform and can be easily specialized to that of a circular planform by letting $a = b$.

5.5.2 Circular plates with circular orthotropy

The fundamental formulation of the theory of plates must be revisited when circular plates with circular orthotropy are treated. For such plates, the fundamental equations need to be

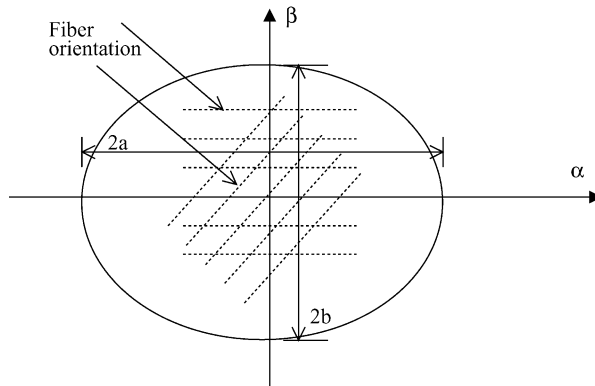


Figure 5.17. Plates having rectangular orthotropy on curvilinear planforms.

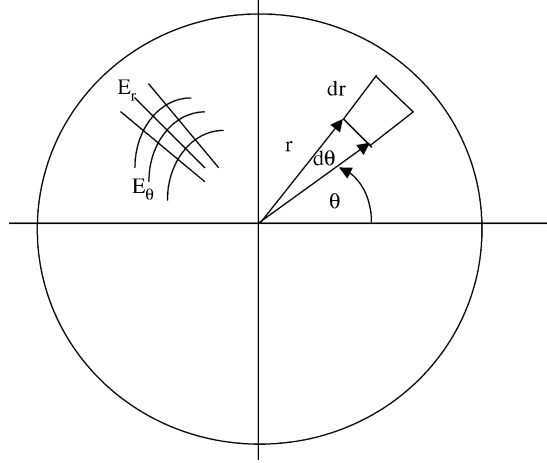


Figure 5.18. Circular plates with circular orthotropy.

re-written in polar coordinates. This can be performed with proper selection of Lamé parameters. Consider the circular plate of Figure 5.18 and its polar coordinates. The following parameters can be applied to the equations derived earlier to obtain equations in polar coordinates:

$$\alpha = r, \quad \beta = \theta, \quad A = 1, \quad B = r \quad (5.73)$$

We will first derive the equations for thin plates.

5.5.2.1 Thin circular plates. The midsurface strains, curvature and twist changes are obtained by substituting Eq. (5.73) into Eqs. (5.2)–(5.4):

$$\begin{aligned} \varepsilon_{0r} &= \frac{\partial u_0}{\partial r} \\ \varepsilon_{0\theta} &= \frac{1}{r} \frac{\partial v_0}{\partial \theta} + \frac{u_0}{r} \\ \gamma_{0\alpha\beta} &= \frac{\partial v_0}{\partial r} + \frac{1}{r} \frac{\partial u_0}{\partial \theta} - \frac{v_0}{r} \end{aligned} \quad (5.74)$$

$$\begin{aligned} \kappa_r &= \frac{\partial \psi_r}{\partial r}, \quad \kappa_\theta = \frac{1}{r} \frac{\partial \psi_\theta}{\partial \theta} + \frac{\psi_r}{r} \\ \tau &= \frac{\partial \psi_\theta}{\partial r} + \frac{1}{r} \frac{\partial \psi_r}{\partial \theta} - \frac{\psi_\theta}{r} \end{aligned} \quad (5.75)$$

where

$$\psi_r = -\frac{\partial w_0}{\partial r}, \quad \psi_\theta = -\frac{1}{r} \frac{\partial w_0}{\partial \theta} \quad (5.76)$$

For laminated circular plates with each layer having circular orthotropy, a transformation matrix can be built from the orthotropic directions 1 and 2 (Figure 1.3) to the (r, θ) coordinates. For that to be done, the angle the fibers make with the principle coordinates (r, θ) must be kept the same as shown in Figure 5.19. This is not a straightforward task, because the additional fibers have to be laid down as one goes farther from the center. This may be the reason why such construction received no attention in the literature. Once done, however, the same lamination theory developed earlier in Chapter 1 (Eqs. (1.3)–(1.9)) can be extended to those for plates laminated of layers each having circular orthotropy. This will yield the following stress resultant equations:

$$\begin{bmatrix} N_r \\ N_\theta \\ N_{r\theta} \\ - \\ M_r \\ M_\theta \\ M_{r\theta} \end{bmatrix} = \begin{bmatrix} A_{11} & A_{12} & A_{16} & B_{11} & B_{12} & B_{16} \\ A_{12} & A_{22} & A_{26} & B_{12} & B_{22} & B_{26} \\ A_{16} & A_{26} & A_{66} & B_{16} & B_{26} & B_{66} \\ - & - & - & - & - & - \\ B_{11} & B_{12} & B_{16} & D_{11} & D_{12} & D_{16} \\ B_{12} & B_{22} & B_{26} & D_{12} & D_{22} & D_{26} \\ B_{16} & B_{26} & B_{66} & D_{16} & D_{26} & D_{66} \end{bmatrix} \begin{bmatrix} \varepsilon_{0r} \\ \varepsilon_{0\theta} \\ \gamma_{0r\theta} \\ - \\ \kappa_r \\ \kappa_\theta \\ \tau \end{bmatrix} \quad (5.77)$$

In real applications of laminated circular plates, the lamination angle is kept as either 0 or 90°. This leads to cross-ply lamination and $A_{16} = A_{26} = B_{16} = B_{26} = D_{16} = D_{26} = 0$.

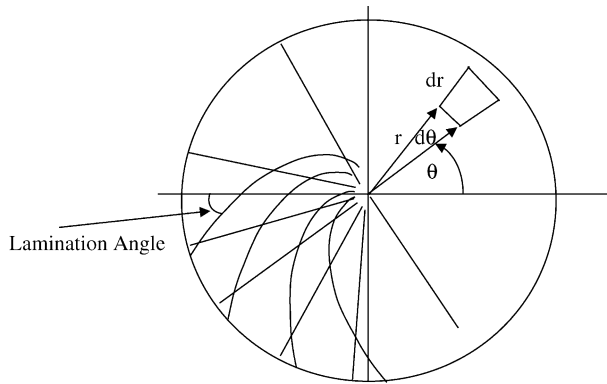


Figure 5.19. Circular plates with circular orthotropy at a lamination angle other than 0 or 90°.

Consider plates constructed with one layer and fibers being in the radial direction (Leissa 1969). The material may be regarded as being homogeneous and orthotropic. Applying the Kirchhoff hypothesis of neglecting shear deformation and the assumption that ε_z is negligible, then the stress-strain equations for an element of material at distance z from the middle surface can be written as

$$\begin{aligned}\varepsilon_r &= \frac{1}{E_r}(\sigma_r - \nu_r \sigma_\theta), \\ \varepsilon_\theta &= \frac{1}{E_\theta}(\sigma_\theta - \nu_\theta \sigma_r) \\ \gamma_{r\theta} &= \tau_{r\theta}/G\end{aligned}\tag{5.78}$$

The stresses over the plate thickness (h) are integrated to obtain the force and moment resultants. Note that for plates, the inplane force resultants are equal (i.e., $N_{r\theta} = N_{\theta r}$), and so are the twisting moments (i.e., $M_{r\theta} = M_{\theta r}$). Thus, the force and moment resultants are

$$\begin{aligned}M_r &= -D_r(\kappa_r + \nu_\theta \kappa_\theta), \\ M_\theta &= -D_\theta(\kappa_\theta + \nu_r \kappa_r) \\ M_{r\theta} &= -2D_g \tau\end{aligned}\tag{5.79}$$

where

$$\begin{aligned}D_r &= \frac{E_r h^3}{12(1 - \nu_r \nu_\theta)}, \\ D_\theta &= \frac{E_\theta h^3}{12(1 - \nu_r \nu_\theta)}, \\ D_g &= \frac{G h^3}{12}\end{aligned}$$

Substituting Eq. (5.73) into Eq. (5.5) yields the following equations of motion for thin plates:

$$\begin{aligned}\frac{\partial}{\partial r}(rN_r) + \frac{\partial}{\partial \theta}(N_{r\theta}) - N_\theta + rq_\alpha &= r(I_1 \ddot{u}_0^2) \\ \frac{\partial}{\partial \theta}(N_\theta) + \frac{\partial}{\partial r}(rN_{r\theta}) + N_{r\theta} + rq_\theta &= r(I_1 \ddot{v}_0^2) \\ \frac{\partial}{\partial r}(rQ_r) + \frac{\partial}{\partial \theta}(Q_\theta) + rq_n &= r(I_1 \ddot{w}_0^2)\end{aligned}\tag{5.80}$$

where

$$\begin{aligned}rQ_r &= \frac{\partial}{\partial r}(rM_r) + \frac{\partial}{\partial \theta}(M_{r\theta}) - M_\theta \\ rQ_\theta &= \frac{\partial}{\partial \theta}(M_\theta) + \frac{\partial}{\partial r}(rM_{r\theta}) + M_{r\theta}\end{aligned}$$

Note that the last two expressions in the above equations are directly derived from the summation of moments in Newton's second law. Note also that the first two equations of motions are generally decoupled from the third bending equation. Boundary conditions can be derived in a similar fashion (Eq. (5.6)).

5.5.2.2 Thick plates. The following expressions are obtained by directly applying Eq. (5.73) into Eqs. (5.22) and (5.28). The midsurface strains are

$$\begin{aligned}
 \varepsilon_{0r} &= \frac{\partial u_0}{\partial r} \\
 \varepsilon_{0\theta} &= \frac{1}{r} \frac{\partial v_0}{\partial \theta} + \frac{u_0}{r} \\
 \gamma_{0r\theta} &= \frac{\partial v_0}{\partial r} + \frac{1}{r} \frac{\partial u_0}{\partial \theta} - \frac{v_0}{r} \\
 \gamma_{0rz} &= \frac{\partial w_0}{\partial r} + \psi_r \\
 \gamma_{0\theta z} &= \frac{1}{r} \frac{\partial w_0}{\partial \theta} + \psi_\theta
 \end{aligned} \tag{5.81}$$

and the curvature and twist changes are

$$\begin{aligned}
 \kappa_r &= \frac{\partial \psi_r}{\partial r} \\
 \kappa_\theta &= \frac{1}{r} \frac{\partial \psi_\theta}{\partial \theta} + \frac{\psi_r}{r} \\
 \tau &= \frac{\partial \psi_\theta}{\partial r} + \frac{1}{r} \frac{\partial \psi_r}{\partial \theta} - \frac{\psi_\theta}{r}
 \end{aligned} \tag{5.82}$$

The force and moment resultants are obtained by integrating the stresses over the plate thickness. The same arguments made earlier for thin plates are valid for thick plates.

The equations of motion for thick plates in polar coordinates are obtained by substituting Eq. (5.73) into Eq. (5.28):

$$\begin{aligned}
 \frac{\partial}{\partial r}(rN_r) + \frac{\partial}{\partial \theta}(N_{r\theta}) - N_\theta + rq_r &= r(I_1\ddot{u}_0 + I_2\ddot{\psi}_r^2) \\
 \frac{\partial}{\partial \theta}(N_\theta) + \frac{\partial}{\partial r}(rN_{r\theta}) + N_{r\theta} + rq_\theta &= r(I_1\ddot{v}_0 + I_2\ddot{\psi}_\theta^2) \\
 \frac{\partial}{\partial r}(rQ_r) + \frac{\partial}{\partial \theta}(Q_\theta) + rq_n &= r(I_1\ddot{w}_0) \\
 \frac{\partial}{\partial r}(rM_r) + \frac{\partial}{\partial \theta}(M_{r\theta}) - M_\theta - rQ_r + rm_r &= r(I_2\ddot{u}_0 + I_3\ddot{\psi}_r^2) \\
 \frac{\partial}{\partial \theta}(M_\theta) + \frac{\partial}{\partial r}(rM_{r\theta}) + M_{r\theta} - rQ_\theta + rm_\theta &= r(I_2\ddot{v}_0 + I_3\ddot{\psi}_\theta^2)
 \end{aligned} \tag{5.83}$$

where the two dots represent the second derivative of these terms with respect to time, and where the inertia terms are defined in Eq. (2.55). The boundary terms for the boundaries with $r = \text{constant}$ can be derived from those given in Eq. (2.58).

Fan and Ye (1990), Srinivasamurthy and Chia (1990), and Xu and Chia (1994b) were among the recent researchers who studied laminated circular plates.

5.6. RECENT ADVANCES

The plates that are discussed in this chapter are rectangular, triangular and circular. Emphasis is given to such plates when made of laminated composite materials with rectangular orthotropy (Qatu 1991a; Chow *et al.* 1992; Takahashi *et al.* 1996; Lee *et al.* 1997). Plates can have other shapes that are rarely discussed in the literature, especially for laminated composite materials. Among these are skewed, elliptic, polygon-shapes and irregular plates. Liew *et al.* (1997b) and Kapania and Lovejoy (1996) studied arbitrary quadrilateral unsymmetrically laminated thick plates. Narita (1985, 1986) and Fu and Chia (1989c) studied orthotropic elliptical plates.

The discussion here was also limited to free undamped linear vibration. Damped vibration of laminated plates received some attention (Taylor and Nayfeh 1997; Zabarar and Pervez 1991; Hu and Dokainish 1994; Bicos and Springer 1989).

Thin plates were analyzed by Kabir *et al.* (2001), and Cinquini *et al.* (1995). Thick plates were discussed by Bhimaraddi (1994), Kabir and Chaudhuri (1994b), Liu (1996), Cederbaum (1992b), Lee *et al.* (1999), Jing and Liao (1991), Yang and Kuo (1994), Liu and Huang (1994), Cho *et al.* (1991) and Maiti and Sinha (1996). Layer-wise theory for plates were used by Nosier *et al.* (1994a, 1994b), Heyliger *et al.* (1996), Saravanos *et al.* (1997) and Adam (2001). Ye (1997) and Cheung and Kong (1993) used three-dimensional elasticity theory to study free vibrations of laminated plates.

Nonlinear analysis of laminated plates received considerable attention. It was performed by Pai and Nayfeh (1992a,b), Bhimaraddi (1990, 1992, 1993), Bhimaraddi and Chandrashekhara (1993), Birman and Zahed (1989), Ganapathi *et al.* (1991), Kuo and Yang (1989), Singh *et al.* (1995), Ribeiro and Petyt (1999), Kim and Kim (2002), Hui (1985), Chia (1985), Chen (2000) and Manoj *et al.* (2000).

Thermal stresses were treated by Hui-Shen Shen (2000), Chang *et al.* (1992), and Librescu and Lin (1999). Stiffened plates were picked up by Lee and Ng (1995). Laminated piezoelectric plates were treated by Batra and Liang (1997), Heyliger and Saravanos (1996) and Miller *et al.* (1997).

Thickness variation was discussed by Lim and Liew (1993). Plates on elastic foundation was treated by Shih and Blotter (1994). Imperfect laminated plates were studied by Chen and Yang (1993), Kapania and Byun (1992), Yang and Chen (1993) and Chia (1990).

The Ritz method (Qatu 1991a; Dawe and Wang 1994) and Galerkin (Gorman and Ding 1996) methods were among the popular methods used to obtain natural frequencies for laminated plates. Finite element methods were used by many researchers including Han and Petyt (1997), Kosmatka (1994), Kant and Mallikarjuna (1990) and Kim and Gupta (1991).

Differential quadrature was used by Farsa *et al.* (1993). Finite strip methods were used by Dawe and Wang (1995), Wang and Lin (1995) and Zhou and Li (1996).

Chapter 6

Shallow Shells

One criterion used in developing composite shell equations is the deepness (or shallowness) of the shell. When the shell has small curvature (i.e., large radius of curvature), it is referred to as a shallow shell. These shells are sometimes referred to as curved plates. The general shell equations can be applied directly to shallow shells. It is noticed, however, that certain additional assumptions valid for shallow shells can be made to the general shell equations. These assumptions will result in a much-reduced complexity in the shell equations. The resulting set of equations is referred to as shallow shell theory or theories. Shallow shell theories were developed mainly for open shells but have been applied to deeper shells, mostly closed cylindrical and conical ones. It has been proven that such use will give results that are not accurate for the lower frequencies when applied to deep shells.

The literature of shallow shells uses often the terminology of “shallow shells” and “extremely shallow shells”. Some researchers used the equations for doubly curved deep shells to analyze shallow shells. While this is correct and accurate, it does not utilize many of the simplifications offered by using a shallow shell theory. In the context of this chapter, we will use the term shallow shells to mean extremely shallow shells.

Shallow shells are defined as shells that have a rise of not more than one-fifth the smallest planform dimension of the shell. It has been widely accepted that extremely shallow shell equations should not be used for maximum span to minimum radius ratio of 0.5 or more. This is actually more restrictive than the earlier definitions. This restriction is needed to make sure that the theory is only applied in the region where it is accurate.

Shallow shells can be thin or thick, and thus, two theories will be presented in this chapter for shallow shells. The first will be a classical shallow shell theory (CSST) and the second will be a shear deformation shallow shell theory (SDSST). Both theories of shallow shells do not offer a reduced order of the shell equations when compared with the general shell theories. They do, however, simplify the equations and reduce the number of terms significantly. Furthermore, unlike deep shells where there are many theories, there is one generally acceptable theory for shallow shells which has been developed and used by many researchers. The root of the equations developed for shallow shells goes back to the equations of Donnell and Mushtari (Leissa 1973a).

Shallow shells can have various types of curvature (e.g., circular cylindrical, spherical, ellipsoidal, conical, hyperbolic paraboloidal, etc.) and various types of planforms (rectangular, triangular, trapezoidal, circular, elliptical, and others). A complete and consistent theory is needed to deal with elastic deformation problems (i.e., static deflections and stresses and free and forced vibrations). This requires equations of equilibrium or

motion, which may be solved either exactly or by an approximate method (e.g., Galerkin, finite differences) and energy functionals which may be used with the Ritz or finite element methods to obtain approximate solutions. Moreover, the equations of motion and energy functionals should be consistent. In other words, they should give the same results for the same problem if the solutions are carried out with sufficient numerical accuracy.

One of the useful sources of previous work is the monograph by Ambartsumian (1964), in which one chapter is devoted to laminated composite shallow shells. No vibration results were presented. Another work by Librescu (1976), in which the primary emphasis is aeroelasticity and flutter, also deals extensively with such structural components. Application of the Ritz method to twisted plates representing turbomachinery blades (Leissa *et al.* 1984a,b) uses energy functionals developed mainly for isotropic shells. This work will extend the previous theories and analyses made for isotropic shallow shells to those made of composite materials.

A complete and consistent set of equations which may be used for the free vibration analyses of laminated composite shallow shells is developed. The theory will employ the usual assumptions made for laminates, i.e. each layer is made of parallel fibers embedded in a matrix material, and each layer may be consequently regarded as being a macroscopically homogeneous, orthotropic, and made of linearly elastic material. The fibers in each layer are assumed to follow the coordinates of the shallow shell or make a constant angle with these coordinates. First, shells sufficiently thin, whose effects of shear deformation and rotary inertia may be neglected, will be considered. This will be followed by consideration of moderately thick shallow shells.

A shallow shell is characterized by its middle surface, which can be defined by

$$z = -\frac{1}{2} \left(\frac{\alpha^2}{R_\alpha} + 2 \frac{\alpha\beta}{R_{\alpha\beta}} + \frac{\beta^2}{R_\beta} \right) \quad (6.1)$$

where the constants R_α , R_β , and $R_{\alpha\beta}$ identify the radii of curvature in the α and β directions and the radius of twist, respectively. We will retain the α , β coordinates in the subsequent analysis for convenience. Such coordinates can be replaced with the Cartesian coordinates for shallow shells with rectangular orthotropy and polar coordinates for shallow shells with circular orthotropy. A typical quadric middle surface described by Eq. (6.1) is depicted in Figure 6.1 for positive values of R_α and R_β .

The theory of shallow shells can be obtained by making the following *additional assumptions* to thin (or classical) and thick (or shear deformation) shell theories

1. The radii of curvature are very large compared to the inplane displacements (i.e., the curvature changes caused by the tangential displacement components u and v are small in a shallow shell, in comparison with changes caused by the normal component w

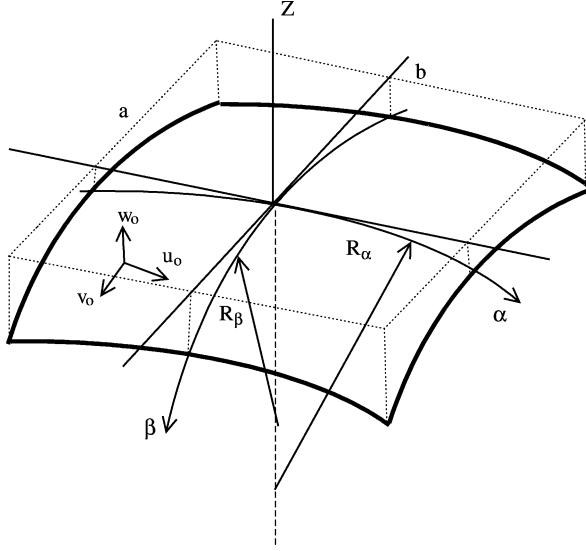


Figure 6.1. Middle surface of a doubly curved shallow shell on rectangular planform.

(Ambartsumian 1964)). Also, the transverse shear forces are much smaller than the term $R_i(\partial N_i/\partial i)$:

$$\frac{u_i}{R_i} \ll 1 \quad \text{and} \quad Q_i \ll R_i \frac{\partial N_i}{\partial i} \quad (6.2)$$

where u_i is either of the inplane displacement components u and v , Q_i is either of the shear forces Q_α , and Q_β , N_i is N_α , N_β , or $N_{\alpha\beta}$, and R_i is R_α , R_β , or $R_{\alpha\beta}$. The term (∂i) indicates derivative with respect to either α or β .

2. The term $(1 + z/R_i)$ is close to 1; where R_i can be R_α , R_β , or $R_{\alpha\beta}$.
3. The shell is shallow enough to be represented by the plane coordinate systems. For the case of rectangular orthotropy, this leads to constant Lamé parameters.

As is customary in shell analysis, an orthogonal set of coordinates α and β are chosen on the middle surface so that the square of the differential of the arc length measured along the surface is given by

$$(ds)^2 = A^2(d\alpha)^2 + B^2(d\beta)^2 \quad (6.3)$$

6.1. FUNDAMENTAL EQUATIONS OF THIN SHALLOW SHELLS

The assumptions made earlier for thin shells of general curvatures (Love's first approximation) are used here to develop the equations for thin shallow shells. Leissa

(1973a) showed that most thin shell theories yield similar results. The exceptions were the membrane theory and that of Donnell and Mushtari, which is classified here as a shallow shell theory. For very thin shells, the assumptions which are used in the previously described thin shell theory (Chapter 2) will be used here. Mainly, it is assumed that the shell is thin enough such that the ratio of the thickness compared to any of the shell's radii of curvature or its width or length is negligible compared to unity, the normals to the middle surface remain straight and normal to the midsurface when the shell undergoes deformation, and no normal strain exists in the direction normal to the middle surface.

6.1.1 Kinematic relations

The first of the above assumptions assures that certain parameters in the shell equations (including the z/R term) can be neglected. The second of the above assumptions allows for neglecting shear deformation in the kinematics equations. It also allows for making the inplane displacement to be linearly varying through the shell's thickness:

$$\begin{aligned}\varepsilon_\alpha &= \varepsilon_{0\alpha} + z\kappa_\alpha \\ \varepsilon_\beta &= \varepsilon_{0\beta} + z\kappa_\beta \\ \gamma_{\alpha\beta} &= \gamma_{0\alpha\beta} + z\tau_{\alpha\beta}\end{aligned}\tag{6.4 (2.59, 5.1)}$$

where the midsurface strains, curvature, and twist changes are given in Eq. (2.60). Using the assumptions of Eq. (6.2), the slopes of Eq. (2.61) when specialized for shallow shells become

$$\psi_\alpha = -\frac{1}{A} \frac{\partial w}{\partial \alpha}, \quad \psi_\beta = -\frac{1}{B} \frac{\partial w}{\partial \beta}\tag{6.5}$$

Notice the difference between the above equations for thin shallow shells (Eq. (6.5)) and those obtained earlier for general shells (Eq. (2.61)). The simplification is a direct results of the assumptions made earlier for shallow shells.

6.1.2 Stress resultants

The stress resultants for thin shallow shells are the same as those derived earlier for thin shells (Eqs. (2.64) and (2.65)). Note that these equations are the same as those obtained for plates. Ignoring the z/R term in stress resultant equations resulted in these simplifications.

6.1.3 Equations of motion

Applying the fundamental assumptions mentioned earlier for shallow shells (Eqs. (6.2)) to the generalized thin shell equations, the equations of motion become

$$\frac{\partial}{\partial \alpha}(BN_\alpha) + \frac{\partial}{\partial \beta}(AN_{\beta\alpha}) + \frac{\partial A}{\partial \beta}N_{\alpha\beta} - \frac{\partial B}{\partial \alpha}N_\beta + ABq_\alpha = AB(I_1\ddot{u}_0^2)$$

$$\begin{aligned} \frac{\partial}{\partial \beta}(AN_\beta) + \frac{\partial}{\partial \alpha}(BN_{\alpha\beta}) + \frac{\partial B}{\partial \alpha}N_{\beta\alpha} - \frac{\partial A}{\partial \beta}N_\alpha + ABq_\beta = AB(I_1\ddot{v}_0^2) \\ -AB\left(\frac{N_\alpha}{R_\alpha} + \frac{N_\beta}{R_\beta} + \frac{N_{\alpha\beta} + N_{\beta\alpha}}{R_{\alpha\beta}}\right) + \frac{\partial}{\partial \alpha}(BQ_\alpha) + \frac{\partial}{\partial \beta}(AQ_\beta) + ABq_n = AB(I_1\ddot{w}_0^2) \end{aligned} \quad (6.6)$$

where

$$\begin{aligned} ABQ_\alpha &= \frac{\partial}{\partial \alpha}(BM_\alpha) + \frac{\partial}{\partial \beta}(AM_{\beta\alpha}) + \frac{\partial A}{\partial \beta}M_{\alpha\beta} - \frac{\partial B}{\partial \alpha}M_\beta \\ ABQ_\beta &= \frac{\partial}{\partial \beta}(AM_\beta) + \frac{\partial}{\partial \alpha}(BM_{\alpha\beta}) + \frac{\partial B}{\partial \alpha}M_{\beta\alpha} - \frac{\partial A}{\partial \beta}M_\alpha \end{aligned}$$

where I_i is defined in Eq. (2.55). Eq. (5.6) gives the boundary conditions for thin shallow shells (for $\alpha = \text{constant}$). In addition, the classification of these boundary conditions shown in Eqs. (2.73)–(2.75) will be adopted here.

It should be noted that the second of the two possible boundary conditions in Eq. (5.6), which will occur at a free edge, does not contain a term M_{nt}/R_t as it would in the case of a deep shell (Eq. (2.72)). This term is negligible to the same order of approximation made elsewhere in the thin shallow shell theory; *viz.*, neglecting curvature changes due to tangential displacement components (Qatu 1989; Leissa and Qatu 1991).

6.1.4 Equations for thin shallow shells with rectangular orthotropy

Consider thin laminated shallow shells with projections of the fibers in each layer to the planform being straight. It simplifies the equations and the subsequent treatment of the problem considerably to represent the equations of such shells using the rectangular coordinates (i.e., planform coordinates). This is true even if the boundaries of such shells are not rectangular in shape.

Consider now a shallow shell with the radii of curvature R_α , R_β , and $R_{\alpha\beta}$ being constant. The curvilinear coordinates (α, β) are the Cartesian coordinates (x, y) . The coordinates (α, β) are maintained here for convenience. This will result in the Lamé parameters $A = B = 1$. Midsurface strains can then be written as

$$\begin{aligned} \varepsilon_{0\alpha} &= \frac{\partial u_0}{\partial \alpha} + \frac{w_0}{R_\alpha} \\ \varepsilon_{0\beta} &= \frac{\partial v_0}{\partial \beta} + \frac{w_0}{R_\beta} \\ \gamma_{0\alpha\beta} &= \frac{\partial v_0}{\partial \alpha} + \frac{\partial u_0}{\partial \beta} + \frac{2w_0}{R_{\alpha\beta}} \end{aligned} \quad (6.7)$$

$$k_\alpha = -\frac{\partial^2 w_0}{\partial \alpha^2}, \quad k_\beta = -\frac{\partial^2 w_0}{\partial \beta^2}, \quad \tau = -2\frac{\partial^2 w_0}{\partial \alpha \partial \beta} \quad (6.8)$$

Deleting the body couples, the reduced equations of motion become (for unit Lamé parameters A and B)

$$\begin{aligned} \frac{\partial N_\alpha}{\partial \alpha} + \frac{\partial N_{\alpha\beta}}{\partial \beta} + p_\alpha &= -\rho \frac{\partial^2 u_0}{\partial t^2} \\ \frac{\partial N_\beta}{\partial \beta} + \frac{\partial N_{\alpha\beta}}{\partial \alpha} + p_\beta &= -\rho \frac{\partial^2 v_0}{\partial t^2} \\ -\left(\frac{2N_{\alpha\beta}}{R_{\alpha\beta}} + \frac{N_\alpha}{R_\alpha} + \frac{N_\beta}{R_\beta}\right) + \frac{\partial^2 M_\alpha}{\partial \alpha^2} + 2\frac{\partial^2 M_{\alpha\beta}}{\partial \beta \partial \alpha} + \frac{\partial^2 M_\beta}{\partial \beta^2} + (p_n) &= -\rho \frac{\partial^2 w_0}{\partial t^2} \end{aligned} \quad (6.9)$$

Substituting Eqs. (6.7) and (6.8) (as well as Eq. (2.64)) in the above Eq. (6.9), and multiplying the last equation by -1 , yields Eq. (5.10). The L_{ij} coefficients for thin shallow shells are

$$\begin{aligned} L_{11} &= \{A_{11}\} \frac{\partial^2}{\partial \alpha^2} + \{2A_{16}\} \frac{\partial^2}{\partial \alpha \partial \beta} + \{A_{66}\} \frac{\partial^2}{\partial \beta^2} \\ L_{12} = L_{21} &= \{A_{16}\} \frac{\partial^2}{\partial \alpha^2} + (A_{12} + A_{66}) \frac{\partial^2}{\partial \alpha \partial \beta} + \{A_{26}\} \frac{\partial^2}{\partial \beta^2} \\ L_{22} &= \{A_{66}\} \frac{\partial^2}{\partial \alpha^2} + \{2A_{26}\} \frac{\partial^2}{\partial \alpha \partial \beta} + \{A_{22}\} \frac{\partial^2}{\partial \beta^2} \\ L_{13} = L_{31} &= -\left\{ \{B_{11}\} \frac{\partial^3}{\partial \alpha^3} + \{B_{26}\} \frac{\partial^3}{\partial \beta^3} + \{3B_{16}\} \frac{\partial^3}{\partial \alpha^2 \partial \beta} + \{B_{12} + 2B_{66}\} \frac{\partial^3}{\partial \alpha \partial \beta^2} \right\} \\ &\quad + \left\{ \frac{A_{11}}{R_\alpha} + \frac{A_{12}}{R_\beta} + 2\frac{A_{16}}{R_{\alpha\beta}} \right\} \frac{\partial}{\partial \alpha} + \left\{ \frac{A_{16}}{R_\alpha} + \frac{A_{26}}{R_\beta} + 2\frac{A_{66}}{R_{\alpha\beta}} \right\} \frac{\partial}{\partial \beta} \\ L_{23} = L_{32} &= -\left\{ \{B_{16}\} \frac{\partial^3}{\partial \alpha^3} + \{B_{22}\} \frac{\partial^3}{\partial \beta^3} + \{3B_{26}\} \frac{\partial^3}{\partial \alpha \partial \beta^2} + \{B_{12} + 2B_{66}\} \frac{\partial^3}{\partial \alpha^2 \partial \beta} \right\} \\ &\quad + \left\{ \frac{A_{16}}{R_\alpha} + \frac{A_{26}}{R_\beta} + 2\frac{A_{66}}{R_{\alpha\beta}} \right\} \frac{\partial}{\partial \alpha} + \left\{ \frac{A_{12}}{R_\alpha} + \frac{A_{22}}{R_\beta} + \frac{A_{26}}{R_{\alpha\beta}} \right\} \frac{\partial}{\partial \beta} \\ L_{33} &= \left\{ D_{11} \frac{\partial^4}{\partial \alpha^4} + 4D_{16} \frac{\partial^4}{\partial \alpha^3 \partial \beta} + 2(D_{12} + 2D_{66}) \frac{\partial^4}{\partial \alpha^2 \partial \beta^2} + 4D_{26} \frac{\partial^4}{\partial \alpha \partial \beta^3} + D_{22} \frac{\partial^4}{\partial \beta^4} \right\} \\ &\quad - 2\left\{ \left(\frac{B_{11}}{R_\alpha} + \frac{B_{12}}{R_\beta} + 2\frac{B_{16}}{R_{\alpha\beta}} \right) \frac{\partial^2}{\partial \alpha^2} + 2\left(\frac{B_{16}}{R_\alpha} + \frac{A_{26}}{R_\beta} + 2\frac{B_{66}}{R_{\alpha\beta}} \right) \frac{\partial^2}{\partial \alpha \partial \beta} \right\} \end{aligned}$$

$$\begin{aligned}
& + \left(\frac{B_{12}}{R_\alpha} + \frac{B_{22}}{R_\beta} + 2 \frac{B_{26}}{R_{\alpha\beta}} \right) \frac{\partial^2}{\partial \beta^2} \Bigg\} \\
& + \left\{ \frac{A_{11}}{R_\alpha^2} + 2 \frac{A_{12}}{R_\alpha R_\beta} + \frac{A_{22}}{R_\beta^2} + 4 \left(\frac{A_{16}}{R_{\alpha\beta} R_\alpha} + \frac{A_{26}}{R_{\alpha\beta} R_\beta} + \frac{A_{66}}{R_{\alpha\beta}^2} \right) \right\} \quad (6.10)
\end{aligned}$$

For symmetrically laminated shells, all terms containing B_{ij} vanish. The above equations can be used to obtain exact solutions as well as approximate ones using methods like the weighted residual methods including the Galerkin's method. Energy functionals that are consistent with the above equations of motion are provided next.

The strain energy functional for a shallow shell can be written as in Eq. (5.12). Substituting the strain- and curvature-displacement equations into the above equation yields the strain energy in terms of the displacements. This may be expressed as the sum of three parts:

$$U = U_s + U_b + U_{bs} \quad (6.11 \text{ (5.13)})$$

where U_s is the part due to stretching alone,

$$\begin{aligned}
U_s = \frac{1}{2} \int_A & \left\{ A_{11} \left(\frac{\partial u_0}{\partial \alpha} + \frac{w_0}{R_\alpha} \right)^2 + A_{22} \left(\frac{\partial v_0}{\partial \beta} + \frac{w_0}{R_\beta} \right)^2 + A_{66} \left(\frac{\partial v_0}{\partial \alpha} + \frac{\partial u_0}{\partial \beta} + \frac{2w_0}{R_{\alpha\beta}} \right)^2 \right. \\
& + 2A_{12} \left(\frac{\partial u_0}{\partial \alpha} + \frac{w_0}{R_\alpha} \right) \left(\frac{\partial v_0}{\partial \beta} + \frac{w_0}{R_\beta} \right) + 2A_{16} \left(\frac{\partial u_0}{\partial \alpha} + \frac{w_0}{R_\alpha} \right) \left(\frac{\partial v_0}{\partial \alpha} + \frac{\partial u_0}{\partial \beta} + \frac{2w_0}{R_{\alpha\beta}} \right) \\
& \left. + 2A_{26} \left(\frac{\partial v_0}{\partial \beta} + \frac{w_0}{R_\beta} \right) \left(\frac{\partial v_0}{\partial \alpha} + \frac{\partial u_0}{\partial \beta} + \frac{2w_0}{R_{\alpha\beta}} \right) \right\} dA \quad (6.12)
\end{aligned}$$

U_b is the part due to bending alone,

$$\begin{aligned}
U_b = \frac{1}{2} \int_A & \left\{ D_{11} \left(\frac{\partial^2 w_0}{\partial \alpha^2} \right)^2 + D_{22} \left(\frac{\partial^2 w_0}{\partial \beta^2} \right)^2 + 4D_{66} \left(\frac{\partial^2 w_0}{\partial \alpha \partial \beta} \right)^2 + 2D_{12} \left(\frac{\partial^2 w_0}{\partial \alpha^2} \right) \left(\frac{\partial^2 w_0}{\partial \beta^2} \right) \right. \\
& \left. + 4D_{16} \left(\frac{\partial^2 w_0}{\partial \alpha^2} \right) \left(\frac{\partial^2 w_0}{\partial \alpha \partial \beta} \right) + 4D_{26} \left(\frac{\partial^2 w_0}{\partial \beta^2} \right) \left(\frac{\partial^2 w_0}{\partial \alpha \partial \beta} \right) \right\} dA \quad (6.13)
\end{aligned}$$

and U_{bs} is the part due to bending–stretching coupling,

$$\begin{aligned}
U_{bs} = - \int_A & \left\{ B_{11} \left(\frac{\partial u_0}{\partial \alpha} + \frac{w_0}{R_\alpha} \right) \left(\frac{\partial^2 w_0}{\partial \alpha^2} \right) + B_{22} \left(\frac{\partial v_0}{\partial \beta} + \frac{w_0}{R_\beta} \right) \left(\frac{\partial^2 w_0}{\partial \beta^2} \right) \right. \\
& \left. + 2B_{66} \left(\frac{\partial v_0}{\partial \alpha} + \frac{\partial u_0}{\partial \beta} + \frac{2w_0}{R_{\alpha\beta}} \right) \left(\frac{\partial^2 w_0}{\partial \alpha \partial \beta} \right) \right\} dA
\end{aligned}$$

$$\begin{aligned}
& +B_{12} \left[\left(\frac{\partial u_0}{\partial \alpha} + \frac{w_0}{R_\alpha} \right) \left(\frac{\partial^2 w_0}{\partial \beta^2} \right) + \left(\frac{\partial v_0}{\partial \beta} + \frac{w_0}{R_\beta} \right) \left(\frac{\partial^2 w_0}{\partial \alpha^2} \right) \right] \\
& +B_{16} \left[2 \left(\frac{\partial u_0}{\partial \alpha} + \frac{w_0}{R_\alpha} \right) \left(\frac{\partial^2 w_0}{\partial \alpha \partial \beta} \right) + \left(\frac{\partial v_0}{\partial \alpha} + \frac{\partial u_0}{\partial \beta} + \frac{2w_0}{R_{\alpha\beta}} \right) \left(\frac{\partial^2 w_0}{\partial \alpha^2} \right) \right] \\
& +B_{26} \left[2 \left(\frac{\partial v_0}{\partial \beta} + \frac{w_0}{R_\beta} \right) \left(\frac{\partial^2 w_0}{\partial \alpha \partial \beta} \right) + \left(\frac{\partial v_0}{\partial \alpha} + \frac{\partial u_0}{\partial \beta} + \frac{2w_0}{R_{\alpha\beta}} \right) \left(\frac{\partial^2 w_0}{\partial \beta^2} \right) \right] \Big\} dA \quad (6.14)
\end{aligned}$$

Note that for symmetrically laminated shells, $B_{ij}=0$, and hence, $U_{bs}=0$. Using the distributed external force components p_α and p_β in the tangential directions, and p_z in the normal direction, the work done by the external forces (W) as the shell displaces is given in Eq. (5.17). Therefore, the total potential energy of the shell in its deformed shape is $\Pi=U-W$. The kinetic energy of the entire shell is then found to be (neglecting rotary inertia terms) the same as given in Eq. (5.18) for plates.

6.2. FUNDAMENTAL EQUATIONS OF THICK SHALLOW SHELLS

Thick shells are shells with a thickness smaller by approximately one order of magnitude when compared with other shell parameters, like its vibration mode shape wavelength and/or radii of curvature. Like general thick shells and plates, thick shallow shells require the inclusion of shear deformation and rotary inertia factors in their equations when compared with thin shallow shells. Thin shallow shell theories are applicable where the thickness is smaller than (1/20)th of the smallest of the wave lengths and/or radii of curvature.

6.2.1 Kinematic relations

As was done for general thick shells, we will assume that normals to the midsurface strains remain straight during deformation but not normal to the midsurface, the displacements can be written as

$$\begin{aligned}
u(\alpha, \beta, z) &= u_0(\alpha, \beta) + z\psi_\alpha(\alpha, \beta) \\
v(\alpha, \beta, z) &= v_0(\alpha, \beta) + z\psi_\beta(\alpha, \beta) \\
w(\alpha, \beta, z) &= w_0(\alpha, \beta)
\end{aligned} \quad (6.15 \text{ (2.35, 5.20)})$$

where u_0 , v_0 , and w_0 are midsurface displacements of the shell, and ψ_α and ψ_β are midsurface rotations. The third of the above equations yields $\varepsilon_z = 0$. Deleting the z/R term in Eq. (2.36) for shallow thick shells (Qatu 1999a) and the terms ψ_α/R_α and ψ_β/R_β ,

the strains at any point in shallow shells can then be written in terms of midsurface strains and curvature changes as

$$\begin{aligned}
 \varepsilon_\alpha &= (\varepsilon_{0\alpha} + z\kappa_\alpha) \\
 \varepsilon_\beta &= (\varepsilon_{0\beta} + z\kappa_\beta) \\
 \varepsilon_{\alpha\beta} &= (\varepsilon_{0\alpha\beta} + z\kappa_{\alpha\beta}) \\
 \varepsilon_{\beta\alpha} &= (\varepsilon_{0\beta\alpha} + z\kappa_{\beta\alpha}) \\
 \gamma_{\alpha z} &= (\gamma_{0\alpha z}) \\
 \gamma_{\beta z} &= (\gamma_{0\beta z})
 \end{aligned} \tag{6.16}$$

Applying the shallow shell assumption (Eq. (6.2)) to Eq. (2.37), the midsurface strains become

$$\begin{aligned}
 \varepsilon_{0\alpha} &= \frac{1}{A} \frac{\partial u_0}{\partial \alpha} + \frac{v_0}{AB} \frac{\partial A}{\partial \beta} + \frac{w_0}{R_\alpha}, & \varepsilon_{0\beta} &= \frac{1}{B} \frac{\partial v_0}{\partial \beta} + \frac{u_0}{AB} \frac{\partial B}{\partial \alpha} + \frac{w_0}{R_\beta} \\
 \varepsilon_{0\alpha\beta} &= \frac{1}{A} \frac{\partial v_0}{\partial \alpha} - \frac{u_0}{AB} \frac{\partial A}{\partial \beta} + \frac{w_0}{R_{\alpha\beta}}, & \varepsilon_{0\beta\alpha} &= \frac{1}{B} \frac{\partial u_0}{\partial \beta} - \frac{v_0}{AB} \frac{\partial B}{\partial \alpha} + \frac{w_0}{R_{\alpha\beta}} \\
 \gamma_{0\alpha z} &= \frac{1}{A} \frac{\partial w_0}{\partial \alpha} + \psi_\alpha, & \gamma_{0\beta z} &= \frac{1}{B} \frac{\partial w_0}{\partial \beta} + \psi_\beta
 \end{aligned} \tag{6.17}$$

The curvature and twist changes are the same as those for plates:

$$\begin{aligned}
 \kappa_\alpha &= \frac{1}{A} \frac{\partial \psi_\alpha}{\partial \alpha} + \frac{\psi_\beta}{AB} \frac{\partial A}{\partial \beta}, & \kappa_\beta &= \frac{1}{B} \frac{\partial \psi_\beta}{\partial \beta} + \frac{\psi_\alpha}{AB} \frac{\partial B}{\partial \alpha} \\
 \kappa_{\alpha\beta} &= \frac{1}{A} \frac{\partial \psi_\beta}{\partial \alpha} - \frac{\psi_\alpha}{AB} \frac{\partial A}{\partial \beta}, & \kappa_{\beta\alpha} &= \frac{1}{B} \frac{\partial \psi_\alpha}{\partial \beta} - \frac{\psi_\beta}{AB} \frac{\partial B}{\partial \alpha}
 \end{aligned} \tag{6.18 (5.23, 2.38)}$$

Note that the major difference between the above equations and those derived for general shells is in the slopes ψ_α and ψ_β .

6.2.2 Stress resultants

The force and moment resultants are obtained by integrating the stresses over the shell thickness. Using the assumption made in Eq. (6.2) for shallow shells, the normal and shear force resultants of shallow shells reduce to those of plates (Eq. (5.24)). It was found that for the limits of shallow shell theory, the term $1 + z/R$ does not add considerable accuracy for thick shallow shells (Qatu 1999a). The difference in the stiffness parameters between the equations used for plates (Eqs. (5.26) and (5.27)) and those used for deep shells (Eqs. (2.41) and (2.42)) is small when shallow shells are considered. Table 6.1 shows a comparison between these stiffness parameters for laminated composite thick shallow shells. The curvature is taken at the limit of shallow shell theory ($a/R = 0.5$). As can be seen from the table, the plate approximate equations lead to a maximum of 4% error for hyperbolic paraboloidal shallow shells. Thus the accurate deep shell equations (Eqs. (2.41)

Table 6.1. Nondimensional stiffness parameters for $[0^\circ, 90^\circ]$ laminated thick shallow shells.

Plate approx.	accurate Eq. (2.41)			Er ^a	Plate approx.	accurate Eq. (2.41)			Er ^a	Plate approx.	accurate Eq. (2.41)			Er ^a
Cylindrical shells ($R_\alpha/R_\beta = 0$)														
(i,j)	$\frac{A_{ij}}{E_2 a^2}$	$\frac{\bar{A}_{ij}}{E_2 a^2}$	$\frac{\hat{A}_{ij}}{E_2 a^2}$		$\frac{100B_{ij}}{E_2 a^3}$	$\frac{100\bar{B}_{ij}}{E_2 a^3}$	$\frac{100\hat{B}_{ij}}{E_2 a^3}$		$\frac{1000D_{ij}}{E_2 a^4}$	$\frac{1000\bar{D}_{ij}}{E_2 a^4}$	$\frac{1000\hat{D}_{ij}}{E_2 a^4}$			
(1,1)	0.804829	0.796043	NA	1.1	−1.760563	−1.727094	NA	1.9	0.670691	0.659080	NA	1.8		
(2,2)	0.804829	NA	0.796208	1.1	1.760563	NA	1.727633	1.9	0.670691	NA	0.659956	1.6		
(6,6)	0.050000	0.050000	0.050000	0.0	0	0.002079	−0.002080	100	0.041667	0.041973	0.041682	0.6		
Hyperbolic paraboloidal shells ($R_\alpha/R_\beta = -1$)														
(1,1)	0.804829	0.787553	NA	2.2	−1.760563	−1.694570	NA	3.9	0.670690	0.649178	NA	3.3		
(2,2)	0.804829	NA	0.787553	2.2	1.760563	NA	1.694570	3.9	0.670690	NA	0.649178	3.3		
(6,6)	0.050000	0.050021	0.050021	0.0	0	0.004168	−0.004168	100	0.041666	0.041698	0.041698	0.1		

$E_1/E_2 = 15$, $G_{12}/E_2 = 0.5$, $G_{13}/E_2 = 0.5$, $\nu_{12} = 0.3$, $a/b = 1$, $a/R_\beta = 0.5$, $a/R_{\alpha\beta} = 0$, $a/h = 10$.

^ae.g., $Error = |(\bar{A}_{ij} - A_{ij}) \times 100/\bar{A}_{ij}|$.

and (2.42)) are not necessary for laminated shallow shells. The equations for plates (Eqs. (5.26) and (5.27)) will be adopted here for shallow shells.

It should be mentioned that both the inplane shear stresses and forces are equal for shallow shells (i.e., $\sigma_{\alpha\beta} = \sigma_{\beta\alpha}$, $N_{\alpha\beta} = N_{\beta\alpha}$). In addition, the twisting moments are equal for shallow shells (i.e., $M_{\alpha\beta} = M_{\beta\alpha}$). This is a direct result of ignoring the $(1 + z/R)$ term in the stress resultants of shallow shells.

6.2.3 Equations of motion

Hamilton's principle can be used to derive the consistent equations of motion and boundary conditions. The equations of motion for thick shallow shells are

$$\begin{aligned}
 & \frac{\partial}{\partial \alpha}(BN_\alpha) + \frac{\partial}{\partial \beta}(AN_{\beta\alpha}) + \frac{\partial A}{\partial \beta}N_{\alpha\beta} - \frac{\partial B}{\partial \alpha}N_\beta + ABq_\alpha = AB(I_1\ddot{u}_0^2 + I_2\ddot{\psi}_\alpha^2) \\
 & \frac{\partial}{\partial \beta}(AN_\beta) + \frac{\partial}{\partial \alpha}(BN_{\alpha\beta}) + \frac{\partial B}{\partial \alpha}N_{\beta\alpha} - \frac{\partial A}{\partial \beta}N_\alpha + ABq_\beta = AB(I_1\ddot{v}_0^2 + I_2\ddot{\psi}_\beta^2) \\
 & -AB\left(\frac{N_\alpha}{R_\alpha} + \frac{N_\beta}{R_\beta} + \frac{N_{\alpha\beta} + N_{\beta\alpha}}{R_{\alpha\beta}}\right) + \frac{\partial}{\partial \alpha}(BQ_\alpha) + \frac{\partial}{\partial \beta}(AQ_\beta) + ABq_n = AB(I_1\ddot{w}_0^2) \quad (6.19) \\
 & \frac{\partial}{\partial \alpha}(BM_\alpha) + \frac{\partial}{\partial \beta}(AM_{\beta\alpha}) + \frac{\partial A}{\partial \beta}M_{\alpha\beta} - \frac{\partial B}{\partial \alpha}M_\beta - ABQ_\alpha + ABm_\alpha = AB(I_2\ddot{u}_0^2 + I_3\ddot{\psi}_\alpha^2) \\
 & \frac{\partial}{\partial \beta}(AM_\beta) + \frac{\partial}{\partial \alpha}(BM_{\alpha\beta}) + \frac{\partial B}{\partial \alpha}M_{\beta\alpha} - \frac{\partial A}{\partial \beta}M_\alpha - ABQ_\beta + ABm_\beta = AB(I_2\ddot{v}_0^2 + I_3\ddot{\psi}_\beta^2)
 \end{aligned}$$

where the two dots represent the second derivative with respect to time, and where the inertia terms are given by Eq. (2.55). Notice the simplification made in the equations of motion with those obtained earlier for general thick shells (Eq. (2.56)).

The boundary terms for the boundaries with $\alpha = \text{constant}$ are given in Eq. (2.58). Similar equations can be obtained for $\beta = \text{constant}$. The classification given in Table 2.1 will be used for shallow shells.

6.2.4 Equations for thick shallow shells with rectangular orthotropy

Consider thick shallow shells which have straight fibers when projected to the planform. The curvilinear coordinates (α, β) are typically replaced by the Cartesian coordinates (x, y) , but will be maintained here for convenience. This will result in $A = B = 1$. The midsurface strains and the curvature and twist changes become

$$\varepsilon_{0\alpha} = \frac{\partial u_0}{\partial \alpha} + \frac{w_0}{R_\alpha}$$

$$\begin{aligned}\varepsilon_{0\beta} &= \frac{\partial v_0}{\partial \beta} + \frac{w_0}{R_\beta} \\ \varepsilon_{0\alpha\beta} &= \frac{\partial u_0}{\partial \beta} + \frac{w_0}{R_{\alpha\beta}}, \quad \varepsilon_{0\beta\alpha} = \frac{\partial v_0}{\partial \alpha} + \frac{w_0}{R_{\alpha\beta}}\end{aligned}\tag{6.20}$$

or

$$\begin{aligned}\gamma_{0\alpha\beta} &= \frac{\partial v_0}{\partial \alpha} + \frac{\partial u_0}{\partial \beta} + \frac{2w_0}{R_{\alpha\beta}} \\ \gamma_{0\alpha z} &= \frac{\partial w_0}{\partial \alpha} + \psi_\alpha, \quad \gamma_{0\beta z} = \frac{\partial w_0}{\partial \beta} + \psi_\beta \\ \kappa_\alpha &= \frac{\partial \psi_\alpha}{\partial \alpha} \\ \kappa_\beta &= \frac{\partial \psi_\beta}{\partial \beta} \\ \kappa_{\alpha\beta} &= \frac{\partial \psi_\beta}{\partial \alpha}, \quad \kappa_{\beta\alpha} = \frac{\partial \psi_\alpha}{\partial \beta}\end{aligned}$$

The equations of motion are:

$$\begin{aligned}\frac{\partial}{\partial \alpha}(N_\alpha) + \frac{\partial}{\partial \beta}(N_{\beta\alpha}) + q_\alpha &= (I_1 \ddot{u}_0^2 + I_2 \ddot{\psi}_\alpha^2) \\ \frac{\partial}{\partial \beta}(N_\beta) + \frac{\partial}{\partial \alpha}(N_{\alpha\beta}) + q_\beta &= (I_1 \ddot{v}_0^2 + I_2 \ddot{\psi}_\beta^2) \\ - \left(\frac{N_\alpha}{R_\alpha} + \frac{N_\beta}{R_\beta} + \frac{N_{\alpha\beta} + N_{\beta\alpha}}{R_{\alpha\beta}} \right) + \frac{\partial}{\partial \alpha}(Q_\alpha) + \frac{\partial}{\partial \beta}(Q_\beta) + q_n &= (I_1 \ddot{w}_0^2) \\ \frac{\partial}{\partial \alpha}(M_\alpha) + \frac{\partial}{\partial \beta}(M_{\beta\alpha}) - Q_\alpha + m_\alpha &= (I_2 \ddot{u}_0^2 + I_3 \ddot{\psi}_\alpha^2) \\ \frac{\partial}{\partial \beta}(M_\beta) + \frac{\partial}{\partial \alpha}(M_{\alpha\beta}) - Q_\beta + m_\beta &= (I_2 \ddot{v}_0^2 + I_3 \ddot{\psi}_\beta^2)\end{aligned}\tag{6.21}$$

The equilibrium equations can be written in terms of displacements ($L_{ij}u_i + M_{ij}\ddot{u}_i = q$), where the L_{ij} are listed below, and the M_{ij} coefficients are given in Eq. (5.33).

$$\begin{aligned}L_{11} &= A_{11} \frac{\partial^2}{\partial \alpha^2} + 2A_{16} \frac{\partial^2}{\partial \alpha \partial \beta} + A_{66} \frac{\partial^2}{\partial \beta^2} \\ L_{12} &= A_{16} \frac{\partial^2}{\partial \alpha^2} + (A_{12} + A_{66}) \frac{\partial^2}{\partial \alpha \partial \beta} + A_{26} \frac{\partial^2}{\partial \beta^2} \\ L_{13} &= \left[\frac{A_{11}}{R_\alpha} + \frac{A_{12}}{R_\beta} + \frac{2A_{16}}{R_{\alpha\beta}} \right] \frac{\partial}{\partial \alpha} + \left[\frac{A_{16}}{R_\alpha} + \frac{A_{26}}{R_\beta} + \frac{2A_{66}}{R_{\alpha\beta}} \right] \frac{\partial}{\partial \beta}\end{aligned}$$

$$\begin{aligned}
L_{14} &= B_{11} \frac{\partial^2}{\partial \alpha^2} + 2B_{16} \frac{\partial^2}{\partial \alpha \partial \beta} + B_{66} \frac{\partial^2}{\partial \beta^2} \\
L_{15} &= B_{16} \frac{\partial^2}{\partial \alpha^2} + (B_{12} + B_{66}) \frac{\partial^2}{\partial \alpha \partial \beta} + B_{26} \frac{\partial^2}{\partial \beta^2} \\
L_{22} &= A_{66} \frac{\partial^2}{\partial \alpha^2} + 2A_{26} \frac{\partial^2}{\partial \alpha \partial \beta} + A_{22} \frac{\partial^2}{\partial \beta^2} \\
L_{23} &= \left[\frac{A_{26}}{R_\beta} + \frac{A_{16}}{R_\alpha} + \frac{2A_{66}}{R_{\alpha\beta}} \right] \frac{\partial}{\partial \alpha} + \left[\frac{A_{22}}{R_\beta} + \frac{A_{12}}{R_\alpha} + \frac{2A_{26}}{R_{\alpha\beta}} \right] \frac{\partial}{\partial \beta} \\
L_{24} &= B_{16} \frac{\partial^2}{\partial \alpha^2} + (B_{12} + B_{66}) \frac{\partial^2}{\partial \alpha \partial \beta} + B_{26} \frac{\partial^2}{\partial \beta^2} \\
L_{25} &= B_{66} \frac{\partial^2}{\partial \alpha^2} + 2B_{26} \frac{\partial^2}{\partial \alpha \partial \beta} + B_{22} \frac{\partial^2}{\partial \beta^2} \\
L_{33} &= -A_{55} \frac{\partial^2}{\partial \alpha^2} - 2A_{45} \frac{\partial^2}{\partial \alpha \partial \beta} - A_{44} \frac{\partial^2}{\partial \beta^2} + \frac{A_{11}}{R_\alpha^2} + \frac{2A_{12}}{R_\alpha R_\beta} + \frac{A_{22}}{R_\beta^2} \\
&\quad + \frac{4}{R_{\alpha\beta}} \left[\frac{A_{16}}{R_\alpha} + \frac{A_{26}}{R_\beta} + \frac{A_{66}}{R_{\alpha\beta}} \right] \\
L_{34} &= \left[-A_{55} + \frac{B_{11}}{R_\alpha} + \frac{B_{12}}{R_\beta} + \frac{2B_{16}}{R_{\alpha\beta}} \right] \frac{\partial}{\partial \alpha} + \left[-A_{45} + \frac{B_{16}}{R_\alpha} + \frac{B_{26}}{R_\beta} + \frac{2B_{66}}{R_{\alpha\beta}} \right] \frac{\partial}{\partial \beta} \\
L_{35} &= \left[-A_{45} + \frac{B_{16}}{R_\alpha} + \frac{B_{26}}{R_\beta} + \frac{2B_{66}}{R_{\alpha\beta}} \right] \frac{\partial}{\partial \alpha} + \left[-A_{44} + \frac{B_{12}}{R_\alpha} + \frac{B_{22}}{R_\beta} + \frac{2B_{26}}{R_{\alpha\beta}} \right] \frac{\partial}{\partial \beta} \\
L_{44} &= -A_{55} + D_{11} \frac{\partial^2}{\partial \alpha^2} + 2D_{16} \frac{\partial^2}{\partial \alpha \partial \beta} + D_{66} \frac{\partial^2}{\partial \beta^2} \\
L_{45} &= -A_{45} + D_{16} \frac{\partial^2}{\partial \alpha^2} + (D_{12} + D_{66}) \frac{\partial^2}{\partial \alpha \partial \beta} + D_{26} \frac{\partial^2}{\partial \beta^2} \\
L_{55} &= -A_{44} + D_{66} \frac{\partial^2}{\partial \alpha^2} + 2D_{26} \frac{\partial^2}{\partial \alpha \partial \beta} + D_{22} \frac{\partial^2}{\partial \beta^2}
\end{aligned} \tag{6.22}$$

6.3. SHALLOW SHELLS WITH RECTANGULAR PLANFORM

Shallow shells, constructed with composite materials having rectangular orthotropy, on rectangular planforms will be considered. Such shells are best represented with Cartesian coordinates. Figure 5.1 shows the fundamental parameters used in these shallow shells (dimensions a and b , and thickness h).

Unlike thin rectangular plates with symmetric lamination which can have four possible boundary conditions at each edge, shallow shells can have up to 16 boundary

conditions at each edge for both symmetric and unsymmetric lamination sequences. Twelve of these are classical boundary conditions (i.e., free, simply supported, and clamped). With 24 possible classical boundary conditions at each edge (Table 2.1), thick shallow shells can have higher number of combinations of boundary conditions.

Like plates, only those shallow shells that have two opposite edges simply supported can permit exact solutions (for homogeneous shallow shells). When the solution procedure is extended to laminated composite shallow shells, it is found that such exact solution can only be applied to cross-ply shells. Unlike plates, shallow shells with antisymmetric angle-ply lamination and S3 boundaries do not have exact solutions.

Similar to plates, the problem with all edges being simply supported have a direct, relatively straightforward, solution referred to as the Navier solution.

6.3.1 Simply supported shallow shells

An early study by Leissa and Kadi (1971) treated isotropic shallow shells supported on all four edges by shear diaphragms. That work is expanded here for laminated thin shallow shells.

6.3.1.1 Thin shallow shells. Consider a shallow shell that is made of a cross-ply laminate, thus $A_{16} = A_{26} = B_{16} = B_{26} = D_{16} = D_{26} = 0$. Assuming the radius of twist to be infinity, (i.e., $R_{\alpha\beta} = \infty$), Eq. (5.31) ($L_{ij}u_i + M_{ij}\ddot{u}_i = q$) for plates can be used for shallow shells with the following differential operators L_{ij} :

$$\begin{aligned}
 L_{11} &= A_{11} \frac{\partial^2}{\partial \alpha^2} + A_{66} \frac{\partial^2}{\partial \beta^2} \\
 L_{12} &= L_{21} = (A_{12} + A_{66}) \frac{\partial^2}{\partial \alpha \partial \beta} \\
 L_{22} &= A_{66} \frac{\partial^2}{\partial \alpha^2} + A_{22} \frac{\partial^2}{\partial \beta^2} \\
 L_{13} &= L_{31} = -B_{11} \frac{\partial^3}{\partial \alpha^3} - (B_{12} + 2B_{66}) \frac{\partial^3}{\partial \alpha \partial \beta^2} + \left\{ \frac{A_{11}}{R_\alpha} + \frac{A_{12}}{R_\beta} \right\} \frac{\partial}{\partial \alpha} \\
 L_{23} &= L_{32} = -B_{22} \frac{\partial^3}{\partial \beta^3} - (B_{12} + 2B_{66}) \frac{\partial^3}{\partial \alpha^2 \partial \beta} + \left\{ \frac{A_{12}}{R_\alpha} + \frac{A_{22}}{R_\beta} \right\} \frac{\partial}{\partial \beta} \\
 L_{33} &= \left\{ D_{11} \frac{\partial^4}{\partial \alpha^4} + 2(D_{12} + 2D_{66}) \frac{\partial^4}{\partial \alpha^2 \partial \beta^2} + D_{22} \frac{\partial^4}{\partial \beta^4} \right\} \\
 &\quad - 2 \left\{ \left(\frac{B_{11}}{R_\alpha} + \frac{B_{12}}{R_\beta} \right) \frac{\partial^2}{\partial \alpha^2} + \left(\frac{B_{12}}{R_\alpha} + \frac{B_{22}}{R_\beta} \right) \frac{\partial^2}{\partial \beta^2} \right\} + \left\{ \frac{A_{11}}{R_\alpha^2} + 2 \frac{A_{12}}{R_\alpha R_\beta} + \frac{A_{22}}{R_\beta^2} \right\}
 \end{aligned} \tag{6.23}$$

The mass parameters are given in Eq. (5.33). Consider an open shell with shear diaphragm (S2) boundaries on all four edges (Eq. (2.74)). Eq. (5.38) gives a solution that satisfies the boundary conditions and the equations of motion exactly. Also, the external forces can be expanded in a Fourier series, as in Eq. (5.39). Substitute the solution of Eq. (5.38) in the above equations of motions; these equations of motion can then be written as

$$\begin{bmatrix} C_{11} & C_{12} & C_{13} \\ C_{21} & C_{22} & C_{23} \\ C_{31} & C_{32} & C_{33} \end{bmatrix} \begin{bmatrix} U_{mn} \\ V_{mn} \\ W_{mn} \end{bmatrix} + \omega_{mn}^2 \begin{bmatrix} I_1 & 0 & 0 \\ 0 & I_1 & 0 \\ 0 & 0 & -I_1 \end{bmatrix} \begin{bmatrix} U_{mn} \\ V_{mn} \\ W_{mn} \end{bmatrix} = \begin{bmatrix} -p_{\alpha mn} \\ -p_{\beta mn} \\ p_{zmn} \end{bmatrix} \quad (6.24 \text{ (5.40)})$$

where

$$C_{11} = -A_{11}\alpha_m^2 - A_{66}\beta_n^2$$

$$C_{12} = C_{21} = -(A_{12} + A_{66})\alpha_m\beta_n$$

$$C_{22} = -A_{66}\alpha_m^2 - A_{22}\beta_n^2$$

$$C_{13} = C_{31} = B_{11}\alpha_m^3 + (B_{12} + 2B_{66})\alpha_m\beta_n^2 + \left\{ \frac{A_{11}}{R_\alpha} + \frac{A_{12}}{R_\beta} \right\} \alpha_m$$

$$C_{23} = C_{32} = B_{22}\beta_n^3 + (B_{12} + 2B_{66})\alpha_m^2\beta_n + \left\{ \frac{A_{12}}{R_\alpha} + \frac{A_{22}}{R_\beta} \right\} \beta_n$$

$$C_{33} = D_{11}\alpha_m^4 + 2(D_{12} + 2D_{66})\alpha_m^2\beta_n^2 + D_{22}\beta_n^4 + 2\left\{ \left(\frac{B_{11}}{R_\alpha} + \frac{B_{12}}{R_\beta} \right) \alpha_m^2 + \left(\frac{B_{12}}{R_\alpha} + \frac{B_{22}}{R_\beta} \right) \beta_n^2 \right\} \\ + \left\{ \frac{A_{11}}{R_\alpha^2} + 2\frac{A_{12}}{R_\alpha R_\beta} + \frac{A_{22}}{R_\beta^2} \right\}$$

The above equations are valid for forced vibration problems. They reduce to static problems if the natural frequency is set to zero and to free vibrations if the loads are set to zero.

6.3.1.2 Thick shallow shells. Consider again cross-ply laminates, with $A_{16} = A_{26} = B_{16} = B_{26} = D_{16} = D_{26} = 0$. A Navier-type solution can be applied to obtain an exact solution. This solution (Eq. (5.44)) can be employed for thick shallow shells with shear diaphragm supports at $\alpha = 0$ and a , and $\beta = 0$ and b (similar to plates). Substituting Eq. (5.44) into the equations of motion and using a Fourier expansion for the loading functions yields the equations

$$[K]\{\Delta\} + (\omega_{mn})^2[M]\{\Delta\} = -\{F\} \quad (6.25 \text{ (5.45)})$$

where $[K]$ and $[M]$ are the stiffness and mass symmetric 5×5 matrices, respectively, ω_{mn} is the frequency, $\{F\}$ the forcing function, and $\{\Delta\} = \{U_{mn}, V_{mn}, W_{mn}, \psi_{\alpha mn}, \psi_{\beta mn}\}^T$.

The K_{ij} coefficients for shallow shells are

$$\begin{aligned}
 K_{11} &= -A_{11}\alpha_m^2 - A_{66}\beta_n^2 \\
 K_{12} &= -(A_{12} + A_{66})\alpha_m\beta_n \\
 K_{13} &= \left[\frac{A_{11}}{R_\alpha} + \frac{A_{12}}{R_\beta} \right] \alpha_m \\
 K_{14} &= -B_{11}\alpha_m^2 - B_{66}\beta_n^2 \\
 K_{15} &= -(B_{12} + B_{66})\alpha_m\beta_n \\
 K_{22} &= -A_{66}\alpha_m^2 - A_{22}\beta_n^2 \\
 K_{23} &= \left[\frac{A_{22}}{R_\beta} + \frac{A_{12}}{R_\alpha} \right] \beta_n \\
 K_{24} &= -(B_{12} + B_{66})\alpha_m\beta_n \\
 K_{25} &= -B_{66}\alpha_m^2 + B_{22}\beta_n^2 \\
 K_{33} &= -A_{55}\alpha_m^2 - A_{44}\beta_n^2 - \left[\frac{A_{11}}{R_\alpha^2} + \frac{2A_{12}}{R_\alpha R_\beta} + \frac{A_{22}}{R_\beta^2} \right] \\
 K_{34} &= \left[-A_{55} + \frac{B_{11}}{R_\alpha} + \frac{B_{12}}{R_\beta} \right] \alpha_m \\
 K_{35} &= \left[-A_{44} + \frac{B_{12}}{R_\alpha} + \frac{B_{22}}{R_\beta} \right] \beta_n \\
 K_{44} &= -A_{55} - D_{11}\alpha_m^2 - D_{66}\beta_n^2 \\
 K_{45} &= -(D_{12} + D_{66})\alpha_m\beta_n \\
 K_{55} &= -A_{44} - D_{66}\alpha_m^2 - D_{22}\beta_n^2
 \end{aligned} \tag{6.26}$$

The above equations reduce to static problems if the natural frequency is set to zero and to free vibrations if the loads are set to zero.

Table 6.2 shows the frequency parameter $\Omega = \omega a^2 \sqrt{\rho/E_2 h^2}$ for cross-ply *hyperbolic paraboloidal* shallow shells on square planform ($a/b = 1$), and with material properties representative of graphite/epoxy ($E_1/E_2 = 15$, $G_{12}/E_2 = 0.5$, $G_{13}/E_2 = 0.5$, $G_{23}/E_2 = 0.5$, $\nu_{12} = 0.25$). A typical shear correction factor is used ($K^2 = 5/6$). Results are presented by using SDSST and CSST. Cross-ply laminates with both symmetric $[0^\circ, 90^\circ, 90^\circ, 0^\circ]$ and asymmetric $[0^\circ, 90^\circ]$ and $[90^\circ, 0^\circ]$ lamination sequences are used in the analysis. Curvature ratios are varied from a flat plate to that of the limit of shallow shell theory ($a/R = 0.5$). Tables 6.3 and 6.4 show similar results for both cylindrical and spherical shells, respectively.

The first observation made here is the difference between the shear deformation theory (SDSST) and the classical theory (CSST). Both theories gave results that agree to the third

Table 6.2. Frequency parameter $\Omega = \omega a^2 \sqrt{\rho/E_2 h^2}$ for cross-ply *hyperbolic paraboloidal* shallow shells ($a/b = 1$, $E_1/E_2 = 15$, $G_{12}/E_2 = 0.5$, $G_{13}/E_2 = 0.5$, $G_{23}/E_2 = 0.5$, $\nu_{12} = 0.25$, $K^2 = 5/6$) for shear deformation shallow shell theory (SDSST) and classical shallow shell theory (CSST).

a/h	a/R	Lamination					
		$[0^\circ, 90^\circ, 90^\circ, 0^\circ]$		$[0^\circ, 90^\circ]$		$[90^\circ, 0^\circ]$	
		SDSST	CSST	SDSST	CSST	SDSST	CSST
100	0	12.2615	12.3773	8.56394	8.56847	8.56394	8.56847
	0.1	12.2491	12.2649	8.55914	8.56847	8.55143	8.55594
	0.2	12.2121	12.2279	8.53710	8.54161	8.52183	8.52632
	0.5	11.9622	11.9776	8.37296	8.37737	8.33708	8.34143
20	0	11.9010	12.2773	8.44807	8.55811	8.44807	8.55811
	0.1	11.8890	12.2649	8.45815	8.56879	8.42109	8.53026
	0.2	11.8530	12.2276	8.45115	8.56208	8.37769	8.48572
	0.5	11.6104	11.9763	8.33038	8.44045	8.15772	8.26102
10	0	10.9716	12.2773	8.11956	8.52569	8.11956	8.52569
	0.1	10.9605	12.2647	8.14483	8.55570	8.07848	8.47898
	0.2	10.9273	12.2269	8.15383	8.56844	8.02233	8.41638
	0.5	10.7031	11.9722	8.08313	8.50237	7.77388	8.14496

significant figure for a thickness ratio of 100. The difference between the two theories reaches 3% for hyperbolic paraboloidal shells, 2.5% for cylindrical shells, and 1.5% for spherical shells when a thickness ratio of 20 is used, indicating the validity of the classical theory for shells with this thickness ratio. When the thickness ratio of 10 is used, the difference between the two theories exceeds 10% for the most parts, showing the lack of accuracy of the classical theory in predicting frequencies for such moderately thick shallow shells.

The second important observation to be made is on the impact of asymmetric lamination. Lower frequency parameters were obtained for asymmetrically laminated cross-ply plates when compared with symmetrically laminated ones. The asymmetric lamination decreases the frequencies significantly for almost all results presented here except the thin moderately deep, spherical shells, where its impact is noticed to be minimal. This can be due to the high influence of membrane forces of these shells on the frequency parameter. Furthermore, the $[0^\circ, 90^\circ]$ lamination gave slightly higher frequencies than the $[90^\circ, 0^\circ]$ lamination. This is particularly true for thicker and deeper shells and more so for hyperbolic paraboloidal shells than cylindrical shells. The two lamination sequences showed no difference for spherical shells.

The third observation made here is on the influence of curvature. The influence of curvature is noticed to be the strongest for spherical shells and the weakest for hyperbolic

Table 6.3. Frequency parameter $\Omega = \omega a^2 \sqrt{\rho/E_2 h^2}$ for cross-ply cylindrical shallow shells ($a/b = 1, E_1/E_2 = 15, G_{12}/E_2 = 0.5, G_{13}/E_2 = 0.5, G_{23}/E_2 = 0.5, \nu_{12} = 0.25, K^2 = 5/6$) for shear deformation shallow shell theory (SDSST) and classical shallow shell theory (CSST).

a/h	a/R	Lamination					
		[0°, 90°, 90°, 0°]		[0°, 90°]		[90°, 0°]	
		SDSST	CSST	SDSST	CSST	SDSST	CSST
100	0	12.2615	12.3773	8.56394	8.56847	8.56394	8.56847
	0.1	13.9561	13.9703	10.8575	10.8616	10.8526	10.8567
	0.2	18.0992	18.1107	15.8445	15.8484	15.8303	15.8342
	0.5	35.1759	35.1838	28.2155	28.2471	27.7925	27.8270
20	0	11.9010	12.2773	8.44807	8.55811	8.44807	8.55811
	0.1	11.9700	12.3442	8.55769	8.66733	8.53889	8.64780
	0.2	12.1740	12.5418	8.86048	8.96840	8.82171	8.92813
	0.5	13.4883	13.8195	10.6898	10.7893	10.5752	10.6707
10	0	10.9716	12.2773	8.11956	8.52569	8.11956	8.52569
	0.1	10.9867	12.2897	8.15924	8.56701	8.12590	8.52847
	0.2	11.0316	12.3270	8.24451	8.65203	8.17744	8.57455
	0.5	11.3342	12.5784	8.75225	9.14960	8.57836	8.94972

paraboloidal shells. For the later shells, increasing the curvature is observed to reduce the frequency parameter slightly. For spherical shells, a slight curvature increase to a curvature ratio of $a/R = 0.1$ results in 50% increase in the frequency parameters associated with thin shells. Its impact is less for thicker shells. Additional detailed results can be found in the dissertation of Chang (1992).

6.3.2 Shallow shells with two opposite edges simply supported

Similar to plates, exact solutions can be found for shallow shells having two opposite edges simply supported. This is true only for cross-ply (symmetric and asymmetric) lamination sequence and shear diaphragm opposite boundaries. It is not true for shells with S3 boundaries and anti-symmetric angle ply lamination. The same notation used earlier for plates to describe boundaries is used for shallow shells (Figure 5.4).

6.3.2.1 Thin shallow shells. Consider shallow shells made of a cross-ply laminate. Thus Eq. (5.35) applies for the stiffness parameters, and Eq. (6.23) applies for the differential operator in the equations of motion. Consider further a shallow shell with shear diaphragm (S2) boundaries on the two opposite edges $\beta = 0, b$ (i.e., $N_\beta = w_0 = u_0 = M_\beta = 0$; for

Table 6.4. Frequency parameter $\Omega = \omega a^2 \sqrt{\rho/E_2 h^2}$ for cross-ply *spherical* shallow shells ($a/b = 1$, $E_1/E_2 = 15$, $G_{12}/E_2 = 0.5$, $G_{13}/E_2 = 0.5$, $G_{23}/E_2 = 0.5$, $\nu_{12} = 0.25$, $K^2 = 5/6$) for shear deformation shallow shell theory (SDSST) and classical shallow shell theory (CSST).

a/h	a/R	Lamination			
		[0°, 90°, 90°, 0°]		[0°, 90°]	
		SDSST	CSST	SDSST	CSST
100	0	12.2615	12.3773	8.56394	8.56847
	0.1	18.1175	18.1290	15.8534	15.8573
	0.2	29.3005	29.3090	27.9620	27.9666
	0.5	66.5695	66.5774	66.0054	66.0139
20	0	11.9010	12.2773	8.44807	8.55811
	0.1	12.1863	12.5545	8.84994	8.95725
	0.2	13.0000	13.3466	9.95202	10.0534
	0.5	17.5209	17.7854	15.4499	15.5392
10	0	10.9716	12.2773	8.11956	8.52569
	0.1	11.0428	12.3397	8.21896	8.62173
	0.2	11.2522	12.5236	8.50843	8.90183
	0.5	12.5718	13.6975	10.2492	10.5975

the edges $\beta = 0, b$), and the other edges $\alpha = -a/2, a/2$ have arbitrary conditions. The displacement field of Eq. (5.57) can be chosen to satisfy the simply supported boundaries.

One needs to substitute Eq. (5.57) into equations $L_{ij}u_i + M_{ij}\ddot{u}_i = q$ with the L_{ij} operators described in Eq. (6.23). One can solve the resulting equations either by the direct method described in Chapter 4 or the state space method (Librescu *et al.* 1989a). This has been described in Section 5.3.3.

6.3.2.2 Thick shallow shells. For thick shallow shells made of cross play laminates, a solution procedure similar to that described for plates can be followed. Let the boundaries on the two opposite edges $\beta = 0, b$ be shear diaphragm (S2) (i.e., $N_\beta = w_0 = u_0 = M_\beta = \psi_\alpha = 0$; for the edges $\beta = 0, b$), and the other edges $\alpha = -a/2, +a/2$ have arbitrary conditions. The displacement field of Eq. (5.58) can be applied to the equations of motion of thick shallow shells. The resulting equations can be addressed in a manner similar to that of curved beams discussed in Chapter 4 (Lin and King 1974). Alternatively, Librescu *et al.* (1989a) used the state space approach (Brogan 1985) for the procedure to obtain solutions to the resulting equations. This approach was described in Section 5.3.3 on plates.

Table 6.5 shows the natural frequency parameters $\Omega = \omega a^2 \sqrt{\rho/E_2 h^2}$ of the asymmetric cross-ply $[0^\circ, 90^\circ]$ square shallow shells as well as the symmetric cross-ply $[0^\circ, 90^\circ, 0^\circ]$ with various boundaries at $\alpha = -a/2, a/2$. The table is written starting with the shallow shell having less constraints (FSFS) and ending with that having more constraints (CSCS). The first observation is the lack of accuracy obtained with the classical theory for such moderately thick shallow shells ($a/h = 10$). The second observation is to note how the frequencies actually increase with the added constraints, particularly when the clamped edges are considered. Another observation is to note how asymmetric lamination sequence actually has different behavior when compared with symmetric lamination. Unsymmetric lamination produced lower frequency parameters for simply supported (SSSS) shallow shells as well as the SSSC and SCSC boundaries, and produced higher frequency parameters for the SFSE, SFSS and SFSC boundaries.

The added curvature is showing significant impact on the shallow shells with higher constraints (SCSC) than it does on the ones with lower constraints (SFSE). This is understandable because such curvature introduces higher membrane stresses which will stiffen the shell and thus produce higher frequencies. The effect of such membrane forces is noticed to be higher for spherical shells than it is for cylindrical shells (Table 6.6).

Table 6.5. Natural frequency parameters $\Omega = \omega a^2 \sqrt{\rho/E_2 h^2}$ for a cross-ply square laminated shallow spherical shells with $E_1/E_2 = 25$, $G_{12}/E_2 = G_{13}/E_2 = 0.5$, $G_{23}/E_2 = 0.2$, $\nu_{12} = \nu_{13} = 0.25$, $K^2 = 5/6$, $a/h = 10$ and various boundaries at $\alpha = -a/2, a/2$ (Librescu *et al.* 1989a).

Theory	a/r (mode no.)	SFSF	SFSS	SFSC	SSSS	SSSC	SCSC
$[0^\circ, 90^\circ]$							
CSST	0	6.136	6.500	7.014	8.566	12.145	15.771
SDSST	0	5.774	6.100	6.544	8.900	10.612	12.622
CSST	0.05	6.132	6.493	7.002	9.588	12.165	15.822
SDSST	0.05	5.768	6.093	6.535	8.922	10.640	12.713
CSST	0.2	6.162	6.510	6.971	9.903	12.465	16.820
SDSST	0.2	5.787	6.105	6.511	9.247	11.004	14.081
$[0^\circ, 90^\circ, 0^\circ]$							
CSST	0	3.902	4.485	6.863	15.104	22.557	32.093
SDSST	0	3.788	4.320	6.144	12.163	14.248	16.383
CSST	0.05	3.909	4.490	6.863	15.116	22.562	32.136
SDSST	0.05	3.794	4.325	6.146	12.178	14.264	16.487
CSST	0.2	4.009	4.562	6.861	15.290	22.640	32.785
SDSST	0.2	3.891	4.397	6.163	12.394	14.499	17.959

6.3.3 General boundary conditions

Exact solutions for the free vibration problem of the boundary conditions other than those having two opposite edges simply supported (e.g., completely free, cantilever, clamped) do not exist. Approximate methods must be employed to obtain natural frequencies for these shallow shells. Results can be obtained by the Ritz method to any degree of accuracy needed. This method has been applied successfully before for plates and proved to be more efficient than the finite element method and reasonably accurate when compared with experimental results.

The Ritz method with algebraic polynomial displacement functions is used. Convergence studies are made which demonstrate that reasonably accurate results are obtainable before ill-conditioning starts to cause problems. Shallow shells with spherical, circular cylindrical, and hyperbolic paraboloidal curvatures and completely free, cantilevered, and doubly cantilevered (i.e., two adjacent edges clamped and the others free) boundary conditions are studied at length. The effects of the fiber orientation, curvature and boundary conditions upon the mode shapes are studied.

Studies that treated isotropic shallow shells are available in the literature. These studies treated cantilevered (Leissa *et al.* 1981), corner supported (Narita and Leissa 1984), completely free (Leissa and Narita 1984) and doubly cantilevered (Qatu and Leissa 1993) isotropic shallow shells. Effects of various edge constraints were also studied (Qatu and Leissa 1992). The analysis of shallow shell was extended to laminated composites (Qatu 1989). Analysis was performed on such shells having shear diaphragm (Qatu 1991b),

Table 6.6. Natural frequency parameters $\Omega = \omega a^2 \sqrt{\rho/E_2 h^2}$ for a cross-ply square laminated shallow cylindrical shells with $E_1/E_2 = 25$, $G_{12}/E_2 = G_{13}/E_2 = 0.5$, $G_{23}/E_2 = 0.2$, $\nu_{12} = \nu_{13} = 0.25$, $K^2 = 5/6$, $a/h = 10$ and various boundaries at $\alpha = -a/2, a/2$ (Librescu *et al.* 1989a).

Theory	a/R (mode no.)	SFSF	SFSS	SFSC	SSSS	SSSC	SCSC
$[0^\circ, 90^\circ]$							
CSST	0.05	6.128	6.489	7.008	9.560	12.136	15.757
SDSST	0.05	5.763	6.087	6.535	8.894	10.609	12.623
CSST	0.2	6.096	6.444	7.014	9.598	12.154	15.747
SDSST	0.2	5.716	6.030	6.524	8.931	10.647	12.663
$[0^\circ, 90^\circ, 0^\circ]$							
CSST	0.05	3.902	4.484	6.866	15.106	22.557	32.091
SDSST	0.05	3.787	4.318	6.146	12.166	14.250	16.385
CSST	0.2	3.894	4.472	6.901	15.136	22.560	32.062
SDSST	0.2	3.773	4.301	6.176	12.212	14.284	16.408

completely free (Qatu and Leissa 1991a), cantilevered (Qatu and Leissa 1991b), and doubly cantilevered (Qatu 1991) boundary configurations.

The analysis of the natural mode shapes for these structures received less interest. Some mode shapes for isotropic shallow shells are given in some studies (e.g., Leissa and Narita 1984) in the literature. The Ritz method with algebraic polynomials was used to find the accurate mode shapes for laminated composite shallow shells (Qatu 1992c).

It was shown in previous sections that shallow shells supported on all four edges by shear diaphragm boundaries and having spherical and circular cylindrical curvatures resulted in frequencies much higher than those of plates, whereas for hyperbolic paraboloidal curvatures, deviation from flatness had no significant effect. It is interesting to find how shallow shells will behave under other boundary conditions.

Figure 6.1 shows the midsurface displacements u_0 and v_0 which are tangent to the shell midsurface at a typical point, and w_0 which is the displacement component normal to the midsurface. The displacements are assumed to be sinusoidal in time in the free vibration analysis. These displacements are assumed to take the forms

$$\begin{aligned} u_0(\alpha, \beta, t) &= U(\alpha, \beta) \sin \omega t \\ v_0(\alpha, \beta, t) &= V(\alpha, \beta) \sin \omega t \\ w_0(\alpha, \beta, t) &= W(\alpha, \beta) \sin \omega t \end{aligned} \quad (6.27 \text{ (5.63)})$$

Algebraic trial functions are used in the analysis, similar to that of plates. The displacement functions U , V , and W can be written in terms of the nondimensional coordinates ξ and η (Figure 5.5) as shown in Eq. (5.64) for plates. Keeping in mind that the Ritz method requires the satisfaction of geometrical constraints only, the lower indices of the displacement polynomials shown in Eq. (5.64) are carefully chosen so that these constraints are exactly satisfied for the particular boundary conditions treated here. When using the Ritz method, there is no need to satisfy the free edge conditions. Several boundary conditions can be treated by the same analysis (Table 5.9).

The energy functional $T_{\max} - U_{\max}$ is generated for the shallow shell from the Eqs. (6.11)–(6.14) during a vibratory cycle. The eigenvalue problem of the free vibration is solved by minimizing $T_{\max} - U_{\max}$ with respect to the coefficients α_{ij} , β_{kl} , and γ_{mn} in the manner similar to that done for plates (Eq. (5.67)). This yields simultaneous, linear, homogenous equations in an equal number of unknowns α_{ij} , β_{kl} , and γ_{mn} . Avoiding the trivial solution of zero coefficients, the determinant of the matrix is set equal to zero, which yields the eigenvalues (nondimensional frequencies). The substitution of a particular eigenvalue back into the simultaneous equations gives the corresponding eigenvector. The mode shape which corresponds to a certain frequency parameter is obtained by substituting the corresponding eigenvector (vector of the coefficients α_{ij} , β_{kl} , and γ_{mn}) back into the displacement fields. The displacement in the normal direction is then calculated at various points on the shell. In the following analysis, these

displacements are calculated at 441 points which form a 21×21 grid on the shell planform. These are further normalized by making the maximum displacement as unity. The difference between the contour lines is taken as one-fifth of the maximum displacement. The contour lines of zero displacement (nodal lines) are distinguished by heavier lines. The dashed lines represent displacement opposite to that of solid lines. In the following sections, the completely free, cantilevered and doubly cantilevered boundary conditions will be studied.

6.3.4 Completely free shallow shells

Convergence studies are made for a series of composite plates and shallow shells representative of those to be analyzed subsequently. These include four-layer symmetric laminates with stacking sequence $[\theta, -\theta, -\theta, \theta]$. The angle θ lies between the fibers and the projection of the α -axis upon the shell. Filamentary composite materials of graphite/epoxy are considered. Other stacking sequence and materials are considered by Qatu and Leissa (1991a).

Convergence studies for moderately thin ($b/h = 100$) plates and shallow shells having square planform ($a/b = 1$) were made. Other aspect ratios were considered in the literature (Qatu 1989). Three types of shell curvatures were considered; these were spherical ($R_\beta/R_\alpha = +1$), cylindrical ($R_\beta/R_\alpha = 0$) and hyperbolic paraboloidal ($R_\beta/R_\alpha = -1$). Figure 6.2 shows these types of curvatures. A moderate shallowness ($a/R = 0.5$) ratio is taken.

Table 6.7 shows a convergence study of the frequency parameter $\Omega = \omega a^2 \sqrt{\rho/E_1 h^2}$ for free composite plates and shallow shells. It is observed that the material with the smaller orthotropy (i.e., E-glass/epoxy) yields slightly faster convergence than that with the larger orthotropy ratio (i.e., graphite/epoxy) on the average (Qatu and Leissa 1991a). The maximum difference between the 64-term and 144-term solutions is about 5% for graphite/epoxy. For the remaining frequencies, convergence occurred for three significant figures only. From these studies, it was decided to choose 64 terms (i.e., $M = N = 7$) for subsequent solutions for plates.

The maximum difference between the 147-term solution and the 192-term solution for spherical shells is 5.3% (for the tenth frequency) and that for cylindrical shells is 2.4%, while it is only 1.8% for hyperbolic paraboloidal shells. Unlike plates, convergence occurred for the first three significant figures only for most of the fundamental frequencies with 192 terms. For the rest of the frequencies, convergence occurred for the first two figures only. From these studies, it was decided to use 192-terms for laminated shallow shells (i.e., $I = J = K = L = M = N = 7$). This is also consistent with using $192/3 = 64$ terms for laminated plates (where only w is needed).

Comparisons were made with analytical results published by Leissa and Narita (1984) for isotropic shells. The agreement was excellent; the results agreed to the fifth significant

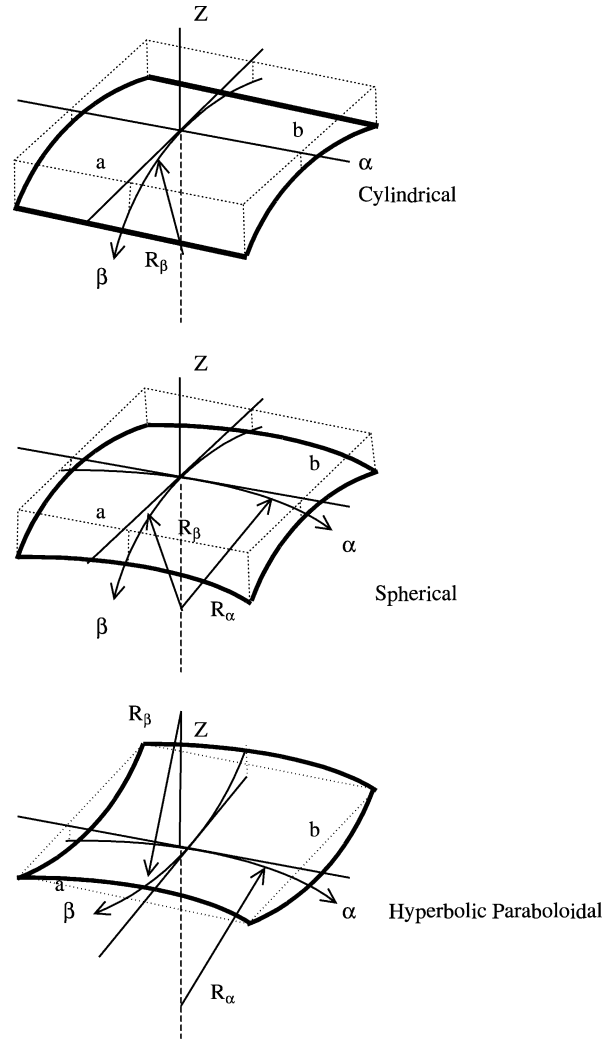


Figure 6.2. Types of curvatures for shallow shells on rectangular planforms.

figure. This is because the same method was used in their study. Comparison among various studies made for laminated plates with free boundaries were shown in Chapter 5.

6.3.4.1 Effect of varying θ upon the frequencies. Studies are made for symmetrically laminated plates and shallow shells of square planform ($a/b = 1$) having various numbers

Table 6.7. Convergence of the frequency parameter for graphite/epoxy [30°, −30°, −30°, 30°] plates and shallow shells on square planform.

R_β/R_α	Determinant size	$\Omega = \omega a^2 \sqrt{\rho/E_1 h^2}$									
		1	2	3	4	5	6	7	8	9	10
Plate	36	1.926	2.260	4.763	5.173	5.580	8.191	9.023	10.815	13.550	16.152
	64	1.914	2.255	4.664	5.098	5.470	7.929	8.548	10.217	13.049	13.692
	100	1.914	2.255	4.664	5.097	5.468	7.923	8.518	10.137	12.966	13.030
	144	1.914	2.255	4.664	5.097	5.468	7.923	8.517	10.135	12.944	13.029
+1	108	2.292	3.333	6.020	6.886	8.756	11.903	13.867	17.323	19.293	24.595
	147	2.284	3.325	5.886	6.796	8.421	11.342	13.205	15.713	18.050	21.318
	192	2.283	3.323	5.871	6.781	8.394	11.118	12.806	15.316	17.120	20.700
0	108	2.221	5.204	5.641	7.863	8.238	13.417	13.802	14.605	16.118	18.636
	147	2.217	5.134	5.575	7.717	8.018	12.911	13.318	14.278	15.380	17.629
	192	2.216	5.124	5.568	7.682	7.991	12.551	12.982	13.997	14.926	17.194
−1	108	2.122	4.961	4.975	8.940	9.655	14.824	15.675	16.975	20.190	20.496
	147	2.117	4.886	4.898	8.853	9.202	13.853	15.239	16.812	18.978	19.827
	192	2.115	4.882	4.887	8.809	9.106	13.363	14.940	16.774	18.276	19.460

Shallow Shells

of layers in angle-ply stacking sequence. Table 6.8 gives the first eight nondimensional frequencies for four-layer $[\theta, -\theta, -\theta, \theta]$ angle-ply plates and shallow shells. The fiber angle varies between 0 and 45°. Because of the symmetry of the problem, frequencies for $\theta = 60, 75$, and 90° are the same as those for $\theta = 30, 15$, and 0°, respectively, when $a/b = 1$. Additional results have been reported in the literature (Qatu and Leissa 1991a). It is found that the fundamental frequencies of shallow shells are virtually the same as those of the plate when $\theta = 0^\circ$. This is due to the fact that the fundamental mode shape in such cases has node lines along the two symmetry axes, requiring no significant stretching of the middle surface. However, the higher frequencies are all significantly affected by curvature.

Increasing θ causes the fundamental frequency to increase for all the shell geometries used here (Figure 6.3). The exception was found only for single-layer G/E plates and hyperbolic paraboloidal shells (Qatu and Leissa 1991a). The maximum fundamental frequency is obtained at $\theta = 45^\circ$ for all cases studied here except for the previously mentioned two cases where it is 0°. For higher frequencies, the maximum frequency can exist at any angle θ between 0 and 45°.

Table 6.8. Effect of varying θ upon the frequency parameters Ω of graphite/epoxy four layer $[\theta, -\theta, -\theta, \theta]$ shallow shells. $a/b = 1$, $a/h = 100$, $a/R_\beta = 0.5$.

R_α/R_β	θ (degrees)	$\Omega = \omega a^2 \sqrt{\rho/E_1} h^2$							
		1	2	3	4	5	6	7	8
–	0	1.491	1.646	3.459	4.538	6.424	6.471	7.132	8.854
	15	1.653	1.843	3.904	4.773	5.902	7.217	7.237	9.185
	30	1.914	2.255	4.664	5.097	5.468	7.923	8.517	10.135
	45	2.233	2.275	4.655	5.043	5.934	9.183	9.423	10.204
+1	0	1.509	3.961	4.233	6.781	7.652	8.553	9.974	14.683
	15	1.836	3.829	4.834	6.768	7.715	9.774	10.992	15.638
	30	2.283	3.323	5.871	6.781	8.394	11.119	12.806	15.316
	45	2.296	3.093	6.459	6.712	9.001	11.172	13.484	14.841
0	0	1.514	4.514	6.455	6.755	7.092	9.198	10.647	12.175
	15	1.805	4.959	6.070	7.126	7.258	10.748	11.517	13.224
	30	2.216	5.124	5.568	7.682	7.991	12.551	12.982	13.997
	45	2.243	4.007	5.586	8.129	8.578	10.409	11.706	15.364
–1	0	1.507	4.235	4.541	7.056	8.956	9.062	11.758	13.358
	15	1.762	4.457	4.678	7.657	8.441	11.671	12.197	14.615
	30	2.115	4.882	4.887	8.809	9.106	13.363	14.940	16.774
	45	2.240	4.968	5.102	9.450	9.481	13.873	16.450	18.223

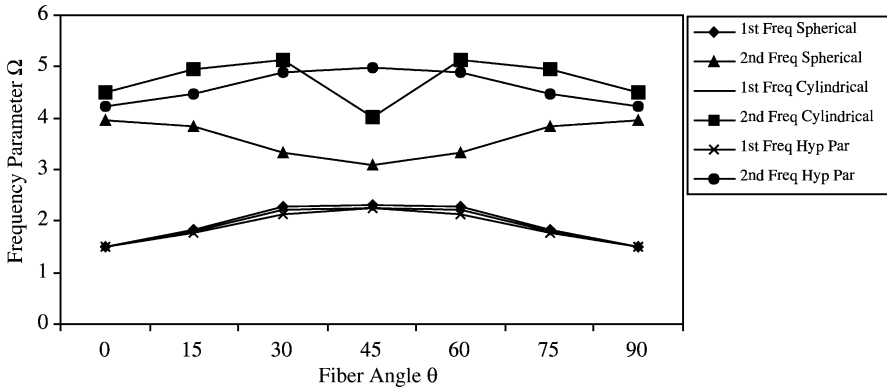


Figure 6.3. Effect of varying θ upon the frequency parameters Ω of graphite/epoxy four layer $[\theta, -\theta, -\theta, \theta]$ shallow shells; $a/b = 1$, $a/h = 100$, $a/R_\beta = 0.5$.

Maximum fundamental frequencies are obtained for spherical shells, and minimum frequencies are found for plates and/or hyperbolic paraboloidal shells. The maximum difference between the fundamental frequency for $\theta = 0^\circ$ and that for $\theta = 45^\circ$ occurs always for spherical shells, and the least difference occurs for plates and/or hyperbolic paraboloidal shells. For spherical shells, changing the angle from 0 to 45° increases the fundamental frequency by almost 50%.

6.3.4.2 Frequencies for cross-ply plates and shallow shells. Studies are made for symmetrically laminated cross-ply plates and shallow shells of square planform. $[0^\circ]$, $[0^\circ, 90^\circ, 0^\circ]$ and $[90^\circ, 0^\circ, 90^\circ]$ laminates are considered with graphite/epoxy material. Two shallowness ratios (a/R) were used for each type of shell. Table 6.9 gives the fundamental nondimensional frequency parameters. Because of the symmetry of the problem, both laminates $[0^\circ, 90^\circ, 0^\circ]$ and $[90^\circ, 0^\circ, 90^\circ]$ give the same results, except for cylindrical shells, when the aspect ratio of 1 is used. Both three-layer laminates give slightly higher fundamental frequencies than the single-layer. For circular cylindrical shells, the $[0^\circ, 90^\circ, 0^\circ]$ laminate gave slightly higher frequencies than the $[90^\circ, 0^\circ, 90^\circ]$ laminate. This is because, for the latter, the outer fibers lie in the direction of the curvature. This causes the chordwise stiffness of the shell to increase considerably, but at the expense of the spanwise stiffness. The mode shapes in the two cases are considerably different, even though the frequencies are nearly the same.

Increasing the curvature increases the fundamental frequencies for all shells except $[90^\circ, 0^\circ, 90^\circ]$ G/E circular cylindrical shells. Increasing the curvature here decreases the fundamental frequency slightly. For higher frequencies, increasing the curvature always

Table 6.9. Frequency parameters Ω of completely free cross-ply graphite/epoxy shallow shells. $a/b = 1$, $a/h = 100$.

R_α/R_β	a/R_α	$\Omega = \omega a^2 \sqrt{\rho/E_1 h^2}$							
		1	2	3	4	5	6	7	8
<i>[0°] Single layer</i>									
–	–	1.491	1.646	3.460	4.539	6.4276	6.471	7.132	9.009
+1	0.1	1.493	2.319	3.511	5.534	6.577	6.706	7.340	9.345
	0.5	1.509	3.961	4.232	6.781	7.652	8.553	9.974	14.68
0	0.1	1.493	2.420	3.509	5.694	6.472	6.572	7.145	9.099
	0.5	1.514	4.514	6.445	6.755	7.092	9.198	10.65	12.17
–1	0.1	1.493	2.398	3.505	5.732	6.565	6.753	7.208	9.038
	0.5	1.507	4.235	4.541	7.056	8.956	9.062	11.76	13.36
<i>[0°, 90°, 0°]</i>									
	–	1.504	2.040	3.682	5.622	6.361	7.042	7.245	9.070
+1	0.1	1.507	3.071	3.840	6.506	6.868	7.504	7.518	9.890
	0.5	1.521	4.373	5.032	6.954	7.912	10.21	11.31	16.73
0	0.1	1.507	3.394	3.840	6.361	6.830	7.142	7.512	9.255
	0.5	1.525	6.344	6.413	7.015	7.910	11.72	12.28	16.77
–1	0.1	1.506	3.245	3.823	6.826	7.042	7.275	7.501	9.086
	0.5	1.518	4.814	5.140	7.042	9.217	11.041	12.97	18.05
<i>[90°, 0°, 90°]*</i>									
0	0.1	1.504	2.040	3.681	5.625	6.908	7.161	7.247	9.280
	0.5	1.501	2.036	3.670	5.656	7.284	9.039	9.051	11.79

*Results for [90°, 0°, 90°] laminate are the same as those for [0°, 90°, 0°] laminate for spherical and hyperbolic paraboloidal shells.

increases the frequencies except for the case mentioned above, where increasing the curvature is observed to decrease the frequencies slightly for the first three frequencies, but increases in the rest.

6.3.4.3 Frequencies for angle-ply plates and shallow shells. Symmetrically laminated plates and shallow shells having $a/b = 1$ are studied. A single-layer [45°] and an angle-ply laminate [45°, –45°, 45°] are used. Two curvature ratios and three types of shells, as well as plates, are studied. It is important to notice that, because of the symmetry of the problem [45°, –45°, 45°] and [–45°, 45°, –45°] laminates give the same results for all the cases.

Table 6.10 gives the fundamental nondimensional frequencies. Even more strongly than what was found for cross-ply laminates, the three-layer angle-ply laminates give higher frequencies than the single-layer configurations in every case.

For the material used, increasing the curvature increases the fundamental frequencies for spherical and cylindrical shells and decreases them slightly for hyperbolic paraboloidal shells when the single-layer configurations are used. Increasing the curvature ratio is found to have larger effects on the single-layer configuration than the multi-layer one (Qatu and Leissa 1991a).

It is also observed that a slight curvature ($a/R = 0.1$, corresponding to an arc length of 5.7°) causes a large increase in the fundamental frequency for the spherical shell. It is observed that the 45° angle-ply laminates give higher frequencies than cross-ply laminates for most of the results when the aspect ratio is 1. When the aspect ratio is 2, it is found that the cross-ply laminates give higher frequencies than those of the angle-ply laminates in all the results (Qatu 1989).

Table 6.10. Frequency parameters Ω of completely free angle-ply graphite/epoxy shallow shells; $a/b = 1$, $a/h = 100$.

2	a/R_α	$\Omega = \omega a^2 \sqrt{\rho/E_1 h^2}$							
		1	2	3	4	5	6	7	8
<i>[45°] Single layer</i>									
1	—	1.378	2.215	3.120	4.565	4.777	6.086	7.938	7.960
	0.1	1.881	2.219	3.557	4.753	4.911	7.278	8.047	8.135
	0.5	2.247	2.824	5.484	5.932	6.868	9.397	10.15	12.13
0	0.1	1.486	2.615	3.235	4.621	4.961	6.412	8.048	8.088
	0.5	1.582	3.903	4.043	5.836	6.724	9.089	9.287	11.96
-1	0.1	1.378	3.121	3.541	4.580	5.352	6.097	8.096	8.388
	0.5	1.376	3.119	4.754	6.216	8.701	9.354	12.648	12.68
<i>[45°, -45°, 45°] and [-45°, 45°, -45°] Laminate</i>									
1	—	1.689	2.240	3.825	4.681	5.197	7.234	8.697	8.786
	0.1	2.245	2.288	4.301	5.242	5.376	8.488	8.903	8.932
	0.5	2.276	2.963	5.973	6.336	8.202	10.21	12.03	13.68
0	0.1	1.785	2.887	3.946	4.873	5.533	7.555	8.866	8.969
	0.5	1.814	4.094	4.606	7.117	7.534	10.03	10.75	13.76
-1	0.1	1.690	3.827	4.270	4.708	5.916	7.242	9.129	9.345
	0.5	1.691	3.843	5.001	7.314	9.591	10.67	14.85	17.97

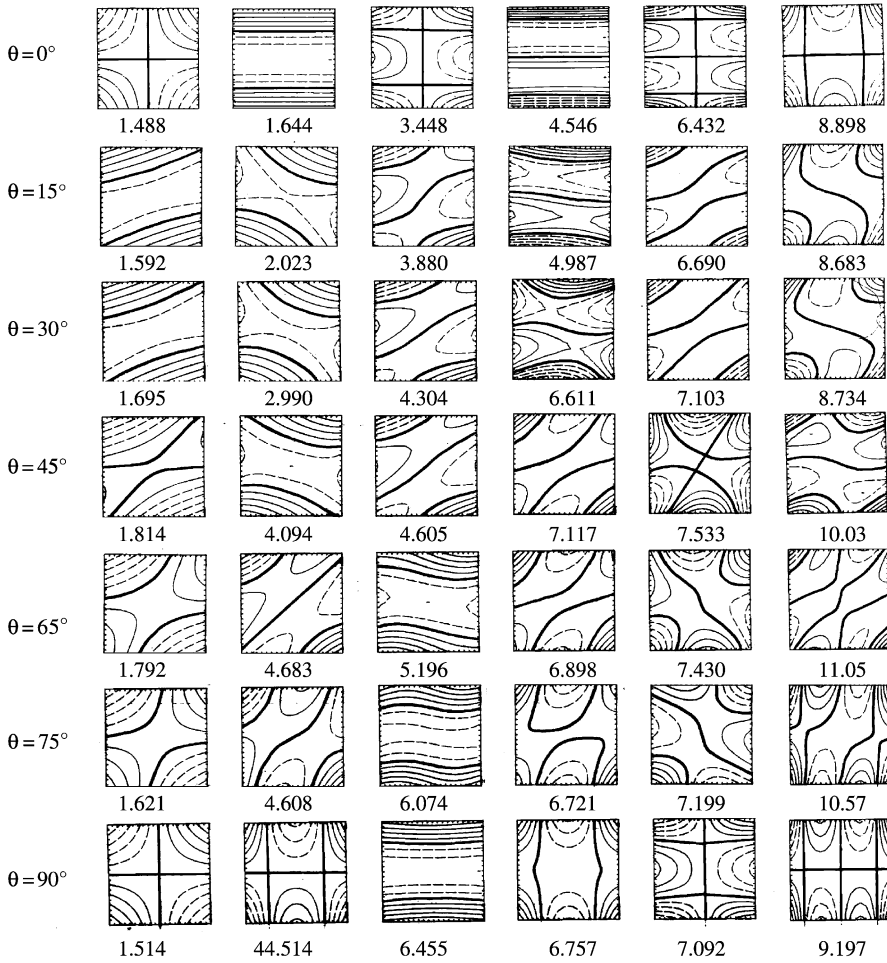


Figure 6.5. Mode shapes for free $[\theta, -\theta, \theta]$, G/E cylindrical shells, $a/b = 1$, $a/h = 100$, $a/R = 0.5$ (Qatu 1992c; reproduced with permission).

sixth mode for $\theta = 0^\circ$. For hyperbolic paraboloidal shells, the fourth mode is becoming the fifth when θ exceeds 15° . There is a tendency for the nodal lines to go in the direction of the fibers (i.e., lamination angle). Taking the cylindrical shell as an example, when $\theta = 0^\circ$ there are 12 horizontal nodal lines (i.e., in the direction of the fibers) and only four vertical nodal lines (i.e., perpendicular to that direction) for the first six mode shapes. When $\theta = 90^\circ$, the horizontal nodal lines decreased to seven, and the vertical nodal line increased to nine. For spherical and hyperbolic paraboloidal shell with diagonal orthotropy (i.e., $\theta = 45^\circ$), almost all the nodal lines are diagonal.

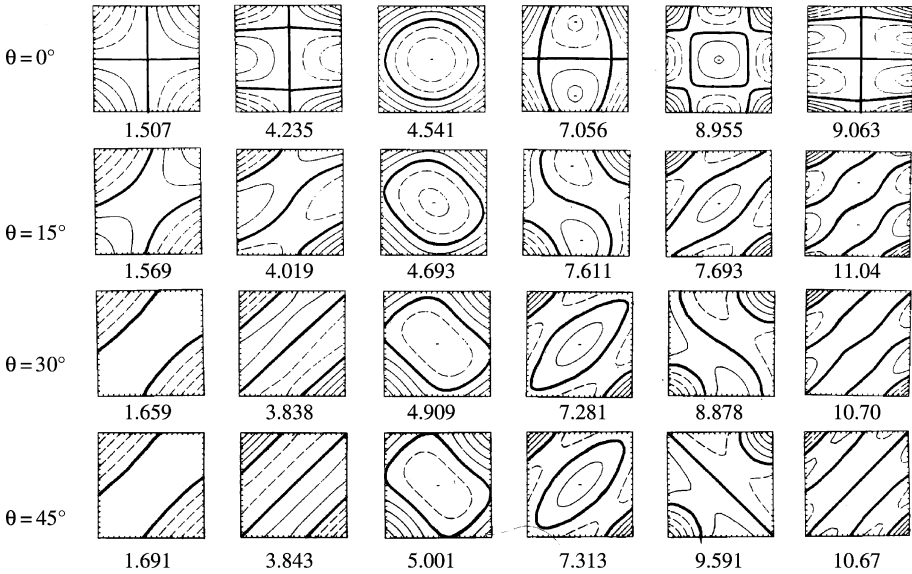


Figure 6.6. Mode shapes for completely free graphite/epoxy hyperbolic paraboloidal shells; $a/b = 1$, $a/h = 100$, $a/R = 0.5$ (Qatu 1992c; reproduced with permission).

Furthermore, it is observed that the crossing of the nodal lines for orthotropic materials (i.e., $\theta = 0$ or 90°) is replaced by curve veering for angle-ply laminates for most of the mode shapes.

The mode shapes can also be used to explain the natural frequencies. For spherical shells, changing the angle from 0 to 45° gradually changes the first mode shape to one similar to the second mode shape which has a considerably larger natural frequency. That is why the first frequency parameter increases considerably as the lamination angle increases. Changing the lamination angle from 0 to 45° does the opposite for the second mode shape which becomes similar to the first mode shape. This explains why the second natural frequency decreases as the lamination angle increases.

6.3.5 Cantilevered shallow shells

A cantilevered doubly curved shallow shell is shown in Figure 6.7. Convergence studies are made for a series of cantilevered plates and shallow shells representative of those to be analyzed subsequently. Filamentary composite materials of graphite/epoxy were considered. Three curvatures are treated: spherical, circular cylindrical, and hyperbolic paraboloidal shells. A moderate thickness ($b/h = 100$) and shallowness ($b/R = 0.5$) ratio

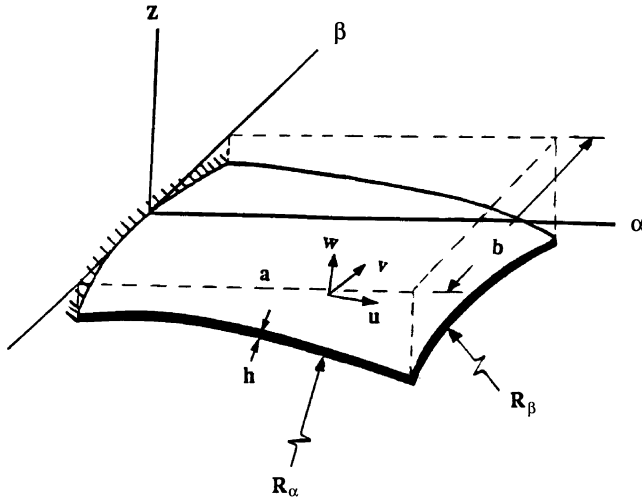


Figure 6.7. A doubly curved cantilevered shallow shell.

and square planform ($a/b = 1$) are used. Convergence studies for cylindrical shells having the fixation along the straight edge are also available (Qatu 1989).

Table 6.11 shows a convergence study of lowest frequency parameters for composite plates and shallow shells. It was observed that the solutions for the multi-layer laminates converge a little more rapidly than for single layers (Qatu and Leissa 1991b). It is also observed that the material with the smaller orthotropy ratio yields faster convergence than that with the higher orthotropy ratio. While the maximum difference between the 64-term and 100-term solution for the tenth frequency is less than 0.1% for E-glass/epoxy, it is about 2.6% for graphite/epoxy (Leissa and Qatu 1991). Because of these studies, unless stated otherwise, 64 terms ($M = 9$, $N = 7$) will be used for plates.

It is found that the convergence is faster as the ratio R_β/R_α decreases. For E-glass/epoxy hyperbolic paraboloidal shells ($R_\beta/R_\alpha = -1$), the difference between the 147-term solution and the 192-term one is 2.5% in the tenth frequency, for cylindrical shells ($R_\beta/R_\alpha = 0$) it is 2.2%, for spherical shells ($R_\beta/R_\alpha = 1$) it is 1.4%, and for the other type of cylindrical shells, where fixation is along the straight edge, it is 0.12% (Qatu 1989). From these studies, it was decided to use 192-terms for subsequent laminated shallow shell results (i.e., $I = K = 8$, $J = L = N = 7$, and $M = 9$). This is also consistent with using 64 terms for laminated plates (where only w_0 is needed).

Table 6.11. Convergence of the frequency parameter for cantilevered graphite/epoxy [30°, − 30°, − 30°, 30°] plates and shallow shells on square planform.

R_β/R_α	Determinant size	$\Omega = \omega a^2 \sqrt{\rho/E_1 h^2}$							
		1	2	3	4	5	6	7	8
Plate	36	0.710	1.615	3.503	4.569	6.025	7.530	9.705	12.754
	64	0.708	1.613	3.464	4.556	5.986	7.294	9.535	12.475
	100	0.707	1.613	3.464	4.555	5.983	7.289	9.520	12.227
+1	108	1.628	2.060	5.261	6.422	8.835	12.407	15.628	17.718
	147	1.613	2.046	5.198	6.365	8.670	12.080	15.265	16.978
	192	1.606	2.044	5.189	6.352	8.646	11.865	15.137	16.605
0	108	2.080	2.965	5.110	7.515	8.015	9.958	14.897	15.416
	147	2.069	2.936	5.099	7.230	7.926	9.660	14.249	14.945
	192	2.066	2.931	5.084	7.091	7.890	9.508	13.744	14.890
−1	108	1.222	2.165	5.293	8.359	11.573	14.264	18.056	18.970
	147	1.212	2.151	5.200	8.276	11.418	14.015	17.786	18.591
	192	1.209	2.146	5.179	8.248	11.354	13.869	17.638	18.414

6.3.5.1 Comparison with other studies. Comparisons were made with analytical results published by Leissa *et al.* (1983) for isotropic shells. The agreement was excellent; the results agreed to the fifth significant figure. Results for cantilevered plates obtained by various methods were discussed in Chapter 5.

Table 6.12 shows a comparison for composite cylindrical shallow shell panels. Finite element and experimental results were obtained by Crawley (1979). Different lamination sequences were used. It is found true for shells (as was earlier found for plates) that the Ritz method yields a closer upper bound to the exact solution than the finite element method, with fewer degrees of freedom (192 used in the Ritz method and 365 used in the finite element method). The maximum difference between the results obtained by using the Ritz method and the experimental methods is within 10%, except for one mode for one configuration, which was apparently missed altogether in both the finite element and experimental investigations.

6.3.5.2 Effect of varying θ upon the frequencies. Studies are made for symmetrically laminated plates and shallow shells of square planform ($a/b = 1$) having either a single layer or four layers in an angle-ply stacking sequence. Results are presented for the strongly orthotropic G/E composites. Table 6.13 presents the fundamental

Table 6.12. Comparison of analytical and experimental natural frequencies (Hz) for cantilevered cylindrical panels.

Qatu and Leissa (1991b)		Crawley (1979)	
Ritz 64 DOF	FEA 365 DOF		Test
$[0, 0, 30, -30]_s$			
163.8	165.7		161.0
269.5	289.6		254.1
593.0	597.0		555.6
702.5	718.5		670.0
824.8	833.3		794.0
$[0, 45, -45, 90]_s$			
190.8	192.4		177.0
217.5	236.1		201.8
695.5	705.8		645.0
804.8	808.2		745.0
954.1	980.6		884.0
$[45, -45, -45, 45]_s$			
133.1	147.0		145.3
236.2	238.0		222.0
746.6	768.1		712.0
758.8	—		—
1037.0	1038.0		997.0

$E_1 = 128 \text{ GPa}$, $E_2 = 11 \text{ GPa}$, $G_{12} = 4.48 \text{ GPa}$, $\nu_{12} = 0.25$, $h/\text{ply} = 0.13 \text{ mm}$, $\rho = 1500 \text{ kg/m}^3$, $R_\beta = 127.5 \text{ mm}$, $a = 152.4 \text{ mm}$, $b = 76.2 \text{ mm}$.

nondimensional frequency parameters for four-layer angle-ply plates and shallow shells. Other materials and lamination sequences are considered by Qatu and Leissa (1991b). The fiber orientation angle varies between 0 and 90° by an angle of 15° in the table. It is observed that increasing θ causes the fundamental frequency to decrease monotonically for the plates and for most of the shells considered. However, for spherical and cylindrical shells, the maximum fundamental frequency occurs in the vicinity of $\theta = 15^\circ$ (Figure 6.8).

It is interesting to notice that the percent change in the fundamental frequency between the 0° and the 90° angle is considerably more for G/E than that for E/E materials (Qatu and Leissa 1991b). It is also observed that changing the fiber angle has a much greater effect upon plates than for shells. The least change in the frequency parameter with increasing θ occurs for hyperbolic paraboloidal shells.

Table 6.13. Effect of varying θ upon the frequency parameters Ω of graphite/epoxy four layer $[\theta, -\theta, -\theta, \theta]$ cantilevered shallow shells. $a/b = 1$, $a/h = 100$, $b/R_\beta = 0.5$.

θ (degrees)	$\Omega = \omega a^2 \sqrt{\rho/E_1 h^2}$							
	1	2	3	4	5	6	7	8
<i>Plates</i>								
0	1.018	1.372	2.639	5.315	6.376	6.835	8.246	10.22
15	0.906	1.470	2.946	5.652	5.817	6.697	8.695	10.71
30	0.708	1.613	3.464	4.556	5.986	7.294	9.535	12.47
45	0.501	1.599	3.012	4.173	5.665	8.447	9.485	9.944
60	0.346	1.368	2.134	4.057	5.369	6.835	7.893	9.638
75	0.274	1.038	1.714	3.361	4.798	6.230	6.795	8.694
90	0.259	0.862	1.623	2.923	4.543	5.973	6.670	8.197
<i>Spherical shells</i>								
0	1.547	1.888	4.420	6.650	8.223	9.257	15.18	18.24
15	1.664	1.967	4.800	6.637	8.414	10.42	16.30	17.03
30	1.606	2.044	5.189	6.352	8.646	11.86	15.14	16.60
45	1.349	1.986	4.723	6.112	8.654	11.54	13.95	16.16
60	1.161	1.673	4.349	5.456	7.820	10.71	12.48	15.52
75	1.052	1.273	3.989	4.659	7.254	8.952	10.52	14.60
90	0.991	1.076	3.517	4.369	7.197	7.769	9.534	13.16
<i>Cylindrical shells</i>								
0	1.962	2.334	4.558	5.518	8.193	8.210	10.26	11.80
15	2.081	2.628	5.180	6.026	7.854	8.875	11.20	13.13
30	2.066	2.931	5.084	7.091	7.890	9.508	13.74	14.89
45	1.866	2.606	4.847	7.334	7.761	10.95	14.28	14.75
60	1.552	2.014	5.041	6.395	7.416	12.30	12.53	13.53
75	1.208	1.674	4.442	6.193	6.838	9.914	10.59	12.03
90	1.027	1.555	3.899	5.973	6.825	8.482	9.701	10.70
<i>Hyperbolic paraboloidal shells</i>								
0	1.473	1.512	5.693	6.956	10.09	10.83	15.93	16.50
15	1.273	1.881	5.348	7.697	10.86	11.95	16.84	17.63
30	1.209	2.146	5.179	8.248	11.35	13.87	17.64	18.41
45	1.150	2.092	4.983	7.988	11.01	15.15	16.63	18.17
60	1.038	1.747	4.497	7.019	9.893	13.73	14.24	15.34
75	0.947	1.311	3.914	5.931	8.561	10.68	12.26	13.23
90	0.973	1.023	3.578	5.340	8.141	8.845	11.28	12.41

Increasing the fiber orientation angle has its largest effects typically in the neighborhood of $\theta = 30^\circ$. However, for cylindrical shells the most rapid change of the frequency parameter occurs near 45 or 60°. The effect of changing the angle upon higher frequencies is less than that for the fundamental frequency.

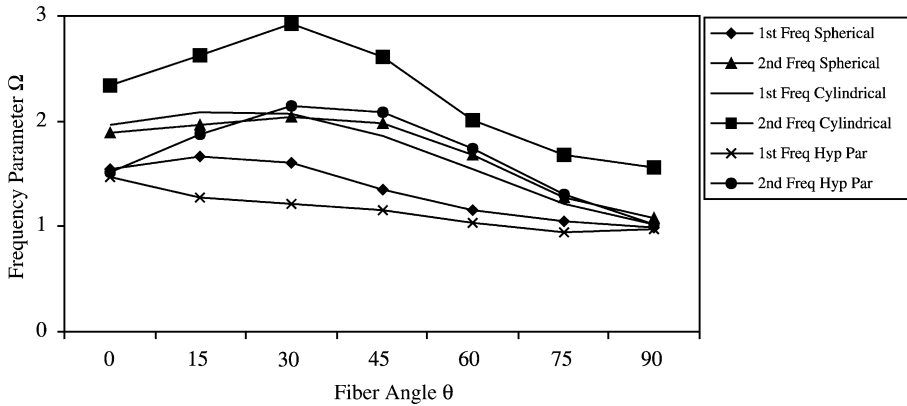


Figure 6.8. Effect of varying θ upon the frequency parameters Ω of graphite/epoxy four layer $[\theta, -\theta, -\theta, \theta]$ cantilevered shallow shells; $a/b = 1$, $a/h = 100$, $b/R_\beta = 0.5$.

6.3.5.3 Frequencies for angle-ply plates and shallow shells. Symmetrically laminated angle-ply plates and shallow shells having $a/b = 1$ are studied. A single-layer, and a three-layer laminate $[45^\circ, -45^\circ, 45^\circ]$ are used in this study. Results are given for flat plates and for shallow shells having two curvature ratios ($b/R = 0.1$ and 0.5). Thus, frequency changes due to curvature are clearly seen. Again, three types of curvature are considered. It is important to notice that, because of the symmetry of the problem, $[45^\circ, -45^\circ, 45^\circ]$ and $[-45^\circ, 45^\circ, -45^\circ]$ laminates give the same results for all the cases. Results for $a/b = 0.5$ and 2.0 are also available (Qatu 1989).

Table 6.14 lists the lowest nondimensional frequencies for G/E materials. The single layers were seen to give slightly lower fundamental frequencies than the three-layer laminates in every case (Qatu and Leissa 1991b). Curvature effects are greatest for cylindrical shells and least for hyperbolic paraboloidal shells.

6.3.5.4 Frequencies for cross-ply plates and shallow shells. Four types of laminates are used: $[0^\circ]$, $[0^\circ, 90^\circ, 0^\circ]$, $[90^\circ, 0^\circ, 90^\circ]$ and $[90^\circ]$. Results are given here for graphite/epoxy (G/E) materials. Results for E-glass/epoxy (E/E) materials are available in the literature. Two curvature ratios ($b/R = 0.1$ and 0.5) are used for each type of shell. Tables 6.14 gives the lowest nondimensional frequency parameters. Results for other aspect ratios are also available (Qatu 1989).

Increasing the curvature increases the frequencies considerably for all cases studied here. Its effect is maximum for cylindrical shells and minimum for hyperbolic paraboloidal shells.

For all cases studied here, the fundamental frequencies obtained for $[0^\circ]$ are more than those found for other laminates. Fundamental frequencies obtained for $[90^\circ, 0^\circ, 90^\circ]$,

Table 6.14. Frequency parameters Ω of cantilevered graphite/epoxy shallow shells; $a/b = 1$, $a/h = 100$.

R_β/R_α	b/R_β	$\Omega = \omega a^2 \sqrt{\rho/E_1 h^2}$							
		1	2	3	4	5	6	7	8
<i>[45°, -45°, 45°] and [-45°, 45°, -45°] laminates</i>									
	–	0.461	1.371	2.844	3.475	5.259	6.877	8.802	9.157
+1	0.1	0.685	1.559	3.044	4.092	5.550	8.262	9.050	9.497
	0.5	1.306	1.917	4.501	5.764	8.039	10.64	12.83	14.771
0	0.1	0.720	1.452	3.367	3.735	5.476	7.198	9.005	9.418
	0.5	1.657	2.543	4.625	6.578	7.035	10.36	12.71	13.706
–1	0.1	0.645	1.470	3.488	4.326	5.665	7.196	9.312	9.624
	0.5	0.923	2.070	4.028	7.942	9.165	13.84	15.86	16.914
<i>[0°, 90°, 0°] laminate</i>									
	–	1.000	1.363	2.898	6.246	6.266	6.755	8.280	11.29
+1	0.1	1.172	1.381	3.616	6.565	6.603	7.425	9.785	12.55
	0.5	1.536	1.919	5.019	6.725	8.520	10.69	17.34	18.32
0	0.1	1.248	1.388	2.936	6.256	6.641	6.831	8.426	11.32
	0.5	1.865	2.454	4.564	6.431	8.164	8.224	12.38	12.38
–1	0.1	1.148	1.384	4.107	6.704	6.767	7.423	8.865	12.03
	0.5	1.465	1.558	6.034	6.946	11.37	12.55	16.96	18.80

where fewer fibers are in the direction perpendicular to the fixed edge and closer to the middle surface of the shell, are considerably below those seen for other laminates (Leissa and Qatu 1991).

Table 6.14 also shows that the effect of curvature is smaller on the second frequencies of spherical and hyperbolic paraboloidal shells than for cylindrical shells. This is predominantly a torsional mode in each case.

It is observed that the cross-ply laminates (when the fibers having 0° are farther from the middle surface like [0°, 90°, 0°] laminates) give higher frequencies than angle-ply laminates.

6.3.5.5 Mode shapes for the cantilevered shells. Figures 6.9–6.11 give the first six mode shapes with various lamination angles for spherical, cylindrical, and hyperbolic paraboloidal curvatures, respectively. Unlike the completely free case, there is no diagonal symmetry here. The mode shapes for all the lamination angles of the three types of shells are considered.

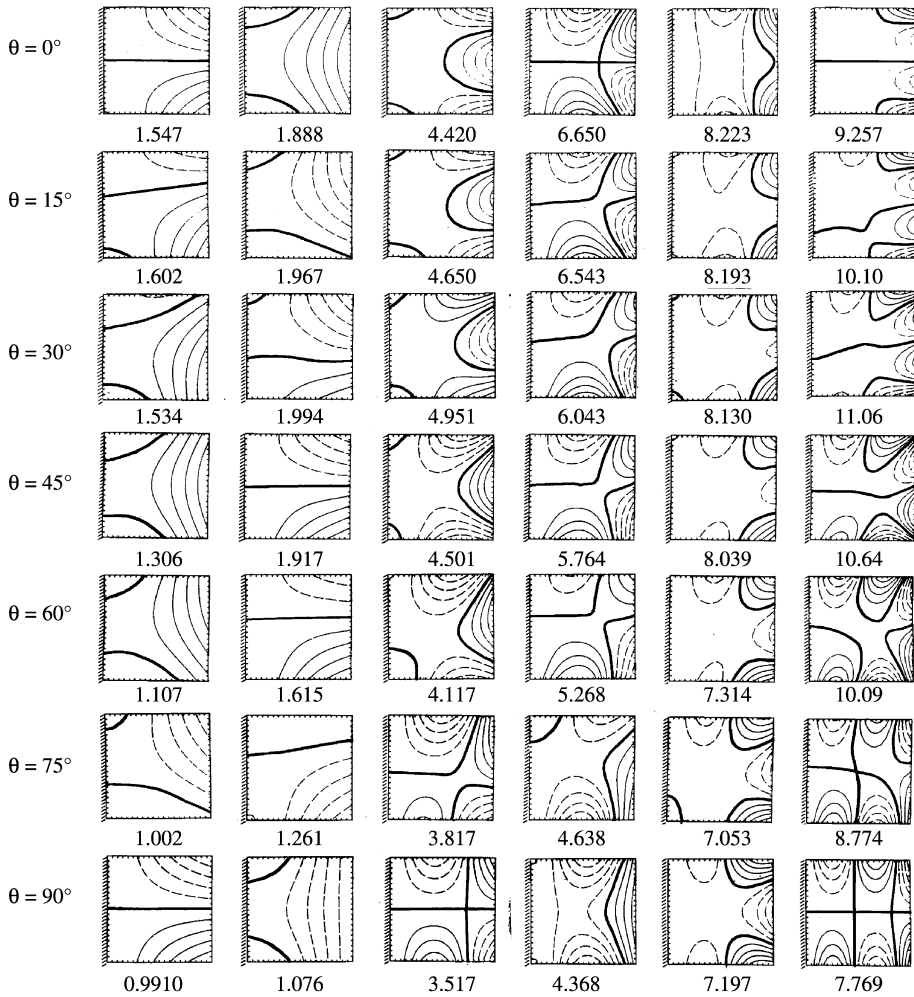


Figure 6.9. Mode shapes for cantilever G/E spherical shells; $a/b = 1$, $a/h = 100$, $a/R = 0.5$ (Qatu 1992c; reproduced with permission).

For cantilevered cross-ply shells, two classes of symmetry are possible in the displacement functions. The displacements can be either symmetric or antisymmetric about the α -axis.

For the flat plate and when $\theta = 0^\circ$, the first six mode shapes were, in order, the first spanwise bending mode (1B), the first torsional mode (1T), the first chordwise bending mode (1C), the second chordwise bending mode (2C), the second torsional mode (2T) and finally the second bending mode (2B). Unlike flat plates, for all the shells considered here,

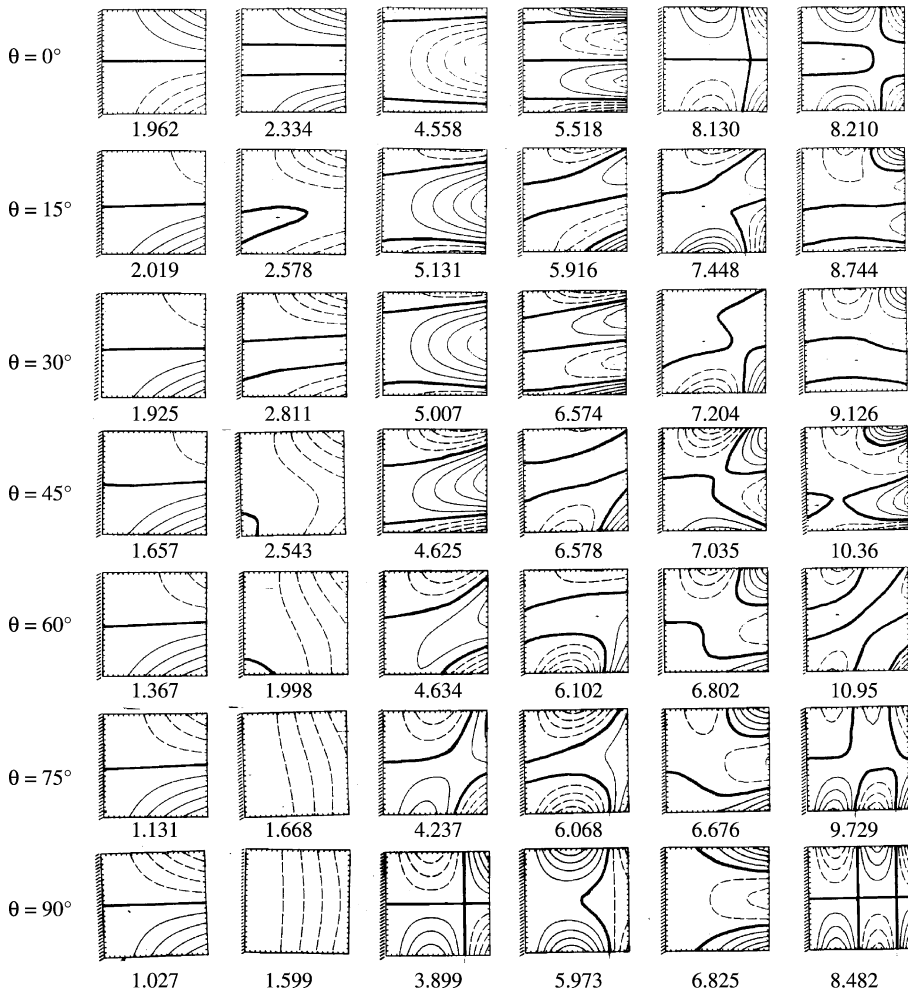


Figure 6.10. Mode shapes for cantilever G/E cylindrical shells, $a/b = 1$, $a/h = 100$, $a/R = 0.5$ (Qatu 1992c; reproduced with permission).

the first mode is the first torsional mode when $\theta = 0$ or 90° . The shape of the mode for shells is not as clear as that for plates. For the lamination angle $\theta = 0^\circ$, the order of the mode shapes is

- (a) For spherical shells 1T, 1B, 1C, 2T, 2B, 2C;
- (b) For cylindrical shells 1T, 1C, 1B, 2C, 2T, 3C;
- (c) For hyperbolic paraboloidal shells 1T, 1B, 1C, 2T, 2B, 2C.

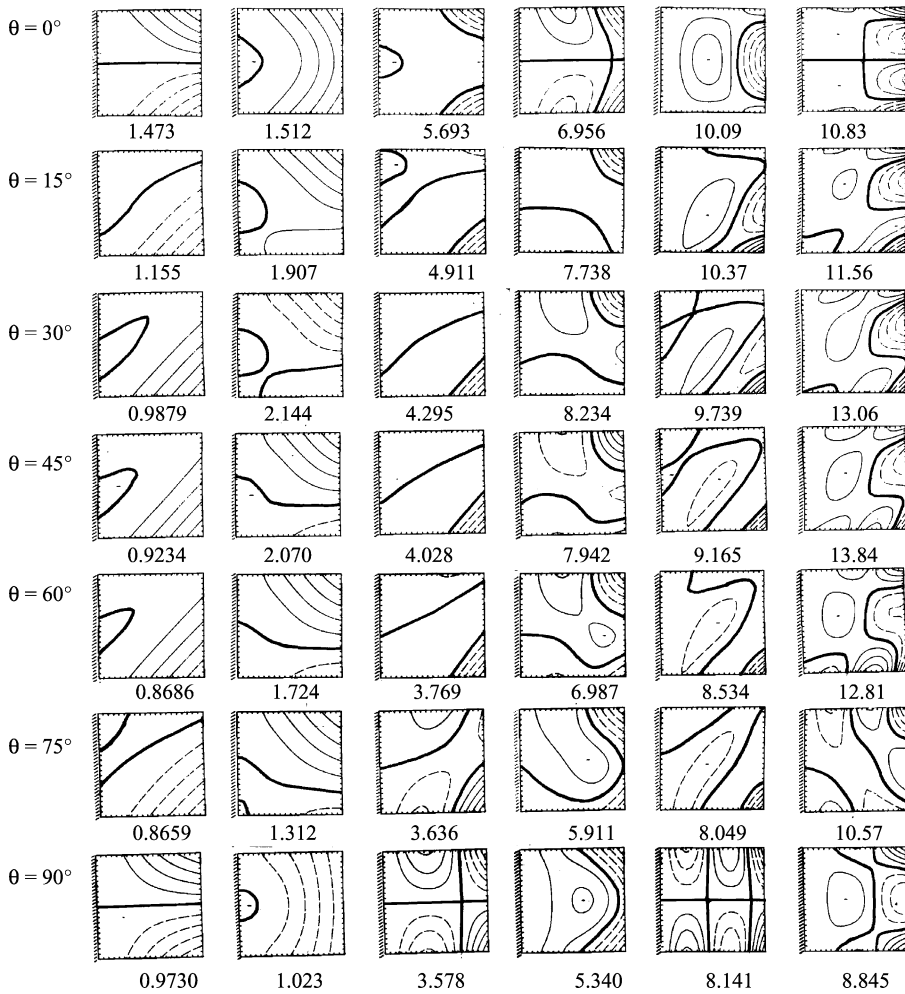


Figure 6.11. Mode shapes for cantilever G/E hyperbolic paraboloidal shells, $a/b = 1$, $a/h = 100$, $a/R = 0.5$ (Qatu 1992c; reproduced with permission).

The order of the mode shapes changes for the 90° lamination angle, but the first mode shape remains the torsional one. More chordwise bending modes tend to exist for the 0° lamination angle than the 90° one.

For lamination angles between 0 and 90° , the fundamental modes are combinations of the above modes. A gradual change in the mode shapes is observed as the lamination angle increases. In some cases, this gradual change in the mode shapes results in a completely different one when the lamination angle becomes 90° .

Looking at these mode shapes more closely, one observes that for most of the mode shapes large displacements are observed in limited regions of the shell, such as at a corner, whereas most of the shell displaces very little. This is characteristic of thin shells, where one observes much more activity near the edges or corners of the shell.

An interesting phenomenon is observed for spherical shells with $\theta = 45^\circ$. For these shells, the mode shapes can be approximately divided into two categories of symmetric and antisymmetric about the α -axis. For this special angle, the first mode is the 1B mode and the second one is 1T, unlike those with $\theta = 0$ or 90° . The difference between the first frequency parameter and the second is the maximum at this angle. For cylindrical shells, the first mode shape is the first torsional mode (i.e., 1T) for all the lamination angles.

6.3.6 Cantilevered pretwisted plates

A twisted plate is actually a shell. In one set of coordinates it is only twisted. But in other coordinates it has curvatures as well. The cantilevered twisted plate is a mechanical element of considerable technical significance. It has many applications such as in turbomachinery, impeller, and fan blades. Considerable literature can be found which relates to the vibration of turbomachinery blades (Leissa 1981a,b, 1986). However, the vast majority treated blades as cantilevered beams. Such representation is inaccurate if higher frequencies are needed or the blade is short. A more accurate model can be made with twisted plates.

Almost all the literature on the vibrations of turbomachinery blades is about isotropic blades (Kielb *et al.* 1985a,b; Leissa *et al.* 1984a,b; MacBain *et al.* 1984). Chamis (1977) compared frequencies obtained for some complex composite fan blades using finite element with those obtained experimentally.

It has been observed that there is a wide disagreement among the natural frequencies obtained for isotropic twisted plate by different analytical methods (Kielb *et al.* 1985a; Leissa *et al.* 1984a,b). This led to experimental investigations (Kielb *et al.* 1985b; MacBain *et al.* 1984) and a three-dimensional study (Leissa and Jacob 1986) of the problem. The agreement of the last two investigations was reasonably good. The three-dimensional solutions yielded slightly higher frequencies than the experimental ones. This can be due to the difficulty in satisfying the clamped edge conditions experimentally. However, the three-dimensional solution is lengthy and not always needed. Another study was made by using shallow shell theory and the Ritz method to solve for the natural frequencies of isotropic twisted plates (Leissa *et al.* 1982). This study concluded that shallow shell theory can be used for twisted plates with an angle of twist not more than 45° .

Natural frequencies and mode shapes of laminated cantilever plates having pretwist is presented here. Laminated shallow shell theory and the Ritz method are used here. The effects of many parameters like twist angle, lamination angle, stacking sequence, and

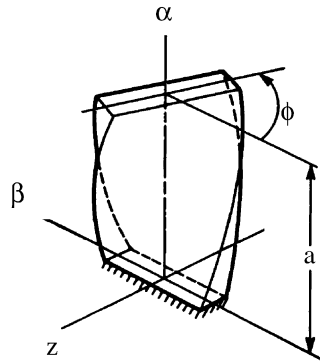


Figure 6.12. A twisted plate.

thickness and orthotropy ratios on the natural frequencies and mode shapes of twisted cantilevered composite plates are also studied (Qatu and Leissa 1991c). Additional studies on twisted plates are available in the literature (Nabi and Ganesan 1993). Pretwisted conical shells were picked up by Lim *et al.* (1997b) Lim and Liew (1995a,b) and Liew and Lim (1996).

A twisted plate is characterized by its middle surface, which is defined by $z = \alpha\beta/R_{\alpha\beta}$. The constant $R_{\alpha\beta}$ identifies the radius of twist. A typical twisted plate is shown in Figure 6.12.

6.3.6.1 Convergence studies. A typical plate of moderate thickness ($b/h = 100$) and twist ($\varphi = 30^\circ$) and square planform ($a/b = 1$) is used. Convergence studies of the lowest frequency parameters $\Omega = \omega a^2 \sqrt{\rho/E_1 h^2}$ for graphite/epoxy are given in Table 6.15. The maximum number of terms used is 192 by choosing eight terms in both α and β directions for all the three components of displacements. Studies conducted earlier (Qatu and Leissa 1991c) concluded that better convergence is obtained when the number of terms in the axis perpendicular to the clamped boundary are higher than those in the direction parallel to the clamped boundary.

As the number of terms increases, rapid convergence is observed. The maximum difference between the $3 \times 7 \times 7 = 147$ -term and the $3 \times 8 \times 8 = 192$ -term solutions for the tenth frequency is 2.5%. It is observed to be even faster for E-glass/epoxy materials (Qatu and Leissa 1991c). It has been decided to use $3 \times 6 \times 8 = 144$ terms in the subsequent analysis. The maximum difference between this solution and the more accurate 192-term solution is less than 2.5%. Comparisons were made with analytical results published by Leissa *et al.* (1982) for isotropic twisted plates. The agreement was excellent.

Table 6.15. Convergence of the frequency parameter for cantilevered graphite/epoxy $[30^\circ, -30^\circ, 30^\circ]$ twisted plates ($\varphi = 30^\circ$) on square planform.

Terms	Determinant size	$\Omega = \omega a^2 \sqrt{\rho/E_1 h^2}$									
		1	2	3	4	5	6	7	8	9	10
$3 \times 5 \times 5$	75	0.7308	4.360	9.236	10.48	11.67	15.62	19.21	20.59	23.13	27.90
$3 \times 6 \times 6$	108	0.7238	4.283	8.487	10.15	10.77	13.26	17.70	18.88	21.08	25.17
$3 \times 8 \times 6$	144	0.7240	4.279	8.488	10.14	10.75	13.19	17.61	18.69	20.64	24.49
$3 \times 7 \times 7$	149	0.7222	4.248	8.246	9.897	10.50	13.11	17.32	17.49	20.17	20.44
$3 \times 6 \times 8$	144	0.7205	4.249	8.203	9.740	10.50	13.12	16.50	17.39	19.75	20.14
$3 \times 8 \times 8$	192	0.7205	4.242	8.203	9.731	10.48	13.04	16.42	17.32	19.64	19.80

6.3.6.2 Natural frequencies and mode shapes. The first natural frequency parameters were obtained for twisted plates having different materials, thickness ratios, and fiber orientations (Qatu and Leissa 1991c). Results were also obtained for square single-layered thin plates. The natural frequencies obtained for single-layer laminates are slightly lower (by less than 3%) than those obtained for the multi-layer ones.

The maximum fundamental frequencies are observed when the fibers are perpendicular to the clamped edge (i.e., $\theta = 0^\circ$) in all cases. Frequencies and mode shapes were given in Figure 5.8 for untwisted cantilevered plates. For the fundamental frequency, which corresponds to the first spanwise bending mode, increasing the fiber angle has a very large effect. The natural frequencies when $\theta = 90^\circ$ are about one quarter of those when $\theta = 0^\circ$ when G/E material is used for all twist angles. This difference is much less for E/E materials. For higher frequencies, the maximum frequency parameters can be found at a fiber angle between 0 and 30° , and occasionally at a fiber angle of 45° , with some exceptions for E/E materials. Although thin untwisted plate theory predicts the same transverse vibration frequency parameters $\Omega = \omega a^2 \sqrt{\rho/E_1 h^2}$ when the thickness ratio is changed, new mode shapes can be introduced for some modes of the thicker plates, which correspond to inplane vibration modes and not transverse ones. This could not be seen if the inplane terms (i.e., U and V) are removed, which is normally done in vibration studies made for untwisted symmetrically laminated thin plates.

Figures 6.13–6.15 show the fundamental six frequency parameters and corresponding mode shapes for laminated twisted graphite/epoxy square plates for angles of twist of 15, 30, and 45° , respectively. As was found earlier (Leissa *et al.* 1982) for isotropic plates, increasing the angle of twist decreases the fundamental bending frequency. For isotropic plates, increasing the angle of twist increases the second frequency, which corresponds to the first torsional mode. This phenomenon is not obvious for laminated twisted plates. The maximum second frequency is obtained when $\varphi = 30^\circ$ for the plates with the fibers perpendicular to the clamped edge (i.e., $\theta = 0^\circ$) and when $\varphi = 15^\circ$ for those with the fibers parallel to the clamped edge (i.e., $\theta = 90^\circ$). Careful analysis of the mode shapes corresponding to these frequencies shows that the second mode shape is not always the first torsional mode. For the same example mentioned above when the angle of twist is 15° , the second frequency corresponds to the first torsional mode when $\theta = 0^\circ$, but it corresponds to the second bending mode when $\theta = 90^\circ$.

For the untwisted plate and when $\theta = 0^\circ$, the first six mode shapes (Figure 5.8) are, in order, the first spanwise bending mode (1B), the first torsional mode (1T), the first chordwise bending mode (1C), the second chordwise bending mode (2C), the second torsional mode (2T) and finally the second bending mode (2B). For this particular fiber angle, there exists a material symmetry about the α -axis, and it is seen that the mode shapes are all either symmetric or antisymmetric about the α -axis. As the fiber orientation angle increases, this symmetry/antisymmetry in the mode shapes is lost, and a gradual

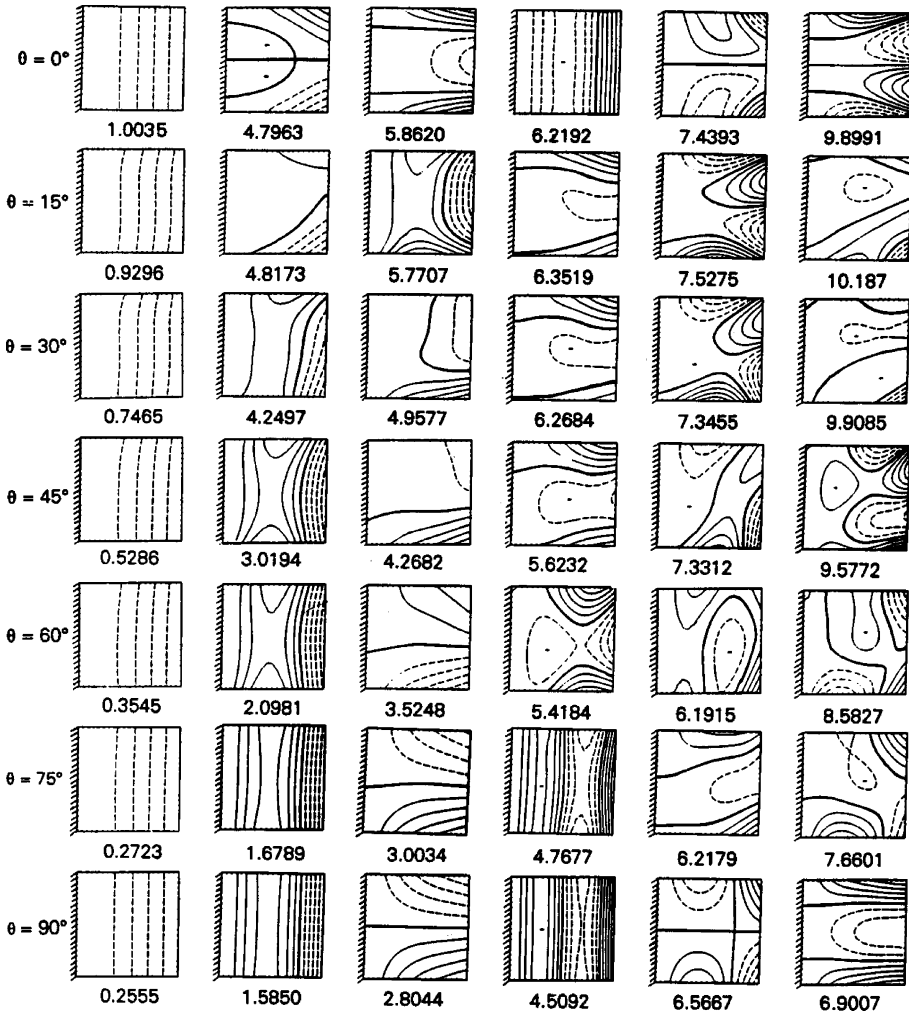


Figure 6.13. Mode shapes for graphite/epoxy cantilever plates with a 15° twist angle.

change in the contour lines is observed. When the angle of fibers become 90° , the material symmetry is recovered, and the mode shapes are again either symmetric or antisymmetric. However, the order of the mode shapes is not the same as that of $\theta = 0^\circ$. The first six mode shapes are 1B, 1T, 2B, 2T, 3T, and 3B. The chordwise bending modes are higher frequency modes because the fibers here all lie parallel to the clamped edge. For plates with $\theta = 0^\circ$, the second, third, and fourth mode shapes have one, two, and three nodal lines parallel to the α -axis, respectively. When the fiber orientation angle becomes 90° (i.e., the fibers are parallel to the clamped edge), the second mode still has one nodal

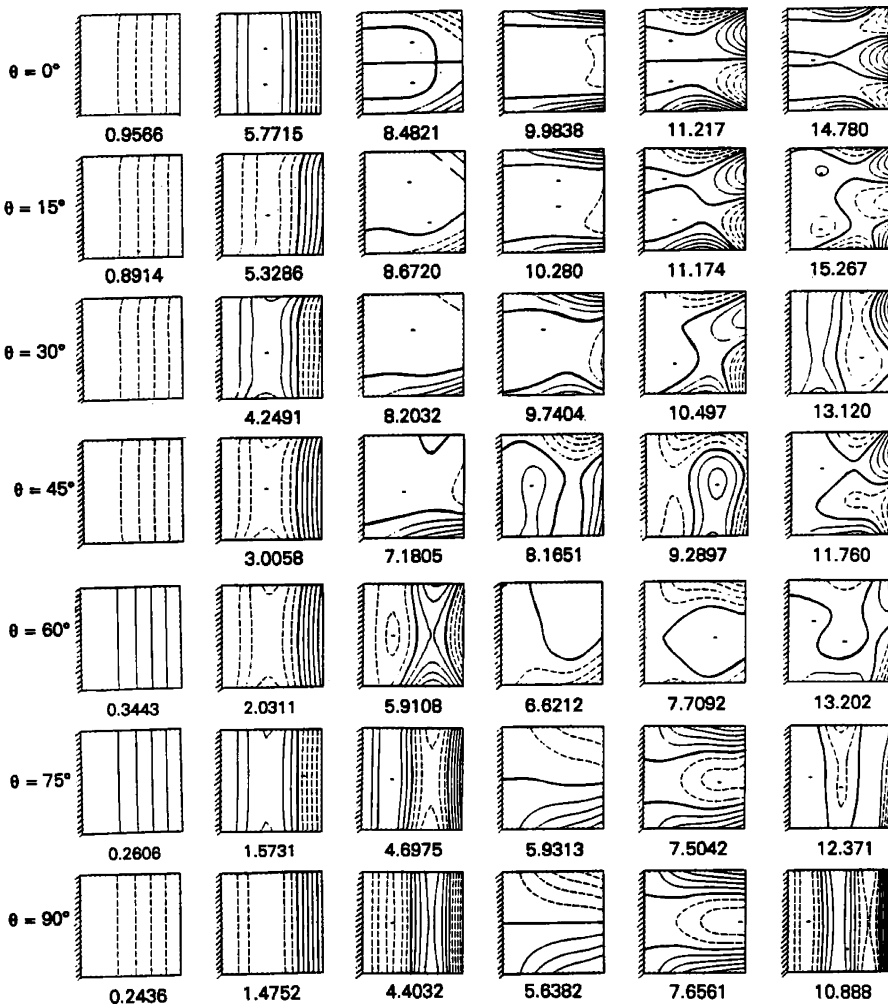


Figure 6.14. Mode shapes for graphite/epoxy cantilever plates with a 30° twist angle.

line parallel to the α -axis; but the third and fourth modes have one nodal line parallel to the β -axis (i.e., fiber direction). This shows that more nodal lines tend to appear parallel to the direction of the fibers, i.e., perpendicular to the direction of least bending stiffness.

Looking carefully at the gradual changes in the contour plots progressing from Figures 6.13–6.15, one can see that the third mode when $\theta = 0^\circ$ gradually changes and becomes the fourth mode when $\theta = 45^\circ$ and eventually becomes the second twisting mode when the fiber angle becomes 90° , which means that a certain mode shape may gradually change to a completely different mode shape as the fiber angle is increased. This is also

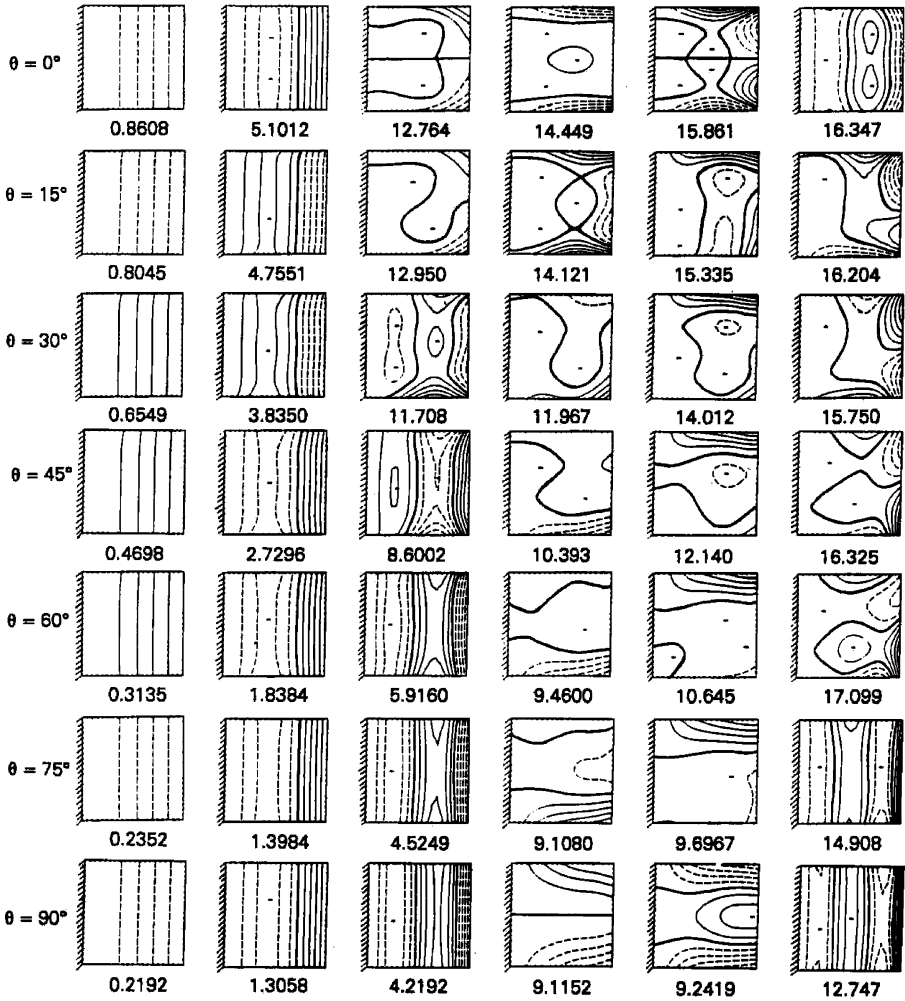


Figure 6.15. Mode shapes for graphite/epoxy cantilever plates with a 45° twist angle.

true for the fourth mode shape when $\theta = 0^\circ$, which is the 2C mode. It gradually changes as θ increases and becomes the third mode (which is 2B) when $\theta = 45^\circ$.

When the plate starts to have an initial twist, the second mode does not remain in the torsional mode. In fact, for $\varphi = 30$ and 45° , the second mode is the second bending mode; the first torsional mode is the third mode when $\theta = 0^\circ$ and the fourth one when $\theta = 90^\circ$, being preceded by three bending modes. The number of symmetric modes such as 1B, 2B,

3B, 1C, and 2C when $\theta = 90^\circ$ increases as the angle of twist increases. For $\varphi = 0^\circ$, three of the first six mode shapes are symmetric, whereas for $\varphi = 45^\circ$, five are symmetric.

For fiber angles between 0 and 90° , coupling between the modes exists, and the strength of the coupling increases both with increasing fiber angle and increasing twist angle. With large twist angle (Figure 6.15), one observes many modes where large displacements occur only in limited regions of the plate such as in a corner, whereas most of the plate displaces very little. This is characteristic of thin shells, and the twisted plate is in actuality a shell.

6.3.7 Doubly cantilevered

A doubly cantilevered shallow shell (i.e., two adjacent edges clamped and the others free) is shown in Figure 6.16. A convergence study for moderately thin ($b/h = 100$) plates and shallow shells having square planform ($a/b = 1$) is performed. The depth of the shell is taken at the limits of shallow shell theory ($b/R_\beta = 0.5$), which is found to yield slower convergence than for shallower shells. Results for the flat plate are shown for comparison. Three layer $[\theta, -\theta, \theta]$ laminates are considered in the analysis. A representative lamination angle of 30° has been adopted in the convergence studies.

Table 6.16 shows a convergence study of the lowest eight nondimensional frequency parameters for composite graphite/epoxy plates and the three types of shells. Convergence for laminated plates is observed to be the best. The maximum difference between the 36-term solution and the 49-term solution is 3.9% for graphite/epoxy. Earlier studies

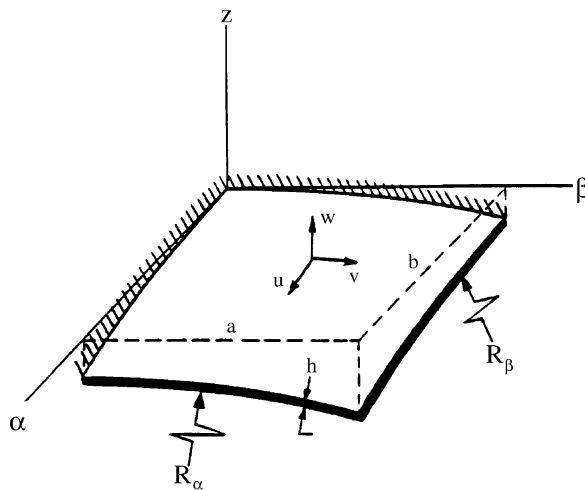


Figure 6.16. A doubly cantilevered shallow shell.

Table 6.16. Convergence of the frequency parameter for doubly cantilevered graphite/epoxy [30, −30, 30] plates and shallow shells on square planform, $b/h = 100$, $b/R_\beta = 0.5$.

R_β/R_α	Determinant size	$\Omega = \omega \alpha^2 \sqrt{\rho/E_1 h^2}$							
		1	2	3	4	5	6	7	8
−	25	1.293	3.057	5.580	6.396	8.833	10.82	13.99	15.44
	36	1.291	3.054	5.556	6.278	8.590	10.37	13.46	14.94
	49	1.291	3.052	5.554	6.273	8.574	10.24	12.99	14.57
+1	75	3.750	4.827	11.74	12.92	20.49	25.00	26.52	30.66
	108	3.677	4.745	10.99	11.54	18.05	21.54	24.21	29.73
	147	3.652	4.726	10.78	11.40	17.44	19.77	23.88	29.32
0	75	2.723	6.535	8.760	10.87	14.39	15.84	16.68	19.30
	108	2.713	6.223	8.582	10.06	13.87	15.31	16.38	18.58
	147	2.709	6.209	8.572	10.02	13.31	14.37	16.28	17.94
−1	75	2.257	8.159	13.80	15.95	18.04	20.25	23.43	25.95
	108	2.242	8.104	13.30	15.29	17.00	18.77	20.93	23.94
	147	2.229	8.050	13.20	15.15	16.56	18.56	20.86	22.85

showed that convergence for the material with the lower inplane orthotropy ratio is faster than that with the higher orthotropy ratio (Qatu 1993a). Similar observation is made for shells. From these studies, the 49-term solution (i.e., $M = 8$, $N = 8$) gives good results for engineering purposes and will be adopted in the subsequent analysis of plates. Convergence for shells is slower than that of plates. It was necessary to use up to a 147-term solution to obtain results of reasonable accuracy. Convergence is slower as the ratio R_β/R_α increases. Interestingly enough, this is opposite to what was found previously for cantilevered shallow shells.

For graphite/epoxy hyperbolic paraboloidal shells ($R_\beta/R_\alpha = -1$), the difference between the 108-term solution and the 147-term solution is 4.7% in the eighth frequency, for cylindrical shells ($R_\beta/R_\alpha = 0$), it is 6.5% in the sixth frequency, and for spherical shells ($R_\beta/R_\alpha = 1$), it is 8.9%, also in the sixth frequency. These differences are less for E-glass/epoxy (Qatu 1993a). From these studies, it was decided to use 147-terms for subsequent analyses (i.e., $I = J = K = L = 8$, $M = N = 9$). This is also consistent with using $147/3 = 49$ terms used for laminated plates.

6.3.7.1 Effect of varying θ upon the frequencies. Studies are made for symmetrically laminated plates and shallow shells of square planform ($a/b = 1$) having a three-layer angle-ply stacking sequence. Results are presented for the strongly orthotropic graphite/epoxy (G/E) composites (Figure 6.17).

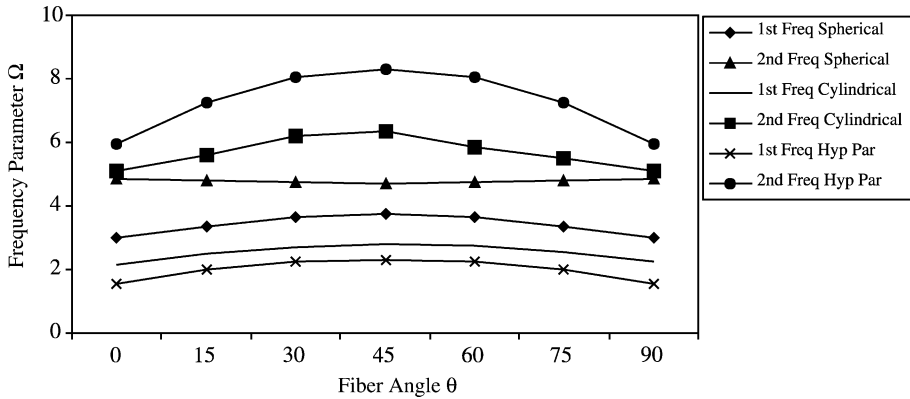


Figure 6.17. Effect of varying θ upon the frequency parameters Ω of graphite/epoxy three layer $[\theta, -\theta, \theta]$ doubly cantilevered shallow shells, $a/b = 1$, $b/h = 100$, $b/R_\beta = 0.5$.

Table 6.17 presents the first eight nondimensional frequency parameters for three-layer plates and shallow shells of moderate curvature ($b/R_\beta = 0.2$) for graphite/epoxy materials. Table 6.18 shows the same thing for shallow shells with relatively deep curvature ($b/R_\beta = 0.5$). The fiber orientation angle varies between 0 and 90° by an angle increment of 15° in all the tables.

Natural frequencies for spherical and hyperbolic paraboloidal shells as well as those for plates are the same when the fiber angle θ is 60, 75, and 90° as those when it is 30, 15, and 0°, respectively. This is due to the symmetry of the problem about the diagonal for the shallow shells of square planform studied here.

It is observed that increasing θ has its largest effect on the fundamental frequencies of hyperbolic paraboloidal shells for all the results. The effect of increasing the lamination angle from 0 to 45° is a 36% increase in fundamental frequencies for hyperbolic paraboloidal, 22% for cylindrical, 24% for spherical shells, compared with only 9.3% for plates. For deeper shallow shells ($b/R_\beta = 0.5$), it is observed that increasing the angle from 0 to 45° causes the fundamental frequencies to increase by 24, 29, and 48% for spherical, cylindrical, and hyperbolic paraboloidal shells, respectively. This leads to the conclusion that increasing the angle has even larger effect on the fundamental frequencies of deeper shells than shallower ones. Interestingly enough, this is opposite to what was found earlier for cantilevered shallow shells, where the effect of increasing θ on the fundamental frequencies is greater for plates than shells.

The maximum frequencies are obtained in the vicinity of $\theta = 45^\circ$ (except for very few numbers of the higher frequencies). Furthermore, the effect of changing the lamination angle decreases for higher frequencies. Better understanding of these results can be

Table 6.17. Effect of varying θ upon the frequency parameters Ω of graphite/epoxy three layer $[\theta, -\theta, \theta]$ doubly cantilevered shallow shells; $a/b = 1$, $b/h = 100$, $b/R_\beta = 0.2$.

θ (degrees)	$\Omega = \omega a^2 \sqrt{\rho/E_1 h^2}$							
	1	2	3	4	5	6	7	8
<i>Plates</i>								
0	1.179	2.413	5.156	6.5157	7.761	9.444	10.14	14.03
15	1.280	2.672	5.438	6.3718	7.998	9.557	11.30	14.23
30	1.291	3.052	5.554	6.273	8.574	10.24	12.99	14.57
45	1.293	3.293	5.218	6.591	9.269	10.85	12.28	14.81
<i>Spherical shells</i>								
0	2.188	3.525	6.908	7.301	10.96	11.70	15.18	18.30
15	2.392	3.635	7.052	8.087	11.79	12.79	16.12	17.67
30	2.614	3.765	7.358	9.154	12.43	14.24	15.68	17.31
45	2.715	3.747	7.633	9.886	11.89	15.04	15.54	17.66
<i>Cylindrical shells</i>								
0	1.668	3.318	5.370	7.105	8.485	9.508	10.45	14.15
15	1.906	3.686	5.756	7.344	8.788	9.847	11.54	14.46
30	2.004	4.135	6.288	7.668	9.432	10.98	13.30	15.31
45	2.023	4.391	6.375	8.925	9.997	12.57	13.37	15.89
60	1.919	4.375	6.450	8.922	10.51	13.87	14.08	16.06
75	1.716	4.130	6.662	7.877	10.39	12.73	14.91	17.20
90	1.492	3.797	6.729	7.145	9.676	11.75	14.14	18.00
<i>Hyperbolic paraboloidal shells</i>								
0	1.386	4.837	7.477	7.660	9.579	11.99	13.55	18.05
15	1.713	5.659	7.422	8.378	10.40	12.78	14.48	17.47
30	1.869	6.331	7.221	9.194	10.91	13.27	14.40	16.40
45	1.883	6.408	7.388	9.132	11.32	12.93	13.46	16.02

achieved by studying the mode shapes corresponding to these frequencies. The previous phenomenon can be observed for all curvatures considered. It is less strong for deeper and cylindrical shells than for other curvatures.

6.3.7.2 Mode shapes. Figures 6.18–6.20 give the first six mode shapes with various lamination angles for spherical, cylindrical, and hyperbolic paraboloidal curvatures, respectively. Similar to the completely free case, there is diagonal symmetry here, and only the mode shapes for $\theta = 0, 15, 30$, and 45° are shown for spherical and hyperbolic paraboloidal shells. For these shells, the mode shapes for $\theta = 60, 75$, and 90° are similar to

Table 6.18. Effect of varying θ upon the frequency parameters Ω of graphite/epoxy three layer $[\theta, -\theta, \theta]$ doubly cantilevered shallow shells; $a/b = 1$, $b/h = 100$, $b/R_\beta = 0.5$.

θ (degrees)	$\Omega = \omega a^2 \sqrt{\rho/E_1 h^2}$							
	1	2	3	4	5	6	7	8
<i>Spherical shells</i>								
0	3.015	4.875	8.933	9.932	14.75	18.9	20.41	23.00
15	3.344	4.782	9.806	10.52	16.18	19.19	21.41	25.65
30	3.652	4.726	10.78	11.40	17.44	19.77	23.88	27.44
45	3.754	4.692	11.41	11.45	17.85	20.53	25.70	28.04
<i>Cylindrical shells</i>								
0	2.162	5.091	7.247	8.171	9.938	11.72	12.84	15.07
15	2.490	5.603	8.002	8.894	11.00	12.93	13.85	15.72
30	2.709	6.209	8.472	10.02	13.31	14.37	16.28	17.94
45	2.787	6.358	8.738	11.54	13.59	16.24	19.39	20.77
60	2.774	5.870	8.698	11.93	14.32	16.08	21.74	21.74
75	2.564	5.519	8.116	10.23	15.64	15.76	18.13	22.15
90	2.248	5.098	7.735	9.229	14.68	15.22	18.14	21.36
<i>Hyperbolic paraboloidal shells</i>								
0	1.551	5.970	10.38	11.90	15.23	15.81	19.41	20.73
15	1.976	7.273	11.49	13.94	15.57	17.92	18.95	21.51
30	2.229	8.050	13.20	15.15	16.56	18.56	20.86	22.85
45	2.306	8.316	14.87	16.26	17.12	18.70	21.54	21.66

those given for $\theta = 30$, 15 , and 0° , respectively, and can be obtained by changing the coordinates.

For this boundary condition, symmetry about the diagonal $\alpha = \beta$ exists only for isotropic and diagonally orthotropic (with layers making a 45° angle with the α -axis) plates and spherical and hyperbolic paraboloidal shells. Mode shapes are either symmetric or antisymmetric about $\alpha = \beta$.

Two adjacent edges are completely clamped for these boundary conditions. This clamping decreases the activity of the displacement near the clamped edges. In addition to this, the fact that shells have considerably more internal stiffness when compared with flat plates makes most of the displacement activity close to the completely free edges.

It is also clear here that more nodal lines tend to exist in the longitudinal direction of the cylindrical shells and parallel to the direction of the fibers. This is shown clearly for cylindrical shells with 0° lamination angle, where almost all the nodal lines are parallel to the α -axis which is both the longitudinal direction of the cylindrical shell and the direction of the fibers.

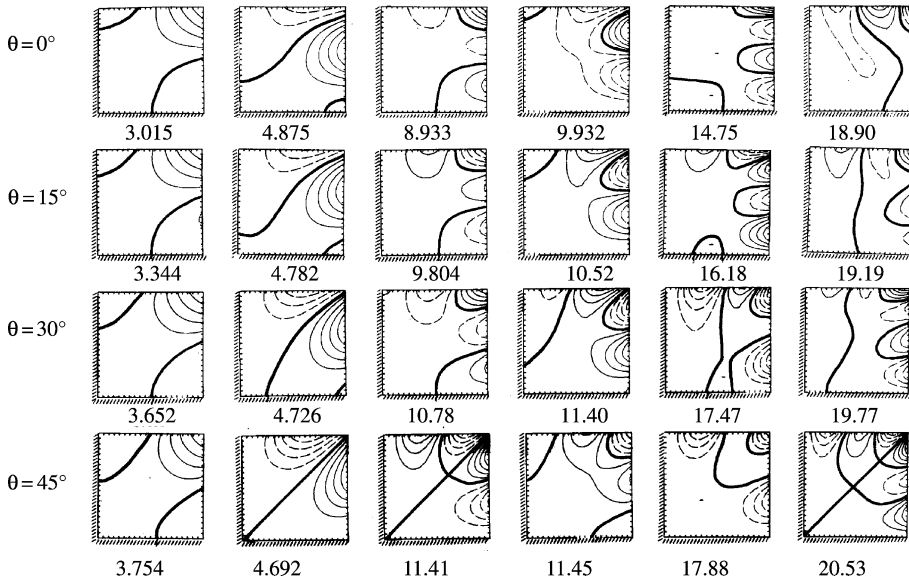


Figure 6.18. Mode shapes for doubly cantilever graphite/epoxy spherical shells; $a/b = 1$, $a/h = 100$, $a/R = 0.5$. (Qatu, 1992c; reproduced with permission).

It is observed that nodal lines cross frequently for the shells with diagonal symmetry (spherical and hyperbolic paraboloidal shells with $\theta = 45^\circ$). This phenomenon is replaced by curve veering for other lamination angles of the same shells and all lamination angles of the cylindrical shells.

An interesting phenomenon is observed for these shells concerning the nodal lines. It is observed that most of the nodal lines start usually almost perpendicular to the clamped boundaries and gradually change its direction to that of the fibers. This is mostly clear for spherical shells. For cylindrical shells, the nodal lines have a direction between the longitudinal axis (i.e., α -axis) of the shell and the lamination angle.

Unlike flat plates, where the first mode shapes have no nodal line and the second mode shape have only one nodal line, almost all the first two mode shapes for these shells have two nodal lines. This can explain more clearly why these shells have considerably higher frequency parameters than flat plates.

6.3.8 Shallow shells with other boundary conditions

Shallow shells with rectangular planforms can have any combination of boundary conditions that laminated plates have. Symmetrically laminated rectangular plates have

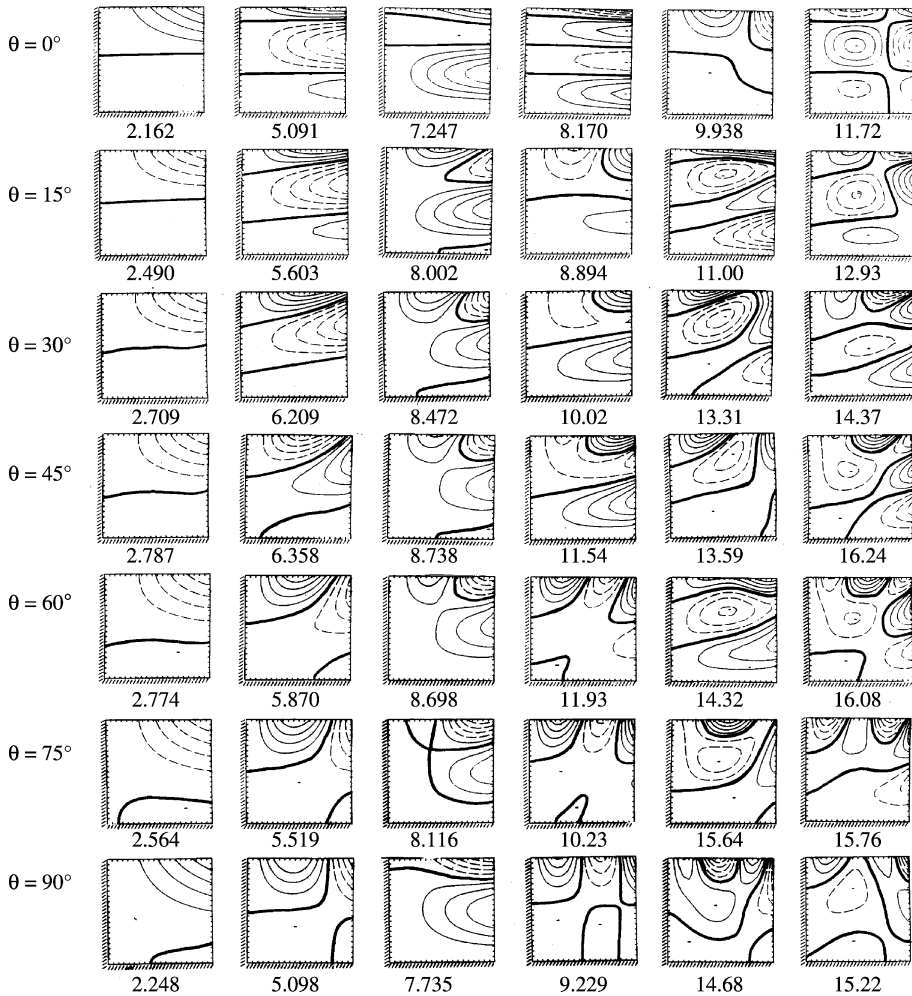


Figure 6.19. Mode shapes for doubly cantilever graphite/epoxy cylindrical shells; $a/b = 1$, $a/h = 100$, $a/R = 0.5$. (Qatu, 1992c; reproduced with permission).

three possible boundary conditions per edge, and 21 combinations of classical boundary conditions for isotropic plates.

Shallow shells have 12 classical boundary conditions per edge. This yields numerous possible combinations of boundary conditions for such shells. Not all of these are necessarily practical. At each edge, the completely free and completely clamped are well understood and used in many applications. In addition, the shear diaphragm boundary (S2) is well recognized for simple supports. Unless stated otherwise, these boundaries will be

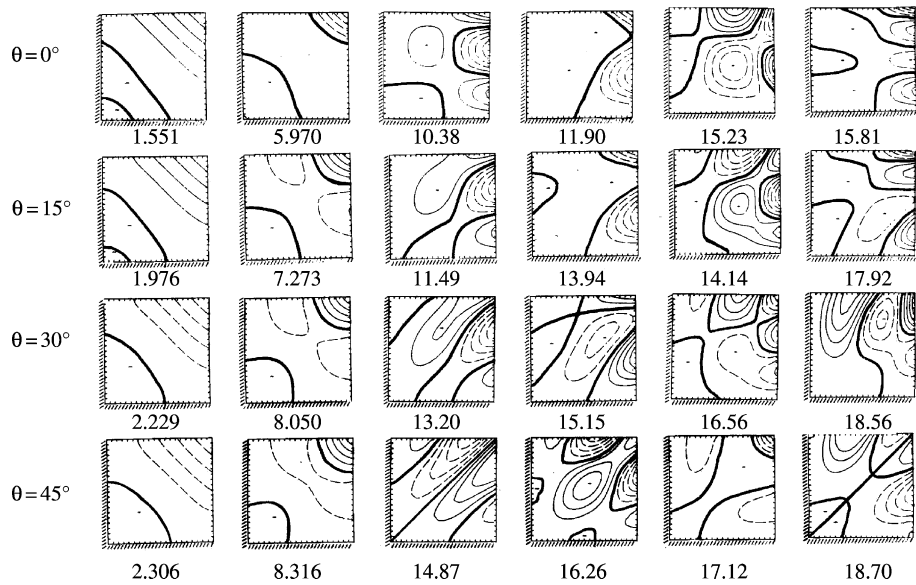


Figure 6.20. Mode shapes for doubly cantilever G/E hyperbolic paraboloidal shells; $a/b = 1$, $a/h = 100$, $a/R = 0.5$. (Qatu, 1992c; reproduced with permission).

studied here. In other words, free will mean completely free (i.e., F4), clamped will mean completely clamped (i.e., C1), and finally simply supported will mean shear diaphragm boundaries (S2). With this simplification, the number of possible combinations of boundary conditions is reduced. We will study the 21 possible combinations known for homogeneous plates.

For symmetrically laminated thin plates, the frequency parameter does not change when the thickness of the plate changes. This is not the case when the lamination sequence for the plate becomes asymmetrical or when we have shells (both symmetrically laminated and unsymmetrically laminated ones). In addition to thickness complexity, shells may have double curvatures and/or a twist. It is thus difficult to actually study all possible combinations or configurations. In real practice, the engineer will have to optimize the system at hand with its given constraints which usually involve given curvatures and/or boundary conditions.

Before we have a detailed study of various boundary conditions, we need to establish the accuracy of the Ritz method with elastic constraints used at $\alpha = a$ and $\beta = b$. Eq. (5.66) gives the energy functionals needed to treat such supports.

E-glass/Epoxy materials made of cross-ply $[0^\circ, 90^\circ, 0^\circ]$ laminates are chosen to perform a comparison among different analyses. Table 6.19 shows a comparison among frequency parameters $\Omega = \omega a^2 \sqrt{\rho/E_1 h^2}$ obtained by various methods and theories for the

Table 6.19. Frequency parameter $\Omega = \omega a^2 \sqrt{\rho/E_1 h^2}$ of laminated shallow shell with shear diaphragm boundaries. $a/b = 1$, $[0^\circ, 90^\circ, 0^\circ]$ E-glass/Epoxy, $a/h = 20$.

<i>Cylindrical shells ($a/R_\alpha = 0.5$)</i>						
m	n	Exact SDSST	Exact CSST	Error (%)	Ritz CSST	Error
1	1	5.588	5.633	0.81	5.685	0.92
1	2	11.445	11.634	1.65	11.676	0.36
2	1	12.444	12.826	3.07	12.932	0.83
2	2	17.343	18.001	3.79	18.201	1.11
1	3	19.899	20.580	3.42	20.732	0.74
3	1	25.325	26.962	6.46	27.009	0.17
2	3	25.651	27.000	5.26	27.437	1.62
3	2	29.502	31.610	7.15	32.599	3.13
1	4	31.502	33.361	5.90		
2	4	37.087	39.859	7.47		
3	3	36.875	39.966	8.38		
<i>Spherical shells ($a/R_\alpha = 0.5$, $a/R_\beta = 0.5$)</i>						
		Exact SDSST	Exact CSST		Ritz CSST	
1	1	8.350	8.383	0.40	8.420	0.44
1	2	12.343	12.512	1.37	12.561	0.39
2	1	14.336	14.680	2.40	14.751	0.48
2	2	18.420	19.044	3.39	19.126	0.43
1	3	20.179	20.838	3.27	21.173	1.61
2	3	26.195	27.512	5.03	27.512	0.00
3	1	26.373	27.961	6.02	27.961	0.00
3	2	30.268	32.334	6.83	32.913	1.79
1	4	31.579	33.417	5.82		
2	4	37.352	40.094	7.34		
3	3	37.383	40.435	8.16		

analysis of such shells. The maximum difference between CSST and SDSST is less than 1% for the fundamental frequency and less than 10% for the 10th frequency for shells with moderate thickness ($a/h = 20$). The Ritz method converged well for the lowest six frequencies. Table 6.20 shows similar results for thin shells with thickness ratio a/h of 100. For such shells, the difference between CSST and SDSST is less than 1% for the fundamental 10 frequencies. The Ritz method shows good convergence.

One important observation should be made here regarding the Ritz analysis. As can be seen from the table and actual convergence studies, convergence may be faster with the Ritz method for some higher modes than it is for the lower modes. This is interesting because it is against the conventional knowledge about the Ritz method. The reason is that

Table 6.20. Frequency parameter $\Omega = \omega a^2 \sqrt{\rho/E_1 h^2}$ of laminated shallow shell with shear diaphragm boundaries. $a/b = 1$, $[0^\circ, 90^\circ, 0^\circ]$ E-glass/Epoxy, $a/h = 100$.

m	n	Exact SDSST	Exact CSST	Error (%)	Ritz (108 DOF) CSST	Error (%)
<i>Cylindrical shells ($a/R_\alpha = 0.5$)</i>						
2	1	14.682	14.700	0.12	15.292	4.03
1	1	18.517	18.522	0.03	18.522	0.00
2	2	25.267	25.300	0.13	25.706	1.60
3	1	27.142	27.216	0.27	28.446	4.52
1	2	32.910	32.923	0.04	33.120	0.60
3	2	33.349	33.447	0.29	33.899	1.35
2	3	37.166	37.229	0.17	37.947	1.93
1	3	42.014	42.047	0.08	42.288	0.57
3	3	43.610	43.756	0.33		
4	1	46.717	46.938	0.47		
<i>Spherical shells ($a/R_\alpha = 0.5$, $a/R_\beta = 0.5$)</i>						
1	1	36.212	36.215	0.01	36.221	0.02
2	1	38.746	38.758	0.03	38.921	0.42
1	2	40.432	40.442	0.02	40.445	0.01
2	2	40.294	40.317	0.06	40.536	0.54
1	3	45.701	45.728	0.06	46.186	1.00
2	3	46.065	46.115	0.11	46.935	1.78
3	1	46.166	46.22	0.12	48.000	3.85
3	2	47.921	47.998	0.16	48.000	0.00
1	4	53.521	53.595	0.14		
3	3	53.749	53.872	0.23		

some higher modes actually have less half sine waves than lower modes. This is only a characteristic for shells and does not happen for plates.

It is also worth mentioning that for both case studies here, convergence for spherical shells is slightly faster than that of cylindrical shells.

Having established the accuracy of the Ritz method in analyzing thin shells using energy functionals described earlier with elastic constraints at some edges, we can treat other boundary conditions. Appendix B lists the fundamental six frequency parameter $\Omega = \omega a^2 \sqrt{\rho/E_1 h^2}$ for three layer $[\theta, -\theta, \theta]$ laminated cylindrical shells with the angle θ varying from 0 to 90° with 15° increments. A moderate thickness ratio (a/h) of 20 is used with moderate curvature a/R_α of 0.5. Notice that for these cylindrical shells with FFFF, SSFF, CCFF, SSSS, CCSS, and CCCC boundary condition, the results obtained for 60, 75, and 90° are not the same as those obtained for 30, 15, and 0°, respectively; as was

found for plates. Appendix C shows similar results for spherical shells. Note there that the mentioned symmetry is retained.

6.4. SHALLOW SHELLS ON TRAPEZOIDAL AND TRIANGULAR PLANFORM

Shallow shells are basically open shells which share similarities with plates. Like plates, shallow shells can virtually have any planform a flat plate may have. This includes rectangular, triangular, trapezoidal, circular, elliptical, and others. As was stated earlier for plates, it is difficult to construct a lamination using fiber-reinforced composites in coordinates other than rectangular. Subsequently, the treatment that follows will emphasize on shallow shells having rectangular orthotropy on nonrectangular planforms. The focus of this section will be shallow shells on triangular and trapezoidal planforms. Isotropic shallow shells were considered for completely free boundary conditions (Qatu 1995b) as well as cantilevered ones (Qatu 1996).

6.4.1 Completely free

A shallow shell with a triangular planform is shown in Figure 6.21 and one with trapezoidal planform is shown in Figure 6.22. The planform boundary is defined by the four straight lines of Eq. (5.69); $\alpha = a_1$, $\alpha = a$, $\beta = b\alpha/a$, and $\beta = -c\alpha/a$; where a_1 , a , b , and c are defined in Figures 6.21 and 6.22. A triangular shape is achieved if one chooses a_1 to be zero; other values of a_1 less than a will result in a trapezoidal planform.

6.4.1.1 Convergence studies. Spherical, cylindrical, and hyperbolic paraboloidal shell curvatures are considered. Moderate curvature is treated ($b/R_\beta = 0.5$). Symmetric, three-layer $[\theta, -\theta, \theta]$, graphite/epoxy laminates are considered.

An equal number of terms is taken in both directions (e.g., $I = J$) of the polynomials. This yields the least upper bound for most frequencies (Leissa and Jaber 1992). The $3 \times 6 \times 6$ (108-term) results are compared with those obtained from the more accurate $3 \times 7 \times 7$ (147-term) and $3 \times 8 \times 8$ (192-term) ones. The first zero frequencies corresponding to rigid body modes are deleted.

Table 6.21 shows a convergence study for the nondimensional frequencies of a laminated right (i.e., $c = 0$) triangular ($a_1/a = 0$) and trapezoidal ($a_1/a = 0.25$) shallow shells. Results for trapezoidal shallow shells with $a_1/a = 0.5$ are available in the literature (Qatu 1995c). A representative lamination angle of 30° is considered in the three-layer $[\theta, -\theta, \theta]$ laminates treated. The first (i.e., lowest) six frequencies are given for various solution sizes. Similar convergence study is available for symmetrical ($c = b$) shallow shells (Qatu 1995c).

Table 6.21. Convergence of the frequency parameters $\Omega = \omega a^2 \sqrt{\rho/E_1 h^2}$ for right triangular and trapezoidal composite shallow shells, $a/R_\beta = 0.5$, $a/h = 100$, $a/b = 1$, $[30^\circ, -30^\circ, 30^\circ]$ graphite/epoxy laminate.

a_1/a	R_β/R_α	No. of terms	Mode number					
			1	2	3	4	5	6
0	+1	108	3.140	5.795	6.477	10.57	12.83	16.23
		147	3.133	5.776	6.410	10.22	12.66	15.52
		192	3.131	5.772	6.404	10.13	12.58	15.24
	0	108	3.194	6.595	7.620	11.70	13.70	19.23
		147	3.186	6.526	7.571	11.23	13.55	18.10
		192	3.184	6.520	7.560	11.10	13.49	17.49
	-1	108	3.310	7.181	8.617	14.40	17.07	23.70
		147	3.301	7.137	8.409	13.95	16.07	21.25
		192	3.299	7.133	8.358	13.57	15.68	20.78
0.25	+1	108	2.850	5.492	7.565	8.308	11.99	16.81
		147	2.836	5.469	7.401	8.224	11.72	14.56
		192	2.835	5.460	7.318	8.198	11.57	14.28
	0	108	2.894	5.847	7.611	10.55	13.40	17.29
		147	2.880	5.809	7.463	10.37	12.84	15.18
		192	2.879	5.792	7.387	10.29	12.64	14.97
	-1	108	2.831	5.985	7.864	13.10	16.38	23.23
		147	2.814	5.930	7.717	12.42	14.51	20.37
		192	2.813	5.892	7.642	12.19	14.32	19.96

Convergence of the frequencies obtained for right shallow shells is observed to be good. The maximum difference between the 147-term solution and the 192-term solution is less than 5% for all the results. The convergence of the fundamental frequency is the best where the frequencies converged to the first three significant figures in almost all cases. No special effects of curvature or the (a_1/a) ratio is observed. Convergence of frequencies obtained for symmetrical shallow shells (i.e., $c = b$) is observed to be slightly worse (Qatu 1995c). Increasing the (a_1/a) ratio made the convergence slower for these shells. The convergence of the first two frequencies of these shells is particularly good. Unfortunately, increasing the number of terms further will introduce ill-conditioning in the stiffness matrix and may lead to worthless results in addition to increasing the computational time. Based on this analysis, the 192-term solution will be used in all subsequent analyses.

6.4.1.2 Effect of varying θ upon the frequencies. In this section, studies are made for symmetrically laminated shallow shells of various planforms having a three-layer angle-ply stacking sequence $[\theta, -\theta, \theta]$. Results are presented for the relatively strong orthotropic graphite/epoxy (G/E) composites.

Shallow shells with right triangular and trapezoidal planforms are first considered. For these shells $c = 0$. An aspect ratio (a/b) of 1 is used because it gives rise to the interesting configuration with a shell “opening” angle (at the left corner of the shell) of 45° . One triangular planform ($a_1/a = 0$) and one trapezoidal ($a_1/a = 0.25$) planform are studied. Results are presented for the triangular planform in Table 6.22 and for the trapezoidal planform in Table 6.23. In each of these tables, the lamination angle in a three-layer laminate $[\theta, -\theta, \theta]$ is varied from 0 to 90° by an increment of 15° . Spherical, cylindrical,

Table 6.22. Effect of varying the lamination angle θ on the frequency parameters of three-layer $[\theta, -\theta, \theta]$ graphite/epoxy right ($c = 0$) triangular shallow shells; $a/R_\beta = 0.5$, $a/h = 100$, $a/b = 1$.

R_β/R_α	Lamination angle (degrees)	Mode number, $\Omega = \omega a^2 \sqrt{\rho/E_1} h^2$					
		1	2	3	4	5	6
+1	0	2.319	3.966	7.085	7.760	9.236	12.52
	15	2.610	4.908	7.122	8.718	10.23	14.60
	30	3.131	5.772	6.404	10.13	12.58	15.24
	45	3.581	4.816	7.544	11.21	12.88	13.69
	60	3.131	5.772	6.405	10.13	12.58	15.24
	75	2.610	4.908	7.122	8.718	10.23	14.61
	90	2.319	3.967	7.085	7.760	9.235	12.52
0	0	1.812	3.669	5.021	7.345	9.666	10.07
	15	2.151	4.552	5.574	8.930	9.691	10.88
	30	2.835	5.460	7.318	8.198	11.57	14.28
	45	4.076	5.208	7.256	10.52	12.48	13.78
	60	3.932	5.478	6.637	10.69	13.03	14.41
	75	2.931	4.887	7.577	9.140	10.53	14.73
	90	2.343	4.051	7.659	8.059	9.427	13.06
-1	0	2.274	4.024	7.492	7.818	10.35	13.06
	15	3.107	4.687	7.204	9.956	11.22	15.23
	30	4.289	5.136	7.648	11.87	13.69	14.68
	45	4.698	5.647	8.298	11.86	15.08	16.44
	60	4.289	5.136	7.648	11.87	13.69	14.68
	75	3.108	4.686	7.200	9.961	11.22	15.19
	90	2.274	4.024	7.492	7.817	10.35	13.05

Table 6.23. Effect of varying the lamination angle θ on the frequency parameters of three-layer $[\theta, -\theta, \theta]$ graphite/epoxy right ($c = 0$) trapezoidal shells: $a_1/a = 0.25$, $a/R_\beta = 0.5$, $a/h = 100$, $a/b = 1$.

R_β/R_α	Lamination angle (degrees)	Mode number, $\Omega = \omega a^2 \sqrt{\rho/E_1 h^2}$					
		1	2	3	4	5	6
+1	0	2.528	4.361	7.182	8.725	11.71	14.24
	15	2.744	5.148	7.822	9.725	12.54	15.00
	30	3.184	6.520	7.560	11.10	13.49	17.49
	45	3.809	6.401	8.094	12.82	13.69	17.84
	60	4.261	6.020	8.000	12.97	15.33	15.56
	75	3.567	6.382	7.738	10.36	13.74	17.39
	90	2.973	5.704	7.785	8.901	12.81	13.65
0	0	1.923	4.117	5.040	8.174	9.957	13.18
	15	2.233	4.838	5.634	9.489	10.87	13.36
	30	2.879	5.792	7.387	10.29	12.64	14.97
	45	4.051	6.149	9.517	10.52	13.87	17.67
	60	4.897	6.196	8.346	13.30	14.33	16.73
	75	3.855	6.875	7.862	10.89	14.25	17.15
	90	2.963	6.128	7.957	9.555	13.11	13.78
-1	0	2.491	4.431	7.809	9.074	12.52	14.52
	15	3.313	4.779	8.285	11.17	12.88	16.28
	30	4.606	5.186	9.499	13.56	14.79	15.38
	45	5.149	6.149	10.77	14.05	15.71	17.12
	60	5.174	6.017	10.63	13.19	14.74	19.33
	75	4.061	6.026	8.874	11.60	14.96	16.48
	90	2.895	5.986	7.664	10.83	12.34	15.55

and hyperbolic paraboloidal curvatures are considered. A thickness ratio (a/h) of 100 and a curvature ratio (b/R_β) of 0.5 are considered.

The 45° lamination angle resulted in the maximum first, third, fourth, and fifth frequencies for spherical right triangular shells with an aspect ratio of 1 (Table 6.22). The maximum second and sixth frequencies are obtained at angles 30 and 60° . For these shells, results obtained for $\theta = 0, 15$, and 30° are the same as those obtained for $\theta = 90, 75$, and 60° , respectively due to symmetry. This symmetry is lost for cylindrical shells where maximum frequencies are obtained at $\theta > 45^\circ$. Almost all maximum frequencies are obtained for $\theta = 45^\circ$ for hyperbolic paraboloidal shells. For these shells with aspect ratio of 1.732 (Qatu 1995c), the symmetry is lost, and maximum frequencies are obtained at angles of lamination between 15 and 45° for all curvatures. For right trapezoidal shells with $a_1/a = 0.25$, the maximum frequencies are obtained when $45^\circ < \theta < 60^\circ$ for almost all results for $a/b = 1$ (Table 6.23).

Table 6.24 presents the natural frequencies of shallow shells having symmetrical triangular planforms ($c = b$). Results for symmetrical shallow shells with trapezoidal planform are available (Qatu 1995c). The value of $a/b = 1.732$ is considered, which corresponds to opening angles of 60° at the origin. This ratio presents the interesting equilateral planform for triangular shallow shells. Three-layer laminates with various angles of lamination θ are considered. Frequencies for the three types of curvature are included.

Interestingly enough, for almost all the frequencies obtained for symmetrical shells (including those obtained for trapezoidal shapes which are not reported here), the maximum frequencies occur at a lamination angle equal to or more than 45° . In many cases, no smooth trends in the frequencies are obtained as the lamination angle is increased. Taking the fifth frequency of spherical shells in Table 6.24 as an example, a frequency parameter of 11.08 is obtained at $\theta = 0^\circ$. Increasing the lamination angle to 30°

Table 6.24. Effect of varying the lamination angle θ on the frequency parameters of three-layer $[\theta, -\theta, \theta]$ graphite/epoxy symmetrical ($c = b$) triangular shells: $a/R = 0.5$, $a/h = 100$, $a/b = 1.732$.

R_β/R_α	Lamination angle (degrees)	Mode number $\Omega = \omega a^2 \sqrt{\rho/E_1} h^2$					
		1	2	3	4	5	6
+1	0	3.047	3.486	6.548	6.782	11.08	11.10
	15	3.215	3.783	6.512	7.488	9.905	12.23
	30	3.224	4.375	6.673	8.391	9.020	14.49
	45	3.089	4.442	6.638	8.636	9.966	13.65
	60	3.203	4.021	6.627	7.921	11.53	12.38
	75	3.210	3.716	6.547	7.613	9.438	12.29
	90	3.067	3.613	6.689	7.675	7.820	12.74
0	0	2.109	2.907	5.341	6.110	9.227	9.971
	15	2.173	3.453	5.661	6.549	9.240	10.71
	30	2.376	4.658	6.382	7.810	8.923	12.07
	45	2.675	5.755	6.865	7.181	10.86	12.59
	60	2.958	5.011	6.725	7.873	11.76	12.49
	75	3.095	4.254	6.394	8.537	10.09	11.70
	90	3.100	3.922	6.541	7.769	9.368	12.54
- 1	0	3.039	3.352	6.727	8.910	11.61	12.55
	15	2.726	4.373	6.617	9.758	11.53	12.91
	30	2.655	5.671	6.794	9.629	13.20	14.75
	45	2.662	5.818	7.154	9.430	13.48	15.61
	60	2.702	5.252	6.525	9.413	12.01	13.88
	75	2.709	4.352	6.123	8.875	10.84	12.32
	90	3.091	3.681	6.406	7.650	10.53	13.42

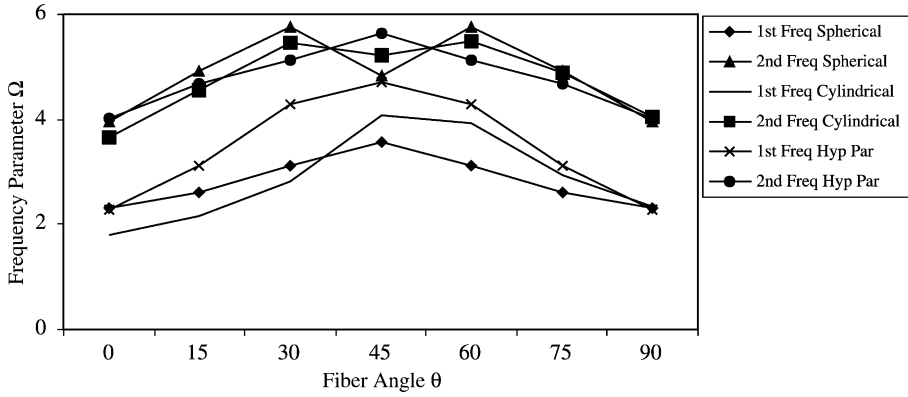


Figure 6.23. Effect of varying the lamination angle θ on the frequency parameters of three-layer $[\theta, -\theta, \theta]$ graphite/epoxy right ($c = 0$) triangular shallow shells: $a/R_\beta = 0.5$, $a/h = 100$, $a/b = 1$.

decreases the frequency to 9.02. Increasing the angle further to 60° increases the frequency to its maximum at 11.53. Further increase in the lamination angle decreases the frequency to a minimum (Figure 6.23).

6.4.2 Cantilevered

A cantilevered shallow shell with a right triangular or trapezoidal planform is shown in Figure 6.24. The planform boundary is defined by the four straight lines $\alpha = a_1$, $\alpha = a$, $\beta = b\alpha/a$, and $\beta = 0$ as in Eq. (5.71). The parameters a_1 , a , and b are defined in Figure 6.24.

6.4.2.1 Convergence studies. Spherical, cylindrical, and hyperbolic paraboloidal shells with moderate depth ($b/R_\beta = 0.5$) are considered. The laminates considered here are symmetric, graphite/epoxy, of three-layers, with stacking sequence $[\theta, -\theta, \theta]$. An equal number of terms is taken in both directions ($I = J$) of the polynomials. The frequencies obtained by using $3 \times 6 \times 6$ (108 term) are compared with those obtained from the more accurate $3 \times 7 \times 7$ (147-term) and $3 \times 8 \times 8$ (192-term) solutions. Table 6.25 shows a convergence study for the nondimensional frequencies $\Omega = \omega a^2 \sqrt{\rho/E_1 h^2}$ of a cantilevered composite triangular ($a_1/a = 0$) and trapezoidal ($a_1/a = 0.25$) shallow shells. The lowest six nondimensional frequency parameters are given for various solution sizes.

Convergence is observed to be very good in all the results. The difference between the 147-term solution and the more accurate 192-term solution did not exceed 1% in almost all the results.

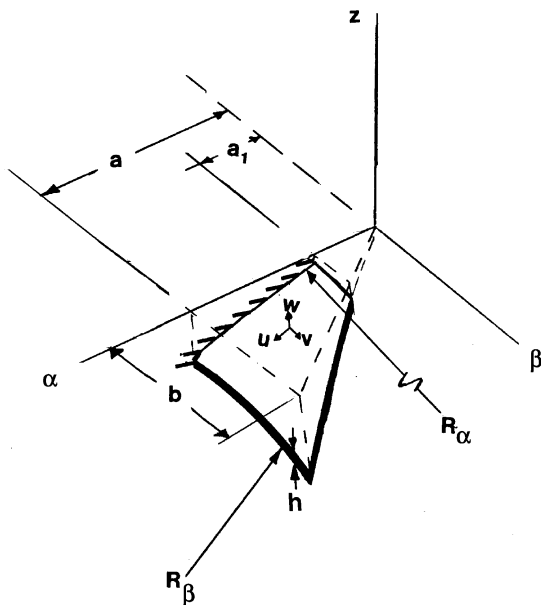


Figure 6.24. A cantilevered shallow shell on right trapezoidal planform (Qatu 1995d).

The fundamental frequencies converged to the first three significant figures in most of the cases. No significant effect of the curvature or the planform shape is observed on the convergence characteristics. Based on this study the 192-term solution will be used in all subsequent results.

6.4.2.2 Effect of varying θ upon the frequencies. Studies are made for symmetrically laminated triangular and trapezoidal shallow shells of various planforms having a three-layer, angle-ply stacking sequence $[\theta, -\theta, \theta]$. All possible shapes of right triangular and trapezoidal planforms may be achieved by varying the parameters a_1/a , and a/b . Shallow shells with right triangular and trapezoidal planforms and an a/b ratio of 1 are considered. Other a/b ratios were considered in the literature (Qatu 1995d). Results for a triangular planform ($a_1/a = 0$) and a trapezoidal planform ($a_1/a = 0.25$) are presented in Tables 6.26 and 6.27. A thickness ratio (a/h) of 100 and a curvature ratio (b/R_β) of 0.5 representing thin shallow shells are considered.

In all results the maximum frequencies occur at a lamination angle other than 0° (Figure 6.25). In fact, the maximum frequency is between double and triple of that found for a lamination angle of 0° . Maximum frequencies are observed at lamination angles of 60 and 75° in all the results except the second frequency for spherical shells (where it is at $\theta = 45^\circ$) and the second and fifth frequencies of cylindrical shells (where the maximum

Table 6.25. Convergence of the frequency parameters for triangular and trapezoidal cantilevered shallow shells, $a/R_\beta = 0.5$, $a/h = 100$, $a/b = 1$, $[30, -30, 30]$ graphite/epoxy laminate (Qatu 1995d).

a_1/a	R_β/R_α	No. of terms	Mode number, $\Omega = \omega a^2 \sqrt{\rho/E_1 h^2}$					
			1	2	3	4	5	6
0	+1	108	1.382	4.741	5.937	10.78	14.12	19.07
		147	1.380	4.723	5.920	10.64	13.92	18.06
		192	1.379	4.717	5.914	10.63	13.87	17.85
	0	108	0.7351	3.101	4.290	7.615	11.16	14.80
		147	0.7349	3.098	4.285	7.602	11.06	14.23
		192	0.7347	3.097	4.283	7.596	11.05	14.20
	-1	108	1.774	5.531	7.582	11.85	15.90	17.98
		147	1.768	5.516	7.574	11.81	15.71	17.80
		192	1.767	5.509	7.567	11.79	15.69	17.74
	+1	108	1.272	4.636	5.005	9.773	11.72	17.40
		147	1.269	4.617	4.990	9.688	11.63	16.58
		192	1.264	4.609	4.979	9.671	11.60	16.39
0.25	0	108	0.6728	2.977	3.904	7.372	10.66	14.42
		147	0.6721	2.974	3.897	7.359	10.59	13.85
		192	0.6721	2.974	3.888	7.353	10.58	13.81
	-1	108	1.680	4.349	5.488	11.68	13.19	17.24
		147	1.674	4.320	5.472	11.63	13.11	17.09
		192	1.672	4.316	5.463	11.62	13.07	17.02

frequency is at $\theta = 90^\circ$). Similar observation is made for triangular shells with a 0.577 aspect ratio (Qatu 1995d). For trapezoidal shells with $a_1/a = 0.25$, the maximum frequencies occur at or around $\theta = 75^\circ$. Similar observation was made when the ratio $a_1/a = 0.5$ (Qatu 1995d).

6.5. SHALLOW SHELLS ON CIRCULAR PLANFORMS (SPHERICAL CAPS)

As was stated earlier, shallow shells are like plates due to the fact that they can have practically any planform. Among the planforms treated for shallow shells is the circular planform. Shallow shells on a circular planform (Figure 6.26) can still have the double curvature and twist. The only problems, however, which are treated in the literature for such shells are when they are spherical in curvature. This will give the interesting problem of a spherical cap, which has useful applications in many industries.

Table 6.26. Effect of varying the lamination angle θ on the frequency parameters of three-layer $[\theta, -\theta, \theta]$ graphite/epoxy triangular shallow shells: $a/R_\beta = 0.5$, $a/h = 100$, $a/b = 1$ (Qatu 1995d).

R_β/R_α	Lamination angle	Mode number, $\Omega = \omega a^2 \sqrt{\rho/E_1 h^2}$					
		1	2	3	4	5	6
+1	0	1.046	3.455	3.920	7.538	9.252	12.84
	15	1.117	3.893	4.906	8.520	11.58	14.42
	30	1.379	4.717	5.914	10.63	13.87	17.85
	45	1.802	5.228	7.088	13.06	15.10	22.52
	60	2.212	5.162	8.060	13.78	16.78	23.50
	75	2.231	4.801	8.555	12.13	19.77	19.96
	90	1.916	4.518	8.067	10.77	15.93	21.34
0	0	0.4812	2.035	3.009	5.041	7.567	9.618
	15	0.5444	2.335	3.548	5.717	9.115	10.65
	30	0.7347	3.097	4.283	7.596	11.05	14.20
	45	1.108	4.330	4.989	11.02	12.74	20.40
	60	1.537	4.785	6.487	13.02	15.52	23.09
	75	1.712	4.667	7.797	11.91	19.28	19.87
	90	1.514	4.361	7.743	10.81	15.79	21.06
-1	0	0.9900	3.354	5.185	7.459	10.45	12.96
	15	1.301	4.115	5.981	9.002	12.63	15.36
	30	1.767	5.509	7.567	11.79	15.69	17.74
	45	2.242	7.396	9.127	14.79	17.30	19.73
	60	2.443	8.309	9.267	15.91	18.42	22.04
	75	2.220	8.045	8.903	14.62	19.86	21.54
	90	1.699	6.588	8.731	13.21	16.54	21.64

Such shells have received some attention when made of isotropic materials and less attention when made of orthotropic materials. A limited number of references treated these shells when made of laminated composite materials. As was stated earlier for plates, the difficulty of manufacturing these structures from fiber-reinforced materials, which require nonstraight fibers may be the cause of such lack of attention. Layers made of isotropic materials are easy to manufacture and the same is true for layers made of orthotropic materials.

The treatment of shallow shells made of layers with rectangular orthotropy on circular planforms is similar to the treatment made for similar circular plates. Shallow shells with circular orthotropy on circular planforms will be treated here.

Similar to plates, the fundamental formulation of the theory of shallow shells must be revisited when they are on circular planforms having circular orthotropy. For such shells, the fundamental equations need to be re-written in polar coordinates. This can be treated with proper selection of Lamé parameters. Consider the plate of Figure 5.16 and the polar

Table 6.27. Effect of varying the lamination angle θ on the frequency parameters of three-layer $[\theta, -\theta, \theta]$ graphite/epoxy trapezoidal shallow shells: $a_1/a = 0.25$, $a/R_\beta = 0.5$, $a/h = 100$, $a/b = 1$ (Qatu 1995d).

R_β/R_α	Lamination angle	Mode number, $\Omega = \omega a^2 \sqrt{\rho/E_1 h^2}$					
		1	2	3	4	5	6
+1	0	1.013	3.204	3.390	7.266	8.030	12.31
	15	1.046	3.777	3.953	8.050	9.821	13.59
	30	1.264	4.609	4.979	9.671	11.60	16.39
	45	1.700	5.098	6.410	12.11	12.99	20.65
	60	2.156	4.986	7.843	12.73	16.34	20.87
	75	2.203	4.692	8.509	11.65	18.18	19.93
	90	1.904	4.438	8.021	10.56	15.24	20.83
0	0	0.4698	1.948	2.789	5.005	7.380	9.683
	15	0.6718	2.241	3.171	5.640	8.795	10.64
	30	0.6724	2.974	3.889	7.353	10.58	13.81
	45	0.9934	4.270	4.473	10.87	11.77	19.99
	60	1.443	4.311	6.387	12.35	15.41	21.70
	75	1.700	4.315	7.791	11.44	18.51	19.55
	90	1.514	4.279	7.665	10.70	15.31	20.64
-1	0	0.9833	3.324	3.544	7.424	8.859	12.92
	15	1.271	3.607	4.065	8.934	10.47	15.32
	30	1.672	4.316	5.463	11.62	13.07	17.02
	45	2.112	5.078	7.493	13.85	15.87	23.72
	60	2.377	5.681	8.764	14.11	18.25	21.12
	75	2.210	6.298	8.830	13.10	19.09	21.11
	90	1.698	6.277	8.119	12.70	15.80	20.97

coordinates shown there. The following parameters can be applied to the equations derived earlier for shallow shells to obtain these equations in polar coordinates:

$$\alpha = r, \quad \beta = \theta \quad A = 1, \quad B = r \quad (6.28)$$

6.5.1 Thin shallow shells on circular planforms

For very thin shallow shells, where Kirchhoff's hypothesis applies, the midsurface strains, curvature, and twist changes are

$$\begin{aligned} \varepsilon_{0r} &= \frac{\partial u_0}{\partial r} + \frac{w_0}{R} \\ \varepsilon_{0\theta} &= \frac{1}{r} \frac{\partial v_0}{\partial \theta} + \frac{u_0}{r} + \frac{w_0}{R} \\ \gamma_{0r\theta} &= \frac{\partial v_0}{\partial r} + \frac{1}{r} \frac{\partial u_0}{\partial \theta} - \frac{v_0}{r} \end{aligned}$$

6.3.4.4 Mode shapes. In the subsequent analysis, the aspect ratio (a/b) is taken as 1, and the thickness ratio (a/h) is taken as 100 representing a typical thin shell. The curvature ratio (a/R) is taken as 0.5 for moderately shallow shells. Three-layer laminates ($\theta, -\theta, \theta$) are considered. The corresponding frequency parameter is given below the mode shape. Figures 6.4–6.6 give the first six mode shapes with various lamination angles for spherical, cylindrical, and hyperbolic paraboloidal curvatures, respectively. Mode shapes are shown for $\theta = 0, 15, 30$, and 45° only for spherical and hyperbolic paraboloidal shells. For these shells, mode shapes for $\theta = 60, 75$, and 90° are similar to those given for the $\theta = 30, 15$, and 0° , respectively, and can be obtained easily by changing the coordinates.

For the completely free boundary condition, symmetry exists about the inplane axes for the isotropic and orthotropic (e.g., cross-ply) shells. This symmetry is lost for shells with angle-ply lamination. For the special case of diagonally orthotropic angle-ply laminates which are made of 45° angle layers, symmetry exists about the diagonals for spherical and hyperbolic paraboloidal shells only. The gradual change in contour lines with increasing θ is evident in the figures.

As the lamination angle increases, the order of the mode shapes may vary. For example, the second mode shape for cylindrical shells is becoming the third one when the lamination angle exceeds 45° , and its shape remains the same. The third mode shape changes gradually as θ increases to end up with a mode shape for $\theta = 90^\circ$ similar to the

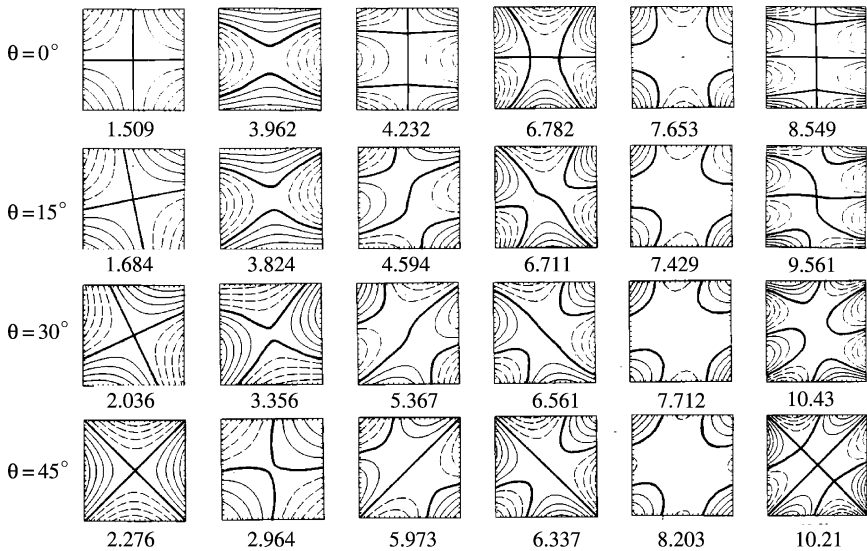


Figure 6.4. Mode shapes and frequency parameters for completely free $[\theta, -\theta, \theta]$, G/E spherical shells, $a/b = 1$, $a/h = 100$, $a/R = 0.5$ (Qatu 1992c; reproduced with permission).

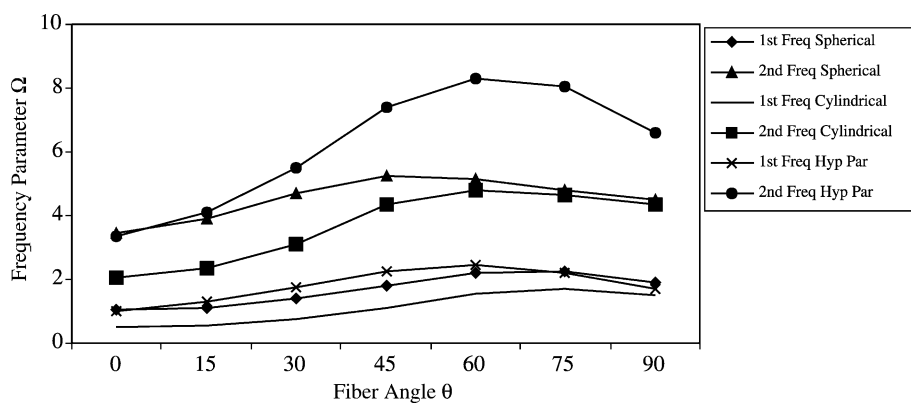


Figure 6.25. Effect of varying the lamination angle θ on the frequency parameters of three-layer $[\theta, -\theta, \theta]$ graphite/epoxy triangular shallow shells: $a/R_\beta = 0.5$, $a/h = 100$, $a/b = 1$.

$$\begin{aligned}\kappa_r &= \frac{\partial \psi_r}{\partial r}, & \kappa_\theta &= \frac{1}{r} \frac{\partial \psi_\theta}{\partial \theta} + \frac{\psi_r}{r} \\ \tau &= \frac{\partial \psi_\theta}{\partial r} + \frac{1}{r} \frac{\partial \psi_r}{\partial \theta} - \frac{\psi_\theta}{r}\end{aligned}\quad (6.29)$$

where

$$\psi_r = \frac{\partial w_0}{\partial r}, \quad \psi_\theta = -\frac{1}{r} \frac{\partial w_0}{\partial \theta} \quad (6.30)$$

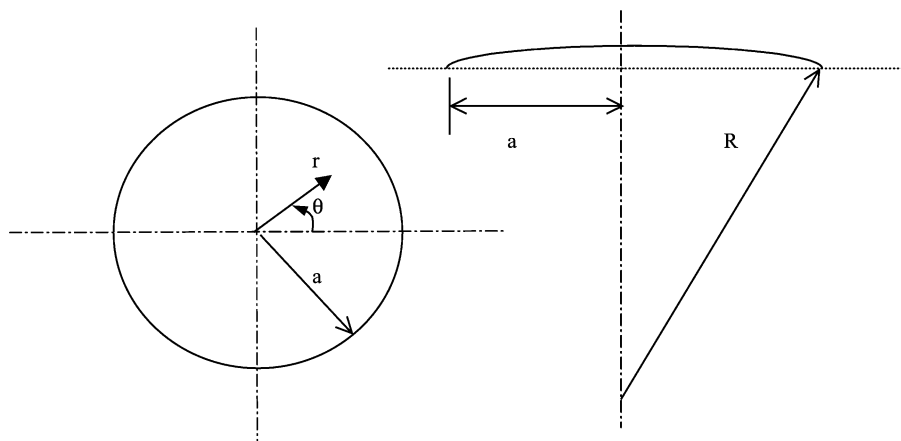


Figure 6.26. A spherical cap.

For laminated shallow shells on a circular planform with each layer having circular orthotropy, a transformation matrix can be built from the orthotropic directions 1 and 2 (Figure 1.3) to the polar (r, θ) coordinates, in a manner similar to that of plates. Eq. (5.76) will then be applied for composite shallow shells.

Substitute Eq. (6.28) into Eq. (6.6) yields the following equations of motion for thin shallow shell on circular planform

$$\begin{aligned} \frac{\partial}{\partial r}(rN_r) + \frac{\partial}{\partial \theta}(N_{\theta r}) - N_\theta + rq_r &= r(I_1 \ddot{u}_0) \\ \frac{\partial}{\partial \theta}(N_\theta) + \frac{\partial}{\partial r}(rN_{r\theta}) + N_{\theta r} + rq_\theta &= r(I_1 \ddot{v}_0) \\ -r\left(\frac{N_r}{R} + \frac{N_\theta}{R}\right) + \frac{\partial}{\partial r}(rQ_r) + \frac{\partial}{\partial \theta}(Q_\theta) + rq_n &= r(I_1 \ddot{w}_0) \end{aligned} \quad (6.31)$$

where

$$\begin{aligned} rQ_r &= \frac{\partial}{\partial r}(rM_r) + \frac{\partial}{\partial \theta}(M_{\theta r}) - M_\theta \\ rQ_\theta &= \frac{\partial}{\partial \theta}(M_\theta) + \frac{\partial}{\partial r}(rM_{r\theta}) + M_{\theta r} \end{aligned}$$

Boundary conditions can be derived in a similar fashion.

$$\begin{aligned} N_{0r} - N_r &= 0 \quad \text{or} \quad u_0 = 0 \\ \left(N_{0r\theta} - \frac{N_{0r\theta}}{R}\right) - \left(N_{r\theta} - \frac{N_{r\theta}}{R}\right) &= 0 \quad \text{or} \quad v_0 = 0 \\ \left(Q_{0r} - \frac{1}{r} \frac{\partial M_{0r\theta}}{\partial \theta}\right) - \left(Q_{\alpha} - \frac{1}{r} \frac{\partial M_{r\theta}}{\partial \theta}\right) &= 0 \quad \text{or} \quad w_0 = 0 \\ M_{0r} - M_r &= 0 \quad \text{or} \quad \psi_r = 0 \\ M_{0r\theta} w_{\theta_1}^{\theta_2} &= 0 \end{aligned} \quad (6.32)$$

6.5.2 Thick shallow shells on circular planforms

For thick shallow spherical caps, where shear deformation and rotary inertia are considered, the midsurface strains can be derived by substituting Eq. (6.28) into Eq. (6.17)

$$\begin{aligned} \varepsilon_{0r} &= \frac{\partial u_0}{\partial r} + \frac{w_0}{R} \\ \varepsilon_{0\theta} &= \frac{1}{r} \frac{\partial v_0}{\partial \theta} + \frac{u_0}{r} + \frac{w_0}{R} \\ \varepsilon_{0r\theta} &= \frac{\partial v_0}{\partial r} \\ \varepsilon_{0\theta r} &= \frac{1}{r} \frac{\partial u_0}{\partial \theta} - \frac{v_0}{r} \end{aligned}$$

$$\begin{aligned}\gamma_{0rz} &= \frac{\partial w_0}{\partial r} + \psi_r \\ \gamma_{0\theta z} &= \frac{1}{r} \frac{\partial w_0}{\partial \theta} + \psi_\theta\end{aligned}\quad (6.33)$$

and the curvature and twist changes are:

$$\begin{aligned}\kappa_r &= \frac{\partial \psi_r}{\partial r}, \quad \kappa_\theta = \frac{1}{r} \frac{\partial \psi_\theta}{\partial \theta} + \frac{\psi_r}{r} \\ \kappa_{r\theta} &= \frac{\partial \psi_\theta}{\partial r}, \quad \kappa_{\theta r} = \frac{1}{r} \frac{\partial \psi_r}{\partial \theta} - \frac{\psi_\theta}{r}\end{aligned}\quad (6.34)$$

The force and moment resultants are obtained by integrating the stresses over the plate thickness.

The equations of motion for thick spherical caps in polar coordinates are obtained by substituting Eq. (6.28) into Eq. (6.19):

$$\begin{aligned}\frac{\partial}{\partial r}(rN_r) + \frac{\partial}{\partial \theta}(N_{\theta r}) - N_\theta + rq_r &= r(\bar{I}_1 \ddot{u}_0^2 + \bar{I}_2 \ddot{\psi}_r^2) \\ \frac{\partial}{\partial \theta}(N_\theta) + \frac{\partial}{\partial r}(rN_{r\theta}) + N_{\theta r} + rq_\theta &= r(\bar{I}_1 \ddot{v}_0^2 + \bar{I}_2 \ddot{\psi}_\theta^2) \\ -r\left(\frac{N_r}{R} + \frac{N_\theta}{R}\right) + \frac{\partial}{\partial r}(rQ_r) + \frac{\partial}{\partial \theta}(Q_\theta) + rq_n &= r(\bar{I}_1 \ddot{w}_0^2) \\ \frac{\partial}{\partial r}(rM_r) + \frac{\partial}{\partial \theta}(M_{\theta r}) - M_\theta - rQ_r + rm_r &= r(\bar{I}_2 \ddot{u}_0^2 + \bar{I}_3 \ddot{\psi}_r^2) \\ \frac{\partial}{\partial \theta}(M_\theta) + \frac{\partial}{\partial r}(rM_{r\theta}) + M_{\theta r} - rQ_\theta + rm_\theta &= r(\bar{I}_2 \ddot{v}_0^2 + \bar{I}_3 \ddot{\psi}_\theta^2)\end{aligned}\quad (6.35)$$

where q_r , q_θ , and q_n represent external forces (per unit area) applied either to the surface or as body forces.

On each boundary, one must specify five conditions. The boundary terms for the boundaries with $r = \text{constant}$ are

$$\begin{aligned}N_{0r} - N_r &= 0 & \text{or} & & u_0 &= 0 \\ N_{0r\theta} - N_{r\theta} &= 0 & \text{or} & & v_0 &= 0 \\ Q_{0r} - Q_r &= 0 & \text{or} & & w_0 &= 0 \\ M_{0r} - M_r &= 0 & \text{or} & & \psi_r &= 0 \\ M_{0r\theta} - M_{r\theta} &= 0 & \text{or} & & \psi_\theta &= 0\end{aligned}\quad (6.36)$$

6.5.3 Free vibration of spherical caps

Table 6.28 shows results obtained for a spherical cap with a/R (where a is the radius of the planform, as shown in Figure 6.26 and R the radius of the shell) of 0.19802. This constitutes a “rise” in the spherical cap at the center of 0.1, the radius of the planform.

Table 6.28. Frequency parameter for $\Omega = \omega R \sqrt{\rho/E_2}$ for clamped spherical cap ($a/R = 0.19802$).

a/h	$[0^\circ]$	$[90^\circ]$	$[0^\circ, 90^\circ]$	$[0^\circ, 90^\circ, 0^\circ]$	$[90^\circ, 0^\circ, 90^\circ]$
100	2.127	1.453	2.070	2.374	1.986
50	2.907	1.603	2.464	2.855	2.239
20	3.721	2.040	3.522	3.908	3.906
14.2	4.142	2.369	4.307	4.314	3.528
10	4.815	2.886	5.107	4.955	3.954

Graphite/epoxy: $E_1 = 13.8 \times 10^6 \text{ N/cm}^2$, $E_2 = 1.06 \times 10^6 \text{ N/cm}^2$, $G_{12} = 0.6 \times 10^6 \text{ N/cm}^2$, $G_{13} = G_{23} = 0.39 \times 10^6 \text{ N/cm}^2$, $\nu_{23} = \nu_{13} = 0.34$, $\rho = 1.5 \text{ kg/m}^3$. Circumferential wave number = 1 (Gautham and Ganesan 1997).

The results are obtained by Gautham and Ganesan (1997) who used finite element methods in their analysis. Graphite/epoxy materials are used with material parameters different to those used earlier. The material properties are listed in the table. Various thickness ratios are used with various lamination sequences.

Compare the results obtained for single layer shells ($[0^\circ]$ and $[90^\circ]$ laminates). The first observation made is that the frequencies are higher when the fibers are oriented in the radial direction than those obtained when the fibers are oriented in the circular direction. This is the case for all thickness ratios studied. Interestingly, for the $[0^\circ, 90^\circ]$ laminate, it gave lower frequencies than those obtained for the $[0^\circ]$ when the shell is thin but slightly higher frequencies for thicker shells. In fact, the $[0^\circ, 90^\circ]$ laminate gave the highest frequencies when compared with all other lamination sequences studied for shells with the thickness ratio a/h of 0.1.

It is also interesting to notice that the $[0^\circ, 90^\circ, 0^\circ]$ lamination sequence gave the highest frequencies when the shell is very thin ($a/h = 100$), and the single layer $[0^\circ]$ gave the highest frequencies for the thickness ratio of 50. As expected, the $[0^\circ, 90^\circ, 0^\circ]$ lamination sequence gave higher frequencies than the $[90^\circ, 0^\circ, 90^\circ]$ lamination sequence.

Chapter 7

Cylindrical Shells

Shells may have different geometrical shapes based mainly on their curvature characteristics. For most shell geometries, the fundamental equations have to be derived at a very basic level. The type of shell curvature makes it necessary to derive equations, which are driven by

1. the choice of the coordinate system (Cartesian, polar, spherical or curvilinear);
2. the characteristics of the Lamé parameters (constant, or function of the coordinates);
3. curvature (constant or varying curvature).

Equations for some shell geometries can be obtained as special cases of a more general shell geometry. For example, equations for cylindrical, spherical, conical and barrel shells can be derived from the equations of the more general case of shells of revolution. Equations for cylindrical, barrel, twisted and shallow shells as well as those for plates can be derived from the general equations of doubly curved open shells.

Cylindrical shells are a special case of the general case of shells of revolution. In shells of revolution, the surface of the shell is constructed by starting with a line, straight or curved, and revolving this line around a certain axis. The surface that the line “sweeps” as a result of this rotation defined the shell’s middle surface. In most shells of revolutions treated in the literature, each point on the line maintains a constant distance from the axis of revolution. This will produce shells of revolutions with circular cross-section. If each point generates a shape other than circular, like elliptic, the shell is referred to by the shape of the cross-section or simply as a shell of revolution with non-circular cross-section. Cylindrical shells are formed by revolving a straight line around an axis parallel to the line itself.

Cylindrical shells have received the most attention in the literature when compared with other shells. The literature on the vibration of these shells is vast. The free vibrations of thin isotropic cylindrical shells was the subject of more than 200 papers published by 1970 (Leissa 1973a). Orthotropic single-layer shells and stiffened ones were the subject of more than 20 papers before 1970. A very limited number of these seemed to have dealt with laminated composite cylindrical shells. Much more information on cylindrical shell vibration, including laminated composite ones, is available now in many journal publications, reports, or other books since 1973. Although some of the recent publications still treat thin isotropic cylindrical shells (Lim *et al.* 1998a,b) and thick ones (Lim and Liew 1995a,b), special interest has been given to shells made of laminated composite materials (Qatu 2002a,b). The theory of such shells was developed before 1964 (Ambartsumian 1964). This attention is due to the promising potential and diverse

applications of laminated composites in the aerospace, marine, automotive and other industries. The ease of manufacturing and widespread usage of cylindrical shells are other reasons for such attention. Other shell geometries were also investigated.

Earlier studies on vibrations of composite shells dealt almost exclusively with stiffened or orthotropic shells. Weingarten (1964) considered a shell made of three isotropic layers and studied its free vibrations using Donnell's shell theory (a shallow shell theory). The first analytical vibration analysis of laminated cylindrical shells is probably that of Dong (1968). Recent studies dealt with generally laminated shells (Qatu 2002a).

A considerable amount of information on the free and forced vibration of cylindrical shells can be found in the books of Leissa (1973a,b) and Soedel (1993). The first of these books studied various shell theories and compared their results with those obtained using the three-dimensional (3D) theory of elasticity. A general conclusion made there was that all thin deep shell theories yield similar results in vibration analysis. The assumptions that were made there for various shell theories are used here for laminated deep thin shells. Certain results obtained there using the 3D theory of elasticity will also be used here for comparison. The book by Soedel (1993) emphasized more on forced vibrations, shell's interaction with fluids and other problems.

A consistent set of equations for generally laminated, deep, circular cylindrical shells will be derived. A more general approach to the analysis of shells of revolution can be found in Suzuki *et al.* (1995a,b). Open as well as closed cylindrical shells will be included in the present analysis.

Consider a shell of revolution, for which the middle surface is shown in Figure 7.1. The fundamental form can be written as

$$(ds)^2 = (d\alpha)^2 + \sin^2 \phi (d\beta)^2 \quad \text{where } d\alpha = R_\alpha d\phi, d\beta = R_\beta d\theta \quad (7.1)$$

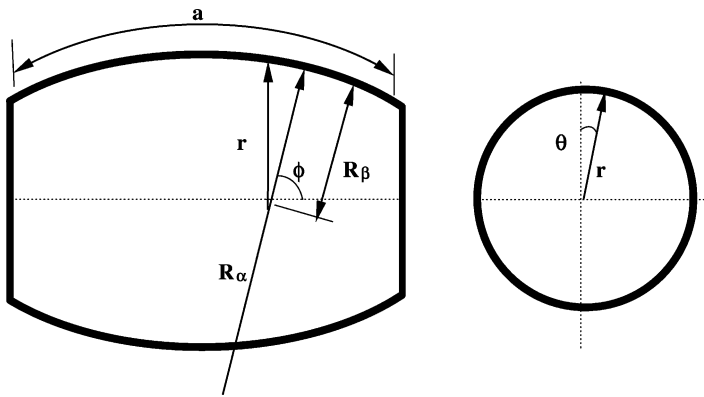


Figure 7.1. Fundamental parameters in shells of revolutions (Qatu 1999b).

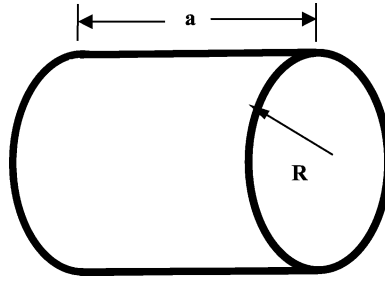


Figure 7.2. Closed cylindrical shell.

We will maintain the α and β coordinates in the subsequent analysis for convenience. The Lamé parameters are

$$A = 1, \quad B = \sin \phi \quad (7.2)$$

Consider further a cylindrical shell with constant radius of curvature R_β , and infinite radii of curvature R_α and $R_{\alpha\beta}$ (Figure 7.2). This leads to constant Lamé parameters. The fundamental form for cylindrical shells become

$$(ds)^2 = (d\alpha)^2 + (d\beta)^2 \quad \text{where } d\beta = R_\beta d\theta \quad (7.3)$$

and the Lamé parameters are

$$A = 1, \quad B = 1 \quad (7.4)$$

It should be mentioned that the midsurface coordinates (α, β) are maintained in the above equations and subsequent derivation. This results in unit Lamé parameters. In most derivations available in the literature, the axes (x, θ) are chosen. For such choice of coordinates, one can either replace β by $(R_\beta \theta)$ and α by x in the following equations and obtain the equations in the (x, θ) coordinates or derive the equations again by replacing α with x and β with θ . In the latter case, the Lamé parameters will be $A = 1$ and $B = R_\beta$. Both approaches yield the same set of equations in the (x, θ) coordinates.

7.1. EQUATIONS FOR THIN CYLINDRICAL SHELLS

The equations are developed for the general dynamic analysis of laminated cylindrical shells and can be reduced to the static and free vibration analyses. We will only consider laminated composite materials that have cylindrical orthotropy.

7.1.1 Kinematic relations

The formulation of Eq. (7.3) can be used to treat both open and closed shells. Closed cylindrical shells can be treated as a special case of open shells. This is done by replacing the coordinate β with $R\theta$. The present formulation accounts for any b/R_β ratio. In fact, the present formulation accounts for the cases when $b > 2\pi R_\beta$ (Qatu 1999b). These cases are seldom treated in the literature.

When the general equations derived earlier for general shells in Chapter 2 are specialized to those of cylindrical shells, the following midsurface strains and curvature changes are obtained:

$$\begin{aligned} \varepsilon_{0\alpha} &= \frac{\partial u_0}{\partial \alpha}, & \varepsilon_{0\beta} &= \frac{\partial v_0}{\partial \beta} + \frac{w_0}{R}, & \gamma_{0\alpha\beta} &= \frac{\partial v_0}{\partial \alpha} + \frac{\partial u_0}{\partial \beta} \\ k_\alpha &= -\frac{\partial^2 w_0}{\partial \alpha^2}, & k_\beta &= \frac{\partial}{\partial \beta} \left(\frac{v_0}{R} \right) - \frac{\partial^2 w_0}{\partial \beta^2} \\ \tau &= \frac{\partial}{\partial \alpha} \left(\frac{v_0}{R} \right) - 2 \frac{\partial^2 w_0}{\partial \beta \partial \alpha} \end{aligned} \quad (7.5)$$

The β subscript is dropped because there is only one radius of curvature for cylindrical shells ($R = R_\beta$).

7.1.2 Stress resultants

Consider a laminated composite thin shell constructed with very thin layers of composite material laminae. Applying the Kirchhoff hypothesis of neglecting shear deformation, assuming that ε_z is negligible, as is customarily done in thin shell theory (or classical shell theory, CST), and integrating the stresses over the thickness of the shell yields Eqs. (2.64) and (2.65). Note that these equations are the same as those for laminated plates, which are valid for *thin* shells (as shown in Chapter 2). Note also that the orthotropy of each layer is assumed to follow the coordinate system or the fibers of each layer make a constant angle with the coordinate.

7.1.3 Equations of motion

By deleting the body couples and implementing unit values for the Lamé parameters A and B , the reduced equations of motion become

$$\begin{aligned} \frac{\partial N_\alpha}{\partial \alpha} + \frac{\partial N_{\alpha\beta}}{\partial \beta} + p_\alpha &= -\bar{I}_1 \frac{\partial^2 u_0}{\partial t^2} \\ \frac{\partial N_\beta}{\partial \beta} + \frac{\partial N_{\alpha\beta}}{\partial \alpha} + \frac{1}{R} \left[\frac{\partial M_\beta}{\partial \beta} + \frac{\partial M_{\alpha\beta}}{\partial \alpha} \right] + p_\beta &= -\bar{I}_1 \frac{\partial^2 v_0}{\partial t^2} \\ -\frac{N_\beta}{R} + \frac{\partial^2 M_\alpha}{\partial \alpha^2} + 2 \frac{\partial^2 M_{\alpha\beta}}{\partial \beta \partial \alpha} + \frac{\partial^2 M_\beta}{\partial \beta^2} + p_n &= -\bar{I}_1 \frac{\partial^2 w_0}{\partial t^2} \end{aligned} \quad (7.6)$$

where p_α , p_β , and p_n are external pressure components. The above equations can be written in term of the coordinates (x, θ) by substituting the following expression into them:

$$\frac{\partial}{\partial \beta} = \frac{1}{R} \frac{\partial}{\partial \theta} \quad (7.7)$$

Substituting Eqs. (7.5) and (2.64) into Eq. (7.6) yields the equations of motion in terms of displacement. Multiplying the last equation by -1 , yields Eq. (5.10). The L_{ij} coefficients of these equations are

$$\begin{aligned} L_{11} &= A_{11} \frac{\partial^2}{\partial \alpha^2} + 2A_{16} \frac{\partial^2}{\partial \alpha \partial \beta} + A_{66} \frac{\partial^2}{\partial \beta^2} \\ L_{12} = L_{21} &= \left\{ A_{16} + \frac{B_{16}}{R} \right\} \frac{\partial^2}{\partial \alpha^2} + \left\{ (A_{12} + A_{66}) + \frac{(B_{12} + B_{66})}{R} \right\} \frac{\partial^2}{\partial \alpha \partial \beta} \\ &\quad + \left\{ A_{26} + \frac{B_{26}}{R} \right\} \frac{\partial^2}{\partial \beta^2} \\ L_{22} &= \left\{ A_{66} + 2 \frac{B_{66}}{R} \right\} \frac{\partial^2}{\partial \alpha^2} + \left\{ 2A_{26} + 4 \frac{B_{26}}{R} \right\} \frac{\partial^2}{\partial \alpha \partial \beta} + \left\{ A_{22} + 2 \frac{B_{22}}{R} \right\} \frac{\partial^2}{\partial \beta^2} \\ L_{13} = L_{31} &= -B_{11} \frac{\partial^3}{\partial \alpha^3} - B_{26} \frac{\partial^3}{\partial \beta^3} - 3B_{16} \frac{\partial^3}{\partial \alpha^2 \partial \beta} - (B_{12} + 2B_{66}) \frac{\partial^3}{\partial \alpha \partial \beta^2} \\ &\quad + \left\{ \frac{A_{12}}{R} \right\} \frac{\partial}{\partial \alpha} + \left\{ \frac{A_{26}}{R} \right\} \frac{\partial}{\partial \beta} \\ L_{23} = L_{32} &= \left\{ -B_{16} - \frac{D_{16}}{R} \right\} \frac{\partial^3}{\partial \alpha^3} + \left\{ -B_{22} - \frac{D_{22}}{R} \right\} \frac{\partial^3}{\partial \beta^3} + \left\{ -3B_{26} - 3 \frac{D_{26}}{R} \right\} \frac{\partial^3}{\partial \alpha \partial \beta^2} \\ &\quad + \left\{ -(B_{12} + 2B_{66}) - \frac{(D_{12} + 2D_{66})}{R} \right\} \frac{\partial^3}{\partial \alpha^2 \partial \beta} \\ &\quad + \left\{ \frac{A_{26}}{R} + \frac{B_{26}}{R^2} \right\} \frac{\partial}{\partial \alpha} + \left\{ \frac{A_{22}}{R} + \frac{B_{22}}{R^2} \right\} \frac{\partial}{\partial \beta} \\ L_{33} &= \left\{ D_{11} \frac{\partial^4}{\partial \alpha^4} + 4D_{16} \frac{\partial^4}{\partial \alpha^3 \partial \beta} + 2(D_{12} + 2D_{66}) \frac{\partial^4}{\partial \alpha^2 \partial \beta^2} + 4D_{26} \frac{\partial^4}{\partial \alpha \partial \beta^3} + D_{22} \frac{\partial^4}{\partial \beta^4} \right\} \\ &\quad - 2 \left\{ \left(\frac{B_{12}}{R} \right) \frac{\partial^2}{\partial \alpha^2} + 2 \left(\frac{A_{26}}{R} \right) \frac{\partial^2}{\partial \alpha \partial \beta} + \left(\frac{B_{22}}{R} \right) \frac{\partial^2}{\partial \beta^2} \right\} + \left\{ \frac{A_{22}}{R^2} \right\} \end{aligned} \quad (7.8)$$

The above equations can be used for exact solutions and approximate weighted residual methods like Galerkin's method.

7.1.4 Energy functionals for cylindrical shells

The strain energy functional for a cylindrical shell made of laminated composite can be written as in Eqs. (5.12) and (5.13) ($U = U_s + U_b + U_{bs}$); where U_s is the part due to

stretching alone,

$$\begin{aligned}
 U_s = \frac{1}{2} \int_A \left\{ A_{11} \left(\frac{\partial u_0}{\partial \alpha} \right)^2 + A_{22} \left(\frac{\partial v_0}{\partial \beta} + \frac{w_0}{R} \right)^2 + A_{66} \left(\frac{\partial v_0}{\partial \alpha} + \frac{\partial u_0}{\partial \beta} \right)^2 \right. \\
 + 2A_{12} \left(\frac{\partial u_0}{\partial \alpha} \right) \left(\frac{\partial v_0}{\partial \beta} + \frac{w_0}{R} \right) + 2A_{16} \left(\frac{\partial u_0}{\partial \alpha} \right) \left(\frac{\partial v_0}{\partial \alpha} + \frac{\partial u_0}{\partial \beta} \right) \\
 \left. + 2A_{26} \left(\frac{\partial v_0}{\partial \beta} + \frac{w_0}{R} \right) \left(\frac{\partial v_0}{\partial \alpha} + \frac{\partial u_0}{\partial \beta} \right) \right\} dA
 \end{aligned} \quad (7.9)$$

U_b is the part due to bending alone,

$$\begin{aligned}
 U_b = \frac{1}{2} \int_A \left\{ D_{11} \left(\frac{\partial^2 w_0}{\partial \alpha^2} \right)^2 + D_{22} \left(\frac{1}{R} \frac{\partial v_0}{\partial \beta} - \frac{\partial^2 w_0}{\partial \beta^2} \right)^2 + D_{66} \left(\frac{1}{R} \frac{\partial v_0}{\partial \alpha} - 2 \frac{\partial^2 w_0}{\partial \alpha \partial \beta} \right)^2 \right. \\
 + 2D_{12} \left(-\frac{\partial^2 w_0}{\partial \alpha^2} \right) \left(\frac{1}{R} \frac{\partial v_0}{\partial \beta} - \frac{\partial^2 w_0}{\partial \beta^2} \right) + 2D_{16} \left(-\frac{\partial^2 w_0}{\partial \alpha^2} \right) \left(\frac{1}{R} \frac{\partial v_0}{\partial \alpha} - 2 \frac{\partial^2 w_0}{\partial \alpha \partial \beta} \right) \\
 \left. + 2D_{26} \left(\frac{1}{R} \frac{\partial v_0}{\partial \beta} - \frac{\partial^2 w_0}{\partial \beta^2} \right) \left(\frac{1}{R} \frac{\partial v_0}{\partial \alpha} - 2 \frac{\partial^2 w_0}{\partial \alpha \partial \beta} \right) \right\} dA
 \end{aligned} \quad (7.10)$$

and U_{bs} is the part due to bending–stretching coupling,

$$\begin{aligned}
 U_{bs} = \int_A \left\{ -B_{11} \left(\frac{\partial u_0}{\partial \alpha} \right) \left(\frac{\partial^2 w_0}{\partial \alpha^2} \right) + B_{22} \left(\frac{\partial v_0}{\partial \beta} + \frac{w_0}{R} \right) \left(\frac{1}{R} \frac{\partial v_0}{\partial \beta} - \frac{\partial^2 w_0}{\partial \beta^2} \right) \right. \\
 + B_{66} \left(\frac{\partial v_0}{\partial \alpha} + \frac{\partial u_0}{\partial \beta} \right) \left(\frac{1}{R} \frac{\partial v_0}{\partial \alpha} - 2 \frac{\partial^2 w_0}{\partial \alpha \partial \beta} \right) \\
 + B_{12} \left[\left(\frac{\partial u_0}{\partial \alpha} \right) \left(\frac{1}{R} \frac{\partial v_0}{\partial \beta} - \frac{\partial^2 w_0}{\partial \beta^2} \right) - \left(\frac{\partial v_0}{\partial \beta} + \frac{w_0}{R} \right) \left(\frac{\partial^2 w_0}{\partial \alpha^2} \right) \right] \\
 + B_{16} \left[\left(\frac{\partial u_0}{\partial \alpha} \right) \left(\frac{1}{R} \frac{\partial v_0}{\partial \alpha} - 2 \frac{\partial^2 w_0}{\partial \alpha \partial \beta} \right) - \left(\frac{\partial v_0}{\partial \alpha} + \frac{\partial u_0}{\partial \beta} \right) \left(\frac{\partial^2 w_0}{\partial \alpha^2} \right) \right] \\
 \left. + B_{26} \left[\left(\frac{\partial v_0}{\partial \beta} + \frac{w_0}{R} \right) \left(\frac{1}{R} \frac{\partial v_0}{\partial \alpha} - 2 \frac{\partial^2 w_0}{\partial \alpha \partial \beta} \right) + \left(\frac{\partial v_0}{\partial \alpha} + \frac{\partial u_0}{\partial \beta} \right) \left(\frac{1}{R} \frac{\partial v_0}{\partial \beta} - \frac{\partial^2 w_0}{\partial \beta^2} \right) \right] \right\} dA
 \end{aligned} \quad (7.11)$$

Note that for symmetrically laminated shells, $B_{ij} = 0$ and, hence, $U_{bs} = 0$. The work done by the external forces as the shell displaces is the same as in Eq. (5.17) and the kinetic

energy of the entire cylindrical shell is expressed with the same equations used for plates (Eq. (5.18)).

7.2. THICK CYLINDRICAL SHELLS

Thick cylindrical shells are shells with a thickness smaller than (1/10)th of the smallest of the wave lengths and/or radii of curvature. Note that CST is applicable only when the thickness is smaller than (1/20)th of the smallest of the wave lengths and/or radii of curvature. Equations for laminated composite deep, thick circular cylindrical shells are derived from the previous general shell equations described in Chapter 2. This is done by imposing the unit Lamé parameters of Eq. (7.3) to the general shell equations and setting both R_α and $R_{\alpha\beta}$ to infinity, while maintaining R_β .

7.2.1 Kinematic relations

Using Eqs. (7.3) and (7.4), the middle surface strains and curvature changes for thick cylindrical shells having constant radius R are

$$\begin{aligned}
 \varepsilon_{0\alpha} &= \frac{\partial u_0}{\partial \alpha}, & \varepsilon_{0\beta} &= \frac{\partial v_0}{\partial \beta} + \frac{w_0}{R} \\
 \varepsilon_{0\alpha\beta} &= \frac{\partial v_0}{\partial \alpha}, & \varepsilon_{0\beta\alpha} &= \frac{\partial u_0}{\partial \beta} \\
 \gamma_{0\alpha z} &= \frac{\partial w_0}{\partial \alpha} + \psi_\alpha, & \gamma_{0\beta z} &= \frac{\partial w_0}{\partial \beta} - \frac{v_0}{R} + \psi_\beta \\
 \kappa_\alpha &= \frac{\partial \psi_\alpha}{\partial \alpha}, & \kappa_\beta &= \frac{\partial \psi_\beta}{\partial \beta}, & \kappa_{\alpha\beta} &= \frac{\partial \psi_\beta}{\partial \alpha}, & \kappa_{\beta\alpha} &= \frac{\partial \psi_\alpha}{\partial \beta}
 \end{aligned} \tag{7.12}$$

7.2.2 Stress resultants

The force and moment resultants are obtained by integrating the stresses over the shell thickness. They are defined in Eqs. (2.39) and (2.40). These equations include the term $(1 + z/R)$ in the denominator. The force and moment resultants of general thick shells are specialized to those for cylindrical shells. For cylindrical shells Eq. (2.41) applies and Eq. (2.42) becomes (after neglecting the term (Ψ_β/R) and higher order shear terms)

$$\begin{bmatrix} Q_\alpha \\ Q_\beta \end{bmatrix} = \begin{bmatrix} \bar{A}_{55} & A_{45} \\ A_{45} & \hat{A}_{44} \end{bmatrix} \begin{bmatrix} \gamma_{0\alpha z} \\ \gamma_{0\beta z} \end{bmatrix} \tag{7.13}$$

where A_{ij} , B_{ij} , and D_{ij} are given in Eqs. (2.43) and (2.44). The terms \bar{A}_{ij} , \bar{B}_{ij} , \bar{D}_{ij} , \hat{A}_{ij} , \hat{B}_{ij} , and \hat{D}_{ij} are specialized for cylindrical shells

$$\left. \begin{aligned} \bar{A}_{ij} &= A_{ij} + \frac{B_{ij}}{R}, & \hat{A}_{ij} &= A_{ij\beta}, \\ \bar{B}_{ij} &= B_{ij} + \frac{D_{ij}}{R}, & \hat{B}_{ij} &= B_{ij\beta}, \\ \bar{D}_{ij} &= D_{ij} + \frac{E_{ij}}{R}, & \hat{D}_{ij} &= D_{ij\beta} \end{aligned} \right\} \quad i, j = 1, 2, 4, 5, 6 \quad (7.14)$$

and where equations $A_{ij\beta}$, $B_{ij\beta}$, and $D_{ij\beta}$, are defined in Eq. (2.44).

One can also use the truncated equations (Leissa and Chang 1996; Qatu 1999a)

$$\left. \begin{aligned} \bar{A}_{ij} &= A_{ij} + \frac{B_{ij}}{R}, & \hat{A}_{ij} &= A_{ij} - \frac{B_{ij}}{R}, \\ \bar{B}_{ij} &= B_{ij} + \frac{D_{ij}}{R}, & \hat{B}_{ij} &= B_{ij} - \frac{D_{ij}}{R}, \\ \bar{D}_{ij} &= D_{ij} + \frac{E_{ij}}{R}, & \hat{D}_{ij} &= D_{ij} - \frac{E_{ij}}{R} \end{aligned} \right\} \quad i, j = 1, 2, 4, 5, 6 \quad (7.15)$$

where A_{ij} , B_{ij} , D_{ij} , and E_{ij} are defined in Eqs. (2.46) and (2.47).

7.2.3 Equations of motion

The equations of motion for cylindrical thick shells are

$$\begin{aligned} \frac{\partial N_\alpha}{\partial \alpha} + \frac{\partial N_{\beta\alpha}}{\partial \beta} + q_\alpha &= (\bar{I}_1 \ddot{u}_0^2 + \bar{I}_2 \ddot{\psi}_\alpha^2) \\ \frac{\partial N_\beta}{\partial \beta} + \frac{\partial N_{\alpha\beta}}{\partial \alpha} + \frac{Q_\beta}{R} + q_\beta &= (\bar{I}_1 \ddot{v}_0^2 + \bar{I}_2 \ddot{\psi}_\beta^2) \\ -\frac{N_\beta}{R} + \frac{\partial Q_\alpha}{\partial \alpha} + \frac{\partial Q_\beta}{\partial \beta} + q_n &= (\bar{I}_1 \ddot{w}_0^2) \\ \frac{\partial M_\alpha}{\partial \alpha} + \frac{\partial M_{\beta\alpha}}{\partial \beta} - Q_\alpha + m_\alpha &= (\bar{I}_2 \ddot{u}_0^2 + \bar{I}_3 \ddot{\psi}_\alpha^2) \\ \frac{\partial M_\beta}{\partial \beta} + \frac{\partial M_{\alpha\beta}}{\partial \alpha} - Q_\beta + m_\beta &= (\bar{I}_2 \ddot{v}_0^2 + \bar{I}_3 \ddot{\psi}_\beta^2) \end{aligned} \quad (7.16)$$

The equilibrium equations can be written in terms of displacements as $L_{ij}u_i + M_{ij}\ddot{u}_i = q$ (Eq. (5.31)). The L_{ij} and the M_{ij} coefficients are given below. Eq. (2.72) represent the

correct boundary conditions for thick cylindrical shells.

$$M_{ji} = M_{ij}$$

$$M_{11} = M_{22} = M_{33} = -\left(I_1 + \frac{I_2}{R}\right)$$

$$M_{14} = M_{25} = -\left(I_2 + \frac{I_3}{R}\right) \quad (7.17)$$

$$M_{44} = M_{55} = -\left(I_3 + \frac{I_4}{R}\right)$$

$$\text{all other} \quad M_{ij} = 0$$

$$\text{and} \quad [I_1, I_2, I_3, I_4] = \sum_{k=1}^N \int_{h_{k-1}}^{h_k} \rho^{(k)} [1, z, z^2, z^3] dz$$

$$L_{11} = \bar{A}_{11} \frac{\partial^2}{\partial \alpha^2} + 2A_{16} \frac{\partial^2}{\partial \alpha \partial \beta} + \hat{A}_{66} \frac{\partial^2}{\partial \beta^2}$$

$$L_{12} = \bar{A}_{16} \frac{\partial^2}{\partial \alpha^2} + (A_{12} + A_{66}) \frac{\partial^2}{\partial \alpha \partial \beta} + \hat{A}_{26} \frac{\partial^2}{\partial \beta^2}$$

$$L_{13} = \left[\frac{A_{12}}{R} \right] \frac{\partial}{\partial \alpha} + \left[\frac{\hat{A}_{26}}{R} \right] \frac{\partial}{\partial \beta}$$

$$L_{14} = \bar{B}_{11} \frac{\partial^2}{\partial \alpha^2} + 2B_{16} \frac{\partial^2}{\partial \alpha \partial \beta} + \hat{B}_{66} \frac{\partial^2}{\partial \beta^2}$$

$$L_{15} = \bar{B}_{16} \frac{\partial^2}{\partial \alpha^2} + (B_{12} + B_{66}) \frac{\partial^2}{\partial \alpha \partial \beta} + \hat{B}_{26} \frac{\partial^2}{\partial \beta^2}$$

$$L_{22} = \bar{A}_{66} \frac{\partial^2}{\partial \alpha^2} + 2A_{26} \frac{\partial^2}{\partial \alpha \partial \beta} + \hat{A}_{22} \frac{\partial^2}{\partial \beta^2} - \frac{\hat{A}_{44}}{R^2}$$

$$L_{23} = \left[\frac{A_{26} + A_{45}}{R} \right] \frac{\partial}{\partial \alpha} + \left[\frac{\hat{A}_{22} + \hat{A}_{44}}{R} \right] \frac{\partial}{\partial \beta}$$

$$L_{24} = \bar{B}_{16} \frac{\partial^2}{\partial \alpha^2} + (B_{12} + B_{66}) \frac{\partial^2}{\partial \alpha \partial \beta} + \hat{B}_{26} \frac{\partial^2}{\partial \beta^2} + \frac{A_{45}}{R}$$

$$L_{25} = \bar{B}_{66} \frac{\partial^2}{\partial \alpha^2} + 2B_{26} \frac{\partial^2}{\partial \alpha \partial \beta} + \hat{B}_{22} \frac{\partial^2}{\partial \beta^2} + \frac{\hat{A}_{44}}{R}$$

$$L_{33} = -\bar{A}_{55} \frac{\partial^2}{\partial \alpha^2} - 2A_{45} \frac{\partial^2}{\partial \alpha \partial \beta} - \hat{A}_{44} \frac{\partial^2}{\partial \beta^2} + \frac{\hat{A}_{22}}{R^2}$$

$$L_{34} = \left[-\bar{A}_{55} + \frac{B_{12}}{R} \right] \frac{\partial}{\partial \alpha} + \left[-A_{45} + \frac{\hat{B}_{26}}{R} \right] \frac{\partial}{\partial \beta}$$

$$L_{35} = \left[-A_{45} + \frac{B_{26}}{R} \right] \frac{\partial}{\partial \alpha} + \left[-\hat{A}_{44} + \frac{\hat{B}_{22}}{R} \right] \frac{\partial}{\partial \beta}$$

$$\begin{aligned}
L_{44} &= -\bar{A}_{55} + \bar{D}_{11} \frac{\partial^2}{\partial \alpha^2} + 2\bar{D}_{16} \frac{\partial^2}{\partial \alpha \partial \beta} + \hat{D}_{66} \frac{\partial^2}{\partial \beta^2} \\
L_{45} &= -A_{45} + \bar{D}_{16} \frac{\partial^2}{\partial \alpha^2} + (D_{12} + D_{66}) \frac{\partial^2}{\partial \alpha \partial \beta} + \hat{D}_{26} \frac{\partial^2}{\partial \beta^2} \\
L_{55} &= -\hat{A}_{44} + \bar{D}_{66} \frac{\partial^2}{\partial \alpha^2} + 2D_{26} \frac{\partial^2}{\partial \alpha \partial \beta} + \hat{D}_{22} \frac{\partial^2}{\partial \beta^2}
\end{aligned} \tag{7.18}$$

7.3. SIMPLY SUPPORTED CYLINDRICAL SHELLS

Cylindrical shells, constructed with composite materials, will be considered in the subsequent analysis. Figure 7.2 shows the fundamental parameters used in these shells when they are closed (length a , and radius R).

Thin cylindrical shells are like shallow shells and can have up to 16 boundary conditions at each edge. Twelve of these are classical boundary conditions (i.e., free, simply supported and clamped). This leads to numerous combinations of boundary conditions, particularly when the shells are open. Thick shells can have 24 possible classical boundary conditions at each edge (Table 2.1). This yields a higher number of combinations of boundary conditions for such shells.

Like shallow shells, only those open cylindrical shells that have two opposite edges simply supported can permit exact solutions (for cross-ply lamination). Interestingly, for closed shells, this constitutes all possible boundary conditions the shell may have. The problem with all edges being simply supported with shear diaphragm boundaries has a direct, relatively straightforward solution, referred to as the Navier solution. Interestingly enough, closed shells with shear diaphragm boundaries at each of the opposing two edges permit the same exact solution. The reason is that conditions at the nodal lines of these shells simulate a shear diaphragm boundary. This can be mathematically proven with the obtained exact solution.

7.3.1 Thin shells

Consider a cylindrical shell that is made of a cross-ply laminate, thus $A_{16} = A_{26} = B_{16} = B_{26} = D_{16} = D_{26} = 0$. The differential parameters in the equations of motion L_{ij} become

$$\begin{aligned}
L_{11} &= A_{11} \frac{\partial^2}{\partial \alpha^2} + A_{66} \frac{\partial^2}{\partial \beta^2} \\
L_{12} = L_{21} &= \left\{ (A_{12} + A_{66}) + \frac{(B_{12} + B_{66})}{R} \right\} \frac{\partial^2}{\partial \alpha \partial \beta}
\end{aligned}$$

$$\begin{aligned}
L_{22} &= \left\{ A_{66} + 2\frac{B_{66}}{R} + \frac{D_{66}}{R^2} \right\} \frac{\partial^2}{\partial \alpha^2} + \left\{ A_{22} + 2\frac{B_{22}}{R} + \frac{D_{22}}{R^2} \right\} \frac{\partial^2}{\partial \beta^2} \\
L_{13} = L_{31} &= -B_{11} \frac{\partial^3}{\partial \alpha^3} - (B_{12} + 2B_{66}) \frac{\partial^3}{\partial \alpha \partial \beta^2} + \frac{A_{12}}{R} \frac{\partial}{\partial \alpha} \\
L_{23} = L_{32} &= -\left\{ B_{22} + \frac{D_{22}}{R} \right\} \frac{\partial^3}{\partial \beta^3} - \left\{ (B_{12} + 2B_{66}) + \frac{(D_{12} + 2D_{66})}{R} \right\} \frac{\partial^3}{\partial \alpha^2 \partial \beta} \\
&\quad + \left\{ \frac{A_{22}}{R} + \frac{B_{22}}{R^2} \right\} \frac{\partial}{\partial \beta} \\
L_{33} &= D_{11} \frac{\partial^4}{\partial \alpha^4} + 2(D_{12} + 2D_{66}) \frac{\partial^4}{\partial \alpha^2 \partial \beta^2} + D_{22} \frac{\partial^4}{\partial \beta^4} \\
&\quad - 2 \left\{ \left(\frac{B_{12}}{R} \right) \frac{\partial^2}{\partial \alpha^2} + \left(\frac{B_{22}}{R} \right) \frac{\partial^2}{\partial \beta^2} \right\} + \frac{A_{22}}{R^2}
\end{aligned} \tag{7.19}$$

Consider an open cylindrical shell (Figure 7.3), with shear diaphragm (S2) boundaries on all four edges. That is, the boundary conditions of Eq. (2.62) for S2 boundaries apply here.

The solution in Eq. (5.38) satisfies the boundary conditions and the equations of motion exactly for open cylindrical shells. These equations can be used in analyzing closed shells by substituting b with πR . With $\beta = R\theta$; the above solution can be written in terms of θ for closed cylindrical shells as

$$\begin{aligned}
u_0(\alpha, \beta, t) &= \sum_{m=0}^M \sum_{n=0}^N U_{mn} \cos(\alpha_m \alpha) \sin(n\theta) \sin(\omega_{mn} t) \\
v_0(\alpha, \beta, t) &= \sum_{m=0}^M \sum_{n=0}^N V_{mn} \sin(\alpha_m \alpha) \cos(n\theta) \sin(\omega_{mn} t) \\
w_0(\alpha, \beta, t) &= \sum_{m=0}^M \sum_{n=0}^N W_{mn} \sin(\alpha_m \alpha) \sin(n\theta) \sin(\omega_{mn} t)
\end{aligned} \tag{7.20}$$

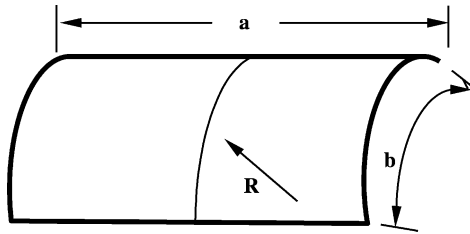


Figure 7.3. Open cylindrical shell (Qatu 1999b).

where

$$\alpha_m = \frac{m\pi}{a}$$

ω_{mn} is the natural frequency. Note also that for such shells, at the nodal points, where $\theta = 0$ and π/n (for each n), analysis yields the inplane displacement u_0 (which is tangential to the boundaries $\theta = 0$ and π/n (i.e., $\beta = 0, R\pi/n$) and transverse displacement w_0 to be zero. The other inplane displacement v_0 normal to the boundaries $\theta = 0$ and π/n (i.e., $\beta = 0, R\pi/n$) is not zero. These are the geometric constraints for shear diaphragm boundaries. The forces and moments at these nodal lines can be determined from Eq. (2.64) together with Eq. (7.5). This yields

$$\begin{aligned} N_\beta &= A_{12} \frac{\partial u_0}{\partial \alpha} + A_{22} \left(\frac{\partial v_0}{\partial \beta} + \frac{w_0}{R} \right) - B_{11} \frac{\partial^2 w_0}{\partial \alpha^2} + B_{12} \left(\frac{1}{R} \frac{\partial v_0}{\partial \beta} - \frac{\partial^2 w_0}{\partial \beta^2} \right) \\ M_\beta &= B_{12} \frac{\partial u_0}{\partial \alpha} + B_{22} \left(\frac{\partial v_0}{\partial \beta} + \frac{w_0}{R} \right) - D_{11} \frac{\partial^2 w_0}{\partial \alpha^2} + D_{12} \left(\frac{1}{R} \frac{\partial v_0}{\partial \beta} - \frac{\partial^2 w_0}{\partial \beta^2} \right) \end{aligned} \quad (7.21)$$

Substituting Eq. (7.20) into the above equations, one gets expressions for these stress resultants. Note that these expressions will yield zero values at the nodal lines. Zero N_β and M_β stress resultants are the forced boundary conditions for shear diaphragm edge supports. For higher modes, each segment of the shell containing double half-sine waves can actually be treated as an independent shell with shear diaphragm boundary conditions vibrating at its fundamental frequency. As will be seen later, this is an important observation for treating closed cylindrical shells having arbitrary boundaries at $\alpha = 0$ and a .

Substitute the general solution of open shells (Eq. (5.38)) into the equations of motion in terms of displacement yields Eq. (5.40) with the following coefficients

$$\begin{aligned} C_{11} &= -A_{11}\alpha_m^2 - A_{66}\beta_n^2 \\ C_{12} = C_{21} &= -\left\{ (A_{12} + A_{66}) + \frac{(B_{12} + B_{66})}{R} \right\} \alpha_m \beta_n \\ C_{22} &= -\left\{ A_{66} + 2\frac{B_{66}}{R} + \frac{D_{66}}{R^2} \right\} \alpha_m^2 - \left\{ A_{22} + 2\frac{B_{22}}{R} + \frac{D_{22}}{R^2} \right\} \beta_n^2 \\ C_{13} = C_{31} &= B_{11}\alpha_m^3 + (B_{12} + 2B_{66})\alpha_m \beta_n^2 + \left\{ \frac{A_{12}}{R} \right\} \alpha_m \\ C_{23} = C_{32} &= \left\{ B_{22} + \frac{D_{22}}{R} \right\} \beta_n^3 + \left\{ (B_{12} + 2B_{66}) + \frac{(D_{12} + 2D_{66})}{R} \right\} \alpha_m^2 \beta_n + \left\{ \frac{A_{22}}{R} + \frac{B_{22}}{R^2} \right\} \beta_n \\ C_{33} &= \{ D_{11}\alpha_m^4 + 2(D_{12} + 2D_{66})\alpha_m^2 \beta_n^2 + D_{22}\beta_n^4 \} + 2\left\{ \left(\frac{B_{12}}{R} \right) \alpha_m^2 + \left(\frac{B_{22}}{R} \right) \beta_n^2 \right\} + \left\{ \frac{A_{22}}{R^2} \right\} \end{aligned} \quad (7.22)$$

7.3.1.1 Comparisons with previous results. Table 7.1 shows a comparison between the results obtained by Bert *et al.* using Love's shell theory (which is a CST), the results of Rath and Das who included shear deformation and rotary inertia, the experimental results obtained by Bray and Egle, as well as those made in this study (also found in Qatu (1999b)). The studies were made for isotropic steel. A nondimensional frequency parameter Ω is used in the present analysis, and the dimensional frequency in Hertz is calculated from the nondimensional frequency parameter $\Omega = \omega R \sqrt{\rho/E_1}$.

Table 7.1. Comparison between the natural frequencies obtained by using various methods ($h = 0.02$ in., $a = 11.74$ in., $R = 5.836$ in., $\rho = 734 \times 10^{-6}$ lb s²/in.⁴, $E = 29.5 \times 10^6$ lb/in.², $\nu = 0.285$) (Qatu 1999b).

m		$n\Omega = \omega R \sqrt{\rho/E_1}$		ω (Hz)		
		(Classical shell theory)	Bert <i>et al.</i> (Love's)	Rath and Das (SDST)	Bray and Egle (Test)	
1	0	0.96852	5295.13	—	5325.97	—
	1	0.59729	3265.53	3271.0	3270.53	—
	2	0.34038	1860.93	1862.3	1861.95	—
	3	0.20149	1101.59	1102.0	1101.75	1001
	4	0.12908	705.71	705.9	706.66	715
	5	0.09104	497.74	497.9	497.47	534
	6	0.07329	400.69	400.3	400.08	410
	7	0.06984	381.83	380.9	380.71	393
	8	0.07652	418.35	416.8	416.69	426
	9	0.08977	490.79	488.7	488.54	495
	10	0.10730	586.63	583.9	583.78	587
	11	0.12796	699.26			
	12	0.15120	826.64	822.9	822.46	821
2	0	0.99501	5439.95	—	5442.54	—
	1	0.88441	4835.28	4837.9	4837.67	—
	2	0.68107	3723.57	3725.5	3424.98	—
	3	0.50153	2741.98	2743.1	2742.61	—
	4	0.36908	2017.85	2018.5	2018.02	—
	5	0.27711	1515.03	1515.4	1514.96	1527
	6	0.21495	1175.18	1175.2	1174.85	—
	7	0.17454	954.25	953.9	953.56	—
	8	0.15096	825.33	824.6	824.19	—
	9	0.14122	772.08	770.6	770.28	744
	10	0.14281	780.77	778.6	778.17	782
	11	0.15317	837.17			
	12	0.17000	929.43	925.7	925.20	927

Table 7.2. Comparison of the frequency parameter $\Omega = \omega R \sqrt{\rho/E_1}$ using CST and 3D elasticity theories.

R/h	a/mR	Analysis	n				
			0	1	2	3	4
20	4	CST	0.48713	0.26941	0.12756	0.13709	0.23147
		3D	0.48708	0.26942	0.12710	0.13615	0.22968
	1	CST	1.00604	0.89941	0.71014	0.56855	0.52145
		3D	1.00434	0.89777	0.70810	0.56533	0.51612
500	4	CST	0.48708	0.26929	0.11813	0.06081	0.03711
		3D	0.48708	0.26929	0.11813	0.06081	0.03710
	1	CST	0.99504	0.88575	0.68364	0.50426	0.37122
		3D	0.99504	0.88575	0.68364	0.50425	0.37122

Comparing the results obtained, one can conclude that the present analysis yields accurate results when compared with those obtained experimentally, analytically using Love's CST, and shear deformation shell theory (SDST). This further shows that indeed for such thin shells, shear deformations can be neglected.

Table 7.2 shows a comparison of the frequency parameter between results obtained here (also found in Qatu (1999b)) and those obtained using the 3D theory of elasticity (Leissa 1973a) for isotropic cylindrical shells. Even for relatively thicker shells with R_β/h ratio of 20, the comparison indicates that the present theory is still relatively accurate. Caution should be observed here because for composite shells, comparisons between the 3D theory of elasticity and thin shell theory show larger difference (Bhimaraddi 1991). These comparisons build confidence in the equations presented here for thin shells.

7.3.1.2 Vibration of cylindrical thin shells. The fundamental natural frequencies are listed for each a/mR ratio. The a/mR ratios are selected so that they include problems that can be encountered in practical applications. CST would yield inaccurate results for shells having the ratio $a/mR < 0.5$ because of end effects (Leissa 1973a). Furthermore, such shells in typical applications are left free along the edges $\alpha = -a/2, +a/2$ and are treated as laminated rings (Chapter 4). For higher ratios of a/mR , the shell may be treated as a beam.

The nondimensional frequency parameter $\Omega = \omega R \sqrt{\rho/E_1}$ is used in all subsequent results. In the results obtained for laminated composite shells, the $[0^\circ, 90^\circ]$ and $[90^\circ, 0^\circ]$

lamination sequences are used in most of these results because they generally represent a shell with the maximum stretching–bending coupling effects (i.e., B_{ij} terms are the highest).

Tables 7.3 and 7.4 present results for graphite/epoxy closed and open $[0^\circ, 90^\circ]$ laminated shells. The material properties for graphite/epoxy are

$$\begin{aligned} E_1 &= 20.02 \times 10^6 \text{ psi}, & E_2 &= 1.3 \times 10^6 \text{ psi} \\ G_{12} &= 1.03 \times 10^6 \text{ psi}, & \nu_{12} &= 0.3 \end{aligned} \quad (7.23 \text{ (5.68)})$$

Figure 7.4 shows the sine waves and possible mode shapes along the circumferential direction of the shell.

7.3.1.3 Effects of the thickness ratio. Table 7.5 lists the natural frequencies for $[0^\circ, 90^\circ]$ graphite/epoxy closed shells with two different thickness ratios ($R/h = 20$ and 500). These represent a thicker shell and a very thin shell, respectively. Results obtained from Table 7.3 are used for shells with a thickness ratio of 100 are not repeated here.

As can be seen from the table, thicker shells have lower frequency parameters than thinner shells for shorter shells ($a/mR = 1$ and 2). It is interesting to note that the thickness ratio has minimal effects on the natural frequencies when $n = 0$ and 1. For $n > 1$, the thickness ratio has a much greater effect. It is also observed that the fundamental frequency occurs at lower n value for higher thickness ratios.

7.3.1.4 Effects of the lamination sequence. Table 7.6 lists the natural frequencies for $[90^\circ, 0^\circ]$, $[0^\circ, 90^\circ]_s$, and $[90^\circ, 0^\circ]_s$ graphite/epoxy closed cylindrical shells. The thickness ratio of ($R/h = 100$) is used. Results obtained previously for $[0^\circ, 90^\circ]$ shells are not repeated here but can be used for comparisons.

The first important observation is that unsymmetric lamination does not always yield lower frequencies. For example, when $a/mR > 2.0$, the unsymmetric lamination sequence $[90^\circ, 0^\circ]$ yielded higher fundamental frequency than the symmetric lamination $[0^\circ, 90^\circ]_s$. This is generally not the case for plates.

Shells with the outer fibers in the circumferential direction of the shell ($[90^\circ, 0^\circ]$ and $[90^\circ, 0^\circ]_s$) give higher frequencies when compared with shells having the outer fibers in the longitudinal direction (i.e., $[0^\circ, 90^\circ]$ and $[0^\circ, 90^\circ]_s$). The effect of lamination sequence is observed to be less for higher frequencies and/or lower length

Table 7.3. Frequency parameters for $[0^\circ, 90^\circ]$ graphite/epoxy closed cylindrical shells, $R/h = 100$.

a/mR_β	n										
	0	1	2	3	4	5	6	7	8	9	10
8	0.08907	0.04903	0.02140	0.01482	0.02075	0.03235	0.04723	0.06495	0.08543	0.10865	0.13460
4	0.17815	0.11600	0.06212	0.03740	0.03013	0.03561	0.04846	0.06552	0.08578	0.10891	0.13483
2	0.35629	0.23975	0.14556	0.09650	0.07025	0.05915	0.06070	0.07187	0.08936	0.11121	0.13651
1	0.71259	0.44205	0.29163	0.20869	0.15935	0.12928	0.11295	0.10837	0.11412	0.12826	0.14882
0.5	0.73565	0.63822	0.49616	0.38973	0.31622	0.26575	0.23171	0.21047	0.20015	0.19960	0.20777

Table 7.4. Frequency parameters for $[0^\circ, 90^\circ]$ graphite/epoxy open cylindrical shells, $b/R = 2.0$, $R/h = 100$.

a/mR_β	n										
	0	1	2	3	4	5	6	7	8	9	10
8	0.08907	0.02984	0.01508	0.02864	0.05197	0.08227	0.11934	0.16314	0.21367	0.27093	0.33490
4	0.17815	0.08060	0.03544	0.03305	0.05293	0.08263	0.11958	0.16337	0.21390	0.27117	0.33515
2	0.35629	0.17846	0.09168	0.06095	0.06305	0.08650	0.12156	0.16474	0.21507	0.27227	0.33623
1	0.71259	0.34488	0.20014	0.13638	0.11052	0.11270	0.13631	0.17420	0.22209	0.27813	0.34152
0.5	0.73565	0.55382	0.37757	0.27836	0.22450	0.20102	0.20207	0.22342	0.26061	0.31001	0.36929

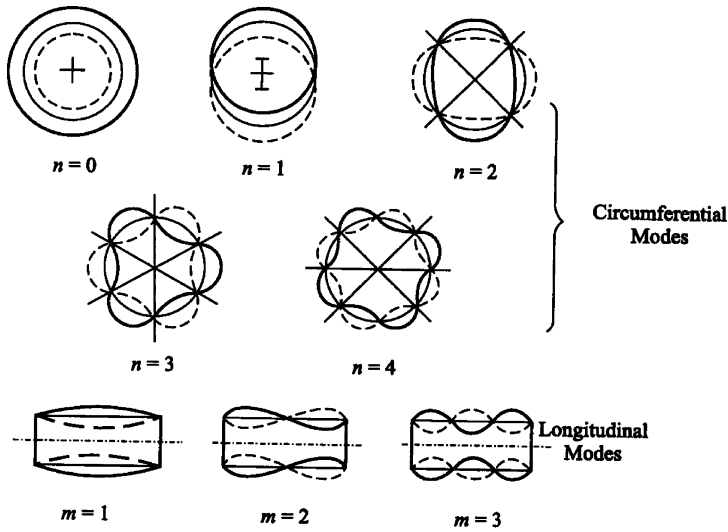


Figure 7.4. Mode shapes along the circumferential direction (Leissa 1973a, reproduced with permission).

ratio (a/mR_β) . Also, lamination sequence effects are insignificant for frequencies with $n < 2$.

7.3.1.5 Effects of the orthotropy ratio. Table 7.7 shows the natural frequency parameters for various E_1/E_2 ratios. To isolate the orthotropy ratio from the effects of shear and Poisson's ratio, constant ratios of G_{12} and ν_{12} are chosen. Two orthotropy ratios, one weak $E_1/E_2 = 3$ and the other strong $E_1/E_2 = 40$, are treated. The thickness ratio of $R/h = 100$, and the $[0^\circ, 90^\circ]$ lamination sequence are used for all the results.

The orthotropy ratio has a considerable effect on all the frequencies. Its effects on the fundamental frequency parameters are found to be higher for short shells ($a/mR = 0.5$) than longer ones. This is reversed when $n = 0$, where the orthotropy effects are found to be higher for longer shells ($a/mR = 8$) than shorter ones.

The fundamental frequencies are observed to occur at a lower n value for lower orthotropy ratios. Similar studies of the effect of the orthotropy ratio on $[90^\circ, 0^\circ]$ laminates yielded similar results.

Table 7.5. Thickness effects on the frequencies for graphite/epoxy $[0^\circ, 90^\circ]$ closed cylindrical shells.

a/mR_β	n										
	0	1	2	3	4	5	6	7	8	9	10
$R/h = 20$											
8	0.08907	0.04912	0.02125	0.01106	0.00751	0.00761	0.00983	0.01315	0.01717	0.02180	0.02700
4	0.17815	0.11621	0.06225	0.03627	0.02330	0.01685	0.01457	0.01537	0.01821	0.02231	0.02726
2	0.35629	0.24015	0.14590	0.09623	0.06761	0.04991	0.03870	0.03199	0.02888	0.02882	0.03116
1	0.71258	0.44245	0.29191	0.20838	0.15753	0.12393	0.10043	0.08346	0.07116	0.06255	0.05461 (11)
0.5	0.73190	0.63517	0.49310	0.38561	0.31000	0.25597	0.21613	0.18590	0.16244	0.14401	0.10433 (13)
$R/h = 500$											
8	0.08908	0.04861	0.02743	0.05217	0.09813	0.15823	0.23177	0.31859	0.41861	0.53176	0.65795
4	0.17816	0.11501	0.06398	0.06289	0.10140	0.15997	0.23315	0.31989	0.41990	0.53305	0.65924
2	0.35633	0.23799	0.14609	0.11114	0.12399	0.17190	0.24126	0.32654	0.42594	0.53880	0.66485
1	0.71266	0.44283	0.29705	0.22751	0.20855	0.23095	0.28502	0.36201	0.45682	0.56700	0.69137
0.5	0.78908	0.69140	0.56195	0.48080	0.44477	0.44535	0.47644	0.53329	0.61211	0.71000	0.82492

Values in brackets give the n values for the last frequency parameter.

Table 7.6. Lamination effects on the frequency parameter for graphite/epoxy $[0^\circ, 90^\circ]$ closed cylindrical shells.

a/mR_β		n										
		0	1	2	3	4	5	6	7	8	9	10
$[90^\circ, 0^\circ]$	8	0.08907	0.04925	0.02182	0.01553	0.02143	0.03298	0.04789	0.06570	0.08632	0.10971	0.13587
	4	0.17815	0.11653	0.06276	0.03836	0.03147	0.03699	0.04975	0.06678	0.08707	0.11030	0.13637
	2	0.35629	0.24079	0.14668	0.09770	0.07184	0.06126	0.06312	0.07433	0.09177	0.11359	0.13892
	1	0.71259	0.44339	0.29322	0.21025	0.16105	0.13136	0.11560	0.11160	0.11777	0.13216	0.15284
	0.5	0.73090	0.63573	0.49559	0.38999	0.31694	0.26689	0.23335	0.21273	0.20311	0.20327	0.21208
$[0^\circ, 90^\circ]_s$	8	0.08907	0.04914	0.02155	0.01449	0.01923	0.02949	0.04285	0.05883	0.07732	0.09829	0.12174
	4	0.17815	0.11627	0.06244	0.03765	0.02961	0.03354	0.04462	0.05980	0.07798	0.09882	0.12220
	2	0.35629	0.24031	0.14621	0.09717	0.07079	0.05892	0.05880	0.06778	0.08289	0.10222	0.12483
	1	0.71259	0.44316	0.29322	0.21064	0.16165	0.13173	0.11501	0.10915	0.11271	0.12405	0.14149
	0.5	0.73919	0.64338	0.50396	0.40026	0.32947	0.28158	0.24969	0.22981	0.21966	0.21786	0.22343
$[90^\circ, 0^\circ]$	8	0.08907	0.04914	0.02251	0.02341	0.04017	0.06422	0.09403	0.12935	0.17014	0.21638	0.26807
	4	0.17815	0.11627	0.06276	0.04187	0.04602	0.06615	0.09483	0.12978	0.17043	0.21661	0.26827
	2	0.35629	0.24027	0.14626	0.09875	0.07888	0.08180	0.10211	0.13351	0.17262	0.21809	0.26940
	1	0.71259	0.44270	0.29247	0.21022	0.16385	0.14166	0.14031	0.15694	0.18738	0.22800	0.27656
	0.5	0.73296	0.63664	0.49550	0.38978	0.31790	0.27151	0.24589	0.23906	0.24950	0.27500	0.31295

Table 7.7. Orthotropy effects on the frequencies for $[0^\circ, 90^\circ]$ closed barrel shells $G_{12}/E_2 = 0.5$, $\nu_{12} = 0.3$.

E_1/E_2	a/mR_β	n										
		0	1	2	3	4	5	6	7	8	9	10
3	8	0.16032	0.06945	0.02655	0.02025	0.03190	0.05076	0.07436	0.10233	0.13463	0.17122	0.21211
	4	0.32064	0.18883	0.08860	0.04928	0.04162	0.05371	0.07549	0.10298	0.13514	0.17172	0.21262
	2	0.64128	0.40679	0.23744	0.14725	0.10112	0.08418	0.08977	0.11021	0.13954	0.17495	0.21538
	1	0.82060	0.66262	0.47548	0.34567	0.25969	0.20480	0.17458	0.16604	0.17601	0.20005	0.23416
	0.5	0.83010	0.79006	0.69832	0.59750	0.50859	0.43735	0.38416	0.34841	0.32951	0.32670	0.33861
40	8	0.04391	0.02876	0.01559	0.01247	0.01783	0.02770	0.04037	0.05549	0.07298	0.09281	0.11498
	4	0.08781	0.06065	0.03644	0.02530	0.02369	0.02999	0.04131	0.05592	0.07320	0.09295	0.11507
	2	0.17562	0.12240	0.07652	0.05371	0.04302	0.04140	0.04751	0.05933	0.07520	0.09420	0.11593
	1	0.35124	0.24021	0.15331	0.10935	0.08547	0.07324	0.06999	0.07452	0.08546	0.10137	0.12117
	0.5	0.70248	0.43769	0.29410	0.21698	0.17233	0.14545	0.13014	0.12376	0.12504	0.13301	0.14671

7.3.2 Thick shells

Consider again cross-ply laminates, with $A_{16} = A_{26} = B_{16} = B_{26} = D_{16} = D_{26} = 0$. The differential parameters L_{ij} in Eq. (7.18) become

$$\begin{aligned}
 L_{11} &= \bar{A}_{11} \frac{\partial^2}{\partial \alpha^2} + \hat{A}_{66} \frac{\partial^2}{\partial \beta^2}, & L_{12} &= (A_{12} + A_{66}) \frac{\partial^2}{\partial \alpha \partial \beta} \\
 L_{13} &= \left[\frac{A_{12}}{R} \right] \frac{\partial}{\partial \alpha}, & L_{14} &= \bar{B}_{11} \frac{\partial^2}{\partial \alpha^2} + \hat{B}_{66} \frac{\partial^2}{\partial \beta^2} \\
 L_{15} &= \bar{B}_{16} \frac{\partial^2}{\partial \alpha^2} + (B_{12} + B_{66}) \frac{\partial^2}{\partial \alpha \partial \beta} \\
 L_{22} &= \bar{A}_{66} \frac{\partial^2}{\partial \alpha^2} + \hat{A}_{22} \frac{\partial^2}{\partial \beta^2} - \frac{\hat{A}_{44}}{R^2} \\
 L_{23} &= \left[\frac{A_{45}}{R} \right] \frac{\partial}{\partial \alpha} + \left[\frac{\hat{A}_{22} + \hat{A}_{44}}{R} \right] \frac{\partial}{\partial \beta} \\
 L_{24} &= (B_{12} + B_{66}) \frac{\partial^2}{\partial \alpha \partial \beta} + \frac{A_{45}}{R} \\
 L_{25} &= \bar{B}_{66} \frac{\partial^2}{\partial \alpha^2} + \hat{B}_{22} \frac{\partial^2}{\partial \beta^2} + \frac{\hat{A}_{44}}{R} \\
 L_{33} &= -\bar{A}_{55} \frac{\partial^2}{\partial \alpha^2} - \hat{A}_{44} \frac{\partial^2}{\partial \beta^2} + \frac{\hat{A}_{22}}{R^2} \\
 L_{34} &= \left[-\bar{A}_{55} + \frac{B_{12}}{R} \right] \frac{\partial}{\partial \alpha} + [-A_{45}] \frac{\partial}{\partial \beta} \\
 L_{35} &= [-A_{45}] \frac{\partial}{\partial \alpha} + \left[-\hat{A}_{44} + \frac{\hat{B}_{22}}{R} \right] \frac{\partial}{\partial \beta} \\
 L_{44} &= -\bar{A}_{55} + \bar{D}_{11} \frac{\partial^2}{\partial \alpha^2} + \hat{D}_{66} \frac{\partial^2}{\partial \beta^2} \\
 L_{45} &= -A_{45} + (D_{12} + D_{66}) \frac{\partial^2}{\partial \alpha \partial \beta} \\
 L_{55} &= -\hat{A}_{44} + \bar{D}_{66} \frac{\partial^2}{\partial \alpha^2} + \hat{D}_{22} \frac{\partial^2}{\partial \beta^2}
 \end{aligned} \tag{7.24}$$

The well-known Navier-type solution can be applied to obtain an exact solution for cross-ply lamination and shear diaphragm boundaries at $\alpha = 0$ and a , and $\beta = 0$ and b ; as was performed for plates and shallow shells. Eq. (5.44) is the exact solution that needs to be substituted in the equations of motion in terms of displacement for cylindrical shells. This yields the equation $[K]\{\Delta\} + (\omega_{mn})^2[M]\{\Delta\} = 1$ for free vibration analysis; where $[K]$, $[M]$ are the stiffness and mass symmetric 5×5 matrices, respectively, ω_{mn} is

the frequency, and $\{\Delta\} = \{U_{mn}, V_{mn}, W_{mn}, \psi_{\alpha mn}, \psi_{\beta mn}\}^T$. The K_{ij} factors are

$$\begin{aligned}
 K_{11} &= -\bar{A}_{11}\alpha_m^2 - \hat{A}_{66}\beta_n^2, & K_{12} &= -(A_{12} + A_{66})\alpha_m\beta_n \\
 K_{13} &= \left[\frac{A_{12}}{R}\right]\alpha_m, & K_{14} &= -\bar{B}_{11}\alpha_m^2 - \hat{B}_{66}\beta_n^2 \\
 K_{15} &= -(B_{12} + B_{66})\alpha_m\beta_n \\
 K_{22} &= -\bar{A}_{66}\alpha_m^2 - \hat{A}_{22}\beta_n^2 - \frac{\hat{A}_{44}}{R} \\
 K_{23} &= \left[\frac{\hat{A}_{22} + \hat{A}_{44}}{R}\right]\beta_n, & K_{24} &= -(B_{12} + B_{66})\alpha_m\beta_n \\
 K_{25} &= -\bar{B}_{66}\alpha_m^2 + \hat{B}_{22}\beta_n^2 + \frac{\hat{A}_{44}}{R} \\
 K_{33} &= -\bar{A}_{55}\alpha_m^2 - \hat{A}_{44}\beta_n^2 - \left[\frac{\hat{A}_{22}}{R}\right] \\
 K_{34} &= \left[-\bar{A}_{55} + \frac{B_{12}}{R}\right]\alpha_m, & K_{35} &= \left[-\hat{A}_{44} + \frac{\hat{B}_{22}}{R}\right]\beta_n \\
 K_{44} &= -\bar{A}_{55} - \bar{D}_{11}\alpha_m^2 - \hat{D}_{66}\beta_n^2 \\
 K_{45} &= -(D_{12} + D_{66})\alpha_m\beta_n \\
 K_{55} &= -\hat{A}_{44} - \bar{D}_{66}\alpha_m^2 - \hat{D}_{22}\beta_n^2
 \end{aligned} \tag{7.25}$$

Table 7.8 shows comparisons of the natural frequency parameters obtained using the present theory with previously published results for cylindrical open shells having shear diaphragm boundaries. First order SDST were used by Librescu *et al.* (1989a,b) and

Table 7.8. Nondimensional frequency parameters $\Omega = \omega a^2 \sqrt{\rho/E_2 h^2}$ for $[0^\circ, 90^\circ]$ cylindrical shells ($E_1/E_2 = 25$, $G_{12}/E_2 = 0.5$, $G_{13}/E_2 = 0.5$, $G_{23}/E_2 = 0.2$, $\nu_{12} = 0.3$, $k^2 = 5/6$, $a/b = 1$, $a/h = 10$) (Qatu 2002a; reproduced with permission).

R/a	Present	Ye and Soldatos (1994)	Bhimaraddi (1991)			Librescu (1989a,b)	
	SDST	3D	3D	SDST	HSDST	SDST	HSDST
1	10.643	10.6973	10.409	10.748	10.919		
2	9.4428	9.4951	9.3627	9.3653	9.5664		
3	9.1755	9.1155	9.1442	9.0563	9.2642		
4	9.0731		9.0613	8.9403	9.1506		
5	9.0221	9.0616	9.0200	8.8840	9.0953	8.931	8.959
10	8.9446	8.9778	8.9564	8.8026	9.0150	8.897	8.933
20	8.9194	8.9477	8.9341	8.7779	8.9904	8.894	8.934
∞	8.9001	8.9248	8.9179	8.7640	8.9761	8.900	8.944

Bhimaraddi (1991), who also used higher-order shear deformation shell theories (HSDT). Bhimaraddi (1991) also used the 3D theory of elasticity to obtain exact analytical solutions. It should be mentioned that Bhimaraddi (1991) made certain assumptions, which reduced his analysis to that of shallow shells. The previously described Navier solution was used to obtain these 3D results. Ye and Soldatos (1994) used the 3D theory of elasticity and obtained exact solutions for cylindrical shells without making the assumption of shallowness made by Bhimaraddi (1991).

In the HSDT theories of both Librescu *et al.* and Bhimaraddi, boundary conditions at the upper and lower surface of the shell can be satisfied and there is no need for shear correction factors. They do introduce, however, boundary terms that are not easily understandable in real applications. Despite their added complexity, the results shown indicate that HSDST theories do not always yield better results than first order SDST theories (when compared with the 3D theory of elasticity). In all SDST and HSDST theories of both Librescu *et al.* and Bhimaraddi, the results deviate from the 3D theory of elasticity as the shell becomes deeper. This indicates that the error in these theories may very well be due to the fact that the term $1 + z/R$ was ignored in the stiffness coefficients. The results of the present theory (Qatu 1999a, 2002a) on the other hand, show closer approximation to the 3D results when compared with the SDST theories of Librescu *et al.* and Bhimaraddi. It also shows better approximation than HSDT theories. This shows again the importance of obtaining accurate stress resultant equations for laminated deep thick shells.

Table 7.9 shows the frequency parameter $\Omega = \omega a^2 \sqrt{\rho/E_2 h^2}$ for cross-ply cylindrical open shells obtained using a shear deformation theory with shallow shell assumptions (Reddy 1984a) and both deep thin and thick shell theories presented here (CST and SDST). The purpose of this comparison is to show how a shear deformation theory can yield inaccurate results when the term $(1 + z/R)$ term is neglected. As can be seen from the table, the thin shell (i.e., classical) theory presented here delivers accurate results for the thinner shell with thickness ratio of 100. This theory, however, was not able to deliver accurate results for the thicker shell with a thickness ratio of 10.

The theory of Reddy, which was derived based on the deep shell equations of Sander's but later ignored the term $(1 + z/R)$ in the stiffness parameters and introduced other assumptions, gave less accurate results for the deeper shells. When Reddy's equations are used with accurate stress resultant's equation, closer agreement for deep shells was obtained (Chang 1992).

7.3.2.1 Vibrations of thick cylindrical shells. Open and closed cylindrical shells are considered (Qatu 2004). For each of these shells, detailed studies of the curvature and thickness effects on the frequency parameters are conducted. The first 11 natural frequencies are listed for different a/mR ratios. It should be noted here that a particular

Table 7.9. Frequency parameter $\Omega = \omega a^2 \sqrt{\rho/E_2 h^2}$ for cross-ply cylindrical shallow shells ($a/b = 1$, $R_\beta/R_\alpha = 0$, $E_1/E_2 = 25$, $G_{12}/E_2 = 0.5$, $G_{13}/E_2 = 0.5$, $G_{23}/E_2 = 0.2$, $\nu_{12} = 0.25$, $K^2 = 5/6$) for cylindrical shells using shear deformation shallow shell theory (SDSST) of Reddy (1984a), shear deformation deep shell theory (SDST) and classical deep shell theory (CST) (Qatu 2004).

Theory	a/R	Lamination								
		[0°, 90°] Reddy (1984a)	SDST	CST	[0°, 90°, 0°] Reddy (1984a)	SDST	CST	[0°, 90°, 90°, 0°] Reddy (1984a)	SDST	CST
$a/h = 100$	0	9.6873	9.6873	9.6960	15.183	15.183	15.228	12.226	15.184	15.228
	0.1	11.831	11.841	11.851	16.625	16.613	16.667	16.634	16.625	16.677
	0.2	16.668	16.697	16.709	20.332	20.295	20.370	20.361	20.333	20.404
	0.5	34.914	31.330	31.489	36.770	36.629	36.787	36.858	36.761	36.908
	1.0	65.474	41.768	42.111	66.583	62.629	64.416	66.704	61.196	62.890
$a/h = 10$	0	8.8998	8.9001	9.6436	12.163	12.163	15.228	12.226	12.226	15.228
	0.1	8.8879	8.9479	9.6856	12.173	12.165	15.236	12.236	12.231	15.236
	0.2	8.9092	9.0286	9.7659	12.207	12.172	15.259	12.267	12.242	15.259
	0.5	9.1476	9.4577	10.222	12.438	12.223	15.415	12.471	12.317	15.421
	1.0	9.9986	10.667	11.520	13.172	12.421	15.915	13.128	12.592	15.935

shell configuration will yield frequencies for various m values. This is because of the repeated nature of the shear diaphragm boundary conditions at the nodal points. As was proven earlier, the half-sine mode shape can be treated as an independent shell configuration. The a/mR ratios studied vary between 0.5 and 8. A ratio of 0.5 represents a short shell and that of 8 represent a long one. As it is known, for shells having the ratio $a/mR_\beta < 0.5$, shell theories could yield inaccurate results because of end effects (Leissa 1973a). For each of the cases studied here the minimum natural frequency is underlined.

The nondimensional frequency parameter $\Omega = \omega R \sqrt{\rho/E_1}$ is used in the subsequent results. In the results obtained for laminated composite shells, the $[0^\circ, 90^\circ]$ lamination sequences are used in most of these results because it generally represents a shell with the maximum stretching–bending coupling effects. The graphite epoxy (G/E) material, which has high orthotropy ratio is used in all studies. Isotropic cylindrical shells were studied by Chang (1992) and Qatu (2004).

7.3.2.2 Effects of the thickness ratio. Comparison among shell theories made for isotropic closed cylindrical shells for various thickness ratios show that the difference between thin and thick shell theories is within 1% for thickness ratio of 20 and frequency parameters associated with $n = 0, 1, \dots, 5$ (Qatu 2004). For higher frequencies ($n > 5$), significant differences appear between both theories. Such differences reach 5% for $n = 10$ and shorter shells. Results are also presented for a thickness ratio of 5. While the accuracy of thick shell theory may be questionable in this range, the frequencies are listed for possible future comparisons with 3D analyses.

Table 7.10 lists the natural frequencies for $[0^\circ, 90^\circ]$ graphite/epoxy closed shell. These results are plotted in Figures 7.5 and 7.6 for long composite shells ($a/mR = 8$) and short ones ($a/mR = 0.5$), respectively. The results show clearly that gross error can occur when using CST especially for thicker and shorter shells. One important observation is that thin shell theory predicted a fundamental frequency at $n = 4$ for the short shells with a thickness ratio of 20. Thick shell theory predicted the fundamental frequency to be associated with $n = 5$ for such shells. For shorter shells, the fundamental frequency tends to occur at higher n values. It is worth noting that the fundamental mode occurs at $n = 2$ for longer shells, at $n = 3$ for intermediate shells, and at $n = 3$ or 4 for shorter shells.

7.3.2.3 Curvature effects on shells frequencies. Tables 7.11 and 7.12 present the natural frequencies of graphite/epoxy shells with a $[0^\circ, 90^\circ]$ lamination sequence and a thickness ratio (R/h) of 10 for closed and open shell configurations, respectively. Figure 7.7 shows the effect of varying the circumferential curvature (a/mR). Cylindrical shells with $[0^\circ, 90^\circ]$ lamination sequence and G/E materials are used.

Table 7.10. Comparisons among shell theories for $[0^\circ, 90^\circ]$ closed cylindrical shells $G_{12}/E_2 = 0.5$, $\nu_{12} = 0.3$ (Qatu 2004).

Theory	R_β/h	a/mR_β	n										
			0	1	2	3	4	5	6	7	8	9	10
CT	20	8	0.08908	0.04861	0.02743	0.05217	0.09813	0.15823	0.23177	0.31859	0.41861	0.53176	0.65795
		4	0.17816	0.11501	0.06398	0.06289	0.10140	0.15997	0.23315	0.31989	0.41990	0.53305	0.65924
		2	0.35633	0.23799	0.14609	0.11114	0.12399	0.17190	0.24126	0.32654	0.42594	0.53880	0.66485
		1	0.71266	0.44283	0.29705	0.22751	0.20855	0.23095	0.28502	0.36201	0.45682	0.56700	0.69137
		0.5	0.78908	0.69140	0.56195	0.48080	0.44477	0.44535	0.47644	0.53329	0.61211	0.71000	0.82492
SDT	20	8	0.08907	0.04850	0.02726	0.05180	0.09709	0.15575	0.22669	0.30930	0.40302	0.50726	0.62139
		4	0.17815	0.11490	0.06373	0.06239	0.10026	0.15740	0.22798	0.31050	0.40420	0.50843	0.62255
		2	0.35629	0.23783	0.14576	0.11047	0.12257	0.16900	0.23573	0.31675	0.40979	0.51367	0.62759
		1	0.71258	0.44180	0.29614	0.22619	0.20628	0.22690	0.27805	0.35049	0.43866	0.53959	0.65155
		0.5	0.77998	0.68421	0.55564	0.47389	0.43619	0.43405	0.46112	0.51230	0.58331	0.67076	0.77209
CT	10	8	0.08911	0.04810	0.04115	0.10098	0.19178	0.30881	0.45132	0.61884	0.81087	1.02687	1.26620
		4	0.17822	0.11386	0.07120	0.10845	0.19525	0.31151	0.45383	0.62128	0.81324	1.02916	1.26839
		2	0.35644	0.23644	0.15148	0.14888	0.21639	0.32633	0.46632	0.63268	0.82399	1.03936	1.27806
		1	0.71288	0.44995	0.31809	0.28021	0.31421	0.40272	0.53077	0.69013	0.87686	1.08886	1.32475
		0.5	0.92024	0.82358	0.72155	0.68285	0.69753	0.75633	0.85381	0.98615	1.15019	1.34327	1.56317
SDT	10	8	0.08907	0.04787	0.04057	0.09878	0.18492	0.29238	0.41839	0.56051	0.71644	0.88410	1.06163
		4	0.17815	0.11364	0.07039	0.10592	0.18807	0.29474	0.42053	0.56254	0.71838	0.88596	1.06341
		2	0.35629	0.23605	0.15033	0.14556	0.20804	0.30813	0.43137	0.57211	0.72715	0.89413	1.07108
		1	0.71258	0.44696	0.31433	0.27329	0.30084	0.37807	0.48809	0.62072	0.77029	0.93321	1.10697
		0.5	0.87845	0.78699	0.68362	0.63829	0.64250	0.68613	0.76206	0.86455	0.98873	1.13051	1.28659
SDT	5	8	0.08907	0.04668	0.06964	0.18006	0.32593	0.49617	0.68369	0.88327	1.09116	1.30470	1.52199
		4	0.17815	0.11145	0.09153	0.18649	0.32999	0.49952	0.68664	0.88592	1.09356	1.30688	1.52399
		2	0.35629	0.23444	0.16910	0.22425	0.35338	0.51725	0.70132	0.89857	1.10471	1.31684	1.53299
		1	0.71258	0.46932	0.37110	0.38351	0.47318	0.61117	0.77834	0.96382	1.16127	1.36670	1.57752
		0.5	1.07170	0.98124	0.91073	0.90474	0.94794	1.03049	1.14508	1.28503	1.44442	1.61838	1.80315

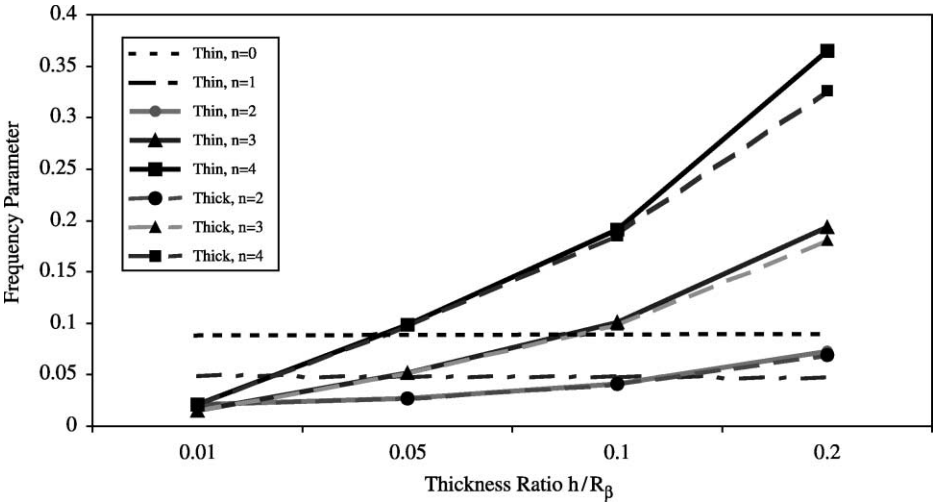


Figure 7.5. Thin *versus* thick shell theories for G/E [0°, 90°] closed cylindrical shells, $a/mR_\beta = 8$ (Qatu 2004).

7.4. CLOSED CYLINDRICAL SHELLS WITH ARBITRARY BOUNDARIES

The exact solution found and implemented for shallow shells and flat plates having two opposite edges simply supported and cross-ply lamination can be expanded to both open

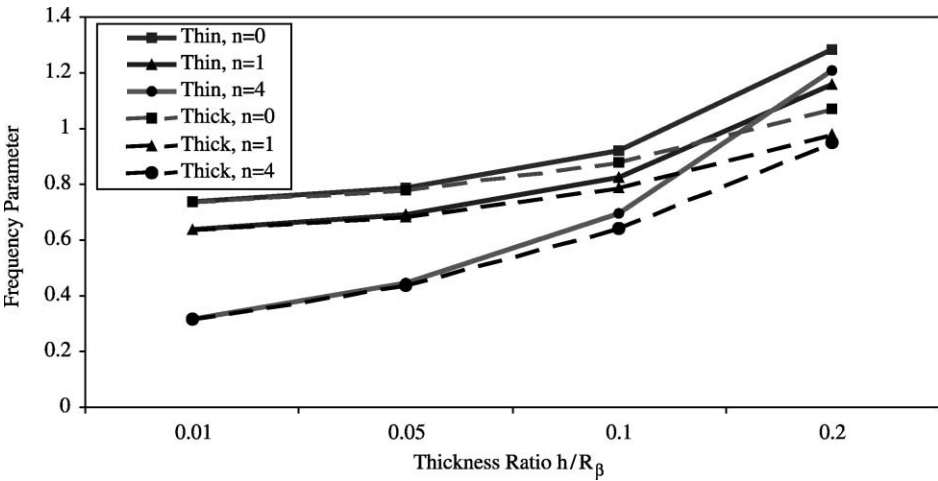


Figure 7.6. Thin *versus* thick shell theory for G/E [0°, 90°] closed cylindrical shells, $a/mR_\beta = 0.5$ (Qatu 2004).

Table 7.11. Natural frequency parameters for $[0^\circ, 90^\circ]$ graphite/epoxy closed barrel shells, $R_\beta/h = 10$.

a/R_α	a/mR_β	n										
		0	1	2	3	4	5	6	7	8	9	10
0	8	0.08907	0.04787	0.04057	0.09878	0.18492	0.29238	0.41839	0.56051	0.71644	0.88410	1.06163
	4	0.17815	0.11364	0.07039	0.10592	0.18807	0.29474	0.42053	0.56254	0.71838	0.88596	1.06341
	2	0.35629	0.23605	0.15033	0.14556	0.20804	0.30813	0.43137	0.57211	0.72715	0.89413	1.07108
	1	0.71258	0.44696	0.31433	0.27329	0.30084	0.37807	0.48809	0.62072	0.77029	0.93321	1.10697
	0.5	0.87845	0.78699	0.68362	0.63829	0.64250	0.68613	0.76206	0.86455	0.98873	1.13051	1.28659

Table 7.12. Natural frequency parameters for $[0^\circ, 90^\circ]$ graphite/epoxy open barrel shells, $b/R_\beta = 2.0$, $R_\beta/h = 10$.

a/R_α	a/mR_β	n										
		0	1	2	3	4	5	6	7	8	9	10
0	8	0.08907	0.03293	0.10955	0.25946	0.45710	0.69289	0.95840	1.24659	1.55182	1.86973	2.19697
	4	0.17815	0.08022	0.11561	0.26195	0.45921	0.69485	0.96023	1.24829	1.55340	1.87119	2.19834
	2	0.35629	0.17713	0.15107	0.27660	0.46961	0.70372	0.96818	1.25552	1.56003	1.87729	2.20397
	1	0.71258	0.35782	0.27342	0.35188	0.52365	0.74753	1.00581	1.28876	1.58986	1.90435	2.22871
	0.5	0.87840	0.72110	0.63609	0.66993	0.78854	0.96932	1.19515	1.45345	1.73534	2.03448	2.34631

and closed cylindrical shells. This exact solution will take the following form for closed cylindrical thin shells:

$$\begin{aligned}
 u_0(\alpha, \beta, t) &= \sum_{m=0}^M \sum_{n=0}^N U_{mn} X_m(\alpha) \sin(n\theta) \sin(\omega_{mn}t) \\
 v_0(\alpha, \beta, t) &= \sum_{m=0}^M \sum_{n=0}^N V_{mn} Y_m(\alpha) \cos(n\theta) \sin(\omega_{mn}t) \\
 w_0(\alpha, \beta, t) &= \sum_{m=0}^M \sum_{n=0}^N W_{mn} Z_m(\alpha) \sin(n\theta) \sin(\omega_{mn}t)
 \end{aligned} \tag{7.26}$$

where ω_{mn} is the natural frequency.

The above solution needs to be substituted into the equations of motion in terms of displacement. This will reduce the system of partial differential equations to that of ordinary differential equations. Any of the solution procedure described earlier for plates and shallow shells can be implemented to find the exact solution.

It should be noted here that the above solution will yield, as proven earlier, shear diaphragm boundary conditions at the longitudinal nodal lines. It is further observed that the vibrating shell segment will act as an independent shell with its own shear diaphragm boundaries. This important observation will enable us to break the shell into two halves at $\theta = 0$ and π and analyze only the upper (or lower) half with actual shear diaphragm boundaries at the cut edges. Approximate methods can then be used to analyze this half with algebraic polynomials in both the α and θ directions, as shown in Figure 7.8.

7.4.1 Comparison with exact solutions

We will use the Ritz method with algebraic polynomials and elastic constraints as described earlier to analyze closed cylindrical shells. We will first establish the accuracy of the described Ritz procedure in analyzing simply supported closed cylindrical shells.

E-glass/epoxy materials made of cross-ply $[0^\circ, 90^\circ, 0^\circ]$ laminates are chosen to perform a comparison among different analyses. Table 7.13 shows frequency parameters $\Omega = \omega a^2 \sqrt{\rho/E_1 h^2}$ obtained by various methods and theories. A shell of the dimensions $a = 2R$ and thickness $h = a/20$ is chosen for the analysis. Note that $b = \pi R$ for closed cylindrical shells. The maximum difference between CST and SDST is less than 1% for the fundamental frequency and less than 7% for the eighth frequency. Error is defined here as the percentage difference between the results obtained by CST and those obtained by the more accurate SDST. Interestingly, for higher frequency but lower number of half-sine waves, the difference between the two theories is less than some of the smaller frequencies with higher number of half-sine waves. This is expected as the contribution of the shear deformation becomes higher when the double half-sine waves get smaller in dimension.

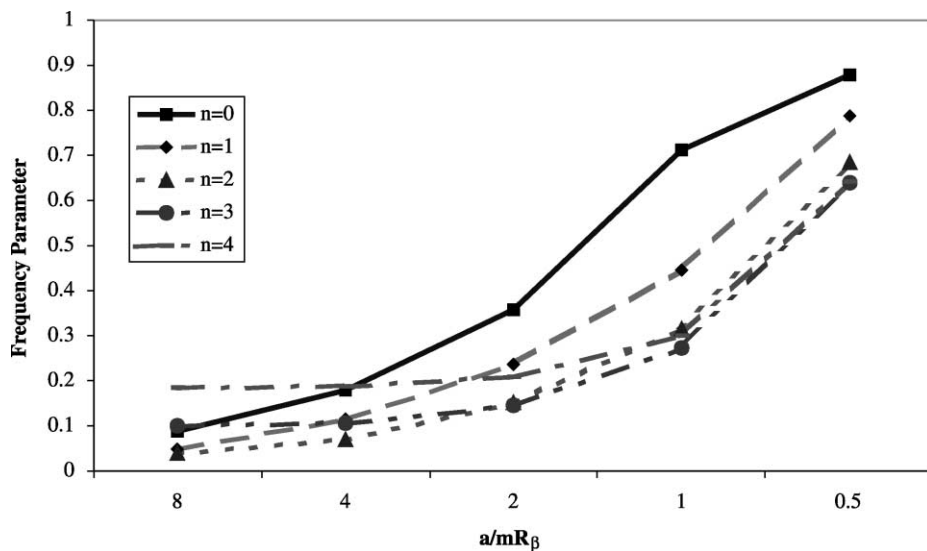


Figure 7.7. Curvature effects (a/mR) on frequency of $[0^\circ, 90^\circ]$ G/E closed cylindrical shells, $R/h = 10$ (Qatu 2004).

The Ritz method converged well for the lowest six frequencies. The difference between the Ritz analysis and the exact solution is less than 5% for these frequencies. Error is defined here as the percentage difference between the exact solution and the Ritz solution.

7.4.2 Convergence studies

Convergence studies are needed in a Ritz analysis to establish the number of terms that should be used to obtain accurate results. The same E-glass/epoxy materials and cross-ply

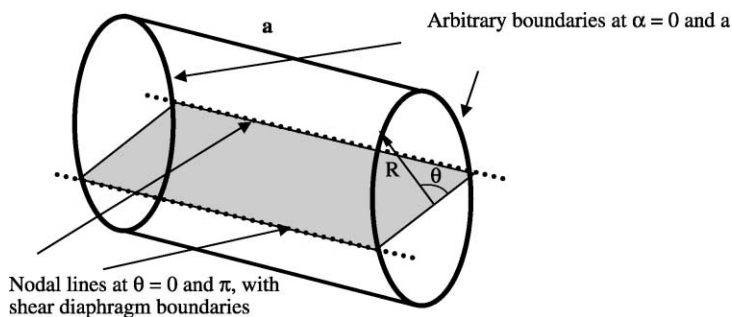


Figure 7.8. Closed cross-ply cylindrical shell with arbitrary boundaries.

Table 7.13. Frequency parameter $\Omega = \omega R \sqrt{\rho/E_1}$ of laminated closed cylindrical shell with shear diaphragm boundaries. $a/R = 2$, $[90^\circ, 0^\circ, 90^\circ]$ E-glass/epoxy, $a/h = 20$.

m	n	Exact SDST	Exact CST	Error (%)	Ritz CST	Error (%)
2	1	0.27433	0.276	0.68	0.28395	2.81
3	1	0.28798	0.295	2.40	0.30937	4.92
1	1	0.44506	0.445	0.05	0.44683	0.35
4	1	0.44390	0.463	4.41	0.46608	0.56
3	2	0.51782	0.531	2.47	0.53564	0.95
2	2	0.57139	0.577	1.04	0.58014	0.49
4	2	0.60392	0.632	4.70	0.69821	10.43
5	1	0.66958	0.715	6.76	0.73539	2.87
1	2	0.75211	0.756	0.50		
3	3	0.78224	0.810	3.55		

$[90^\circ, 0^\circ, 90^\circ]$ lamination, thickness ratio and length to radius ratio which were used in Section 7.4.1 are used here for the convergence studies. Table 7.14 lists the fundamental six frequency parameters for these closed shells. It is noted that except for a handful of frequencies, where the convergence was slow, the frequencies converge well to the exact solution with maximum difference less than 5% for most frequencies.

It should be noted here that convergence characteristics of the Ritz method with algebraic polynomials in vibration analysis of laminated shells is different than that experienced for plates or shallow shells. Convergence is observed to be faster for frequencies other than the fundamental frequency. Having lower frequencies for higher number of half-sine waves for these closed shells is thought to be the reason.

Another observation should be made here about ill conditioning. It starts to occur when higher number of terms are used. Ill conditioning manifests itself by giving higher frequencies for higher number of terms. As mentioned earlier, the Ritz method guarantees convergence of the frequencies from above. Meaning, as the number of terms increases, lower frequencies are expected. If higher frequencies are obtained, then that is due to ill conditioning. Ill conditioning can be improved with the use of orthogonal polynomials or by using higher precision computations. Inaccurate results are not reported.

7.4.3 Frequencies for cross-ply closed shells

Vibration studies are performed for the same shell described in Section 7.4.2 with a/R ratio of 2 and a/h ratio of 20. Three additional lamination sequences were studied. In particular, the lamination $[90^\circ]$, $[0^\circ]$, $[0^\circ, 90^\circ, 0^\circ]$ sequences were studied for all six boundary conditions. The results are listed in Table 7.15.

Table 7.14. Convergence of the frequency parameter $\Omega = \omega R \sqrt{\rho/E_1}$ of laminated closed cylindrical shell. $a/R = 2$, $[90^\circ, 0^\circ, 90^\circ]$ E-glass/epoxy, $a/h = 20$.

B.C.	DOF	1	2	3	4	5	6
SFSF	$3 \times 5 \times 5 = 75$	0.02195	0.02426	0.11487	0.13041	0.52173	0.58559
	$3 \times 6 \times 6 = 108$	0.02037	0.02364	0.11487	0.13027	0.27371	0.29661
	$3 \times 7 \times 7 = 147$	0.02036	0.02364	–	–	0.27371	0.29661
	Error (%)	0.02	0.00	0.00	0.11	0.00	0.00
SFSS	$3 \times 5 \times 5 = 75$	0.02305	0.11949	0.34910	0.39122	0.44299	0.63522
	$3 \times 6 \times 6 = 108$	0.02194	0.11944	0.28003	0.34910	0.39002	0.40414
	$3 \times 7 \times 7 = 147$	0.02193	–	0.27901	0.34910	0.38739	0.40221
	Error (%)	0.05	0.04	0.37	0.00	0.68	0.48
SSSS	$3 \times 5 \times 5 = 75$	0.28779	0.44581	0.44794	0.47114	0.58022	0.69821
	$3 \times 6 \times 6 = 108$	0.28777	0.33918	0.44683	0.46719	0.55548	0.69821
	$3 \times 7 \times 7 = 147$	0.28395	0.33903	–	0.46608	0.53564	–
	Error (%)	1.35	0.04	0.25	0.24	3.71	0.00
SSSC	$3 \times 5 \times 5 = 75$	0.32851	0.45514	0.63128	0.69821	0.71533	0.74887
	$3 \times 6 \times 6 = 108$	0.32314	0.45170	0.61809	0.63133	0.69820	0.74873
	$3 \times 7 \times 7 = 147$	0.32087	0.45167	0.57013	0.63062	0.69816	0.74868
	Error (%)	0.71	0.76	8.41	0.11	0.00	0.01
SCSF	$3 \times 5 \times 5 = 75$	0.16478	0.21858	0.34918	0.40494	0.56261	0.68067
	$3 \times 6 \times 6 = 108$	0.16474	0.21839	0.34910	0.40494	0.43584	0.68067
	$3 \times 7 \times 7 = 147$	0.15729	0.21838	0.34910	–	0.43307	–
	Error (%)	4.73	0.00	0.00	0.00	0.64	0.00
SCSC	$3 \times 5 \times 5 = 75$	0.34258	0.38502	0.46820	0.63169	0.69821	0.71567
	$3 \times 6 \times 6 = 108$	0.34246	0.38189	0.46820	0.61357	0.63091	0.69821
	$3 \times 7 \times 7 = 147$	0.33990	0.38176	–	0.61326	0.62921	–
	Error (%)	0.75	0.03	0.00	0.05	0.27	2.50

Note that for both laminates $[90^\circ]$, and $[90^\circ, 0^\circ, 90^\circ]$, more fibers are in the circumferential direction. For the second laminate, two thirds of the fibers are in the circumferential direction of the shell. These two-thirds are closer to the shell outer surfaces rather than the middle surface, which makes their contribution to the overall stiffness of the shell significant. Obviously, the $[90^\circ]$ laminate is stiffer and yields slightly higher frequencies. Both laminates, however, yield significantly higher frequencies than those of $[0^\circ]$ and $[0^\circ, 90^\circ, 0^\circ]$, where more fibers are in the longitudinal direction of the shell.

The second observation that needs to be made here is that the effect of the lamination is much higher for the free cylindrical shells than it is for the clamped one. The fundamental frequencies for the free cylindrical shells having $[90^\circ]$, and $[90^\circ, 0^\circ, 90^\circ]$

Table 7.15. Frequency parameters $\Omega = \omega R \sqrt{\rho/E_1}$ of laminated closed cylindrical shell with two opposite edges simply supported and the others arbitrary. $a/R = 2$, E-glass/epoxy, $a/h = 20$.

Lamination	B.C.	1	2	3	4	5	6
[90°]	FF	0.02060	0.02373	0.1043	0.1221	0.2808	0.3028
	FS	0.02209	0.1096	0.2868	0.3491	0.3680	0.3963
	SS	0.2685	0.3374	0.4338	0.4445	0.5440	0.5484
	SC	0.3114	0.3738	0.4444	0.5649	0.6252	0.6386
	CF	0.1499	0.2070	0.2932	0.3492	0.3878	0.4197
	CC	0.3383	0.3890	0.4722	0.6158	0.6342	0.6676
[0°]	FF	0.01314	0.02149	0.0666	0.0964	0.1792	0.2159
	FS	0.01747	0.07615	0.1895	0.3491	0.3712	0.3918
	SS	0.2892	0.2896	0.4232	0.4445	0.5550	0.5693
	SC	0.3254	0.3327	0.4453	0.6682	0.6982	0.7252
	CF	0.1489	0.2071	0.2260	0.3459	0.4046	0.4174
	CC	0.3448	0.3450	0.4502	0.6665	0.6744	0.6982
[0°, 90°, 0°]	FF	0.01351	0.02159	0.0684	0.0976	0.1894	0.2255
	FS	0.01770	0.07765	0.1988	0.3491	0.3724	0.3948
	SS	0.2856	0.2858	0.4389	0.4445	0.5574	0.5946
	SC	0.3334	0.3368	0.4593	0.6375	0.6862	0.6982
	CF	0.1454	0.2137	0.2247	0.3492	0.3610	0.4196
	CC	0.3493	0.3553	0.4680	0.6877	0.6982	0.7967

lamination sequence are about 50% higher than those of [0°], and [0°, 90°, 0°]. The impact of lamination on higher frequencies for FF shells is generally less than that on the fundamental frequencies but can still be significant for some frequencies like the third one. The impact of lamination on the second frequency is particularly smaller than other frequencies for these shells. Studies on the mode shapes will yield a better understanding of the reason.

The difference between various lamination sequences is much less for the clamped cylindrical shells. This difference between the stiffer [90°] laminate and the weaker [0°] one is about 10% for the first two frequencies of the simply supported shell and less than that for the higher frequencies. It is also worth mentioning how the simple supports at both ends introduce considerable stiffness to the shell. The frequencies obtained for the SS boundaries are closer to the SC and the stiffest CC boundaries than the CF boundary.

7.5. VIBRATIONS OF OPEN CYLINDRICAL SHELLS

Open cylindrical shells can have any combinations of boundary conditions that shallow shells or plates have. Cylindrical shells can have 12 possible classical boundary conditions

per edge. This yields numerous potential combinations of boundary conditions for open cylindrical shells. As was done previously for shallow shells, and unless stated otherwise, free will mean completely free (i.e., F4), clamped will mean completely clamped (i.e., C1) and simply supported will mean shear diaphragm boundaries (S2). Even with this simplification, we are not back to the 21 possible combinations of boundary conditions that a plate has. The reason is curvature. For example, a circular cylindrical shell that has a CFFF boundary (i.e., cantilever) will mean that the clamped edge is on the curved surface of the shell, which is considerably stiffer than the same shell having a FCFF boundary where the clamping is on the straight edge of the shell. These two boundary configurations (CFFF and FCFF) will yield the same results for flat plates and spherical shallow shells but will yield significantly different results for cylindrical shells.

7.5.1 Comparison with exact solutions

The accuracy of the Ritz method with elastic constraints used at $\alpha = a$ and $\beta = b$ will be established first for these open shells. Eq. (5.66) gives the energy functionals needed to treat such supports.

E-glass/epoxy materials made of cross-ply $[90^\circ, 0^\circ, 90^\circ]$ laminates are chosen to perform a comparison among different analyses. Table 7.16 shows a comparison among frequency parameters $\Omega = \omega a^2 \sqrt{\rho/E_1 h^2}$ obtained by various methods and theories for the analysis of such shells. This frequency parameter is chosen for the treatment of open cylindrical shells to allow for direct comparison between these shells and shallow shells as well as flat plates discussed in previous chapters. The maximum difference between CST and SDST is less than 1% for the fundamental frequency and less than 10% for the 10th frequency. Furthermore, the Ritz method converged well for the lowest six frequencies.

Table 7.16. Frequency parameter $\Omega = \omega a^2 \sqrt{\rho/E_1 h^2}$ of laminated cylindrical open shell with shear diaphragm boundaries. $a/b = 1$, $[90^\circ, 0^\circ, 90^\circ]$ E-glass/epoxy, $a/h = 20$, $a/R = 0.5$.

<i>m</i>	<i>n</i>	Exact SDST	Exact CST	Error (%)	Ritz CST	Error (%)
1	2	12.106	12.438	2.74	13.163	5.83
1	1	12.914	12.951	0.29	13.393	3.41
2	2	20.744	21.332	2.83	21.948	2.89
2	1	25.147	25.334	0.74	25.496	0.64
1	3	23.940	25.422	6.19	26.965	6.07
2	3	29.123	31.065	6.67	31.762	2.24
3	2	31.203	32.431	3.94	32.754	1.00
3	1	34.010	34.644	1.86	34.706	0.18
3	3	37.885	40.767	7.61		
4	2	43.431	45.133	3.92		

The observation made earlier about the Ritz method converging faster for some higher frequencies than it is for the lower ones is observed here as well. In particular, the convergence is observed to be slower when higher number of half-sine waves exist in the circumferential direction of the shell.

7.5.2 Convergence studies

Convergence studies are needed to establish the number of terms used to obtain accurate results. E-glass/epoxy materials and a typical lamination sequence $[30^\circ, -30^\circ, 30^\circ]$, aspect ratio (a/b) of 1.0, thickness ratio (a/h) of 20 and length to radius ratio (a/R) of 1.0 are used in the following convergence studies.

Seven boundary configurations representative of those to be encountered later are used in these convergence studies. The completely free (FFFF), simply supported (SSSS) and completely clamped (CCCC) boundary configurations are studied. In addition, the boundary conditions of cantilevered (CFFF), SFSF, CFCF and CSCS are analyzed.

Table 7.17 lists the fundamental frequency parameters for these seven boundary conditions. Equal number of terms in the α and β directions are used with equal terms for the inplane displacements and out of plane displacement. This led to a total number of terms of 75, 108 and 147 terms analyzed for convergence.

The first important observation is that ill conditioning starts to appear when the 147 terms solution is used. This is recognized either when the frequencies start to go higher, which contradicts the proven understanding of the Ritz method, or when the results are far off those obtained by the previous solution. Inaccurate results are not reported. It is thus seen that the most accurate solution can only be obtained with 108 terms.

Error is also reported in the table. It is defined as the percentage difference between the last two accurate solutions. For example, for the first frequency of the FFFF boundary, where accurate results were obtained with the 147-term solution, the error is defined as the percentage difference between the 147- and 108-term solutions. For the fourth frequency, error is defined as the percentage difference between the 108 and 75-term solutions. Most frequencies compared well with the 108-term solution. This 108-term solution is adopted for the detailed studies on the behavior of laminated composite cylindrical shells.

7.5.3 Frequencies for deep cylindrical shells

Having established the accuracy of the Ritz method for analyzing composite shells with simple support boundaries, the method will now be extended to analyze these shells when under different boundary conditions. Appendix D lists the fundamental six frequency parameters for three-layered $[\theta, -\theta, \theta]$ E-glass/epoxy cylindrical shells with $a/b = 1$, a thickness ratio (a/h) of 20, and curvature ratio (a/R) of 1.0. The Ritz method was used with algebraic polynomials having equal number of terms in the α and β directions, and

Table 7.17. Convergence of the frequency parameter $\Omega = \omega R \sqrt{\rho/E_1}$ of laminated open cylindrical shell with selected boundaries. $a/R = 1$, $[90^\circ, 0^\circ, 90^\circ]$ E-glass/epoxy, $a/h = 20$.

B.C.	DOF	1	2	3	4	5	6
FFFF	$3 \times 5 \times 5 = 75$	3.262	4.520	7.674	9.049	9.727	16.195
	$3 \times 6 \times 6 = 108$	3.251	4.435	7.668	9.049	9.599	12.856
	$3 \times 7 \times 7 = 147$	3.248	4.399	7.555	—	9.468	12.683
	Error (%)	0.07	0.80	1.49	0.00	1.38	1.36
CFFF	$3 \times 5 \times 5 = 75$	1.972	2.244	5.897	7.842	8.671	10.630
	$3 \times 6 \times 6 = 108$	1.972	2.244	5.848	7.842	8.671	10.630
	$3 \times 7 \times 7 = 147$	—	2.243	5.793	—	8.668	—
	Error (%)	0.00	0.04	0.94	0.00	0.04	0.00
SFSF	$3 \times 5 \times 5 = 75$	4.311	4.601	8.950	12.599	12.956	18.059
	$3 \times 6 \times 6 = 108$	4.311	4.601	8.984	12.631	12.848	16.549
	$3 \times 7 \times 7 = 147$	—	—	8.904	12.488	12.785	16.390
	Error (%)	0.00	0.00	0.90	1.15	0.49	0.97
CFCF	$3 \times 5 \times 5 = 75$	7.271	7.791	11.527	17.939	18.232	22.056
	$3 \times 6 \times 6 = 108$	7.154	7.737	11.497	17.354	17.745	18.539
	$3 \times 7 \times 7 = 147$	6.773	7.507	—	16.245	17.668	18.303
	Error (%)	5.63	3.07	0.26	6.83	0.44	1.29
SSSS	$3 \times 5 \times 5 = 75$	8.832	11.049	16.623	19.778	30.065	31.147
	$3 \times 6 \times 6 = 108$	9.040	11.096	16.823	19.430	21.472	28.245
	$3 \times 7 \times 7 = 147$	9.004	11.021	16.741	19.358	21.472	28.137
	Error (%)	0.39	0.68	0.49	0.37	0.00	0.38
CSCS	$3 \times 5 \times 5 = 75$	10.550	12.817	20.913	23.722	30.982	31.223
	$3 \times 6 \times 6 = 108$	10.550	12.817	20.890	21.610	24.408	31.223
	$3 \times 7 \times 7 = 147$	—	—	20.881	21.610	24.383	—
	Error (%)	0.00	0.00	0.04	0.00	0.10	0.00
CCCC	$3 \times 5 \times 5 = 75$	14.301	17.173	22.160	26.967	30.289	37.582
	$3 \times 6 \times 6 = 108$	14.301	16.849	21.957	26.431	30.289	37.582
	$3 \times 7 \times 7 = 147$	—	—	—	—	—	—
	Error (%)	0.00	1.92	0.92	2.03	0.00	0.00

equal terms for the displacements u_0 , v_0 , and w_0 . A total of 108 degrees of freedom (DOF), with six terms in each direction for each displacement function, were used in the analysis. The zero frequencies corresponding to rigid body modes for some boundary configurations are not listed.

It is interesting to see how curvature, fibers' orientation and boundary conditions interact. It is generally known that additional fixation will yield higher frequencies (note that the zero frequencies have to be accounted for here). Furthermore, fixation on a curved edge will result in higher frequencies when compared with fixation on a straight edge.

It is also observed that when more fibers, particularly those farther away from the shell's middle surface, are oriented in the circumferential direction of the shell yields higher frequencies. It is also found that when fibers are perpendicular to a fixed boundary, it yields higher frequencies than when they are parallel to that boundary. The previous two observations yield an interesting interaction between the impact of the boundary conditions, curvature and fiber orientation on the fundamental frequencies.

In general, deeper shells yield higher frequencies than shallower ones. There were some exceptions to this for some boundary configurations like SSFF, where shallower shells yielded slightly higher frequencies than deeper shells.

Among the important observation that should be reported are that maximum fundamental frequencies were obtained at different lamination angles for different boundary conditions. Maximum fundamental frequencies were obtained at 0° for CFFF, CSFF, CFSF, CFCF, CSCF, and CCCF boundaries. These were obtained at 15° for SFSF, SSSF, CSSF, CCSF, and SCSF conditions. Maximum fundamental frequencies were obtained at 45° for FFFF, SFFF, SSFF, CCFF, CSSS, CSCS and SSSS boundaries. CCCS, CSSS and CCSS yielded maximum fundamental frequencies at a lamination angle higher than 45° . In particular, the completely clamped shell was the only shell that gave maximum fundamental frequencies at 90° . Among the general conclusions that can be drawn from the above observation is that shells with the two opposite curved edges being simply supported or clamped tend to give maximum fundamental frequencies when the lamination angle is closer to 0° ; with the exception of CCCS, SSSS and completely clamped boundaries. Shells with two adjacent edges free tend to give maximum fundamental frequencies close to 45° . Minor deviations are found in these observations when the curvature is increased. In particular, the CSFF boundary gave maximum fundamental frequency at 0° for deeper shells and at 15° for shallower ones; both the CSSS and CSCS gave maximum fundamental frequencies at 45° for shallow shells and at 60° for deeper shells.

One should be careful when comparing the results in Appendix D with those in Appendix B for shallow shells. The results in Appendix B were obtained with $a/R_\alpha = 2.0$ and $a/R_\beta = 0$. Thus a CFFF boundary, for example, in Appendix B will mean that the clamped support is at the straight edge while the same boundary in Appendix D will mean that the clamped boundary is at the curved edge.

7.6. EQUATIONS AND ANALYSIS OF BARREL SHELLS

Barrel shells are essentially cylindrical shells for which the meridional direction of the shell has some initial curvature. The curvature may be due to imperfection in manufacturing, or is a part of the design as is the case in barrel shells.

Soedel (1993) presented a treatment to deal with isotropic barrel shells and simplified equations were derived. Barrel shells are treated as a special case of shells of revolution in which the angle that the radius of curvature along the shell direction makes with the center of revolution axis is close to 90° . This simplified the equations and introduced constant Lamé parameters. This approach to the treatment of barrel shells is adopted here. A similar approach was adopted earlier using shallow shell theory (McElman and Knoell 1971). A more general approach to the analysis of shells of revolution can be found in Suzuki *et al.* (1995a,b).

7.6.1 Thin barrel shells

We will first treat thin barrel shells. Thick shells will be considered next.

7.6.1.1 Fundamental equations. Consider a shell of revolution as shown in Figure 7.1, and the associated fundamental form of Eqs. (7.1) and (7.2). For barrel shells of revolution (Figure 7.1), the angle ϕ is assumed to vary between 75 and 105° . Thus, the following approximation is reasonable

$$\sin(\phi) \approx 1 \quad (7.27a)$$

Keeping the curvilinear coordinates, the fundamental form can then be approximated as

$$A = 1, \quad B \approx 1 \quad (7.27b)$$

Based on these assumptions, we will only be able to consider barrel shells that have a small length to curvature ratio in the α -direction (i.e., $|a/R_\alpha| \leq 0.5$). Note that R_α can be a negative value. There is a geometric constraint for shells having negative R_α , and that is $|R_\alpha(1 - \cos(a/2R_\alpha))| > R_\beta$. This is necessary for the shell surfaces to remain non-intersecting.

For the case of open shells (Figure 7.9), the shell might have an initial pretwist. The radius of twist ($R_{\alpha\beta}$) is included in the development of the equations.

With constant and unit Lamé parameters, midsurface strains can be simplified from Eq. (2.53) and expressed as

$$\begin{aligned} \varepsilon_\alpha^0 &= \frac{\partial u_0}{\partial \alpha} + \frac{w_0}{R_\alpha} \\ \varepsilon_\beta^0 &= \frac{\partial v_0}{\partial \beta} + \frac{w_0}{R_\beta} \\ \gamma_{\alpha\beta}^0 &= \frac{\partial v_0}{\partial \alpha} + \frac{\partial u_0}{\partial \beta} + \frac{2w_0}{R_{\alpha\beta}} \end{aligned} \quad (7.28)$$

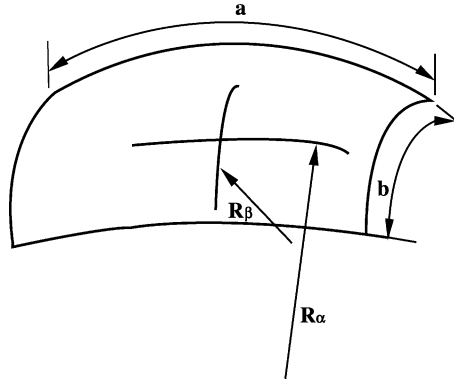


Figure 7.9. Open barrel shell.

Curvature changes can be written as

$$\begin{aligned}
 k_\alpha &= \frac{\partial}{\partial \alpha} \left(\frac{u_0}{R_\alpha} + \frac{v_0}{R_{\alpha\beta}} - \frac{\partial w_0}{\partial \alpha} \right) \\
 k_\beta &= \frac{\partial}{\partial \beta} \left(\frac{u_0}{R_{\alpha\beta}} + \frac{v_0}{R_\beta} - \frac{\partial w_0}{\partial \beta} \right) \\
 \tau &= \frac{\partial}{\partial \alpha} \left(\frac{u_0}{R_{\alpha\beta}} + \frac{v_0}{R_\beta} - \frac{\partial w_0}{\partial \beta} \right) + \frac{\partial}{\partial \beta} \left(\frac{v_0}{R_{\alpha\beta}} + \frac{u_0}{R_\alpha} - \frac{\partial w_0}{\partial \alpha} \right)
 \end{aligned} \tag{7.29}$$

Force and moment resultants for thin shells derived in Chapter 2 (Eqs. (2.64) and (2.65)) and applied to plates, shallow shells and cylindrical shells also apply for barrel thin shells.

Deleting the body couples, the reduced equations of motion become (for unit values of the Lamé parameters A and B)

$$\begin{aligned}
 \frac{\partial N_\alpha}{\partial \alpha} + \frac{\partial N_{\alpha\beta}}{\partial \beta} + \frac{1}{R_\alpha} \left[\frac{\partial M_\alpha}{\partial \alpha} + \frac{\partial M_{\alpha\beta}}{\partial \beta} \right] + \frac{1}{R_{\alpha\beta}} \left[\frac{\partial M_\beta}{\partial \beta} + \frac{\partial M_{\alpha\beta}}{\partial \alpha} \right] + p_\alpha &= -\rho \frac{\partial^2 u_0}{\partial t^2} \\
 \frac{\partial N_\beta}{\partial \beta} + \frac{\partial N_{\alpha\beta}}{\partial \alpha} + \frac{1}{R_{\alpha\beta}} \left[\frac{\partial M_\alpha}{\partial \alpha} + \frac{\partial M_{\alpha\beta}}{\partial \beta} \right] + \frac{1}{R_\beta} \left[\frac{\partial M_\beta}{\partial \beta} + \frac{\partial M_{\alpha\beta}}{\partial \alpha} \right] + p_\beta &= -\rho \frac{\partial^2 v_0}{\partial t^2} \\
 - \left(\frac{2N_{\alpha\beta}}{R_{\alpha\beta}} + \frac{N_\alpha}{R_\alpha} + \frac{N_\beta}{R_\beta} \right) + \frac{\partial^2 M_\alpha}{\partial \alpha^2} + 2 \frac{\partial^2 M_{\alpha\beta}}{\partial \beta \partial \alpha} + \frac{\partial^2 M_\beta}{\partial \beta^2} + p_n &= -\rho \frac{\partial^2 w_0}{\partial t^2}
 \end{aligned} \tag{7.30}$$

The above equations can be written in terms of displacement yielding Eq. (5.10), with the L_{ij} differential operators

$$\begin{aligned}
 L_{11} &= \left\{ A_{11} + 2\frac{B_{11}}{R_\alpha} + 2\frac{B_{16}}{R_{\alpha\beta}} + \frac{D_{11}}{R_\alpha^2} + 2\frac{D_{16}}{R_\alpha R_{\alpha\beta}} + \frac{D_{66}}{R_{\alpha\beta}^2} \right\} \frac{\partial^2}{\partial \alpha^2} \\
 &+ \left\{ 2A_{16} + 2\frac{(B_{12} + B_{66})}{R_{\alpha\beta}} + 4\frac{B_{16}}{R_\alpha} + 2\frac{(D_{12} + D_{66})}{R_\alpha R_{\alpha\beta}} + 2\frac{D_{16}}{R_\alpha^2} + 2\frac{D_{26}}{R_{\alpha\beta}^2} \right\} \frac{\partial^2}{\partial \alpha \partial \beta} \\
 &+ \left\{ A_{66} + 2\frac{B_{66}}{R_\alpha} + 2\frac{B_{26}}{R_{\alpha\beta}} + \frac{D_{66}}{R_\alpha^2} + 2\frac{D_{26}}{R_\alpha R_{\alpha\beta}} + \frac{D_{22}}{R_{\alpha\beta}^2} \right\} \frac{\partial^2}{\partial \beta^2} \\
 L_{12} = L_{21} &= \left\{ A_{16} + \frac{(B_{11} + B_{66})}{R_{\alpha\beta}} + \frac{B_{16}}{R_\beta} + \frac{B_{16}}{R_\alpha} + \frac{D_{11}}{R_\alpha R_{\alpha\beta}} + \frac{D_{16}}{R_\alpha R_\beta} + \frac{D_{16}}{R_{\alpha\beta}^2} \right. \\
 &+ \left. \frac{D_{66}}{R_\beta R_{\alpha\beta}} \right\} \frac{\partial^2}{\partial \alpha^2} + \left\{ (A_{12} + A_{66}) + \frac{(B_{12} + B_{66})}{R_\beta} + \frac{(B_{12} + B_{66})}{R_\alpha} \right. \\
 &+ 2\frac{(B_{16} + B_{26})}{R_{\alpha\beta}} + \frac{(D_{12} + D_{66})}{R_\alpha R_\beta} + \frac{(D_{12} + D_{66})}{R_{\alpha\beta}^2} + 2\frac{D_{26}}{R_\beta R_{\alpha\beta}} \\
 &+ 2\frac{D_{16}}{R_\alpha R_{\alpha\beta}} \left. \right\} \frac{\partial^2}{\partial \alpha \partial \beta} + \left\{ A_{26} + \frac{(B_{22} + B_{66})}{R_{\alpha\beta}} + \frac{B_{26}}{R_\beta} + \frac{B_{26}}{R_\alpha} \right. \\
 &+ \left. \frac{D_{66}}{R_\alpha R_{\alpha\beta}} + \frac{D_{26}}{R_\alpha R_\beta} + \frac{D_{26}}{R_{\alpha\beta}^2} + \frac{D_{22}}{R_\beta R_{\alpha\beta}} \right\} \frac{\partial^2}{\partial \beta^2} \\
 L_{22} &= \left\{ A_{66} + 2\frac{B_{66}}{R_\beta} + 2\frac{B_{16}}{R_{\alpha\beta}} + \frac{D_{66}}{R_\beta^2} + 2\frac{D_{16}}{R_\beta R_{\alpha\beta}} + \frac{D_{11}}{R_{\alpha\beta}^2} \right\} \frac{\partial^2}{\partial \alpha^2} \\
 &+ \left\{ 2A_{26} + 2\frac{(B_{12} + B_{66})}{R_{\alpha\beta}} + 4\frac{B_{26}}{R_\beta} + 2\frac{(D_{12} + D_{66})}{R_\beta R_{\alpha\beta}} + 2\frac{D_{26}}{R_\beta^2} + 2\frac{D_{16}}{R_{\alpha\beta}^2} \right\} \frac{\partial^2}{\partial \alpha \partial \beta} \\
 &+ \left\{ A_{22} + 2\frac{B_{22}}{R_\beta} + 2\frac{B_{26}}{R_{\alpha\beta}} + \frac{D_{66}}{R_{\alpha\beta}^2} + 2\frac{D_{26}}{R_\beta R_{\alpha\beta}} + \frac{D_{22}}{R_\beta^2} \right\} \frac{\partial^2}{\partial \beta^2} \\
 L_{13} = L_{31} &= \left\{ -B_{11} - \frac{D_{11}}{R_\alpha} - \frac{D_{16}}{R_{\alpha\beta}} \right\} \frac{\partial^3}{\partial \alpha^3} + \left\{ -B_{26} - \frac{D_{26}}{R_\alpha} - \frac{D_{22}}{R_{\alpha\beta}} \right\} \frac{\partial^3}{\partial \beta^3} \\
 &+ \left\{ -3B_{16} - 3\frac{D_{16}}{R_\alpha} - \frac{(D_{12} + 2D_{66})}{R_{\alpha\beta}} \right\} \frac{\partial^3}{\partial \alpha^2 \partial \beta} \\
 &+ \left\{ -(B_{12} + 2B_{66}) - 3\frac{D_{26}}{R_{\alpha\beta}} - \frac{(D_{12} + 2D_{66})}{R_\alpha} \right\} \frac{\partial^3}{\partial \alpha \partial \beta^2} \\
 &+ \left\{ \frac{A_{11}}{R_\alpha} + \frac{A_{12}}{R_\beta} + 2\frac{A_{16}}{R_{\alpha\beta}} + \frac{B_{11}}{R_\alpha^2} + 2\frac{B_{66}}{R_{\alpha\beta}^2} + 3\frac{B_{16}}{R_\alpha R_{\alpha\beta}} + \frac{B_{26}}{R_\beta R_{\alpha\beta}} + \frac{B_{12}}{R_\alpha R_\beta} \right\} \frac{\partial}{\partial \alpha}
 \end{aligned}$$

$$\begin{aligned}
& + \left\{ \frac{A_{16}}{R_\alpha} + \frac{A_{26}}{R_\beta} + 2 \frac{A_{66}}{R_{\alpha\beta}} + \frac{(2B_{66} + B_{12})}{R_\alpha R_{\alpha\beta}} + \frac{B_{22}}{R_\beta R_{\alpha\beta}} + \frac{B_{16}}{R_\alpha^2} + 2 \frac{B_{26}}{R_{\alpha\beta}^2} + \frac{B_{26}}{R_\alpha R_\beta} \right\} \frac{\partial}{\partial \beta} \\
L_{23} = L_{32} = & \left\{ -B_{16} - \frac{D_{11}}{R_{\alpha\beta}} - \frac{D_{16}}{R_\beta} \right\} \frac{\partial^3}{\partial \alpha^3} + \left\{ -B_{22} - \frac{D_{26}}{R_{\alpha\beta}} - \frac{D_{22}}{R_\beta} \right\} \frac{\partial^3}{\partial \beta^3} \\
& + \left\{ -3B_{26} - 3 \frac{D_{26}}{R_\beta} - \frac{(D_{12} + 2D_{66})}{R_{\alpha\beta}} \right\} \frac{\partial^3}{\partial \alpha \partial \beta^2} \\
& + \left\{ -(B_{12} + 2B_{66}) - 3 \frac{D_{16}}{R_{\alpha\beta}} - \frac{(D_{12} + 2D_{66})}{R_\beta} \right\} \frac{\partial^3}{\partial \alpha^2 \partial \beta} \\
& + \left\{ \frac{A_{16}}{R_\alpha} + \frac{A_{26}}{R_\beta} + 2 \frac{A_{66}}{R_{\alpha\beta}} + \frac{B_{11}}{R_\alpha R_{\alpha\beta}} + \frac{(B_{12} + 2B_{66})}{R_\beta R_{\alpha\beta}} + \frac{B_{26}}{R_\beta^2} \right. \\
& + 2 \frac{B_{16}}{R_{\alpha\beta}^2} + \frac{B_{16}}{R_\alpha R_\beta} \left. \right\} \frac{\partial}{\partial \alpha} + \left\{ \frac{A_{12}}{R_\alpha} + \frac{A_{22}}{R_\beta} + \frac{A_{26}}{R_{\alpha\beta}} + \frac{B_{16}}{R_\alpha R_{\alpha\beta}} \right. \\
& + 3 \frac{B_{26}}{R_\beta R_{\alpha\beta}} + \frac{B_{22}}{R_\beta^2} + 2 \frac{B_{66}}{R_{\alpha\beta}^2} + \frac{B_{12}}{R_\alpha R_\beta} \left. \right\} \frac{\partial}{\partial \beta} \\
L_{33} = & \left\{ D_{11} \frac{\partial^4}{\partial \alpha^4} + 4D_{16} \frac{\partial^4}{\partial \alpha^3 \partial \beta} + 2(D_{12} + 2D_{66}) \frac{\partial^4}{\partial \alpha^2 \partial \beta^2} + 4D_{26} \frac{\partial^4}{\partial \alpha \partial \beta^3} + D_{22} \frac{\partial^4}{\partial \beta^4} \right\} \\
& - 2 \left\{ \left(\frac{B_{11}}{R_\alpha} + \frac{B_{12}}{R_\beta} + 2 \frac{B_{16}}{R_{\alpha\beta}} \right) \frac{\partial^2}{\partial \alpha^2} + 2 \left(\frac{B_{16}}{R_\alpha} + \frac{A_{26}}{R_\beta} + 2 \frac{B_{66}}{R_{\alpha\beta}} \right) \frac{\partial^2}{\partial \alpha \partial \beta} \right. \\
& + \left. \left(\frac{B_{12}}{R_\alpha} + \frac{B_{22}}{R_\beta} + 2 \frac{B_{26}}{R_{\alpha\beta}} \right) \frac{\partial^2}{\partial \beta^2} \right\} + \left\{ \frac{A_{11}}{R_\alpha^2} + 2 \frac{A_{12}}{R_\alpha R_\beta} + \frac{A_{22}}{R_\beta^2} + 4 \left(\frac{A_{16}}{R_{\alpha\beta} R_\alpha} + \frac{A_{26}}{R_{\alpha\beta} R_\beta} + \frac{A_{66}}{R_{\alpha\beta}^2} \right) \right\} \\
& \quad \quad \quad (7.31)
\end{aligned}$$

Conducting the proper substitutions in the general thin shell equations to specialize them to those for barrel shells (Qatu 1999b), the strain energy may be expressed in Eqs. (5.12) and (5.13) ($U = U_s + U_b + U_{bs}$) where U_s is the part due to stretching alone,

$$\begin{aligned}
U_s = & \frac{1}{2} \int_A \left\{ A_{11} \left(\frac{\partial u_0}{\partial \alpha} + \frac{w_0}{R_\alpha} \right)^2 + A_{22} \left(\frac{\partial v_0}{\partial \beta} + \frac{w_0}{R_\beta} \right)^2 + A_{66} \left(\frac{\partial v_0}{\partial \alpha} + \frac{\partial u_0}{\partial \beta} + \frac{2w_0}{R_{\alpha\beta}} \right)^2 \right. \\
& + 2A_{12} \left(\frac{\partial u_0}{\partial \alpha} + \frac{w_0}{R_\alpha} \right) \left(\frac{\partial v_0}{\partial \beta} + \frac{w_0}{R_\beta} \right) + 2A_{16} \left(\frac{\partial u_0}{\partial \alpha} + \frac{w_0}{R_\alpha} \right) \left(\frac{\partial v_0}{\partial \alpha} + \frac{\partial u_0}{\partial \beta} + \frac{2w_0}{R_{\alpha\beta}} \right) \\
& + 2A_{26} \left(\frac{\partial v_0}{\partial \beta} + \frac{w_0}{R_\beta} \right) \left(\frac{\partial v_0}{\partial \alpha} + \frac{\partial u_0}{\partial \beta} + \frac{2w_0}{R_{\alpha\beta}} \right) \left. \right\} dA \\
& \quad \quad \quad (7.32)
\end{aligned}$$

U_b is the part due to bending alone,

$$\begin{aligned}
 U_b = \frac{1}{2} \int_A \bigg\{ & D_{11} \left(\frac{\partial}{\partial \alpha} \left(\frac{u_0}{R_\alpha} + \frac{v_0}{R_{\alpha\beta}} - \frac{\partial w_0}{\partial \alpha} \right) \right)^2 + D_{22} \left(\frac{\partial}{\partial \beta} \left(\frac{u_0}{R_{\alpha\beta}} + \frac{v_0}{R_\beta} - \frac{\partial w_0}{\partial \beta} \right) \right)^2 \\
 & + D_{66} \left(\frac{\partial}{\partial \alpha} \left(\frac{u_0}{R_{\alpha\beta}} + \frac{v_0}{R_\beta} - \frac{\partial w_0}{\partial \beta} \right) + \frac{\partial}{\partial \beta} \left(\frac{v_0}{R_{\alpha\beta}} + \frac{u_0}{R_\alpha} - \frac{\partial w_0}{\partial \alpha} \right) \right)^2 \\
 & + 2D_{12} \left\{ \frac{\partial}{\partial \alpha} \left(\frac{u_0}{R_\alpha} + \frac{v_0}{R_{\alpha\beta}} - \frac{\partial w_0}{\partial \alpha} \right) \times \frac{\partial}{\partial \beta} \left(\frac{u_0}{R_{\alpha\beta}} + \frac{v_0}{R_\beta} - \frac{\partial w_0}{\partial \beta} \right) \right\} \\
 & + 2D_{16} \left(\frac{\partial}{\partial \alpha} \left(\frac{u_0}{R_\alpha} + \frac{v_0}{R_{\alpha\beta}} - \frac{\partial w_0}{\partial \alpha} \right) \right) \\
 & \times \left\{ \frac{\partial}{\partial \alpha} \left(\frac{u_0}{R_{\alpha\beta}} + \frac{v_0}{R_\beta} - \frac{\partial w_0}{\partial \beta} \right) + \frac{\partial}{\partial \beta} \left(\frac{v_0}{R_{\alpha\beta}} + \frac{u_0}{R_\alpha} - \frac{\partial w_0}{\partial \alpha} \right) \right\} \\
 & + 2D_{26} \left(\frac{\partial}{\partial \beta} \left(\frac{u_0}{R_{\alpha\beta}} + \frac{v_0}{R_\beta} - \frac{\partial w_0}{\partial \beta} \right) \right) \\
 & \left. \left\{ \frac{\partial}{\partial \alpha} \left(\frac{u_0}{R_{\alpha\beta}} + \frac{v_0}{R_\beta} - \frac{\partial w_0}{\partial \beta} \right) + \frac{\partial}{\partial \beta} \left(\frac{v_0}{R_{\alpha\beta}} + \frac{u_0}{R_\alpha} - \frac{\partial w_0}{\partial \alpha} \right) \right\} \right\} dA \quad (7.33)
 \end{aligned}$$

and U_{bs} is the part due to bending–stretching coupling,

$$\begin{aligned}
 U_{bs} = - \int_A \bigg\{ & B_{11} \left(\frac{\partial u_0}{\partial \alpha} + \frac{w_0}{R_\alpha} \right) \frac{\partial}{\partial \alpha} \left(\frac{u_0}{R_\alpha} + \frac{v_0}{R_{\alpha\beta}} - \frac{\partial w_0}{\partial \alpha} \right) + B_{22} \left(\frac{\partial v_0}{\partial \beta} + \frac{w_0}{R_\beta} \right) \frac{\partial}{\partial \beta} \left(\frac{u_0}{R_{\alpha\beta}} + \frac{v_0}{R_\beta} - \frac{\partial w_0}{\partial \beta} \right) \\
 & + B_{66} \left(\frac{\partial v_0}{\partial \alpha} + \frac{\partial u_0}{\partial \beta} + \frac{2w_0}{R_{\alpha\beta}} \right) \left\{ \frac{\partial}{\partial \alpha} \left(\frac{u_0}{R_{\alpha\beta}} + \frac{v_0}{R_\beta} - \frac{\partial w_0}{\partial \beta} \right) + \frac{\partial}{\partial \beta} \left(\frac{v_0}{R_{\alpha\beta}} + \frac{u_0}{R_\alpha} - \frac{\partial w_0}{\partial \alpha} \right) \right\} \\
 & + B_{12} \left[\left(\frac{\partial u_0}{\partial \alpha} + \frac{w_0}{R_\alpha} \right) \frac{\partial}{\partial \beta} \left(\frac{u_0}{R_{\alpha\beta}} + \frac{v_0}{R_\beta} - \frac{\partial w_0}{\partial \beta} \right) + \left(\frac{\partial v_0}{\partial \beta} + \frac{w_0}{R_\beta} \right) \frac{\partial}{\partial \alpha} \left(\frac{u_0}{R_\alpha} + \frac{v_0}{R_{\alpha\beta}} - \frac{\partial w_0}{\partial \alpha} \right) \right] \\
 & + B_{16} \left[\left(\frac{\partial u_0}{\partial \alpha} + \frac{w_0}{R_\alpha} \right) \left\{ \frac{\partial}{\partial \alpha} \left(\frac{u_0}{R_{\alpha\beta}} + \frac{v_0}{R_\beta} - \frac{\partial w_0}{\partial \beta} \right) + \frac{\partial}{\partial \beta} \left(\frac{v_0}{R_{\alpha\beta}} + \frac{u_0}{R_\alpha} - \frac{\partial w_0}{\partial \alpha} \right) \right\} \right. \\
 & \quad \left. + \left(\frac{\partial v_0}{\partial \alpha} + \frac{\partial u_0}{\partial \beta} + \frac{2w_0}{R_{\alpha\beta}} \right) \frac{\partial}{\partial \alpha} \left(\frac{u_0}{R_\alpha} + \frac{v_0}{R_{\alpha\beta}} - \frac{\partial w_0}{\partial \alpha} \right) \right] \\
 & + B_{26} \left[\left(\frac{\partial v_0}{\partial \beta} + \frac{w_0}{R_\beta} \right) \left\{ \frac{\partial}{\partial \alpha} \left(\frac{u_0}{R_{\alpha\beta}} + \frac{v_0}{R_\beta} - \frac{\partial w_0}{\partial \beta} \right) + \frac{\partial}{\partial \beta} \left(\frac{v_0}{R_{\alpha\beta}} + \frac{u_0}{R_\alpha} - \frac{\partial w_0}{\partial \alpha} \right) \right\} \right. \\
 & \quad \left. + \left(\frac{\partial v_0}{\partial \alpha} + \frac{\partial u_0}{\partial \beta} + \frac{2w_0}{R_{\alpha\beta}} \right) \frac{\partial}{\partial \beta} \left(\frac{u_0}{R_{\alpha\beta}} + \frac{v_0}{R_\beta} - \frac{\partial w_0}{\partial \beta} \right) \right] \bigg\} dA \quad (7.34)
 \end{aligned}$$

The work done by the external forces W and the kinetic energy equations are similar to those derived earlier for thin cylindrical shells. Therefore, the total potential energy of the shell in its deformed shape is $\Pi = U - W$.

7.6.1.2 Simply supported cross-ply thin barrel shells. Consider a barrel shell that is made of a cross-ply laminate, and assume the radius of twist to be infinity, (i.e., $R_{\alpha\beta} = \infty$). The differential parameters L_{ij} in the Eq. (7.31) become

$$\begin{aligned}
 L_{11} &= \left\{ A_{11} + 2 \frac{B_{11}}{R_\alpha} + \frac{D_{11}}{R_\alpha^2} \right\} \frac{\partial^2}{\partial \alpha^2} + \left\{ A_{66} + 2 \frac{B_{66}}{R_\alpha} + \frac{D_{66}}{R_\alpha^2} \right\} \frac{\partial^2}{\partial \beta^2} \\
 L_{12} = L_{21} &= \left\{ (A_{12} + A_{66}) + \frac{(B_{12} + B_{66})}{R_\beta} + \frac{(B_{12} + B_{66})}{R_\alpha} + \frac{(D_{12} + D_{66})}{R_\alpha R_\beta} \right\} \frac{\partial^2}{\partial \alpha \partial \beta} \\
 L_{22} &= \left\{ A_{66} + 2 \frac{B_{66}}{R_\beta} + \frac{D_{66}}{R_\beta^2} \right\} \frac{\partial^2}{\partial \alpha^2} + \left\{ A_{22} + 2 \frac{B_{22}}{R_\beta} + \frac{D_{22}}{R_\beta^2} \right\} \frac{\partial^2}{\partial \beta^2} \\
 L_{13} = L_{31} &= - \left\{ B_{11} + \frac{D_{11}}{R_\alpha} \right\} \frac{\partial^3}{\partial \alpha^3} - \left\{ (B_{12} + 2B_{66}) + \frac{(D_{12} + 2D_{66})}{R_\alpha} \right\} \frac{\partial^3}{\partial \alpha \partial \beta^2} \\
 &\quad + \left\{ \frac{A_{11}}{R_\alpha} + \frac{A_{12}}{R_\beta} + \frac{B_{11}}{R_\alpha^2} + \frac{B_{12}}{R_\alpha R_\beta} \right\} \frac{\partial}{\partial \alpha} \\
 L_{23} = L_{32} &= - \left\{ B_{22} + \frac{D_{22}}{R_\beta} \right\} \frac{\partial^3}{\partial \beta^3} - \left\{ (B_{12} + 2B_{66}) + \frac{(D_{12} + 2D_{66})}{R_\beta} \right\} \frac{\partial^3}{\partial \alpha^2 \partial \beta} \\
 &\quad + \left\{ \frac{A_{12}}{R_\alpha} + \frac{A_{22}}{R_\beta} + \frac{B_{22}}{R_\beta^2} + \frac{B_{12}}{R_\alpha R_\beta} \right\} \frac{\partial}{\partial \beta} \\
 L_{33} &= \left\{ D_{11} \frac{\partial^4}{\partial \alpha^4} + 2(D_{12} + 2D_{66}) \frac{\partial^4}{\partial \alpha^2 \partial \beta^2} + D_{22} \frac{\partial^4}{\partial \beta^4} \right\} \\
 &\quad - 2 \left\{ \left(\frac{B_{11}}{R_\alpha} + \frac{B_{12}}{R_\beta} \right) \frac{\partial^2}{\partial \alpha^2} + \left(\frac{B_{12}}{R_\alpha} + \frac{B_{22}}{R_\beta} \right) \frac{\partial^2}{\partial \beta^2} \right\} + \left\{ \frac{A_{11}}{R_\alpha^2} + 2 \frac{A_{12}}{R_\alpha R_\beta} + \frac{A_{22}}{R_\beta^2} \right\}
 \end{aligned} \tag{7.35}$$

Consider an open barrel shell, with shear diaphragm (S2) boundaries on all four edges (Eq. (2.74)). Eq. (5.38) presents a solution that satisfies both the boundary conditions and the equations of motion exactly. Substitute Eq. (5.38) into the equations of motion would result in Eq. (5.40), where

$$\begin{aligned}
 C_{11} &= - \left\{ A_{11} + 2 \frac{B_{11}}{R_\alpha} + \frac{D_{11}}{R_\alpha^2} \right\} \alpha_m^2 - \left\{ A_{66} + 2 \frac{B_{66}}{R_\alpha} + \frac{D_{66}}{R_\alpha^2} \right\} \beta_n^2 \\
 C_{12} = C_{21} &= - \left\{ (A_{12} + A_{66}) + \frac{(B_{12} + B_{66})}{R_\beta} + \frac{(B_{12} + B_{66})}{R_\alpha} + \frac{(D_{12} + D_{66})}{R_\alpha R_\beta} \right\} \alpha_m \beta_n \\
 C_{22} &= - \left\{ A_{66} + 2 \frac{B_{66}}{R_\beta} + \frac{D_{66}}{R_\beta^2} \right\} \alpha_m^2 - \left\{ A_{22} + 2 \frac{B_{22}}{R_\beta} + \frac{D_{22}}{R_\beta^2} \right\} \beta_n^2
 \end{aligned}$$

$$\begin{aligned}
C_{13} = C_{31} &= -\left\{-B_{11} - \frac{D_{11}}{R_\alpha}\right\}\alpha_m^3 - \left\{-(B_{12} + 2B_{66}) - \frac{(D_{12} + 2D_{66})}{R_\alpha}\right\}\alpha_m\beta_n^2 \\
&\quad + \left\{\frac{A_{11}}{R_\alpha} + \frac{A_{12}}{R_\beta} + \frac{B_{11}}{R_\alpha^2} + \frac{B_{12}}{R_\alpha R_\beta}\right\}\alpha_m \\
C_{23} = C_{32} &= -\left\{-B_{22} - \frac{D_{22}}{R_\beta}\right\}\beta_n^3 - \left\{-(B_{12} + 2B_{66}) - \frac{(D_{12} + 2D_{66})}{R_\beta}\right\}\alpha_m^2\beta_n \\
&\quad + \left\{\frac{A_{12}}{R_\alpha} + \frac{A_{22}}{R_\beta} + \frac{B_{22}}{R_\beta^2} + \frac{B_{12}}{R_\alpha R_\beta}\right\}\beta_n \\
C_{33} &= \{D_{11}\alpha_m^4 + 2(D_{12} + 2D_{66})\alpha_m^2\beta_n^2 + D_{22}\beta_n^4\} \\
&\quad + 2\left\{\left(\frac{B_{11}}{R_\alpha} + \frac{B_{12}}{R_\beta}\right)\alpha_m^2 + \left(\frac{B_{12}}{R_\alpha} + \frac{B_{22}}{R_\beta}\right)\beta_n^2\right\} + \left\{\frac{A_{11}}{R_\alpha^2} + 2\frac{A_{12}}{R_\alpha R_\beta} + \frac{A_{22}}{R_\beta^2}\right\}
\end{aligned} \tag{7.36}$$

Various curvature ratios in the longitudinal direction of the shell are treated including both negative and positive curvature. The first 11 natural frequencies are listed for each a/mR_β ratio. For higher ratios of a/mR , the shell may be treated as a beam with a varying moment of inertia. For each case, the minimum natural frequency is underlined. The curvature ratio (a/R_α) along the longitudinal axis varies from -0.5 to 0.5 . The ratio $+0.5$ (with $a/mR_\beta = 0.5$, and $m = 1$) yields a spherical shells that is “chopped” from bottom and top. When a/R_α is taken as zero (i.e., $R_\alpha = \infty$) the special case of cylindrical shell occurs.

Tables 7.18 and 7.19 present results for graphite/epoxy closed and open $[0^\circ, 90^\circ]$ laminated shells. The curvature ratio (a/R_α) along the longitudinal axis varies from -0.5 to 0.5 . As was found for isotropic shells (Qatu 1999b), increasing the curvature a/R_α increases all the natural frequencies with its maximum effect on the fundamental natural frequency. For example, increasing the curvature a/R_α from 0.0 to 0.1 increased the fundamental frequency by 43% for $a/mR_\beta = 8$. Such an increase is less for lower a/mR_β and/or higher frequencies.

Introducing a negative curvature R_α in laminated composite shells has similar effects on the frequencies when compared with isotropic shells (Qatu 1999b). The fundamental frequency is observed to reach a minimum value at a certain a/R_α ratio. This minimum depends on a/mR_β , as well as the thickness ratio (Qatu 1999b). For higher frequencies, introducing a negative curvature increases the frequencies. Vibration studies on the effects of the thickness ratio, orthotropy ratio and lamination sequence were made and available in the literature (Qatu 1999b).

Table 7.18. Frequency parameters for $[0^\circ, 90^\circ]$ graphite/epoxy closed barrel shells, $R_\beta/h = 100$ (Qatu 1999b).

a/R_α	a/mR_β	n										
		0	1	2	3	4	5	6	7	8	9	10
-0.5	8	0.08907	0.02882	0.01384	0.03115	0.04160	0.05169	0.06386	0.07898	0.09730	0.11879	0.14339
	4	0.17815	0.10359	0.03684	0.01109	0.02524	0.04126	0.05727	0.07478	0.09458	0.11702	0.14221
	2	0.35629	0.23298	0.13045	0.07467	0.04497	0.03790	0.04882	0.06717	0.08876	0.11280	0.13926
	1	0.71259	0.43859	0.28386	0.19667	0.14358	0.11078	0.09365	0.09091	0.10033	0.11837	0.14216
	0.5	0.73555	0.63692	0.49277	0.38409	0.30840	0.25596	0.22030	0.19801	0.18739	0.18734	0.19663
-0.1	8	0.08907	0.04498	0.01466	0.01075	0.02015	0.03273	0.04785	0.06563	0.08610	0.10929	0.13521
	4	0.17815	0.11353	0.05705	0.03112	0.02510	0.03317	0.04754	0.06531	0.08589	0.10919	0.13520
	2	0.35629	0.23841	0.14255	0.09212	0.06505	0.05411	0.05688	0.06943	0.08792	0.11040	0.13611
	1	0.71259	0.44137	0.29008	0.20629	0.15619	0.12555	0.10898	0.10461	0.11093	0.12577	0.14696
	0.5	0.73563	0.63796	0.49549	0.38860	0.31465	0.26379	0.22942	0.20796	0.19756	0.19708	0.20544
0.1	8	0.08907	0.05309	0.02822	0.02123	0.02445	0.03425	0.04823	0.06549	0.08570	0.10875	0.13459
	4	0.17815	0.11847	0.06720	0.04378	0.03602	0.03954	0.05074	0.06683	0.08652	0.10933	0.13504
	2	0.35629	0.24108	0.14858	0.10088	0.07549	0.06441	0.06503	0.07494	0.09142	0.11256	0.13739
	1	0.71259	0.44273	0.29317	0.21109	0.16251	0.13302	0.11696	0.11223	0.11748	0.13098	0.15093
	0.5	0.73566	0.63847	0.49684	0.39085	0.31778	0.26771	0.23400	0.21299	0.20276	0.20216	0.21016
0.5	8	0.08907	0.06932	0.05573	0.05146	0.05187	0.05641	0.06526	0.07841	0.09553	0.11631	0.14045
	4	0.17815	0.12824	0.08751	0.06978	0.06306	0.06340	0.06967	0.08124	0.09743	0.11763	0.14144
	2	0.35629	0.24634	0.16061	0.11841	0.09672	0.08682	0.08574	0.09216	0.10495	0.12300	0.14544
	1	0.71259	0.44540	0.29932	0.22067	0.17516	0.14807	0.13336	0.12858	0.13245	0.14386	0.16160
	0.5	0.73567	0.63945	0.49952	0.39534	0.32402	0.27556	0.24320	0.22315	0.21339	0.21270	0.22014

Table 7.19. Frequency parameters for $[0^\circ, 90^\circ]$ graphite/epoxy open barrel shells, $b/R_\beta = 2.0$, $R_\beta/h = 100$ (Qatu 1999b).

a/R_α	a/mR_β	n										
		0	1	2	3	4	5	6	7	8	9	10
− 0.5	8	0.08907	0.00178	0.03282	0.04864	0.06782	0.09442	0.12887	0.17087	0.22014	0.27650	0.33982
	4	0.17815	0.06008	0.01193	0.03674	0.06203	0.09153	0.12738	0.17009	0.21976	0.27634	0.33979
	2	0.35629	0.16679	0.06910	0.03762	0.05356	0.08545	0.12374	0.16808	0.21876	0.27599	0.33986
	1	0.71259	0.33900	0.18755	0.11851	0.09147	0.09833	0.12789	0.16994	0.22037	0.27792	0.34223
	0.5	0.73555	0.55136	0.37161	0.26910	0.21273	0.18826	0.19022	0.21371	0.25325	0.30468	0.36554
− 0.1	8	0.08907	0.02385	0.01173	0.02885	0.05262	0.08294	0.11996	0.16372	0.21422	0.27145	0.33540
	4	0.17815	0.07649	0.02915	0.02995	0.05227	0.08272	0.11991	0.16378	0.21435	0.27162	0.33561
	2	0.35629	0.17613	0.08715	0.05574	0.05964	0.08494	0.12095	0.16459	0.21515	0.27248	0.33652
	1	0.71259	0.34371	0.19762	0.13279	0.10656	0.10942	0.13410	0.17284	0.22130	0.27769	0.34132
	0.5	0.73563	0.55333	0.37638	0.27651	0.22214	0.19843	0.19962	0.22134	0.25898	0.30878	0.36838
0.1	8	0.08907	0.03584	0.02115	0.03093	0.05281	0.08257	0.11939	0.16306	0.21351	0.27071	0.33465
	4	0.17815	0.08471	0.04188	0.03757	0.05488	0.08345	0.11990	0.16343	0.21383	0.27101	0.33494
	2	0.35629	0.18078	0.09622	0.06631	0.06702	0.08869	0.12269	0.16531	0.21532	0.27233	0.33617
	1	0.71259	0.34605	0.20265	0.13998	0.11453	0.11615	0.13876	0.17580	0.22311	0.27876	0.34189
	0.5	0.73566	0.55430	0.37876	0.28021	0.22687	0.20363	0.20457	0.22555	0.26231	0.31132	0.37028
0.5	8	0.08907	0.05988	0.05127	0.05467	0.06856	0.09280	0.12616	0.16765	0.21665	0.27286	0.33609
	4	0.17815	0.10111	0.06831	0.06266	0.07244	0.09480	0.12733	0.16842	0.21723	0.27333	0.33650
	2	0.35629	0.19001	0.11440	0.08868	0.08684	0.10273	0.13204	0.17155	0.21956	0.27523	0.33815
	1	0.71259	0.35068	0.21270	0.15443	0.13106	0.13139	0.15069	0.18448	0.22932	0.28319	0.34505
	0.5	0.73567	0.55622	0.38350	0.28762	0.23638	0.21422	0.21492	0.23468	0.26985	0.31736	0.37505

7.6.2 Thick barrel shells

7.6.2.1 Fundamental equations. The middle surface strains and curvature changes for thick barrel shells having constant R_α , R_β and unit values for Lamé parameters are

$$\begin{aligned}
 \varepsilon_{0\alpha} &= \frac{\partial u_0}{\partial \alpha} + \frac{w_0}{R_\alpha}, & \varepsilon_{0\beta} &= \frac{\partial v_0}{\partial \beta} + \frac{w_0}{R_\beta} \\
 \varepsilon_{0\alpha\beta} &= \frac{\partial v_0}{\partial \alpha} + \frac{w_0}{R_{\alpha\beta}}, & \varepsilon_{0\beta\alpha} &= \frac{\partial u_0}{\partial \beta} + \frac{w_0}{R_{\alpha\beta}} \\
 \gamma_{0\alpha z} &= \frac{\partial w_0}{\partial \alpha} - \frac{u_0}{R_\alpha} - \frac{v_0}{R_{\alpha\beta}} + \psi_\alpha, & \gamma_{0\beta z} &= \frac{\partial w_0}{\partial \beta} - \frac{v_0}{R_\beta} - \frac{u_0}{R_{\alpha\beta}} + \psi_\beta \\
 \kappa_\alpha &= \frac{\partial \psi_\alpha}{\partial \alpha}, & \kappa_\beta &= \frac{\partial \psi_\beta}{\partial \beta}, & \kappa_{\alpha\beta} &= \frac{\partial \psi_\beta}{\partial \alpha}, & \kappa_{\beta\alpha} &= \frac{\partial \psi_\alpha}{\partial \beta}
 \end{aligned} \tag{7.37}$$

With infinite radius of twist (yielding barrel shells equations) the above equations become

$$\begin{aligned}
 \varepsilon_{0\alpha} &= \frac{\partial u_0}{\partial \alpha} + \frac{w_0}{R_\alpha}, & \varepsilon_{0\beta} &= \frac{\partial v_0}{\partial \beta} + \frac{w_0}{R_\beta}, & \varepsilon_{0\alpha\beta} &= \frac{\partial v_0}{\partial \alpha}, & \varepsilon_{0\beta\alpha} &= \frac{\partial u_0}{\partial \beta} \\
 \gamma_{0\alpha z} &= \frac{\partial w_0}{\partial \alpha} - \frac{u_0}{R_\alpha} + \psi_\alpha, & \gamma_{0\beta z} &= \frac{\partial w_0}{\partial \beta} - \frac{v_0}{R_\beta} + \psi_\beta \\
 \kappa_\alpha &= \frac{\partial \psi_\alpha}{\partial \alpha}, & \kappa_\beta &= \frac{\partial \psi_\beta}{\partial \beta}, & \kappa_{\alpha\beta} &= \frac{\partial \psi_\beta}{\partial \alpha}, & \kappa_{\beta\alpha} &= \frac{\partial \psi_\alpha}{\partial \beta}
 \end{aligned} \tag{7.38}$$

The force and moment resultants are obtained by integrating the stresses over the shell thickness. The $1 + z/R$ term should be included, as well as shear deformation. This yields Eqs. (2.41)–(2.44). One can also use the truncated equations for better numerical stability, which yields Eqs. (2.45)–(2.48).

The equations of motion for barrel shells are

$$\begin{aligned}
 \frac{\partial N_\alpha}{\partial \alpha} + \frac{\partial N_{\beta\alpha}}{\partial \beta} + \frac{Q_\alpha}{R_\alpha} + \frac{Q_\beta}{R_{\alpha\beta}} + q_\alpha &= AB(\bar{I}_1 \ddot{u}_0^2 + \bar{I}_2 \ddot{\psi}_\alpha^2) \\
 \frac{\partial N_\beta}{\partial \beta} + \frac{\partial N_{\alpha\beta}}{\partial \alpha} + \frac{Q_\beta}{R_\beta} + \frac{Q_\alpha}{R_{\alpha\beta}} + q_\beta &= (\bar{I}_1 \ddot{v}_0^2 + \bar{I}_2 \ddot{\psi}_\beta^2) \\
 - \left(\frac{N_\alpha}{R_\alpha} + \frac{N_\beta}{R_\beta} + \frac{N_{\alpha\beta} + N_{\beta\alpha}}{R_{\alpha\beta}} \right) + \frac{\partial Q_\alpha}{\partial \alpha} + \frac{\partial Q_\beta}{\partial \beta} + q_n &= (\bar{I}_1 \ddot{w}_0^2) \\
 \frac{\partial M_\alpha}{\partial \alpha} + \frac{\partial M_{\beta\alpha}}{\partial \beta} - Q_\alpha + \frac{P_\beta}{R_{\alpha\beta}} + m_\alpha &= (\bar{I}_2 \ddot{u}_0^2 + \bar{I}_3 \ddot{\psi}_\alpha^2) \\
 \frac{\partial M_\beta}{\partial \beta} + \frac{\partial M_{\alpha\beta}}{\partial \alpha} - Q_\beta + \frac{P_\alpha}{R_{\alpha\beta}} + m_\beta &= (\bar{I}_2 \ddot{v}_0^2 + \bar{I}_3 \ddot{\psi}_\beta^2)
 \end{aligned} \tag{7.39}$$

The equilibrium equations can be written in terms of displacements ($L_{ij}u_i + M_{ij}\ddot{u}_i = q$) where the L_{ij} and the M_{ij} coefficients are listed below (\bar{I}_i are defined in Eq. (2.57)). Eq. (2.72) represents the correct boundary conditions for thick cylindrical or barrel shells.

The coefficients of the inertia matrix are

$$\begin{aligned} M_{ji} &= M_{ij} \\ M_{11} &= M_{22} = M_{33} = -\bar{I}_1 \\ M_{14} &= M_{25} = -\bar{I}_2 \\ M_{44} &= M_{55} = -\bar{I}_3 \\ \text{all other } M_{ij} &= 0 \end{aligned} \quad (7.40)$$

The coefficients of the stiffness differential operators are

$$\begin{aligned} L_{11} &= \bar{A}_{11} \frac{\partial^2}{\partial \alpha^2} + 2A_{16} \frac{\partial^2}{\partial \alpha \partial \beta} + \hat{A}_{66} \frac{\partial^2}{\partial \beta^2} - \frac{\bar{A}_{55}}{R_\alpha^2} \\ L_{12} &= \bar{A}_{16} \frac{\partial^2}{\partial \alpha^2} + (A_{12} + A_{66}) \frac{\partial^2}{\partial \alpha \partial \beta} + \hat{A}_{26} \frac{\partial^2}{\partial \beta^2} - \frac{A_{45}}{R_\alpha R_\beta} \\ L_{13} &= \left[\frac{\bar{A}_{11} + \bar{A}_{55}}{R_\alpha} + \frac{A_{12}}{R_\beta} \right] \frac{\partial}{\partial \alpha} + \left[\frac{A_{16} + A_{45}}{R_\alpha} + \frac{\hat{A}_{26}}{R_\beta} \right] \frac{\partial}{\partial \beta} \\ L_{14} &= \bar{B}_{11} \frac{\partial^2}{\partial \alpha^2} + 2B_{16} \frac{\partial^2}{\partial \alpha \partial \beta} + \hat{B}_{66} \frac{\partial^2}{\partial \beta^2} + \frac{\bar{A}_{55}}{R_\alpha} \\ L_{15} &= \bar{B}_{16} \frac{\partial^2}{\partial \alpha^2} + (B_{12} + B_{66}) \frac{\partial^2}{\partial \alpha \partial \beta} + \hat{B}_{26} \frac{\partial^2}{\partial \beta^2} - \frac{\hat{A}_{45}}{R_\alpha} \\ L_{22} &= \bar{A}_{66} \frac{\partial^2}{\partial \alpha^2} + 2A_{26} \frac{\partial^2}{\partial \alpha \partial \beta} + \hat{A}_{22} \frac{\partial^2}{\partial \beta^2} - \frac{\hat{A}_{44}}{R_\beta^2} \\ L_{23} &= \left[\frac{A_{26} + A_{45}}{R_\beta} + \frac{\bar{A}_{16}}{R_\alpha} \right] \frac{\partial}{\partial \alpha} + \left[\frac{\hat{A}_{22} + \hat{A}_{44}}{R_\beta} + \frac{A_{12}}{R_\alpha} \right] \frac{\partial}{\partial \beta} \\ L_{24} &= \bar{B}_{16} \frac{\partial^2}{\partial \alpha^2} + (B_{12} + B_{66}) \frac{\partial^2}{\partial \alpha \partial \beta} + \hat{B}_{26} \frac{\partial^2}{\partial \beta^2} + \frac{A_{45}}{R_\beta} \\ L_{25} &= \bar{B}_{66} \frac{\partial^2}{\partial \alpha^2} + 2B_{26} \frac{\partial^2}{\partial \alpha \partial \beta} + \hat{B}_{22} \frac{\partial^2}{\partial \beta^2} + \frac{\hat{A}_{44}}{R_\beta} \\ L_{33} &= -\bar{A}_{55} \frac{\partial^2}{\partial \alpha^2} - 2A_{45} \frac{\partial^2}{\partial \alpha \partial \beta} - \hat{A}_{44} \frac{\partial^2}{\partial \beta^2} + \frac{\bar{A}_{11}}{R_\alpha^2} + \frac{2A_{12}}{R_\alpha R_\beta} + \frac{\hat{A}_{22}}{R_\beta^2} \\ L_{34} &= \left[-\bar{A}_{55} + \frac{\bar{B}_{11}}{R_\alpha} + \frac{B_{12}}{R_\beta} \right] \frac{\partial}{\partial \alpha} + \left[-A_{45} + \frac{B_{16}}{R_\alpha} + \frac{\hat{B}_{26}}{R_\beta} \right] \frac{\partial}{\partial \beta} \end{aligned}$$

$$\begin{aligned}
L_{35} &= \left[-A_{45} + \frac{\bar{B}_{16}}{R_\alpha} + \frac{B_{26}}{R_\beta} \right] \frac{\partial}{\partial \alpha} + \left[-\hat{A}_{44} + \frac{B_{12}}{R_\alpha} + \frac{\hat{B}_{22}}{R_\beta} \right] \frac{\partial}{\partial \beta} \\
L_{44} &= -\bar{A}_{55} + \bar{D}_{11} \frac{\partial^2}{\partial \alpha^2} + 2\bar{D}_{16} \frac{\partial^2}{\partial \alpha \partial \beta} + \hat{D}_{66} \frac{\partial^2}{\partial \beta^2} \\
L_{45} &= -A_{45} + \bar{D}_{16} \frac{\partial^2}{\partial \alpha^2} + (D_{12} + D_{66}) \frac{\partial^2}{\partial \alpha \partial \beta} + \hat{D}_{26} \frac{\partial^2}{\partial \beta^2} \\
L_{55} &= -\hat{A}_{44} + \bar{D}_{66} \frac{\partial^2}{\partial \alpha^2} + 2D_{26} \frac{\partial^2}{\partial \alpha \partial \beta} + \hat{D}_{22} \frac{\partial^2}{\partial \beta^2}
\end{aligned} \tag{7.41}$$

7.6.2.2 Simply supported cross-ply thick barrel shells. The same exact solution used earlier for thick plates, shallow shells and cylindrical shells can be extended for barrel shells having shear diaphragm edges and cross-ply lamination (Qatu 2004).

The displacement fields represented by Eq. (5.44) are used for barrel shells. This yields the equation $[K]\{\Delta\} + \omega^2[M]\{\Delta\} = 0$ for free vibration analysis where $[K]$ and $[M]$ are the stiffness and mass symmetric 5×5 matrices, respectively, and ω is the frequency. The stiffness coefficients K_{ij} are

$$\begin{aligned}
K_{11} &= -\bar{A}_{11}\alpha_m^2 - \hat{A}_{66}\beta_n^2 - \frac{\bar{A}_{55}}{R_\alpha} \\
K_{12} &= -(A_{12} + A_{66})\alpha_m\beta_n \\
K_{13} &= \left[\frac{\bar{A}_{11} + \bar{A}_{55}}{R_\alpha} + \frac{A_{12}}{R_\beta} \right] \alpha_m \\
K_{14} &= -\bar{B}_{11}\alpha_m^2 - \hat{B}_{66}\beta_n^2 + \frac{\bar{A}_{55}}{R_\alpha} \\
K_{15} &= -(B_{12} + B_{66})\alpha_m\beta_n - \frac{\hat{A}_{45}}{R_\alpha} \\
K_{22} &= -\bar{A}_{66}\alpha_m^2 - \hat{A}_{22}\beta_n^2 - \frac{\hat{A}_{44}}{R_\beta^2} \\
K_{23} &= \left[\frac{\hat{A}_{22} + \hat{A}_{44}}{R_\beta} + \frac{A_{12}}{R_\alpha} \right] \beta_n \\
K_{24} &= -(B_{12} + B_{66})\alpha_m\beta_n \\
K_{25} &= -\bar{B}_{66}\alpha_m^2 + \hat{B}_{22}\beta_n^2 + \frac{\hat{A}_{44}}{R_\beta}
\end{aligned}$$

$$\begin{aligned}
K_{33} &= -\bar{A}_{55}\alpha_m^2 - \hat{A}_{44}\beta_n^2 - \left[\frac{\bar{A}_{11}}{R_\alpha^2} + \frac{2A_{12}}{R_\alpha R_\beta} + \frac{\hat{A}_{22}}{R_\beta^2} \right] \\
K_{34} &= \left[-\bar{A}_{55} + \frac{\bar{B}_{11}}{R_\alpha} + \frac{B_{12}}{R_\beta} \right] \alpha_m \\
K_{35} &= \left[-\hat{A}_{44} + \frac{B_{12}}{R_\alpha} + \frac{\hat{B}_{22}}{R_\beta} \right] \beta_n \\
K_{44} &= -\bar{A}_{55} - \bar{D}_{11}\alpha_m^2 - \hat{D}_{66}\beta_n^2 \\
K_{45} &= -(D_{12} + D_{66})\alpha_m\beta_n \\
K_{55} &= -\hat{A}_{44} - \bar{D}_{66}\alpha_m^2 - \hat{D}_{22}\beta_n^2
\end{aligned} \tag{7.42}$$

The nondimensional frequency parameter ($\Omega = \omega R \sqrt{\rho/E_1}$) is used in all subsequent results. In the results obtained for laminated composite shells, the $[0^\circ, 90^\circ]$ lamination sequence is used in most of these results. The moderately orthotropic graphite/epoxy (G/E) materials is used.

Table 7.20 lists the natural frequencies for $[0^\circ, 90^\circ]$ graphite/epoxy closed barrel shells with (a/R_α) ratios of 0.5. The table shows comparison between results obtained using SDST and those obtained using CST for various thickness ratios. Similar to cylindrical shells, the results show clearly that gross error can occur when using thin shell theory especially for thicker and shorter shells.

Tables 7.21 and 7.22 present the natural frequencies of graphite/epoxy shells with a $[0^\circ, 90^\circ]$ lamination sequence and a thickness ratio of $R_\beta/h = 10$ for closed and open shell configurations; respectively. The curvature ratio (a/R_α) along the α -axis varies from -0.5 to 0.5 . Figure 7.10 shows the effect of varying the curvature (a/R_α) for different circumferential curvature ratios (a/mR_β) .

The first observation made here is that a slight curvature in the barrel shell with $a/R_\alpha = 0.1$ resulted in a considerable change in the natural frequencies. This is similar to observations made earlier for isotropic shells Qatu (2004). For longer closed shells with $a/mR_\beta = 8$, changing a/R_α from 0 (i.e., perfect cylindrical shells) to 0.1 resulted in increasing the natural frequency parameter by 5%. For open shells, such change resulted in a higher deviation.

Another important observation is that increasing the curvature a/R_α increased the frequencies associated with $n = 1, 2$ and 3 of the shells with moderate length $a/mR_\beta = 2$. For longer shells with $a/mR_\beta = 8$, increasing curvature increased the frequency associated with $n = 1$. The other frequencies associated with $n = 2$ and 3 seem to have minimum values at $a/R_\alpha = -0.3$ and 0, respectively.

Introducing a negative curvature R_α in laminated composite shells has effects on the frequencies which are similar to those found for isotropic shells. The fundamental

Table 7.20. Comparisons of frequency parameters obtained using different shell theories for $[0^\circ, 90^\circ]$ closed barrel shells $a/R_\alpha = 0.5$, $G_{12}/E_2 = 0.5$, $\nu_{12} = 0.3$.

Theory	R_β/h	a/mR_β	n										
			0	1	2	3	4	5	6	7	8	9	10
CST	20	8	0.08908	0.06889	0.05765	0.07058	0.10761	0.16333	0.23457	0.32005	0.41923	0.53182	0.65761
		4	0.17816	0.12725	0.08835	0.08527	0.11439	0.16707	0.23712	0.32209	0.42101	0.53346	0.65917
		2	0.35633	0.24464	0.16084	0.13013	0.14000	0.18247	0.24786	0.33064	0.42846	0.54029	0.66563
		1	0.71266	0.44632	0.30464	0.23845	0.22066	0.24171	0.29341	0.36823	0.46139	0.57035	0.69381
		0.5	0.78961	0.69301	0.56533	0.48574	0.45070	0.45160	0.48246	0.53876	0.61691	0.71415	0.82851
SDST	20	8	0.08907	0.06874	0.05742	0.07017	0.10660	0.16092	0.22958	0.31089	0.40380	0.50749	0.62125
		4	0.17814	0.12715	0.08811	0.08480	0.11331	0.16458	0.23205	0.31283	0.40547	0.50901	0.62267
		2	0.35628	0.24449	0.16054	0.12952	0.13869	0.17969	0.24245	0.32099	0.41246	0.51532	0.62854
		1	0.71256	0.44533	0.30376	0.23719	0.21850	0.23782	0.28661	0.35688	0.44338	0.54307	0.65412
		0.5	0.78071	0.68593	0.55908	0.47889	0.44223	0.44046	0.46733	0.51797	0.58830	0.67508	0.77582
CST	10	8	0.08911	0.06836	0.06459	0.11071	0.19588	0.31052	0.45183	0.61866	0.81026	1.02597	1.26510
		4	0.17822	0.12611	0.09317	0.12209	0.20159	0.31451	0.45516	0.62168	0.81308	1.02863	1.26762
		2	0.35644	0.24313	0.16550	0.16315	0.22560	0.33173	0.46951	0.63457	0.82507	1.03994	1.27831
		1	0.71288	0.45361	0.32532	0.28924	0.32250	0.40920	0.53564	0.69385	0.87981	1.09129	1.32685
		0.5	0.92183	0.82605	0.72531	0.68750	0.70255	0.76132	0.85858	0.99062	1.15440	1.34729	1.56708
SDST	10	8	0.08906	0.06808	0.06399	0.10859	0.18919	0.29433	0.41920	0.56068	0.71623	0.88366	1.06104
		4	0.17812	0.12590	0.09246	0.11975	0.19463	0.29798	0.42213	0.56325	0.71857	0.88582	1.06307
		2	0.35625	0.24276	0.16444	0.16010	0.21756	0.31380	0.43480	0.57421	0.72844	0.89488	1.07148
		1	0.71249	0.45066	0.32164	0.28255	0.30946	0.38489	0.49323	0.62460	0.77327	0.93554	1.10882
		0.5	0.88006	0.78934	0.68724	0.64289	0.64756	0.69120	0.76686	0.86897	0.99274	1.13415	1.28989
SDST	5	8	0.08903	0.06680	0.08438	0.18480	0.32772	0.49681	0.68378	0.88308	1.09081	1.30424	1.52147
		4	0.17805	0.12368	0.10862	0.19411	0.33339	0.50118	0.68745	0.88627	1.09364	1.30679	1.52378
		2	0.35611	0.24118	0.18149	0.23382	0.35915	0.52088	0.70375	0.90028	1.10595	1.31776	1.53367
		1	0.71222	0.47330	0.37788	0.39091	0.47959	0.61638	0.78259	0.96736	1.16427	1.36930	1.57979
		0.5	1.07481	0.98465	0.91514	0.90987	0.95338	1.03594	1.15034	1.29001	1.44908	1.62273	1.80721

Table 7.21. Frequency parameters for $[0^\circ, 90^\circ]$ graphite/epoxy closed barrel shells, $R_\beta/h = 10$ (Qatu 2004).

a/R_α	a/mR_β	n										
		0	1	2	3	4	5	6	7	8	9	10
− 0.5	8	0.08908	0.02778	0.03845	0.10352	0.18952	0.29633	0.42181	0.56352	0.71915	0.88657	1.06391
	4	0.17817	0.10126	0.05113	0.10080	0.18826	0.29641	0.42261	0.56469	0.72049	0.88799	1.06535
	2	0.35634	0.22920	0.13633	0.13286	0.20148	0.30523	0.43030	0.57200	0.72756	0.89483	1.07195
	1	0.71268	0.44313	0.30696	0.26416	0.29269	0.37197	0.48373	0.61762	0.76805	0.93158	1.10577
	0.5	0.87667	0.78449	0.67984	0.63355	0.63733	0.68099	0.75722	0.86012	0.98473	1.12691	1.28334
− 0.1	8	0.08908	0.04383	0.03783	0.09854	0.18514	0.29270	0.41874	0.56086	0.71678	0.88443	1.06195
	4	0.17815	0.11117	0.06623	0.10413	0.18756	0.29468	0.42065	0.56274	0.71862	0.88622	1.06367
	2	0.35630	0.23470	0.14751	0.14285	0.20648	0.30733	0.43097	0.57193	0.72710	0.89415	1.07116
	1	0.71260	0.44620	0.31286	0.27146	0.29917	0.37679	0.48715	0.62003	0.76977	0.93283	1.10667
	0.5	0.87809	0.78648	0.68285	0.63732	0.64144	0.68507	0.76106	0.86363	0.98788	1.12975	1.28589
0.1	8	0.08907	0.05191	0.04418	0.09962	0.18507	0.29229	0.41821	0.56028	0.71619	0.88385	1.06138
	4	0.17814	0.11611	0.07466	0.10807	0.18885	0.29500	0.42056	0.56245	0.71824	0.88578	1.06322
	2	0.35628	0.23741	0.15314	0.14833	0.20972	0.30905	0.43187	0.57237	0.72727	0.89416	1.07106
	1	0.71257	0.44771	0.31580	0.27513	0.30253	0.37938	0.48905	0.62143	0.77082	0.93362	1.10728
	0.5	0.87877	0.78745	0.68433	0.63919	0.64349	0.68712	0.76299	0.86540	0.98949	1.13119	1.28721
0.5	8	0.08906	0.06808	0.06399	0.10859	0.18919	0.29433	0.41920	0.56068	0.71623	0.88366	1.06104
	4	0.17812	0.12590	0.09246	0.11975	0.19463	0.29798	0.42213	0.56325	0.71857	0.88582	1.06307
	2	0.35625	0.24276	0.16444	0.16010	0.21756	0.31380	0.43480	0.57421	0.72844	0.89488	1.07148
	1	0.71249	0.45066	0.32164	0.28255	0.30946	0.38489	0.49323	0.62460	0.77327	0.93554	1.10882
	0.5	0.88006	0.78934	0.68724	0.64289	0.64756	0.69120	0.76686	0.86897	0.99274	1.13415	1.28989

Table 7.22. Frequency parameters for $[0^\circ, 90^\circ]$ graphite/epoxy open barrel shells, $b/R_\beta = 2.0$, $R_\beta/h = 10$ (Qatu 2004).

a/R_α	a/mR_β	n										
		0	1	2	3	4	5	6	7	8	9	10
−0.5	8	0.08908	0.01671	0.11438	0.26359	0.46040	0.69564	0.96079	1.24872	1.55375	1.87149	2.19861
	4	0.17817	0.06070	0.11172	0.26336	0.46133	0.69697	0.96222	1.25014	1.55512	1.87280	2.19984
	2	0.35634	0.16570	0.13927	0.27289	0.46888	0.70407	0.96896	1.25649	1.56106	1.87834	2.20501
	1	0.71268	0.35188	0.26428	0.34519	0.51970	0.74520	1.00439	1.28789	1.58932	1.90404	2.22856
	0.5	0.87667	0.71791	0.63132	0.66481	0.78388	0.96535	1.19179	1.45059	1.73286	2.03230	2.34437
−0.1	8	0.08908	0.02800	0.10942	0.25976	0.45745	0.69323	0.95873	1.24690	1.55211	1.87000	2.19723
	4	0.17815	0.07628	0.11410	0.26180	0.45936	0.69508	0.96049	1.24855	1.55366	1.87144	2.19857
	2	0.35630	0.17484	0.14852	0.27562	0.46928	0.70365	0.96823	1.25563	1.56016	1.87744	2.20413
	1	0.71260	0.35664	0.27158	0.35049	0.52280	0.74701	1.00548	1.28855	1.58971	1.90425	2.22865
	0.5	0.87809	0.72049	0.63517	0.66893	0.78763	0.96855	1.19450	1.45290	1.73487	2.03407	2.34594
0.1	8	0.08907	0.03815	0.11023	0.25942	0.45691	0.69265	0.95815	1.24634	1.55157	1.86949	2.19674
	4	0.17814	0.08417	0.11748	0.26231	0.45919	0.69471	0.96004	1.24808	1.55319	1.87098	2.19813
	2	0.35628	0.17940	0.15370	0.27769	0.47003	0.70386	0.96819	1.25546	1.55993	1.87718	2.20385
	1	0.71257	0.35899	0.27527	0.35330	0.52454	0.74810	1.00618	1.28902	1.59004	1.90448	2.22881
	0.5	0.87877	0.72175	0.63707	0.67099	0.78952	0.97018	1.19588	1.45409	1.73591	2.03499	2.34676
0.5	8	0.08906	0.06036	0.11821	0.26191	0.45769	0.69273	0.95789	1.24591	1.55105	1.86892	2.19616
	4	0.17812	0.10007	0.12807	0.26590	0.46050	0.69510	0.95999	1.24781	1.55279	1.87051	2.19762
	2	0.35625	0.18849	0.16500	0.28318	0.47259	0.70510	0.96877	1.25568	1.55993	1.87704	2.20363
	1	0.71249	0.36366	0.28274	0.35924	0.52840	0.75064	1.00793	1.29027	1.59096	1.90517	2.22933
	0.5	0.88006	0.72423	0.64085	0.67510	0.79332	0.97348	1.19872	1.45655	1.73806	2.03689	2.34847

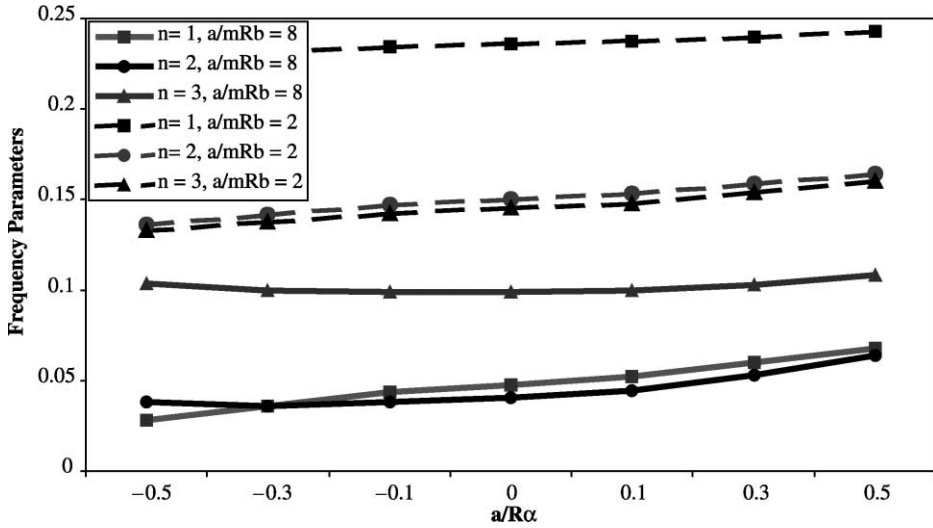


Figure 7.10. Effects of curvature on $[0^\circ, 90^\circ]$ G/E barrel shell frequencies, $R/h = 10$ (Qatu 2004).

frequency is observed to reach a minimum value at a certain a/R_α ratio (Figure 7.10). For higher frequencies, introducing a negative curvature increases the frequencies.

7.7. NON CIRCULAR CYLINDRICAL SHELLS

This chapter has so far dealt with cylindrical shells having circular cross-sections. The circular cross-section of the cylindrical shell is a direct result of constant curvature. Cylindrical shells and other shells of revolutions can be built with variable curvature in the circumferential direction. This will result in cylindrical shells with a non-circular cross-section. The literature on the mechanics of such shells was reviewed by Soldatos (1999). Among the widely studied non-circular cylindrical shells are shells with elliptic cross-section.

Vibration analysis of laminated composite non-circular cylindrical shells received limited attention. Suzuki *et al.* (1994, 1996) developed the fundamental equations for thin and thick laminated non-circular cylindrical shells and presented solutions.

Consider the non-circular cylindrical shell shown in Figure 7.11. The curvature can be taken as

$$\frac{d\theta}{d\beta} = \frac{1}{r} = G\Phi(\theta) \quad (7.43)$$

where G is a constant and Φ a function of θ .

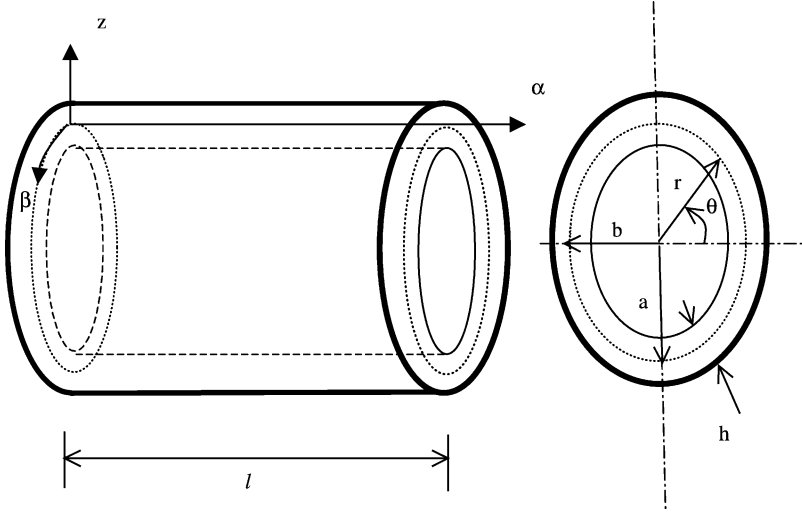


Figure 7.11. Non-circular cylindrical shell.

7.7.1 Thin non-circular cylindrical shells

Eq. (2.61) of Chapter 2 can be specialized for non-circular cylindrical shells to give the following slopes

$$\psi_\alpha = -\frac{\partial w_0}{\partial \alpha}, \quad \psi_\beta = G\Phi\left(v_0 - \frac{\partial w_0}{\partial \theta}\right) \quad (7.44)$$

When the general equations derived earlier for general shells in Chapter 2 are specialized to those of non-circular cylindrical shells, the following midsurface strains and curvature changes are obtained

$$\begin{aligned} \varepsilon_{0\alpha} &= \frac{\partial u_0}{\partial \alpha}, & \varepsilon_{0\theta} &= G\Phi\left(\frac{\partial v_0}{\partial \theta} + w_0\right), & \gamma_{0\alpha\theta} &= \frac{\partial v_0}{\partial \alpha} + G\Phi\frac{\partial u_0}{\partial \theta} \\ k_\alpha &= -\frac{\partial^2 w_0}{\partial \alpha^2}, & k_\beta &= -G\Phi\frac{\partial}{\partial \theta}\left(G\Phi\left(\frac{\partial w_0}{\partial \theta} - v_0\right)\right) \\ \tau &= G\Phi\frac{\partial}{\partial \alpha}\left(v_0 - 2\frac{\partial^2 w_0}{\partial \theta \partial \alpha}\right) \end{aligned} \quad (7.45)$$

Eqs. (2.64) and (2.65) are valid for the stress resultants of non-circular cylindrical

shells. The equations of motion are

$$\begin{aligned}
 \frac{\partial N_\alpha}{\partial \alpha} + G\Phi \frac{\partial N_{\alpha\theta}}{\partial \theta} + p_\alpha &= I_1 \frac{\partial^2 u_0}{\partial t^2} \\
 G\Phi \frac{\partial N_\theta}{\partial \theta} + \frac{\partial N_{\alpha\theta}}{\partial \alpha} + G\Phi \left[G\Phi \frac{\partial M_\theta}{\partial \theta} + \frac{\partial M_{\alpha\theta}}{\partial \alpha} \right] + p_\theta &= I_1 \frac{\partial^2 v_0}{\partial t^2} \\
 -G\Phi N_\theta + \frac{\partial^2 M_\alpha}{\partial \alpha^2} + 2G\Phi \frac{\partial^2 M_{\alpha\theta}}{\partial \theta \partial \alpha} + (G\Phi)^2 \frac{\partial^2 M_\theta}{\partial \theta^2} + p_n &= I_1 \frac{\partial^2 w_0}{\partial t^2}
 \end{aligned} \tag{7.46}$$

Substituting Eqs. (7.45) and (2.64) into Eq. (7.46) yields the equations of motion in terms of displacement (Suzuki *et al.* 1994). Strain energy can also be derived in a manner similar to that done for plates and circular cylindrical shells using Eqs. (5.12) and (5.13).

7.7.2 Thick non-circular cylindrical shells

The middle surface strains and curvature changes for thick non-circular cylindrical shells are

$$\begin{aligned}
 \varepsilon_{0\alpha} &= \frac{\partial u_0}{\partial \alpha}, & \varepsilon_{0\theta} &= G\Phi \left(\frac{\partial v_0}{\partial \theta} + w_0 \right) \\
 \varepsilon_{0\alpha\theta} &= \frac{\partial v_0}{\partial \alpha}, & \varepsilon_{0\theta\alpha} &= G\Phi \frac{\partial u_0}{\partial \theta} \\
 \gamma_{0\alpha z} &= \frac{\partial w_0}{\partial \alpha} + \psi_\alpha, & \gamma_{0\beta z} &= G\Phi \left(\frac{\partial w_0}{\partial \beta} - v_0 \right) + \psi_\theta \\
 \kappa_\alpha &= \frac{\partial \psi_\alpha}{\partial \alpha}, & \kappa_\theta &= G\Phi \frac{\partial \psi_\theta}{\partial \theta}, & \kappa_{\alpha\theta} &= \frac{\partial \psi_\theta}{\partial \alpha}, & \kappa_{\theta\alpha} &= G\Phi \frac{\partial \psi_\alpha}{\partial \theta}
 \end{aligned} \tag{7.47}$$

Eqs. (2.41) and (7.13) can be applied for non-circular cylindrical shells. The terms \bar{A}_{ij} , \bar{B}_{ij} , \bar{D}_{ij} , \bar{A}_{ij} , \bar{B}_{ij} , and \bar{D}_{ij} as specialized in Eqs. (7.14) and/or (7.15) can be expanded to treat the problem of non-circular cylindrical shells. This will introduce the difficulty of having the stress resultants as functions of the coordinate θ , which would complicate the equations. It is proposed to use the average radius of curvature of the shell for R in these equations.

The equations of motion for non-circular cylindrical thick shells are

$$\begin{aligned}
 \frac{\partial N_\alpha}{\partial \alpha} + G\Phi \frac{\partial N_{\alpha\theta}}{\partial \theta} + q_\alpha &= (\bar{I}_1 \ddot{u}_0 + \bar{I}_2 \ddot{\psi}_\alpha^2) \\
 G\Phi \frac{\partial N_\theta}{\partial \theta} + \frac{\partial N_{\alpha\theta}}{\partial \alpha} + G\Phi Q_\theta + q_\theta &= (\bar{I}_1 \ddot{v}_0 + \bar{I}_2 \ddot{\psi}_\theta^2) \\
 -G\Phi N_\theta + \frac{\partial Q_\alpha}{\partial \alpha} + G\Phi \frac{\partial Q_\theta}{\partial \theta} + q_n &= (\bar{I}_1 \ddot{w}_0) \\
 \frac{\partial M_\alpha}{\partial \alpha} + G\Phi \frac{\partial M_{\alpha\theta}}{\partial \theta} - Q_\alpha + m_\alpha &= (\bar{I}_2 \ddot{u}_0 + \bar{I}_3 \ddot{\psi}_\alpha^2) \\
 G\Phi \frac{\partial M_\theta}{\partial \theta} + \frac{\partial M_{\alpha\theta}}{\partial \alpha} - Q_\theta + m_\theta &= (\bar{I}_2 \ddot{v}_0 + \bar{I}_3 \ddot{\psi}_\theta^2)
 \end{aligned} \tag{7.48}$$

The equilibrium equations can be written in terms of displacements as $L_{ij}u_i + M_{ij}\ddot{u}_i = q$ (Eq. (5.31)).

7.7.3 Vibration of non-circular cylindrical shells

Closed non-circular thin cylindrical shells were considered by Suzuki *et al.* (1994), and later thick ones were treated by Suzuki *et al.* (1996). The shells considered had symmetrical lamination and cross-ply sequence. This results in $A_{16} = A_{26} = A_{45} = D_{26} = 0$. In addition, all the B_{ij} terms are zeros. The shell had shear diaphragm at both open ends.

The procedure described by Suzuki for obtaining exact solutions is based on the Levy solution presented earlier for shells and plates with two opposite edges having shear diaphragm boundaries. For thin shells the solution takes the form

$$\begin{aligned} u_0(\alpha, \theta, t) &= u_m(\theta)\cos\left(\frac{m\pi}{l}\alpha\right)\sin(\omega t) \\ v_0(\alpha, \theta, t) &= v_m(\theta)\sin\left(\frac{m\pi}{l}\alpha\right)\sin(\omega t) \\ w_0(\alpha, \theta, t) &= w_m(\theta)\sin\left(\frac{m\pi}{l}\alpha\right)\sin(\omega t) \end{aligned} \quad (7.49)$$

This solution satisfies the shear diaphragm boundaries at $\alpha = 0$ and l . A similar solution can be obtained for thick shells

$$\begin{aligned} u_0(\alpha, \theta, t) &= u_m(\theta)\cos\left(\frac{m\pi}{l}\alpha\right)\sin(\omega t) \\ v_0(\alpha, \theta, t) &= v_m(\theta)\sin\left(\frac{m\pi}{l}\alpha\right)\sin(\omega t) \\ w_0(\alpha, \theta, t) &= w_m(\theta)\sin\left(\frac{m\pi}{l}\alpha\right)\sin(\omega t) \\ \psi_\alpha(\alpha, \theta, t) &= \psi_{cm}(\theta)\cos\left(\frac{m\pi}{l}\alpha\right)\sin(\omega t) \\ \psi_\theta(\alpha, \theta, t) &= \psi_{\theta m}(\theta)\sin\left(\frac{m\pi}{l}\alpha\right)\sin(\omega t) \end{aligned} \quad (7.50)$$

The above solutions can be substituted in the equations of motion (when written in terms of displacements). This will reduce the system of partial differential equations with α and θ as variables to a system of ordinary differential equations with only θ as a variable. The solution is found by expressing the function Φ as an infinite power series in θ and assuming the functions u_m , v_m , w_m , ψ_{cm} , and $\psi_{\theta m}$ as infinite power series of θ . Then the problem is divided into different classes of symmetry and each class is treated independently (Suzuki *et al.* 1994, 1996).

Let us define a representative radius and ellipticity of the cross-section as

$$r_0 = \sqrt{\frac{a^2 + b^2}{2}} \quad (7.51)$$

$$\mu_0 = \frac{a^2 - b^2}{a^2 + b^2}$$

one obtains

$$\Phi(\theta) = (1 + \mu_0 \cos(2\theta))^{3/2}$$

$$G = \frac{1}{1 - \mu_0^2} \quad (7.52)$$

Graphite/epoxy materials (G/E) with $E_1 = 138$ GPa, $E_2 = 8.96$ GPa, $G_{12} = G_{13} = 7.1$ GPa, $G_{23} = 3.45$ GPa, $\nu_{12} = \nu_{13} = \nu_{23} = 0.3$ are considered by Suzuki *et al.* (1994, 1996). Results were obtained for non-circular cylindrical shells with various symmetries in θ . If symmetry about both axes ($\theta = 0$ and $\pi/2$) is considered, the resulting modes will be referred to as SS modes. Similarly, one obtains SA, AS and AA modes, where in the last, antisymmetry exists around the two axes.

Table 7.23 gives the results obtained for a three layer $[0^\circ, 90^\circ, 0^\circ]$. For various lengths and ellipticity values. Moderately thick shells are considered with $r_0 = 6h$. The frequency parameter $\Omega = \omega r_0^2 \sqrt{12\rho(1 - \nu_{12}\nu_{21})/E_1}$ is used. Some results were not reported because of computational limitations.

7.8. RECENT DEVELOPMENTS

Recent advances in the research performed on laminated composite cylindrical shells can be found in the review article by Qatu (2002a). Thin cylindrical shells were analyzed by many researchers including Rezaeepazhand *et al.* (1996), Christoforou and Swanson (1990), Lakshminarayana and Dwarakanath (1992), Narita *et al.* (1993), Heyliger and Jilani (1993), Chen, *et al.* (1998a,b), Tighe and Palazotto (1994), Kubala and Markus (1994), Sorokin (1995), Birman and Magid (1994), Lam and Loy (1995a,b), Zarutsky (1995), Bercin (1996), Ip *et al.* (1996), Besspalova and Kitaigorodsky (1996), Hu *et al.* (1997), Lam *et al.* (2000), and Lee and Lee (1997). Loy *et al.* (1999) studied the vibrations of antisymmetric angle-ply laminated cylindrical panels with different boundary conditions.

Thick cylindrical shells were considered in various articles including Khdeir and Reddy (1990), Carrera (1991), Chun and Dong (1992a,b), Ganapathi *et al.* (1994), Tarn (1994), Mizusawa and Kito (1995), Suzuki *et al.* (1996), Mizusawa (1996), Kumar and Singh (1996), Shulga *et al.* (1999) and Xi *et al.* (1996). Point supported cylindrical shells

Table 7.23. Frequency parameters $\Omega = \omega r_0^2 \sqrt{12\rho(1 - \nu_{12}\nu_{21})/E_1}$ of a three layer $[0^\circ, 90^\circ, 0^\circ]$ graphite/epoxy non-circular cylindrical shells. $r_0/h = 6h$ (SDST) (Suzuki *et al.* 1994, 1996).

Symmetry	$m\pi/l$	Mode no.	Ellipticity, μ_0			
			0.1	0.2	0.3	0.4
SS modes	0.5	First	0.172	0.171	0.169	0.167
		Second	3.085	3.079	3.069	3.054
	1.0	First	0.253	0.248	0.241	0.232
		Second	3.129	3.125	3.116	3.101
	2.0	First	0.660	0.639	0.606	0.562
		Second	3.394	3.390	3.381	3.363
	3.0	First	1.386	1.331	1.248	1.144
		Second	3.944	3.944	3.935	3.909
SA modes	0.5	First	0.053	0.056	0.060	0.063
		Second	1.056	1.050	1.041	1.029
	1.0	First	0.288	0.307	0.326	0.345
		Second	1.105	1.099	1.089	1.075
	2.0	First	1.217	1.267	1.272	–
		Second	1.403	1.437	1.509	1.598
	3.0	First	1.963	1.921	1.865	1.800
		Second	2.663	2.916	3.179	3.446
AS modes	0.5	First	0.046	0.042	0.038	0.034
		Second	1.056	1.050	1.041	1.028
	1.0	First	0.247	0.226	0.204	0.182
		Second	1.105	1.099	1.089	1.076
	2.0	First	1.037	0.938	0.838	0.737
		Second	1.399	1.397	1.391	1.377
	3.0	First	1.947	1.816	1.632	1.439
		Second	2.250	2.164	2.129	2.098
SS modes	0.5	First	0.179	0.192	0.208	0.227
		Second	3.085	3.080	3.073	3.066
	1.0	First	0.253	0.250	0.245	0.237
		Second	3.129	3.126	3.120	3.115
	2.0	First	0.664	0.654	0.638	0.615
		Second	3.394	3.392	3.392	–
	3.0	First	1.398	1.375	1.337	1.285
		Second	3.944	3.947	3.949	–

were treated by Chakravorty *et al.* (1995a,b). Recently, Soldatos and Messina (2001) studied cylindrical shells under different boundaries.

Layer-wise theory was used by Ramesh and Ganesan (1992), Zenkour (1998), and Dasgupta and Huang (1997). The 3D theory of elasticity was used by Ye and Soldatos

(1994) and Jiang (1997). Various theories were used and compared for the analysis of cylindrical shells by Timarci and Soldatos (1995). Ye and Soldatos (1996) used 3D elasticity theory to treat cylindrical shells with arbitrary point supports. Ding and Tang (1999) presented 3D free vibration analysis of thick laminated cylindrical shells with clamped edges. Non-circular cylindrical shells were analyzed by Suzuki *et al.* (1994, 1996) and Kumar and Singh (1995). The literature on this subject was reviewed by Soldatos (1999).

Wang and Vaicaitis (1998) studied active control of vibrations and noise of double wall cylindrical shells. Grigorenko (1998), Reddy and Tajuddin (2000) and Soldatos and Ye (1994) studied hollow cylinders. Effects of boundary conditions on shell vibrations were studied by Messina and Soldatos (1999a,b).

A nonlinear cylindrical shell theory was introduced by Pai and Nayfeh (1992a,b). Nonlinear analysis of cylindrical shells was carried out by various authors including Tsai (1991), Raouf and Palazotto (1992, 1994), Soldatos (1992), Fu and Chia (1993) and Ganapathi and Varadan (1995). Dynamic stability analysis of cylindrical shells was performed in various studies like those of Lam and Ng (1998), Ng and Lam (1999) and Ng *et al.* (1998).

Chapter 8

Conical Shells

Conical shells constitute another special type of shells of revolution. They are formed by revolving a straight line around an axis that is not parallel to the line. If the axis of revolution is parallel to the line, the special case of cylindrical shells is obtained. Figure 8.1 shows a typical closed conical shell of revolution. Conical shells can have circular and elliptic cross-sections. Only conical shells with circular cross-sections are considered here. Open conical shells can be produced by cutting a segment of the closed conical shell. An example of an open conical shell can be obtained by considering the shell between $\theta = \theta_1$ and θ_2 (Figure 8.1). If the side lengths of the open conical shell (for the fundamental mode) are less than half the minimum radius of curvature, a shallow conical shell theory can be developed to treat such shells (Lim *et al.* 1998). This will not be done here.

The equation of conical shells can be obtained by deriving and substituting the proper Lamé parameters of conical shells in the general shell equations. Consider Figure 8.2, which is a side view of the conical shell described in Figure 8.1. The fundamental form can be written as

$$(ds)^2 = (d\alpha)^2 + \alpha^2 \sin^2(\varphi)(d\theta)^2 \quad (8.1)$$

which yields the following Lamé parameters and radii of curvature are

$$\begin{aligned} A &= 1 \\ B &= \alpha \sin(\varphi) \\ R_\alpha &= \infty \\ R_\beta &= \alpha \tan(\varphi) \end{aligned} \quad (8.2)$$

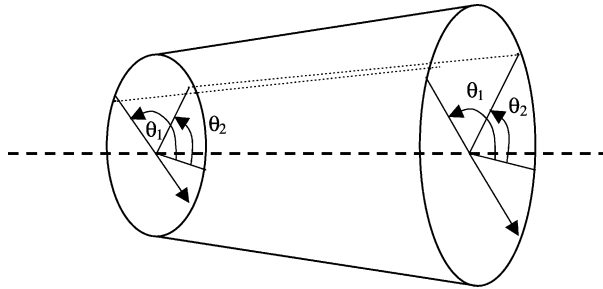


Figure 8.1. A closed conical shell.

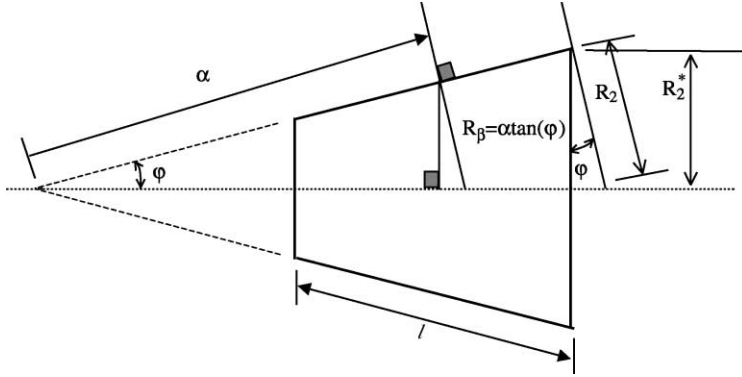


Figure 8.2. Side view of a closed conical shell.

8.1. THIN CONICAL SHELLS

We will first discuss thin conical shells. The fundamental equations of such shells will be derived by substituting Eq. (8.2) into the general equations derived in Chapter 2.

8.1.1 Kinematic relations

Substituting Eq. (8.2) into the general Eqs. (2.60) and (2.61) yield the midsurface strains and curvature changes for a thin conical shell

$$\begin{aligned}
 \varepsilon_{0\alpha} &= \frac{\partial u_0}{\partial \alpha} \\
 \varepsilon_{0\theta} &= \frac{1}{\alpha \sin(\varphi)} \frac{\partial v_0}{\partial \theta} + \frac{u_0}{\alpha} + \frac{w_0}{\alpha \tan(\varphi)} \\
 \gamma_{0\alpha\theta} &= \frac{\partial v_0}{\partial \alpha} + \frac{1}{\alpha \sin(\varphi)} \frac{\partial u_0}{\partial \theta} - \frac{v_0}{\alpha} \\
 \kappa_\alpha &= \frac{\partial \psi_\alpha}{\partial \alpha}, \quad \kappa_\theta = \frac{1}{\alpha \sin(\varphi)} \frac{\partial \psi_\theta}{\partial \theta} + \frac{\psi_\alpha}{\alpha} \\
 \tau &= \frac{\partial \psi_\theta}{\partial \alpha} + \frac{1}{\alpha \sin(\varphi)} \frac{\partial \psi_\alpha}{\partial \theta} - \frac{\psi_\theta}{\alpha}
 \end{aligned} \tag{8.3}$$

where

$$\psi_\alpha = -\frac{\partial w_0}{\partial \alpha}, \quad \psi_\theta = \frac{v_0}{\alpha \tan(\varphi)} - \frac{1}{\alpha \sin(\varphi)} \frac{\partial w_0}{\partial \theta} \tag{8.4}$$

8.1.2 Stress resultants

The equations derived earlier for the general thin shells (Eq. (2.64)) can be applied for conical shells with proper change in the coordinates. The material considered here have conical orthotropy. Note that the assumption of constant stiffness parameters is made here. More fibers farther from the axis of revolution may be needed to maintain constant stiffness.

8.1.3 Equations of motion

The equations of motion of thin conical shells can be obtained by substituting Eq. (8.2) into Eq. (2.71). The resulting equations are (after being divided by $B = R \sin(\varphi)$)

$$\begin{aligned} \frac{\partial N_\alpha}{\partial \alpha} + \frac{N_\alpha - N_\theta}{\alpha} + \frac{1}{\alpha \sin(\varphi)} \frac{\partial N_{\alpha\theta}}{\partial \theta} + q_\alpha &= (I_1 \ddot{u}_0^2) \\ \frac{1}{\alpha \sin(\varphi)} \frac{\partial N_\theta}{\partial \theta} + \frac{\partial N_{\alpha\theta}}{\partial \alpha} + \frac{2N_{\alpha\theta}}{\alpha} + \frac{Q_\theta}{\alpha \tan(\varphi)} + q_\theta &= (I_1 \ddot{v}_0^2) \\ -\left(\frac{N_\theta}{\alpha \tan(\varphi)}\right) + \frac{\partial Q_\alpha}{\partial \alpha} + \frac{Q_\alpha}{\alpha} + \frac{1}{\alpha \sin(\varphi)} \frac{\partial Q_\theta}{\partial \theta} + q_n &= (I_1 \ddot{w}_0^2) \end{aligned} \quad (8.5)$$

where

$$\begin{aligned} Q_\alpha &= \frac{M_\alpha}{\alpha} + \frac{\partial M_\alpha}{\partial \alpha} + \frac{1}{\alpha \sin(\varphi)} \frac{\partial M_{\theta\alpha}}{\partial \theta} - \frac{M_\theta}{\alpha} \\ Q_\theta &= \frac{1}{\alpha \sin(\varphi)} \frac{\partial M_\theta}{\partial \theta} + \frac{\partial M_{\alpha\theta}}{\partial \alpha} + \frac{2M_{\alpha\theta}}{\alpha} \end{aligned}$$

The boundary conditions for thin shallow shells are obtained by substituting Eq. (8.2) into Eq. (2.72). For $\alpha = \text{constant}$, the boundary conditions are

$$\begin{aligned} N_{0\alpha} - N_\alpha &= 0 \quad \text{or} \quad u_0 = 0 \\ \left(N_{0\alpha\theta} - \frac{N_{0\alpha\theta}}{\alpha \tan(\varphi)}\right) - \left(N_{\alpha\theta} - \frac{N_{\alpha\theta}}{\alpha \tan(\varphi)}\right) &= 0 \quad \text{or} \quad v_0 = 0 \\ \left(Q_{0\alpha} - \frac{1}{\alpha \sin(\varphi)} \frac{\partial M_{0\alpha\theta}}{\partial \theta}\right) - \left(Q_\alpha - \frac{1}{\alpha \sin(\varphi)} \frac{\partial M_{\alpha\theta}}{\partial \theta}\right) &= 0 \quad \text{or} \quad w_0 = 0 \\ M_{0\alpha} - M_\alpha &= 0 \quad \text{or} \quad \psi_\alpha = 0 \\ M_{0\alpha\theta} w_{\theta_1}^{\theta_2} &= 0 \end{aligned} \quad (8.6)$$

Substituting Eqs. (8.3) and (2.64) into Eq. (8.5) yields the equations of motion in terms of displacement. These can be written as

$$\begin{bmatrix} L_{11} & L_{12} & L_{13} \\ L_{21} & L_{22} & L_{23} \\ L_{31} & L_{32} & L_{33} \end{bmatrix} \begin{bmatrix} u_0 \\ v_0 \\ w_0 \end{bmatrix} + \begin{bmatrix} -I_1 & 0 & 0 \\ 0 & -I_1 & 0 \\ 0 & 0 & -I_1 \end{bmatrix} \frac{\partial^2}{\partial t^2} \begin{bmatrix} u_0 \\ v_0 \\ w_0 \end{bmatrix} = \begin{bmatrix} -p_\alpha \\ -p_\beta \\ -p_n \end{bmatrix} \quad (8.7)$$

The L_{ij} coefficients of the above equations are

$$\begin{aligned} L_{11} = & \frac{\partial}{\partial \alpha} \left(A_{11} \left(\frac{\partial}{\partial \alpha} \right) + A_{12} \left(\frac{1}{\alpha} \right) + A_{16} \left(\frac{1}{\alpha \sin(\varphi)} \frac{\partial}{\partial \theta} \right) \right) \\ & + \frac{1}{\alpha} \left(A_{11} \left(\frac{\partial}{\partial \alpha} \right) + A_{12} \left(\frac{1}{\alpha} \right) + A_{16} \left(\frac{1}{\alpha \sin(\varphi)} \frac{\partial}{\partial \theta} \right) \right) \\ & - \frac{1}{\alpha} \left(A_{12} \left(\frac{\partial}{\partial \alpha} \right) + A_{22} \left(\frac{1}{\alpha} \right) + A_{26} \left(\frac{1}{\alpha \sin(\varphi)} \frac{\partial}{\partial \theta} \right) \right) \\ & + \frac{1}{\alpha \sin(\varphi)} \frac{\partial}{\partial \theta} \left(A_{16} \left(\frac{\partial}{\partial \alpha} \right) + A_{26} \left(\frac{1}{\alpha} \right) + A_{66} \left(\frac{1}{\alpha \sin(\varphi)} \frac{\partial}{\partial \theta} \right) \right) \\ L_{12} = & \frac{\partial}{\partial \alpha} \left(A_{12} \left(\frac{1}{\alpha \sin(\varphi)} \frac{\partial}{\partial \theta} \right) + A_{16} \left(\frac{\partial}{\partial \alpha} - \frac{1}{\alpha} \right) + B_{12} \left(\frac{\cot(\varphi)}{\alpha^2 \sin(\varphi)} \frac{\partial}{\partial \theta} \right) \right) \\ & + B_{16} \left(\frac{\cot(\varphi)}{\alpha} \frac{\partial}{\partial \alpha} - \frac{2 \cot(\varphi)}{\alpha^2} \right) \\ & + \frac{1}{\alpha} \left(A_{12} \left(\frac{1}{\alpha \sin(\varphi)} \frac{\partial}{\partial \theta} \right) + A_{16} \left(\frac{\partial}{\partial \alpha} - \frac{1}{\alpha} \right) + B_{12} \left(\frac{\cot(\varphi)}{\alpha^2 \sin(\varphi)} \frac{\partial}{\partial \theta} \right) \right) \\ & + B_{16} \left(\frac{\cot(\varphi)}{\alpha} \frac{\partial}{\partial \alpha} - \frac{2 \cot(\varphi)}{\alpha^2} \right) \\ & - \frac{1}{\alpha} \left(A_{22} \left(\frac{1}{\alpha \sin(\varphi)} \frac{\partial}{\partial \theta} \right) + A_{26} \left(\frac{\partial}{\partial \alpha} - \frac{1}{\alpha} \right) + B_{22} \left(\frac{\cot(\varphi)}{\alpha^2 \sin(\varphi)} \frac{\partial}{\partial \theta} \right) \right) \\ & + B_{26} \left(\frac{\cot(\varphi)}{\alpha} \frac{\partial}{\partial \alpha} - \frac{2 \cot(\varphi)}{\alpha^2} \right) \\ & + \frac{1}{\alpha \sin(\varphi)} \frac{\partial}{\partial \theta} \left(A_{26} \left(\frac{1}{\alpha \sin(\varphi)} \frac{\partial}{\partial \theta} \right) + A_{66} \left(\frac{\partial}{\partial \alpha} - \frac{1}{\alpha} \right) + B_{26} \left(\frac{\cot(\varphi)}{\alpha^2 \sin(\varphi)} \frac{\partial}{\partial \theta} \right) \right) \\ & + B_{66} \left(\frac{\cot(\varphi)}{\alpha} \frac{\partial}{\partial \alpha} - \frac{2 \cot(\varphi)}{\alpha^2} \right) \end{aligned}$$

$$\begin{aligned}
L_{13} = & \frac{\partial}{\partial \alpha} \left(A_{12} \left(\frac{1}{\alpha \tan(\varphi)} \right) - B_{11} \left(\frac{\partial^2}{\partial \alpha^2} \right) - B_{12} \left(\frac{1}{\alpha^2 \sin^2(\varphi)} \frac{\partial^2}{\partial \theta^2} + \frac{1}{\alpha} \frac{\partial}{\partial \alpha} \right) \right. \\
& \left. + B_{16} \left(-\frac{2}{\alpha \sin(\varphi)} \frac{\partial^2}{\partial \theta \partial \alpha} + \frac{2}{\alpha^2 \sin(\varphi)} \frac{\partial}{\partial \theta} \right) \right) \\
& + \frac{1}{\alpha} \left(A_{12} \left(\frac{1}{\alpha \tan(\varphi)} \right) - B_{11} \left(\frac{\partial^2}{\partial \alpha^2} \right) - B_{12} \left(\frac{1}{\alpha^2 \sin^2(\varphi)} \frac{\partial^2}{\partial \theta^2} + \frac{1}{\alpha} \frac{\partial}{\partial \alpha} \right) \right. \\
& \left. + B_{16} \left(-\frac{2}{\alpha \sin(\varphi)} \frac{\partial^2}{\partial \theta \partial \alpha} + \frac{2}{\alpha^2 \sin(\varphi)} \frac{\partial}{\partial \theta} \right) \right) \\
& - \frac{1}{\alpha} \left(A_{22} \left(\frac{1}{\alpha \tan(\varphi)} \right) - B_{12} \left(\frac{\partial^2}{\partial \alpha^2} \right) - B_{22} \left(\frac{1}{\alpha^2 \sin^2(\varphi)} \frac{\partial^2}{\partial \theta^2} + \frac{1}{\alpha} \frac{\partial}{\partial \alpha} \right) \right. \\
& \left. + B_{26} \left(-\frac{2}{\alpha \sin(\varphi)} \frac{\partial^2}{\partial \theta \partial \alpha} + \frac{2}{\alpha^2 \sin(\varphi)} \frac{\partial}{\partial \theta} \right) \right) \\
& + \frac{1}{\alpha \sin(\varphi)} \frac{\partial}{\partial \theta} \left(A_{26} \left(\frac{1}{\alpha \tan(\varphi)} \right) - B_{16} \left(\frac{\partial^2}{\partial \alpha^2} \right) - B_{26} \left(\frac{1}{\alpha^2 \sin^2(\varphi)} \frac{\partial^2}{\partial \theta^2} + \frac{1}{\alpha} \frac{\partial}{\partial \alpha} \right) \right. \\
& \left. + B_{66} \left(-\frac{2}{\alpha \sin(\varphi)} \frac{\partial^2}{\partial \theta \partial \alpha} + \frac{2}{\alpha^2 \sin(\varphi)} \frac{\partial}{\partial \theta} \right) \right) \\
L_{21} = & \frac{1}{\alpha \sin(\varphi)} \frac{\partial}{\partial \theta} \left(A_{12} \left(\frac{\partial}{\partial \alpha} \right) + A_{22} \left(\frac{1}{\alpha} \right) + A_{26} \left(\frac{1}{\alpha \sin(\varphi)} \frac{\partial}{\partial \theta} \right) \right) \\
& + \frac{\partial}{\partial \alpha} \left(A_{16} \left(\frac{\partial}{\partial \alpha} \right) + A_{26} \left(\frac{1}{\alpha} \right) + A_{66} \left(\frac{1}{\alpha \sin(\varphi)} \frac{\partial}{\partial \theta} \right) \right) \\
& + \frac{2}{\alpha} \left(A_{16} \left(\frac{\partial}{\partial \alpha} \right) + A_{26} \left(\frac{1}{\alpha} \right) + A_{66} \left(\frac{1}{\alpha \sin(\varphi)} \frac{\partial}{\partial \theta} \right) \right) \\
& + \frac{\cos(\varphi)}{\alpha^2 \sin^2(\varphi)} \frac{\partial}{\partial \theta} \left(B_{12} \left(\frac{1}{\partial \alpha} \right) + B_{22} \left(\frac{u_0}{\alpha} \right) + B_{26} \left(\frac{1}{\alpha \sin(\varphi)} \frac{\partial}{\partial \theta} \right) \right) \\
& + \frac{1}{\alpha \tan(\varphi)} \frac{\partial}{\partial \alpha} \left(B_{16} \left(\frac{\partial}{\partial \alpha} \right) + B_{26} \left(\frac{1}{\alpha} \right) + B_{66} \left(\frac{1}{\alpha \sin(\varphi)} \frac{\partial}{\partial \theta} \right) \right) \\
& + \frac{2}{\alpha^2 \tan(\varphi)} \left(B_{16} \left(\frac{\partial}{\partial \alpha} \right) + B_{26} \left(\frac{1}{\alpha} \right) + B_{66} \left(\frac{1}{\alpha \sin(\varphi)} \frac{\partial}{\partial \theta} \right) \right)
\end{aligned}$$

$$\begin{aligned}
L_{22} = & \frac{1}{\alpha \sin(\varphi)} \frac{\partial}{\partial \theta} \left(A_{22} \left(\frac{1}{\alpha \sin(\varphi)} \frac{\partial}{\partial \theta} \right) + A_{26} \left(\frac{\partial}{\partial \alpha} - \frac{1}{\alpha} \right) + B_{22} \left(\frac{\cot(\varphi)}{\alpha^2 \sin(\varphi)} \frac{\partial}{\partial \theta} \right) \right. \\
& \left. + B_{26} \left(\frac{\cot(\varphi)}{\alpha} \frac{\partial}{\partial \alpha} - \frac{2 \cot(\varphi)}{\alpha^2} \right) \right) \\
& + \frac{\partial}{\partial \alpha} \left(A_{26} \left(\frac{1}{\alpha \sin(\varphi)} \frac{\partial}{\partial \theta} \right) + A_{66} \left(\frac{\partial}{\partial \alpha} - \frac{1}{\alpha} \right) + B_{26} \left(\frac{\cot(\varphi)}{\alpha^2 \sin(\varphi)} \frac{\partial}{\partial \theta} \right) \right. \\
& \left. + B_{66} \left(\frac{\cot(\varphi)}{\alpha} \frac{\partial}{\partial \alpha} - \frac{2 \cot(\varphi)}{\alpha^2} \right) \right) \\
& + \frac{2}{\alpha} \left(A_{26} \left(\frac{1}{\alpha \sin(\varphi)} \frac{\partial}{\partial \theta} \right) + A_{66} \left(\frac{\partial}{\partial \alpha} - \frac{1}{\alpha} \right) + B_{26} \left(\frac{\cot(\varphi)}{\alpha^2 \sin(\varphi)} \frac{\partial}{\partial \theta} \right) \right. \\
& \left. + B_{66} \left(\frac{\cot(\varphi)}{\alpha} \frac{\partial}{\partial \alpha} - \frac{2 \cot(\varphi)}{\alpha^2} \right) \right) \\
& + \frac{\cos(\varphi)}{\alpha^2 \sin^2(\varphi)} \frac{\partial}{\partial \theta} \left(B_{22} \left(\frac{1}{\alpha \sin(\varphi)} \frac{\partial}{\partial \theta} \right) + B_{26} \left(\frac{\partial}{\partial \alpha} - \frac{1}{\alpha} \right) + D_{22} \left(\frac{\cot(\varphi)}{\alpha^2 \sin(\varphi)} \frac{\partial}{\partial \theta} \right) \right. \\
& \left. + D_{26} \left(\frac{\cot(\varphi)}{\alpha} \frac{\partial}{\partial \alpha} - \frac{2 \cot(\varphi)}{\alpha^2} \right) \right) \\
& + \frac{1}{\alpha \tan(\varphi)} \frac{\partial}{\partial \alpha} \left(B_{26} \left(\frac{1}{\alpha \sin(\varphi)} \frac{\partial}{\partial \theta} \right) + B_{66} \left(\frac{\partial}{\partial \alpha} - \frac{1}{\alpha} \right) + D_{26} \left(\frac{\cot(\varphi)}{\alpha^2 \sin(\varphi)} \frac{\partial}{\partial \theta} \right) \right. \\
& \left. + D_{66} \left(\frac{\cot(\varphi)}{\alpha} \frac{\partial}{\partial \alpha} - \frac{2 \cot(\varphi)}{\alpha^2} \right) \right) \\
& + \frac{2}{\alpha^2 \tan(\varphi)} \left(B_{26} \left(\frac{1}{\alpha \sin(\varphi)} \frac{\partial}{\partial \theta} \right) + B_{66} \left(\frac{\partial}{\partial \alpha} - \frac{1}{\alpha} \right) + D_{26} \left(\frac{\cot(\varphi)}{\alpha^2 \sin(\varphi)} \frac{\partial}{\partial \theta} \right) \right. \\
& \left. + D_{66} \left(\frac{\cot(\varphi)}{\alpha} \frac{\partial}{\partial \alpha} - \frac{2 \cot(\varphi)}{\alpha^2} \right) \right) \\
\\
L_{23} = & \frac{1}{\alpha \sin(\varphi)} \frac{\partial}{\partial \theta} \left(A_{22} \left(\frac{1}{\alpha \tan(\varphi)} \right) - B_{12} \left(\frac{\partial^2}{\partial \alpha^2} \right) - B_{22} \left(\frac{1}{\alpha^2 \sin^2(\varphi)} \frac{\partial^2}{\partial \theta^2} + \frac{1}{\alpha} \frac{\partial}{\partial \alpha} \right) \right. \\
& \left. + B_{26} \left(-\frac{2}{\alpha \sin(\varphi)} \frac{\partial^2}{\partial \theta \partial \alpha} + \frac{2}{\alpha^2 \sin(\varphi)} \frac{\partial}{\partial \theta} \right) \right) \\
& + \frac{\partial}{\partial \alpha} \left(A_{26} \left(\frac{1}{\alpha \tan(\varphi)} \right) - B_{16} \left(\frac{\partial^2}{\partial \alpha^2} \right) - B_{26} \left(\frac{1}{\alpha^2 \sin^2(\varphi)} \frac{\partial^2}{\partial \theta^2} + \frac{1}{\alpha} \frac{\partial}{\partial \alpha} \right) \right. \\
& \left. + B_{66} \left(-\frac{2}{\alpha \sin(\varphi)} \frac{\partial^2}{\partial \theta \partial \alpha} + \frac{2}{\alpha^2 \sin(\varphi)} \frac{\partial}{\partial \theta} \right) \right)
\end{aligned}$$

$$\begin{aligned}
& + \frac{2}{\alpha} \left(A_{26} \left(\frac{1}{\alpha \tan(\varphi)} \right) - B_{16} \left(\frac{\partial^2}{\partial \alpha^2} \right) - B_{26} \left(\frac{1}{\alpha^2 \sin^2(\varphi)} \frac{\partial^2}{\partial \theta^2} + \frac{1}{\alpha} \frac{\partial}{\partial \alpha} \right) \right. \\
& \quad \left. + B_{66} \left(-\frac{2}{\alpha \sin(\varphi)} \frac{\partial^2}{\partial \theta \partial \alpha} + \frac{2}{\alpha^2 \sin(\varphi)} \frac{\partial}{\partial \theta} \right) \right) \\
& + \frac{\cos(\varphi)}{\alpha^2 \sin^2(\varphi)} \frac{\partial}{\partial \theta} \left(B_{22} \left(\frac{1}{\alpha \tan(\varphi)} \right) - D_{12} \left(\frac{\partial^2}{\partial \alpha^2} \right) - D_{22} \left(\frac{1}{\alpha^2 \sin^2(\varphi)} \frac{\partial^2}{\partial \theta^2} + \frac{1}{\alpha} \frac{\partial}{\partial \alpha} \right) \right. \\
& \quad \left. + D_{26} \left(-\frac{2}{\alpha \sin(\varphi)} \frac{\partial^2}{\partial \theta \partial \alpha} + \frac{2}{\alpha^2 \sin(\varphi)} \frac{\partial}{\partial \theta} \right) \right) \\
& + \frac{1}{\alpha \tan(\varphi)} \frac{\partial}{\partial \alpha} \left(B_{26} \left(\frac{1}{\alpha \tan(\varphi)} \right) - D_{16} \left(\frac{\partial^2}{\partial \alpha^2} \right) - D_{26} \left(\frac{1}{\alpha^2 \sin^2(\varphi)} \frac{\partial^2}{\partial \theta^2} + \frac{1}{\alpha} \frac{\partial}{\partial \alpha} \right) \right. \\
& \quad \left. + D_{66} \left(-\frac{2}{\alpha \sin(\varphi)} \frac{\partial^2}{\partial \theta \partial \alpha} + \frac{2}{\alpha^2 \sin(\varphi)} \frac{\partial}{\partial \theta} \right) \right) \\
& + \frac{2}{\alpha^2 \tan(\varphi)} \left(B_{26} \left(\frac{1}{\alpha \tan(\varphi)} \right) - D_{16} \left(\frac{\partial^2}{\partial \alpha^2} \right) - D_{26} \left(\frac{1}{\alpha^2 \sin^2(\varphi)} \frac{\partial^2}{\partial \theta^2} + \frac{1}{\alpha} \frac{\partial}{\partial \alpha} \right) \right. \\
& \quad \left. + D_{66} \left(-\frac{2}{\alpha \sin(\varphi)} \frac{\partial^2}{\partial \theta \partial \alpha} + \frac{2}{\alpha^2 \sin(\varphi)} \frac{\partial}{\partial \theta} \right) \right) \\
\\
L_{31} = & - \frac{1}{\alpha \tan(\varphi)} \left(A_{12} \left(\frac{\partial}{\partial \alpha} \right) + A_{22} \left(\frac{1}{\alpha} \right) + A_{26} \left(\frac{1}{\alpha \sin(\varphi)} \frac{\partial}{\partial \theta} \right) \right) \\
& + \frac{\partial^2}{\partial \alpha^2} \left(B_{11} \left(\frac{\partial}{\partial \alpha} \right) + B_{12} \left(\frac{1}{\alpha} \right) + B_{16} \left(\frac{1}{\alpha \sin(\varphi)} \frac{\partial}{\partial \theta} \right) \right) \\
& + \frac{2}{\alpha \sin(\varphi)} \frac{\partial^2}{\partial \theta \partial \alpha} \left(B_{16} \left(\frac{\partial}{\partial \alpha} \right) + B_{26} \left(\frac{1}{\alpha} \right) + B_{66} \left(\frac{1}{\alpha \sin(\varphi)} \frac{\partial}{\partial \theta} \right) \right) \\
& - \frac{1}{\alpha} \frac{\partial}{\partial \alpha} \left(B_{12} \left(\frac{\partial}{\partial \alpha} \right) + B_{22} \left(\frac{1}{\alpha} \right) + B_{26} \left(\frac{1}{\alpha \sin(\varphi)} \frac{\partial}{\partial \theta} \right) \right) \\
& + \frac{2}{\alpha} \frac{\partial}{\partial \alpha} \left(B_{11} \left(\frac{\partial}{\partial \alpha} \right) + B_{12} \left(\frac{1}{\alpha} \right) + B_{16} \left(\frac{1}{\alpha \sin(\varphi)} \frac{\partial}{\partial \theta} \right) \right) \\
& + \frac{1}{\alpha^2 \sin^2(\varphi)} \frac{\partial^2}{\partial \theta^2} \left(B_{12} \left(\frac{\partial}{\partial \alpha} \right) + B_{22} \left(\frac{1}{\alpha} \right) + B_{26} \left(\frac{1}{\alpha \sin(\varphi)} \frac{\partial}{\partial \theta} \right) \right) \\
& + \frac{2}{\alpha^2 \sin(\varphi)} \frac{\partial}{\partial \theta} \left(B_{16} \left(\frac{\partial}{\partial \alpha} \right) + B_{26} \left(\frac{1}{\alpha} \right) + B_{66} \left(\frac{1}{\alpha \sin(\varphi)} \frac{\partial}{\partial \theta} \right) \right)
\end{aligned}$$

$$\begin{aligned}
L_{32} = & -\frac{1}{\alpha \tan(\varphi)} \left(A_{22} \left(\frac{1}{\alpha \sin(\varphi)} \frac{\partial}{\partial \theta} \right) + A_{26} \left(\frac{\partial}{\partial \alpha} - \frac{1}{\alpha} \right) + B_{22} \left(\frac{\cot(\varphi)}{\alpha^2 \sin(\varphi)} \frac{\partial}{\partial \theta} \right) \right. \\
& \left. + B_{26} \left(\frac{\cot(\varphi)}{\alpha} \frac{\partial}{\partial \alpha} - \frac{2 \cot(\varphi)}{\alpha^2} \right) \right) \\
& + \frac{\partial^2}{\partial \alpha^2} \left(B_{12} \left(\frac{1}{\alpha \sin(\varphi)} \frac{\partial}{\partial \theta} \right) + B_{16} \left(\frac{\partial}{\partial \alpha} - \frac{1}{\alpha} \right) + D_{12} \left(\frac{\cot(\varphi)}{\alpha^2 \sin(\varphi)} \frac{\partial}{\partial \theta} \right) \right. \\
& \left. + D_{16} \left(\frac{\cot(\varphi)}{\alpha} \frac{\partial}{\partial \alpha} - \frac{2 \cot(\varphi)}{\alpha^2} \right) \right) \\
& + \frac{2}{\alpha \sin(\varphi)} \frac{\partial^2}{\partial \theta \partial \alpha} \left(B_{26} \left(\frac{1}{\alpha \sin(\varphi)} \frac{\partial}{\partial \theta} \right) + B_{66} \left(\frac{\partial}{\partial \alpha} - \frac{1}{\alpha} \right) + D_{26} \left(\frac{\cot(\varphi)}{\alpha^2 \sin(\varphi)} \frac{\partial}{\partial \theta} \right) \right. \\
& \left. + D_{66} \left(\frac{\cot(\varphi)}{\alpha} \frac{\partial}{\partial \alpha} - \frac{2 \cot(\varphi)}{\alpha^2} \right) \right) \\
& - \frac{1}{\alpha} \frac{\partial}{\partial \alpha} \left(B_{22} \left(\frac{1}{\alpha \sin(\varphi)} \frac{\partial}{\partial \theta} \right) + B_{26} \left(\frac{\partial}{\partial \alpha} - \frac{1}{\alpha} \right) + D_{22} \left(\frac{\cot(\varphi)}{\alpha^2 \sin(\varphi)} \frac{\partial}{\partial \theta} \right) \right. \\
& \left. + D_{26} \left(\frac{\cot(\varphi)}{\alpha} \frac{\partial}{\partial \alpha} - \frac{2 \cot(\varphi)}{\alpha^2} \right) \right) \\
& + \frac{2}{\alpha} \frac{\partial}{\partial \alpha} \left(+ B_{12} \left(\frac{1}{\alpha \sin(\varphi)} \frac{\partial}{\partial \theta} \right) + B_{16} \left(\frac{\partial}{\partial \alpha} - \frac{1}{\alpha} \right) + D_{12} \left(\frac{\cot(\varphi)}{\alpha^2 \sin(\varphi)} \frac{\partial}{\partial \theta} \right) \right. \\
& \left. + D_{16} \left(\frac{\cot(\varphi)}{\alpha} \frac{\partial}{\partial \alpha} - \frac{2 \cot(\varphi)}{\alpha^2} \right) \right) \\
& + \frac{1}{\alpha^2 \sin^2(\varphi)} \frac{\partial^2}{\partial \theta^2} \left(B_{22} \left(\frac{1}{\alpha \sin(\varphi)} \frac{\partial}{\partial \theta} \right) + B_{26} \left(\frac{\partial}{\partial \alpha} - \frac{1}{\alpha} \right) + D_{22} \left(\frac{\cot(\varphi)}{\alpha^2 \sin(\varphi)} \frac{\partial}{\partial \theta} \right) \right. \\
& \left. + D_{26} \left(\frac{\cot(\varphi)}{\alpha} \frac{\partial}{\partial \alpha} - \frac{2 \cot(\varphi)}{\alpha^2} \right) \right) \\
& + \frac{2}{\alpha^2 \sin(\varphi)} \frac{\partial}{\partial \theta} \left(B_{26} \left(\frac{1}{\alpha \sin(\varphi)} \frac{\partial}{\partial \theta} \right) + B_{66} \left(\frac{\partial}{\partial \alpha} - \frac{1}{\alpha} \right) + D_{26} \left(\frac{\cot(\varphi)}{\alpha^2 \sin(\varphi)} \frac{\partial}{\partial \theta} \right) \right. \\
& \left. + D_{66} \left(\frac{\cot(\varphi)}{\alpha} \frac{\partial}{\partial \alpha} - \frac{2 \cot(\varphi)}{\alpha^2} \right) \right) \\
L_{33} = & -\frac{1}{\alpha \tan(\varphi)} \left(A_{22} \left(\frac{1}{\alpha \tan(\varphi)} \right) - B_{12} \left(\frac{\partial^2}{\partial \alpha^2} \right) - B_{22} \left(\frac{1}{\alpha^2 \sin^2(\varphi)} \frac{\partial^2}{\partial \theta^2} + \frac{1}{\alpha} \frac{\partial}{\partial \alpha} \right) \right. \\
& \left. + B_{26} \left(-\frac{2}{\alpha \sin(\varphi)} \frac{\partial^2}{\partial \theta \partial \alpha} + \frac{2}{\alpha^2 \sin(\varphi)} \frac{\partial}{\partial \theta} \right) \right)
\end{aligned}$$

$$\begin{aligned}
& + \frac{\partial^2}{\partial \alpha^2} \left(B_{12} \left(\frac{1}{\alpha \tan(\varphi)} \right) - D_{11} \left(\frac{\partial^2}{\partial \alpha^2} \right) - D_{12} \left(\frac{1}{\alpha^2 \sin^2(\varphi)} \frac{\partial^2}{\partial \theta^2} + \frac{1}{\alpha} \frac{\partial}{\partial \alpha} \right) \right. \\
& \quad \left. + D_{16} \left(-\frac{2}{\alpha \sin(\varphi)} \frac{\partial^2}{\partial \theta \partial \alpha} + \frac{2}{\alpha^2 \sin(\varphi)} \frac{\partial}{\partial \theta} \right) \right) \\
& + \frac{2}{\alpha \sin(\varphi)} \frac{\partial^2}{\partial \theta \partial \alpha} \left(B_{26} \left(\frac{1}{\alpha \tan(\varphi)} \right) - D_{16} \left(\frac{\partial^2}{\partial \alpha^2} \right) - D_{26} \left(\frac{1}{\alpha^2 \sin^2(\varphi)} \frac{\partial^2}{\partial \theta^2} + \frac{1}{\alpha} \frac{\partial w_0}{\partial \alpha} \right) \right. \\
& \quad \left. + D_{66} \left(-\frac{2}{\alpha \sin(\varphi)} \frac{\partial^2}{\partial \theta \partial \alpha} + \frac{2}{\alpha^2 \sin(\varphi)} \frac{\partial}{\partial \theta} \right) \right) \\
& - \frac{1}{\alpha} \frac{\partial}{\partial \alpha} \left(B_{22} \left(\frac{1}{\alpha \tan(\varphi)} \right) - D_{12} \left(\frac{\partial^2}{\partial \alpha^2} \right) - D_{22} \left(\frac{1}{\alpha^2 \sin^2(\varphi)} \frac{\partial^2}{\partial \theta^2} + \frac{1}{\alpha} \frac{\partial w_0}{\partial \alpha} \right) \right. \\
& \quad \left. + D_{26} \left(-\frac{2}{\alpha \sin(\varphi)} \frac{\partial^2}{\partial \theta \partial \alpha} + \frac{2}{\alpha^2 \sin(\varphi)} \frac{\partial}{\partial \theta} \right) \right) \\
& + \frac{2}{\alpha} \frac{\partial}{\partial \alpha} \left(B_{12} \left(\frac{1}{\alpha \tan(\varphi)} \right) - D_{11} \left(\frac{\partial^2}{\partial \alpha^2} \right) - D_{12} \left(\frac{1}{\alpha^2 \sin^2(\varphi)} \frac{\partial^2}{\partial \theta^2} + \frac{1}{\alpha} \frac{\partial}{\partial \alpha} \right) \right. \\
& \quad \left. + D_{16} \left(-\frac{2}{\alpha \sin(\varphi)} \frac{\partial^2}{\partial \theta \partial \alpha} + \frac{2}{\alpha^2 \sin(\varphi)} \frac{\partial}{\partial \theta} \right) \right) \\
& + \frac{1}{\alpha^2 \sin^2(\varphi)} \frac{\partial^2}{\partial \theta^2} \left(B_{22} \left(\frac{1}{\alpha \tan(\varphi)} \right) - D_{12} \left(\frac{\partial^2}{\partial \alpha^2} \right) - D_{22} \left(\frac{1}{\alpha^2 \sin^2(\varphi)} \frac{\partial^2}{\partial \theta^2} + \frac{1}{\alpha} \frac{\partial}{\partial \alpha} \right) \right. \\
& \quad \left. + D_{26} \left(-\frac{2}{\alpha \sin(\varphi)} \frac{\partial^2}{\partial \theta \partial \alpha} + \frac{2}{\alpha^2 \sin(\varphi)} \frac{\partial}{\partial \theta} \right) \right) \\
& + \frac{2}{\alpha^2 \sin(\varphi)} \frac{\partial}{\partial \theta} \left(B_{26} \left(\frac{1}{\alpha \tan(\varphi)} \right) - D_{16} \left(\frac{\partial^2}{\partial \alpha^2} \right) - D_{26} \left(\frac{1}{\alpha^2 \sin^2(\varphi)} \frac{\partial^2}{\partial \theta^2} + \frac{1}{\alpha} \frac{\partial}{\partial \alpha} \right) \right. \\
& \quad \left. + D_{66} \left(-\frac{2}{\alpha \sin(\varphi)} \frac{\partial^2}{\partial \theta \partial \alpha} + \frac{2}{\alpha^2 \sin(\varphi)} \frac{\partial}{\partial \theta} \right) \right)
\end{aligned} \tag{8.8}$$

The level of complexity of above equations is notable. The equations are much simplified when symmetrically laminated conical shells are treated. The above equations can be used for approximate weighted residual methods like Galerkin's method.

8.1.4 Energy functionals for conical shells

The strain energy functional for a cylindrical shell made of laminated composite can be written as in Eqs. (5.12) and (5.13) ($U = U_s + U_b + U_{bs}$) where U_s is the part due to

stretching alone,

$$\begin{aligned}
 U_s = \frac{1}{2} \int_A \left\{ A_{11} \left(\frac{\partial u_0}{\partial \alpha} \right)^2 + 2A_{12} \left(\frac{1}{\alpha \sin(\varphi)} \frac{\partial v_0}{\partial \theta} + \frac{u_0}{\alpha} + \frac{w_0}{\alpha \tan(\varphi)} \right) \left(\frac{\partial u_0}{\partial \alpha} \right) \right. \\
 + 2A_{16} \left(\frac{\partial v_0}{\partial \alpha} + \frac{1}{\alpha \sin(\varphi)} \frac{\partial u_0}{\partial \theta} - \frac{v_0}{\alpha} \right) \left(\frac{\partial u_0}{\partial \alpha} \right) \\
 + A_{22} \left(\frac{1}{\alpha \sin(\varphi)} \frac{\partial v_0}{\partial \theta} + \frac{u_0}{\alpha} + \frac{w_0}{\alpha \tan(\varphi)} \right)^2 \\
 + A_{66} \left(\frac{\partial v_0}{\partial \alpha} + \frac{1}{\alpha \sin(\varphi)} \frac{\partial u_0}{\partial \theta} - \frac{v_0}{\alpha} \right)^2 \\
 \left. + 2A_{26} \left(\frac{\partial v_0}{\partial \alpha} + \frac{1}{\alpha \sin(\varphi)} \frac{\partial u_0}{\partial \theta} - \frac{v_0}{\alpha} \right) \left(\frac{1}{\alpha \sin(\varphi)} \frac{\partial v_0}{\partial \theta} + \frac{u_0}{\alpha} + \frac{w_0}{\alpha \tan(\varphi)} \right) \right\} dA \quad (8.9)
 \end{aligned}$$

U_b is the part due to bending alone,

$$\begin{aligned}
 U_b = \frac{1}{2} \int_A \left\{ D_{11} \left(-\frac{\partial^2 w_0}{\partial \alpha^2} \right)^2 + D_{22} \left(\frac{\cot(\varphi)}{\alpha^2 \sin(\varphi)} \frac{\partial v_0}{\partial \theta} - \frac{1}{\alpha^2 \sin^2(\varphi)} \frac{\partial^2 w_0}{\partial \theta^2} - \frac{1}{\alpha} \frac{\partial w_0}{\partial \alpha} \right)^2 \right. \\
 + D_{66} \left(\frac{\cot(\varphi)}{\alpha} \frac{\partial v_0}{\partial \alpha} - \frac{2 \cot(\varphi)}{\alpha^2} v_0 - \frac{2}{\alpha \sin(\varphi)} \frac{\partial^2 w_0}{\partial \theta \partial \alpha} + \frac{2}{\alpha^2 \sin(\varphi)} \frac{\partial w_0}{\partial \theta} \right)^2 \\
 + 2D_{12} \left(\frac{\cot(\varphi)}{\alpha^2 \sin(\varphi)} \frac{\partial v_0}{\partial \theta} - \frac{1}{\alpha^2 \sin^2(\varphi)} \frac{\partial^2 w_0}{\partial \theta^2} - \frac{1}{\alpha} \frac{\partial w_0}{\partial \alpha} \right) \left(-\frac{\partial^2 w_0}{\partial \alpha^2} \right) \\
 + 2D_{16} \left(\frac{\cot(\varphi)}{\alpha} \frac{\partial v_0}{\partial \alpha} - \frac{2 \cot(\varphi)}{\alpha^2} v_0 - \frac{2}{\alpha \sin(\varphi)} \frac{\partial^2 w_0}{\partial \theta \partial \alpha} + \frac{2}{\alpha^2 \sin(\varphi)} \frac{\partial w_0}{\partial \theta} \right) \\
 \times \left(-\frac{\partial^2 w_0}{\partial \alpha^2} \right) + 2D_{26} \left(\frac{\cot(\varphi)}{\alpha} \frac{\partial v_0}{\partial \alpha} - \frac{2 \cot(\varphi)}{\alpha^2} v_0 \right. \\
 \left. - \frac{2}{\alpha \sin(\varphi)} \frac{\partial^2 w_0}{\partial \theta \partial \alpha} + \frac{2}{\alpha^2 \sin(\varphi)} \frac{\partial w_0}{\partial \theta} \right) \\
 \left. \times \left(\frac{\cot(\varphi)}{\alpha^2 \sin(\varphi)} \frac{\partial v_0}{\partial \theta} - \frac{1}{\alpha^2 \sin^2(\varphi)} \frac{\partial^2 w_0}{\partial \theta^2} - \frac{1}{\alpha} \frac{\partial w_0}{\partial \alpha} \right) \right\} dA \quad (8.10)
 \end{aligned}$$

and U_{bs} is the part due to bending–stretching coupling,

$$\begin{aligned}
 U_{bs} = \frac{1}{2} \int_A \left\{ 2B_{11} \left(-\frac{\partial^2 w_0}{\partial \alpha^2} \right) \left(\frac{\partial u_0}{\partial \alpha} \right) \right. \\
 + 2B_{22} \left(\frac{\cot(\varphi)}{\alpha^2 \sin(\varphi)} \frac{\partial v_0}{\partial \theta} - \frac{1}{\alpha^2 \sin^2(\varphi)} \frac{\partial^2 w_0}{\partial \theta^2} - \frac{1}{\alpha} \frac{\partial w_0}{\partial \alpha} \right) \\
 \left. \times \left(\frac{1}{\alpha \sin(\varphi)} \frac{\partial v_0}{\partial \theta} + \frac{u_0}{\alpha} + \frac{w_0}{\alpha \tan(\varphi)} \right) \right\}
 \end{aligned}$$

$$\begin{aligned}
& + 2B_{66} \left(\frac{\cot(\varphi)}{\alpha} \frac{\partial v_0}{\partial \alpha} - \frac{2 \cot(\varphi)}{\alpha^2} v_0 - \frac{2}{\alpha \sin(\varphi)} \frac{\partial^2 w_0}{\partial \theta \partial \alpha} + \frac{2}{\alpha^2 \sin(\varphi)} \frac{\partial w_0}{\partial \theta} \right) \\
& \times \left(\frac{\partial v_0}{\partial \alpha} + \frac{1}{\alpha \sin(\varphi)} \frac{\partial u_0}{\partial \theta} - \frac{v_0}{\alpha} \right) \\
& + 2B_{12} \left(\frac{\cot(\varphi)}{\alpha^2 \sin(\varphi)} \frac{\partial v_0}{\partial \theta} - \frac{1}{\alpha^2 \sin^2(\varphi)} \frac{\partial^2 w_0}{\partial \theta^2} - \frac{1}{\alpha} \frac{\partial w_0}{\partial \alpha} \right) \left(\frac{\partial u_0}{\partial \alpha} \right) \\
& + 2B_{12} \left(-\frac{\partial^2 w_0}{\partial \alpha^2} \right) \left(\frac{1}{\alpha \sin(\varphi)} \frac{\partial v_0}{\partial \theta} + \frac{u_0}{\alpha} + \frac{w_0}{\alpha \tan(\varphi)} \right) \\
& + 2B_{16} \left(\frac{\cot(\varphi)}{\alpha} \frac{\partial v_0}{\partial \alpha} - \frac{2 \cot(\varphi)}{\alpha^2} v_0 - \frac{2}{\alpha \sin(\varphi)} \frac{\partial^2 w_0}{\partial \theta \partial \alpha} + \frac{2}{\alpha^2 \sin(\varphi)} \frac{\partial w_0}{\partial \theta} \right) \\
& \times \left(\frac{\partial u_0}{\partial \alpha} \right) + 2B_{16} \left(-\frac{\partial^2 w_0}{\partial \alpha^2} \right) \left(\frac{\partial v_0}{\partial \alpha} + \frac{1}{\alpha \sin(\varphi)} \frac{\partial u_0}{\partial \theta} - \frac{v_0}{\alpha} \right) \\
& + 2B_{26} \left(\frac{\cot(\varphi)}{\alpha} \frac{\partial v_0}{\partial \alpha} - \frac{2 \cot(\varphi)}{\alpha^2} v_0 - \frac{2}{\alpha \sin(\varphi)} \frac{\partial^2 w_0}{\partial \theta \partial \alpha} + \frac{2}{\alpha^2 \sin(\varphi)} \frac{\partial w_0}{\partial \theta} \right) \\
& \times \left(\frac{1}{\alpha \sin(\varphi)} \frac{\partial v_0}{\partial \theta} + \frac{u_0}{\alpha} + \frac{w_0}{\alpha \tan(\varphi)} \right) \\
& + 2B_{26} \left(\frac{\cot(\varphi)}{\alpha^2 \sin(\varphi)} \frac{\partial v_0}{\partial \theta} - \frac{1}{\alpha^2 \sin^2(\varphi)} \frac{\partial^2 w_0}{\partial \theta^2} - \frac{1}{\alpha} \frac{\partial w_0}{\partial \alpha} \right) \\
& \times \left(\frac{\partial v_0}{\partial \alpha} + \frac{1}{\alpha \sin(\varphi)} \frac{\partial u_0}{\partial \theta} - \frac{v_0}{\alpha} \right) \Big\} dA
\end{aligned} \tag{8.11}$$

Note that for symmetrically laminated shells, $B_{ij} = 0$ and, hence, $U_{bs} = 0$. The work done by the external forces as the shell displaces is the same as in Eq. (5.17), and the kinetic energy of the entire thin conical shell is expressed with the same equations used for plates (Eq. (5.18)).

8.2. THICK CONICAL SHELLS

The fundamental equations of thick conical shells will be derived by substituting the Lamé parameters and radii of curvature of Eq. (8.2) into the general equations derived for thick shells in Chapter 2.

8.2.1 Kinematic relations

Substituting Eq. (8.2) into the general equations (2.37) and (2.38) yields the midsurface strains and curvature changes for a thick conical shell are

$$\begin{aligned}
 \varepsilon_{0\alpha} &= \frac{\partial u_0}{\partial \alpha} \\
 \varepsilon_{0\theta} &= \frac{1}{\alpha \sin(\varphi)} \frac{\partial v_0}{\partial \theta} + \frac{u_0}{\alpha} + \frac{w_0}{\alpha \tan(\varphi)} \\
 \varepsilon_{0\alpha\theta} &= \frac{\partial v_0}{\partial \alpha} \\
 \varepsilon_{0\beta\alpha} &= \frac{1}{\alpha \sin(\varphi)} \frac{\partial u_0}{\partial \theta} - \frac{v_0}{\alpha}
 \end{aligned} \tag{8.12}$$

$$\begin{aligned}
 \gamma_{0\alpha z} &= \frac{\partial w_0}{\partial \alpha} + \psi_\alpha \\
 \gamma_{0\theta z} &= \frac{1}{\alpha \sin(\varphi)} \frac{\partial w_0}{\partial \theta} - \frac{v_0}{\alpha \tan(\varphi)} + \psi_\theta \\
 \kappa_\alpha &= \frac{\partial \psi_\alpha}{\partial \alpha}, \quad \kappa_\theta = \frac{1}{\alpha \sin(\varphi)} \frac{\partial \psi_\theta}{\partial \theta} + \frac{\psi_\alpha}{\alpha} \\
 \kappa_{\alpha\theta} &= \frac{\partial \psi_\theta}{\partial \alpha}, \quad \kappa_{\theta\alpha} = \frac{1}{\alpha \sin(\varphi)} \frac{\partial \psi_\alpha}{\partial \theta} - \frac{\psi_\theta}{\alpha}
 \end{aligned} \tag{8.13}$$

8.2.2 Stress resultants

The equations derived earlier for the general thick shells (Eqs. (2.41)–(2.44)) are applicable for the special case of conical shells. The resulting stiffness parameters will be functions of the coordinates. This is because the radius of curvature is not constant for conical shells. This will yield equations that may not be attractive for practicing engineers and researchers. It is proposed here to take the average curvature of the conical shells when using these equations. Once this is done, Eqs. (2.41)–(2.44) can be reduced to those of conical shells. This yields equations similar to those found earlier for cylindrical shells (Eq. (7.14)). Alternatively, the truncated equations (2.46)–(2.48) can also be used which will yield equations similar to those found for cylindrical shells (Eq. (7.15)). In both cases, R should be taken as the average curvature.

8.2.3 Equations of motion

The equations of motion of thick conical shells can be obtained by substituting Eq. (8.2) into Eq. (2.56) derived earlier for shells in curvilinear coordinates. The resulting

equations, when divided by $B (= \alpha \sin(\varphi))$, are

$$\begin{aligned}
 \frac{\partial N_\alpha}{\partial \alpha} + \frac{N_\alpha - N_\theta}{\alpha} + \frac{1}{\alpha \sin \varphi} \frac{\partial N_{\theta\alpha}}{\partial \theta} + q_\alpha &= (\bar{I}_1 \ddot{u}_0^2 + \bar{I}_2 \ddot{\psi}_\alpha^2) \\
 \frac{1}{\alpha \sin \varphi} \frac{\partial N_\theta}{\partial \theta} + \frac{\partial N_{\alpha\theta}}{\partial \alpha} + \frac{N_{\alpha\theta} + N_{\theta\alpha}}{\alpha} + \frac{Q_\theta}{\alpha \tan \varphi} + q_\theta &= (\bar{I}_1 \ddot{v}_0^2 + \bar{I}_2 \ddot{\psi}_\beta^2) \\
 -\left(\frac{N_\theta}{\alpha \tan \varphi}\right) + \frac{\partial Q_\alpha}{\partial \alpha} + \frac{Q_\alpha}{\alpha} + \frac{1}{\alpha \sin \varphi} \frac{\partial Q_\theta}{\partial \theta} + q_n &= (\bar{I}_1 \ddot{w}_0^2) \\
 \frac{\partial M_\alpha}{\partial \alpha} + \frac{M_\alpha - M_\theta}{\alpha} + \frac{1}{\alpha \sin \varphi} \frac{\partial M_{\theta\alpha}}{\partial \theta} - Q_\alpha + m_\alpha &= (\bar{I}_2 \ddot{u}_0^2 + \bar{I}_3 \ddot{\psi}_\alpha^2) \\
 \frac{1}{\alpha \sin \varphi} \frac{\partial M_\theta}{\partial \theta} + \frac{\partial M_{\alpha\theta}}{\partial \alpha} + \frac{M_{\alpha\theta} + M_{\theta\alpha}}{\alpha} - Q_\theta + m_\theta &= (\bar{I}_2 \ddot{v}_0^2 + \bar{I}_3 \ddot{\psi}_\beta^2)
 \end{aligned} \tag{8.14}$$

The equilibrium equations can be written in terms of displacements $L_{ij}u_i + M_{ij}\ddot{u}_i = q$. The stiffness parameters L_{ij} are

$$\begin{aligned}
 L_{11} &= \frac{\partial}{\partial \alpha} \left(\bar{A}_{11} \left(\frac{\partial}{\partial \alpha} \right) + A_{12} \left(\frac{1}{\alpha} \right) + A_{16} \left(\frac{1}{\alpha \sin(\varphi)} \frac{\partial}{\partial \theta} \right) \right) \\
 &\quad + \frac{1}{\alpha} \left(\bar{A}_{11} \left(\frac{\partial}{\partial \alpha} \right) + A_{12} \left(\frac{1}{\alpha} \right) + A_{16} \left(\frac{1}{\alpha \sin(\varphi)} \frac{\partial}{\partial \theta} \right) \right) \\
 &\quad - \frac{1}{\alpha} \left(A_{12} \left(\frac{\partial}{\partial \alpha} \right) + \hat{A}_{22} \left(\frac{1}{\alpha} \right) + \hat{A}_{26} \left(\frac{1}{\alpha \sin(\varphi)} \frac{\partial}{\partial \theta} \right) \right) \\
 &\quad + \frac{1}{\alpha \sin \varphi} \frac{\partial}{\partial \theta} \left(A_{16} \left(\frac{\partial}{\partial \alpha} \right) + \hat{A}_{26} \left(\frac{1}{\alpha} \right) + \hat{A}_{66} \left(\frac{1}{\alpha \sin(\varphi)} \frac{\partial}{\partial \theta} \right) \right) \\
 L_{12} &= \frac{\partial}{\partial \alpha} \left(A_{12} \left(\frac{1}{\alpha \sin(\varphi)} \frac{\partial}{\partial \theta} \right) + \bar{A}_{16} \left(\frac{\partial}{\partial \alpha} \right) - A_{16} \left(\frac{1}{\alpha} \right) \right) \\
 &\quad + \frac{1}{\alpha} \left(A_{12} \left(\frac{1}{\alpha \sin(\varphi)} \frac{\partial}{\partial \theta} \right) + \bar{A}_{16} \left(\frac{\partial}{\partial \alpha} \right) - A_{16} \left(\frac{1}{\alpha} \right) \right) \\
 &\quad - \frac{1}{\alpha} \left(\hat{A}_{22} \left(\frac{1}{\alpha \sin(\varphi)} \frac{\partial}{\partial \theta} \right) + A_{26} \left(\frac{\partial}{\partial \alpha} \right) - \hat{A}_{26} \left(\frac{1}{\alpha} \right) \right) \\
 &\quad + \frac{1}{\alpha \sin \varphi} \frac{\partial}{\partial \theta} \left(\hat{A}_{26} \left(\frac{1}{\alpha \sin(\varphi)} \frac{\partial}{\partial \theta} \right) + A_{66} \left(\frac{\partial}{\partial \alpha} \right) - \hat{A}_{66} \left(\frac{1}{\alpha} \right) \right) \\
 L_{13} &= \frac{\partial}{\partial \alpha} \left(A_{12} \left(\frac{1}{\alpha \tan(\varphi)} \right) \right) + \frac{1}{\alpha} \left(A_{12} \left(\frac{1}{\alpha \tan(\varphi)} \right) \right) \\
 &\quad - \frac{1}{\alpha} \left(\hat{A}_{22} \left(\frac{1}{\alpha \tan(\varphi)} \right) \right) + \frac{1}{\alpha \sin \varphi} \frac{\partial}{\partial \theta} \left(\hat{A}_{26} \left(\frac{1}{\alpha \tan(\varphi)} \right) \right)
 \end{aligned}$$

$$\begin{aligned}
L_{14} = & \frac{\partial}{\partial \alpha} \left(\bar{B}_{11} \left(\frac{\partial}{\partial \alpha} \right) + B_{12} \left(\frac{1}{\alpha} \right) + B_{16} \left(\frac{1}{\alpha \sin(\varphi)} \frac{\partial}{\partial \theta} \right) \right) \\
& + \frac{1}{\alpha} \left(\bar{B}_{11} \left(\frac{\partial}{\partial \alpha} \right) + B_{12} \left(\frac{1}{\alpha} \right) + B_{16} \left(\frac{1}{\alpha \sin(\varphi)} \frac{\partial}{\partial \theta} \right) \right) \\
& - \frac{1}{\alpha} \left(B_{12} \left(\frac{\partial}{\partial \alpha} \right) + \hat{B}_{22} \left(\frac{1}{\alpha} \right) + \hat{B}_{26} \left(\frac{1}{\alpha \sin(\varphi)} \frac{\partial}{\partial \theta} \right) \right) \\
& + \frac{1}{\alpha \sin \varphi} \frac{\partial}{\partial \theta} \left(B_{16} \left(\frac{\partial}{\partial \alpha} \right) + \hat{B}_{26} \left(\frac{1}{\alpha} \right) + \hat{B}_{66} \left(\frac{1}{\alpha \sin(\varphi)} \frac{\partial}{\partial \theta} \right) \right)
\end{aligned}$$

$$\begin{aligned}
L_{15} = & \frac{\partial}{\partial \alpha} \left(B_{12} \left(\frac{1}{\alpha \sin(\varphi)} \frac{\partial}{\partial \theta} \right) + \bar{B}_{16} \left(\frac{\partial}{\partial \alpha} \right) + B_{16} \left(-\frac{1}{\alpha} \right) \right) \\
& + \frac{1}{\alpha} \left(B_{12} \left(\frac{1}{\alpha \sin(\varphi)} \frac{\partial}{\partial \theta} \right) + \bar{B}_{16} \left(\frac{\partial \psi_\theta}{\partial \alpha} \right) + B_{16} \left(-\frac{1}{\alpha} \right) \right) \\
& - \frac{1}{\alpha} \left(\hat{B}_{22} \left(\frac{1}{\alpha \sin(\varphi)} \frac{\partial}{\partial \theta} \right) + B_{26} \left(\frac{\partial \psi_\theta}{\partial \alpha} \right) + \hat{B}_{26} \left(-\frac{1}{\alpha} \right) \right) \\
& + \frac{1}{\alpha \sin \varphi} \frac{\partial}{\partial \theta} \left(\hat{B}_{26} \left(\frac{1}{\alpha \sin(\varphi)} \frac{\partial}{\partial \theta} \right) + B_{66} \left(\frac{\partial}{\partial \alpha} \right) + \hat{B}_{66} \left(-\frac{1}{\alpha} \right) \right)
\end{aligned}$$

$$\begin{aligned}
L_{21} = & \frac{1}{\alpha \sin \varphi} \frac{\partial}{\partial \theta} \left(A_{12} \left(\frac{\partial}{\partial \alpha} \right) + \hat{A}_{22} \left(\frac{1}{\alpha} \right) + \hat{A}_{26} \left(\frac{1}{\alpha \sin(\varphi)} \frac{\partial}{\partial \theta} \right) \right) \\
& + \frac{\partial}{\partial \alpha} \left(\bar{A}_{16} \left(\frac{\partial}{\partial \alpha} \right) + A_{26} \left(\frac{1}{\alpha} \right) + A_{66} \left(\frac{1}{\alpha \sin(\varphi)} \frac{\partial}{\partial \theta} \right) \right) \\
& + \frac{1}{\alpha} \left(\bar{A}_{16} \left(\frac{\partial}{\partial \alpha} \right) + A_{26} \left(\frac{1}{\alpha} \right) + A_{66} \left(\frac{1}{\alpha \sin(\varphi)} \frac{\partial}{\partial \theta} \right) \right) \\
& + \frac{1}{\alpha} \left(A_{16} \left(\frac{\partial}{\partial \alpha} \right) + \hat{A}_{26} \left(\frac{1}{\alpha} \right) + \hat{A}_{66} \left(\frac{1}{\alpha \sin(\varphi)} \frac{\partial}{\partial \theta} \right) \right)
\end{aligned}$$

$$\begin{aligned}
L_{22} = & \frac{1}{\alpha \sin \varphi} \frac{\partial}{\partial \theta} \left(\hat{A}_{22} \left(\frac{1}{\alpha \sin(\varphi)} \frac{\partial}{\partial \theta} \right) + A_{26} \left(\frac{\partial}{\partial \alpha} \right) + \hat{A}_{26} \left(-\frac{1}{\alpha} \right) \right) \\
& + \frac{\partial}{\partial \alpha} \left(A_{26} \left(\frac{1}{\alpha \sin(\varphi)} \frac{\partial}{\partial \theta} \right) + \bar{A}_{66} \left(\frac{\partial}{\partial \alpha} \right) + A_{66} \left(-\frac{1}{\alpha} \right) \right) \\
& + \frac{1}{\alpha} \left(A_{26} \left(\frac{1}{\alpha \sin(\varphi)} \frac{\partial}{\partial \theta} \right) + \bar{A}_{66} \left(\frac{\partial}{\partial \alpha} \right) + A_{66} \left(-\frac{1}{\alpha} \right) \right) \\
& + \frac{1}{\alpha} \left(\hat{A}_{26} \left(\frac{1}{\alpha \sin(\varphi)} \frac{\partial}{\partial \theta} \right) + A_{66} \left(\frac{\partial}{\partial \alpha} \right) + \hat{A}_{66} \left(-\frac{1}{\alpha} \right) \right) \\
& + \frac{1}{\alpha \tan \varphi} \left(\hat{A}_{44} \left(-\frac{1}{\alpha \tan(\varphi)} \right) \right)
\end{aligned}$$

$$\begin{aligned}
L_{23} = & \frac{1}{\alpha \sin \varphi} \frac{\partial}{\partial \theta} \left(\hat{A}_{22} \left(\frac{1}{\alpha \tan(\varphi)} \right) \right) + \frac{\partial}{\partial \alpha} \left(A_{26} \left(\frac{1}{\alpha \tan(\varphi)} \right) \right) \\
& + \frac{1}{\alpha} \left(A_{26} \left(\frac{1}{\alpha \tan(\varphi)} \right) \right) + \frac{1}{\alpha} \left(\hat{A}_{26} \left(\frac{1}{\alpha \tan(\varphi)} \right) \right) \\
& + \frac{1}{\alpha \tan \varphi} \left(A_{45} \left(\frac{\partial}{\partial \alpha} \right) + \hat{A}_{44} \left(\frac{1}{\alpha \sin(\varphi)} \frac{\partial}{\partial \theta} \right) \right)
\end{aligned}$$

$$\begin{aligned}
L_{24} = & \frac{1}{\alpha \sin \varphi} \frac{\partial}{\partial \theta} \left(B_{12} \left(\frac{\partial}{\partial \alpha} \right) + \hat{B}_{22} \left(\frac{1}{\alpha} \right) + \hat{B}_{26} \left(\frac{1}{\alpha \sin(\varphi)} \frac{\partial}{\partial \theta} \right) \right) \\
& + \frac{\partial}{\partial \alpha} \left(\bar{B}_{16} \left(\frac{\partial}{\partial \alpha} \right) + B_{16} \left(\frac{1}{\alpha} \right) + B_{66} \left(\frac{1}{\alpha \sin(\varphi)} \frac{\partial}{\partial \theta} \right) \right) \\
& + \frac{1}{\alpha} \left(\bar{B}_{16} \left(\frac{\partial}{\partial \alpha} \right) + B_{16} \left(\frac{1}{\alpha} \right) + B_{66} \left(\frac{1}{\alpha \sin(\varphi)} \frac{\partial}{\partial \theta} \right) \right) \\
& + \frac{1}{\alpha} \left(B_{16} \left(\frac{\partial}{\partial \alpha} \right) + \hat{B}_{26} \left(\frac{1}{\alpha} \right) + \hat{B}_{66} \left(\frac{1}{\alpha \sin(\varphi)} \frac{\partial}{\partial \theta} \right) \right) + \frac{1}{\alpha \tan \varphi} (A_{45})
\end{aligned}$$

$$\begin{aligned}
L_{25} = & \frac{1}{\alpha \sin \varphi} \frac{\partial}{\partial \theta} \left(\hat{B}_{22} \left(\frac{1}{\alpha \sin(\varphi)} \frac{\partial}{\partial \theta} \right) + B_{26} \left(\frac{\partial}{\partial \alpha} \right) - \hat{B}_{26} \left(\frac{1}{\alpha} \right) \right) \\
& + \frac{\partial}{\partial \alpha} \left(B_{16} \left(\frac{1}{\alpha \sin(\varphi)} \frac{\partial}{\partial \theta} \right) + \bar{B}_{66} \left(\frac{\partial}{\partial \alpha} \right) - B_{66} \left(\frac{1}{\alpha} \right) \right) \\
& + \frac{1}{\alpha} \left(B_{16} \left(\frac{1}{\alpha \sin(\varphi)} \frac{\partial}{\partial \theta} \right) + \bar{B}_{66} \left(\frac{\partial}{\partial \alpha} \right) - B_{66} \left(\frac{1}{\alpha} \right) \right) \\
& + \frac{1}{\alpha} \left(\hat{B}_{26} \left(\frac{1}{\alpha \sin(\varphi)} \frac{\partial}{\partial \theta} \right) + B_{66} \left(\frac{\partial}{\partial \alpha} \right) - \hat{B}_{66} \left(\frac{1}{\alpha} \right) \right) + \frac{1}{\alpha \tan \varphi} (\hat{A}_{44})
\end{aligned}$$

$$L_{31} = - \left(\frac{1}{\alpha \tan \varphi} \left(A_{12} \left(\frac{\partial}{\partial \alpha} \right) + \hat{A}_{22} \left(\frac{1}{\alpha} \right) + \hat{A}_{26} \left(\frac{1}{\alpha \sin(\varphi)} \frac{\partial}{\partial \theta} \right) \right) \right)$$

$$\begin{aligned}
L_{32} = & - \left(\frac{1}{\alpha \tan \varphi} \left(\hat{A}_{22} \left(\frac{1}{\alpha \sin(\varphi)} \frac{\partial}{\partial \theta} \right) + A_{26} \left(\frac{\partial}{\partial \alpha} \right) + \hat{A}_{26} \left(-\frac{1}{\alpha} \right) \right) \right) \\
& - \frac{\partial}{\partial \alpha} \left(A_{45} \left(\frac{1}{\alpha \tan(\varphi)} \right) \right) - \frac{1}{\alpha} \left(A_{45} \left(\frac{1}{\alpha \tan(\varphi)} \right) \right) \\
& - \frac{1}{\alpha \sin \varphi} \frac{\partial}{\partial \theta} \left(\hat{A}_{44} \left(-\frac{1}{\alpha \tan(\varphi)} \right) \right)
\end{aligned}$$

$$\begin{aligned}
L_{33} = & - \left(\frac{1}{\alpha \tan \varphi} \left(\hat{A}_{22} \left(\frac{1}{\alpha \tan(\varphi)} \right) \right) \right) + \frac{\partial}{\partial \alpha} \left(\bar{A}_{55} \left(\frac{\partial}{\partial \alpha} \right) + A_{45} \left(\frac{1}{\alpha \sin(\varphi)} \frac{\partial}{\partial \theta} \right) \right) \\
& + \frac{1}{\alpha} \left(\bar{A}_{55} \left(\frac{\partial}{\partial \alpha} \right) + A_{45} \left(\frac{1}{\alpha \sin(\varphi)} \frac{\partial}{\partial \theta} \right) \right) \\
& + \frac{1}{\alpha \sin \varphi} \frac{\partial}{\partial \theta} \left(A_{45} \left(\frac{\partial}{\partial \alpha} \right) + \hat{A}_{44} \left(\frac{1}{\alpha \sin(\varphi)} \frac{\partial}{\partial \theta} \right) \right)
\end{aligned}$$

$$\begin{aligned}
L_{34} &= -\left(\frac{1}{\alpha \tan \varphi} \left(B_{12} \left(\frac{\partial}{\partial \alpha} \right) + \hat{B}_{22} \left(\frac{1}{\alpha} \right) + \hat{B}_{26} \left(\frac{1}{\alpha \sin(\varphi)} \frac{\partial}{\partial \theta} \right) \right) \right) \\
&\quad + \frac{\partial}{\partial \alpha} (\bar{A}_{55}) + \frac{1}{\alpha} (\bar{A}_{55}) + \frac{1}{\alpha \sin \varphi} \frac{\partial}{\partial \theta} (A_{45}) \\
L_{35} &= -\left(\frac{1}{\alpha \tan \varphi} \left(\hat{B}_{22} \left(\frac{1}{\alpha \sin(\varphi)} \frac{\partial}{\partial \theta} \right) + B_{26} \left(\frac{\partial}{\partial \alpha} \right) + \hat{B}_{26} \left(-\frac{1}{\alpha} \right) \right) \right) + \frac{\partial}{\partial \alpha} (A_{45}) \\
&\quad + \frac{1}{\alpha} (+A_{45}) + \frac{1}{\alpha \sin \varphi} \frac{\partial}{\partial \theta} (\hat{A}_{44}) \\
L_{41} &= \frac{\partial}{\partial \alpha} \left(\bar{B}_{11} \left(\frac{\partial}{\partial \alpha} \right) + B_{12} \left(\frac{1}{\alpha} \right) + B_{16} \left(\frac{1}{\alpha \sin(\varphi)} \frac{\partial}{\partial \theta} \right) \right) \\
&\quad + \frac{1}{\alpha} \left(\bar{B}_{11} \left(\frac{\partial}{\partial \alpha} \right) + B_{12} \left(\frac{1}{\alpha} \right) + B_{16} \left(\frac{1}{\alpha \sin(\varphi)} \frac{\partial}{\partial \theta} \right) \right) \\
&\quad - \frac{1}{\alpha} \left(B_{12} \left(\frac{\partial}{\partial \alpha} \right) + \hat{B}_{22} \left(\frac{1}{\alpha} \right) + \hat{B}_{26} \left(\frac{1}{\alpha \sin(\varphi)} \frac{\partial}{\partial \theta} \right) \right) \\
&\quad + \frac{1}{\alpha \sin \varphi} \frac{\partial}{\partial \theta} \left(\bar{B}_{16} \left(\frac{\partial}{\partial \alpha} \right) + B_{26} \left(\frac{1}{\alpha} \right) + B_{66} \left(\frac{1}{\alpha \sin(\varphi)} \frac{\partial}{\partial \theta} \right) \right) \\
L_{42} &= \frac{\partial}{\partial \alpha} \left(B_{12} \left(\frac{1}{\alpha \sin(\varphi)} \frac{\partial}{\partial \theta} \right) + \bar{B}_{16} \left(\frac{\partial}{\partial \alpha} \right) - B_{16} \left(\frac{1}{\alpha} \right) \right) \\
&\quad + \frac{1}{\alpha} \left(B_{12} \left(\frac{1}{\alpha \sin(\varphi)} \frac{\partial}{\partial \theta} \right) + \bar{B}_{16} \left(\frac{\partial}{\partial \alpha} \right) - B_{16} \left(\frac{1}{\alpha} \right) \right) \\
&\quad - \frac{1}{\alpha} \left(+\hat{B}_{22} \left(\frac{1}{\alpha \sin(\varphi)} \frac{\partial}{\partial \theta} \right) + B_{26} \left(\frac{\partial}{\partial \alpha} \right) - \hat{B}_{26} \left(\frac{1}{\alpha} \right) \right) \\
&\quad + \frac{1}{\alpha \sin \varphi} \frac{\partial}{\partial \theta} \left(B_{26} \left(\frac{1}{\alpha \sin(\varphi)} \frac{\partial}{\partial \theta} \right) + \bar{B}_{66} \left(\frac{\partial}{\partial \alpha} \right) - B_{66} \left(\frac{1}{\alpha} \right) \right) + \left(A_{45} \left(\frac{1}{\alpha \tan(\varphi)} \right) \right) \\
L_{43} &= \frac{\partial}{\partial \alpha} \left(B_{12} \left(\frac{1}{\alpha \tan(\varphi)} \right) \right) + \frac{1}{\alpha} \left(B_{12} \left(\frac{1}{\alpha \tan(\varphi)} \right) \right) - \frac{1}{\alpha} \left(\hat{B}_{22} \left(\frac{1}{\alpha \tan(\varphi)} \right) \right) \\
&\quad + \frac{1}{\alpha \sin \varphi} \frac{\partial}{\partial \theta} \left(B_{26} \left(\frac{1}{\alpha \tan(\varphi)} \right) \right) - \left(\bar{A}_{55} \left(\frac{\partial}{\partial \alpha} \right) + A_{45} \left(\frac{1}{\alpha \sin(\varphi)} \frac{\partial}{\partial \theta} \right) \right) \\
L_{44} &= \frac{\partial}{\partial \alpha} \left(\bar{D}_{11} \left(\frac{\partial}{\partial \alpha} \right) + D_{12} \left(\frac{1}{\alpha} \right) + D_{16} \left(\frac{1}{\alpha \sin(\varphi)} \frac{\partial}{\partial \theta} \right) \right) \\
&\quad + \frac{1}{\alpha} \left(\bar{D}_{11} \left(\frac{\partial}{\partial \alpha} \right) + D_{12} \left(\frac{1}{\alpha} \right) + D_{16} \left(\frac{1}{\alpha \sin(\varphi)} \frac{\partial}{\partial \theta} \right) \right) \\
&\quad - \frac{1}{\alpha} \left(D_{12} \left(\frac{\partial}{\partial \alpha} \right) + \hat{D}_{22} \left(\frac{1}{\alpha} \right) + \hat{D}_{26} \left(\frac{1}{\alpha \sin(\varphi)} \frac{\partial}{\partial \theta} \right) \right) \\
&\quad + \frac{1}{\alpha \sin \varphi} \frac{\partial}{\partial \theta} \left(\bar{D}_{16} \left(\frac{\partial}{\partial \alpha} \right) + D_{16} \left(\frac{1}{\alpha} \right) + D_{66} \left(\frac{1}{\alpha \sin(\varphi)} \frac{\partial}{\partial \theta} \right) \right) - (\bar{A}_{55})
\end{aligned}$$

$$\begin{aligned}
L_{55} = & \frac{1}{\alpha \sin \varphi} \frac{\partial}{\partial \theta} \left(\hat{D}_{22} \left(\frac{1}{\alpha \sin(\varphi)} \frac{\partial}{\partial \theta} \right) + D_{26} \left(\frac{\partial}{\partial \alpha} \right) - \hat{D}_{26} \left(\frac{1}{\alpha} \right) \right) \\
& + \frac{\partial}{\partial \alpha} \left(D_{16} \left(\frac{1}{\alpha \sin(\varphi)} \frac{\partial}{\partial \theta} \right) + \bar{D}_{66} \left(\frac{\partial}{\partial \alpha} \right) - D_{66} \left(\frac{1}{\alpha} \right) \right) \\
& + \frac{1}{\alpha} \left(D_{16} \left(\frac{1}{\alpha \sin(\varphi)} \frac{\partial}{\partial \theta} \right) + \bar{D}_{66} \left(\frac{\partial}{\partial \alpha} \right) - D_{66} \left(\frac{1}{\alpha} \right) \right) \\
& + \frac{1}{\alpha} \left(\hat{D}_{26} \left(\frac{1}{\alpha \sin(\varphi)} \frac{\partial}{\partial \theta} \right) + D_{66} \left(\frac{\partial}{\partial \alpha} \right) - \hat{D}_{66} \left(\frac{1}{\alpha} \right) \right) - (\hat{A}_{44})
\end{aligned} \tag{8.15}$$

Eq. (7.17) gives the coefficients of the mass matrix. Note that the average radius of curvature should be used for R . The boundary conditions for thick conical shells are given in Eq. (2.58).

8.3. FREE VIBRATIONS

The free vibrations of conical shells can permit exact solution in a manner similar to that described earlier for flat plates and shallow shells having two opposite edges simply supported with shear diaphragm boundaries and cross-ply lamination method. Tong (1993a) obtained such exact solution for thin conical shells and later (Tong 1994a) for thick conical shells. Shu (1996) used differential quadrature to obtain natural frequencies. Lim *et al.* (1997b, 1998) obtained results for untwisted and twisted cantilevered shallow conical shells using the Ritz method.

Table 8.1 shows frequency parameter for $\Omega = \omega R_2 \sqrt{\rho h / A_{11}}$ for closed cones with S2 boundary conditions. Antisymmetric cross-ply $[0^\circ, 90^\circ]$ lamination was used. The results were obtained by Tong *et al.* (1994a) using exact solutions. Both a thin (classical) shell theory (CST) and a thick (shear deformation) shell theory (SDST) were used to obtain results for various thickness ratios. As was observed earlier, the difference between both theories is minimal for very thin shells (h/R_2^*) of 0.01. This difference reaches 4% for a thickness ratio of 0.05 (corresponding to $R_2^*/h = 20$) for $\varphi = 30^\circ$ and 8% for the same thickness ratio and $\varphi = 45^\circ$. The difference between both theories doubles for moderately thick shells with a thickness ratio (h/R_2^*) of 0.1, which is not acceptable for engineering applications, and SDST should be used for such a thickness ratio.

Table 8.2 shows the same frequency parameter for closed cones with different boundary condition. The results are obtained by using the differential quadrature method (Shu 1996). Four boundary conditions are analyzed. One cone angle ($\varphi = 30^\circ$) is used in these results. An SC boundary condition represents a cone that is simply supported at the end having smaller radius of curvature and clamped at the other end having larger radius of curvature.

The first observation made here is that the effect of the thickness ratio is much higher for cones with higher degree of fixation. Changing the thickness ratio from 0.01 to 0.1 in the clamped cone resulted in frequency parameters that are five times higher. Doing

Table 8.1. Frequency parameter for $\Omega = \omega R_2 \sqrt{\rho h / A_{11}}$ for closed cones with S2 boundary conditions.

$h/(R_2^*)$	SDST	CST
$\varphi = 30^\circ$		
0.01	0.1768	0.1769
0.02	0.2091	0.2119
0.03	0.2304	0.2360
0.04	0.2495	0.2578
0.05	0.2681	0.2794
0.06	0.2862	0.3010
0.08	0.3193	0.3426
0.10	0.3469	0.3801
$\varphi = 45^\circ$		
0.01	0.2270	0.2321
0.02	0.2691	0.2797
0.03	0.3000	0.3164
0.04	0.3302	0.3529
0.05	0.3610	0.3905
0.06	0.3914	0.4290
0.08	0.3193	0.3426
0.10	0.3469	0.3801

Antisymmetric cross-ply $[0^\circ, 90^\circ]$, $E_1/E_2 = 15.0$, $G_{12}/E_2 = 0.5$, $\nu_{12} = 0.25$, $\nu_{13} = \nu_{23} = 0.3$, $G_{13}/E_2 = G_{23}/E_2 = 0.3846$, $l/(R_2^*) = 0.5$ (Tong 1994a).

the same for the simply supported cones resulted only in doubling the frequency. Both cones with SC and CS boundaries gave results in between, but they were closer to the completely clamped cone.

Table 8.2. Frequency parameter for $\Omega = \omega R_2^* \sqrt{\rho h / A_{11}}$ for closed cones.

$h/(R_2^*)$	SS	SC	CS	CC
0.01	0.1799	0.2656	0.2641	0.2986
0.02	0.2153	0.3852	0.2894	0.4625
0.03	0.2397	0.4958	0.5027	0.6210
0.04	0.2620	0.5975	0.6141	0.7752
0.05	0.2841	0.7044	0.7246	0.9331
0.06	0.3061	0.8059	0.8381	1.0843
0.08	0.3484	1.0045	1.0466	1.3845
1.00	0.3863	1.2036	1.2571	1.5737

Antisymmetric cross-ply $[0^\circ, 90^\circ]$, $E_1/E_2 = 15.0$, $\nu_{12} = 0.25$, $G_{12}/E_2 = 0.5$; $l \sin(\varphi)/(R_2^*) = 0.5$, $\varphi = 30^\circ$ (Shu 1996).

The second observation made here is that the fundamental frequency occurs at a higher number of circumferential half sine waves for thin shells than it does for thick shells. This was observed earlier for cylindrical and barrel shells.

Table 8.3 shows results obtained for open shallow conical shells by Lim *et al.* (1998). A shallow conical shell with $\theta_1 - \theta_2 = 30^\circ$ (see Figure 8.1) is used in the analysis, with $\varphi = 15^\circ$. The shell is cantilevered at the wider end. E-glass/epoxy materials are used in the analysis. The lamination angle is varied from 0 to 90° in 15° increments. The lamination sequences of $[-\theta, \theta, \theta, -\theta]$ which are symmetrically laminated and $[-\theta, \theta, -\theta, \theta]$ which are antisymmetrically laminated have been used. Shell's aspect ratio (l/b) is 1.5 with the length of the shell (l) being 1.5 times the curved clamped edge (b). A thin shell with a thickness ratio (l/h) of 100 is used. The Ritz method is used in this analysis.

Interestingly, the unsymmetric lamination yielded slightly higher fundamental frequencies. The maximum fundamental frequency was obtained at a lamination angle of 30° . The difference, however, between the symmetric and unsymmetric lamination sequences studied here is very small.

It is also noticed that a lamination angle other than 0° yielded higher frequencies. The fundamental frequency can be maximized by about 10% with the optimal choice of fiber angle. The second frequency was obtained at a lamination angle of 0° . A study of the mode

Table 8.3. Frequency parameter for $\Omega = \omega l \sqrt{\rho/E_1}$ for an open cantilevered (the wider curved boundary is clamped and the others free) conical shell with E-glass/epoxy materials.

θ (degrees)	1	2	3	4
<i>$[-\theta, \theta, \theta, -\theta]$ lamination</i>				
0	0.033727	0.044772	0.12099	0.12207
15	0.034688	0.043762	0.12107	0.12473
30	0.035949	0.040259	0.12079	0.13008
45	0.034834	0.036298	0.11712	0.13574
60	0.032148	0.033685	0.11017	0.13669
75	0.030752	0.031168	0.10277	0.13404
90	0.029683	0.030690	0.099392	0.13229
<i>$[-\theta, \theta, -\theta, \theta]$ lamination</i>				
0	0.033727	0.044772	0.12099	0.12207
15	0.034638	0.043723	0.12223	0.12366
30	0.036082	0.040105	0.12319	0.12826
45	0.035393	0.036092	0.11994	0.13451
60	0.032286	0.034065	0.11233	0.13649
75	0.031013	0.031146	0.10354	0.13400
90	0.029683	0.030690	0.099392	0.13229

$l/h = 100$, $\varphi = 15^\circ$, $\theta_1 - \theta_2 = 30^\circ$ (see Figure 8.1), Lim *et al.* (1998).

shapes published by Lim *et al.* (1998) revealed some skewness in the nodal lines, similar to that observed earlier for shallow shells.

8.4. RECENT DEVELOPMENTS

Thin conical composite shells were treated by many researchers (Ganapathi *et al.* 1999; Kayran and Vinson 1990a,b; Sivadas and Ganesan 1992, 1993; Wu and Wu 2000; Shu 1994; Kumar and Singh 1996; Lim *et al.* 1998). Thick conical shells were studied in several articles including those by Ramesh and Ganesan (1992, 1993), Tong (1993a,b, 1994a,b, 1996), Xi *et al.* (1996) and Lu *et al.* (1996). Lim *et al.* (1997b, 1998) addressed the vibration behavior of cantilevered laminated composite shallow conical shells. Liu *et al.* (1997) studied vibrations of joined conical shells. Gofman (1998) examined the steady-state torsional oscillations of multilayer truncated cones.

Korjakin *et al.* (1998) looked at damped vibrations of laminated composite conical shells. Stiffened conical shells were discussed by Khatri (1995). Sivadas and Ganesan (1991b, 1992) studied composite conical shells with variable thickness. Khatri and Asnani (1995, 1996) treated damping in multilayered conical shells. Prestressed conical shells were treated by Sivadas (1995a,b). Nonlinear analysis of composite conical shells was discussed by Xu *et al.* (1996) and Liu and Li (1995).

Chapter 9

Spherical Shells

Spherical shells are another special case of shells of revolution. For these shells, a circular arc, rather than a straight line, revolves about an axis to generate the surface. If the circular arc is half a circle and the axis of rotation is the circle's own diameter, a closed sphere will result.

Shallow spherical shells on both rectangular and circular planforms were treated in Chapter 6. Such shells were referred to as spherical caps when they possess circular planforms. These shallow shells can have both rectangular orthotropy as well as spherical orthotropy. The treatment of both was described in the earlier chapter.

The emphasis in this chapter is on closed or deep spherical shells composed of layers having spherical orthotropy. The literature on closed composite spherical shells is limited. This could be due to the difficulty of producing laminates that form closed spheres.

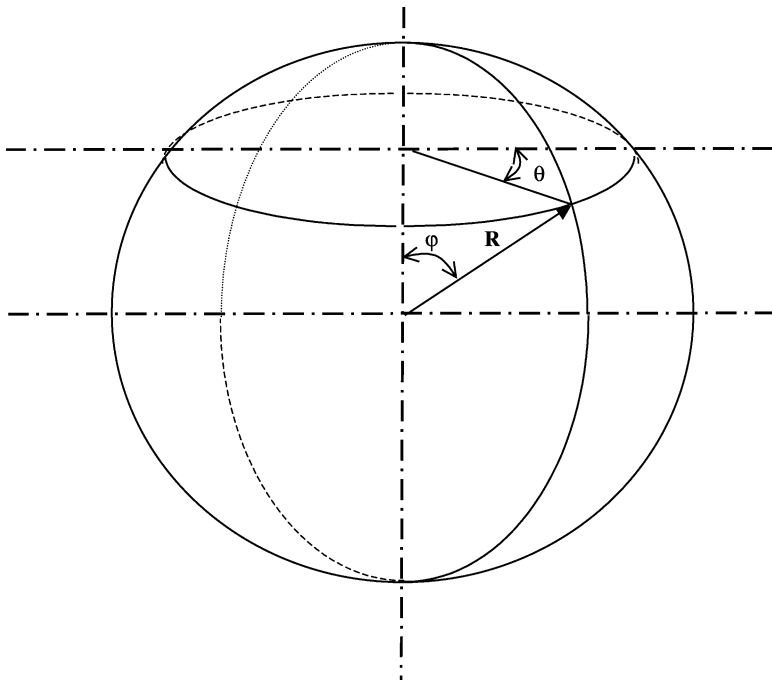


Figure 9.1. A closed spherical shell.

The equation of spherical shells can be obtained by deriving and substituting the proper Lamé parameters of such shells in the general shell equations. Considering Figure 9.1, the fundamental form can be written as

$$(ds)^2 = R^2(d\varphi)^2 + R^2 \sin^2(\varphi)(d\theta)^2 \quad (9.1)$$

which yields the following Lamé parameters and radii of curvature

$$\begin{aligned} A &= R \\ B &= R \sin(\varphi) \\ R_\alpha &= R \\ R_\beta &= R \end{aligned} \quad (9.2)$$

9.1. THIN SPHERICAL SHELLS

Consider first thin spherical shells. The fundamental equations of such shells will be derived by substituting Eq. (9.2) into the general equations derived in Chapter 2.

9.1.1 Kinematic relations

Substituting Eq. (9.2) into Eqs. (2.60) and (2.61) yields the midsurface strains and curvature changes for a thin conical shell

$$\begin{aligned} \varepsilon_{0\varphi} &= \frac{1}{R} \left(\frac{\partial u_0}{\partial \varphi} + w_0 \right) \\ \varepsilon_{0\theta} &= \frac{1}{R} \left(\frac{1}{\sin(\varphi)} \frac{\partial v_0}{\partial \theta} + u_0 \cot \varphi + w_0 \right) \\ \gamma_{0\varphi\theta} &= \frac{1}{R} \left(\frac{\partial v_0}{\partial \varphi} + \frac{1}{\sin(\varphi)} \frac{\partial u_0}{\partial \theta} - v_0 \cot(\varphi) \right) \\ \kappa_\phi &= \frac{1}{R} \frac{\partial \psi_\varphi}{\partial \varphi}, \quad \kappa_\theta = \frac{1}{R} \left(\frac{1}{\sin(\varphi)} \frac{\partial \psi_\theta}{\partial \theta} + \psi_\varphi \cot(\varphi) \right) \\ \tau &= \frac{1}{R} \left(\frac{\partial \psi_\theta}{\partial \varphi} + \frac{1}{\sin(\varphi)} \frac{\partial \psi_\varphi}{\partial \theta} - \psi_\theta \cot(\varphi) \right) \end{aligned} \quad (9.3)$$

where

$$\psi_\varphi = \frac{1}{R} \left(u_0 - \frac{\partial w_0}{\partial \varphi} \right), \quad \psi_\theta = \frac{1}{R} \left(v_0 - \frac{1}{\sin(\varphi)} \frac{\partial w_0}{\partial \theta} \right) \quad (9.4)$$

9.1.2 Stress resultants

The equations derived earlier for the general thin shells (Eq. (2.64)) are applicable for spherical shells with the appropriate change in the coordinate system to that of spherical

shells. The orthotropy of the material treated here is spherical orthotropy. Similar to conical shells, the assumption is made that the stiffness parameters are constant.

9.1.3 Equations of motion

The equations of motion of thin conical shells can be obtained by substituting Eq. (9.2) into Eq. (2.71) derived earlier for shells in curvilinear coordinates. The resulting equations are divided by $B = \alpha \sin(\varphi)$ to become

$$\begin{aligned} \frac{\partial N_\varphi}{\partial \varphi} + (N_\varphi - N_\theta) \cot(\varphi) + \frac{1}{\sin(\varphi)} \frac{\partial N_{\varphi\theta}}{\partial \theta} + Q_\varphi + Rq_\alpha &= R(I_1 \ddot{u}_0^2) \\ \frac{1}{\sin(\varphi)} \frac{\partial N_\theta}{\partial \theta} + \frac{\partial N_{\varphi\theta}}{\partial \varphi} + 2N_{\varphi\theta} \cot(\varphi) + Q_\theta + Rq_\theta &= R(I_1 \ddot{v}_0^2) \\ -(N_\varphi + N_\theta) + \frac{\partial Q_\varphi}{\partial \varphi} + Q_\varphi \cot(\varphi) + \frac{1}{\sin(\varphi)} \frac{\partial Q_\theta}{\partial \theta} + Rq_n &= R(I_1 \ddot{w}_0^2) \end{aligned} \quad (9.5)$$

where

$$\begin{aligned} Q_\varphi &= \frac{1}{R} \left(M_\varphi \cot(\varphi) + \frac{\partial M_\varphi}{\partial \varphi} + \frac{1}{\sin(\varphi)} \frac{\partial M_{\theta\varphi}}{\partial \theta} - M_\theta \cot(\varphi) \right) \\ Q_\theta &= \frac{1}{R} \left(\frac{1}{\sin(\varphi)} \frac{\partial M_\theta}{\partial \theta} + \frac{\partial M_{\varphi\theta}}{\partial \varphi} + 2M_{\varphi\theta} \cot(\varphi) \right) \end{aligned}$$

The equations of motion in terms of displacement can be obtained by substituting Eqs. (2.64) and (9.3) into the above equations.

The boundary conditions for thin shallow shells are obtained by substituting Eq. (8.2) into Eq. (2.72). For $\varphi = \text{constant}$, the boundary conditions are

$$\begin{aligned} N_{0\varphi} - N_\varphi &= 0 \quad \text{or} \quad u_0 = 0 \\ \left(N_{0\varphi\theta} - \frac{N_{0\varphi\theta}}{R} \right) - \left(N_{\varphi\theta} - \frac{N_{\varphi\theta}}{R} \right) &= 0 \quad \text{or} \quad v_0 = 0 \\ \left(Q_{0\varphi} - \frac{1}{R \sin(\varphi)} \frac{\partial M_{0\varphi\theta}}{\partial \theta} \right) - \left(Q_\varphi - \frac{1}{R \sin(\varphi)} \frac{\partial M_{\varphi\theta}}{\partial \theta} \right) &= 0 \quad \text{or} \quad w_0 = 0 \\ M_{0\varphi} - M_\varphi &= 0 \quad \text{or} \quad \psi_\varphi = 0 \\ M_{0\varphi\theta} w \Big|_{\theta_1}^{\theta_2} &= 0 \end{aligned} \quad (8.6)$$

Energy functional can be obtained by substituting Eqs. (2.64) and (9.3) into Eq. (2.67) for the strain energy. Work and kinetic energy expressions are given in Eqs. (2.68) and (2.69), respectively.

9.2. THICK SPHERICAL SHELLS

The fundamental equations of thick spherical shells will be derived by substituting the Lamé parameters and radii of curvature of Eq. (9.2) into the general equations derived for thick shells in Chapter 2.

9.2.1 Kinematic relations

Substituting Eq. (9.2) into the general equations (2.37) and (2.38) yields the midsurface normal, inplane and shear strains for a thick spherical shell:

$$\begin{aligned}
 \varepsilon_{0\varphi} &= \frac{1}{R} \left(\frac{\partial u_0}{\partial \varphi} + w_0 \right) \\
 \varepsilon_{0\theta} &= \frac{1}{R} \left(\frac{1}{\sin(\varphi)} \frac{\partial v_0}{\partial \theta} + u_0 \cot(\varphi) + w_0 \right) \\
 \varepsilon_{0\varphi\theta} &= \frac{1}{R} \left(\frac{\partial v_0}{\partial \varphi} \right) \\
 \varepsilon_{0\theta\varphi} &= \frac{1}{R} \left(\frac{1}{\sin(\varphi)} \frac{\partial u_0}{\partial \theta} - v_0 \cot(\varphi) \right) \\
 \gamma_{0\varphi z} &= \frac{1}{R} \left(\frac{\partial w_0}{\partial \varphi} - u_0 \right) + \psi_\alpha \\
 \gamma_{0\theta z} &= \frac{1}{R} \left(\frac{1}{\sin(\varphi)} \frac{\partial w_0}{\partial \theta} - v_0 \right) + \psi_\theta
 \end{aligned} \tag{9.6}$$

The curvature changes of a thick spherical shell are

$$\begin{aligned}
 \kappa_\varphi &= \frac{1}{R} \frac{\partial \psi_\varphi}{\partial \varphi}, & \kappa_\theta &= \frac{1}{R} \left(\frac{1}{\sin(\varphi)} \frac{\partial \psi_\theta}{\partial \theta} + \psi_\varphi \cot(\varphi) \right) \\
 \kappa_{\alpha\theta} &= \frac{1}{R} \frac{\partial \psi_\theta}{\partial \varphi}, & \kappa_{\theta\alpha} &= \frac{1}{R} \left(\frac{1}{\sin(\varphi)} \frac{\partial \psi_\varphi}{\partial \theta} - \psi_\theta \cot(\varphi) \right)
 \end{aligned} \tag{9.7}$$

9.2.2 Stress resultants

The general thick shell stress resultant Eqs. (2.41)–(2.44) are applicable for the special case of spherical shells. They should, however, be simplified for spherical shells. The term $(1 + z/R)$ exists in both the numerator and denominator of the stress resultant equations and can be eliminated for spherical shells. Even when the truncated Eqs. (2.46)–(2.48) are used, the C_0 parameter of Eq. (2.48) is equal to 0. This will effectively reduce the equations to those of plates (Eqs. (5.26) and (5.27)) with the proper change of the coordinates (α becomes φ and β becomes θ).

9.2.3 Equations of motion

The equations of motion of thick spherical shells are obtained by substituting Eq. (9.2) into Eq. (2.56) derived earlier for shells in curvilinear coordinates. The resulting equations, after being divided by $B (= \alpha \sin(\varphi))$, become:

$$\begin{aligned}
 \frac{\partial N_\varphi}{\partial \varphi} + (N_\varphi - N_\theta) \cot(\varphi) + \frac{1}{\sin(\varphi)} \frac{\partial N_{\varphi\theta}}{\partial \theta} + Q_\varphi + Rq_\alpha &= R(I_1 \ddot{u}_0^2) \\
 \frac{1}{\sin(\varphi)} \frac{\partial N_\theta}{\partial \theta} + \frac{\partial N_{\varphi\theta}}{\partial \varphi} + (N_{\varphi\theta} + N_{\theta\varphi}) \cot(\varphi) + Q_\theta + Rq_\theta &= R(I_1 \ddot{v}_0^2) \\
 -(N_\varphi + N_\theta) + \frac{\partial Q_\varphi}{\partial \varphi} + Q_\varphi \cot(\varphi) + \frac{1}{\sin(\varphi)} \frac{\partial Q_\theta}{\partial \theta} + Rq_n &= R(I_1 \ddot{w}_0^2) \\
 M_\varphi \cot(\varphi) + \frac{\partial M_\varphi}{\partial \varphi} + \frac{1}{\sin(\varphi)} \frac{\partial M_{\varphi\theta}}{\partial \theta} - M_\theta \cot(\varphi) + RQ_\varphi + Rm_\varphi &= R(\bar{I}_2 \ddot{u}_0^2 + \bar{I}_3 \ddot{\psi}_\varphi^2) \\
 \frac{1}{\sin(\varphi)} \frac{\partial M_\theta}{\partial \theta} + \frac{\partial M_{\varphi\theta}}{\partial \varphi} + (M_{\varphi\theta} + M_{\theta\varphi}) \cot(\varphi) + RQ_\theta + Rm_\theta &= R(\bar{I}_2 \ddot{v}_0^2 + \bar{I}_3 \ddot{\psi}_\theta^2)
 \end{aligned} \tag{9.8}$$

where q_φ , q_θ and q_n represent external forces (per unit area) applied either to the surface or as body forces, where the two dots represent the second derivative of these terms with respect to time, and where

$$\bar{I}_i = \left(I_i + \frac{2I_{i+1}}{R} + \frac{I_{i+2}}{R^2} \right), \quad i = 1, 2, 3 \tag{9.9}$$

$$[I_1, I_2, I_3, I_4, I_5] = \sum_{k=1}^N \int_{h_{k-1}}^{h_k} \rho^{(k)} [1, z, z^2, z^3, z^4] dz$$

$\rho^{(k)}$ is the mass density of the k th layer of the shell per unit midsurface area. The boundary conditions for thick shallow shells are similar to those of Eq. (2.58).

9.3. FREE VIBRATIONS

The free vibrations of spherical shells were tackled by different methods. Gautham and Ganesan (1997) used finite elements to solve for vibrations of spherical shells. Graphite/epoxy materials were used with material parameters different from those used earlier. The material properties are listed in Table 9.1. Various thickness ratios were used with various lamination sequences.

Compare the results obtained for single-layer shells with $[0^\circ]$ and $[90^\circ]$ laminates. The first observation made is that the frequencies are higher when the fibers are oriented in the φ direction (i.e., $[0^\circ]$) than those obtained when the fibers are oriented in the θ direction (i.e., $[90^\circ]$). This is the case for all thickness ratios studied. Interestingly, the two-layer,

Table 9.1. Frequency parameter for $\Omega = \omega R \sqrt{\rho/E_2}$ for clamped hemispherical shell.

R/h	$[0^\circ]$	$[90^\circ]$	$[0^\circ, 90^\circ]$	$[0^\circ, 90^\circ, 0^\circ]$	$[90^\circ, 0^\circ, 90^\circ]$
100	0.884	0.976	1.157	1.133	1.125
50	0.932	0.978	1.183	1.180	1.145
20	1.130	0.983	1.237	1.284	1.185
14.2	1.253	0.988	1.263	1.340	1.202
10	1.386	0.995	1.292	1.404	1.222

Graphite/epoxy: $E_1 = 13.8 \times 10^6 \text{ N/cm}^2$, $E_2 = 1.06 \times 10^6 \text{ N/cm}^2$, $G_{12} = 0.6 \times 10^6 \text{ N/cm}^2$, $G_{13} = G_{23} = 0.39 \times 10^6 \text{ N/cm}^2$, $\nu_{23} = \nu_{13} = 0.34$, $\rho = 1.5 \text{ kg/m}^3$, circumferential wave number = 1, (Gautham and Ganesan 1997).

unsymmetrically laminated $[0^\circ, 90^\circ]$ laminate gave the highest frequencies when the shell is thin ($a/h = 50$ and 100). This was not the case when such a shell was shallow (Table 6.28). The three-layer lamination $[0^\circ, 90^\circ, 0^\circ]$ gave the highest frequencies for the thicker shells.

Narasimhan and Alwar (1992) used the Galerkin method with Shybyshev polynomials and obtained frequencies for laminated annular spherical shells having clamped and simple support edges at both the inner and outer boundaries.

Figure 9.2 shows a cross-section of an open annular spherical shell. It defined both the opening angle (φ_1) and annular angle (φ_0) of such shells. Figure 9.3 shows results obtained by Narasimhan and Alwar (1992) for annular spherical shells with different annular angles (φ_0) and various wave numbers (in the circumferential direction). It is observed that such shells with less annular angle have lower frequencies for lower wave numbers and higher frequencies for higher wave numbers when compared with annular shell with larger annular angle.

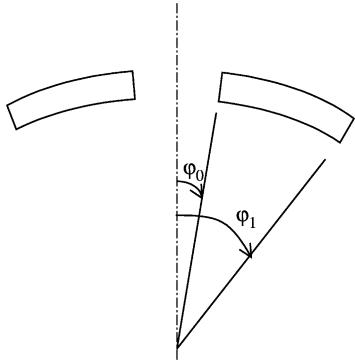


Figure 9.2. Cross-section of annular spherical open shell.

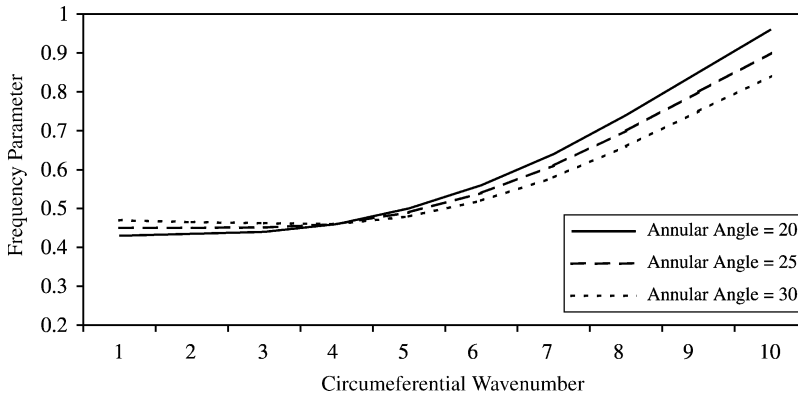


Figure 9.3. Effect of the annular angle on the frequency parameter of a $[0^\circ, 90^\circ, 0^\circ, 90^\circ]$ laminated spherical shell. $\varphi_1 = 60^\circ$, $R/h = 20$, $E_1/E_2 = 11$, $G_{12}/E_2 = 0.275$, $G_{13}/E_2 = G_{23}/E_2 = 0.2$, $\nu_{12} = 0.0275$ (Narasimhan and Alwar 1992).

9.4. RECENT DEVELOPMENTS

Thin spherical shell vibration was considered by Narashimhan and Alwar (1992), Kumar and Singh (1996), Chen and Ding (1997) and Gautham and Ganesan (1997). Thick spherical shells were taken up by Chao and Chern (1988), Chao and Tung (1989) and Chao *et al.* (1999). Gupta and Prasad (1999) studied dynamic axial compression of glass–polyester composite hemispherical shells. Birman *et al.* (2000) analyzed composite spherical shells with active piezoelectric and composite stiffeners. Heated spherical composite shells were studied by Babich *et al.* (1996) and Senitsky (1994) considered fluid-filled spherical shells. Nonlinear dynamic analysis of spherical composite shells was undertaken by Sandeep and Nath (2000). Acoustic radiation of spherical shells was treated by Slepyan and Sorokin (1995).

Chapter 10

Complicating Effects

Free vibration of laminated thin and thick shells was the focus of previous chapters. The complexity of the treatment of these shells can be much higher if one or some of the complicating effects are considered. In a classical sense, both anisotropy and shear deformation are complicating effects (Leissa 1973a). In the context of this book, they were considered as a part of the theory or standard effects. Thus all theories presented here for thin plates and shells like classical plate theory (CPT), classical shallow shell theory (CSST) and classical shell theory (CST) as well as shear deformation plate theory (SDPT), shear deformation shallow shell theory (SDSST) and shear deformation shell theory (SDST) were a part of these standard plate and shell theories. The treatments made here focus further on linear free vibration analysis. The literature on nonlinear theories was reviewed earlier in Chapter 2. Nonlinearity, mainly in the sense large deformation (and strains), constitutes an added complexity to the treatment of laminated shells.

For general shells, the most occurring geometries of doubly curved, cylindrical, spherical and conical shells were treated. Cylindrical, spherical and conical shells belong to the general case of shells of revolution. Both open and closed shells were considered in previous chapters.

General shell shapes and geometries can be more complicated than the types of shells studied here. In fact, many of these complicated shapes do exist in real applications in civil, mechanical, aerospace and submarine engineering. The vibration analysis of such structures has been performed by many working engineers using powerful finite element packages. In most cases, a doubly curved shell element with constant curvature is used. Such an element makes the curvature of the shells discrete and not continuous. Thus, for shells with variable curvature, like conical and noncircular cylindrical shells, a fine mesh must be used to simulate the actual curvature of the shell. The analytical treatment of some of these general shaped shells is possible but may be mathematically demanding, especially for laminated composite structures. As has been seen for the treatment of barrel, noncircular cylindrical, conical and spherical shells, such treatment will require going back to the fundamental shell equations and specializing them to the particular geometry at hand.

In addition to the complexity of curvature, many other complexities can exist in the treatment of laminated shell structures. Among these complexities that researchers have treated in the open literature are initial loading, dynamic loading, thermal stresses, rotating shells, stiffened shells, imperfect shells, piezoelectric shells, damped and viscoelastic shells and shells imbedded in (or filled with) elastic or fluid media. Also, shells on elastic supports and/or foundations, or with variable thickness, or with cutouts

constitute other dimensions of complexities shells may have. More than one complexity can exist in the treatment of some shell problems.

Other complexities may exist for laminated shells that have received limited, if any, treatment in the literature. Variable fiber spacing, material nonlinearity and shells with delaminated layers are examples of such added complexities.

The remainder of this chapter summarizes these complexities and reviews highlights of the most recent research done regarding them. A more comprehensive literature survey can be found in the recent article by the author (Qatu 2002a). There will be no attempt here to cover the analytical treatment of such complexities.

10.1. SHELLS CURVATURE

Other types of curvature that were treated in some of the literature on laminated shells include other shells of revolution which were discussed by Kayran and Vinson (1994), Visscher *et al.* (1991), Singh and Mirza (1991), Rao *et al.* (1993) and Xi *et al.* (1999). Patel *et al.* (2000) studied conical/cylindrical complex structures. Kayran and Vinson (1990a,b) picked up other types of paraboloidal shells.

10.2. INITIAL AND DYNAMIC LOADING

Initial axial loading for cylindrical shells was treated in several research studies (Chang and Lin 1992; Sivadas and Ganesan 1993; Argento 1993; Williams *et al.* 1996). Vibrations of stationary and rotating prestressed conical shells were treated by Sivadas (1995a,b).

Various impulsive loadings were considered by Lee and Lee (1997). Stability and instability of cylindrical shells were treated by Argento (1993). Nemoto and Kasuya (1994) discussed the dynamic response of cylindrical shells subjected to periodic external pressure. Suzuki and Shikanai (1998) studied the vibration of a composite circular cylindrical pressurized vessel.

10.3. THERMAL LOADING

The effects of thermal stresses upon the free vibration or dynamic response of cylindrical shells were discussed by several researchers (Huang and Tauchert 1992; Chang and Shyong 1994; Birman and Bert 1990; Gotsis and Guptill 1995; Xu *et al.* 1997). Argyris *et al.* (1998) studied the chaotic oscillations of laminated composite cylinders subject to periodic application of temperature. Large flexural vibrations of thermally stressed

layered shallow shells were discussed by Heuer (1994). Babich *et al.* (1996) treated heated spherical shells. Noor and Burton (1992) reviewed computational models for high-temperature multilayered composite plates and shells.

10.4. ROTATING, STIFFENED AND IMPERFECT SHELLS

Rotating cylindrical shells were studied by many researchers including Kadivar and Samani (2000) and Lam and Loy (1995b). Rotating conical shells were treated by Sivadas (1995b) and Lam and Hua (2000) studied rotating multilayered conical shell. Lee and Kim (1998) studied rotating composite cylindrical shells with orthogonal stiffeners.

Stiffened cylindrical shells were studied by several researchers including Blocka (1988), Nabi and Ganesan (1993), Bert *et al.* (1993), Liao and Cheng (1994a,b), Goswami and Mukhopadhyay (1995) and Bouabdallah and Batoz (1996). Liao and Cheng (1994a,b) considered stiffened laminated composite plates and shells.

Vibration analysis of imperfect laminated panels under complex preloading conditions was carried out by Kapania and Byun (1992), Cheng *et al.* (2000) and Librescu and Chang (1993). Fu and Chia (1989a,b) studied the multimode nonlinear vibration and postbuckling of antisymmetric imperfect cylindrical thick panels.

10.5. PIEZOELECTRIC SHELLS

Shells made either partially or completely with piezoelectric materials to actively control noise were the subject of interesting research recently. A finite element model was developed for such shells by Heyliger *et al.* (1996). Tzou and Ye (1996) developed a triangular element and used it in vibration analysis of piezoelectric shells. Other advanced materials like shape memory alloys were treated by Hurlbut and Regelbrugge (1996). Application of a finite shell element for composites containing piezoelectric polymers in vibration control was discussed by Lammering (1991) and Berger and Gabbert (2000). Piezoelectric actuators effects on cylindrical shell response were studied by Hussein and Heyliger (1996), Sonti and Jones (1996a,b), Dube *et al.* (1999a,b) and Tzou and Bao (1995). Chen and Shen (1998) used three-dimensional analysis to examine the free vibration of orthotropic piezoelectric circular cylindrical shells. Birman *et al.* (2000) studied the axisymmetric motion of composite spherical shells with active piezoelectric and composite stiffeners. Much of the literature on piezoelectric composite shells has been recently reviewed by Saravanos and Heyliger (1999).

10.6. DAMPED AND VISCOELASTIC SHELLS

Vibrations of thick elastic and viscoelastic tubes were considered by Moore (1990). Damping of cylindrical shells was considered by many authors (Bicos and Springer 1989; Birlik and Mengi 1989; Singh and Gupta 1994a,b; Ramesh and Ganesan 1994). Hu and Huang (2000a,b) investigated the application of constrained layer damping on the cylindrical shells conveying fluid. Korjakin *et al.* (1998) studied damped vibrations of conical shells.

10.7. SHELLS IMBEDDED IN (OR FILLED WITH) ELASTIC OR FLUID MEDIA

Open cylindrical shells subjected to a flowing fluid were discussed by Selmane and Lakis (1997b). Influence of enclosed air on vibration modes of a shell structure was investigated by Isaksson *et al.* (1995). Vibrational modes of submerged bodies were found by Barbone and Crighton (1994). Other studies on submerged shells include those of Gong and Lam (1998).

Fluid-filled cylindrical shells were examined by Lakis and Laveau (1991), Sharma *et al.* (1996) and others. Submerged shells were discussed by Barbone and Crighton (1994).

Acoustic radiation of cylindrical or spherical shells was treated in many studies (Blaise *et al.* 1991; Blaise and Lesueur 1992).

10.8. OTHER COMPLEXITIES

Vibration of an orthotropic shallow spherical shell on a Pasternak foundation was discussed by Paliwal *et al.* (1995a), and on a Kerr foundation by Paliwal *et al.* (1995b). Paliwal and Pandey (1998) studied the free vibration of a cylindrical shell on an elastic foundation.

Cylindrical shells with variable thickness were discussed by Ganesan and Sivadas (1989, 1990), and Suzuki *et al.* (1994, 1996). Conical shells with variable thickness were examined by Sivadas and Ganesan (1991a,b). Patel *et al.* (2000) studied conical/cylindrical complex structures. Shells with discontinuously variable cross-section were analyzed by Drewko and Sperski (1991). Panels with cutouts were picked up by Levraea *et al.* (1993).

Examples of wave propagation in composite plates and shells can be found in the books of Nayfeh (1995) and Ye (2003).

Dynamic instability of layered anisotropic shells received considerable attention. Argento and Scott (1993a,b) presented formulation and results for the case of dynamic

stability of laminated cylindrical shells. Lam and Ng (1998) and Ng *et al.* (1998) studied dynamic stability of laminated composite cylindrical shells subjected to conservative periodic axial loads using various shell theories.

Lee and Saravanos (2000) used a mixed, multifield FEM formulation for a study of thermopiezoelectric composite shells. Sensitivity analysis was performed by Noor *et al.* (1995).

10.9. CONCLUDING REMARKS

There is a general trend among researchers in the field of composite shell vibrations to include shear deformation and rotary inertia. This is understandable because the effects of shear deformation are found to be greater for composite shells than they are for isotropic, homogeneous ones. For that purpose, and the convenience of avoiding having to use the three-dimensional theory of elasticity, most researchers looked for, developed and used thick, or shear deformation, shell theories.

Flat plates, doubly curved shallow shells and cylindrical shells are the subject of research of most recent articles. Complicating effects of various kinds have received considerable interest. Piezoelectric shells, with their advanced applications in controlling vibrations in the aerospace industry have received considerable attention. Shell interaction with elastic or fluid media is receiving more interest recently. In particular, attention has been given to fluid-filled shells and shell vibration in an acoustical medium. Damping is also becoming another corner of interesting research. This can be due to the increasing sensitivity of the public to noise and vibrations in engineering products, and to reduce vibration stresses to increase fatigue life.

The Ritz method for the linear analysis of composite shells and the Galerkin method for the nonlinear analysis of such shells are still frequently used. Their accuracy and ease of use with today's high-performance digital computational tools have made them attractive to researchers. On the other hand, finite element methods are being used successfully in many engineering applications, including composite shell vibrations. Special attention is still needed when nonclassical curvature or boundary conditions are treated, as these are not yet covered by most computational finite element packages. Furthermore, convergence studies are needed for finite element analyses to show the accuracy of the results obtained.

Recent research seems to be more oriented towards developing and using advanced theories that, in some cases, may not be needed for the problem at hand. Less attention is being given towards experimental verification of such theories, the interpretation of the results and finding new applications for such structures. The parameters of the lamination material and sequence, fiber orientation, as well as curvature, are giving more freedom to engineers to design superior and more economical structures. More attention should be

given to the fundamental understanding of the behavior of laminated composite shells and the effects of the various parameters that the engineer controls. Attention is also needed for experimental verification and correlation with current analytical methods and theories. As is shown here, articles that are dedicated to obtaining experimental results are extremely limited.

Appendix A

Frequency parameter $\Omega = \omega a^2 \sqrt{\rho/E_1 h^2}$ for three-layered $[\theta, -\theta, \theta]$ E/E square plates (49 DOF).

B.C.	θ	1	2	3	4	5	6
FFFF	0	2.926	4.123	6.531	7.222	8.734	11.85
	15	3.002	4.137	6.344	7.271	8.838	12.02
	30	3.155	4.200	5.928	7.390	8.962	12.74
	45	3.231	4.263	5.686	7.462	8.980	13.91
SFFF	0	1.455	4.437	5.129	6.283	10.84	12.65
	15	1.498	4.271	5.172	6.335	10.91	12.89
	30	1.593	3.842	5.299	6.464	11.07	12.64
	45	1.664	3.348	5.444	6.642	11.01	11.32
	60	1.625	3.007	5.483	6.849	9.942	11.26
	75	1.501	2.877	5.354	7.039	9.410	11.25
	90	1.435	2.853	5.255	7.124	9.294	11.40
CFFF	0	1.024	2.014	5.373	6.441	7.992	12.30
	15	0.9744	2.051	5.441	6.187	7.914	12.24
	30	0.8668	2.107	5.309	5.883	7.756	12.39
	45	0.7617	2.095	4.719	6.035	7.596	12.41
	60	0.6919	1.985	4.297	6.214	7.434	12.12
	75	0.6607	1.844	4.122	6.298	7.302	11.59
	90	0.6535	1.782	4.085	6.293	7.270	11.46
SSFF	0	0.7315	3.604	5.001	8.559	9.973	14.94
	15	0.7401	3.603	5.027	8.589	10.25	14.44
	30	0.7814	3.655	4.966	8.651	10.94	13.51
	45	0.8037	3.682	4.928	8.676	11.58	12.75
CSFF	0	1.356	3.947	6.846	9.980	10.28	14.23
	15	1.401	4.022	6.811	9.876	10.74	16.53
	30	1.386	4.172	6.469	9.857	11.45	16.28
	45	1.307	4.326	6.022	9.796	12.36	14.82
	60	1.201	4.468	5.638	9.660	12.94	13.96
	75	1.120	4.590	5.382	9.499	12.35	14.69
	90	1.097	4.700	5.187	9.419	12.08	15.07
CCFF	0	1.610	5.008	6.975	10.85	12.26	18.01
	15	1.688	5.086	7.003	10.95	12.60	17.79
	30	1.734	5.262	6.789	11.03	13.43	16.63
	45	1.748	5.369	6.645	11.06	14.26	15.57

(continued)

Appendix A. (continued).

B.C.	θ	1	2	3	4	5	6
SFSF	0	2.866	3.988	7.693	11.49	12.74	15.23
	15	2.755	3.974	7.813	11.04	12.49	15.28
	30	2.470	3.947	8.111	9.964	11.91	15.45
	45	2.149	3.904	8.444	8.733	11.21	15.70
	60	1.932	3.751	7.822	8.668	10.44	15.74
	75	1.845	3.477	7.420	8.791	9.644	15.41
	90	1.828	3.331	7.335	8.936	9.186	15.15
CFSF	0	4.490	5.389	8.699	14.56	15.64	15.92
	15	4.295	5.305	8.814	13.95	15.20	15.75
	30	3.837	5.114	9.081	12.55	14.21	16.71
	45	3.358	4.884	9.327	11.02	13.11	17.11
	60	3.035	4.593	9.420	9.902	12.08	17.15
	75	2.895	4.279	9.398	9.423	11.27	16.77
	90	2.864	4.135	9.293	9.412	10.93	16.50
SSSF	0	3.184	5.952	11.82	12.16	14.61	20.64
	15	3.115	6.060	11.41	12.39	14.65	20.66
	30	2.939	6.307	10.51	12.77	14.85	20.83
	45	2.732	6.541	9.452	13.02	15.24	20.51
	60	2.529	6.633	8.555	12.91	15.73	18.68
	75	2.364	6.590	8.011	12.47	16.20	17.61
	90	2.296	6.545	7.843	12.20	16.40	17.32
CSSF	0	4.739	7.061	12.85	14.86	17.21	22.09
	15	4.672	7.216	13.15	14.44	17.23	22.61
	30	4.367	7.368	13.14	13.79	16.92	22.69
	45	3.959	7.433	11.76	14.23	16.57	22.76
	60	3.585	7.355	10.59	14.33	16.44	21.48
	75	3.332	7.184	9.935	13.96	16.60	20.24
	90	3.227	7.080	9.723	13.69	16.71	19.90
CCSF	0	4.842	7.897	14.72	14.90	17.85	24.19
	15	4.806	8.058	14.46	15.00	17.85	24.19
	30	4.521	8.301	13.30	15.46	17.85	24.25
	45	4.164	8.509	11.92	15.75	18.24	23.90
	60	3.834	8.613	10.78	15.55	19.04	21.34
	75	3.602	8.670	10.11	15.18	19.58	20.39
	90	3.508	8.670	9.896	14.89	19.88	20.01
CFCF	0	6.498	7.338	9.982	16.74	17.93	18.91
	15	6.255	7.016	10.08	16.94	17.43	18.30
	30	5.620	6.586	10.20	15.51	16.88	17.78
	45	4.923	6.112	10.26	13.62	15.34	18.35
	60	4.432	5.674	10.19	12.25	14.10	18.58

(continued)

Appendix A. (continued).

B.C.	θ	1	2	3	4	5	6
SCSF	75	4.212	5.324	10.07	11.62	13.24	18.31
	90	4.161	5.181	10.02	11.48	12.93	18.07
	0	3.339	6.884	11.90	14.08	15.23	22.11
	15	3.275	6.994	11.53	14.12	15.46	22.17
	30	3.127	7.285	10.66	14.20	16.18	22.28
	45	2.980	7.654	9.736	14.26	17.39	20.95
	60	2.829	7.862	8.876	14.10	18.27	18.90
	75	2.708	7.987	8.384	13.73	17.74	19.28
CSCF	90	2.655	8.032	8.209	13.50	17.44	19.63
	0	6.692	8.601	13.89	18.21	20.39	23.88
	15	6.467	8.578	14.10	17.55	20.05	24.06
	30	5.893	8.486	14.58	15.95	19.24	24.35
	45	5.268	8.354	14.12	15.17	18.33	24.41
	60	4.788	8.111	12.76	15.56	17.46	24.29
	75	4.524	7.896	12.06	15.59	17.00	23.32
	90	4.440	7.798	11.86	15.44	17.11	22.97
CCCF	0	6.768	9.296	15.62	18.26	20.86	26.06
	15	6.553	9.296	15.85	17.61	20.51	26.02
	30	5.998	9.312	15.96	16.48	19.93	26.08
	45	5.398	9.341	14.22	17.00	19.47	26.20
	60	4.962	9.349	12.87	17.12	19.46	24.78
	75	4.720	9.292	12.19	16.75	19.95	23.40
	90	4.650	9.266	11.99	16.50	20.25	23.06
SSSS	0	4.434	9.717	12.96	17.73	19.09	26.55
	15	4.499	9.942	12.80	17.76	19.70	26.94
	30	4.631	10.45	12.44	17.91	21.17	25.37
	45	4.696	10.76	12.18	18.02	22.79	23.62
CSSS	0	5.734	10.53	15.83	19.62	20.13	28.43
	15	5.720	10.73	15.52	19.55	20.70	28.63
	30	5.675	11.21	14.76	19.64	22.00	28.87
	45	5.553	11.70	13.81	19.54	23.64	26.12
	60	5.513	11.90	13.80	20.11	21.77	25.44
	75	5.156	11.55	13.20	19.02	22.09	27.29
	90	5.078	11.41	13.29	18.91	21.53	27.97
CCSS	0	6.235	12.05	16.11	21.20	21.95	30.10
	15	6.276	12.32	15.83	20.99	22.81	30.90
	30	6.369	12.81	15.22	21.00	24.21	29.41
	45	6.416	13.19	14.84	21.15	26.16	26.43

(continued)

Appendix A. (continued).

B.C.	θ	1	2	3	4	5	6
CSCS	0	7.483	11.66	19.08	20.31	22.96	28.62
	15	7.365	11.80	18.61	20.54	23.06	30.59
	30	7.142	12.19	17.50	21.04	23.81	31.94
	45	6.709	12.52	16.05	21.18	24.30	29.66
	60	6.372	12.91	14.81	20.81	26.01	26.91
	75	6.062	13.23	13.97	20.46	25.03	27.63
	90	5.964	13.35	13.72	20.26	24.46	28.21
CCCS	0	7.925	13.17	19.36	22.56	23.87	32.49
	15	7.840	13.40	18.87	22.90	24.19	32.12
	30	7.590	13.58	17.78	22.82	25.05	32.81
	45	7.364	14.12	16.72	22.78	27.19	30.00
	60	7.193	14.45	16.03	22.69	27.23	30.08
	75	7.030	14.14	16.35	22.94	25.26	31.24
	90	7.000	13.95	16.49	22.49	25.07	32.19
CCCC	0	8.498	14.81	19.81	24.56	25.71	33.08
	15	8.444	15.19	19.31	24.64	35.73	37.45
	30	8.418	15.42	18.42	24.56	27.98	33.49
	45	8.334	15.95	17.57	24.37	29.75	30.18

Appendix B

Frequency parameter $\Omega = \omega a^2 \sqrt{\rho/E_1 h^2}$ for three-layered $[\theta, -\theta, \theta]$ E/E shallow cylindrical shells on square planforms ($a/h = 20$, $a/R_\alpha = 0.5$), 108 DOF.

B.C.	θ	1	2	3	4	5	6
FFFF	0	2.922	5.542	6.592	7.452	8.806	13.24
	15	2.998	5.546	6.442	7.480	8.959	13.39
	30	3.164	5.344	6.293	7.580	9.176	13.93
	45	3.280	4.813	6.535	7.654	9.231	14.18
	60	3.224	4.368	6.993	7.563	9.222	12.78
	75	3.025	4.192	7.386	7.415	9.116	12.05
	90	2.919	4.160	7.304	7.581	9.020	11.87
SFFF	0	1.437	4.449	6.230	6.405	11.67	13.87
	15	1.479	4.283	6.045	6.711	11.76	14.05
	30	1.573	3.860	5.917	7.086	11.91	12.81
	45	1.645	3.367	5.829	7.393	11.26	11.99
	60	1.612	3.012	5.647	7.693	10.10	11.91
	75	1.485	2.868	5.360	7.958	9.540	11.78
	90	1.415	2.841	5.211	8.064	9.413	11.86
CFFF	0	1.012	1.963	6.236	6.714	7.392	11.57
	15	0.963	2.002	5.977	6.677	7.476	11.77
	30	0.857	2.061	5.343	6.612	7.591	11.73
	45	0.754	2.052	4.677	6.466	7.699	11.09
	60	0.684	1.943	4.232	6.218	7.873	10.34
	75	0.653	1.797	4.043	5.941	8.074	9.730
	90	0.646	1.729	4.002	5.814	8.170	9.429
SSFF	0	0.730	4.518	5.026	9.023	11.27	15.14
	15	0.741	4.407	5.217	9.097	11.53	14.71
	30	0.787	4.235	5.423	9.246	12.04	13.79
	45	0.816	3.997	5.625	9.298	12.02	13.45
	60	0.794	3.770	5.787	9.227	11.11	14.25
	75	0.743	3.614	5.863	9.107	10.37	14.98
	90	0.725	3.583	5.814	9.067	10.08	15.30
CSFF	0	1.350	4.683	6.803	10.46	11.38	17.24
	15	1.403	4.758	6.809	10.47	11.76	17.34
	30	1.400	4.887	6.549	10.49	12.43	16.53
	45	1.327	4.908	6.257	10.41	13.18	15.02
	60	1.216	4.798	6.095	10.22	13.15	14.63

(continued)

Appendix B. (continued).

B.C.	θ	1	2	3	4	5	6
CCFF	75	1.121	4.687	6.004	9.997	12.42	15.39
	90	1.089	4.683	5.878	9.899	12.14	15.79
	0	1.897	5.930	7.113	11.74	13.32	18.28
	15	1.986	5.946	7.254	11.81	13.65	17.85
	30	2.066	5.947	7.274	11.86	14.33	16.69
	45	2.113	5.821	7.366	11.79	14.54	16.11
	60	2.123	5.607	7.574	11.66	13.50	17.22
	75	2.081	5.402	7.733	11.54	12.65	18.12
SFSF	90	2.007	5.314	7.644	11.50	12.27	18.17
	0	2.833	3.885	9.912	11.53	12.76	17.06
	15	2.725	3.871	10.00	11.10	12.60	16.59
	30	2.447	3.844	10.02	10.03	12.24	16.43
	45	2.132	3.803	8.777	9.879	11.77	16.45
	60	1.915	3.653	7.854	9.662	11.15	16.36
	75	1.826	3.384	7.447	9.363	10.60	15.95
	90	1.807	3.241	7.361	9.191	10.39	15.67
CFSF	0	4.357	6.647	11.28	14.38	15.77	17.89
	15	4.185	6.630	11.33	13.82	15.41	18.01
	30	3.758	6.471	11.31	12.46	14.50	18.11
	45	3.286	6.183	10.91	11.20	13.50	18.12
	60	2.957	5.773	9.799	10.98	12.41	17.88
	75	2.813	5.399	9.295	10.86	11.56	17.38
	90	2.781	5.221	9.184	10.91	11.10	17.07
SSSF	0	3.140	7.597	11.86	13.97	14.24	14.75
	15	3.070	7.783	11.49	14.08	14.89	15.17
	30	2.897	8.098	10.61	13.85	15.86	16.62
	45	2.692	8.182	9.631	13.62	16.42	17.43
	60	2.493	8.020	8.782	13.27	16.61	16.89
	75	2.330	7.853	8.185	12.72	14.89	17.29
	90	2.264	7.863	7.873	12.43	13.97	17.32
CSSF	0	4.662	8.446	13.97	14.83	14.87	17.42
	15	4.616	8.648	14.41	14.89	15.11	17.39
	30	4.317	8.929	13.24	15.30	16.62	17.36
	45	3.914	8.973	11.83	15.18	17.25	17.44
	60	3.540	8.763	10.65	14.78	16.61	17.40
	75	3.283	8.463	9.959	14.20	14.89	17.64
	90	3.185	8.297	9.747	13.88	13.97	17.74
CCSF	0	5.530	10.03	14.86	16.71	18.17	24.83
	15	5.549	10.21	14.47	16.77	18.32	24.88

(continued)

Appendix B. (continued).

B.C.	θ	1	2	3	4	5	6
	30	5.418	10.31	13.37	16.70	18.64	24.98
	45	5.154	10.23	12.06	16.41	19.05	24.41
	60	4.839	10.07	10.95	16.05	19.76	22.10
	75	4.559	9.940	10.347	15.66	20.49	21.00
	90	4.403	9.939	9.961	15.17	20.42	20.68
CFCF	0	10.53	10.97	13.29	17.84	18.96	19.01
	15	10.10	10.57	13.13	17.14	18.41	19.15
	30	9.024	9.615	12.75	15.44	17.08	19.39
	45	7.849	8.613	12.27	13.54	15.60	19.54
	60	7.088	7.922	11.94	12.16	14.33	19.47
	75	6.785	7.539	11.53	11.69	13.42	19.00
	90	6.723	7.414	11.39	11.63	13.07	18.69
SCSF	0	3.656	8.423	11.94	13.97	15.39	15.87
	15	3.624	8.597	11.60	14.89	15.06	16.48
	30	3.546	8.882	10.81	14.80	16.61	17.38
	45	3.470	8.869	10.05	14.59	17.43	18.14
	60	3.404	8.521	9.665	14.39	16.63	18.79
	75	3.296	8.196	9.440	13.97	14.90	17.74
	90	3.229	8.080	9.350	13.72	13.97	17.44
CSCF	0	7.028	10.71	16.10	18.29	20.71	25.72
	15	6.905	10.71	16.22	17.67	20.39	25.66
	30	6.530	10.57	16.01	16.48	19.68	25.57
	45	6.002	10.20	14.27	16.51	18.87	25.30
	60	5.491	9.736	12.90	16.42	18.14	24.11
	75	5.118	9.372	12.16	16.00	18.07	22.79
	90	4.978	9.235	11.953	15.746	18.16	22.20
CCCF	0	10.702	12.62	17.91	18.21	21.20	27.48
	15	10.279	12.40	17.54	17.98	20.96	27.04
	30	9.254	11.90	16.01	18.10	20.44	26.24
	45	8.150	11.40	14.28	18.05	19.99	26.46
	60	7.400	10.96	12.96	17.65	20.42	26.30
	75	7.139	10.86	12.26	16.63	16.63	18.14
	90	7.054	10.84	12.01	16.87	21.06	24.42
SSSS	0	5.601	11.71	13.05	18.10	20.69	27.09
	15	5.759	11.92	12.96	18.24	21.20	27.11
	30	6.073	11.89	13.05	18.48	22.44	25.44
	45	6.252	11.35	13.37	18.60	23.17	24.38
	60	6.097	10.70	13.65	18.39	21.26	26.16
	75	5.785	10.11	13.90	18.16	19.75	27.16
	90	5.626	9.863	14.00	18.11	19.11	26.70

(continued)

Appendix B. (continued).

B.C.	θ	1	2	3	4	5	6
CSSS	0	6.623	12.34	15.91	20.45	21.16	27.93
	15	6.704	12.60	15.63	20.36	22.00	29.74
	30	6.850	12.97	14.90	20.33	23.34	26.94
	45	6.857	12.91	14.53	20.12	24.47	25.84
	60	6.620	12.36	14.12	19.71	24.17	26.44
	75	6.274	11.78	14.22	19.30	22.56	27.94
	90	6.106	11.52	14.29	19.19	22.07	27.93
CCSS	0	8.028	14.13	16.31	21.59	24.05	32.05
	15	8.157	14.30	16.09	21.37	24.42	30.31
	30	8.284	14.41	15.74	21.66	25.85	29.82
	45	8.185	13.94	15.95	21.87	27.17	28.91
	60	7.924	13.19	16.24	21.34	25.10	30.52
	75	7.659	12.61	16.77	21.39	23.27	30.56
	90	7.537	12.38	16.94	21.33	22.35	30.01
CSCS	0	9.068	13.86	19.31	22.00	23.43	27.93
	15	9.080	13.98	18.87	22.09	23.64	29.76
	30	8.958	14.10	17.79	22.19	24.72	31.98
	45	8.533	14.08	16.32	21.87	25.45	30.93
	60	7.980	14.01	15.28	21.36	26.77	27.95
	75	7.529	13.76	14.82	20.90	26.13	28.21
	90	7.358	13.57	14.80	20.69	25.56	27.93
CCCS	0	11.54	15.75	19.46	24.86	24.86	32.43
	15	11.29	15.68	19.10	24.19	25.44	32.38
	30	10.60	15.67	18.11	23.65	26.16	33.11
	45	9.824	15.57	17.59	23.94	28.66	32.23
	60	9.229	15.05	16.94	23.38	28.55	31.07
	75	8.969	14.50	17.09	22.47	25.75	31.93
	90	8.885	14.18	17.45	22.89	26.16	33.38
CCCC	0	11.97	17.21	19.79	25.76	28.24	38.47
	15	11.58	17.23	17.23	21.26	21.26	28.70
	30	11.16	17.12	18.80	25.38	30.88	35.40
	45	10.56	16.73	18.70	25.42	31.37	33.01
	60	10.19	15.89	19.33	25.08	29.42	36.05
	75	10.03	15.35	16.10	20.23	25.03	29.06
	90	10.22	10.22	16.07	20.50	26.12	27.96

Appendix C

Frequency parameter $\Omega = \omega a^2 \sqrt{\rho/E_1 h^2}$ for three-layered $[\theta, -\theta, \theta]$ E/E shallow spherical shells on square planforms ($a/h = 20, a/R_\alpha = 0.5, b/R_\beta = 0.5$).

B.C.	θ	1	2	3	4	5	6
FFFF	0	2.915	4.733	7.412	7.907	8.852	13.32
	15	3.016	4.649	7.504	7.829	8.932	13.47
	30	3.259	4.418	7.673	7.711	9.039	13.99
	45	3.429	4.243	7.596	7.831	9.060	14.79
SFFF	0	1.437	4.489	6.327	6.735	12.699	13.81
	15	1.490	4.361	6.220	6.940	12.819	13.97
	30	1.613	4.027	6.125	7.223	12.926	13.57
	45	1.696	3.669	6.034	7.423	12.157	12.96
	60	1.633	3.486	5.793	7.630	11.265	12.68
	75	1.487	3.464	5.452	7.851	10.837	12.29
	90	1.415	3.473	5.287	7.952	10.715	12.10
CFFF	0	1.333	1.994	5.799	7.417	7.426	11.60
	15	1.294	2.039	5.720	7.061	7.704	11.80
	30	1.190	2.112	5.399	6.805	7.825	11.76
	45	1.068	2.103	4.981	6.611	7.857	11.11
	60	0.9822	1.978	4.742	6.323	7.926	10.37
	75	0.9438	1.822	4.675	6.007	8.053	9.750
	90	0.9344	1.754	4.665	5.862	8.128	9.451
SSFF	0	0.7243	3.983	5.856	10.59	11.25	15.73
	15	0.7488	3.858	6.014	10.69	11.52	15.32
	30	0.8102	3.783	6.093	10.97	11.99	14.57
	45	0.8423	3.755	6.112	11.11	12.26	14.14
CSFF	0	1.369	4.316	7.362	11.22	11.99	17.53
	15	1.402	4.312	7.468	11.31	12.33	17.88
	30	1.389	4.371	7.300	11.58	12.84	17.15
	45	1.318	4.419	7.018	11.82	13.33	15.91
	60	1.217	4.485	6.736	11.77	13.64	15.21
	75	1.138	4.610	6.463	11.49	13.34	15.55
	90	1.123	4.772	6.198	11.35	13.12	15.81
CCFF	0	2.553	5.445	7.835	12.95	13.24	18.75
	15	2.616	5.385	8.061	12.99	13.59	18.35
	30	2.684	5.378	8.154	13.14	14.19	17.35
	45	2.707	5.376	8.172	13.21	14.60	16.68

(continued)

Appendix C. (continued).

B.C.	θ	1	2	3	4	5	6
SFSF	0	3.146	3.966	11.07	12.10	12.97	17.54
	15	3.053	3.961	11.14	11.70	12.88	17.34
	30	2.813	3.947	10.71	10.98	12.72	17.33
	45	2.540	3.899	9.626	10.57	12.37	17.46
	60	2.359	3.718	8.866	10.12	11.81	17.45
	75	2.294	3.431	8.505	9.641	11.31	17.04
	90	2.282	3.285	8.406	9.410	11.11	16.72
CFSF	0	4.806	6.763	12.10	14.88	15.98	18.27
	15	4.668	6.753	12.18	14.34	15.64	18.47
	30	4.315	6.601	12.18	13.07	14.78	18.71
	45	3.909	6.269	11.60	12.06	13.74	18.84
	60	3.609	5.863	10.70	11.67	12.74	18.76
	75	3.453	5.477	10.26	11.41	11.90	18.30
	90	3.407	5.296	10.14	11.33	11.52	17.96
SSSF	0	3.478	9.398	12.41	13.97	14.91	15.79
	15	3.426	9.667	12.07	14.87	15.05	16.04
	30	3.293	10.03	11.34	15.09	16.54	16.68
	45	3.126	9.816	10.72	15.12	17.02	17.44
	60	2.944	9.333	10.13	15.00	16.61	17.35
	75	2.776	8.962	9.561	14.49	14.89	17.64
	90	2.704	8.818	9.297	13.97	14.14	17.77
CSSF	0	4.930	10.10	13.97	15.31	15.50	18.31
	15	4.939	10.37	14.88	14.92	15.85	18.31
	30	4.698	10.76	13.85	16.17	16.64	18.21
	45	4.320	10.75	12.57	16.29	17.43	17.91
	60	3.952	10.41	11.49	16.22	16.61	17.96
	75	3.687	9.94	10.81	14.89	15.77	18.01
	90	3.583	9.685	10.58	13.97	15.43	18.06
CCSF	0	5.752	11.38	15.30	17.16	18.98	25.19
	15	5.701	11.02	15.02	17.31	19.00	24.70
	30	5.662	11.83	13.96	17.54	19.35	25.78
	45	5.370	11.78	12.74	17.58	19.36	24.10
	60	4.981	11.43	11.95	17.41	20.16	22.78
	75	4.648	10.95	11.50	17.10	20.67	21.50
	90	4.510	10.72	11.34	16.84	20.89	21.19
CFCF	0	10.829	11.04	13.76	18.26	19.15	19.26
	15	10.455	10.66	13.68	17.56	18.62	19.45
	30	9.512	9.740	13.43	15.95	17.33	19.78
	45	8.424	8.741	13.03	14.20	15.89	20.05

(continued)

Appendix C. (continued).

B.C.	θ	1	2	3	4	5	6
SCSF	60	7.657	8.023	12.55	13.00	14.61	20.15
	75	7.292	7.619	12.21	12.43	13.68	19.78
	90	7.197	7.485	12.08	12.28	13.31	19.47
	0	3.562	10.27	12.44	13.97	16.41	16.44
	15	3.519	10.46	12.15	14.90	16.11	17.09
	30	3.407	10.57	11.67	16.03	16.62	17.97
	45	3.266	10.03	11.56	16.12	17.42	18.81
	60	3.100	9.437	11.36	16.14	16.64	19.45
	75	2.943	9.031	11.09	14.90	15.86	18.61
CSCF	90	2.873	8.876	10.95	13.97	15.63	18.32
	0	7.412	11.77	16.57	18.70	21.44	25.91
	15	7.341	11.87	16.69	18.13	21.19	26.07
	30	7.043	11.90	16.44	17.15	20.57	26.16
	45	6.562	11.61	14.92	17.18	19.77	25.75
	60	6.023	10.84	13.71	17.87	19.21	24.24
	75	5.641	10.52	12.96	17.29	18.50	22.91
	90	5.470	10.29	12.74	17.04	18.47	22.32
CCCF	0	10.930	13.50	18.23	18.58	21.89	27.84
	15	10.588	13.38	17.85	18.41	21.63	26.47
	30	9.635	13.24	16.49	18.65	21.24	27.62
	45	8.497	13.01	14.86	18.89	21.29	28.82
	60	7.870	12.56	13.67	18.98	20.93	26.91
	75	7.513	12.18	12.96	18.59	21.08	25.45
	90	7.407	12.03	12.73	18.32	21.30	25.11
SSSS	0	8.238	12.70	14.53	19.10	21.05	27.63
	15	8.566	13.00	14.48	19.32	21.56	27.89
	30	9.209	13.38	14.44	19.74	22.78	26.35
	45	9.542	13.44	14.45	19.93	24.10	24.82
CSSS	0	8.975	13.31	17.14	21.34	21.57	27.93
	15	9.237	13.59	16.94	21.21	22.27	29.75
	30	9.744	14.02	16.40	21.27	23.46	30.32
	45	9.974	14.20	15.90	21.34	24.95	27.94
	60	9.598	14.29	15.33	21.00	25.60	26.74
	75	8.951	14.24	14.90	20.44	24.27	28.10
	90	8.626	14.03	14.82	20.18	23.76	27.93
CCSS	0	9.967	14.92	17.51	22.55	24.42	33.06
	15	10.23	15.57	18.04	22.65	25.15	32.05
	30	10.68	15.44	17.04	22.71	26.16	30.81
	45	10.90	15.56	16.60	21.90	27.13	27.52

(continued)

Appendix C. (continued).

B.C.	θ	1	2	3	4	5	6
CSCS	0	10.72	14.55	20.34	22.32	24.21	27.93
	15	10.88	14.69	19.99	22.51	24.30	29.76
	30	11.08	14.88	19.10	22.83	24.93	32.72
	45	10.89	14.88	18.04	22.88	25.71	31.88
	60	10.28	14.90	17.05	22.39	27.07	29.08
	75	9.599	15.08	16.18	21.63	27.39	28.32
	90	9.301	15.24	15.74	21.53	27.01	27.93
CCCS	0	12.69	16.18	20.48	25.05	25.29	34.41
	15	12.61	16.28	20.16	24.70	26.61	35.87
	30	12.50	16.68	18.89	23.89	23.89	29.26
	45	11.97	16.58	18.40	24.79	29.05	32.70
	60	11.42	16.84	17.89	24.47	28.75	31.34
	75	10.93	16.68	17.69	23.62	28.12	32.90
	90	10.70	16.45	17.87	23.85	27.45	33.13
CCCC	0	13.61	17.65	20.75	26.37	27.96	33.97
	15	13.58	17.72	20.46	25.96	28.83	37.12
	30	13.44	18.00	19.84	26.06	31.31	35.91
	45	13.41	18.16	19.54	26.63	32.17	34.18

Appendix D

Frequency parameter $\Omega = \omega a^2 \sqrt{\rho/E_1 h^2}$ for three-layered $[\theta, -\theta, \theta]$ E/E deep cylindrical shells ($a/b = 1$, $a/h = 20$, $a/R = 1.0$, 108 DOF).

B.C.	θ	1	2	3	4	5	6
FFFF	0	2.899	4.138	7.227	9.536	9.609	11.94
	15	3.032	4.185	7.379	9.494	9.586	12.11
	30	3.251	4.435	7.668	9.176	9.599	12.86
	45	3.281	5.006	7.799	8.771	9.526	14.32
	60	3.150	5.706	7.760	8.416	9.336	15.63
	75	2.982	6.263	7.748	8.160	8.961	15.48
	90	2.906	6.475	7.792	8.051	8.720	15.50
SFFF	0	1.450	5.049	6.773	7.167	11.90	12.73
	15	1.523	5.122	6.775	7.174	12.03	13.01
	30	1.664	5.306	6.713	7.130	12.24	13.77
	45	1.723	5.516	6.468	7.083	12.30	14.47
	60	1.641	5.657	6.130	7.072	12.16	13.90
	75	1.500	5.632	5.864	7.112	11.98	13.24
	90	1.432	5.556	5.767	7.155	11.95	12.78
CFFF	0	2.115	2.221	5.548	8.493	8.772	10.91
	15	2.121	2.221	5.644	8.275	8.826	11.15
	30	2.015	2.244	5.848	7.956	8.704	11.16
	45	1.822	2.202	6.070	7.660	8.397	10.46
	60	1.676	2.061	6.327	7.341	8.022	9.663
	75	1.605	1.908	6.565	7.019	7.688	9.080
	90	1.583	1.843	6.681	6.843	7.553	8.820
SSFF	0	0.7057	3.523	6.993	10.07	10.86	15.56
	15	0.7310	3.579	7.059	10.23	11.15	15.49
	30	0.7874	3.793	6.998	10.67	11.76	15.28
	45	0.8063	4.097	6.817	11.09	12.48	14.79
	60	0.7726	4.426	6.548	11.04	13.26	14.47
	75	0.7247	4.702	6.208	10.72	13.30	14.88
	90	0.7129	4.829	5.952	10.54	13.12	15.16
CSFF	0	1.487	3.883	8.544	10.27	12.13	16.79
	15	1.501	3.991	8.626	10.49	12.36	17.00
	30	1.472	4.208	8.407	11.00	12.77	17.23
	45	1.394	4.462	8.001	11.59	13.17	16.82
	60	1.300	4.730	7.541	11.73	13.87	16.04

(continued)

Appendix D. (continued).

B.C.	θ	1	2	3	4	5	6
CCFF	75	1.229	4.955	7.114	11.46	14.62	15.46
	90	1.212	5.017	6.868	11.30	14.79	15.31
	0	2.530	6.076	8.714	12.23	13.51	18.68
	15	2.611	6.166	8.892	12.45	13.76	18.78
	30	2.672	6.348	8.826	13.01	14.31	18.46
	45	2.668	6.506	8.596	13.67	15.05	17.61
	60	2.609	6.657	8.299	14.06	15.64	17.25
	75	2.503	6.792	7.949	14.04	15.42	17.77
SFSF	90	2.395	6.913	7.581	14.00	15.10	17.97
	0	4.324	4.910	8.487	13.54	13.77	15.38
	15	4.331	4.891	8.656	13.35	13.38	15.79
	30	4.318	4.751	8.984	12.63	12.85	16.55
	45	4.225	4.455	9.222	11.94	12.11	17.31
	60	3.989	4.164	9.301	11.23	11.44	17.70
	75	3.678	3.982	9.286	10.38	11.08	17.36
	90	3.528	3.913	9.296	9.99	10.92	17.01
CFSF	0	5.792	6.352	9.594	16.10	16.33	16.49
	15	5.708	6.335	9.797	15.70	16.03	16.77
	30	5.519	6.196	10.17	14.70	15.25	17.45
	45	5.267	5.874	10.37	13.66	14.21	18.25
	60	4.949	5.535	10.27	12.90	13.27	18.83
	75	4.605	5.270	10.07	12.10	12.76	18.66
	90	4.449	5.159	9.980	11.75	12.59	18.33
SSSF	0	4.672	7.892	12.47	13.63	13.97	16.95
	15	4.677	8.119	12.55	13.60	14.90	17.08
	30	4.645	8.490	12.36	13.90	16.62	17.37
	45	4.522	8.570	11.81	14.63	17.42	17.65
	60	4.312	8.320	11.21	15.44	16.60	17.50
	75	4.092	7.973	10.67	14.89	16.01	16.81
	90	3.990	7.810	10.46	13.97	15.98	16.64
CSSF	0	5.945	8.807	13.22	13.97	16.32	19.24
	15	6.013	9.004	13.50	14.90	16.11	19.25
	30	5.872	9.281	14.02	15.40	16.62	19.21
	45	5.552	9.256	13.82	15.30	17.42	19.08
	60	5.174	8.927	13.00	15.95	16.60	18.69
	75	4.869	8.527	12.34	14.89	16.56	17.80
	90	4.741	8.335	12.06	13.97	16.96	17.15
CCSF	0	6.153	10.52	15.27	16.39	20.15	25.13
	15	6.222	10.77	15.53	16.29	20.05	25.15

(continued)

Appendix D. (continued).

B.C.	θ	1	2	3	4	5	6
	30	6.168	11.23	15.20	16.70	20.11	25.46
	45	5.904	11.59	14.13	17.67	20.30	25.40
	60	5.584	11.68	13.29	18.78	20.41	24.68
	75	5.286	11.50	12.46	19.36	20.18	23.31
	90	5.171	11.33	12.21	19.38	20.10	22.88
CFCF	0	7.640	8.163	10.99	17.03	19.55	19.64
	15	7.502	8.047	11.17	17.30	19.02	19.15
	30	7.154	7.737	11.50	17.35	17.75	18.54
	45	6.679	7.324	11.60	16.16	16.32	19.16
	60	6.174	6.934	11.35	15.04	15.23	19.84
	75	5.766	6.635	11.00	14.11	14.70	20.06
	90	5.602	6.504	10.83	13.76	14.50	19.83
SCSF	0	4.738	9.575	13.63	13.97	14.65	17.85
	15	4.740	9.780	13.31	14.89	15.08	17.97
	30	4.713	10.19	12.70	15.92	16.63	18.30
	45	4.626	10.53	12.03	16.91	17.47	18.75
	60	4.486	10.63	11.40	16.61	17.97	19.31
	75	4.326	10.53	10.83	14.90	18.33	19.61
	90	4.249	10.50	10.51	13.97	18.24	19.79
CSCF	0	7.747	10.15	14.25	19.52	22.06	24.63
	15	7.605	10.31	14.50	18.96	21.90	24.88
	30	7.246	10.59	15.08	17.66	21.51	25.42
	45	6.796	10.56	15.54	16.43	20.90	25.45
	60	6.367	10.14	14.94	16.57	20.17	23.89
	75	6.053	9.605	14.28	17.12	19.21	22.58
	90	5.920	9.340	14.05	17.44	18.63	21.96
CCCF	0	7.921	11.81	16.24	19.59	22.86	27.46
	15	7.791	11.99	16.50	19.03	22.64	27.00
	30	7.456	12.38	17.10	17.93	22.29	26.86
	45	7.059	12.74	16.11	18.47	22.03	27.92
	60	6.673	12.85	15.07	19.43	21.72	27.39
	75	6.395	12.57	14.41	19.97	21.19	26.60
	90	6.289	12.36	14.18	20.67	20.71	26.34
SSSS	0	8.105	10.21	16.58	19.02	19.15	26.94
	15	8.428	10.48	16.66	18.99	19.96	27.42
	30	9.040	11.10	16.82	19.43	21.47	28.25
	45	9.301	11.79	17.10	19.83	23.38	26.89
	60	8.917	12.45	17.16	19.71	25.40	25.99
	75	8.284	12.97	16.56	19.24	25.21	27.13
	90	7.968	13.17	16.09	18.97	24.81	27.77

(continued)

Appendix D. (continued).

B.C.	θ	1	2	3	4	5	6
CSSS	0	8.960	11.02	18.86	19.76	21.31	29.17
	15	9.219	11.25	18.79	19.97	21.63	29.46
	30	9.698	11.78	18.62	20.60	22.59	30.28
	45	9.849	12.36	18.51	21.10	24.00	29.91
	60	9.418	12.89	18.33	20.91	25.85	28.48
	75	8.780	13.35	17.67	20.39	27.39	27.52
	90	8.469	13.52	17.20	20.10	27.09	27.93
CCSS	0	10.06	13.23	19.30	22.27	22.58	28.73
	15	10.36	13.58	19.23	22.42	23.62	31.71
	30	10.97	14.31	19.02	22.47	24.72	31.94
	45	11.51	15.41	19.07	23.29	27.58	30.72
	60	11.71	16.40	19.12	23.19	25.20	28.96
	75	11.44	16.90	18.76	23.41	28.19	31.83
	90	11.17	17.01	18.46	23.34	27.80	32.28
CSCS	0	10.15	12.18	20.42	21.67	23.90	27.93
	15	10.33	12.37	20.80	21.45	24.03	29.77
	30	10.67	12.83	20.89	21.61	24.41	32.36
	45	10.78	13.12	20.36	22.27	23.89	33.24
	60	10.35	13.64	19.83	22.37	26.44	31.69
	75	9.693	13.77	19.18	21.20	26.09	29.81
	90	9.310	14.09	18.59	21.53	27.93	28.30
CCCS	0	11.22	14.21	22.05	23.31	24.94	32.80
	15	11.42	14.62	21.82	23.67	25.45	34.29
	30	11.83	15.15	21.28	24.13	27.21	34.96
	45	12.17	16.13	20.89	26.22	26.22	34.19
	60	12.34	17.00	20.57	25.69	30.45	32.65
	75	12.10	17.37	20.13	25.17	31.00	32.42
	90	11.84	17.48	19.80	22.56	30.43	30.89
CCCC	0	13.80	15.65	22.72	25.52	27.46	38.71
	15	13.82	16.00	22.45	26.24	28.43	37.35
	30	14.35	16.85	21.96	26.43	30.33	37.68
	45	15.32	17.86	21.73	27.84	32.25	37.91
	60	16.59	20.02	21.64	26.85	34.03	36.68
	75	18.07	19.81	22.52	26.64	32.37	38.78
	90	18.56	20.24	22.66	26.96	33.40	36.56

REFERENCES

- Abe, A., Kobayashi, Y. and Yamada, G. (2000) Nonlinear vibration characteristics of clamped laminated shallow shells. *J. Sound Vib.* **234**(3), 405–426.
- Abu-Farsakh, G. and Qatu, M.S. (1995) A triangular conforming element for laminated shells. *Thin-Walled Structures* **21**(1), 31–42.
- Adam, C. (2001) Dynamic analysis of isotropic composite plates using a layerwise theory. *Compos. Struct.* **51**(4), 427–437.
- Ahmed, K.M. (1971) Free vibrations of curved sandwich beams by the method of finite elements. *J. Sound Vib.* **18**(1), 61–74.
- Ahmed, K.M. (1972) Dynamic analysis of sandwich beams. *J. Sound Vib.* **21**(3), 263–276.
- Alghothani, A. (1986) A unified approach to the dynamic analysis of bending and extension of moderately thick laminated composite plates. PhD Dissertation, Ohio State University.
- Ambartsumian, S.A. (1961) Theory of Anisotropic Shells, Fizmargiz, Moskva, English Translation, NACA TTF-118, 1964.
- Ambartsumian, S.A. (1962) Contributions to the theory of anisotropic laminated shells. *Appl. Mech. Rev.* **15**(4), 245–249.
- Ambartsumian, S.A. (1970) Theory of Anisotropic Plates, Fizmargiz, Moskva (Technomic, Stanford).
- Anderson, B.W. (1954) Vibration of a triangular cantilever plate by the Ritz method. *J. Appl. Mech.* **21**, 365–376.
- Argento, A. (1993) Dynamic stability of a composite circular cylindrical shell subjected to combined axial and torsional loading. *J. Compos. Mater.* **27**(18), 1722–1738.
- Argento, A. and Scott, R.A. (1993a) Dynamic instability of layered anisotropic circular cylindrical shells. Part I: theoretical development. *J. Sound Vib.* **162**(2), 311–322.
- Argento, A. and Scott, R.A. (1993b) Dynamic instability of layered anisotropic circular cylindrical shells. Part II: numerical results. *J. Sound Vib.* **162**(2), 323–332.
- Argyris, J. and Tenek, L. (1996) Natural mode method: a practicable and novel approach to the global analysis of laminated composite plates and shells. *Appl. Mech. Rev.* **49**(7), 381–399.
- Argyris, J., Tenek, L., Andreadis, I., Iathanasiou, M. and Pavlos, G. (1998) Chaotic oscillations of a laminated composite cylinder subject to a periodic application of temperature. *Chaos Solitons Fractals* **9**(9), 1529–1554.
- Ashton, J.E. and Whitney, J.M. (1970) Theory of Laminated Plates (Technomic, Stamford).
- Babich, D.V., Shpakova, S.G. and Sheptun, L.A. (1996) Stability and oscillations of heated spherical shells (Russian). *Prikl Mekh (Appl. Mech.)* **32**(3), 34–38.
- Baharlou, B. (1985) Vibration and buckling of laminated composite plates with arbitrary boundary conditions. PhD Dissertation, Ohio State University.
- Baharlou, B. and Leissa, A.W. (1987) Vibration and buckling of generally laminated composite plates with arbitrary edge conditions. *Int. J. Mech. Sci.* **29**, 545–555.
- Barbone, P.E. and Crighton, D.J. (1994) Vibrational modes of submerged elastic bodies. *Appl. Acoust.* **43**(3), 295–317.
- Bardell, N.S., Langley, R.S., Dunsdon, J.M. and Aglietti, G.S. (1999) h-p FE vibration analysis of open conical sandwich panels and conical sandwich frusta. *J. Sound Vib.* **226**(2), 345–377.

- Basar, Y. and Omurtag, M.H. (2000) Free-vibration analysis of thin–thick laminated structures by layer-wise shell models. *Comput. Struct.* **74**(4), 409–427.
- Batra, R.C. and Liang, X.Q. (1997) Vibration of a rectangular laminated elastic plate with embedded piezoelectric sensors and actuators. *Comput. Struct.* **63**(2), 203–216.
- Beakou, A. and Touratier, M. (1993) Rectangular FE for analysing composite multilayered shallow shells in statics, vibration and buckling. *Int. J. Numer. Meth. Engng* **36**(4), 627–653.
- Bercin, A.N. (1996) Natural frequencies of cross-ply laminated singly-curved panels. *Mech. Res. Commun.* **23**(2), 165–170.
- Berger, H. and Gabbert, U. (2000) Finite element analysis and design of piezoelectric controlled smart structures. *J. Theor. Appl. Mech.* **38**(3), 475–498.
- Bert, C.W. (1967) Structural theory of laminated anisotropic elastic shells. *J. Compos. Mater.* **1**(4), 414–423.
- Bert, C.W. (1977) Optimal design of a composite materials plate to maximize its fundamental frequency. *J. Sound Vib.* **50**, 229–237.
- Bert, C.W. and Chen, L.C. (1978) Effect of shear deformation on vibration of antisymmetric angle-ply laminated plates. *Int. J. Solids Struct.* **14**, 465–473.
- Bert, C.W., Baker, J.L. and Egle, D.M. (1969a) Free vibration of multilayer anisotropic cylindrical shells. *J. Compos. Mater.* **3**, 480–500.
- Bert, C.W., Baker, J.L. and Egle, D.M. (1969b) Dynamics of composite, sandwich and stiffened shell-type structures. *J. Space Rockets* **6**(12), 1345–1361.
- Bert, C.W., Kim, C.D. and Birman, V. (1993) Vibration of composite-material cylindrical shells with ring and/or stringer stiffeners. *Compos. Struct.* **25**(1–4), 477–484.
- Beskos, D.E. (1997) Boundary element methods in dynamic analysis – Part II (1986–1996). *Appl. Mech. Rev.* **50**(3), 149–197.
- Bespalova, E.I. and Kitaigorodsky, A.B. (1996) Effect of constructive anisotropy on the vibration frequencies of cylindrical shells (Russian). *Prikl Mekh (Appl. Mech.)* **32**(7), 55–59.
- Bhat, R.B. (1981) Flexural vibration of polygonal plates using characteristic polynomials in two variables. *J. Sound Vib.* **78**, 65–71.
- Bhattacharyya, S.K. and Vendhan, C.P. (1991) Wave propagation in semi-infinite plane anisotropic thin circular shells. *J. Sound Vib.* **149**(1), 71–82.
- Bhimaraddi, A. (1990) Nonlinear vibrations of in-plane loaded, imperfect, orthotropic plates using the perturbation technique. *Int. J. Solids Struct.* **25**(5), 563–575.
- Bhimaraddi, A. (1991) Free vibration analysis of doubly curved shallow shells on rectangular planform using 3-D elasticity theory. *Int. J. Solids Struct.* **27**(7), 897–913.
- Bhimaraddi, A. (1992) Nonlinear free vibration of laminated composite plates. *J. Engng Mech.* **118**(1), 174–189.
- Bhimaraddi, A. (1993) Large amplitude vibrations of imperfect antisymmetric angle-ply laminated plates. *J. Sound Vib.* **162**(3), 457–470.
- Bhimaraddi, A. (1994) Direct ply thickness computation of laminated plates for which the Kirchhoff theory predicts the fundamental frequency within the specified degree of accuracy. *J. Sound Vib.* **164**(3), 445–458.
- Bhimaraddi, A. and Chandrashekhara, K. (1993) Nonlinear vibrations of heated antisymmetric angle-ply laminated plates. *Int. J. Solids Struct.* **30**(9), 1255–1268.

- Bicos, A.S. and Springer, G.S. (1989) Analysis of free damped vibration of laminated composite plates and shells. *Int. J. Solids Struct.* **25**(2), 129–149.
- Birlik, G.A. and Mengi, Y. (1989) Refined dynamic theory for viscoelastic cylindrical shells and cylindrical laminated composites – Part 2: application. *J. Sound Vib.* **130**(1), 69–77.
- Birman, V. and Bert, C.W. (1990) Dynamic stability of reinforced composite cylindrical shells in thermal fields. *J. Sound Vib.* **142**(2), 183–190.
- Birman, V. and Magid, M.G. (1994) Vibrations of generally laminated long cylindrical panels. *J. Sound Vib.* **170**(2), 276–279.
- Birman, V. and Zahed, H. (1989) Nonlinear problems of parametric vibrations of imperfect laminated plates. *Compos. Struct.* **12**(3), 181–191.
- Birman, V., Griffin, S. and Knowle, G. (2000) Axisymmetric dynamics of composite spherical shells with active piezoelectric and composite stiffeners. *Acta Mech.* **141**(1/2), 71–83.
- Blaise, A. and Lesueur, C. (1992) Acoustic transmission through a 2D orthotropic multi-layered infinite cylindrical shell. *J. Sound Vib.* **155**(1), 95–109.
- Blaise, A., Lesueur, C., Gotteland, M. and Barbe, M. (1991) Sound transmission into an orthotropic infinite shell: comparison with Koval's results and understanding of phenomena. *J. Sound Vib.* **150**(2), 233–243.
- Blocka, B. (1988) Free vibrations of thin, elastic, segmented shells of revolution reinforced with circumferential rings. *Arch. Mech.* **40**(2/3), 183–199.
- Bouabdallah, M.S. and Batoz, J.L. (1996) Formulation and evaluation of a FE model for the linear analysis of stiffened composite cylindrical panels. *Finite Elem. Anal. Des.* **21**(4), 265–289.
- Bray, F.M. and Egle, D.M. (1970) An experimental investigation of the free vibration of thin cylindrical shells with discrete longitudinal stiffening. *J. Sound Vib.* **12**, 153–164.
- Brogan, W.L. (1985) *Modern Control Theory* (Prentice-Hall, Englewood Cliffs, NJ).
- Carrera, E. (1991) Effects of shear deformation and curvature on buckling and vibrations of cross-ply laminated composite shells. *J. Sound Vib.* **150**(3), 405–433.
- Carrera, E. (1999a) Reissner's mixed variational theorem applied to vibration analysis of multilayered shells. *J. Appl. Mech.* **66**(1), 69–78.
- Carrera, E. (1999b) Study of transverse normal stress effect on vibration of multilayered plates and shells. *J. Sound Vib.* **225**(5), 803–829.
- Carrera, E. (1999c) Multilayered shell theories accounting for layerwise mixed description. Part 1: governing equations. *AIAA J.* **37**(9), 1107–1116.
- Carrera, E. (1999d) Multilayered shell theories accounting for layerwise mixed description. Part 2: numerical evaluations. *AIAA J.* **37**(9), 1117–1124.
- Carrera, E. (2001) Developments, ideas, and evaluations based upon Reissner's mixed variational theorem in the modeling of multilayered plates and shells. *Appl. Mech. Rev.* **54**(4).
- Carrera, E. (2002) Theories and finite elements for multilayered, anisotropic, composite plates and shells. *Arch. Comput. Math. Engng* **9**(2), 87–140.
- Cederbaum, G. (1992a) Analysis of parametrically excited laminated shells. *Int. J. Mech. Sci.* **34**(3), 241–250.
- Cederbaum, G. (1992b) Parametric instability of laminated plates modeled within a high-order shear-deformation theory. *Acta Mech.* **91**(3/4), 179–191.

- Chakravorty, D., Bandyopadhyay, J.N. and Sinha, P.K. (1995a) Finite element free vibration analysis of point supported laminated composite cylindrical shells. *J. Sound Vib.* **181**(1), 43–52.
- Chakravorty, D., Bandyopadhyay, J.N. and Sinha, P.K. (1995b) Free vibration analysis of point-supported laminated composite doubly curved shells: a FE approach. *Comput. Struct.* **54**(2), 191–198.
- Chakravorty, D., Bandyopadhyay, J.N. and Sinha, P.K. (1996) Finite element free vibration analysis of doubly-curved laminated composite shells. *J. Sound Vib.* **191**(4), 491–504.
- Chamis, C.C. (1977) Vibration characteristics of composite fan blades and comparisons with measured data. *J. Aircraft* **14**, 644.
- Chang, J.-D. (1992) Theory of thick laminated composite shallow shells. PhD Dissertation, Ohio State University, Columbus, OH.
- Chang, J.S. and Lin, C.H. (1992) Buckling and free vibration of cross-ply laminated circular cylindrical shells subjected to axial thrust and lateral pressure loading according to a higher order displacement field. *Thin-Walled Struct.* **13**(3), 177–196.
- Chang, J.S. and Shyong, J.W. (1994) Thermally induced vibration of laminated circular cylindrical shell panels. *Compos. Sci. Tech.* **51**(3), 419–427.
- Chang, J.S., Wang, J.H. and Tsai, T.Z. (1992) Thermally induced vibration of thin laminated plates by FEM. *Comput. Struct.* **42**(1), 117–128.
- Chao, C.C. and Chern, Y.C. (1988) Axisymmetric free vibration of orthotropic complete spherical shells. *J. Compos. Mater.* **22**(12), 1116–1130.
- Chao, C.C. and Tung, T.P. (1989) Step pressure and blast responses of clamped orthotropic hemispherical shells. *Int. J. Impact Eng.* **8**(3), 191–207.
- Chao, C.C., Tung, T.P. and Chern, Y.C. (1991) Axisymmetric free vibration of thick orthotropic hemispherical shells under various edge conditions. *J. Vib. Acoust. Stress Reliab. Des.* **113**(2), 152–159.
- Chaudhuri, R.A. and Kabir, H.R.H. (1992) Boundary-continuous-displacement based Fourier analysis of laminated doubly-curved panels using classical shallow shell theories. *Int. J. Engng Sci.* **30**(11), 1647–1664.
- Chaudhuri, R.A. and Kabir, H.R.H. (1994) Static and dynamic Fourier analysis of finite cross-ply doubly curved panels using classical shallow shell theories. *Compos. Struct.* **28**(1), 73–91.
- Chen, J. (2000) Nonlinear transient analysis of rectangular composite laminated plates. *Compos. Struct.* **49**(2), 129–139.
- Chen, W.Q. and Ding, H.J. (1997) Free vibrations of an embedded anisotropic spherical shells. *J. Pressure Vessel Tech.* **119**(4), 481–487.
- Chen, C.Q. and Shen, Y.P. (1998) Three-dimensional analysis for the free vibration of finite-length orthotropic piezoelectric circular cylindrical shells. *J. Vib. Acoust.* **120**(1), 194–198.
- Chen, L.W. and Yang, J.Y. (1993) Nonlinear vibration of antisymmetric imperfect angle-ply laminated plates. *Compos. Struct.* **23**(1), 39–46.
- Chen, C.I., Mucino, V.H. and Barbero, E.J. (1993) Finite element vibration analysis of a helically wound tubular and laminated composite material beam. *Comput. Struct.* **49**(3), 399–410.
- Chen, W., Cai, J., Ye, G. and Ding, H. (1998) Three-dimensional exact free vibration of transversely isotropic cylindrical panels. *J. Vib. Acoust.* **120**(4), 982–986.

- Chen, W.Q., Ying, J. and Yang, Q.D. (1998) Free vibrations of transversely isotropic cylinders and cylindrical shells. *J. Pressure Vessel Tech.* **120**(4), 321–324.
- Cheng, Z.Q., He, L.H. and Kitipornchai, S. (2000) Influence of imperfect interfaces on bending and vibration of laminated composite shells. *Int. J. Solids Struct.* **37**(15), 2127–2150.
- Chern, Y.C. and Chao, C.C. (2000) Comparison of natural frequencies of laminates by 3D theory – Part II: curved panels. *J. Sound Vib.* **230**(5), 1009–1030.
- Cheung, Y.K. and Kong, J. (1993) Approximate 3D analysis of rectangular thick laminated plates: bending, vibration, and buckling. *Comput. Struct.* **47**(2), 193–199.
- Chia, C.Y. (1985) Non-linear vibration of anisotropic rectangular plates with non-uniform edge constraints. *J. Sound Vib.* **101**, 539–550.
- Chia, C.Y. (1990) Dynamic and static nonlinear analysis of generally laminated imperfect plates having nonuniform boundary conditions and resting on elastic foundation. *Z. Angew Math. Phys.* **40**(5), 628–644.
- Chidamparam, P. and Leissa, A.W. (1993) Vibrations of planar curved beams, rings and arches. *Appl. Mech. Rev.* **46**(9), 467–482.
- Cho, K.N., Bert, C.W. and Striz, A.G. (1991) Free vibrations of laminated rectangular plates analyzed by higher order individual-layer theory. *J. Sound Vib.* **145**(3), 429–442.
- Cho, C., Zhao, G. and Kim, C.B. (2000) Nonlinear FE analysis of composite shell under impact. *KSME Int. J.* **14**(6), 666–674.
- Chonan, S. (1988) Low frequency soundproof characteristics of orthotropic two-layered cylindrical shells. *J. Sound Vib.* **126**(3), 407–415.
- Chow, S.T., Liew, K.M. and Lam, K.Y. (1992) Transverse vibration of symmetrically laminated rectangular composite plates. *Compos. Struct.* **20**(4), 213–226.
- Chowdary, T.V.R., Parthan, S. and Sinha, P.K. (1994) Finite element flutter analysis of laminated composite panels. *Comput. Struct.* **53**(2), 245–251.
- Christoforou, A.P. and Swanson, S.R. (1990) Analysis of simply-supported orthotropic cylindrical shells subject to lateral impact loads. *J. Appl. Mech.* **57**(2), 376–382.
- Chun, C.K. and Dong, S.B. (1992a) Shear constitutive relations for laminated anisotropic shells and plates: Part I – methodology. *J. Appl. Mech.* **59**, 372–379.
- Chun, C.K. and Dong, S.B. (1992b) Shear constitutive relations for laminated anisotropic shells and plates: Part II – vibrations of composite cylinders. *J. Appl. Mech.* **59**, 380–389.
- Chun, C.K. and Dong, S.B. (1998) Finite element analysis of shear deformation in laminated anisotropic shells of revolution. *J. Sound Vib.* **218**(1), 164–176.
- Chun, L. and Lam, K.Y. (1995) Dynamic analysis of clamped laminated curved panels. *Compos. Struct.* **30**(4), 389–398.
- Cinquini, C., Mariani, C. and Venini, P. (1995) Rayleigh-Ritz analysis of elastically constrained thin laminated plates on Winkler inhomogeneous foundations. *Comput. Meth. Appl. Mech. Engng* **123**, 263–286.
- Crawley, E.F. (1978) The natural mode shapes and frequencies of graphite/epoxy cantilevered plates and shells. MS Thesis, MIT.
- Crawley, E.F. (1979) The natural modes of graphite/epoxy cantilever plates and shells. *J. Compos. Mater.* **13**, 195–205.
- Cristensen, R.M. (1963) Vibration of a 45 degrees right triangular plate by a grid work method. *AIAA J.* **1**, 1790–1795.

- Cyr, G.J., Hinrichsen, R.L. and Walley, R.A. (1988) Effects of cutouts on the dynamic response of curved rectangular composite panels. *AIAA J.* **26**(5), 582–588.
- Dasgupta, A. and Huang, K.H. (1997) Layer-wise analysis for free vibrations of thick composite spherical panels. *J. Compos. Mater.* **31**(7), 658–671.
- Dawe, D.J. and Wang, S. (1994) Free vibration of generally-laminated, shear-deformable, composite rectangular plates using a spline Rayleigh-Ritz method. *Compos. Struct.* **25**(1–4), 77–87.
- Dawe, D.J. and Wang, S. (1995) Spline finite strip analysis of the buckling and vibration of rectangular composite laminated plates. *Int. J. Mech. Sci.* **37**, 645–667.
- Ding, K. and Tang, L. (1999) Three-dimensional free vibration of thick laminated cylindrical shells with clamped edges. *J. Sound Vib.* **220**(1), 171–177.
- Ding, K., Tang, L. and Fan, J. (1997) Exact analysis for axisymmetric vibration and buckling of the thick laminated closed cylindrical shells in a Hamilton system. *J. Sound Vib.* **206**(3), 435–441.
- DiTaranto, R.A. (1973) Free and forced response of a laminated ring. *J. Acoust. Soc. Am.* **53**(3), 748–757.
- Dong, S.B. (1968) Free vibration of laminated orthotropic cylindrical shells. *J. Acoust. Soc. Am.* **44**, 1628–1635.
- Donnell, L.H. (1976) *Beams, Plates, and Shells* (McGraw-Hill, New York) 453 pp.
- Drewko, J. and Sperski, M. (1991) Vibration of multi-chamber shell structures with discontinuously variable cross-sections. *Rozprawy Inżynierskie (Eng. Trans.)* **39**(2), 163–180.
- Dube, G.P., Dumir, P.C. and Kumar, C.B. (1999a) Segmented sensors and actuators for thick plates and shells – Part I: analysis using FSDT. *J. Sound Vib.* **226**(4), 739–753.
- Dube, G.P., Dumir, P.C. and Kumar, C.B. (1999b) Segmented sensors and actuators for thick plates and shells – Part II: parametric study. *J. Sound Vib.* **226**(4), 755–767.
- Fan, J. and Ye, J. (1990) Exact solutions for axisymmetric vibration of laminated circular plates. *J. Engng Mech.* **116**(4), 920–927.
- Farsa, J., Kukreti, A.R. and Bert, C.W. (1993) Fundamental frequency analysis of laminated rectangular plates by differential quadrature method. *Int. J. Numer. Meth. Engng* **36**(14), 2341–2356.
- Flügge, W. (1962) *Stresses in Shells* (Springer, Berlin).
- Fu, Y.M. and Chia, C.Y. (1989a) Multi-mode nonlinear vibration and postbuckling of antisymmetric imperfect angle-ply cylindrical thick panels. *Int. J. Non-Linear Mech.* **24**(5), 365–381.
- Fu, Y.M. and Chia, C.Y. (1989b) Nonlinear analysis of unsymmetrically laminated imperfect thick panels on elastic foundation. *Compos. Struct.* **13**(4), 289–314.
- Fu, Y.M. and Chia, C.Y. (1989c) Nonlinear bending and vibration of symmetrically laminated orthotropic elliptical plate with simply supported edge. *Acta Mech.* **4**(1–4), 155–170.
- Fu, Y.M. and Chia, C.Y. (1993) Nonlinear vibration and postbuckling of generally laminated circular cylindrical thick shells with non-uniform boundary conditions. *Int. J. Non-Linear Mech.* **28**(3), 313–327.
- Ganapathi, M. and Varadan, T.K. (1995) Nonlinear free flexural vibrations of laminated circular cylindrical shells. *Compos. Struct.* **30**(1), 33–49.

- Ganapathi, M. and Varadan, T.K. (1996) Large amplitude vibrations of circular cylindrical shells. *J. Sound Vib.* **192**(1), 1–14.
- Ganapathi, M., Varadan, T.K. and Sarma, B.S. (1991) Nonlinear flexural vibrations of laminated orthotropic plates. *Comput. Struct.* **39**(6), 685–688.
- Ganapathi, M., Varadan, T.K. and Balamurugan, V. (1994) Dynamic instability of laminated composite curved panels using FEM. *Comput. Struct.* **53**(2), 335–342.
- Ganapathi, M., Patel, B.P. and Sambandam, C.T. (1999) Dynamic instability analysis of circular conical shells. *Compos. Struct.* **46**(1), 59–64.
- Ganesan, N. and Sivadas, K.R. (1989) Vibration analysis of orthotropic shells. *J. Sound Vib.* **133**(3), 510–514.
- Ganesan, N. and Sivadas, K.R. (1990) Vibration analysis of orthotropic shells with variable thickness. *Comput. Struct.* **35**(3), 239–248.
- Gautham, B.P. and Ganesan, N. (1992) Axisymmetric vibration of layered orthotropic spherical shells of variable thickness. *Comput. Struct.* **45**(5/6), 893–900.
- Gautham, B.P. and Ganesan, N. (1994) Free vibration analysis of orthotropic thick shells of revolution using discrete layer theory. *J. Sound Vib.* **171**(4), 549–556.
- Gautham, B.P. and Ganesan, N. (1997) Free vibration characteristics of isotropic and laminated spherical caps. *J. Sound Vib.* **204**(1), 17–40.
- Gendy, A.S., Saleeb, A.F. and Mikhail, S.N. (1997) Free vibrations and stability analysis of laminated composite plates and shells with hybrid-mixed formulation. *Comput. Struct.* **63**(6), 1149–1163.
- Germain, S. (1821) *Researches sur la theorie des surfaces elastiques*, Paris.
- Gofman, M.N. (1998) Steady-state torsional oscillations of multilayer truncated cones. *Prikl Mekh* **34**(3), 64–68.
- Gol'denveizer, A.L. (1961) *Theory of Elastic Thin Shells* (English Translation) (Pergamon Press, New York).
- Gong, S.W. and Lam, K.Y. (1998) Transient response of stiffened composite submersible hull subjected to underwater explosive shock. *Compos. Struct.* **41**(1), 27–37.
- Gorman, D.J. and Ding, W. (1996) Accurate free vibration analysis of clamped antisymmetric angle-ply laminated rectangular plates by the Superposition-Galerkin method. *Compos. Struct.* **34**(4), 387–395.
- Goswami, S. and Mukhopadhyay, M. (1995) Finite element free vibration analysis of laminated composite stiffened shell. *J. Compos. Mat.* **29**(18), 2388–2422.
- Gotsis, P.K. and Guptill, J.D. (1995) Free vibration of fiber composite thin shells in a hot environment. *J. Reinforced Plastics Compos.* **14**(2), 143–163.
- Grigorenko, A.Y. (1998) Numerical solution of the problem of free axisymmetrical oscillations of a hollow orthotropic cylinder under various adjustment of end-faces (Russian). *Prikl Mekh* **33**(5), 49–54.
- Gummadi, N.B. and Palazotto, A.N. (1999) Nonlinear dynamic FE analysis of composite cylindrical shells considering large rotations. *AIAA J.* **37**(11), 1489–1494.
- Gupta, N.K. and Prasad, G.L. (1999) Quasi-static and dynamic axial compression of glass–polyester composite hemi-spherical shells. *Int. J. Impact Engng* **22**(8), 757–774.
- Gustafson, P.N., Stokey, W.F. and Zorowski, C.F. (1953) An experimental study of natural vibration of cantilever triangular plates. *J. Aero. Sci.* **20**, 331–337.

- Han, W. and Petyt, M. (1997) Geometrically nonlinear vibration analysis of thin, rectangular plates using the hierarchical FEM – II: 1st mode of laminated plates and higher modes of isotropic and laminated plates. *Comput. Struct.* **63**(2), 309–318.
- Hanna, N. (1990) Thick plate theory with application to vibration. PhD Dissertation, Ohio State University.
- Hearmon, R.F.S. (1946) The fundamental frequency of vibration of rectangular of rectangular wood and ply-wood plates. *Proc. Phys. Soc. (London)* **58**, 78–92.
- Heuer, R. (1994) Large flexural vibrations of thermally stressed layered shallow shells. *Nonlinear Dyn.* **5**(1), 25–38.
- Heyliger, P.R. and Jilani, A. (1993) Free vibrations of laminated anisotropic cylindrical shells. *J. Engng Mech.* **119**(5), 1062–1077.
- Heyliger, P. and Saravanan, D.A. (1996) Exact free-vibration analysis of laminated plates with embedded piezoelectric layers. *J. Acoust. Soc. Am.* **98**(3), 1547–1557.
- Heyliger, P., Pei, K.C. and Saravanan, D. (1996) Layerwise mechanics and FE model for laminated piezoelectric shells. *AIAA J.* **34**(11), 2353–2360.
- Hu, B.G. and Dokainish, M.A. (1994) Damped vibrations of laminated composite plates: modeling and FE analysis. *Finite Elem. Anal. Des.* **15**(2), 103–124.
- Hu, Y.C. and Huang, S.C. (2000a) Application of constrained layer damping on the cylindrical shells conveying fluid. *J. Chin. Soc. Mech. Engng* **21**(2), 189–200.
- Hu, Y.C. and Huang, S.C. (2000b) Frequency response and damping effect of three-layer thin shell with viscoelastic core. *Comput. Struct.* **76**(5), 577–591.
- Hu, X., Chen, H. and Wauer, J. (1997) Finite strip dynamic analysis of cylindrical shell sandwich structures. *Chin. J. Mech. Engng* **10**(2), 141–147.
- Huang, K.H. and Dasgupta, A. (1995) Layer-wise analysis for free vibration of thick composite cylindrical shells. *J. Sound Vib.* **186**(2), 207–222.
- Huang, N.N. and Tauchert, T.R. (1992) Thermally induced vibration of doubly curved cross-ply laminated panels. *J. Sound Vib.* **154**(3), 485–494.
- Hui, D. (1985) Soft-spring nonlinear vibrations of antisymmetrically laminated rectangular plates. *Int. J. Mech. Sci.* **27**, 397–408.
- Hurlbut, B.J. and Regelbrugge, M.A. (1996) Evaluation of a constitutive model for shape memory alloys embedded in shell structures. *J. Reinforced Plastics Compos.* **15**(12), 1249–1261.
- Hussein, M. and Heyliger, P.R. (1996) Discrete layer analysis of axisymmetric vibrations of laminated piezoelectric cylinders. *J. Sound Vib.* **192**(5), 995–1013.
- Ip, K.H., Chan, W.K., Tse, P.C. and Lai, T.C. (1996) Vibration analysis of orthotropic thin cylindrical shells with free ends by the Rayleigh-Ritz method. *J. Sound Vib.* **195**(1), 117–135.
- Isaksson, A., Saldner, H.O. and Molin, N.E. (1995) Influence of enclosed air on vibration modes of a shell structure. *J. Sound Vib.* **187**(3), 451–466.
- Iu, V.P. and Chia, C.Y. (1988) Effect of transverse shear on nonlinear vibration and post-buckling of anti-symmetric cross-ply imperfect cylindrical shells. *Int. J. Mech. Sci.* **30**(10), 705–718.
- Jensen, D.W. and Crawley, E.F. (1984) Frequency determination techniques for cantilevered plates with bending–torsion coupling. *AIAA J.* **22**, 415–420.

- Jensen, D.W., Crawley, E.F. and Dugundji, J. (1982) Vibration of cantilevered graphite/epoxy plates with bending-torsion coupling. *J. Reinforced Plastic Compos.* **1**, 254–269.
- Jia, J. and Rogers, C.A. (1990) Formulation of a laminated shell theory incorporating embedded distributed actuators. *J. Mech. Des.* **112**(4), 594–602.
- Jiang, X. (1997) Three-dimensional vibration analysis of fiber reinforced composite laminated cylindrical shells. *J. Vib. Acoust.* **119**(1), 46–51.
- Jing, H.S. and Liao, M.L. (1991) Partial hybrid stress element for vibrations of thick laminated composite plates. *Comput. Struct.* **36**(1), 57–64.
- Jones, R.M. (1973) Buckling and vibration of unsymmetrically laminated cross-ply rectangular plates. *AIAA J.* **11**, 1626–1632.
- Jones, R.M. (1975) *Mechanics of Composite Materials* (Scripta Book, Washington, DC).
- Kabir, H.R.H. (1998) Free vibration response of shear deformable antisymmetric cross-ply cylindrical panel. *J. Sound Vib.* **217**(4), 601–618.
- Kabir, H.R.H. and Chaudhuri, R.A. (1991) Free vibration of shear-flexible anti-symmetric angle-ply doubly curved panels. *Int. J. Solids Struct.* **28**(1), 17–32.
- Kabir, H.R.H. and Chaudhuri, R.A. (1994a) Gibbs-phenomenon-free Fourier solution for finite shear-flexible laminated clamped curved panels. *Int. J. Engng Sci.* **32**(3), 501–520.
- Kabir, H.R.H. and Chaudhuri, R.A. (1994b) Free vibration of clamped, moderately thick, arbitrarily laminated plates using a generalized Navier's approach. *J. Sound Vib.* **171**(3), 397–410.
- Kabir, H.R.H., Al-Khaleefi, A.M. and Chaudhuri, R.A. (2001) Free vibration analysis of thin arbitrarily laminated anisotropic plates using boundary-continuous displacement Fourier approach. *Compos. Struct.* **53**(4), 469–476.
- Kadivar, M.H. and Samani, K. (2000) Free vibration of rotating thick composite cylindrical shells using layerwise laminate theory. *Mech. Res. Commun.* **27**(6), 679–684.
- Kant, T. and Mallikarjuna, (1990) Vibrations of unsymmetrically laminated plates analyzed by using a higher order theory with a C deg finite element formulation. *J. Sound Vib.* **134**(1), 1–16.
- Kantorovich, L.V. and Krylov, V.I. (1964) *Approximate Methods in Higher Analysis* (P. Noordhoff, Gronigen, The Netherlands).
- Kao, J. and Ross, R.J. (1968) Bending of multilayered sandwich beams. *AIAA J.* **6**(8), 1583–1585.
- Kapania, P.K. (1989) Review on the analysis of laminated shells. *J. Pressure Vessel Tech.* **111**(2), 88–96.
- Kapania, P.K. and Byun, C. (1992) Vibrations of imperfect laminated panels under complex preloads. *Int. J. Non-Linear Mech.* **27**(1), 51–62.
- Kapania, R.K. and Lovejoy, A.E. (1996) Free vibration of thick generally laminated cantilever quadrilateral plates. *AIAA J.* **34**(7), 1474–1486.
- Kapania, P.K. and Mohan, P. (1996) Static, free vibration and thermal analysis of composite plates and shells using a flat triangular shell element. *Comput. Mech.* **17**(5), 343–357.
- Kayran, A. and Vinson, J.R. (1990a) Free vibration analysis of laminated composite truncated circular conical shells. *AIAA J.* **28**(7), 1259–1269.
- Kayran, A. and Vinson, J.R. (1990b) Torsional vibrations of layered composite paraboloidal shells. *J. Sound Vib.* **141**(2), 231–244.

- Kayran, A. and Vinson, J.R. (1994) Method for the calculation of natural frequencies of orthotropic axisymmetrically loaded shells of revolution. *ES Ardic Vib. Acoust.* **116**(1), 16–25.
- Khatrri, K.N. (1995) Vibrations of arbitrarily laminated fiber reinforced composite material truncated conical shell. *J. Reinforced Plastics Compos.* **14**(9), 923–948.
- Khatrri, K.N. (1996) Antisymmetric vibrations of multilayered conical shells with constrained viscoelastic layers. *Int. J. Solids Struct.* **33**(16), 2331–2355.
- Khatrri, K.N. and Asnani, N.T. (1995) Vibration and damping analysis of multilayered conical shells. *Compos. Struct.* **33**(3), 143–157.
- Khatrri, K.N. and Asnani, N.T. (1996) Vibration and damping analysis of fiber reinforced composite material conical shells. *J. Sound Vib.* **193**(3), 581–595.
- Khdeir, A.A. (1986) Analytical solutions for the statics and dynamics of rectangular laminated composite plates using shear deformation theories. PhD Dissertation, Virginia Polytechnical Institute and State University, Blacksburg, VA.
- Khdeir, A.A. (1988a) Free vibration of antisymmetric angle-ply laminated plates including various boundary conditions. *J. Sound Vib.* **122**(2), 377–388.
- Khdeir, A.A. (1988b) Free vibration and buckling of symmetric cross-ply laminated plates by an exact method. *J. Sound Vib.* **126**(3), 447–461.
- Khdeir, A.A. (1989) Free vibration and buckling of unsymmetric cross-ply laminated plates using a refined theory. *J. Sound Vib.* **128**(3), 377–395.
- Khdeir, A.A. and Reddy, J.N. (1990) Influence of edge conditions on the modal characteristics of cross-ply laminated shells. *Comput. Struct.* **34**(6), 817–826.
- Kielb, R.E., Leissa, A.W. and MacBain, J.C. (1985a) Vibrations of twisted cantilever plates – a comparison of theoretical results. *Int. J. Numer. Meth. Engng* **21**, 1365.
- Kielb, R.E., Leissa, A.W., MacBain, J.C. and Carney, K.S. (1985b) Joint research effort on vibrations of twisted plates. NASA Reference Publication 1150.
- Kim, C.S. and Dickinson, S.M. (1990b) The free flexural vibration of right triangular isotropic and orthotropic plates. *J. Sound Vib.* **141**, 291–311.
- Kim, C.S. and Dickinson, S.M. (1992) The free flexural vibration of isotropic and orthotropic general triangular shaped plates. *J. Sound Vib.* **152**, 383–403.
- Kim, M.J. and Gupta, A. (1991) Finite element analysis of free vibrations of laminated composite plates. *Int. J. Anal. Exp. Modal Anal.* **5**(3), 195–203.
- Kim, T.W. and Kim, J.H. (2002) Nonlinear vibration of viscoelastic laminated composite plates. *Int. J. Solids Struct.* **39**(10), 2857–2870.
- Klosowski, P., Woznica, K. and Weichert, D. (1995) Comparative study of vibrations of elasto-viscoplastic shells and plates. *Eng Trans* **43**(1–2), 183–204.
- Koiter, W.T. (1967) Foundation and Basic Equations of Shell Theory, *Proceedings of IUTAM, Second Symposium Theory of Thin Shells*, ed. Niordson, F.L. (Springer, New York) 93–05.
- Koiter, W.T. (1969) Theory of Thin Shells, ed. Niordson, F.L. (Springer-Verlag, New York), pp. 93–105.
- Kolesnikov, S.V. (1996) Refined theory of the vibrations of a cylindrical shell based on an expansion in series of the normal displacement. *J. Appl. Math. Mech.* **60**(1), 113–119.
- Korjakin, A., Rikards, R., Chate, A. and Altenbach, H. (1998) Analysis of free damped vibrations of laminated composite conical shells. *Compos. Struct.* **41**(1), 39–47.

- Kosmatka, J.B. (1994) Accurate shear-deformable six-node triangular plate element for laminated composite structures. *Int. J. Numer. Meth. Engng* **37**(3), 431–455.
- Kraus, H. (1967) *Thin Elastic Shells* (Wiley, New York).
- Kreyszig, E. (1989) *Introductory Functional Analysis with Application* (Wiley, New York).
- Kreyszig, E. (1993) *Advanced Engineering Mathematics*, 7th edition (Wiley, New York).
- Kubala, M. and Markus, S. (1994) Distinction of vibration eigenmodes of a cylindrical composite shell (Slovak). *Strojnický Casopis* **45**(4), 299–308.
- Kumar, V. and Singh, A.V. (1995) Vibrations of composite noncircular cylindrical shells. *J. Vib. Acoust.* **117**(4), 470–476.
- Kumar, V. and Singh, A.V. (1996) Vibrations of fiber-reinforced laminated deep shells. *J. Pressure Vessel Tech.* **118**(4), 407–414.
- Kuo, W.S. and Yang, I.H. (1989) Generic nonlinear behavior of antisymmetric angle-ply laminated plates. *Int. J. Mech. Sci.* **31**(2), 131–143.
- Lagrange, J.L. (1811) Note communiquée aux commissaires pour le prix de la surface elastique, Paris.
- Lakis, A.A. and Laveau, A. (1991) Non-linear dynamic analysis of anisotropic cylindrical shells containing a flowing fluid. *Int. J. Solids Struct.* **28**(9), 1079–1094.
- Lakis, A.A. and Sinno, M. (1992) Free vibration of axisymmetric and beam-like cylindrical shells, partially filled with liquid. *Int. J. Numer. Meth. Engng* **33**(2), 235–268.
- Lakis, A.A., Selmane, A. and Toledano, A. (1998) Nonlinear free vibration of laminated orthotropic cylindrical shells. *Int. J. Mech. Sci.* **40**(1), 27–94.
- Lakshminarayana, H.V. and Dwarakanath, K. (1992) Free vibration characteristics of cylindrical shells made of composite material. *J. Sound Vib.* **154**(3), 431–439.
- Lam, K.Y. and Hua, L. (2000) Generalized differential quadrature for frequency of rotating multilayered conical shell. *J. Engng Mech.* **126**(11), 1156–1162.
- Lam, K.Y. and Loy, C.T. (1995a) Influence of boundary conditions and fiber orientation on the natural frequencies of thin orthotropic laminated cylindrical shells. *Compos. Struct.* **31**(1), 21–30.
- Lam, K.Y. and Loy, C.T. (1995b) Analysis of rotating laminated cylindrical shells by different thin shell theories. *J. Sound Vib.* **186**(1), 23–35.
- Lam, K.Y. and Ng, T.Y. (1998) Dynamic stability analysis of laminated composite cylindrical shells subjected to conservative periodic axial loads. *Compos. Part B – Engng* **29**(6), 769–785.
- Lam, K.Y., Ng, T.Y. and Qian, W. (2000) Vibration analysis of thick laminated composite cylindrical shells. *AIAA J.* **38**(6), 1102–1107.
- Lammering, R. (1991) Application of a finite shell element for composites containing piezoelectric polymers in vibration control. *Comput. Struct.* **41**(5), 1101–1109.
- Lanczos, C. (1986) *The Variational Principles in Mechanics*, 4th edition (Fover, New York).
- Langhaar, H.L. (1962) *Energy Methods in Applied Mechanics* (Wiley, New York).
- Laura, P.A.A. and Maurizi, J.A. (1987) Recent research on vibrations of arch-type structures. *Shock Vib. Digest* **19**(1), 6–9.
- Lee, D.G. (1988) Calculation of natural frequencies of vibration of thin orthotropic composite shells by energy method. *J. Compos. Mater.* **22**(12), 1102–1115.
- Lee, Y.S. and Kim, Y.W. (1998) Vibration analysis of rotating composite cylindrical shells with orthogonal stiffeners. *Comput. Struct.* **69**(2), 271–281.

- Lee, D.M. and Lee, I. (1995) Vibration analysis of anisotropic plates with eccentric stiffeners. *Comput. Struct.* **57**(1), 99–105.
- Lee, H.P. and Ng, T.Y. (1995) Vibration of symmetrically laminated rectangular composite plates reinforced by intermediate stiffeners. *Composite Struct.*, **29**, 405–413.
- Lee, Y.S. and Lee, K.D. (1997) Dynamic response of laminated circular cylindrical shells under impulse loads. *Comput. Struct.* **63**(1), 149–157.
- Lee, H.J. and Saravanos, D.A. (2000) Mixed multi-field FE formulation for thermopiezoelectric composite shells. *Int. J. Solids Struct.* **37**(36), 4949–4967.
- Lee, J.M., Chung, J.H. and Chung, T.Y. (1997) Free vibration analysis of symmetrically laminated composite rectangular plates. *J. Sound Vib.* **199**(1), 71–85.
- Lee, Y.S., Lee, Y.W., Yang, M.S. and Park, B.S. (1999) Optimal design of thick laminated composite plates for maximum thermal buckling load. *J. Thermal Stresses* **22**(3), 259–273.
- Leissa, A.W. (1969) *Vibration of Plates*. NASA SP-160 (US Government Printing Office, Washington, DC) 353 pp. Republished in 1993 by The Acoustical Society of America.
- Leissa, A.W. (1973a) *Vibration of Shells*. NASA SP288 (US Government Printing Office, Washington, DC) Republished in 1993 by The Acoustical Society of America.
- Leissa, A.W. (1973b) The free vibration of rectangular plates. *J. Sound Vib.* **31**(3), 257–293.
- Leissa, A.W. (1978) Recent research in plate vibrations, 1973–1976: complicating effects. *Shock Vib. Dig.* **10**, 21–35.
- Leissa, A.W. (1981a) Recent research in plate vibrations, 1976–1980: complicating effects. *Shock Vib. Dig.* **13**, 19–36.
- Leissa, A.W. (1981b) Vibrational aspects of rotating turbomachinery blades. *Appl. Mech. Rev.* **34**, 629–635.
- Leissa, A.W. (1985) Buckling of Laminated Composite Plates and Shell Panels, Flight Dynamics Laboratory Report No. AFWAL-TR-85-3069, Wright-Patterson Air Force Base, 439 pp.
- Leissa, A.W. (1986) Update to vibrational aspects of rotating turbomachinery blades. *Appl. Mech. Update*, 359.
- Leissa, A.W. (1987a) A review of laminated composite plate buckling. *Appl. Mech. Rev.* **40**(5), 575–591.
- Leissa, A.W. (1987b) Recent studies in plate vibrations 1981–1985: complicating effects. *Shock Vib. Digest* **19**, 10–24.
- Leissa, A.W. (1991) *Vibrations of Continuous Systems* (Ohio State University class note).
- Leissa, A.W. and Chang, J. (1996) Elastic deformation of thick, laminated composite shallow shells. *Compos. Struct.* **35**, 53–170.
- Leissa, A.W. and Jaber, N.A. (1992) Vibrations of completely free triangular plates. *Int. J. Mech. Sci.* **34**, 605–616.
- Leissa, A.W. and Jacob, K.I. (1986) Three dimensional vibrations of twisted cantilevered parallelepiped. *J. Appl. Mech.* **53**, 614.
- Leissa, A.W. and Kadi, A.S. (1971) Curvature effects on shallow shell vibrations. *J. Sound Vib.* **16**(2), 173–187.
- Leissa, A.W. and Narita, Y. (1984) Vibrations of completely free shallow shells of rectangular planform. *J. Sound Vib.* **96**(2), 207–218.
- Leissa, A.W. and Narita, Y. (1989) Vibration studies for simply supported symmetrically laminated rectangular plates. *Compos. Struct.* **12**, 113–132.

- Leissa, A.W. and Qatu, M.S. (1991) Equations of elastic deformation for laminated composite shallow shells. *J. Appl. Mech.* **58**, 181–188.
- Leissa, A.W., Lee, J.K. and Wang, A.J. (1981) Vibrations of cantilevered shallow cylindrical shells having rectangular planform. *J. Sound Vib.* **78**(3), 311–328.
- Leissa, A.W., Lee, J.K. and Wang, A.J. (1982) Rotating blade vibration analysis using shells. *J. Engng Power* **104**, 296.
- Leissa, A.W., Lee, J.K. and Wang, A.J. (1983) Vibrations of cantilevered doubly-curved shallow shells. *Int. J. Solid Struct.* **19**, 411–424.
- Leissa, A.W., Lee, J.K. and Wang, A.J. (1984a) Vibrations of twisted rotating blades. *J. Vib. Acoust. Stress Relat. Des.* **106**(2), 251–257.
- Leissa, A.W., MacBain, J.C. and Kielb, R.E. (1984b) Vibrations of twisted cantilever plates – summary of previous and current results. *J. Sound Vib.* **96**, 159.
- Lekhnitski, S.T. (1957) *Anisotropic Plates* (GITTL, Moscow) Also, American Iron and Steel Institute, 1956, New York; Also English translation, Gordon&Breach, New York, 1968.
- Levraea, Jr., V.J., Palazotto, A.N. and Maddux, G.E. (1993) Effect of cutout positioning on the dynamic characteristics of a curved composite panel. *Compos. Struct.* **23**(4), 263–272.
- Li, D. (1992) Nonlinear vibrations of orthotropic shallow shells of revolution. *Appl. Math. Mech.* **13**(4), 331–344.
- Li, D. (1993) Time-mode approach to nonlinear vibrations of orthotropic thin shallow spherical shells. *Int. J. Solids Struct.* **30**(22), 3113–3128.
- Li, L. (1996) Bending instability of composite tubes. *J. Aerospace Engng* **9**(2), 58–61.
- Li, N. and Mirza, S. (1997) Dynamic response of cross-ply laminated shell panels. *J. Pressure Vessel Tech.* **119**(2), 157–160.
- Liao, C.L. and Cheng, C.R. (1994a) Dynamic stability of stiffened laminated composite plates and shells subjected to in-plane pulsating forces. *J. Sound Vib.* **174**(3), 335–351.
- Liao, C.L. and Cheng, C.R. (1994b) Dynamic stability of stiffened laminated composite plates and shells subjected to in-plane pulsating forces. *Int. J. Numer. Meth. Engng* **37**(24), 4167–4183.
- Liao, C.L. and Sun, Y.W. (1993) Flutter analysis of stiffened laminated composite plates and shells in supersonic flow. *AIAA J.* **31**(10), 1897–1905.
- Librescu, L. (1976) *The Elastostatics and Kinetics of Anisotropic and Heterogeneous Shell-Type Structures* (Noordhoff, Leyden, Netherlands).
- Librescu, L. and Chang, M.Y. (1993) Effects of geometric imperfections on vibration of compressed shear deformable laminated composite curved panels. *Acta Mech.* **96**(1–4), 203–224.
- Librescu, L. and Lin, W. (1999) Nonlinear response of laminated plates and shells to thermomechanical loading: implications of violation of interlaminar shear traction continuity requirement. *Int. J. Solids Struct.* **36**(27), 4111–4147.
- Librescu, L., Khdeir, A.A. and Frederick, D. (1989a) A shear-deformable theory for laminated composite shallow shell-type panels and their response analysis I: free vibration and buckling. *Acta Mech.* **76**, 1–33.
- Librescu, L., Khdeir, A.A. and Frederick, D. (1989b) A shear-deformable theory for laminated composite shallow shell-type panels and their response analysis II: static analysis. *Acta Mech.* **77**, 1–12.

- Liew, K.M. and Lim, C.W. (1996) Vibratory characteristics of pretwisted cantilever trapezoids of unsymmetric laminates. *AIAA J.* **34**(5), 1041–1050.
- Liew, K.M., Kitipornchai, S. and Wang, C.M. (1993) Research development in the analysis of plates and shells. *J. Const. Steel Res.* **26**(2/3), 231–248.
- Liew, K.M., Lim, C.W. and Kitipornchai, S. (1997a) Vibration of shallow shells: a review with bibliography. *Appl. Mech. Rev.* **50**(8), 431–444.
- Liew, K.M., Karunasena, W., Kitipornchai, S. and Chen, C.C. (1997b) Vibration analysis of arbitrary quadrilateral unsymmetrically laminated thick plates. *AIAA J.* **35**(7), 1251–1253.
- Lim, C.W. and Liew, K.M. (1993) Effects of boundary constraints and thickness variations on the vibratory response of rectangular plates. *Thin-Walled Struct.* **17**(2), 133–159.
- Lim, C.W. and Liew, K.M. (1995a) Higher order theory for vibration of shear deformable cylindrical shallow shells. *Int. J. Mech. Sci.* **37**, 277–295.
- Lim, C.W. and Liew, K.M. (1995b) Vibration of pretwisted cantilevered trapezoidal symmetric laminates. *Acta Mech.* **111**(3/4), 193–208.
- Lim, C.W., Kitipornchai, S. and Liew, K.M. (1997a) Comparative accuracy of shallow and deep shell theories for vibration of cylindrical shells. *J. Vib. Control* **3**, 119–143.
- Lim, C.W., Liew, K.M. and Kitipornchai, S. (1997b) Free vibration of pretwisted, cantilevered composite shallow conical shells. *AIAA J.* **35**(2), 327–333.
- Lim, C.W., Liew, K.M. and Kitipornchai, S. (1998) Vibration of cantilevered laminated composite shallow conical shells. *Int. J. Solids Struct.* **35**(15), 1695–1707.
- Lin, C.C. (1974) Exact solutions for free transverse vibrations of unsymmetrically laminated rectangular plates. *J. Sci. Engng* **11**, 139–152.
- Lin, C.C. and King, W.W. (1974) Free transverse vibrations of rectangular unsymmetrically laminated plates. *J. Sound Vib.* **36**(1), 91–103.
- Liu, I.W. (1996) Element for static, vibration, and buckling analysis of thick laminated plates. *Comput. Struct.* **59**(6), 1051–1058.
- Liu, W.H. and Huang, C.C. (1994) Free vibrations of thick cantilever laminated plates with step-change of thickness. *J. Sound Vib.* **169**(5), 601–618.
- Liu, R.H. and Li, J. (1995) Nonlinear vibration of shallow conical sandwich shells. *Int. J. Non-Linear Mech.* **30**(2), 97–109.
- Liu, L., Liu, T. and Huang, W.L. (1997) Free vibrations of joined conical shells made of composite materials. *J. Huazhong Univ. Sci. Technol.* **25**(9), 32–34.
- Love, A.E.H. (1892) *A Treatise on the Mathematical Theory of Elasticity*, 1st edition (Cambridge University Press, Cambridge) 4th edition, Dover Publishing, New York, 1944.
- Loy, C.T., Lam, K.Y., Hua, L. and Liu, G.R. (1999) Vibration of antisymmetric angle-ply laminated cylindrical panels with different boundary conditions. *Q. J. Mech. Appl. Math.* **51**(1), 55–71.
- Lu, Y.B. (1976) An analytical formulation of the forced responses of damped rings. *J. Sound Vib.* **48**(1), 27–33.
- Lu, C.H., Mao, R. and Winfield, D.C. (1996) Free vibration of thick-walled laminated conical tubes. *Comput. Struct.* **59**(3), 397–405.
- Lur'ye, A.I. (1940) General theory of elastic shells (in Russian). *Prikl Mat Mekh* **4**(1), 7–34.
- Ma, B.A. and He, J.F. (1998) Vibration analysis of laminated shells using a refined shear deformation theory. *J. Reinforced Plastics Composites* **17**(16), 1431–1449.

- MacBain, J.C., Kielb, R.E. and Leissa, A.W. (1984) Vibrations of twisted cantilever plates – experimental investigation. *J. Engng Gas Turbines Power* **107**, 187.
- Maiti, D.K. and Sinha, P.K. (1996) Bending, free vibration and impact response of thick laminated composite plates. *Comput. Struct.* **59**(1), 115–129.
- Manoj, T., Ayyappan, M., Krishnan, K.S. and Rao, B.N. (2000) Nonlinear vibration analysis of thin laminated rectangular plates on elastic foundations., *Z Angew Math Mech* **80**(3), 183–192.
- Markus, S. and Nanasi, T. (1981) Vibrations of curved beams. *Shock Vib. Dig.* **7**(4), 3–14.
- Martin, C.W. and Lung, S.F. (1991) Finite dynamic element for laminated composite plates and shells. *Comput. Struct.* **40**(5), 1249–1259.
- McElman, J.A. and Knoell, A.C. (1971) Vibration and buckling analysis of composite plates and shells. *J. Compos. Mater.* **5**, 529–531.
- Messina, A. and Soldatos, K.P. (1999a) Ritz-type dynamic analysis of cross-ply laminated circular cylinders subjected to different boundary conditions. *J. Sound Vib.* **227**(4), 749–768.
- Messina, A. and Soldatos, K.P. (1999b) Influence of edge boundary conditions on the free vibrations of cross-ply laminated circular cylindrical panels. *J. Acoust. Soc. Am.* **106**(5), 2608–2620.
- Miller, S.E., Oshman, Y. and Abramovich, H. (1997) Modal control of piezolaminated anisotropic rectangular plates – Part 2: control theory. *AIAA J.* **34**(9), 1876–1884.
- Mindlin, R.D. (1951) Influence of rotary inertia and shear on flexural motions of isotropic elastic plates. *J. Appl. Mech.* **18**(10), 31–38.
- Mirza, S. and Bijlani, M. (1983) Vibration of triangular plates. *AIAA J.* **21**, 1472–1475.
- Mizusawa, T. (1996) Vibration of thick laminated cylindrical panels by the spline strip method. *Comput. Struct.* **61**(3), 441–457.
- Mizusawa, T. and Kito, H. (1995) Vibration of antisymmetric angle-ply laminated cylindrical panels by the spline strip method. *Comput. Struct.* **56**(4), 589–604.
- Mohan, D. and Kingsbury, H.B. (1971) Free vibrations of generally laminated orthotropic plates. *J. Acoust. Soc. Am.* **50**, 266–269.
- Mohd, S. and Dawe, D.J. (1993a) Finite strip vibration analysis of composite prismatic shell structures with diaphragm ends. *Comput. Struct.* **49**(5), 753–765.
- Mohd, S. and Dawe, D.J. (1993b) Buckling and vibration of thin laminated composite, prismatic shell structures. *Composite Struct.* **25**(1–4), 353–362.
- Moore, I.D. (1990) Vibration of thick elastic and viscoelastic tubes. I. Harmonic response. *J. Engng Mech.* **116**(4), 928–942.
- Mushtari, K.h.M. (1961) Basic Theory of Shallow Shells With Fillers, *Izv. Akad. Nauk. SSSR, Otd. Tekh. Nauk. Mekh i Mash* **2**, 24–29.
- Nabi, S.M. and Ganesan, N. (1993) Vibration and damping analysis of pre-twisted composite blades. *Comput. Struct.* **47**(2), 275–280.
- Naghdi, P.M. and Berry, J.G. (1964) On the equations of motion of cylindrical shells. *J. Appl. Mech.* **21**, 160–166.
- Naghdi, P.M. and Cooper, R.M. (1956) Propagation of elastic waves in cylindrical shells, including the effects of transverse shear and rotary inertia. *J. Acoust. Soc. Am.* **28**, 56–63.
- Narasimhan, M.C. and Alwar, R.S. (1992) Free vibration analysis of laminated orthotropic spherical shells. *J. Sound Vib.* **154**(3), 515–529.

- Narita, Y. (1985) Natural frequencies of free, orthotropic elliptical plates. *J. Sound Vib.* **100**, 83–89.
- Narita, Y. (1986) Free-vibration analysis of orthotropic elliptical plates resting on arbitrarily distributed point supports. *J. Sound Vib.* **108**, 1–10.
- Narita, Y. and Iwato, N. (1990) Vibration studies of laminated circular and elliptical plates resting on elastic point supports. *Compos. Sci. Technol.* **39**, 75–88.
- Narita, Y. and Leissa, A.W. (1984) Vibrations of corner supported shallow shells of rectangular planform. *Earthquake Engng Struct. Dyn.* **12**(5), 651–662.
- Narita, Y. and Leissa, A.W. (1986) Vibrations of completely free shallow shells of curvilinear planform. *J. Appl. Mech.* **53**, 647–651.
- Narita, Y., Ohta, Y. and Saito, M. (1993) FE study for natural frequencies of cross-ply laminated cylindrical shells. *Compos. Struct.* **26**(1/2), 55–62.
- Nayfeh, A.H. (1995) *Wave Propagation in Layered Anisotropic Media* (North-Holland, Amsterdam) 346 pp.
- Nayfeh, J.F. and Riveccio, N.J. (2000) Nonlinear vibration of composite shell subjected to resonant excitations. *J. Aerospace Engng* **13**(2), 59–68.
- Nelson, F.C. (1977) The forced vibration of a three-layer damped circular ring. ASME Paper No. 77-DET-154.
- Nemoto, K. and Kasuya, H. (1994) Dynamic response of angle-ply laminated cylindrical shells subjected to periodic external pressure. *J. Soc. Mater. Sci. Jpn* **43**(486), 254–258.
- Ng, T.Y. and Lam, K.Y. (1999) Dynamic stability analysis of cross-ply laminated cylindrical shells using different shell theories. *Acta Mech.* **134**(3/4), 147–167.
- Ng, T.Y., Lam, K.Y. and Reddy, J.N. (1998) Dynamic stability of cross-ply laminated cylindrical shells. *Int. J. Mech. Sci.* **40**(8), 805–823.
- Noor, A.K. (1973) Free vibration of multilayered composite plates. *AIAA J.* **11**, 1038–1039.
- Noor, A.K. (1990) Assessment of computational models for multilayered composite shells. *Appl. Mech. Rev.* **43**(4), 67–96.
- Noor, A.K. and Burton, W.S. (1990) Assessment of computational models for multilayered composite shells. *Appl. Mech. Rev.* **43**(4), 67–97.
- Noor, A.K. and Burton, W.S. (1992) Computational models for high-temperature multilayered composite plates and shells. *Appl. Mech. Rev.* **45**(10), 419–446.
- Noor, A.K., Burton, W.S. and Peters, J.M. (1990) Predictor–corrector procedures for stress and free vibration analyses of multilayered composite plates and shells. *Comput. Meth. Appl. Mech. Engng* **82**(1–3), 341–363.
- Noor, A.K., Burton, W.S. and Peters, J.M. (1991) Assessment of computational models for multilayered composite cylinders. *Int. J. Solids Struct.* **27**(10), 1269–1286.
- Noor, A.K., Peters, J.M. and Andersen, C.M. (1993) Reduced basis technique for non-linear vibration analysis of composite panels. *Comput. Meth. Appl. Mech. Engng* **103**(1/2), 175–186.
- Noor, A.K., Hadian, M.J. and Peters, J.M. (1994) Reduced basis technique for evaluating the sensitivity of the nonlinear vibrational response of composite plates. *Comput. Struct.* **52**(6), 1097–1105.
- Noor, A.K., Burton, W.S. and Peters, J.M. (1995) Hierarchical adaptive modeling of structural sandwiches and multilayered composite panels. *Engng Fracture Mech.* **50**(5/6), 801–817.

- Noor, A.K., Burton, W.S. and Bert, C.W. (1996) Computational models for sandwich panels and shells. *Appl. Mech. Rev.* **49**, 155–199.
- Nosier, A. and Reddy, J.N. (1992) Vibration and stability analyses of cross-ply laminated circular cylindrical shells. *J. Sound Vib.* **157**(1), 139–159.
- Nosier, A., Kapania, R.K. and Reddy, J.N. (1994a) Free vibration analysis of laminated plates using a layerwise theory. *AIAA J.* **31**(12), 2335–2346.
- Nosier, A., Kapania, R.K. and Reddy, J.N. (1994b) Low-velocity impact of laminated composites using a layerwise theory. *Comput. Mech.* **13**(5), 360–379.
- Novozhilov, V.V. (1958) Thin Elastic Shells. Translated from 2nd Russian edition by Lowe, P.G. London.
- Ohnabe, H. (1995) Nonlinear vibration of heated orthotropic sandwich plates and shallow shells. *Int. J. Non-Linear Mech.* **30**(4), 501–508.
- Pagano, N.J. (1970) Influence of shear deformation in cylindrical bending of anisotropic plates. *J. Compos. Mater.* **4**, 330.
- Pai, P.F. and Nayfeh, A.H. (1992a) Nonlinear composite plate theory. *Nonlinear Dyn.* **2**(6), 445–477.
- Pai, P.F. and Nayfeh, A.H. (1992b) Nonlinear composite shell theory. *Nonlinear Dyn.* **3**(6), 431–463.
- Pai, P.F. and Nayfeh, A.H. (1994) Unified nonlinear formulation for plate and shell theories. *Nonlinear Dyn.* **6**(4), 459–500.
- Palazotto, A.N. and Linnemann, P.E. (1991) Vibration and buckling characteristics of composite cylindrical panels incorporating the effects of a higher order shear theory. *Int. J. Solids Struct.* **28**(3), 341–361.
- Paliwal, D.N. and Pandey, R.K. (1998) Free vibration of a cylindrical shell on an elastic foundation. *J. Vib. Acoust.* **120**(1), 63–71.
- Paliwal, D.N., Kanagasabapathy, H. and Gupta, K.M. (1995a) Vibrations of an orthotropic shallow spherical shell on a Pasternak foundation. *Compos. Struct.* **33**(3), 135–142.
- Paliwal, D.N., Kanagasabapathy, H. and Gupta, K.M. (1995b) Vibrations of an orthotropic shallow spherical shell on a Kerr foundation. *Int. J. Pressure Vessels Piping* **64**(1), 17–24.
- Patel, B.P., Ganapathi, M. and Kama, S. (2000) Free vibration characteristics of laminated composite joined conical-cylindrical shells. *J. Sound Vib.* **237**(5), 920–930.
- Piskunov, V.G., Verijenko, V.E., Adali, S. and Tabakov, P.Y. (1994) Transverse shear and normal deformation higher-order theory for the solution of dynamic problems of laminated plates and shells. *Int. J. Solids Struct.* **31**(24), 3345–3374.
- Piskunov, V.G., Fedorenko, Y.M. and Didychenko, I.M. (1995) Dynamics of the non-elastic laminated composite shells. (Russian). *Mech. Composite Mat.* **T31**(1), 72–80.
- Qatu, M.S. (1989) Free vibration and static analysis of laminated composite shallow shells. PhD Dissertation, The Ohio State University.
- Qatu, M.S. (1991a) Free vibration of laminated composite rectangular plates. *Int. J. Solids Struct.* **28**, 941–954.
- Qatu, M.S. (1991b) Curvature effects on the deflection and vibration of cross-ply shallow shells, in *Mechanics and Computing in 90's and Beyond*, eds. Adeli, H. and Sierakowski, R. (ASCE pp. 745–750).
- Qatu, M.S. (1992a) Inplane vibration of slightly curved laminated composite beams. *J. Sound Vib.* **159**, 327–338.

- Qatu, M.S. (1992b) Review of shallow shell vibration research. *Shock Vib. Dig.* **24**, 3–15.
- Qatu, M.S. (1992c) Mode shape analysis of laminated composite shallow shells. *J. Acoust Soc. Am.* **92**, 1509–1520.
- Qatu, M.S. (1993a) Vibration of doubly-cantilevered laminated composite thin shallow shells. *Thin-Walled Struct.* **15**, 235–248.
- Qatu, M.S. (1993b) Theories and analyses of thin and moderately thick laminated composite curved beams. *Int. J. Solids Struct.* **30**(20), 2743–2756.
- Qatu, M.S. (1994a) On the validity of nonlinear shear deformation theories for laminated composite plates and shells. *Compos. Struct.* **27**, 395–401.
- Qatu, M.S. (1994b) Vibrations of laminated composite completely free triangular and trapezoidal plates. *Int. J. Mech. Sci.* **36**(9), 797–809.
- Qatu, M.S. (1994c) Natural frequencies for cantilevered laminated composite right triangular and trapezoidal plates. *Compos. Sci. Tech.* **51**, 441–449.
- Qatu, M.S. (1995a) Accurate stress resultant equations for laminated composite deep, thick shells. *Compos. Pressure Vessel Ind., ASME-PVP* **302**, 39–46.
- Qatu, M.S. (1995b) Vibration studies on completely free shallow shells having triangular and trapezoidal planforms. *Appl. Acoust.* **44**(3), 215–231.
- Qatu, M.S. (1995c) Natural vibration of free laminated composite triangular and trapezoidal shallow shells. *Compo. Struct.* **31**(1), 9–19.
- Qatu, M.S. (1995d) Vibration of cantilevered composite triangular and trapezoidal doubly-curved shallow shells. *Acta Mech.* **108**, 63–75.
- Qatu, M.S. (1996) Vibration analysis of cantilevered shallow shells with right triangular and trapezoidal planforms. *J. Sound Vib.* **191**(2), 219–231.
- Qatu, M.S. (1999a) Accurate theory for laminated composite deep thick shells. *Int. J. Solids Struct.* **36**(19), 2917–2941.
- Qatu, M.S. (1999b) Theory and vibration analysis of laminated barrel thin shells. *J. Vib. Control* **5**, 851–889.
- Qatu, M.S. (2002a) Recent research advances in the dynamic behavior of shells: 1989–2000. Part 1: laminated composite shells. *Appl. Mech. Rev.* **55**(4), 325–351.
- Qatu, M.S. (2002b) Recent research advances in the dynamic behavior of shells: 1989–2000. Part 2: homogeneous shells. *Appl. Mech. Rev.* **55**(5), 415–435.
- Qatu, M.S. (2004) Theory and vibration analysis of laminated barrel thick shells. *J. Vib. Control* to appear.
- Qatu, M.S. and Bataineh, A. (1992) Structural analysis of shallow shells using cray Y-MP supercomputers. *Int. J. Comput. Struct.* **45**(3), 453–459.
- Qatu, M.S. and Elsharkawy, A. (1993) Vibrations of laminated composite arches with deep curvature and arbitrary boundaries. *Comput. Struct.* **47**, 305–311.
- Qatu, M.S. and Leissa, A.W. (1991a) Free vibrations of completely free doubly-curved laminated composite shallow shells. *J. Sound Vib.* **151**(1991), 9–29.
- Qatu, M.S. and Leissa, A.W. (1991b) Natural frequencies for cantilevered doubly-curved laminated composite shallow shells. *Compos. Struct.* **17**(3), 227–256.
- Qatu, M.S. and Leissa, A.W. (1991c) Vibration studies for laminated composite twisted cantilever plates. *Int. J. Mech. Sci.* **33**(11), 927–940.
- Qatu, M.S. and Leissa, A.W. (1992) Effects of edge constraints upon shallow shell frequencies. *Thin-Walled Struct.* **14**, 347–379.

- Qatu, M.S. and Leissa, A.W. (1993) Vibrations of shallow shells with two adjacent edges clamped and the others free. *J. Mech. Struct. Mech.* **21**(3), 285–301.
- Qatu, M.S., Leissa, A.W. and Jaber, N.A. (1993) Natural frequencies for completely free trapezoidal plates. *J. Sound Vib.* **167**(1), 183–191.
- Ramesh, T.C. and Ganesan, N. (1992) FE based on a discretized layer theory for the free vibration analysis of cylindrical shells. *Comput. Struct.* **43**(1), 137–143.
- Ramesh, T.C. and Ganesan, N. (1993) Finite element based on a discrete layer theory for the free vibration analysis of conical shells. *J. Sound Vib.* **166**(3), 531–538.
- Ramesh, T.C. and Ganesan, N. (1994) Orthotropic cylindrical shells with a viscoelastic core: a vibration and damping analysis. *J. Sound Vib.* **175**(4), 535–555.
- Rao, K.P. (1978) A rectangular laminated anisotropic shallow thin shell finite element. *Comput. Meth. Appl. Mech. Engng* **15**(1), 13–33.
- Rao, M.A., Dukkipati, R.V. and Tummala, M. (1993) FE analysis of multilayered shells of revolution. *Comput. Struct.* **47**(2), 253–258.
- Raouf, R.A. and Palazotto, A.N. (1992) Nonlinear free vibrations of symmetrically laminated, slightly compressible cylindrical shell panels. *Compos. Struct.* **20**(4), 249–257.
- Raouf, R.A. and Palazotto, A.N. (1994) Nonlinear free vibrations of curved orthotropic panels. *Int. J. Non-Linear Mech.* **29**(4), 507–514.
- Rath, B.K. and Das, Y.C. (1973) Vibration of layered shells. *J. Sound Vib.* **28**, 737–757.
- Rayleigh, L. (1877) *Theory of Sound*, vols. I and II (Dover Publications, New York).
- Reddy, J.N. (1979) Free vibration of antisymmetric angle-ply laminated plates including transverse shear deformation by the finite element method. *J. Sound Vib.* **66**, 565–576.
- Reddy, J.N. (1984a) Exact solutions of moderately thick laminated shells. *J. Engng Mech.* **110**(5), 794–809.
- Reddy, J.N. (1984b) *Energy and Variational Methods in Applied Mechanics* (McGraw-Hill, New York).
- Reddy, J.N. (1989) Refined computational models of composite laminates. *Int. J. Numer. Meth. Engng* **27**(2), 361–382.
- Reddy, J.N. (2003) *Mechanics of Laminated Composite Plates and Shells: Theory and Analysis*, 2nd edition (CRC Press, Boca Raton, FL).
- Reddy, J.N. and Khdeir, A.A. (1989) Buckling and vibration of laminated composite plates using various plate theories. *AIAA J.* **27**(1), 1808–1816.
- Reddy, J.N. and Liu, C.F. (1985) A higher order shear deformation theory of laminated elastic shells. *Int. J. Engng Sci.* **23**(3), 440–447.
- Reddy, P.M. and Tadjuddin, M. (2000) Exact analysis of the plane-strain vibrations of thick-walled hollow poroelastic cylinders. *Int. J. Solids Struct.* **37**(25), 3439–3456.
- Reissner, E. (1941) New derivation of the equations of the deformation of elastic shells. *Am. J. Math.* **63**, 177–184.
- Reissner, E. (1945) The effect of transverse shear deformation on the bending of elastic plates. *J. Appl. Mech.* **67**, A69–A77.
- Reissner, E. (1952) Stress strain relation in the theory of thin elastic shells. *J. Math. Phys.* **31**, 109–119.
- Reissner, E. and Stavsky, Y. (1961) Bending and stretching of certain types of heterogeneous anisotropic elastic plates. *J. Appl. Mech.* **28**(3), 402–408.

- Rezaeepazhand, J., Simiteses, G.J. and Starnes, Jr., J.H. (1996) Design of scaled down models for predicting shell vibration response. *J. Sound Vib.* **195**(2), 301–311.
- Ribeiro, P. and Petyt, M. (1999) Nonlinear vibration of composite laminated plates by the hierarchical FEM. *Compos. Struct.* **46**(3), 197–208.
- Roussos, N. and Mason, D.P. (1998) Nonlinear radial oscillations of a thin-walled double-layer hyperelastic cylindrical tube. *Int. J. Non-Linear Mech.* **33**(3), 507–530.
- Saada, A. (1974) *Elasticity: Theory and Applications* (Pergamon Press, New York) Reprinted by Robert Kreiger Publishing, Florida, 1983, 1987.
- Sagartz, M.J. (1977) Transient response of three-layered rings. *J. Appl. Mech.* **44**(2), 299–304.
- Sandeep, K. and Nath, Y. (2000) Nonlinear dynamic response of axisymmetric thick laminated shallow spherical shells. *Int. J. Nonlinear Sci. Numer. Simulat.* **1**(3), 225–238.
- Sanders, J. (1959) An Improved First Approximation Theory of Thin Shells. NASA TR-R24.
- Saravanos, D.A. and Heyliger, P.R. (1999) Mechanics and computational models for laminated piezoelectric beams, plates, and shells. *Appl. Mech. Rev.* **52**(10), 305–319.
- Saravanos, D.A., Heyliger, P.R. and Hopkins, D.A. (1997) Layerwise mechanics and FE for the dynamic analysis of piezoelectric composite plates. *Int. J. Solids Struct.* **34**(3), 359–378.
- Sathyamoorthy, M. (1995) Nonlinear vibrations of moderately thick orthotropic shallow spherical shells. *Comput. Struct.* **57**(1), 59–65.
- Selmane, A. and Lakis, A.A. (1997a) Influence of geometric nonlinearities on the free vibrations of orthotropic open cylindrical shells. *Int. J. Numer. Meth. Engng* **40**(6), 1115–1137.
- Selmane, A. and Lakis, A.A. (1997b) Nonlinear dynamic analysis of orthotropic open cylindrical shells subjected to a flowing fluid. *J. Sound Vib.* **202**(1), 67–93.
- Selmane, A. and Lakis, A.A. (1997c) Dynamic analysis of anisotropic open cylindrical shells. *Comput. Struct.* **62**(1), 1–12.
- Selmane, A. and Lakis, A.A. (1997d) Vibration analysis of anisotropic open cylindrical shells subjected to a flowing fluid. *J. Fluids Struct.* **11**(1), 111–134.
- Senitsky, Y.E. (1994) Axisymmetrical dynamic problem for nonhomogeneous shallow spherical shell with finite shift liquid (Russian). *Prikl Mekh (Appl. Mech.)* **30**(9), 50–57.
- Sharma, C.B., Darvizeh, M. and Darvizeh, A. (1996) Free vibration response of multilayered orthotropic fluid-filled circular cylindrical shells. *Compos. Struct.* **34**(2), 349–355.
- Sharma, C.B., Darviseh, M. and Darvizeh, A. (1999) Free vibration behavior of helically wound cylindrical shells. *Compos. Struct.* **44**(1), 55–62.
- Sheinman, I. and Reichman, Y. (1992) Study of buckling and vibration of laminated shallow curved panels. *Int. J. Solids Struct.* **29**(11), 1329–1338.
- Shen, H. (2000) Nonlinear analysis of composite laminated thin plates subjected to lateral pressure and thermal loading and resting on elastic foundations. *Compos. Struct.* **49**(2), 115–128.
- Shih, Y.-S. and Blotter, P.T. (1994) Nonlinear vibration analysis of arbitrarily laminated thin rectangular plates on elastic foundations. *J. Sound Vib.* **167**(3), 433–459.
- Shin, D.K. (1997) Large amplitude free vibration behavior of doubly curved shallow open shells with simply-supported edges. *Comput. Struct.* **62**(1), 35–49.
- Shu, C. (1996) Free vibration analysis of composite laminated conical shells by generalized differential quadrature. *J. Sound Vib.* **194**(4), 587–604.

- Shulga, N.A., Meish, V.F. and Khamrenko, Y.A. (1999) Nonstationary vibrations of three-layered cylindrical shells under axisymmetric loading (Russian). *Prikl Mekh (Appl. Mech.)* **35**(8), 3–9.
- Singh, S.P. and Gupta, K. (1994a) Damped free vibrations of layered composite cylindrical shells. *J. Sound Vib.* **172**(2), 191–209.
- Singh, S.P. and Gupta, K. (1994b) Free damped flexural vibration analysis of composite cylindrical tubes using beam and shell theories. *J. Sound Vib.* **172**(2), 171–190.
- Singh, A.V. and Kumar, V. (1996) Vibration of laminated shallow shells on quadrangular boundary. *J. Aerospace Engng* **9**(2), 52–57.
- Singh, A.V. and Mirza, S. (1991) Asymmetric vibrations of layered orthotropic shells of revolution. *J. Sound Vib.* **148**(2), 265–277.
- Singh, A.V., Mirza, S. and Gupgupoglu, K. (1990) Dynamic response of sandwich shells of revolution. *J. Pressure Vessel Tech.* **112**(1), 98.
- Singh, G., Rao, V.G. and Iyengar, N.G.R. (1995) Finite element analysis of the nonlinear vibrations of moderately thick unsymmetrically laminated composite plates. *J. Sound Vib.* **181**, 315–329.
- Sivadas, K.R. (1995a) Vibration analysis of pre-stressed thick circular conical composite shells. *J. Sound Vib.* **186**(1), 87–97.
- Sivadas, K.R. (1995b) Vibration analysis of pre-stressed rotating thick circular conical shell. *J. Sound Vib.* **186**(1), 99–110.
- Sivadas, K.R. and Ganesan, N. (1991a) Asymmetric vibration analysis of thick composite circular cylindrical shells with variable thickness. *Comput. Struct.* **38**(5/6), 627–635.
- Sivadas, K.R. and Ganesan, N. (1991b) Vibration analysis of laminated conical shells with variable thickness. *J. Sound Vib.* **148**(3), 477–491.
- Sivadas, K.R. and Ganesan, N. (1992) Vibration analysis of thick composite clamped conical shells of varying thickness. *J. Sound Vib.* **152**(1), 27–37.
- Sivadas, K.R. and Ganesan, N. (1993) Effect of coupling between in-plane strains and twist due to anisotropy on vibration of composite shells. *Comput. Struct.* **49**(3), 481–493.
- Sivak, V.F. (1998) Experimental study of resonance and dissipative properties of cylindrical shell of glass fiber reinforced plastic filled with liquid (Russian). *Prikl Mekh* **34**(2), 39–42.
- Sivakumaran, K.S. (1987) Natural frequencies of symmetrically laminated rectangular plates with free edges. *Compos. Struct.* **7**, 191–204.
- Slepyan, L.I. and Sorokin, S.V. (1995) Analysis of structural-acoustic coupling problems by a two-level boundary integral equations method – Part 1: a general formulation and test problems. *J. Sound Vib.* **184**(2), 195–211.
- Smith, C.B. (1953) Some new types of orthotropic plates laminated of orthotropic materials. *J. Appl. Mech.* **20**, 286–288.
- Soares, C.M.M., Correia, V.F., Mateus, H. and Herskovits, J. (1995) Discrete model for the optimal design of thin composite plate-shell type structures using a two-level approach. *Compos. Struct.* **30**(2), 147–157.
- Soedel, W. (1993) *Vibrations of Shells and Plates*, 2nd edition (Marcel Dekker, New York).
- Soldatos, K.P. (1991) Refined laminated plate and shell theory with applications. *J. Sound Vib.* **144**(1), 109–129.

- Soldatos, K.P. (1992) Nonlinear analysis of transverse shear deformable laminated composite cylindrical shells. Part I. Derivation of governing equations. *J. Pressure Vessel Tech.* **114**(1), 105–109.
- Soldatos, K.P. (1994) Review of three dimensional dynamic analyses of circular cylinders and cylindrical shells. *Appl. Mech. Rev.* **47**, 501–516.
- Soldatos, K.P. (1999) Mechanics of cylindrical shells with non-circular cross-section. *Appl. Mech. Rev.* **52**(8), 237–274.
- Soldatos, K.P. and Messina, A. (1998) Vibration studies of cross-ply laminated shear deformable circular cylinders on the basis of orthogonal polynomials. *J. Sound Vib.* **218**(2), 219–243.
- Soldatos, K.P. and Messina, A. (2001) The influence of boundary conditions and transverse shear on the vibration of angle-ply laminates plates, circular cylinder and cylindrical panels. *Comput. Meth. Appl. Mech. Engng* **190**, 2385–2409.
- Soldatos, K.P. and Ye, J. (1994) Wave propagation in anisotropic laminated hollow cylinders of infinite extent. *J. Acoust. Soc. Am.* **96**(6), 3744–3752.
- Sonti, V.R. and Jones, J.D. (1996a) Curved piezoactuator model for active vibration control of cylindrical shells. *AIAA J.* **34**(5), 1034–1040.
- Sonti, V.R. and Jones, J.D. (1996b) Dynamic effects of piezoactuators on the cylindrical shell response. *AIAA J.* **34**(4), 795–801.
- Sorokin, S.V. (1995) Analysis of structural-acoustic coupling problems by a two-level boundary integral equations method – Part 2: vibrations of a cylindrical shell of finite length in an acoustic medium. *J. Sound Vib.* **184**(2), 213–228.
- Srinivas, S., Joga Rao, C.V. and Rao, A.K. (1970) An exact analysis of vibration of simply supported homogeneous and laminated thick rectangular plates. *J. Sound Vib.* **12**, 187–199.
- Srinivasamurthy, K. and Chia, C.Y. (1990) Nonlinear dynamic and static analysis of laminated anisotropic thick circular plates. *Acta Mech.* **82**(3/4), 135–150.
- Sun, G., Bennet, P.N. and Williams, F.W. (1997) Investigation on fundamental frequencies of laminated circular cylinders given by shear deformable FEs. *J. Sound Vib.* **205**(3), 265–273.
- Suzuki, K. and Shikanai, G. (1998) Vibration of composite circular cylindrical vessel. *Int. J. Solids Struct.* **35**(22), 2877–2899.
- Suzuki, K., Shikanai, G. and Leissa, A.W. (1994) Free vibrations of laminated composite noncircular thin cylindrical shells. *J. Appl. Mech.* **61**(4), 861–871.
- Suzuki, K., Shikanai, G., Kosawada, T. and Tabata, M. (1995a) Vibration analysis of laminated composite thin shells of revolution. *Trans. Jpn. Soc. Mech. Engng* **61C**, 849–856. in Japanese.
- Suzuki, K., Shikanai, G. and Nakano, K. (1995b) Vibration analysis of laminated composite thick shells of revolution (in Japanese). *Trans. Jpn. Soc. Mech. Engng* **61C**, 863–870.
- Suzuki, K., Shikanai, G. and Leissa, A.W. (1996) Free vibrations of laminated composite non-circular thick cylindrical shells. *Int. J. Solids Struct.* **33**(27), 4079–4100.
- Swider, P., Le Fichoux, B. and Jacquet-Richardet, G. (1996) Dynamic modeling of a composite shell: a mixed numerical and experimental approach. *Compos. Struct.* **34**(2), 301–308.

- Takahashi, K., Sato, E., Maeda, N. and Abiru, S. (1996) Vibration, buckling and dynamic stability of anti-symmetric angle-ply laminated rectangular plates. *Proc. JSCE* **537**(I-35), 53–60.
- Tang, W. and Chen, T. (1998) Nonlinear dynamic response analysis of laminated composite cylindrical panels (Chinese). *J. Shanghai Jiaotong Univ.* **32**(7), 128–131.
- Tarn, J.Q. (1994) Asymptotic theory for dynamic response of anisotropic inhomogeneous and laminated cylindrical shells. *J. Mech. Phys. Solids* **42**(10), 1633–1650.
- Tatemichi, A., Okazaki, A. and Hikyama, M. (1980) Damping properties of curved sandwich beams with viscoelastic layer. *Bull. Nagaya Inst.* **29**, 309–317.
- Taylor, T.W. and Nayfeh, A.H. (1997) Damping characteristics of laminated thick plates. *J. Appl. Mech.* **64**(1), 132–138.
- Tighe, K.V. and Palazotto, A.N. (1994) Higher order cylindrical panel relationships considering general ply layups. *Compos. Struct.* **27**(3), 225–242.
- Timarci, T. and Soldatos, K.P. (1995) Comparative dynamic studies for symmetric cross-ply circular cylindrical shells on the basis of a unified shear deformable shell theory. *J. Sound Vib.* **187**(4), 609–624.
- Timoshenko, S. (1921) On the correction for shear of the differential equation for transverse vibration of prismatic bars. *Philos. Mag. Ser. 6* **41**, 742.
- Timoshenko, S. (1983) *History of Strength of Materials* (Dover Publication, New York).
- Timoshenko, S. and Goodier, S. (1970) *Theory of Elasticity* (McGraw-Hill, New York).
- Timoshenko, S. and Woinowsky-Krieger, S. (1959) *Theory of Plates and Shells*, 2nd edition (McGraw-Hill, New York).
- Tong, L. (1993a) Free vibration of composite laminated conical shells. *Int. J. Mech. Sci.* **35**(1), 47–61.
- Tong, L. (1993b) Free vibration of orthotropic conical shells. *Int. J. Engng Sci.* **31**(5), 719–733.
- Tong, L. (1994a) Free vibration of laminated conical shells including transverse shear deformation. *Int. J. Solids Struct.* **31**(4), 443–456.
- Tong, L. (1994b) Effect of transverse shear deformation on free vibration of orthotropic conical shells. *Acta Mech.* **107**(1–4), 65–75.
- Tong, L. (1996) Effect of axial load on free vibration of orthotropic truncated conical shells. *J. Vib. Acoust.* **118**(2), 164–168.
- Toorani, M.H. and Lakis, A.A. (2000) General equations of anisotropic plates and shells including transverse shear deformations, rotary inertia and initial curvature effects. *J. Sound Vib.* **237**(4) 561–615.
- Touratier, M. and Faye, J.P. (1995) Refined model in structural mechanics: FE approximation and edge effect analysis for axisymmetric shells. *Comput. Struct.* **54**(5), 897–920.
- Tracy, J.J., Dimis, J.D. and Pardowin, G.C. (1985) The effect of impact damage on the dynamic properties of laminated composite plates. Proceedings of the Fifth International Conference on Composite Materials, San Diego, CA, pp. 111–125.
- Tsai, Y.M. (1991) Longitudinal motion of a thick transversely isotropic hollow cylinder. *J. Pressure Vessel Tech.* **113**(4), 585–589.
- Tsai, C.T. and Palazotto, A.N. (1991) Finite element analysis of non-linear vibration for cylindrical shells with high-order shear deformation theory. *Int. J. Non-Linear Mech.* **26**(3/4), 379–388.

- Tzou, H.S. and Bao, Y. (1995) Dynamics and control of adaptive shells with curvature transformations. *Shock Vib.* **2**(2), 143–154.
- Tzou, H.S. and Gadre, M. (1989) Theoretical analysis of a multi-layered thin shell coupled with piezoelectric shell actuators for distributed vibration controls. *J. Sound Vib.* **132**(3), 433–450.
- Tzou, H.S. and Ye, R. (1996) Analysis of piezoelectric structures with laminated piezoelectric triangle shell elements. *AIAA J.* **34**(1), 110–115.
- Vinson, J.R. and Sierakowski, R.L. (1986) *The Behaviour of Structures Composed of Composite Materials* (Martinus Nijhoff Publishers, Dordrecht, The Netherlands) 323 pp.
- Visscher, W.M., Migliori, A., Bell, T.M. and Reinert, R.A. (1991) Normal modes of free vibration of inhomogeneous and anisotropic elastic objects. *J. Acoust. Soc. Am.* **90**(4 PT 1), 2154–2162.
- Vlasov, V.Z. (1949) *General Theory of Shells and Its Application to Engineering* (GITTL, Moskva-Leningrad) English Translation, NASA Technical Translation TTF-99, 1964.
- Walton, W.C., Jr. (1960) Applications of a general finite difference method for calculating bending deformation of solid plates, NASA TND-536.
- Wang, W.J. and Lin, K.C. (1995) Free vibration of laminated plates using a finite strip method based on a higher-order plate theory. *Comput. Struct.* **53**, 1281–1289.
- Wang, J. and Schweizerhof, K. (1996a) Study on free vibration of moderately thick orthotropic laminated shallow shells by boundary-domain elements. *Appl. Math. Model* **20**(8), 579–584.
- Wang, J. and Schweizerhof, K. (1996b) Boundary-domain element method for free vibration of moderately thick laminated orthotropic shallow shells. *Int. J. Solids Struct.* **33**(1), 11–18.
- Wang, J. and Schweizerhof, K. (1997) Free vibration of laminated anisotropic shallow shells including transverse shear deformation by the boundary-domain element method. *Comput. Struct.* **62**(1), 151–156.
- Wang, C.Y. and Vaicaitis, R. (1998) Active control of vibrations and noise of double wall cylindrical shells. *J. Sound Vib.* **216**(5), 865–888.
- Wang, Z., Zhu, D. and Tang, L. (1995) Semi-analytical solution for free vibration of laminated composite cylindrical panels (Chinese). *J. Vib. Engng* **8**(2), 91–98.
- Wang, Y., Wang, X. and Song, H. (1997) Nonlinear free vibration of orthotropic shallow shells of revolution under the static load. *Appl. Math. Mech.* **18**(6), 585–591.
- Washizu, K. (1982) *Variational Methods in Elasticity and Plasticity*, 3rd edition (Pergamon Press, New York).
- Weingarten, V.I. (1964) Free vibration of multilayered cylindrical shells. *Exp. Mech.* **4**, 200–205.
- Whitney, J.M. (1969) The effect of transverse shear deformation on the bending of laminated plates. *J. Compos. Mater.* **3**, 534–547.
- Whitney, J.M. (1987) *Structural Analysis of Laminated Anisotropic Plates* (Technomic Publishing, Lancaster, PA).
- Whitney, J.M. and Sun, C.T. (1973) A higher order theory for extensional motion of laminated composites. *J. Sound Vib.* **41**(2), 471–476.
- Williams, F.W., Bennett, P.N. and Kennedy, D. (1996) Curves for natural frequencies of axially compressed prismatic plate assemblies. *J. Sound Vib.* **194**(1), 13–24.

- Wilt, T.E., Saleeb, A.F. and Chang, T.Y. (1990) Mixed element for laminated plates and shells. *Comput. Struct.* **37**(4), 597–611.
- Wu, C.P. and Wu, C.H. (2000) Asymptotic differential quadrature solutions for the free vibration of laminated conical shells. *Comput. Mech.* **25**(4), 346–357.
- Xavier, P.B., Chew, C.H. and Lee, K.H. (1995) Buckling and vibration of multilayer orthotropic composite shells using a simple higher-order layerwise theory. *Int. J. Solids Struct.* **32**(23), 3479–3497.
- Xi, Z.C., Yam, L.H. and Leung, T.P. (1996) Semi-analytical study of free vibration of composite shells of revolution based on the Reissner–Mindlin assumption. *Int. J. Solids Struct.* **33**(6), 851–863.
- Xi, Z.C., Yam, L.H. and Leung, T.P. (1999) Free vibration of a laminated composite shell of revolution: effects of shear nonlinearity. *Int. J. Mech. Sci.* **41**(6), 649–661.
- Xu, C.S. and Chia, C.Y. (1994a) Nonlinear analysis of unsymmetrically laminated moderately thick shallow spherical shells. *Int. J. Non-Linear Mech.* **29**(2), 247–259.
- Xu, C.S. and Chia, C.Y. (1994b) Large-amplitude vibrations of unsymmetrically laminated imperfect thick circular plates on an elastic foundation. *Compos. Sci. Tech.* **49**(2), 131–137.
- Xu, C.S. and Chia, C.Y. (1995) Nonlinear vibration and buckling analysis of laminated shallow spherical shells with holes. *Compos. Sci. Tech.* **54**(1), 67–74.
- Xu, C.S., Xia, Z.Q. and Chia, C.Y. (1996) Nonlinear theory and vibration analysis of laminated truncated, thick, conical shells. *Int. J. Non-Linear Mech.* **31**(2), 139–154.
- Xu, K., Noor, A.K. and Burton, W.S. (1997) 3D solutions for free vibration of initially stressed thermoelectroelastic multilayered cylinders. *J. Engng Mech.* **123**(1), 45–51.
- Yang, J.Y. and Chen, L.W. (1993) Large amplitude vibration of antisymmetric imperfect cross-ply laminated plates. *Compos. Struct.* **24**(2), 149–159.
- Yang, I.H. and Kuo, W.S. (1994) Stability and vibration of initially stressed thick laminated plates. *J. Sound Vib.* **168**(2), 285–297.
- Ye, J.Q. (1997) Three-dimensional free vibration analysis of cross-ply laminated rectangular plates with clamped edges. *Comput. Meth. Appl. Mech. Engng* **140**(3/4), 383–392.
- Ye, J.Q. (2003) *Laminated Composite Plates and Shells: 3D Modeling* (Springer, Berlin) p. 288.
- Ye, J.Q. and Soldatos, K.P. (1994) Three-dimensional vibrations of laminated cylinders and cylindrical panels with a symmetric or an antisymmetric cross-ply lay-up. *Compos. Engng* **4**, 429–444.
- Ye, J.Q. and Soldatos, K.P. (1996) Three-dimensional vibration of laminated composite plates and cylindrical panels with arbitrarily located lateral surfaces point supports. *Int. J. Mech. Sci.* **38**(3), 271–281.
- Ye, J.Q. and Soldatos, K.P. (1997) Three-dimensional vibrations of cross-ply laminated hollow cylinders with clamped edge boundaries. *J. Vib. Acoust.* **119**(3), 317–323.
- Yin, X. (1999) Simplification of frequency equation of multilayered cylinders and some recursion formulae of Bessel functions. *Appl. Math. Mech.* **20**(3), 332–337.
- Yong, Y.K. and Cho, Y. (1995) Higher-order, partial hybrid stress, FE formulation for laminated plate and shell analyses. *Comput. Struct.* **57**(5), 817–827.
- Young, P.G. and Dickinson, S.M. (1997) Natural frequencies of vibration of a class of solids composed of layers of isotropic materials. *Int. J. Mech. Sci.* **39**(1), 97–104.

- Zabaras, N. and Pervez, T. (1991) Viscous damping approximation of laminated anisotropic composite plates using the finite element method. *Comput. Meth. Appl. Mech. Engng* **81**(3), 291–316.
- Zarutski, V.A. (1998) Approximate nonlinear equations of motion of cylindrical shells from the composition materials (Russian). *Prikl Mekh (Appl. Mech.)* **34**(10), 55–59.
- Zarutsky, V.A. (1995) Approximate equations for calculation of natural frequencies of oscillations of longitudinally supported cylindrical shells obtained using the precise theory (Russian). *Prikl Mekh (Appl. Mech.)* **31**(3), 40–44.
- Zenkour, A.M. (1998) Vibration of axisymmetric shear deformable cross-ply laminated cylindrical shells: a variational approach. *Int. J. Engng Sci.* **36**(3), 219–231.
- Zhou, H.B. and Li, G. (1996) Free vibration analysis of sandwich plates with laminated faces using spline finite point method. *Comput. Struct.* **59**(2), 257–263.
- Zhu, J. (1996) Free vibration analysis of multilayered composite plates and shells with the natural approach. *Comput. Meth. Appl. Mech. Engng* **130**(1/2), 133–149.

Subject Index

- Algebraic polynomials 63, 66, 204
- Angle of twist 224–231
- Anisotropic 48
- Approximate solutions 60
- Arc length 24, 28, 185

- Bars 75
- Beams
 - Curved 75–105
 - Laminated 75–105
 - Sandwich 75
 - Straight 75
 - Thick 82–87
 - Thin 76–81
- Bending 109, 114, 189, 263
 - Cylindrical 78
- Bending modes (see Mode shapes)
- Bending stretching coupling 115, 167, 189, 263
- Boundary conditions
 - Forced 62
 - Geometric 62
 - Thick beams 86
 - Thick plates 119
 - Thick shallow shells 193
 - Thick shells 44
 - Thin beams 81
 - Thin plates 112
 - Thin shallow shells 186
 - Thin shells 51
 - Three dimensional 12–14
- Boundary element methods 72
- Boundary terms 178

- Cantilevered
 - Pretwisted plates 224–230
 - Rectangular plates 148, 152
 - Shallow shells 214–223
 - Trapezoidal plates 166
 - Trapezoidal shallow shells 247–249
 - Triangular plates 166
 - Triangular shallow shells 247–249
- Cartesian coordinates 6, 121, 187, 193
- Christoffel symbols 26
- Classical beam theory 76–81
- Classical plate theory 4, 109–115
- Classical shallow shell theory 185–190
- Classical shell theory 46–52
- Closed rings 75, 91
- Columns 75
- Compatibility conditions 14–15, 52
- Compatibility equations 14–15
- Completely free
 - Rectangular plates 148
 - Shallow shells 205–213
 - Trapezoidal plates 163
 - Trapezoidal shallow shells 241–247
 - Triangular plates 163
 - Triangular shallow shells 241–247
- Composite (see Laminated)
- Constitutive equations (see Stress-strain relations)
- Continuous systems 64, 99
- Convergence 64, 67, 99, 144, 161, 168, 205, 216, 225, 232, 241, 247
- Cross-ply lamination (see Lamination)
- Curvature changes
 - Thick beams 82
 - Thick cylindrical shells 265
 - Thick plates 110, 113
 - Thick shallow shells 190
 - Thick shells 35
 - Thin beams 77
 - Thin cylindrical shells 262

- Thin plates 117, 119
- Thin shallow shells 186
- Thin shells 47
- Curved plates 183

- Damped ring 75
- Damped shells 360
- Deformation 7, 28
- Degrees of freedom (DOF) 67, 69, 75, 99, 147–149, 217
- Differential quadratures 72, 179
- Displacement field 64, 69
- Doubly cantilevered 231–235
- Dynamic loading 358

- Elastic constraints 81, 142
- Elastic foundation 360
- Elasticity
 - Theory of 19, 260
 - Three dimensional (3D) 6, 12–14, 17, 23–28, 32, 54, 55, 116, 178
- Elements
 - Brick 67
 - Eight noded 67
 - Rectangular 67
 - Shell 67
 - Solid 67
 - Triangular 67
- Energy
 - Kinetic energy 16, 42, 80, 86, 114, 189, 263
 - Potential energy 16, 41, 80, 86, 114, 189, 263
 - Strain energy
 - Thick beams 86
 - Thick shells 41
 - Thin barrel shells 301
 - Thin beams 80
 - Thin conical shells 331
 - Thin cylindrical shells 263
 - Thin plates 114–115
 - Thin shallow shells 189–190
 - Thin shells 49
 - Three dimensional 16
- Energy functionals (see Energy) 61, 63
- Epoxy resin 8
- Equations of motion
 - Thick barrel shells 308
 - Thick beams 84
 - Thick conical shells 334
 - Thick cylindrical shells 266
 - Thick plates 118, 119, 177
 - Thick shallow shells 193, 194, 254
 - Thick shells 42
 - Thick spherical shells 351
 - Thin barrel shells 299
 - Thin beams 78
 - Thin conical shells 325
 - Thin cylindrical shells 262
 - Thin plates 111, 112, 176
 - Thin shallow shells 186, 188, 253
 - Thin shells 50
 - Thin spherical shells 348
 - Three dimensional 12, 32
- Exact solutions 60, 88, 93, 195–201, 268–284, 303, 309
- Existence of a solution 15
- Experimental methods 59
- External work 41

- Fiber 8, 31, 172
- Fiber orientation 8
- Finite differences 184
- Finite element methods 54, 66–72, 140, 146, 148, 149, 169, 184
- First fundamental form 24
- Fluid media 360
- Flutter 5
- Force resultants (see Stress resultants)
- Fourier analysis 72
- Fourier series 197
- Frenet's formula 25

- Galerkin method 65–66, 179, 184
- Gauss characteristic equation 27
- Geometric series 40

- Hamilton's principle 15–19, 32, 43, 81, 111, 112, 262
- Higher order terms 38, 40, 63
- Holography 59
- Homogeneous 9, 109, 112
- Imperfect shells 359
- Impulsive loading 358
- Initial loading 358
- Kinematic equations 7–8
 - Thick barrel shells 307
 - Thick beams 84
 - Thick conical shells 334
 - Thick cylindrical shells 265, 316
 - Thick plates 116, 177
 - Thick shallow shells 190, 252
 - Thick shells 34
 - Thick spherical shells 350
 - Thin barrel shells 298
 - Thin beams 78
 - Thin conical shells 324
 - Thin cylindrical shells 262, 315
 - Thin plates 110, 175
 - Thin shallow shells 186, 251–252
 - Thin shells 46
 - Thin spherical shells 348
 - Three dimensional 28
- Kerr foundation 360
- Kinetics 6
- Kirchhoff hypothesis 77, 110, 111
- Lagrangian 16, 17, 61, 63
- Lamé parameters 29, 111, 112, 119
- Lamination
 - Angle-ply 129, 122, 137, 196
 - Antisymmetric 60, 114, 122, 130, 129, 137
 - Asymmetric (see Unsymmetric)
 - Cross-ply 60, 122, 124, 126, 133, 196–198, 200, 268–284
 - Sequence 60, 139
 - Symmetric 41, 49, 80, 85, 140, 190
 - Unsymmetric 60, 122, 198–199
- Layer-wise theories 52
- Levy solution 122, 200
- Love's approximation 4, 33, 185
- Mainardi-Codazzi equations 27
- Mass parameters 120
- Matrix
 - Mass 70, 98, 198
 - Stiffness 69, 70, 98, 198
 - Transformation 10
- Membrane theory 46
- Midsurface strains (see Curvature changes)
- Modes 102, 103
- Mode shapes
 - Cantilevered pretwisted plates 227–231
 - Cantilevered shallow shells 220–223
 - Cylindrical shells 276
 - Doubly cantilevered shallow shells 234–236
 - Free shallow shells 212–214
 - Plates 150–155
- Moduli of elasticity 8
- Moduli of rigidity 8
- Moment resultants (see Stress resultants)
- Monoclinic 31
- Navier solution 122, 127, 197
- Newton's second law 12, 16, 111
- Nodes 66, 69
- Nonlinear
 - Analysis 178
 - Geometric nonlinearity 53
 - Material nonlinearity 53
 - Terms 29
 - Theories 53
- Orthotropy
 - Circular 8, 174–178, 184
 - Conical 324
 - Cylindrical 261
 - Diagonal 156
 - Elliptical 112
 - Rectangular 8, 112, 119, 173, 184
 - Spherical 348

- Pasternak foundation 360
- Piezoelectric shells 359
- Plates 109–179
 - Circular 112, 172–178
 - Elliptical 112, 178
 - Equilateral 165
 - Isotropic 158–159
 - Rectangular 121–158
 - Right trapezoidal 165
 - Right triangular 163
 - Symmetrical triangular 165
 - Thick 116–121, 126, 130, 135, 177
 - Thin 109–115, 124, 129, 134, 174
 - Trapezoidal 159–171
 - Triangular 159–171
- Preprocessor 66
- Polar coordinates 174, 253, 259
- Postprocessor 70
- Poisson's ratio 9
- Pretwisted (see Plates, pretwisted)
- Radius of twist (see Plates, pretwisted)
- Rayleigh method 61
- Rectangular coordinates
 - (see Cartesian coordinates)
- Resin 8
- Rings 75
- Ritz method 61–64, 95, 140–144, 146, 169, 179, 203–205, 286–297
- Rods 75
- Rotating shells 359
- Second fundamental form 25
- Shafts 75
- Shallow shells
 - Circular planform 249–254
 - Cylindrical 198–248
 - Ellipsoidal 183
 - Elliptical planform 185, 241
 - Equilateral 244–245
 - Hyperbolic paraboloidal 198–248
 - Rectangular planform 195–240
 - Right triangular 244–245
 - Spherical 186, 198–254
 - Symmetrical triangular 244–245
 - Thick 190–195
 - Thin 185–190
 - Trapezoidal 241–248
 - Triangular planform 241–248
- Shear deformation beam theory 82–87
- Shear deformation plate theory 4, 116–121
- Shear deformation shallow shell theory
 - 190–193
- Shear deformation shell theory 33–46
- Shear diaphragm 51, 124, 197–203
- Shear strain 8, 11, 29
- Shells
 - (see Shallow shells)
 - Barrel 297–314
 - Circular cylindrical 261–313
 - Conical 324–343
 - Cylindrical 261–320
 - Non-circular cylindrical 314–318
 - Shells of revolution 260, 324, 348
 - Spherical 348–353
- Similitude 59
- Simply supported
 - Barrel shells 303, 309
 - Beams 88–93
 - Cylindrical shells 268–284
 - Plates 124–137
 - Shallow shells 193–202
- Single layered bodies 14
- Single layered shells 32, 259
- Spherical caps 249–254
- Springs 142
- Stability 5
- State-space 72
- Stiffened shells 359
- Stiffness coefficients 11, 12, 77
- Strain 7
- Strain displacement relations
 - (see Kinematic relations)
- Stress resultants
 - Thick barrel shells 300
 - Thick beams 82

- Thick cylindrical shells 265
- Thick plates 116
- Thick shallow shells 192
- Thick shells 36
- Thin barrel shells 308
- Thin beams 77
- Thin cylindrical shells 262
- Thin plates 111, 113
- Thin shallow shells 186
- Thin shells 48
- Stress-strain relations
 - (see Stress resultants) 36
 - Thin shells 47–48
 - Three dimensional 8–12, 31
- Stretching 113, 114, 189, 263, 302, 331
- Stretching bending coupling
 - (see Bending stretching coupling)
- Superposition 72
- Surface tractions 13
- Surfaces, theory of 23–28
- Taylor series 33
- Theory of surfaces 23–28
- Thermal loading 178
- Three dimensional (see Elasticity)
- Transformation of stress 9
- Trial functions 65
- Trigonometric functions 156
- Twisting modes (see Mode shapes)
- Twisting moments 48, 118
- Undeformed surface 24
- Uniqueness of a solution 15
- Variable thickness 178
- Variational principles 15–19
- Virtual displacement 16
- Viscoelastic 75, 360
- Wavelength 34, 46, 110
- Wave propagation 360
- Weighted residual methods 65
- Weight functions 65
- Weingarten formulas 26
- Work 41, 80, 86
- Zero curvature 109